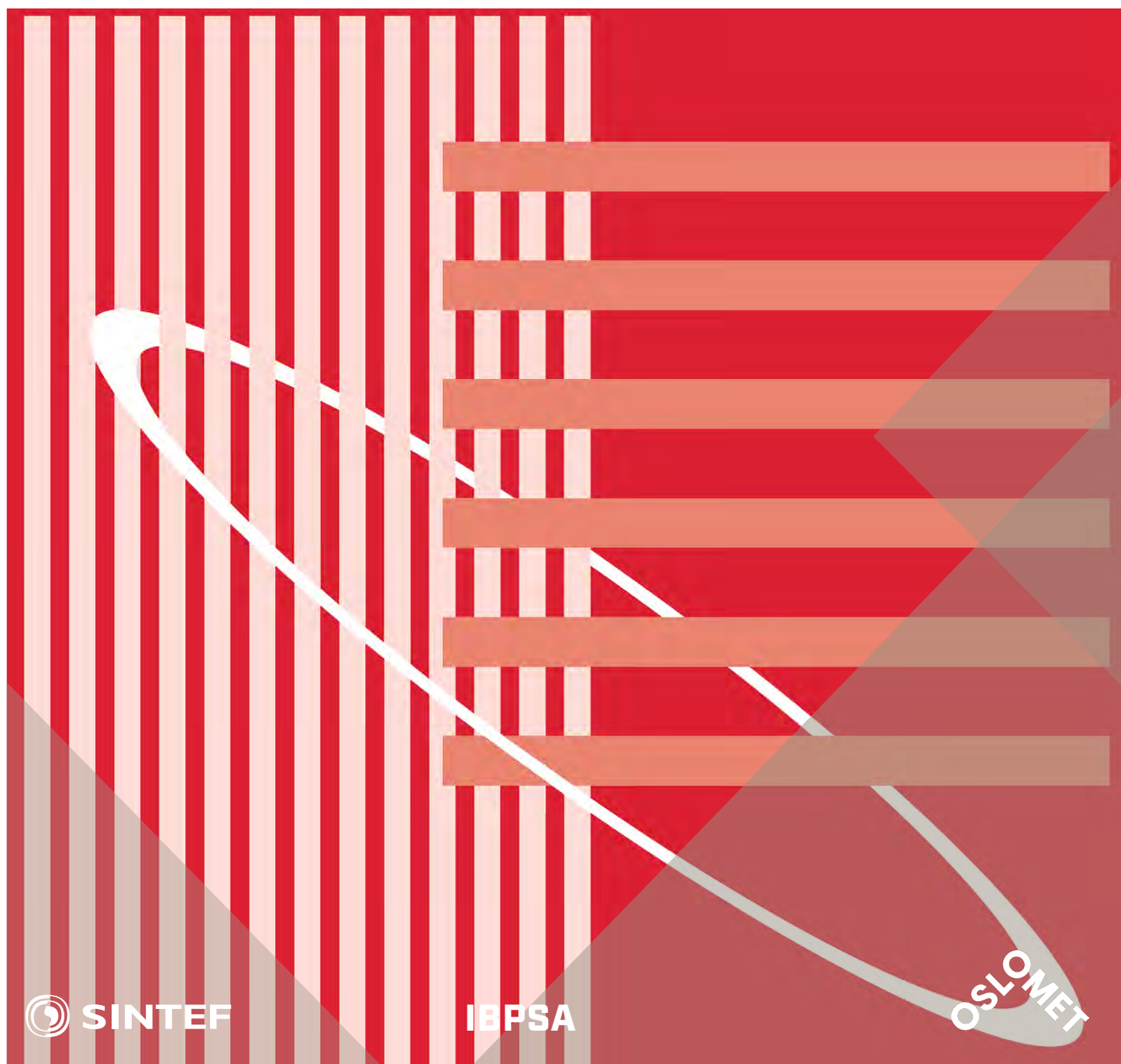International Conference Organised by
IBPSA-Nordic, 13th–14th October 2020,
OsloMet

BuildSIM-Nordic 2020
Selected papers

SINTEF   IBPSA   OSLOMET

SINTEF Proceedings

Editors:
Laurent Georges, Matthias Haase, Vojislav Novakovic and Peter G. Schild

BuildSIM-Nordic 2020

Selected papers

International Conference Organised by IBPSA-Nordic,
13th–14th October 2020, OsloMet

Keywords:
Building acoustics, Building Information Modelling (BIM), Building
physics, CFD and air flow, Commissioning and control, Daylighting and
lighting, Developments in simulation, Education in building performance
simulation, Energy storage, Heating, Ventilation and Air Conditioning
(HVAC), Human behavior in simulation, Indoor Environmental Quality (IEQ),
New software developments, Optimization, Simulation at urban scale,
Simulation to support regulations, Simulation vs reality, Solar energy
systems, Validation, calibration and uncertainty, Weather data & Climate
adaptation, Fenestration (windows & shading), Zero Energy Buildings
(ZEB), Emissions and Life Cycle Analysis

Cover illustration: IBPSA-logo

PREFACE

The BuildSim-Nordic 2020 conference is the first in a series of events with a long-term objective to establish a key biannual international conference in building performance simulation, with a strong focus on Nordic countries. The purpose is to create a platform for exchanging ideas, issues, and research findings that facilitates international collaboration and the meeting of minds between practitioners, researchers, and students.

This book contains selected papers approved by the reviewers and the scientific committee of the BuildSim-Nordic 2020 conference, October 13th & 14th 2020. The conference was hosted by OsloMet University in Oslo, Norway, and organized in cooperation between the Nordic chapter of IBPSA, OsloMet and NORVAC.

All submissions to the conference underwent a review process and presentation type was determined. Two blind reviewers evaluated each paper, a third reviewer was asked for evaluation in cases where the first two reviewers were not in good agreement. The selected full papers are of a high quality theoretical (scientific) nature.

IBPSA-Nordic is a regional affiliate of IBPSA, the International Building Performance Simulation Association, for four countries: Denmark, Finland, Norway and Sweden. IBPSA-Nordic is linked to IBPSA-World association but acts as an independent organization.

 The software company EQUA, known for its famous building simulation package IDA ICE, has sponsored the conference Buildsim-Nordic 2020 (Gold). This is highly appreciated.

Laurent Georges
Norwegian University of Science and Technology (NTNU)

Matthias Haase
Zurich University of Applied Sciences (ZHAW)

Vojislav Novakovic
Norwegian University of Science and Technology (NTNU)

Peter G. Schild
Oslo Metropolitan University (OsloMet)

Contents

UBEM, District Heating and Large Buildings

A top-down digital mapping of spatial energy use for municipality-owned buildings: a case study in Borlänge, Sweden

Samer Quintana [1, 2]*, Pei Huang [1], Mengjie Han [1], Xingxing Zhang [1]

[1] School of Technology and Business Studies, Dalarna University, Falun, Sweden

[2] Department of Engineering Sciences, Uppsala University, Uppsala, Sweden

* corresponding author: ssq@du.se

Abstract

Urban energy mapping plays a crucial role in benchmarking the energy performance of buildings for many stakeholders. This paper studies a set of buildings in the city of Borlänge, Sweden, owned by the municipality. The aim is to present a digital spatial mapping of both electricity use and district heating demand. A toolkit for top-down data processing and analysis is considered based on the energy performance database of municipality-owned buildings. The data is initially cleaned and transformed using the Feature Manipulation Engine tool (FME) and then is geocoded using a python script with an application program interface (API) for OpenStreetMap. The final dataset consists of 221 and 89 geocoded addresses for, respectively, electricity and district heating monthly consumption for the year 2018. The electricity use and heating demand in the building samples is about 24.06 kWh/m^2 and 190.99 kWh/m^2 respectively, where large potential in saving heating energy is observed. The digital mapping reveals a spatial vision of identifiable hotspots for electricity uses in high-occupancy-dense areas and for district heating needs in districts with buildings mostly constructed before 1980. This result will provide a comprehensive understanding of the existing energy distributions to stakeholders and energy advisors. It will also facilitate strategy towards future energy planning in the city such as energy benchmarking policies.

Introduction

Buildings represent large energy end-users worldwide. In the E.U. and U.S, buildings currently consume over 40% of total primary energy usage (Huang et al., 2020). With sights set in the new paradigm shift regarding energy production, efficiency and climate change, Sweden will implement strategies to reach national targets of energy efficiency in the building sector by 2050, According to this target energy use per square metre should decrease by 20% to 2020 and 50% to 2050, in comparison with use in 1995, A national target for energy efficiency in the housing sector is proposed (Ministry of Sustainable Development Sweden, 2006). In 2010, over 50% of the world's population are living in urban areas. By 2050, this number is expected to reach 75% (UN-Habitat, 2009). Urban development and the expansion of cities, through the modification of land uses (from natural to artificial) modify the local energy budget and wind patterns. Such transform has significantly changed the microenvironment and the related energy usage in urban cities (Torabi Moghadam et al., 2019). The mapping of urban building energy plays a crucial role in understanding the multitude of agents that take part in the energy performance of buildings, which will set up the benchmarks in different districts for various stakeholders.

In the context of sustainable cities, spatial visualization is a very effective approach to help decision-makers in the urban planning process to create future energy transition strategies and implement energy efficiency and renewable energy technologies. Geographic Information System (GIS) techniques can be used for visualizing the energy demand or production in buildings, from urban to regional, or even to a national scale. Some of these visualization techniques are: the thematic 2D map (Mhalas et al., 2013); the 'hit maps' (i.e., aggregated data in 3D charts) (Murugesan et al., 2015); the 3D city models with semantic objects (Gröger and Plümer, 2012). There are many studies using GIS techniques to visualize the energy data in building stocks. For instance, Mattinen et al. developed a method for estimating and visualizing the energy use and greenhouse gas emissions from a residential building stock located in Kaukajärvi district, Finland (Mattinen et al., 2014). Using such visualization model, they also analysed the impacts of behavioural and technical changes on the energy performance in the building stock. Finney et al. made a comprehensive mapping of heat sources and sinks in Sheffield City, the UK (Finney et al., 2013). Based on the heat source mapping, they linked these smaller systems to create a combined-heat-and-power based urban-scale network of energy generation and delivery. Huang et al. used GIS technique to obtain the roof area in Kowloon district in Hong Kong. Using the obtained roof are, they evaluated the solar power potentials of the whole district by installing rooftop PV panels. Based on the mapped solar power potentials, they developed an optimal design method to sit the public charging stations (Huang et al., 2019). Similarly, Ramachandra and Shruthi used the GIS technique to map the wind energy resources of Karnataka state, India. Based on the wind power mapping, they analysed their variability considering spatial and seasonal aspects (Ramachandra and Shruthi, 2005).

In Swan and Ugursal's study, the modelling approaches for energy consumption in a number of buildings were classified into bottom-up or top-down approaches (Swan and Ugursal, 2009). The bottom-up approach is more appropriate when there is a need for evaluating the energy consumption based on a high detailed level of data and the ability to model technological systems (Kavgic et al., 2010). Bottom-up models can be divided into two types: deterministic (or engineering) and statistical. The statistical methods search for correlations, utilizing a sample of information in energy bills as a source of data for energy modelling and analysing the link between energy consumption and a range of different variables (e.g. building shape, age, and occupant behaviour) (Nouvel et al., 2015). They can also consider socioeconomic effects in the equations. They calculate reliable consumption based on the available information on the current status of buildings. However, due to their strong dependency on available historical consumption data, these methods are restricted to predict the impact of new technology options and energy saving potential after applying refurbishment measures (Torabi Moghadam et al., 2018). The deterministic methods are detailed models which are based on thermodynamic relationships and heat transfer calculations (Bruse and Fleer, 1998). The main advantage of an engineering-based method is the ability of predicting energy saving potentials for buildings if some renovation measures are to be implemented (Mauree et al., 2017). These modelling approaches require a large amount of information about the building structures and parametric input for estimating the energy usage of a set of reference buildings of the stock based on a numerical model. Additionally, the evaluation of urban planning scenarios is computationally extensive and the availability of construction and geometrical data needed as input for the models is very scarce. The top-down approach treats the entire residential sector as one energy sink. The top-down methods are suitable for a large-scale analysis and not for the identification of the possible improvements at the building at urban and local levels (United Nations, 2015). Compared with the bottom up-approach, the top-down approaches are relatively easy to develop based on the limited information provided by macroeconomic indicators such as price and income, technology development pace, and climate. As summarized by Swan and Ugursal, the top-down approach has advantages including long-term forecasting in the absence of any discontinuity, inclusion of macroeconomic and socioeconomic effects, simple input information required and encompasses trends (Swan and Ugursal, 2009).

Although there are existing studies in mapping energy uses in different cities, a spatial energy analysis in local municipality is necessary as it will be different in various city and culture contexts. Specific consideration in general needs to be paid to the differences between cities when it aims to optimize the integration of urban energy systems operated in buildings, and promote renovation and renewable energy systems. Because cities differ from each other at the local, national and international levels in the perspectives of geography, socio-economy, culture, infrastructure, and information platform. The type of cities and districts will determine the kind of users and needs, and consequently the nature (qualitative and quantitative) of the policy/regulation schemes and the calibration/adjustment of the energy infrastructures. The citizen's behaviours and needs/preference of energy may be different to each other in different cities, which will lead to a great difference in the energy demand. Within the same framework of transforming to sustainable and liveable city, different areas must not only adopt standardized approaches, but also consider the specificities at the local level. A dedicated research into local city and district is therefore of paramount importance to ensure the proper mix between international/national scenarios and local measures.

The urban energy mapping and analysis for Borlänge city have not yet been done. Therefore, this paper aims to cover the research gap by studying a set of buildings owned by the municipality of Borlänge, Sweden. The initial step of the study is to give a spatial mapping of both electricity use and district heating demand. A top-down approach is considered based on the energy consumption data of the municipality-owned buildings. It is expected that this study is able to provide insights that will allow the understanding of the existing local energy distributions. It will also facilitate strategy towards future energy planning in this city.

This paper is structured as the following: Methods, illustrates the data source and the methodology of processing the data; in Results and discussion, both statistical and spatial analysis are presented this case in Borlänge; Conclusion is further depicted after.

Methods

Data sources

Acquiring the necessary data to create an urban model can be a difficult endeavour. New general data protection regulation laws (GDPR) by the European Parliament regulates how the data must be acquired, handled and stored while protecting the privacy of the individuals (European Parliament, 2016). Energy consumption data is sensitive information that fall into the new regulation, greatly complicating the data acquisition. Depending on the data resolution, storing the information can be complicated, may be not kept for large periods of time or stored in obsoletes systems making difficult to be of use.

The primary source of data used for this model is provided by Tunabyggen, a municipality owned company that constructs, manages and rents a set of buildings in the Borlänge municipality. The data is provided in PDF format, containing a total number of 375 pages monthly data for electricity demand, district heating and hot water flow rate for the year 2018. The geographical information is obtained from the official Swedish surveying

institution, Lantmäteriet, specifically, the vector data for the property information and LiDAR data for the Borlänge municipality. Other social statistics and specific data such as building year of construction, percentage of occupation, demographics, typologies, are acquired from hitta.se, which is a Swedish search engine that offers telephone directory, addresses and maps. To complete and validate the model, it is necessary to use some extra information that was obtained by visual inspection including the number of floors, area and shape of the roofs. The flowchart, Figure 1, further describes the processes, databases and validation operations.
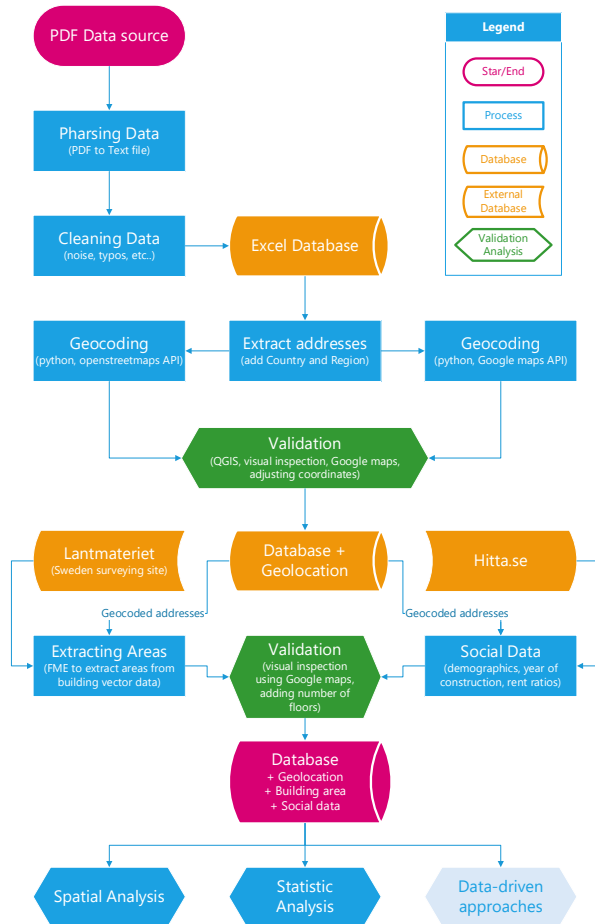
Figure 1 Flowchart for data processing, extraction, geocoding and validation

Data extraction

The first step in the process is to extract the information from the data source provided. The PDF archaic data structure format must be transformed into a common format that can be used by other applications. In order to extract the data a custom python script is written to parse out the information. Then, the data is further inspected for missing data and error correction. From the 375 pages in PDF format, a total of 262 addresses and 463 entry points of monthly data for electricity (kWh), district heating (MWh) and flow rate (m^3) for the year 2018 are extracted.

Geocoding

The extracted addresses from the data source are further expanded to the city and the country. Then, it is run through a python script, using an application program interface (API) for OpenStreetMap, Figure 2, gives the script that uses pandas, geopy libraries. In parallel, another script was used to connect to Google Maps API geocoding services. Two outputs from each geocoding service are obtained with the longitude and latitudes of the addresses. The output format for the coordinate system is the standard LL-WGS84. The location for a total of 222 out of the 262 entry points were found on the first iteration.

```
df=pandas.read_excel ("addresses.xlsx")

from geopy.geocoders import Nominatim

nom=Nominatim(user_agent="my-application")

df["address"]=df["address"]+", "+df["City"]+", "+df["State"]+", "+df["Country"]

df["Coodinates"]=df["address"].apply(nom.geocode)

df["Latitude"]=df["Coodinates"].apply(lambda x: x.latitude if x != None else None)

df["Longitude"]=df["Coodinates"].apply(lambda x: x.longitude if x != None else None)
```

Figure 2 Python script, for OSM API geocoder

Geocoding validation

The results are plotted and further inspected for validation. During this process, the locations are geocoded and manually centred in the property area, as displayed in Figure 3. The green dots are the geocoded locations and the brown dots are the manually centred locations. The output becomes to 238 out of the 262 total addresses, leaving a total of 24 addresses and 31 entry points that are not able to be geocoded due to unspecific naming until manual visual inspection and analysis of the context is performed. The final result generates a total of 250 geocoded addresses and 12 unclarified ones.
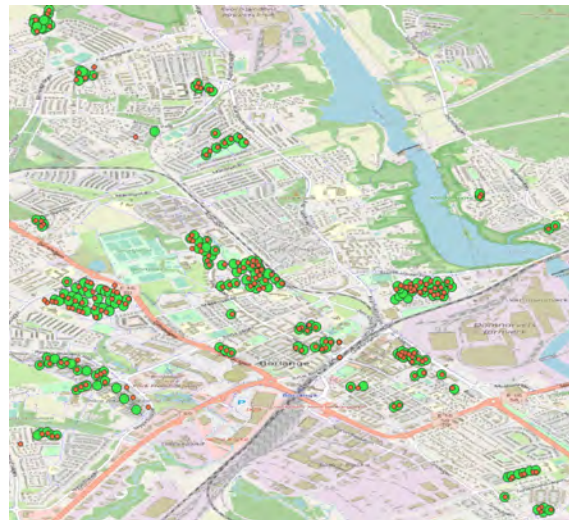
Figure 3 Geocoded data and adjusted coordinates

Area merger code, area validation

Next parameters are extracted from the Swedish survey database Lantmäteriet. The building property vector information is provided in a shapefile (.shp) format, a digital vector storage format for storing geometric location and associated attribute information.

Using the Feature Manipulation Engine (FME) tool, shown in Figure 4, it is possible to extract and calculate the areas for the geocoded addresses points. This information is compared to the visual inspected area, in order to analyse its accuracy. The extra information stored in the shapefile is incorporated to the dataset. This information includes a building description, coordinates in the Swedish reference system SWEREF-99-TM and a unique object identity.
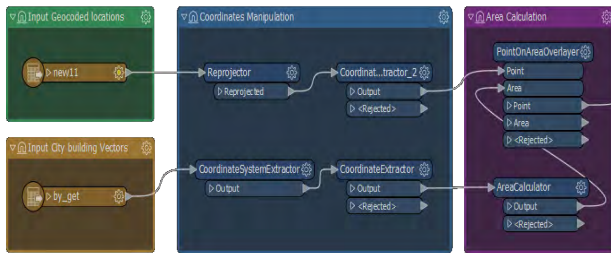
Figure 4 Process of FME area merger workflow

Data processing

All the different sources of information are finally combined together and inspected for errors or inconsistencies. The total building area is calculated using the number of floors and the buildings vector surface areas. Finally, the results for the energy consumption, electricity and district heating in kWh/m^2 for the year 2018 are obtained.

In total, there are 250 addresses that are geocoded, while 28 addresses are excluded from the dataset analysed. This is due missing, erroneous or abnormal information. The final sample dataset consists of 221 buildings for the electricity data and 89 buildings for district heating data.

Results and discussion

Statistic data analysis

In the considered building samples, all of the buildings are residential buildings and the related facility buildings (such as laundries, storage, etc.). The energy use is normalized by dividing the energy use by the heated floor area. The definition of the heated or living floor area has a large impact on the magnitude of the area-specific energy requirement. In Sweden, the heated floor area is defined as the floor area that is heated more than 10ºC. As a result, in this study, we assume the heated floor area is averagely 87% of the total external floor area for the analysis (Mata and Kalagasidis, 2009). In addition, electricity demand is further normalized by considering the occupancy ratio of each building. For heating demand there is no need to consider the occupation ratio, as it is common in Sweden for the heating systems to stay on even there is no occupancy in the building.

The annual electricity demand for lighting and appliance in the building samples are illustrated in Figure 5.
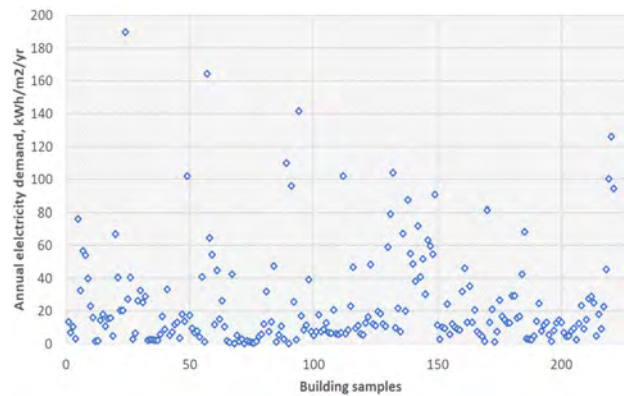
Figure 5 Annual electricity demand for building samples

The mean electricity demand of 222 building samples are 24.06 kWh/m^2, with a total range from minimum 0.02 kWh/m^2 to maximum 189.89 kWh/m^2. Comparing to the average electricity demand of 30-36 kWh/m^2 in Swedish context (Mata et al., 2013), the average electricity demand of the building samples is reasonably low, as most the occupants in the sample's buildings have relatively lower income. The median electricity demand is 12.72 kWh/m^2, which means that 50% of the building samples demand less electricity than this value. Furthermore, over 76% of the building samples achieves lower electricity use than 30 kWh/m^2.

According to the Swedish Housing Agency's building rules (Boverket, 2011), it requires energy performance for buildings depending on their use, end-use heating system and climate zones. The energy performance (heating demand) requirements are given as the specific energy use, comprising the purchased energy for space heating, domestic hot water and electricity for fans and pumps but excluding electricity for household appliances and lighting (Dodoo and Gustavsson, 2014). The annual heating demand for the building samples are displayed in Figure 6.
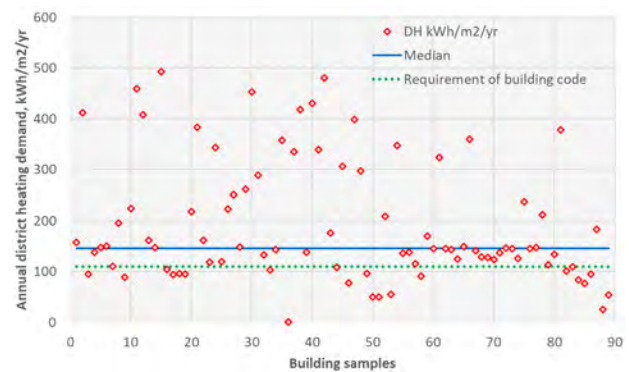
Figure 6 Annual heating demand for building samples

The mean heating demand of 89 building samples are 190.99 kWh/m^2, with a total range from minimum 0.41 kWh/m^2 to maximum 492.52 kWh/m^2. Borlänge city belongs to climate zone II in Sweden, where the new building code requires up to 110 kWh/m^2 energy use for

non-electric heated buildings (with district heating) annually. In addition, passive houses criteria even have higher requirements with up to 35% lower value compared to building code (FEBY, 2012). Thus, the average heating demand in the building samples is much higher than either the building code or the passive house standard, which is about 2 times of the requirement by building code, and 3 times of the requirement by passive house standard. The median heating demand is 145.43 kWh/m^2, which means that 50% of the building samples demand less heating than this value. Approximately 25% of the building samples achieves lower heating demand than 110 kWh/m^2. The difference between the different counties is clear. In Gävleborg, it is found that the average heating demand was about 185 kWh/m^2 in 2010. When across the whole Sweden, the average annual energy use for heating in single- or two-dwelling was reported at about 158 kWh/m^2 per year in 2014 (Swedish Energy Agency, 2015). So, the heating use in Borlänge city stays at a high level when compared to the closed regions and the average figure over the country.

However, this high energy demand can be understood since over 60% of the buildings in the sample were constructed before 1980, and therefore it may not be energy efficient dwellings. The annual heating demand average varies considerably depending on the year of construction of the building. For buildings built after 1980, the heating demand is of about 97-98 kWh/m^2 in 2004, while those built before 1980 used heating from 120 to 133 kWh/m^2 per year (Pallardó, 2011). In the sample, the average heating demand for buildings constructed before 1980 is about 187.98 kWh/m^2 per year, where these buildings account for 90,651 m^2 of the heated floor area. So, there is great potential (about 4,532 - 5,439 MWh/year) for these buildings built before 1980 to improve their energy performance through renovations such as, increasing the thermal insulation of the walls/roofs, upgrading windows and heating radiators for example.

Spatial data analysis

Digital mapping method is applied hereby to compile and format the energy data into a virtual image, which is to produce a general map with energy use in Borlänge city based on building samples, which offers appropriate representations of the dedicated areas and districts. Using a Geographic Information System (GIS) tool - QGIS, it is able to visualize the sample energy data on the spatial map of Borlänge. Using the yearly electricity and heating demand in the unit of kWh/m^2 as the weight factor, longitude and latitude of the addresses, two digital maps are generated as shown in Figure 7 and Figure 8, respectively for electricity use and heating demand.

These digital maps provide an interactive and scalable way of visualizing the energy use across the city, which is used to spot abnormalities or faulty energy data points. These maps also illustrate a spatial idea of identifiable hotspots for electricity uses in high-occupancy/dense

areas. For district heating demands it shows hotspots with buildings mostly constructed before 1980. For instance, some of the hotspots can be easily identified as several student's accommodation areas in the northwest quadrant. These highly dense buildings have high electricity consumption since the occupants remain indoor for the most learning and living activities, but at the same time these buildings have relatively low heating needs as the buildings are well maintained and insulated. It is observed from these two maps that electricity use is mainly relied on the occupancy density, where higher population per floor area usually results in higher electricity use. On the other hand, district heating demand is dependent on the building itself, where poorly-insulated building leads to higher heating need. As a result, electricity use and heating demand do not always appear in the same district/area since they are influenced by different parameters. This offers clear insights for planning of urban energy infrastructure and distributions, as well as the potential contributions from local renewable energy source (RES) systems. For instance, more electricity distribution or RES power generation is necessary for high-dense residential areas, while higher heating should be distributed to those areas with buildings mostly constructed before 1980.
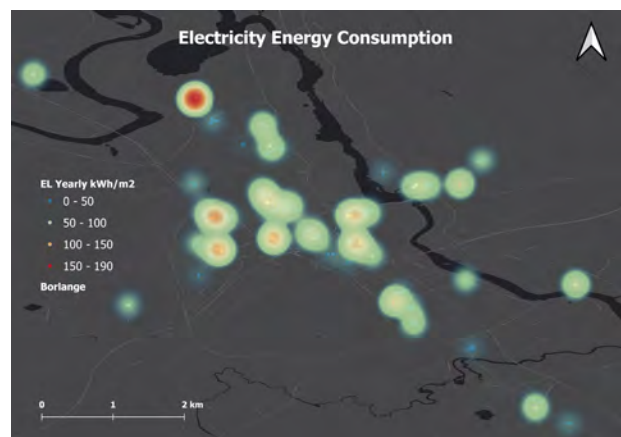
Figure 7 Digital mapping of electricity use in Borlänge city based on building samples
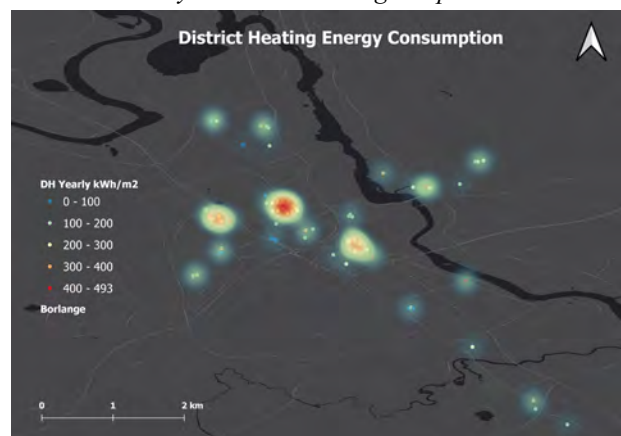
Figure 8 Digital mapping of heating demand in Borlänge city based on building samples

Conclusion

A dedicated spatial analysis of both electricity use and district heating demand in a Swedish local-city context is completed, through a toolkit for top-down digital mapping. The average electricity demand in Borlänge building samples are 24.06 kWh/m^2, which is reasonably lower than the average value in Sweden. The mean value of heating of the building samples is 190.99 kWh/m^2, which is much higher than either the building code or the passive house standard. The heating use in Borlänge city stays at a high level when compared to the closed regions and the average figure over the country. In particular, there are great potentials (about 4,532 - 5,439 MWh/year) for the buildings built before 1980 to improve the energy performance.

The digital maps illustrate a spatial vision of identifiable hotspots for electricity uses in high-occupancy-dense areas and for district heating needs in districts with buildings mostly constructed before 1980. Electricity use and heating demand do not always appear in the same district/area since they are influenced by different parameters. This offers clear insights for planning of urban energy infrastructure and distributions, as well as potential contribution from local RES implementation.

Acknowledgement

References

Boverket, 2011. Boverket´s mandatory provisions and general recommendations, BBR, BFS 2011:6 with amendments up to BFS 2018:4 154.

Bruse, M., Fleer, H., 1998. Simulating surface–plant–air interactions inside urban environments with a three dimensional numerical model. Environmental Modelling & Software 13, 373–384. https://doi.org/10.1016/S1364-8152(98)00042-5

Dodoo, A., Gustavsson, L., 2014. Effect of Energy Efficiency Requirements for Residential Buildings in Sweden on Lifecycle Primary Energy Use. Energy Procedia 61, 1183–1186. https://doi.org/10.1016/j.egypro.2014.11.1049

European Parliament, 2016. Regulation (EU) 2016/ 679 of the European Parliament and of the council - of 27 April 2016 - on the protection of natural persons with regard to the processing of personal data and on the free movement of such data, and repealing Directive 95/46/EC (General Data Protection Regulation) 88.

FEBY, 2012. Specification for zero energy, passive and low-energy houses.

Finney, K.N., Zhou, J., Chen, Q., Zhang, X., Chan, C., Sharifi, V.N., Swithenbank, J., Nolan, A., White, S.,

Ogden, S., Bradford, R., 2013. Modelling and mapping sustainable heating for cities. Applied Thermal Engineering, Includes Special Issue: PRO-TEM Special Issue 53, 246–255. https://doi.org/10.1016/j.applthermaleng.2012.04.009

Gröger, G., Plümer, L., 2012. CityGML – Interoperable semantic 3D city models. ISPRS Journal of Photogrammetry and Remote Sensing 71, 12–33. https://doi.org/10.1016/j.isprsjprs.2012.04.004

Huang, P., Lovati, M., Zhang, X., Bales, C., 2020. A coordinated control to improve performance for a building cluster with energy storage, electric vehicles, and energy sharing considered. Applied Energy 268, 114983. https://doi.org/10.1016/j.apenergy.2020.114983

Huang, P., Ma, Z., Xiao, L., Sun, Y., 2019. Geographic Information System-assisted optimal design of renewable powered electric vehicle charging stations in high-density cities. Applied Energy 255, 113855. https://doi.org/10.1016/j.apenergy.2019.113855

Kavgic, M., Mavrogianni, A., Mumovic, D., Summerfield, A., Stevanovic, Z., Djurovic-Petrovic, M., 2010. A review of bottom-up building stock models for energy consumption in the residential sector. Building and Environment 45, 1683–1697. https://doi.org/10.1016/j.buildenv.2010.01.021

Mata, É., Kalagasidis, A.S., 2009. Calculation of energy use in the Swedish housing 52.

Mata, É., Sasic Kalagasidis, A., Johnsson, F., 2013. Energy usage and technical potential for energy saving measures in the Swedish residential building stock. Energy Policy, Special section: Long Run Transitions to Sustainable Economic Structures in the European Union and Beyond 55, 404–414. https://doi.org/10.1016/j.enpol.2012.12.023

Mattinen, M.K., Heljo, J., Vihola, J., Kurvinen, A., Lehtoranta, S., Nissinen, A., 2014. Modeling and visualization of residential sector energy consumption and greenhouse gas emissions. Journal of Cleaner Production 81, 70–80. https://doi.org/10.1016/j.jclepro.2014.05.054

Mauree, D., Coccolo, S., Kaempf, J., Scartezzini, J.-L., 2017. Multi-scale modelling to evaluate building energy consumption at the neighbourhood scale. PLoS ONE 12, e0183437. https://doi.org/10.1371/journal.pone.0183437

Mhalas, A., Kassem, M., Crosbie, T., Dawood, N., 2013. A visual energy performance assessment and decision support tool for dwellings. Visualization in Engineering 1. https://doi.org/10.1186/2213-7459-1-7

Ministry of Sustainable Development Sweden, 2006. Swedish national roadmap for implementing the European Environmental Technologies Action Plan (ETAP).

Murugesan, L.K., Hoda, R., Salcic, Z., 2015. Design criteria for visualization of energy consumption: A systematic literature review. Sustainable Cities and Society 18, 1–12. https://doi.org/10.1016/j.scs.2015.04.009

Nouvel, R., Mastrucci, A., Leopold, U., Baume, O., Coors, V., Eicker, U., 2015. Combining GIS-based statistical and engineering urban heat consumption models: Towards a new framework for multi-scale policy support. Energy and Buildings 107, 204–212. https://doi.org/10.1016/j.enbuild.2015.08.021

Pallardó, G.G., 2011. Energy Consumption in Tertiary Buildings in Sweden Case-study: M-building at Lund University – LTH, Lund University.

Ramachandra, T.V., Shruthi, B.V., 2005. Wind energy potential mapping in Karnataka, India, using GIS. Energy Conversion and Management 46, 1561–1578. https://doi.org/10.1016/j.enconman.2004.07.009

Swan, L.G., Ugursal, V.I., 2009. Modeling of end-use energy consumption in the residential sector: A review of modeling techniques. Renewable and Sustainable Energy Reviews 13, 1819–1835. https://doi.org/10.1016/j.rser.2008.09.033

Swedish Energy Agency, 2015. New regional energy statistics for single- or two-dwelling buildings [WWW Document]. URL http://www.energimyndigheten.se/en/news/2011/new-regional-energy-statistics-for-single--or-two-dwelling-buildings/ (accessed 5.10.20).

Torabi Moghadam, S., Coccolo, S., Mutani, G., Lombardi, P., Scartezzini, J.-L., Mauree, D., 2019. A new clustering and visualization method to evaluate urban heat energy planning scenarios. Cities 88, 19–36. https://doi.org/10.1016/j.cities.2018.12.007

Torabi Moghadam, S., Toniolo, J., Mutani, G., Lombardi, P., 2018. A GIS-statistical approach for assessing built environment energy use at urban scale. Sustainable Cities and Society 37, 70–84. https://doi.org/10.1016/j.scs.2017.10.002

UN-Habitat, 2009. Global report on human settlements 2009: Planning sustainable cities.

United Nations, 2015. Global Initiative for Resources Efficient Cities.

Requirements for representative models for comfort and energy simulations in districts

Matthias Haase[1*]
[1]SINTEF, Trondheim, Norway

corresponding author: mathaase@gmail.com

Abstract

The energy master planning process for districts requires an analysis of different scenarios, which include new construction to different levels of energy efficiency, major renovation of all or some buildings comprising building stock under consideration with Deep Energy Retrofit of these buildings, minor renovations with energy-related scope of work, or demolition of some old buildings. Such analysis requires building energy modeling. In this research work we collected models of representative buildings from several countries and compared them.

Different baselines and constraints were compared for different countries as Australia, Austria, Canada, Denmark, Finland, Germany, Norway, UK and USA and were put into context (cultural and economic) and pattern were developed. In typical districts in city centres the dominant commercial buildings are often heated, cooled, and ventilated. The same retail units are never connected to other buildings or spaces of activities. Still, large open doorways through which air, odours, light, and noise exchanges occur, effectively linking the different spaces, exist. The next step will be to develop a common approach to calibration of building models to existing energy use data available from metering and sub metering.

Introduction

Climate change challenge the ambitious goals that regulators have put in place by setting more and more aggressive building and community energy-related requirements based on the Sustainable Development Goals of the UN. The concept of Energy Master Planning (EMP) can help to initiate a better planning and implementation process to fulfill these goals. In the EU, reaching for the climate gas reduction goals of the Paris Agreement, stakeholders on all geographical and organizational levels from nations, regions, cities and communities are challenged. Following bottom-up approaches for energy planning on the neighborhood level is a promising attempt to reduce energy demand, increase efficiency and lower the carbon footprint in a multi-stakeholder approach.

In the context of the 2012 EU directive (EED 2012), several important measures have been adopted throughout the EU to improve energy efficiency. These include national long-term renovation strategies for the building stock in each EU country, mandatory energy efficiency certificates accompanying the sale and rental of buildings, the preparation of national energy efficiency action plans (NEEAPs) every three years, minimum energy efficiency standards and labelling for a variety of products, as well as obligation schemes for energy companies (to achieve yearly energy savings of 1.5% of annual sales to final consumers). However, Member States have yet to fully implement the Directive and additional support in building capacity and know-how is needed (EPBD 2018). Significant additional energy savings, reduced emissions, and increased energy security can be realized by considering holistic solutions for the heating, cooling and power needs of communities, on neighbourhood and district scale, comprising collections of buildings. As a result, considerable literature has become available including both guidance and assessment tools aimed at EMP at the neighbourhood and district level as e.g. campuses (DOE 2013; Huang et al. 2015; EnergyPlan 2019; BREEAM 2019; LEED 2019). But the existing guidance and tools do not seem to be fully solving the challenges. The energy planning consists in determining the optimal mix of energy sources to satisfy a given energy demand. The major difficulties of this issue lie in its multi scales aspect (temporal and geographical), but also in the necessity to consider the quantitative (economic, technical) but also qualitative (environmental impact, social criterion) criteria (Schiefelbein et al. 2017).

In order to be able to apply principles of a holistic approach to neighborhood and districts, often coined community energy planning in the literature, and to provide the necessary methods and instruments to master planners, decision makers, and stakeholders, it is essential to identify and frame the constraints that bound the options towards an optimized energy master planning solution (Sharp et al. 2020). Existing master planning guidance available indicates that identifying and establishing project goals is a critical first step (Jank, 2017).

In a new initiative of the European Commission, Positive Energy Districts are envisioned as "*are energy-efficient and energy-flexible urban areas or groups of connected buildings which produce net zero greenhouse gas*

emissions and actively manage an annual local or regional surplus production of renewable energy. They require integration of different systems and infrastructures and interaction between buildings, the users and the regional energy, mobility and ICT systems, while securing the energy supply and a good life for all in line with social, economic and environmental sustainability." (JPI UE 2020).

In many cities, the necessary legal and strategic frameworks for the realization of PED/PENs are not yet in place. Very often, there is also a lack of a planning culture in city administrations or the personnel resources available might be insufficient. In particular, the transformation of large (brownfield) areas to climate neutral city districts has a big potential for the development of PED/PENs but needs cooperation between administration, industry, and research. Especially in case of heterogeneous ownership structures, cooperative planning processes are indispensable. Far less common in EMP guidance and related literature is information on the identification of constraints that limit energy technology options and how stakeholders influence the decision-making process. Literature in this area mentions options analysis or prioritization, or optimization analysis (EED 2012; Jank, 2017; Fox 2016; Zhivov et al. 2014; Robinson et al. 2009), yet, options analysis or optimization is certainly influenced by project energy-related constraints. Sharp et al. (2020) compared EMP in several countries and analysed these constraints (Sharp et al. 20120). The results show that successful energy master planning is highly dependent on a thorough understanding of framing goals and constraints, both local and regional, and their associated limitations that will dictate the optimum master planning design. Haase and Baer (2020) pointed out that as more and more countries push to improve the efficiency, environmental impact, and the resilience of their buildings and neighbourhoods, the need for early and comprehensive energy master planning on neighbourhood and district level is critically important.

The development of districts requires a distinct understanding of the situation now as well as a vision of the future district to be able develop suitable pathways for this transition. In order to be able to do that a district needs to be modelled that consists of several buildings, sufficiently described so that the future district can actively manage their energy consumption and the energy flow between them and the wider energy system. The energy master planning process requires an analysis of different scenarios, which include new construction to different levels of energy efficiency, major renovation of all or some buildings comprising building stock under consideration with Deep Energy Retrofit of these buildings, minor renovations with energy-related scope of work, or demolition of some old buildings. Such analysis requires building energy modeling. In this research work

we developed requirements for representative models of buildings and districts from several countries.

Methods

The paper develops new performance concepts for districts based on the technical functionality of district architecture, and on concepts with functional and organizational element sub-division.

The IPMVP Volume III focuses on energy savings in new constructions, whereas Volume I refers mainly to retrofit constructions. The fundamental difference between M&V in new and retrofit construction is related to the baseline (IPMVP 2002). The baseline in a retrofit project is usually the performance of the building or system prior to modification. This baseline physically exists and can therefore be measured and monitored before the changes are implemented. In new construction, the baseline is usually strictly hypothetical; it does not physically exist, and therefore cannot be measured or monitored. A new construction baseline can be defined or characterized by code or regulations, common practice, or even the documented performance of similar constructed buildings.

Energy codes and standards for buildings can provide a convenient, clearly defined, and consistent baseline to ensure appropriateness. Whole building energy simulation tools require high level of design detail for proper analytical rigor, requiring a well-developed design of each building. M&V requires baselines that are consistent and repeatable, or that can at least be readily adjusted to allow performance comparisons on a broader scale.

An accurate determination of energy savings is a key condition for long term success of energy management projects. Energy savings are determined by comparing measured energy use before and after implementation of an energy saving measurements.

To perform these kinds of analysis, it is necessary to:

- Identify the market segments and the segmentation of the current energy performance requirements (different requirements for different building types) where applicable;
- define and select a sufficient number of reference buildings that are characterised by their functionality, characteristics and regional conditions, including indoor and outdoor climate conditions;
- specify packages of energy saving- energy efficiency- and energy supply measures to be assessed;
- assess the corresponding energy-related investment costs, energy costs and other running costs of relevant packages applied to the selected reference buildings;
- use, when appropriate, the established reference buildings and relevant packages to identify, using the same methodology, cost-optimal energy performance requirements for building elements and technical building systems.

One of the first steps in energy master planning is to determine the framing constraints.

The imposed constraints are constraints that for the most part is relevant for individual buildings or facilities (e.g. requirements on maximum energy consumption, emissions or requirements on specific indoor climate parameters) but the imposed constraints can also apply to the entire district (e.g. local plans or national energy targets). The energy planner, owner or operator of the district could also choose to impose special voluntary operational constraints that are more restrictive than e.g. legislative constraints, e.g. 100% renewables, possibility for islanding for a certain length of time etc. Several constraints were divided into the following five categories (Sharp et al., 2020):

- Natural Locational Constraints – Resources and threats
- Distribution System & Storage Constraints
- Building and Facility Constraints
- Indoor Environment Constraints
- Building Equipment and District System Constraints

These constraints should ideally be specified so that direct implications for energy use can be deducted.

The natural constraints cover e.g. locational threats and resources. Locational threats deal with all natural threats that influence the possible choices of technologies or solutions and could be e.g. regional or local air quality, extreme temperatures or high winds. Locational resources deal with the availability of energy on-site or nearby. It covers both renewable energy sources for the location, e.g. wind, solar etc. and existing available energy infrastructure, e.g. power lines, gas pipes, district heating etc. Harnessing adequate amounts of energy from renewable energy sources usually requires quite a lot of space, e.g. it may be difficult to harness solar energy in big cities where roof or land area is not available and it may be difficult to utilize wind turbines since they require open spaces to be efficient. Therefore, the spatial possibilities are also part of the natural constraints. The constraints analysis shows the link between single building requirements and specific goals that a district might have set. In net zero energy districts e.g. the resources on the one hand have to meet the buildings energy use on the other hand. A miss-match is an important performance indicator.

Results

Architecture encompasses technology, functionality, and aesthetics in districts. However, architectural form has to be considered in context with functions, user and occupant expectations and requirements to build a basis for energy performance indicators that relates to the layout of the buildings in the district, users requirements and cultural context. There are different types of buildings (see Table 1) but there is not a stringent typology associated with the usage that different areas in districts are put to, functional patterns and stakeholder groups are

associated with the areas. The different building types and typologies may vary according to for example location, size and use, for example it may be expected that districts in city centres will have smaller circulation areas and larger public spaces than residential districts, and some districts do not have restaurants, shops or parking areas.

However, there are certain areas within a district that may be considered standard for all districts. Table 1 describes the five main areas in districts, their usage and different locations within a centre and shows an overlap in usage, for example not all commercial activities takes place in clearly defined retail units; some take place in common areas in temporary or permanent units. Restaurants, food courts and cafes may be found within retail units and on occasion stores may be found in restaurants and cafes. In addition, city centre districts that offer leisure activities, or specialised functions like meeting or conference facilities, are typologies not covered in this overview. Typical examples which impose other usages include cinemas, bowling alleys, or swimming complexes. Hotels or apartments may also be located within a district. For these typologies, additional performance indicators may apply.

Table 1: Five main functions in districts (plus outdoor spaces)

Function	Description	Building types
Residence		Single family Multy-family Apartment blocks
Commercial	Commercial activities	Office Shopping mall Shop Restaurants
Service	Public services	Schools Kindergarten Departmental Office
Cultural	Cultural activities	Museum Gallery Theatres Concert hall Sports facilities
Industry	Production sites	Office factory
Common areas	Public and private spaces Squares Parks Outdoor space	

Table 2 summarizes the differences in characteristics in Building Energy Use Limits by Country. There is a large variety of energy use limit characteristics in different countries. While some report site/end energy, others

report primary energy, it is important to make efforts to streamline reporting matrices and calculation methods

Table 1. Typical end energy demand values for non-residential buildings according to EnEV 2012 (average values) in Germany and total net energy requrirements according to TEK17 [20] in Norway

Building usage	ENEV 2012		TEK17
	Heating / DHH	Electricity	Total net energy demand
	kWh/(m²a)	kWh/(m²a)	kWh/(m²a)
Middle class hotel	85	55	170
Restaurant	205	95	180
Cinema	55	80	180
Gyms	120	35	145
Multipurpose Convention Centers	240	40	180
Swimming pool (indoor)	385	105	145
Non-food commerce small	135	45	180
Shopping malls	70	75	180
Hospitals	175	80	225 (265)*
Office building (heating only)	105	35	115
Office building (heating/cooling)	110	85	115
Cultural building			130
Light industry/workshop			140 (160)*
School building			110
University/universiy college			125
Nursing home			195 (230)*
Kindergarten			135

* Numbers in parentheses are buildings with reduced possibility for heat recovery from ventilation

Table 2: Difference in Building Energy Use Limits by Country

Characteristics of building energy use limit	Country						
	Austria	Denmark	Finland	Norway	US	UK*	Germany
Energy use limit	Max heating site/end	Max total site/end	Max total primary	Max total net (site/end or primary?)	Max total site/end or primary	Max fossil, electric, total site	Total site & primary - reference bldg
Format of energy use limit	One number & simple equation	Simple equation	Numbers	Numbers	Numbers	Numbers	Simulation-reference bldg
Limit units (per year)	kWh/m2	kwh/m2 heated	kWh/m2	kwh/m2 heated	kBtu/ft2	kWh/m2	TBD
Limit required?	Required	Required	Required	Required	Voluntary	Voluntary	Required
How limit addresses building types	One equation for all	Two equations - 1. dwellings 2. commercial	Values for 7 types. No limit-hospitals/ others	Values for 12 types.	Values for 53 types.	Values for 10 types.	Reference building varies for every building
How limit varies within a building type	Varies - equation using volume/surface ratio	Varies - equation using building heated floor area	No variance	No variance	No variance	1-4 categories	
How limit addresses different climates	No variance	No variance	No variance	No variance	Numbers for 16 climates.	No variance	
How limit addresses different operations (e.g., operating hrs)	No variance	No variance	No variance	No variance	Multipliers for shifts.	Multipliers for shifts.	

Energy use and flows in complex districts

Complex districts consist of buildings and outdoor spaces with specific needs. The use that different buildings and areas are put to affects energy consumption, whereas the different functional patterns and stakeholder groups influence energy use. They are also associated with specific requirements that make it relevant to consider different types of performance indicators.

In the scope of this analysis both ventilation indicators and requirements with a direct or an indirect effect on energy consumption in districts are identified. When defining the relevance of performance indicators; legal

requirements (i.e. for work environment), ownership or authority over parts of the district (single buildings or a complex of buildings), and cultural context also come into play.

As a result of the underlining complexity of performance requirements in districts, it may also be useful to distinguish between causes of energy use within a functional sub-division, meaning energy divided by the functions which it is used (by end use or supply system), and organizational sub-divisions of energy use distinguished by who pays for the energy and thus is related to billing practice, building owner and tenant agreements, and contracts with energy supply carrier companies.

The first three divisions are mainly linked to the demand side and indicators that represent the requirements that can be found in norms, standards, and the like. While different stakeholder groups, organisation and contextual aspects like climate and energy availability, also define the relevance of performance indicators, and suggest which priorities should be given when performance requirements are in conflict. The latter interest groups and contextual aspects also form billing practices, sub-metering, and indicators for dividing the operational energy costs.
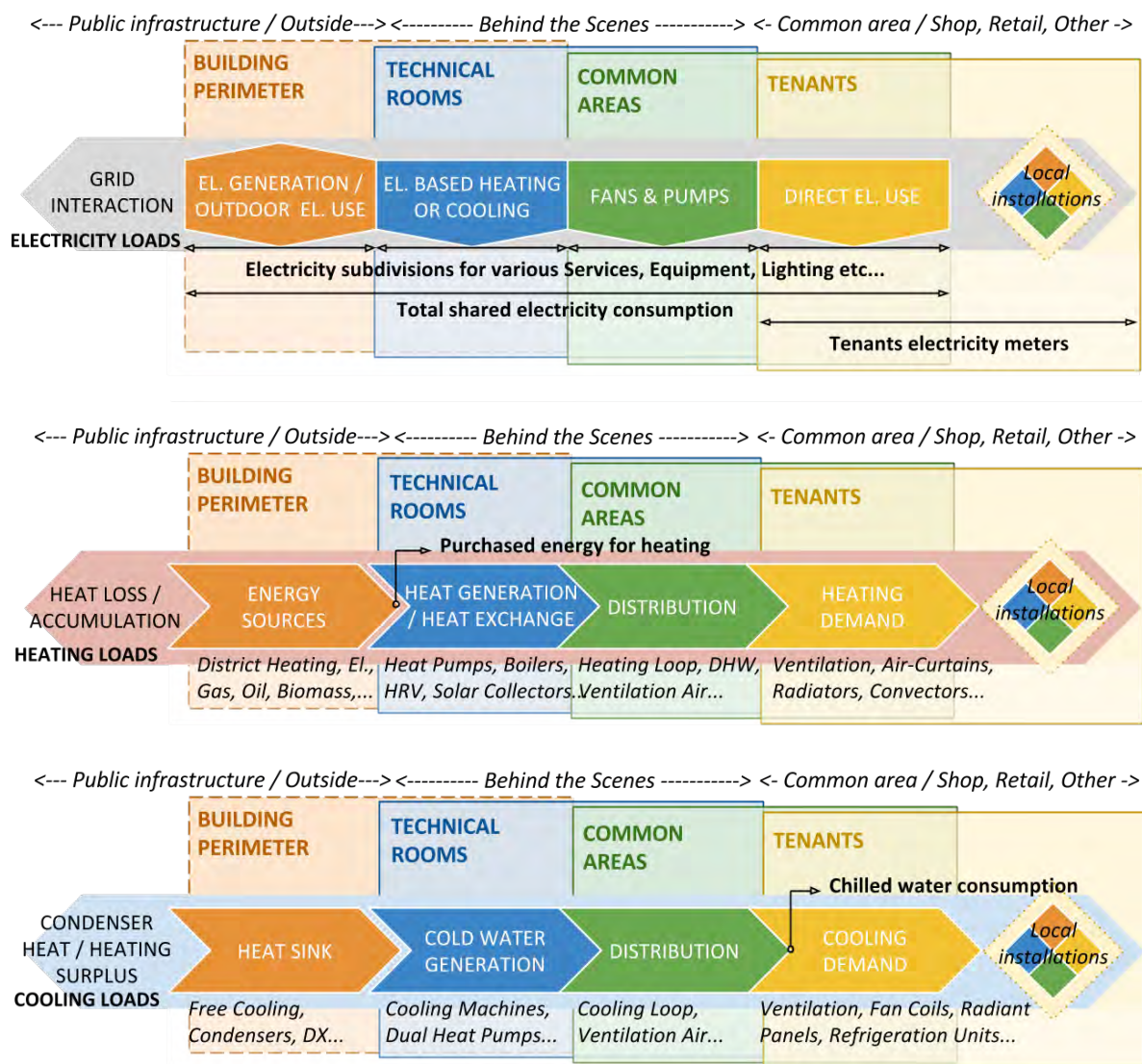
Figure 1 – Sub-division of energy flows (electricity and thermal) associated with different end uses.

Protocol for sub-metering

Figure 1 illustrates a functional sub-division of energy end use within a district. Starting with the energy supply

and the technical services in place, the energy use associated with heating, cooling and electricity are structured by end use. The diagram is easiest to

comprehend for centralized systems, but in principle the structure is the same for all installations localized in private and public space. In a typical district, there will exist several heating, or cooling loops and many electrical subdivisions (distribution boards) on top of various end uses of energy. The different concepts are explained in more detail in Haase et al. (2015).

The illustrated processes are usually in the control of facility managers and technical staff of each building. Multi-owned districts often lack professional skilled workers. A multitude of performance indicators can be related to this structure. Some performance indicators are important in the design and commissioning of the systems, others are of use in the day-to-day running of the buildings. Reading the diagram from left to right, the potential of increasing energy efficiency lies both in production, distribution and end-use. Building performance simulation tools should take these into account and visualize them for their users.

Energy can be considered to follow function because energy in the end is used to meet requirements defined by the activities that take place in a district. In each district, requirements are diversified by the type of activities/functions (residences, commercial (shops, retail), service (schools, restaurants, cafes, etc.), by the sizes of tenants rental spaces, or by the type of spaces (public areas, offices, parking etc.). The different activities can be characterized by functional patterns for various groups; – opening hours for commercial buildings will differ from operational hours for technical services and lighting. Facility operation has to meet the requirements of staff in commercial and cultural or service buildings before they open to the public. In districts, many tasks are performed outside of opening hours which require maintaining health and safety for the workers. Examples are maintenance and cleaning, sanitation and supply infrastructures, mobility and transport. In relation to this, the ratio of full operation of HVAC and lighting vs. opening hours or service hours is one index that could be used as a performance indicator.

Therefore, six performance concepts are identified which form the structure of the next sections, all with contextual relevance to energy use and supply of energy in districts:

Concepts with functional element sub-division:

- Energy follows function
- Energy follows form
- Energy follows user needs

Concepts with organizational element sub-division:

- Energy follows stakeholders
- Energy follows organization
- Energy follows availability

Discussion

In typical districts in city centres the dominant commercial buildings are often heated, cooled, and ventilated. The same retail units are never connected to other buildings or spaces of activities. Still, large open doorways through which air, odours, light, and noise

exchanges occur, effectively linking the different spaces, exist. This limits the accuracy of heating, cooling, and ventilation assessments. Key performance indicators based on floor area can be used, but it is challenging to meet performance requirements, to keep within accepted limits of comfort and meet retailer needs in such an open indoor environment, where different spaces inside the commercial part of a district are effectively linked.

In the transformation process, operation, meetings between tenant associations and management, labour meetings performance indicators can be important quantitative statements to meet user needs regarding comfort and ensure high energy performance. Also building code requirements related to work-space specifications can have an influence on the design and transformation choices (Boermans et al. 2011). An active cooperation with various stakeholders is essential (Haase and Baer 2020). Access to daylight for workers e.g. is of importance for those buildings that do not have direct access to sufficient daylight due to its location within the district.

Organisational forms can be observed in Real Estate companies, property companies, management companies, facilities companies (outsourcing or within the same owner company) and tenant associations. Contracts between those organisations and the indicators used in those agreements are often based on KPIs which offers potential for introducing energy intensity related KPIs.

Nowadays, it is a challenge to transform the current energy system into modular power generation to improve the quality and the reliability of the electricity supply. The renewable energies and efficient solutions can overcome the oversizing problem of the electrical infrastructure for meeting the energy demand peaks as well as the energy transmission losses. It is important to operate with KPIs that can help to distribute energy production within the district. However, the incorporation of renewable system in districts must take into account that some problems in the supply can appear given its dependence of the climate conditions as well as the affections in the quality of the grid since they can generate frequency and voltage fluctuations and outages. Furthermore, any interaction in the grid must consider the grid capacity for admit new compounds.

Individual building computer-based energy models that are currently available for general use buildings are not sufficient and the need for a clear reporting structure of key performance indicators became evident. They need to be further customized to function as archetypes to predict energy use in districts and adapted to different climate conditions and energy use requirements. To be used for community planning, all prototype models must be fully parametrized for common modeling inputs in order to be able to build in energy efficiency measures.

The next step will be to develop a common approach to calibration of building models to existing energy use data available from metering and sub metering.

However, it is important to highlight that districts are not the simple sum about its buildings, but the set of all parties that make up the urban system such as buildings, mobility, public lighting, open spaces, water and waste management. Ideally, Energy Master planning of districts must be programmed according to a long-term vision together with all transformation measures and their possibly assessed impacts. In that sense, the energy policies can lead to various positive social, environmental, and economic impacts that can bring an added value for the choice of the alternative strategies. To facilitate the transformation process, the benefits that can be generated by the requalification measures and the different impacts that they can provide on the whole community must be considered (Ürge-Vorsatz et al. 2014; Bisello and Vettorato 2018).

Conclusion

The HVAC (heating, ventilating, and air conditioning) system is responsible for providing the thermal and hygienic needs of a building in a district. An efficiently designed and operated building and HVAC system reduces the amount of energy needed to control hydrothermal conditions and air flow in a space. In addition to the passive solutions regarding thermal insulation, natural ventilation, and solar gain controls there are specific solutions regarding the HVAC system, that promise to lead to energy savings. To reduce the consumption associated with HVAC the focus must be on:

- energy efficient equipment
- energy flux strategy
- equipment control and management.

Energy efficient equipment and components

The current equipment could be replaced with ones with greater efficiencies.

This is especially true when the existing systems are old, inefficient, or malfunctioning. Some of the main predictor variables include:

- Efficiency of the heating system (boiler, Heat pumps, Combined heat and power (co- and tri-generation, Biomass boiler or District heating)
- Efficiency of air-conditioning systems (e.g., chillers);
- Efficiency of ventilation system
- Presence and efficiency of heat recovery systems;
- Performance parameters of economisers;
- Efficiency of auxiliary devices

The type of distribution system (radiant floor or ceiling, fan coils or primary air) should be also considered as a predictor variable with special attention to the efficiency of auxiliaries (e.g., fans, motors) and to the correct size of equipment and balance systems.

Energy flux strategy and recovery

The recovery factor of the heat waste recovery system and the performance of free cooling should be considered. Thermal layout is important because it influences which thermal synergies (e.g., thermal cascade) can be exploited. For instance, the existence of interconnections and the supply and return temperatures of the refrigeration and heating/cooling duct are important predictor variables.

Equipment control and management

Building system control and management strategies in districts and group of buildings are crucial to ensure correct operation. The operation should therefore be regulated by a central unit (district management system – DMS) acquiring information from the field and deciding the best strategies to deliver the required conditions for each zone and tenant. Control strategies are very powerful predictor variables (on/off set points, temperature and rate set points, etc.). In the scope of this analysis both indicators and requirements with a direct or an indirect effect on energy consumption in districts were identified. When defining the relevance of performance indicators; legal requirements (i.e. for work environment), ownership or authority over parts of the district, and cultural context also come into play. Six performance concepts were identified which have contextual relevance to energy use and supply of energy in districts. As a result of the underlining complexity of performance requirements in districts, it may also be useful to distinguish between causes of energy use within a functional sub-division, meaning energy divided by the functions which it is used (by end use or supply system), and organizational sub-divisions of energy use distinguished by who pays for the energy and thus is related to billing practice, tenant agreements, and contracts with energy supply carrier companies.

A possible task for the future is to identify if and how relevant energy performance indicators can be incorporated in contracts, or other forms of agreements between the stakeholders. Also, other energy use from sectors like mobility should be started to include. This could result in multiple benefits which could help to enhance the district master planning.

Acknowledgement

References

Baer, D. and Haase, M. (2020), Energy Master Planning on neighbourhood level: learnings on stakeholders and constraints from the Norwegian case of Ydalir, Proceedings World Sustainble Built Environment Conference, Gothenburg, Sweden

Bisello, A., & Vettorato, D. (2018). Multiple Benefits of Smart Urban Energy Transition. In: *Urban Energy*

Transition (pp. 467–490). Elsevier. https://doi.org/10.1016/B978-0-08-102074-6.00037-1

Boermans, T., Bettgenhäuser, K., Hermelink,A. and Schimschar, S. Cost optimal building performance requirements, May 2011 © European Council for an Energy Efficient Economy, Commissioned by eceee with financial support from Eurima and the EuropeanClimate Foundation (ECF), access: http://www.ecofys.com/files/files/cost_optimality-eceeereport.pdf; access date: 24.06.2014

BREEAM, *BRE Environmental Assessment Method,* https://www.breeam.com/. Accessed Aug 13, 2019.

EED - Directive 2012/27/EU of the European Parliament and of the Council of 25 October 2012 on energy efficiency, *Energy Efficiency Directive*, https://ec.europa.eu/energy/en/topics/energy-efficiency/targets-directive-and-rules/energy-efficiency-directive, access data: 04.12.2019

EnergyPlan. *Energy systems simulation tool*. https://www.energyplan.eu/. Accessed Aug 13, 2019.

ENEV 2012, Energieeinsparverordnung, http://www.enev-online.com/index.htm, Access date: Feb 2019

EPBD. 2018. Directive (EU) 2018/844 of the European Parliament and of the Council of 30 May 2018 amending Directive 2010/31/EU on the energy performance of buildings. https://eur-lex.europa.eu/legal-content/EN/TXT/?uri=uriserv%3AOJ.L_.2018.156.01.0075.01.ENG

Fox, K. 2016. *Energy Master Planning Perspectives and Best Practices, presentation to the Federal Utility Partnership Working Group*, May 2016, Cincinnati, OH.

Haase and Baer, Constraints, stakeholders and framing goals in Energy master planning (EMP) between neighbourhood and district, accepted for publication in Smart ans Sustainable Planning in Cities and Regions, Volume 5, Springer, 2020

Haase, M. and Lohse, R., Process of Energy Master Planning of Resilient Communities for comfort and energy solutions in districts, IOP Conference Series: Earth and Environmental Science, Volume 352, Number 1, IOP Publishing Ltd, https://iopscience.iop.org/article/10.1088/1755-1315/352/1/012019, access date: 09.02.2020

Haase, M., Skeie, K.S., Woods, R., Mellegård, S., Schlanbusch, R.D., Homolka, S., Gantner, J., Schneider, S., Lam-Nang, F., (2015) Deliverable 2.3 report - Typical functional patterns and socio-cultural context, EU FP7 project CommONEnergy, access date: April 2015

Huang, Zishuo & Yu, Hang & Peng, Zhenwei & Zhao, Mei, 2015. "Methods and tools for community energy planning: A review," *Renewable and Sustainable Energy Reviews,* Elsevier, vol. 42(C), pages 1335-1348.

IPMVP, International Performance Measurement & Verification Protocol - Concepts and Options for Determining Energy and Water Savings, Revised March 2002. DOE/GO-102002-1554, http://www.nrel.gov/docs/fy02osti/31505.pdf, access date: Feb 2017

JPI Urban Europe / SET Plan Action 3.2 (2020). White Paper on PED Reference Framework for Positive Energy Districts and Neighbourhoods. https://jpi-urbaneurope.eu/ped/

Jank, R. (2017) Annex 51: Case studies and guidelines for energy efficient communities. *Energy and Buildings* 154: 529–537.

LEED, *Leadership in Energy and Environmental Design*, http://leed.usgbc.org/leed.html. Accessed Nov 19, 2019.

Robinson, Darren et al. 2009. CITYSIM: Comprehensive Micro-Simulation of Resource Flows for Sustainable Urban Planning, *Building Simulation 2009*, Eleventh International IBPSA Conference, Glasgow, Scotland. July 2009.

Schiefelbein et al. 2017. Implementation of energy strategies in communities – Results within the context of IEA annex 63, 30th International Conference on Efficiency, Cost, Optimization, Simulation and Environmental Impact of Energy Systems, ECOS 2017-San Diego, CA, US.

Sharp, T., Haase, M., Zhivov, A., Rismanchi, B., Lohse, R., Rose, J. Nord, N. (2020), Energy Master Planning: Identifying Framing Constraints That Scope Your Technology Options, ASHRAE Transactions. Atlanta: American Society of Heating, Refrigerating and Air-Conditioning Engineers, Inc

TEK17, Regulations on technical requirements for construction works, DiBK, https://dibk.no/globalassets/byggeregler/regulation-on-technical-requirements-for-construction-works--technical-regulations.pdf, Access date: Feb 2019

Ürge-Vorsatz, D., Herrero, S.T., Dubash, N.K., & Lecocq, F. (2014). Measuring the Co-Benefits of Climate Change Mitigation. *Annual Review of Environment and Resources*, 39, 549–582. https://doi.org/10.1146/annurev-environ-031312-125456

Zhivov et al. 2014. Energy Master Planning Towards Net-Zero Energy Communities/Campuses, *ASHRAE Transactions*. Atlanta: ASHRAE Engineers, Inc.

Zhivov et al. 2017. Technologies Integration to Achieve Resilient, Low-Energy Military Installations. Proposal No. EW18-5281 to the U.S. Department of Defense Environmental Security Technology Certification Program.

Planning a low carbon urban area in Helsinki with dynamic energy simulations

Santeri Siren
Ramboll Finland Oy, Espoo, Finland
santeri.siren@ramboll.fi

Abstract

The city of Helsinki has a target to achieve carbon neutrality in 2035.

The objective of this project was to use energy simulations to study and compare multiple different energy production alternatives for new Malmi airport area in Helsinki and determine which of them would be suitable for achieving low carbon emissions cost efficiently.

Totally 284 energy system variations were simulated.

Results show that the carbon emissions from energy production can be cost effectively decreased compared to local business as usual solution. Ground source heat pump-based systems proved to be one of the most effective solutions.

Introduction

Finland has committed to reduce the greenhouse emissions 40% compared with 1990 levels until 2030, and 80% compared with 1990 levels until 2050 [1], [2]. Most of the major cities in Finland have their own individual carbon neutrality targets and strategies for achieving them.

The city of Helsinki has the target to achieve carbon neutrality in 2035 [3]. This will require major changes in many areas such as local energy production methods, improving energy efficiency in the existing building stock as well as minimizing the energy demand of new construction.

The Malmi airport area is the most significant area in Helsinki for upcoming new construction in near future. According to the city land use plan there will be 1.35 million square meters of new construction in that area during 2020s. In the land use plan this area is divided in to 10 sub areas. All the sub areas will be designed separately using individual themes and they will be built in a specific order during a total 25 – 30-year period. This project concentrated on the first two sub areas: Nallenrinne and Lentoasemakortteli. In these two sub areas there are totally 267 914 m² of planned new construction. The major part of the new buildings will be residential.

	Nallenrinne	Lentoasemakortteli
Appartment buildings [m²]	128 700	95 300
Commercial buildings [m²]	2 600	0
Schools [m²]	1 500	11 500
Car park buildings [m²]	4 400	19 150
Other [m²]	-	4 764
Total [m²]	137 200	130 714

Table 1. New construction building quantities planned in Nallenrinne and Lentoasemakortteli areas

The objective of the project was to compare different solutions for a heating and cooling energy production system that serves Nallenrinne and Lentoasemakortteli sub areas. The focus of the calculations was in the life cycle emissions of produced energy and the life cycle cost of different systems. The results will serve as a guideline in the future planning of the Malmi airport area energy production solutions. Local electricity production with photo voltaic was also included in the study. The idea was that the results of this project can be also applied in general planning of the other sub areas as well.

Methods

This project included a development of a simulation platform for running urban area level dynamic energy simulations that could be used for simulating and comparing different types of energy systems serving the Nallenrinne and Lentoasemakortteli sub areas.

Developing the simulation platform

The simulation platform can be broken down to four main components:

- Energy simulation for modelling urban area energy systems
- Life cycle cost calculation
- Life cycle emission calculation
- Result data reporting and visualization environment

The simulation platform consists of several software's that are connected to each other via interfaces. Scripting was used to automate the data flows between the different components and software's.

IDA ICE (v4.8) was used as the main energy simulation software for running the energy system simulations. IDA ICE is mainly used for building energy simulations but in this case the focus was heavily on urban area energy system modelling.

The energy simulation component of the platform included a lot of different kind of simulation components for modelling a wide variety of energy production systems and a methodology for creating an urban area simulation model including all the building blocks, local building integrated energy production units, area level energy production units, control and adjustment components and also heating, cooling and electricity distribution networks connecting all the building blocks

and energy production components together. Scripting was used for automating the creation of the simulation models of all the predefined scenarios, running the simulations and gathering all the wanted results for post processing purposes. The main results from the dynamic energy simulation included e.g. building block energy demands, energy production of different systems and units and some essential information about occurred maximum power values of different devices during the simulation.

The LCC component of the platform is used for making all the financial calculations related to the different types of energy systems that are being simulated. Investment costs, maintenance costs and renewal costs were specified for every different energy production related technology included in the study. Also, the cost data for building the local heat distribution networks and required heat exchangers etc. were obtained. Most of the cost values were obtained from local Finnish technology suppliers and contractors. The effects of the unit's size on the nominal cost were also considered. E.g. a large heat pump system has as smaller nominal investment cost than a small system [€/kW]. The energy and fuel costs were based on the public pricing of local suppliers. All the cost data was used for creating a cost database that was integrated with the life cycle cost analysis calculator. The results from the energy simulation were used as initial values for the LCC calculations.

The inflation rates for different cost parameters in LCC calculations are always just guesses and thus they cause uncertainties in the results. Because of this a sensitivity analysis function was created in the result visualization environment. With this function the user can easily change any of the interest rates related to LCC and the result charts and diagrams will automatically update accordingly. This makes sensitivity analysis very easy and effortless.

The emission calculation component of the platform is used for determining the CO_2 emissions generated from the heating, cooling and electricity production related to the selected energy production systems. Because estimating the emission factors is not unambiguous, several scenarios were used for different emission factors and the forecast of how they will develop during the lifecycle of 30 years. The long-term annual development of the emission factors as well as the monthly based fluctuation were considered in the calculations.

The simulations produce large amounts of result data and a reporting and data visualization environment was developed to make viewing and analyzing the results easy. Tableau software was used to create an interactive data visualization environment for specialists, client and other stakeholders to study and analyze results. Several dashboards were constructed to present different aspects of the main results such as financial, energy and emissions. The dashboards included an interactive map-based user interface that could be used for easily

navigating all the results from the whole area perspective to single buildings and blocks individually. The visualizations and dashboards can be published online in a cloud-based system and they can be accessed via almost any device that has an internet connection.

A main user interface was also developed for the simulation platform. The UI can be used to quickly set up the main case parameters such as all the buildings and energy demand information, different energy production technologies, automatic system sizing [kW] and setting up different combinations of systems in the area (distributed and centralized). The UI was created so that it is easy to set up as many different parallel scenarios as needed. For example, in this case totally 284 different scenarios were set up and then simulated with a single press of a button.

Determining the energy demand of the buildings

The upcoming buildings planned for the examined area were divided into 6 different building types:

- Residential apartment building
- Commercial buildings
- Schools
- Car park
- Fire station
- Grocery store

Hourly based nominal heating, cooling and electrical energy demand were defined for each building type (kWh/m²). For residential buildings the energy demand values were based on actual measured values of 50 recently built (2013-2018) apartment buildings in Helsinki.

Simulated values were used for all the other building types. The simulated values were average values from several recent design projects made by Ramboll Finland. The hourly based nominal demand profiles included the following individual profiles:

- Space + AHU heating demand
- Domestic hot water heating
- Space + AHU Cooling
- Electricity

The electricity demand consists of all other electrical loads except electrical demand of local heating and cooling production systems (e.g. heat pumps). That part of the demand was calculated separately based on the energy system simulations. The electricity demand profile included also a profile for charging electrical cars.

The simulated energy demand values were based on Helsinki energy test year 2012 weather data [4]. This is an hourly based weather data file published by the Finnish meteorological institute and it represents a typical climate currently in southern Finland. The measured energy demand values were modified to correspond with the same climate data.

The two examined sub areas were divided into 18 individual blocks. These blocks can be seen in Figures 1 and 2.

Figure 1. The area of Nallenrinne and its blocks

Figure 2. The area of Lentoasemakortteli and its blocks

The number of square meters of different types of construction planned for each block were calculated based on the latest Helsinki city planning material.

For each block the total energy demand was based on multiplying the nominal demand profiles with corresponding square meters. The result was hourly based energy demand profiles of heating, cooling and electricity for each block. These results were used as initial values in the energy system simulations.

Simulating energy system variations

Different types of energy production technologies to include in the study were defined together with the project team and client. In the simulations the included technologies could be used as a local building integrated system (B) or a centralized system that serves the whole area of Nallenrinne and Lentoasemakortteli (C). Some of the technologies could be used as both (B/C). The following technologies were selected

1. District heating (B/C)
2. Ground source heat pump system [GSHP] (300 m deep boreholes, B/C])
3. Geothermal heat pump system (2000 m deep boreholes) (B/C)
4. Local heating plant (wood pellets) (C)
5. Gas boilers (bio / natural gas) (B)

6. Electrical boilers (B)
7. Wastewater heat recovery system (B)
8. Two-way heat trade system (with heat pumps) (B)
9. District cooling (B)
10. Air cooled chillers (B)
11. CHC system (B)
12. Free cooling from geothermal boreholes (B)
13. Building integrated photo voltaic [PV] (roof installation, B)

Also, two different options were included for a local low temperature heating distribution network

- Supply temperature of 50 °C
- Supply temperature of 70 °C

The main difference between these two options is that with the 70 °C temperature level domestic hot water (typically 60 °C in Finland) can be directly obtained from the network. With the 50 °C temperature local heat pumps were used to prime the temperature level for the domestic hot water. The temperature level also affects the COP values of all heat pump systems connected to the local heat distribution network. The low temperature option enables better efficiency of heat pumps.

A specific simulation component was created in IDA ICE for every different energy production technology listed above. These components were integrated as a part of the simulation platform. Totally 284 different energy system combinations were defined from the above-mentioned technological solutions. Each of the combinations includes different kinds of heating, cooling and electricity production systems and energy distribution solutions for satisfying the energy demand of Nallenrinne and Lentoasemakortteli sub areas. These combinations included also centralized and de-centralized solutions of different technologies such as ground source heat pump systems etc. The simulation platform was used for sizing the production units, generating corresponding simulation models, running the energy simulations, LCC calculations, emission calculations and extracting specified results for all the 284 alternatives into the reporting environment.

The LCC calculation was conducted including the calculation of net present values of all the scenarios in the study during the specified lifecycle (30 years). All the important factors were included in the calculation such as investment costs, maintenance costs, renewal costs, purchased energy etc.

Results

The calculations and simulations described in the Methods section produced a very large amount of data, including energy, power, financial and emissions related information. Only the very essential values were reported in the final report of the project and will be presented here.
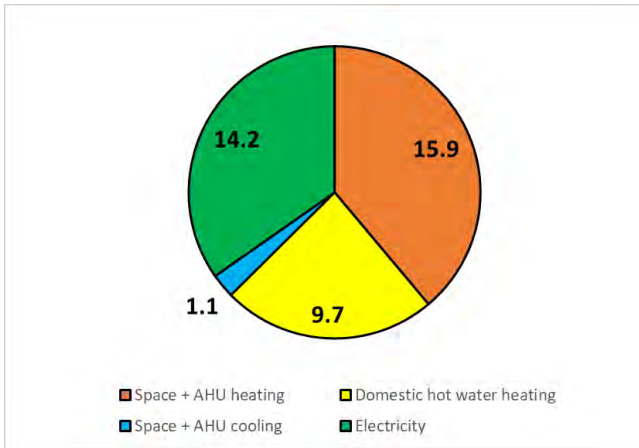
Figure 3. building energy demand of the studied area [GWh/a]

Results show that the major part of the total energy demand comes from heating demand. Domestic hot water

has a significant share because most of the new buildings are residential buildings.

Figure 4 shows how all the simulated 284 cases position themselves on a lifecycle cost vs. life cycle emissions chart. The color of the points represents the type of the system as follows.

- Red: Only decentralized building integrated heating and cooling systems
- Blue: Heating only with district heating
- Green: Heating by both DH and building integrated systems
- Yellow: Only local centralized heating systems (no DH)

Five individual scenarios (marked in figure 4) were selected as recommendations, one from each category except two from green category. Also, scenario no.5 was displayed separately because it represents the typical business as usual option in Helsinki area, which is only district heating and district cooling.
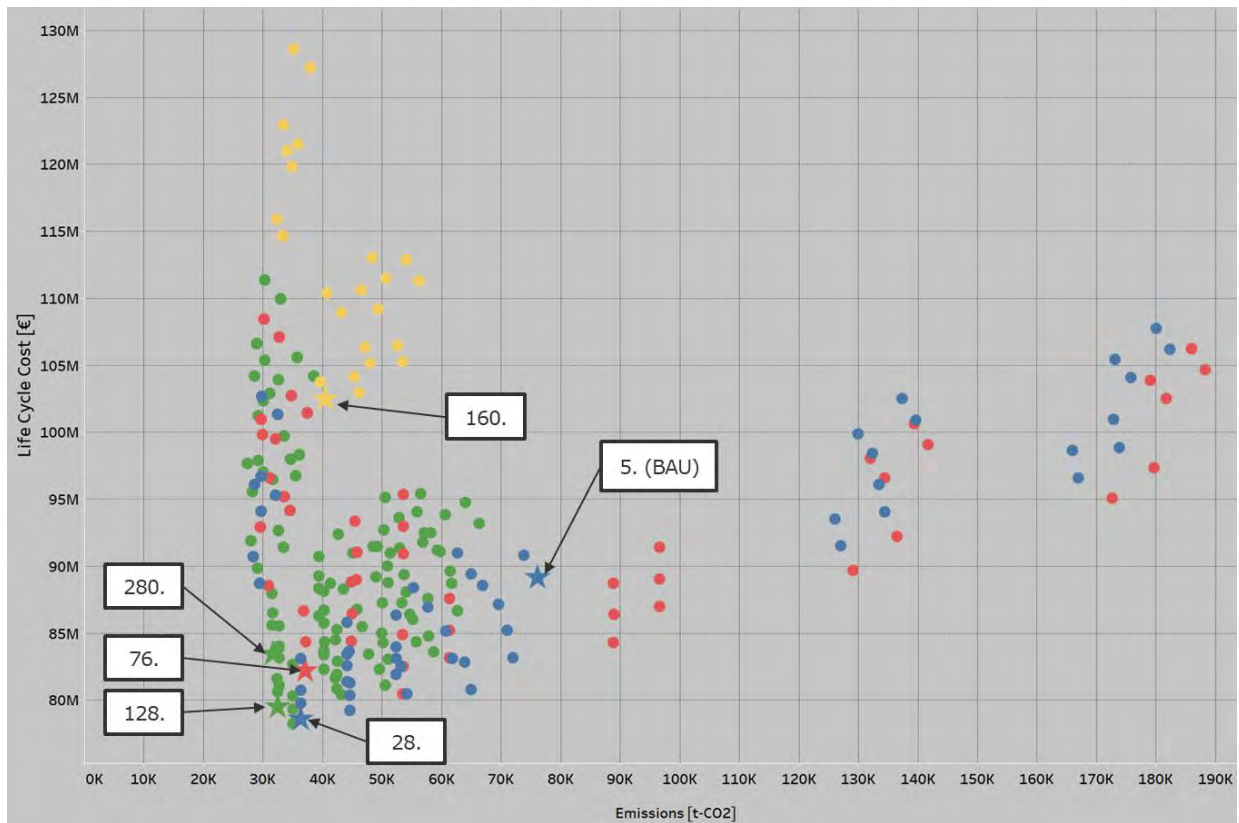
Figure 4. Life cycle cost [M€] and life cycle emissions [t CO2] for a 30-year period for all the 284 simulated scenarios.

Table 2. the technologies used in each of the selected scenarios.

Scenario no.	Centralized Heating systems	Building integrated heating	Cooling	Waste water heat recovery	Photo Voltaic	Heating distribution network
5. (BAU)	DH	-	DC	No	No	District heating network
28	DH	-	Fee cooling + CHC	Yes	Yes	District heating network
76	-	GSHP	Fee cooling + CHC	Yes	Yes	-
128	GSHP + DH	GSHP	Fee cooling + CHC	Yes	Yes	70 °C network
160	GSHP+ local heating plant (biofuel)		CHC	Yes	Yes	70 °C network
280	GSHP + DH	GSHP	Fee cooling + CHC	Yes	Yes	50 °C network

The following figures summarize the main results of the study concerning the six selected system combinations.
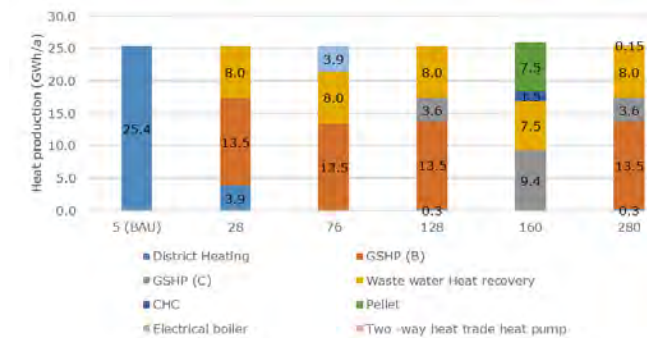
Figure 5. Heating production breakdown of the selected scenarios [GWh/a]
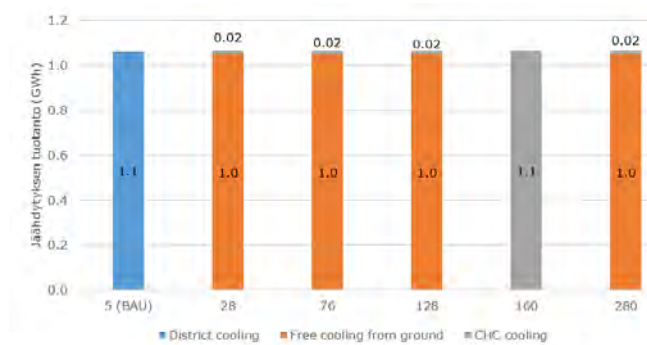
Figure 6. Cooling production breakdown of the selected scenarios [GWh/a]
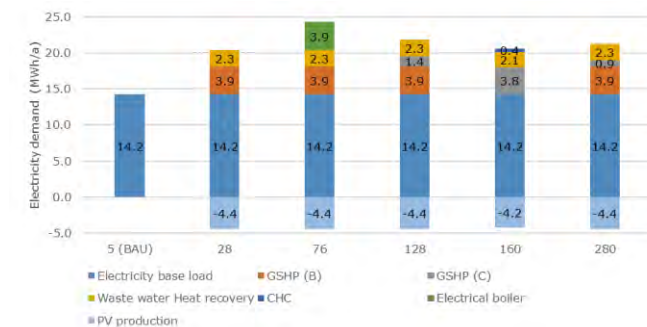
Figure 7. Electricity demand breakdown of the selected scenarios [GWh/a]
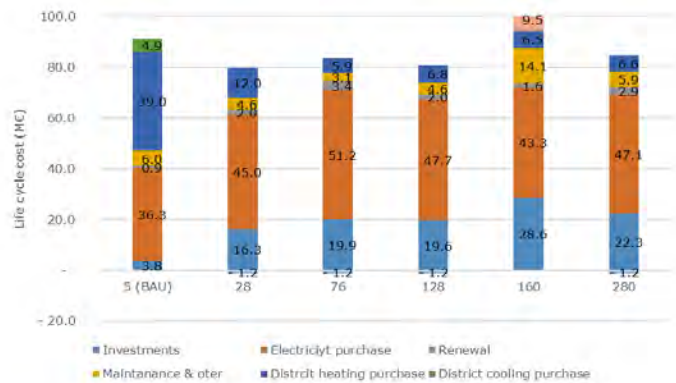
Figure 8. Life cycle cost breakdown of the selected scenarios [M€]
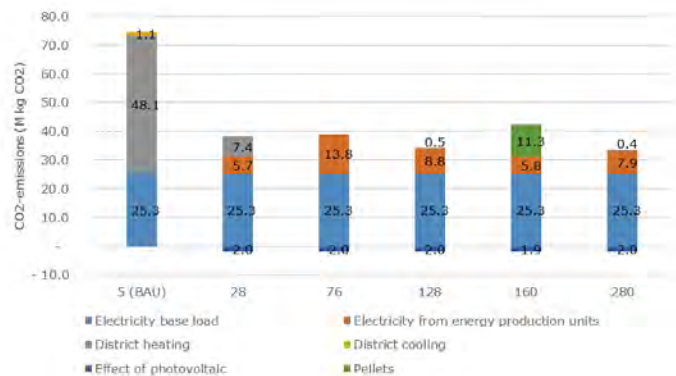
Figure 9. Life cycle emissions of the selected scenarios [M kg CO_2]

There were a lot of other interesting results and details that came out during this project but cannot be presented here due to lack of space.

Discussion

The main challenge in this project was to develop the new simulation platform for running batch based urban area energy simulations semi automatically. A lot of work was put into this and the result was quite satisfying. The simulation platform can now be used relatively easy to generate a lot of different scenarios, automatically generate the corresponding simulation models and running the dynamic simulations. Also, the LCC and CO_2 emission calculations as well as the visualization environment for analyzing the result data were integrated as a part of the simulation platform. The system is very scalable for almost any size of urban area, and it can be used in similar projects in the future.

As figure 4 suggests there were a lot of other interesting results and details that came out during this project but cannot be dealt with here due to lack of space.

The final report of this project was published as a public document on Helsinki's web page [5].

The results are being studied by the city officials for future developing of the Malmi area. Already at least one project has been started on the basis of this study to design a GSHP based semi centralized energy production system in a more detailed level. This could be used in the Malmi area as well as any other areas also.

In future studies it would be interesting to include heating and electrical storages and demand response in the simulations and study their potential. In this project these solutions were framed out because the main study was already very extensive.

Conclusion

Results showed that a significant reduction to emissions can be obtained cost efficiently using the studied energy system options compared to the business as usual case.

Most of the recommended scenarios were based on ground source heat pump systems at some level. Heat pumps are usually a strong option emission vise because they use only one unit of electricity to produce multiple units of heating (or cooling). The local district heating emission factors are just not low enough compared to electricity to compete with this. The major problem with ground source heat pump systems is that they practically always need another heating system to support them, because the maximum power they can produce is quite limited. This is because it is not cost effective to size a GSHP system to cover 100% of heating energy demand.

The supporting system increases the life cycle cost significantly even it is used to produce relatively low share from the total energy demand. The study indicated that there is enough space to drill boreholes on most of the building sites for achieving a 90% heating energy cover when using de-centralized systems. There is also a large park area nearby for the centralized ground source heat pump system options.

The wastewater heat recovery systems show great potential in almost all the cases, mostly because there are so much water usage in the area due to high share of residential buildings. A heat pump is always recommended to be used with the heat recovery system to increase the potential.

Local building integrated PV can compensate a relatively small portion of the total electricity demand (about 4.4 GWh/a). However, the PV systems are financially feasible investment and help to reduce the emissions. The largest restriction for PV in this study was the lack of available installation space on building roof areas. Façade mounted or ground mounted PV systems would be interesting to study further for increasing the local renewable electricity production.

A local bio fueled (wood pellets) heating plant would generate the lowest amount of emissions if pellets were considered emission free. However, in this study this was not the case and the biofuel plant-based scenario had the second highest emissions of all the recommended cases. Also, the local heating plant-based solution was the most expensive of all the recommended scenarios.

The recommended systems have clearly larger investment costs than BAU, but the life cycle costs were lower in most of the cases.

Two-way heat trade didn't have a lot of potential in the studied area because the residential buildings mostly just consume heat and do not produce significant excess heat flows. Two-way heat trade potential could be increased by adding diversity to the building types in the area, such as offices, shopping malls, data centers etc. This would also support better the low temperature heating distribution solutions.

References

[1] Ministry of employment and economy. Energy and climate roadmap 2050; 2014. Available: https://tem.fi/documents/1410877/2628105/Energia-+ja+ilmastotiekartta+2050.pdf/1584025f-c5c7-456c-a912-aba0ee3e5052/Energia-+ja+ilmastotiekartta+2050.pdf [Accessed 2020]

[2] Government report on the National Energy and Climate Strategy for 2030; 2016. Available: https://tem.fi/documents/1410877/3570111/Kansallinen+energia-+ja+ilmastostrategia+vuoteen+2030+24+11+2016+lopull.pdf/a07ba219-f4ef-47f7-ba39-70c9261d2a63/Kansallinen+energia-+ja+ilmastostrategia+vuoteen+2030+24+11+2016+lopull.pdf [Accessed 2020]

[3] City of Helsinki. Carbon neutral Helsinki action plan; 2019. Available: https://www.hel.fi/static/liitteet/kaupunkiymparisto/julkaisut/julkaisut/HNH-2035-toimenpideohjelma.pdf [Accessed 2020]

[4] Finnish meteorological institute. Test reference year 2012 for building energy demand and impacts of climate change; 2011. Available: https://www.ilmatieteenlaitos.fi/energialaskennan-testivuodet-nyky [Accessed 2020]

[5] Hiilineutraalin Malmin lentokentän alueen energiaselvitys. Ramboll Finland Oy; 2019. Available https://www.hel.fi/hel2/ksv/liitteet/2019_kaava/4844_1_energiaselvitys_30102019.pdf [Accessed 2020]:

Integration of a high-temperature borehole thermal energy storage in a local heating grid for a neighborhood

Michael Jokiel[1], Daniel Rohde[1], Hanne Kauko[1], Harald Taxt Walnum[2]
[1]SINTEF Energy Research, P.O. Box 4761 Torgarden, NO-7465 Trondheim, Norway
[2]SINTEF Community, P.O. Box 124 Blindern, NO-0314 Oslo, Norway
corresponding author: Michael.Jokiel@sintef.no

Abstract

A borehole thermal energy storage (BTES) will be built in a refurbished residential district in Oslo, Norway. The new heating demand for the neighborhood is estimated to be 26 GWh/year. To partially meet this heating demand, excess heat from a waste incineration plant will be stored in a BTES. The stored thermal energy can be used as a heat source in winter. A local heating grid connects the heat storage with a district heating grid.

A Modelica model of the BTES system has been created using the results from a design study. Several cases were investigated where the use of the BTES was limited to periods with peaked heating demand. Fluctuating seasonal district heating prices were considered to highlight the economic benefits.

Introduction

With consideration of increasing consumption and depleting fossil-based fuels, the future will most likely bring increased energy prices and both short and long-term energy insecurities. There is a need for better utilization of energy to reach the goals for reducing greenhouse gas emissions. In this context, the future is not just about how energy can be produced as efficient and clean as possible, but also about how to handle the energy that has already been produced. In future neighborhoods, both thermal and electric energy can be managed in a flexible way to achieve reduced power peaks, reduced energy use, reduced CO2-emissions and increased self-consumption of locally produced energy [Jensen17].

For many sites, a seasonal mismatch is at hand between the available waste heat and the heat demand. Typical examples are waste incineration plants with generally uniform amounts of waste heat throughout the year. As waste cannot be stored for several months, it needs to be incinerated in summer as well, leading to great amounts of surplus waste heat available in summer months, while heating demand is greatest during winter. In order to shift heat potentials from summer to winter and thereby enabling the feed-in of otherwise wasted surplus heat in an economically attractive way, this study investigates the storage of waste heat to meet the heat demand for a neighborhood, with the help of a largescale high-temperature borehole thermal energy storage (BTES).

For 4th generation district heating grids, waste heat integration is expected to be a common design element. Integration of waste heat into these grids is technically feasible, as many practical examples were already successfully demonstrated in 2nd/3rd generation grids [Lund14]. However, significant thermal capacities still remain unused due to the required high supply temperatures for 2nd/3rd generation district heating grids.

In this context this study focuses on the case study of Furuset (Oslo, Norway) to explore potentials to improve the local heat supply by using waste heat from a local incineration plant as an additional energy source. The heat is stored in a BTES in summer, and different control strategies for discharging cycles will be highlighted with regard to efficient utilization of the stored heat in winter.

Based on available information about the Furuset area and the plan for the future district heating system, a system model for dynamic simulations of the micro energy grid in Furuset was built to investigate the thermal interaction between the borehole park as a heat source, and the buildings as a heat sink. The focus of the study lies on the evaluation of various operation and control strategies.

Borehole thermal energy storage

A BTES stores large amounts of waste heat for later use to solve the temporary mismatch between energy production and demand. The natural heat capacity in a large volume of underground soil or rock is used to store thermal energy. The subsurface is heated by circulating a fluid like water or brine in a closed system with vertical boreholes that are typically $20 - 200$ m deep, filled with a plastic pipe and grouting [Tabares-Velasco17]. Drawbacks of BTES systems are generally slow response and high thermal losses. The slow response is due to a relatively low heat transfer rate between the ground and the heat transfer fluid. Thermal losses for BTES systems are usually in the order of 30 % [Sibbitt15], depending on the shape of the storage volume and the borehole arrangement.

Storage temperatures for regular BTES range between $30 - 60$ °C during charging and discharging, with up to $70 - 90$°C for high-temperature borehole thermal energy storages [Sibbitt15]. A start-up period of a few years should be expected to heat up the storage and the surroundings for the design system temperature to be reached [Tabares-Velasco17]. The application of BTES has mostly been designed for use in larger building complexes, neighborhoods or as part of district heating grids [Gehlin19].

Existing high temperature BTES systems

Two well-documented cases for high-temperature BTES systems that are well-proven and in operation for several years are integrated in the Drake Landing Solar Community in Canada and at the Emmaboda site in Sweden.

In Drake Landing, heat for 52 high energy-efficiency houses is provided through an integrated system combining solar thermal collectors and a BTES. The BTES system is composed of 144 boreholes with a depth of 35 m [Sibbitt12]. The BTES is connected to solar collectors, auxiliary boilers and two water tanks for short-term storage. The water tanks are used as a buffer between the collector loop, the heating grid, and the BTES field, charging and discharging thermal energy as required to balance both the variations in energy demand and power consumption. The injection and withdrawal temperatures vary from 80 °C to 30 °C. The BTES is providing more than 90 % of the total annual heating demand, which is achieved through a combination of direct use from the solar collectors and indirect use of the stored solar heat in the BTES. The coefficient of performance is over 30. Consistent retrieving efficiencies of above 95 % were achieved for the period 2012 – 2016, with overall ten years of reliable operation with no unscheduled interruptions related to heating delivery operation [Sibbitt12].

The high-temperature BTES in Emmaboda (Sweden) was put in operation in 2010 and consists of 140 boreholes with a depth of 150 m. The system is charged with industrial waste heat from an aluminum foundry. The overall activity at the foundry is rather energy intensive with 45,000 MWh of electricity and 5000 MWh of district heating being purchased for the site annually. The BTES is used to store heat generated in summer when the plant has no heating demand, and to use it in winter to reduce purchased district heating for the site [Nordell15]. The highest achieved values for heat injection and extraction were 2200 MWh and 400 MWh, respectively, yielding a BTES efficiency of 19 % [Nilsson19].

Although the geological conditions in Norway are generally favorable for high-temperature BTES systems [Ramstad17], there is still a lack of integrated high-temperature BTES systems that are in operation. One of the first high-temperature BTES systems in Norway is planned to be built at Furuset in Oslo.

The Furuset case

The site in Furuset is a pilot area within the research center ZEN (Zero Emission Neighborhoods in smart cities) [Baer18]. Furuset is a multi-functional local neighborhood center in the eastern part of Oslo which incorporates about 3.800 residential units from the 1970s. The Furuset project aims to physically upgrade the district towards high environmental ambitions. The renewal includes the whole infrastructure and is taking energy, waste, water, traffic and social issues into consideration.

The development of a micro energy system aims to establish a local energy system with zero-emissions. Furuset lies within the concession area of a local district heating provider. Estimated timeframe for completion is 2030 [Baer18].

The planned micro-energy system in Furuset is depicted in figure 1. It will be used to connect a high-temperature BTES, solar panels and batteries with a local district heating grid to reduce peak loads.
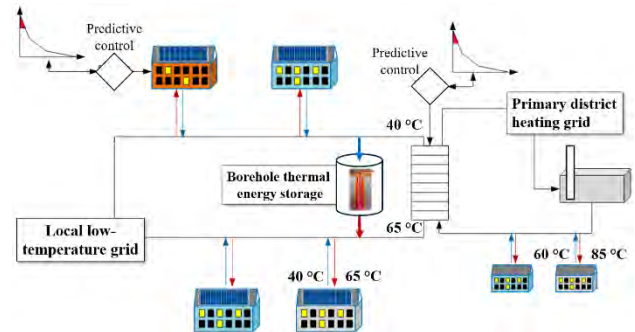
Figure 1: The planned micro energy system in Furuset

The utilization of a BTES is a promising approach to store surplus heat during summer from the local nearby waste incineration plant in Klemetsrud for heating purposes in winter, thus getting a step closer to establish a local energy system with zero-emissions. The stored surplus heat can be used for either direct use in the local thermal grid or as a heat source for a heat pump.

To investigate the dynamic interaction between the BTES, the incineration plant, Furuset's micro energy system and the primary district heating grid, a Modelica-based model was created. With help of the model, several BTES operation cases and control strategies can be assessed to guarantee the most efficient utilization of the stored heat. Both the model and the system design parameters that are used in the model are presented in the following sections.

Dynamic simulation model

A simplified version of Furuset's micro energy system from figure 1 is modelled using the Modelica language. A borehole field model is available in the open-source buildings simulation library IBPSA [Wetter14], which was modified and configured to fit the Furuset design. The Modelica model (figure 2) uses the system design parameters from the following section.

As the Furuset borehole park is planned to be an extensive site with 440 boreholes thermally interacting with each other and the ground, the borehole model needs to provide the possibility for the simulation of both short-term transient thermal effects within the boreholes and long-term thermal interactions within the overall bore field.

A common strategy for the simulation of BTES is to use separate models to evaluate heat transfer inside and around the boreholes, with the borehole wall temperature acting as an interface between the models [Cimmino19a].
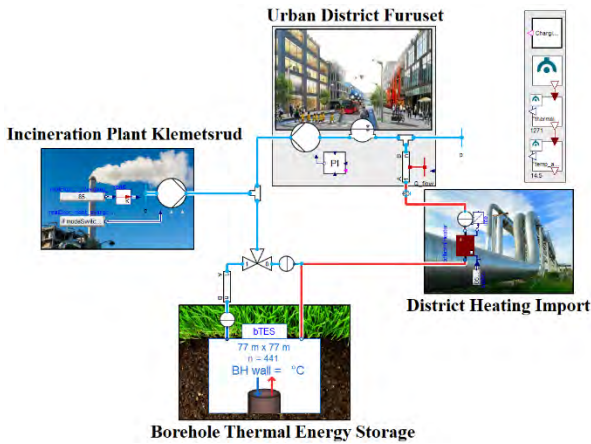
Figure 2: A simplified overview of the modelled micro energy system in Furuset

In general, the borefield model is constructed in two main parts: the borehole and the ground heat transfer. The thermal behavior between the pipes and borehole wall are modeled as a resistance-capacitance network [Bauer11]. Fluid and ground temperatures are predicted by temporally superimposing g-functions, which are step-response functions that estimate the relation between the heat injection rate in the bore field and the resulted average temperature variation at the borehole walls [Eskilon87]. The g-function of a particular bore field needs to be superimposed in time to obtain the effective borehole wall temperature variation due to variable heat extraction rates.

The heat interaction between the particular boreholes is therefore restricted to parallel feeding of the boreholes, as the same borehole wall temperature needs to be assumed at each depth. The ground temperature response model only computes the average borehole wall temperature for all boreholes combined. Except for various first results as for example stated in [Cimmino2019b], there is currently no modelling approach reported that is capable of considering both serial and parallel operation of a borehole park for long-term dynamic simulations. The results of this study shall therefore be assessed in consideration of the usage of a parallel connection setup.

System design parameters

The heat demand for Furuset is estimated based on the expected building mass in 2030. A typical temperature profile for Oslo is used as a base to generate thermal load profiles from a database that contains various large sets of heat load measurements from different building categories and energy efficiency levels. The heating demand includes both space heating und domestic hot water heating. It is mapped based on estimated floor space as well as the age and type of both new and old buildings in the neighborhood [Lindberg13]. As illustrated in figure 3, the maximum value for the heat demand is estimated to be 10.1 MW while the aggregated yearly heating demand is 26 GWh. The Modelica model applies this heat demand profile directly as a heat sink.
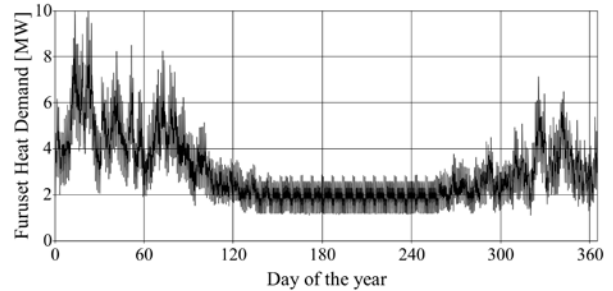
Figure 3: The estimated heat demand profile for Furuset

In addition to the estimated heat demand profile for Furuset, further design parameters are provided by a design study conducted by [Tvärne18]. The supply and return temperatures in the micro energy system are planned to be 65 and 40 °C, respectively. The preliminary design of the high temperature BTES was concluded to consist of 440 boreholes, each 180 m deep with a 3.7 m distance between the boreholes, arranged in a cylindrical shape with both parallel and serial water flow. Further design parameters are summarized in table 1.

Table 1: Design parameters for the planned BTES system in Furuset [Tvärne18][Zari16]

Charging temperature in summer	87 – 90 °C
Mass flow rate in summer/winter	200 m³/h, 1100 m³/h (55 – 305 kg/s)
Pipe material	U-pipe, type PE100-RT, HDPE ISO 24033 Type II (0.42 W/mK, 0.941 g/cm³)
Borehole thermal resistance	0,12 - 0,26 Km/W
Rock type	Granodiorite/Gneiss,
Rock density	2.65 g/cm³
Rock heat capacity	770–979 J/kg K
Rock thermal conductivity	2.7–3.1 W/m K

As for the waste heat quantification, the design study estimates excess heat in the range of 40 MW from the incineration plant in Klemetsrud being available during the summer months June, July and August. During these three months, the BTES system will only be operated in charging mode. Starting from September, the BTES can be used to provide heat to the micro-energy system of Furuset. The maximum charging (injection) and discharging (extraction) effect for the BTES is estimated to be 12 MW and 4 MW, respectively. The total amount of required thermal energy for charging is 13 GWh/year. With an estimated heat loss value of 27 %, 9.5 GWh of heat can be provided per year to Furuset. However, these values only apply for a BTES in equilibrium state, after several years of charging. Table 2 and figure 4 show that a larger amount of heat is needed especially in the very first year of operation:
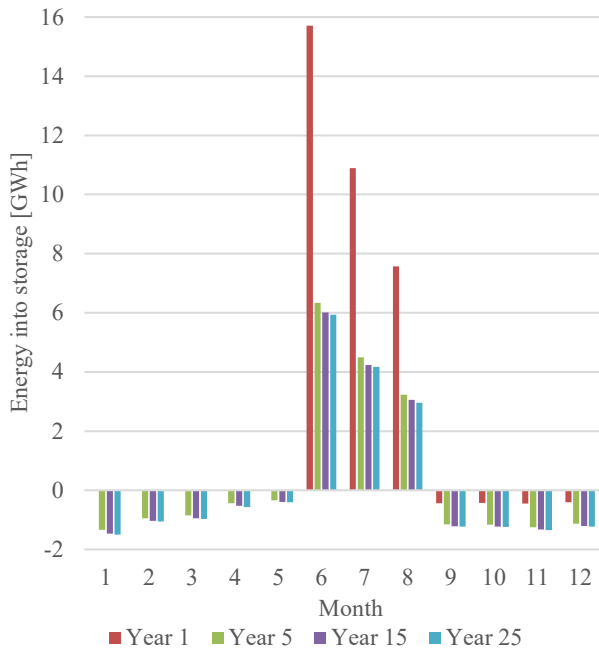
Figure 4: Estimated monthly heat for charging and discharging the BTES for several years of operation [Tvärne18]

After five years of operation (green bars in figure 4), the heat losses have stabilized and the BTES can be used with balanced charging and discharging cycles, as the amount of heat being injected and extracted from the BTES is already close to the equilibrium values that would be reached after 25 years of operation (purple bars in figure 4). In an equilibrium operation, roughly 13 GWh are being charged into the BTES during the three summer months, while 9.5 GWh are being discharged during the remaining months, as summarized in table 2.

Table 2: Estimated aggregated heat for charging (three summer months) and discharging (nine winter months) the BTES for several years of operation [Tvärne18]

Season	Year 1 [GWh]	Year 5 [GWh]	Year 15 [GWh]	Year 25 [GWh]
Charging (Jun-Aug)	34.18	14.06	13.31	13.07
Discharging (Sep-May)	-1.72	-8.61	-9.35	-9.54

Case studies

A Modelica-based model was created towards results from the design study. To assess the most efficient utilization of the high temperature BTES with regards to lowering additional heating costs in form of imported district heat, several BTES operation cases and control strategies need to be evaluated. The first two cases *partial mass flow* and *complete mass flow* focus on general control strategies and the effect of mass flow control on the BTES performance.

The focus for case *September*, case *December*, case *peak 3.4* and case *peak 2.7* lies on discharging strategies, and how the BTES can most effectly reduce the overall energy cost in the micro energy system. With the help of peak shaving, the amount of imported district heating during periods of highest heating prices will be reduced. In all cases, comparisons between the modelled system performance results and the preliminary system performance results from the design study will be conducted.

Mass flow control cases

The first two sets of simulations focus on control strategies for operating the BTES. For the case *partial mass flow*, the BTES is operated to provide an outlet water temperature of 65 °C. To achieve this, the mass flow rate into the BTES is therefore limited and the rest of the flow is bypassed. Additional heat imported from the district heating grid is then used to heat the bypassed flow. The advantage of this approach is that the main district heating system can achieve lower return temperatures. For the case *complete mass flow*, the whole water mass flow which would be required to match the district's heat demand profile is pumped into the BTES, resulting in a lower water outlet temperature out of the BTES. In that case, the district heating system is used to lift the temperature up to the required 65 °C.
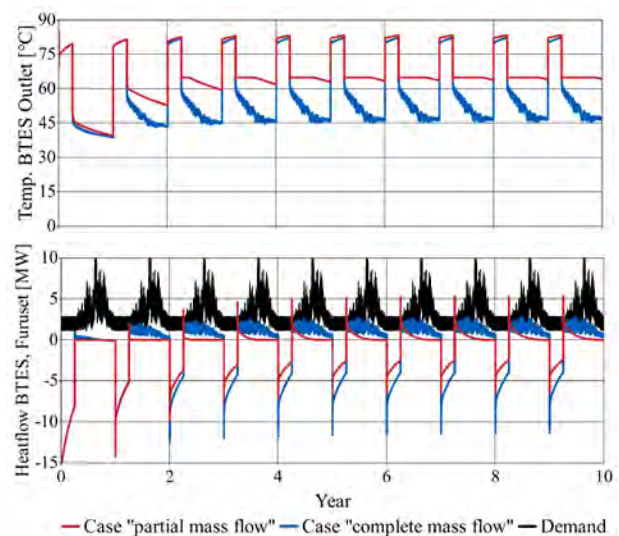
Figure 5: Comparison of two control strategies for BTES discharging over ten years of operation: (a) BTES outlet temperature; (b) heat flow rate into (negative value) and out of (positive value) the BTES in comparison to Furuset's heat demand

Figure 5a shows the BTES outlet temperature for ten years of operation with three months of charging followed by nine months of discharging. Figures 5b is comparing the heat flow rates from and into the BTES with the requested demand by the neighborhood. The modelled maximum charging power for the first year is 15 MW, while 12 MW were anticipated in the design study. The first year (i.e., the first three months) of charging was completed with 25 GWh of heat being stored in the ground, while the design study estimated 32 GWh. The deviation might result from the use of a parallel borehole configuration in the present model, while the design study suggested a serial connected setup, resulting in different values for the mass flow rate and overall heat losses.
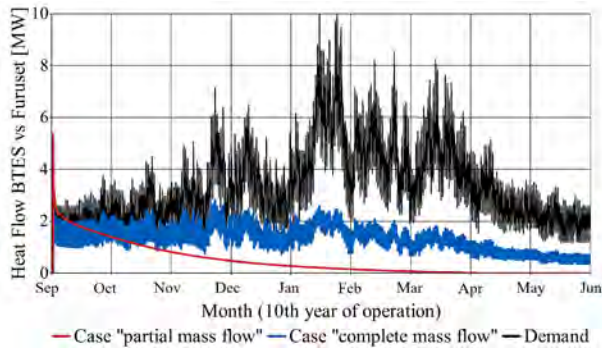
Figure 6: Comparison between Furuset's heat demand and the heat flow rate for the BTES, for nine months of BTES discharging, after ten years of operation

Figures 6 is zooming into figure 5b to focus on the tenth year of operation when an equilibrium operation point can be assumed after the initial years of charging the BTES. The nine discharging months are illustrated and the provided heat by the BTES for both two cases are depicted in comparison to the overall heat demand of the district. The difference between both curves yields therefore the amount of imported district heat to fully cover Furuset's heat demand.

Figure 6 shows that the case *partial mass flow* is not capable of providing sufficient heat to the neighborhood, especially during the periods of peaked demand in January/February. The integrated values yield that in case *partial mass flow* only 7.1 GWh of heat is stored in the BTES during summer and 3.2 GWh are being discharged during the rest of the year. For case *complete mass flow*, 12.1 GWh are charged and 8.9 GWh are discharged, which meets the estimated values from the design study, as stated in table 2 and figure 4. It can be therefore concluded that only case *complete mass flow* is able to reproduce realistic BTES operation, and the BTES system should be operated with higher mass flow rates with less consideration of the BTES outlet temperature.

In case *partial mass flow*, even ten years of BTES operation are apparently not sufficient to provide an outlet temperature of 65 °C with reasonable amounts of mass flow rates, which ultimately results in highly increased imported district heat. This cannot be justified by the lower return temperature in the district heating grid, and it can be therefore recommended to control the BTES with an increased mass flow rate and accepting slightly lower outlet temperatures. In that case, more heat can be retrieved compared with an outlet temperature-controlled BTES system. It shall be however noted that a proper consideration of the pressure loss within the BTES will most likely lead to a more beneficial assessment of the *partial mass flow* case.

However, as shown in figure 6, both operation cases are only covering 2 % (case *partial mass flow*) and 26 % (case *complete mass flow*) of the highest peak load in January. Most of the peak loads are being covered in the beginning of the discharging season in September/October, when import from the district heating grid is not as costly as during winter months. The next cases will therefore focus on reducing the highest peak loads during winter.

Peak shaving cases

For the next cases, the BTES will be mainly used to reduce the amount of imported district heating especially during the most costly time periods of peaked heat demand. To better evaluate the economic benefit when a BTES is applied to reduced transient peak demands, the price for imported heat from the district heating grid needs to be considered. The real economic benefit of this system is a function of the marginal energy production cost for the district heating company. However, this information is considered trade secret and is therefore not publically available. Instead, a comparison of the following cases is performed with a standard pricing scheme for industrial costumers.

The district heating price is typically added together from three terms: a fixed base term, an energy term and a term for the maximum peak demand per month. Up-to-date values for these terms for 2019/2020 for industrial end-users were taken from a local district heating provider in Oslo [Fortum20]. The basic term is 3000 NOK/year, and the remaining monthly terms are summarized in table 3.

Table 3: District heating prices for industry in Oslo, 2019/2020 [Fortum20]

Month	Energy Term [NOK/kWh]	Maximum Demand Term [NOK/kW/month]
January	0.5103	150
February	0.3992	150
March	0.3640	80
April	0.2954	23
May	0.6172	23
June	0.5253	23
July	0.5559	23
August	0.5697	23
September	0.5270	23
October	0.6005	23
November	0.6868	80
December	0.6425	150

The highly increased pricing for district heat import is especially apparent during the winter months of December, January and February. The explicit utilization of the stored heat from summer during these particular months offers therefore the highest possible savings. In the following, four control strategies for an efficient usage of the BTES during peaked demand will be compared. It shall be noted, that based on the results from the previous section, the BTES is supplied with an on/off control for the mass flow in all four cases: If stored heat from the BTES is requested, the complete required mass flow needed to meet the heat demand of the neighborhood is pumped into the BTES, as a partial bypass was considered to be energetically less favorable.

The first case *September* corresponds to the *complete mass flow* case from the previous section, as the BTES discharging starts right after the end of the charging period and lasts for nine months.

For case *December*, a shorter overall discharging period is investigated. The start of BTES discharging is shifted to the beginning of December, when the import of district

heat becomes most costly. Therefore, the BTES is completely bypassed for the first three months September, October and November, and the heat demand for the neighborhood is entirely provided by district heating during the first months.

In the last two cases, *peak 2.7* and *peak 3.4*, the BTES will only be utilized when the neighborhood's heating demand surpasses a specific threshold. The threshold for case *peak 3.4* is set to 3.4 MW to concentrate the utilization of the BTES to periods with highest heating demand. The import from the district heating grid will therefore cover all heating demand under this threshold, while the BTES is providing any heat demand surpassing the 3.4 MW threshold. The shaved off peaks are illustrated in figure 7:
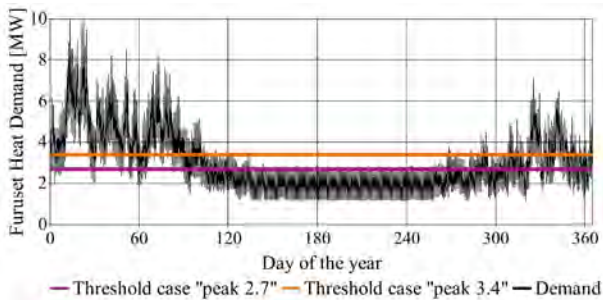
Figure 7: Visualization of both peak shaving thresholds in comparison to Furuset's heat demand profile

The threshold for case *peak 2.7* was calculated considering the known heat demand profile, to ensure that all of the stored heat is utilized in the most efficient way: Since it was shown in table 2 that the BTES is capable to deliver at most 8 – 9 GWh per year, the integrated value for the particular shaved off peaks in the demand profile were set to 8 GWh, to theoretically approach an optimal and complete utilization of the stored heat by the end of the discharging season. With the given heat demand profile, the threshold was calculated to be 2.7 MW.

It shall be noted that this theoretical approach is only applicable because of the assumption of a known heat demand profile. In reality, the district's heat demand cannot be perfectly predicted, leading to a non-optimal usage of the BTES when the stored heat will either diminish before the end of the peaked heating season (overutilization of the BTES) or when valuable stored heat was not fully discharged during periods of peaked demand (underutilization of the BTES). In general, the prediction of future demands for optimal production planning is already well established in the operation of district heating grids, but not in connection with seasonal time horizons.
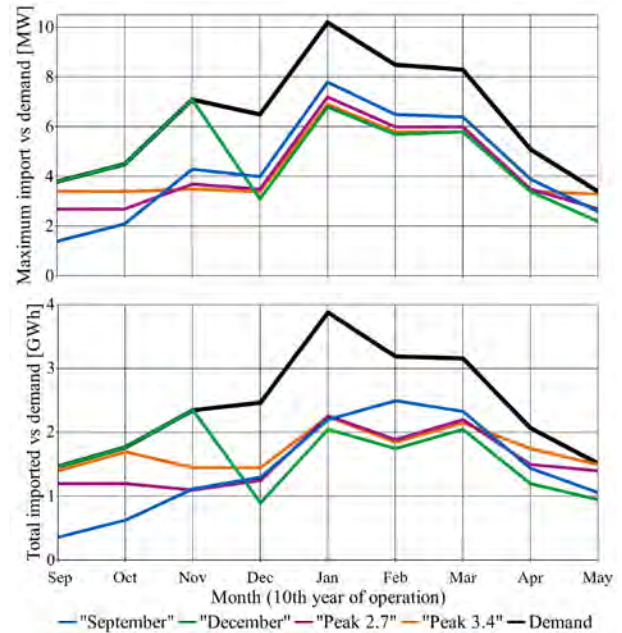
Figure 8: Four cases for peak heating reduction: (a) maximum peak values for Furuset's heating demand vs. imported district heat [MW], (b) overall heat demand of Furuset vs. imported heat from district heating [GWh]

Figure 8a illustrates how much heat in [MW] needs to be imported from the district heating grid for all four cases. Figure 8b illustrates the imported heat in [GWh]. As a comparison, the overall heat demand of Furuset is depicted as well. The difference between the black and the colored lines in figure 8 equals therefore the heat that is provided by the BTES. The bigger the difference between the black and the colored lines, the greater the cost reduction becomes due to reduced import of district heat.

Table 4 and table 5 summarize the reduction in peak heating in percent, both for the monthly maximum imported heat in [MW] and the overall imported heat in [GWh]. The second column in table 5 depicts Furuset's heat demand in [GWh] for each particular month of the discharging season. Without the utilization of any BTES, this amount of heat would be fully covered by import from the district heating grid. The sum for the nine discharging months equals to an annual heat demand of 21.9 GWh and is therefore slightly lower than the estimated 26 GWh from section "*System design parameters*", as the three summer months were excluded. During the summer months, it is assumed that the heat demand of Furuset is fully covered by available surplus heat from the incineration plant.

The amount of imported heat for case *December* equals the overall heat demand of the neighborhood in the first three months, since the BTES is not used before December. However, case *December* offers the biggest peak reductions for the remaining months, when most of the stored heat from summer is finally discharged, as illustrated in figure 8, table 4 and table 5.

Table 4: Furuset's maximum heat demand per month [MW] vs. the reduction of maximum imported heat from the district heating grid [in %] due to BTES usage

Month	Peak heat demand [MW]	Case peak 3.4 [%]	Case peak 2.7 [%]	Case Dec. [%]	Case Sept. [%]
Sep	3.78	-10	-28.5	0	-63.3
Oct	4.5	-24.5	-40	0	-54.4
Nov	7.15	-51.7	-48.1	0	-39.7
Dec	6.49	-47.6	-46.4	-52.8	-38.2
Jan	10.22	-32.4	-29.6	-33.1	-24.1
Feb	8.52	-32.4	-29.4	-32.8	-23.8
Mar	8.26	-30.3	-27.4	-30.4	-22.1
Apr	5.15	-34	-31.4	-34.3	-24.9
May	3.41	-2.3	-20.8	-34.4	-24

Table 5: Furuset's monthly heat demand [GWh] vs. the heat import reduction [in %] due to BTES usage

Month	Heat demand [GWh]	Case peak 3.4 [%]	Case peak 2.7 [%]	Case Dec. [%]	Case Sept. [%]
Sep	1.47	-4.8	-18.4	0	-75.5
Oct	1.77	-4	-32.2	0	-64.4
Nov	2.35	-38.3	-53.2	0	-52.3
Dec	2.47	-41.3	-49.4	-63.6	-47.4
Jan	3.88	-42	-41.8	-47.2	-43.3
Feb	3.19	-42	-40.8	-45.1	-21.6
Mar	3.16	-32	-30.4	-35.1	-26.3
Apr	2.07	-15.5	-27.5	-42	-30.4
May	1.52	-1.3	-7.9	-37.5	-30.3

The effect of peak shaving is lowest for case *September*, especially during highest peak heating periods in winter, as the BTES is constantly being discharged and therefore not capable of providing enough heat during these periods. However, during the first four months and for the very last month, case *September* is capable to provide a larger reduction in heat import as both *peak* cases. This is due to the constant discharging of the BTES which leads to an increased utilization of most of the stored heat, while both *peak* cases appear to underutilize the stored heat:

The total amount of provided heat during the nine months is highest for case *September* (8.94 GWh), and especially case *peak 3.4* underutilizes the stored heat, as only 6.38 GWh of heat are being released in nine months, due to the restricted temporal utilization of the BTES in that case. Case *December* provides 7.39 GWh while case *peak 2.7* provides 7.88 GWh during nine months. The elaborate estimation of proper thresholds for peak shaving resulted therefore only in marginal efficiency improvements: Both *peak* cases provide approximately the same order of magnitude for peak reduction as case *December*, but especially for case *peak 3.4*, at the expense of overall utilization of stored heat potential.

Finally, with consideration of the amount of imported heat from figure 8 and the corresponding price terms from table 3, the overall costs for importing district heat result in: 10.04 MNOK for case *September*, 11.16 MNOK for case *December*, 10.48 MNOK for case *peak 2.7* and 11.26 MNOK for case *peak 3.4*. Without the utilization of BTES, the supply of Furuset's heat demand would be fully covered by import from the district heating grid, resulting in costs of 16.40 MNOK. Therefore, these costs can be reduced by 31.3 – 38.8 % when stored surplus heat from summer is utilized in winter.

It shall be noted that the consideration of a serial connected bore field will most likely result in higher outlet temperatures and therefore increased maximum power output from the storage, resulting in higher potential for cases that focus on peak heating thresholds such as the presented *peak* cases in this study.

Conclusion

BTES systems offer huge potential for storing surplus heat in summer for later use in winter. This simulation-based study was conducted with the help of a Modelica-based model, which utilized the results from a design study. The model was used in combination with aggregated heat demand profiles for a neighborhood in Oslo to get preliminary evaluations on the efficient integration of a BTES within a local micro energy system. The results showed that utilization of stored heat during periods of peaked heat demands provide great potential to reduce the costly heat import from district heating grids.

Two cases for testing general control strategies to discharge the BTES were investigated. Running all the water through the BTES resulted in a decreased borehole outlet temperature, and additional heat from the district heating grid was needed to lift the temperature to the required supply temperature. This operation mode was assessed to be energetically more efficient than the case with decreased water mass flow rates into the BTES, which lead to higher outlet temperatures but also more additional heat needed to be imported.

Several cases for temporally shifting the usage of the stored heat were investigated. It has been shown that with proper BTES utilization, the costs for importing district heat during periods of highest heating demand can be greatly decreased. Depending on the discharging case, the maximum heat demand was reduced by up to 53 % in winter. It was shown that the costs for importing district heat can be reduced by up to 39 % when stored surplus heat from summer is used in winter. The efficient utilization of the stored heat can be highly dependent on the anticipated heat demand profile for the district, as the threshold for starting the BTES discharge can be set too low (overutilization) or too high (underutilization).

In this context, heat demand profiles with more extreme peak demands could be analyzed in the future with their effect on an efficient utilization of the BTES. Furthermore, focus needs to be put on the usage of additional heaters: Heat pumps or electrical heaters can be assessed as an alternative to the import of district heating, and economic comparisons need to be drawn with consideration of both electricity prices and district heating prices. A proper consideration of pressure losses and

pumping power as well as the integration of a BTES connected in serial configuration will further increase the quality of future studies on BTES integration: A storage in serial connection mode would reduce the heat losses to the ground in comparison to a parallel-connected BTES, and therefore increase the maximum power output.

Acknowledgement

References

[Baer18] Baer, D., Andresen, I., (2018). "ZEN Pilot Projects - Mapping of the Pilot Projects within the Research Centre on Zero Emission Neighbourhoods in Smart Cities", ZEN Report No. 10 – 2018, NTNU, SINTEF, ISBN 978-82-536-1601-8, *https://fmezen.no/*

[Bauer11] Bauer, D., Heidemann, W., Müller-Steinhagen, H., Diersch, H.-J., (2011). "Thermal resistance and capacity models for borehole heat exchangers"), Int. J. Energy Res. 35 (4), 312–320. *https://doi.org/10.1002/er.1689*

[Cimmino19a] Cimmino, M., Laferrière, A., Picard, D., Helsen, L., (2019). "Development and validation of a full-time-scale semi-analytical model for the short- and long-term simulation of vertical geothermal bore fields", Polytechnique Montreal, Canada, *https://doi.org/10.1016/j.geothermics.2019.101788*

[Cimmino19b] Cimmino, M, (2019). "Semi-Analytical Method for g-Function Calculation of bore fields with series- and parallel-connected boreholes", Science and Technology for the Built Environment, *https://doi.org/10.1080/23744731.2019.1622937*

[Eskilon87] Eskilson, P., (1987). "Thermal Analysis of Heat Extraction Boreholes", Lund University, Sweden

[Fortum20] Fortum Oslo Varme AS, (2020). "Priser og vilkår", *https://www.fortum.no/bedrift-og-borettslag/fjernvarme/priser-og-vilkar*

[Gehlin19] Gehlin, S., Andersson, O., (2019). "Geothermal Energy Use, Country Update for Sweden", European Geothermal Congress, Den Haag, The Netherlands

[Jensen17] Jensen, S.Ø., Marszal-Pomianowska, A., Lollini, R., Pasut, W., Knotzer, A., Engelmann, P., Reynders, G., (2017). "IEA EBC Annex 67 energy flexible buildings", Energy and Buildings, 155:25-34

[Lindberg13] Lindberg; K. B., Doorman, G., (2013). "Hourly load modelling of non-residential building stock", Dept. of Electric Power Engineering, Norwegian University of Science and Technology, NTNU, Trondheim, Norway

[Lund 14] Lund, W., Werner, S., Wiltshire, R., Svendsen, S., Thorsen, J. E., Hvelplund, F., Mathiesen, B. V., (2014). "4th Generation District Heating (4GDH): Integrating smart thermal grids into future sustainable energy systems", Energy 2014;68:1e11

[Nilsson19] Nilsson, E., Rohdin, P., (2019). "Performance evaluation of an industrial borehole thermal energy storage (BTES) project - Experiences from the first seven years of operation", Renewable Energy, Volume 143, p. 1022-1034

[Nordell15] Nordell, B., Andersson, O., Rydell, L., Liuzzo-Scorpo, A., (2015). "Long-term Performance of the HT-BTES in Emmaboda, Sweden", Greenstock, Beijing, China

[Ramstad17] Ramstad, R.K, Holmberg, H., Bugge, L og Riise, M.H., (2017). "Sluttrapport Fjell2020 konseptutredning miljøløsninger", Asplan Viak-rapport utført for Drammen Eiendom KF

[Sibbitt12] Sibbitt, B., McClenahan, D., Djebbar, R., Thornton, J., Wong, B., Carriere, J., Kokko, J., (2012). "The Performance of a High Solar Fraction Seasonal Storage District Heating System – Five Years of Operation", CanmetENERGY, Natural Resources Canada, Ottawa, Canada, DOI: *https://doi.org/10.1016/j.egypro.2012.11.097*

[Sibbitt15] Sibbet, B., McClenahan, D., (2015) "Seasonal Borehole Thermal Energy Storage—Guidelines for Design & Construction" IEA-Solar Heating & Cooling TECH SHEET 45.B.3.1, page 1-15

[Tabares-Velasco17] Tabares-Velasco, P.C., Lanahan, M., (2017). "Seasonal Thermal-Energy Storage: A Critical Review on BTES Systems, Modeling, and System Design for Higher System Efficiency", Department of Mechanical Engineering, Colorado School of Mines, USA, Energies 2017,10(6), 743; *https://doi.org/10.3390/en10060743*

[Tvärne18] Tvärne, A., Mattsson, P., (2018). "Värmeförsörjning i Furuset med utnyttjande av säsongslager i systemet", Förstudie högtemperatur borrhålslager, SENS Sustainable Energy Solutions AB, Nacka, Sweden

[Wetter14] Wetter, M., Zuo, W., Nouidui, T. S., Pang, X., (2014). "Modelica Buildings Library", Journal of Building Performance Simulation 7(4): 253–70. *https://doi.org/10.1080/19401493.2013.765506*

[Zari16] Zari, N., Jemmal, Y., Maaroufi, M., (2016). "Thermophysical and chemical analysis of gneiss rock as low cost candidate material for thermal energy storage in concentrated solar power plants", Mohammed V University, Morocco *http://dx.doi.org/10.1016/j.solmat.2016.06.00*

A novel modelling approach of ground source heat pump application for district heating and cooling, developed for a case study of an urban district in Finland

Oleg Todorov[1*], Kari Alanne[1], Markku Virtanen[1], Risto Kosonen[1,2]
[1]Aalto University, Helsinki, Finland
[2]Nanjing Tech University, Nanjing, China
* corresponding author: oleg.todorovradoslavov@aalto.fi

Abstract

The world impact of fossil fuels on air pollution is responsible for several millions premature deaths every year. The present study analyses the decarbonization of district heating (DH) and cooling (DC) networks by the integration of ground source heat pump (GSHP) within an urban district in southwestern Finland, in terms of technoeconomic feasibility, efficiency and environmental impact. A novel mathematical modelling for GSHP operation and energy system management is proposed and demonstrated, using hourly-based data for heating and cooling demand. Hydrogeological and geographic data from different Finnish data sources is retrieved in order to calibrate and validate a groundwater model. Three different Scenarios for GSHP operation are investigated, limited by the maximum pumping flow rate of the groundwater area. The additional pre-cooling exchanger in Scenario 2 and 3 resulted in an important advantage, since it increased the heating and cooling demand covered by GSHP by 15% and 16% respectively as well as decreased the energy production cost by 4%. Moreover, Scenario 3 was solved as nonlinear optimization problem resulting in 4% lower pumping rate compared to Scenario 2. Overall, the annually balanced GSHP management in terms of energy and pumping flows, resulted in low long-term environmental impact and is economically feasible (energy production cost below 30 €/MWh).

Introduction

Worldwide, some 4.5 million people die prematurely every year due to air pollution generated by burning fossil fuels and the increased levels of PM2.5, while the overall cost is estimated as 3.3% of world GDP (Greenpeace 2020). Recent study also relates the mortality of Covid-19 and the long-term exposure to air pollution and PM2.5, concluding that small increase in PM2.5 exposure has 20 times more lethal impact in Covid-19 death rate (Wu et al. 2020). Therefore, a decarbonization of our existing energy networks, based primarily on fossil fuels generation, is a necessity for sustainable and healthy future. According to Eurostat, in 2018 the share of renewable energy sources (RES) used for heating and cooling in the European Union was 21% and several countries like Sweden (65%), Latvia (56%), Finland (55%) and Estonia (54%) covered more than half of their

heating and cooling consumption with renewables sources (Eurostat 2020). The variability of renewable generation between heating and cooling seasons, as well as the low coincidence between supply and demand are important challenges for RES penetration, therefore short- and long-term energy storage is needed for maximizing the usage of RES.

Wherever the hydrogeological conditions are favourable, Aquifer Thermal Energy Storage (ATES) is an attractive technological option, suitable for large buildings and utilities (Fleuchaus et al. 2018) as well as capable to enable important thermal storage capacities (Pellegrini et al. 2019). Fleuchaus et al. (2018) presented a complete overview of global ATES development and application: some 3000 ATES systems are operated nowadays worldwide. The Netherlands with 85% of all ATES realizations, followed by Sweden, Denmark and Belgium, are the undisputed frontrunners. From these 3000 ATES applications worldwide, there are some 100 large-scale utility systems, integrated in DH/DC networks (Schmidt et al. 2018).

In the same line, ground-source heat pump (GSHP) is a key technology for a decarbonization of the existing heating and cooling, nowadays mostly based on the utilization of fossil fuels (Paiho et al. 2018; Soltani et al. 2019; Popovski et al. 2019). The work of Paiho et al. 2018 revealed that large-scale heat pumps are crucial for increasing the flexibility of the Finnish energy systems. Within the same research, different examples are presented for heat pump integration in Finnish DH/DC networks: in Turku - the Kakola plant recycling heat from sewage wastewater, and in Helsinki - the Katri Vala plant generating heating and cooling in a single process. Fleuchaus et al. (2019) evaluated the performance of ATES based on different criteria and concluded that ATES integration into heating and cooling systems were rarely addressed. In order to fill this gap, the integration of GSHP in tandem with ATES within the existing DH/DC networks of a Finnish urban district, is presented and developed in the current case study.

The novelty of the present research is to introduce a mathematical modelling of the whole energy chain ATES-GSHP-DH-DC in order to improve system´s energy management, as well as to study its technical

justification, economic feasibility and the long-term impact of GSHP-ATES operation. Finnish public data sources are available, like the Finnish Environmental Institute (SYKE) regarding the hydrological resources; Geological Survey of Finland (GTK) - hydrogeological conditions, and the National Land Survey of Finland (NLSF) for geographical data. The present research also presents a methodology for fetching data from the aforementioned sources for calibrating and validating a groundwater model, which in turn is an essential tool for studying the long-term impact on the aquifer area.

Methods

The modelling procedure of the combined ATES-GSHP-DH-DC system is based on the following steps, namely - i) input data of the target DH/DC networks and the nearby groundwater areas, ii) mathematical modelling of combined ATES-GSHP operation, iii) techno-economic analysis, and iv) impact of ATES-GSHP operation on aquifer areas, by developing and calibrating a specific groundwater model. Groundwater model based on the finite-difference-method software MODFLOW (Harbaugh et al. 2005) is developed in this case study, which is calibrated against long-term data (hydraulic heads of the observation wells) of the studied aquifer.

Input data for GSHP integration

Input data of the DH and DC networks

The target DH/DC networks are located in the central district of Kupittaa in the town of Turku, located in the south-west part of Finland. The available data is hourly-based and the most relevant parameters of both DH and DC networks are summarized in *Table 1* and *Figure 1*.

Table 1. Relevant DH / DC network parameters

Network parameters	DH network	DC network
Annual energy demand, MWh	67,971	12,382
Max./min. load, MW	27.06 / 0.43	6.38 / 0.52
Avg. load (± stand. dev.), MW	7.76 ± 4.8	1.41 ± 0.7
Max./min. supply temp., ºC	110.4 / 56.0	10.0 / 5.3
Avg. supply temperature, ºC	84.3 ± 7.8	6.6 ± 0.3
Max./min. return temp., ºC	51.4 / 22.7	14.8 / 10.0
Avg. return temperature, ºC	40.9 ± 2.8	13.5 ± 0.4
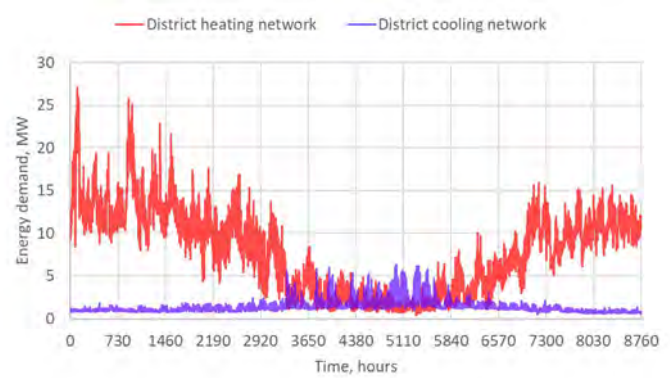
Figure 1. Annual energy demand of DH / DC networks

Input data for a groundwater model

The impact of GSHP-ATES operation is studied by developing a generic groundwater model. Typical data for an esker aquifer located in southwestern Finland is utilized, relative to groundwater areas, monitoring stations and observation wells. Additionally, open data from the National Land Survey of Finland is used, particularly its "10m elevation model". The elevation model is retrieved as Geo-TIFF raster file, transformed to Surfer Grid file (GRD) using QGIS (QSIS, 2019).

GSHP-ATES utilization for DH/DC

Ground-source heat pump (GSHP), operating with groundwater open-loop *well doublet* (comprising groundwater abstraction and injection wells), is considered. The condenser side of the heat pump is connected to DH network while the evaporator side is connected to aquifer pumping stream. Three different scenarios have been investigated. In the first Scenario, the ATES pumping flow path encounters two serial exchangers – HP evaporator and cooling for DC network. In Scenario 2 and 3, a pre-cooling exchanger is added before the HP evaporator, providing 1st stage cooling to the DC network.

As will be shown in the result section, with this configuration the DC demand can be more efficiently covered and HP efficiency (COP) is improved since heat pump inlet temperature increases several degrees after a pre-cooling exchanger. GSHP-ATES integration within existing DH/DC networks is depicted in the general scheme presented in *Figure 2*, where temperature values illustrate the setup of Scenario 2/3.
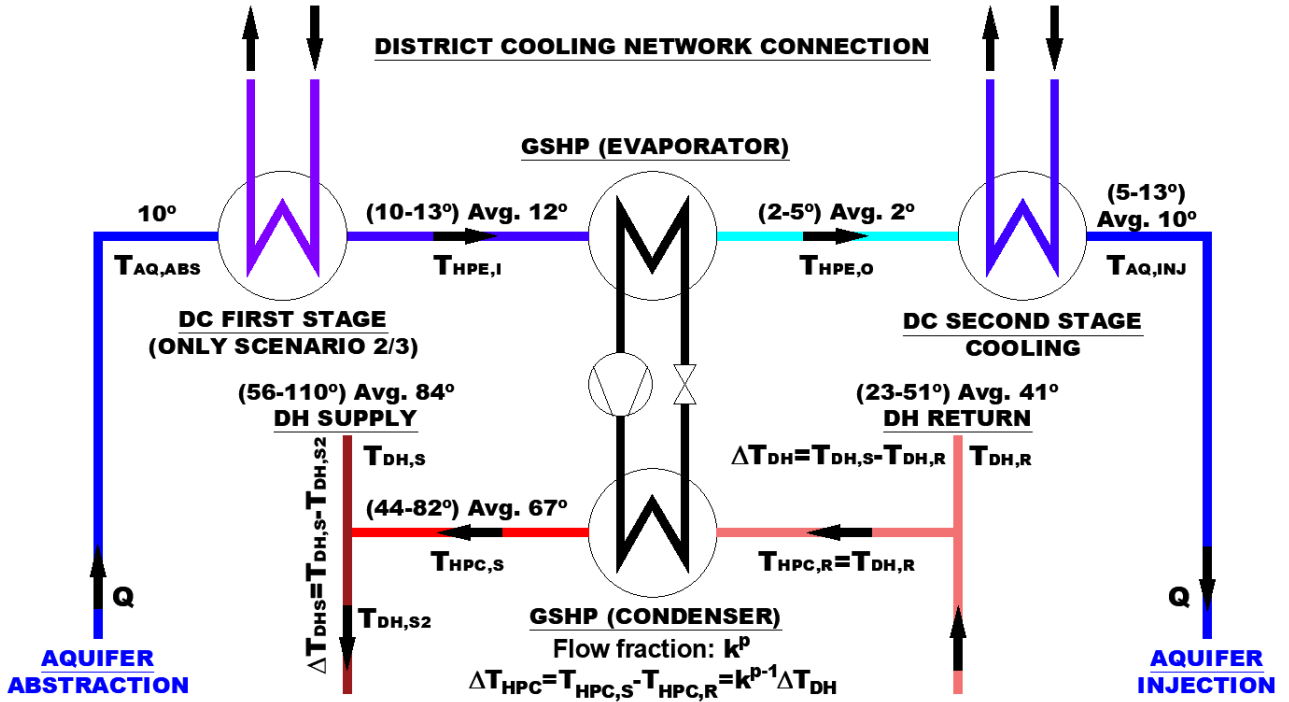
Figure 2. General scheme of GSHP-ATES integration

Modelling tools and methods

GSHP utilization for district heating

GSHP is used to recover and upgrade all excess heat proceeding from the DC network and inject it in DH network. In this context ATES is utilized for balancing the energy system and mitigating the variability and no-coincidence of the simultaneously dispatched heating and cooling loads. To that end, heat pump supply temperature is calculated, based on the demanded power fraction k (the ratio between heat supplied by the heat pump and total heat demanded in the DH branch). The flow fraction recirculated through HP condenser can be calculated as: k^p, where $0 \leq p \leq 1$ is additional exponent parameter. For each hour n, given that $T_{DH,R,n}$ and $T_{DH,S,n}$ are DH return and supply temperatures respectively, the heat pump supply temperature $T_{HPC,S,n}$ can be calculated as follows:

$$T_{HPC,S,n} = T_{DH,R,n} + \left(T_{DH,S,n} - T_{DH,R,n}\right)k^{1-p}$$
$$\Rightarrow \Delta T_{HPC,n} = \Delta T_{DH,n}k^{1-p} \quad (1)$$

And the resulted supply temperature $T_{DH,S2,n}$ after mixing can be computed as:

$$T_{DH,S2,n} = T_{DH,S,n} + \left(T_{DH,S,n} - T_{DH,R,n}\right)(k - k^p)$$
$$\Rightarrow \Delta T_{DHS,n} = T_{DH,S,n} - T_{DH,S2,n} = \Delta T_{DH,n}(k^p - k) \quad (2)$$

The parameter p is chosen equal to 0.6, which can be advantageous in partial load operation. For example, for power fraction $k = 0.4$ and $\Delta T_{DH} = 40$ °C, GSHP should elevate DH return temperature by roughly 28 °C instead of 40 °C. After mixing with supply DH flow, the temperature drop ΔT_{DHS} is around 7 °C.

COP$_H$ estimation model

According to Reinholdt (2018), the maximum theoretical COP of a heat pump can be estimated by calculating Lorentz COP, defined as follows:

$$COP_{Lor} = \frac{T_{lm,H}}{T_{lm,H} - T_{lm,L}}, where$$

$$T_{lm,H} = \frac{T_{HPC,S} - T_{HPC,R}}{ln\left(\frac{T_{HPC,S}}{T_{HPC,R}}\right)}; \; T_{lm,L} = \frac{T_{HPE,O} - T_{HPE,I}}{ln\left(\frac{T_{HPE,O}}{T_{HPE,I}}\right)} \quad (3)$$

In Equation (3), $T_{lm,H}$ and $T_{lm,L}$ are respectively the logarithmic mean temperature of the sink and source, where notations HPC and HPE stand for heat pump´s condenser and evaporator temperatures, while notations I / O stand for inlet / outlet temperatures of the evaporator and S / R stand for supply / return temperatures of the condenser (all values expressed in Kelvin). Based on best industrial refrigeration systems, Reinholdt suggested values for Lorentz efficiency between 50 and 60% of the maximum Lorenz COP. In our case study, more conservative value of 45% is adopted.

GSHP utilization for district cooling

As mentioned previously, part of DC demand can be produced by free cooling in a 1st stage cooling exchanger. After that, GSHP is utilized in the second place for simultaneously cooling of ATES flow in the evaporator and supplying heat to DH network in the condenser (see *Figure 2*). And finally, second stage cooling is applied, and groundwater is injected into the aquifer. For each hour of operation, it is crucial to determine the ATES pumping flow rate Q [m³/s] since there is constraint for pumping of

2500 m³/day (annual average). Due to this limitation, the max. heat output of GSHP condenser is limited to 1.43/1.67 MW respectively in Scenario 1/2(3) and ATES pumping flow rate is calculated according to the algorithm developed below.

Computation of ATES pumping flow rate

Since in the ATES flow path there are two / three exchangers respectively for Scenario 1/2, the needed pumping flow rate Q can be estimated as follows. For each hour n will be determined whether heating or cooling is dominating, given that $\Phi_{heat,n}$ and $\Phi_{cool,n}$ are respectively heating and cooling demand to be covered (notations according to Figure 2):

- Heating dominates:

$$If \quad \frac{\left(1 - \frac{1}{COP_n}\right)\phi_{heat,n}}{S_{VC,wat}\left(T_{HPE,I,n} - T_{HPE,O,n}\right)}$$

$$\geq \frac{\phi_{cool,n}}{S_{VC,wat}\left(T_{HPE,I,n} - T_{AQ,ABS,n} + T_{AQ,INJ,n} - T_{HPE,O,n}\right)}$$

where $T_{HPE,I,n} = T_{AQ,ABS,n}$ (in sc. 1) ;

$T_{HPE,I,n} = max\{T_{AQ,ABS,n}; T_{DC,R,n} - \Delta T_{min}\}$ (in sc. 2);

$T_{AQ,INJ,n,max} = T_{DC,R,n} - \Delta T_{min}$;

$T_{HPE,O,n,min} = 2°C$; $S_{VC,wat} = 4.19 \; MJ/m^3K$

Where $\Delta T_{min} = 2$ °C is the min. pinch point difference in cooling exchangers and $\Delta T_{HPE,O,n,min} = 2$ °C is the min. temperature after GSHP evaporator. COP_n is calculated with Equation (3), assuming avg. value for $T_{HPE,O} = 2$ °C

$$\Rightarrow Q_n = \frac{\left(1 - \frac{1}{COP_n}\right)\phi_{heat,n}}{S_{VC,wat}\left(T_{HPE,I,n} - T_{HPE,O,n}\right)}$$

- Cooling dominates (iteration method):

$$If \quad \frac{\left(1 - \frac{1}{COP_n}\right)\phi_{heat,n}}{S_{VC,wat}\left(T_{HPE,I,n} - T_{HPE,O,n}\right)}$$

$$< \frac{\phi_{cool,n}}{S_{VC,wat}\left(T_{HPE,I,n} - T_{AQ,ABS,n} + T_{AQ,INJ,n} - T_{HPE,O,n}\right)}$$

Iteration step: *initial Q_n is estimated as*

$$\frac{\phi_{cool,n}}{S_{VC,wat}\left(T_{HPE,I,n} - T_{AQ,ABS,n} + T_{AQ,INJ,n} - T_{HPE,O,n}\right)}$$

Recalculation of temperature after HP evaporator

$$T_{HPE,O,n} = T_{HPE,I,n} - \frac{\left(1 - \frac{1}{COP_n}\right)\phi_{heat,n} \cdot Q_n}{S_{VC,wat}}$$

Recalculation of 1ˢᵗ and 2ⁿᵈ stage cooling demands

$$\phi_{cool-1stage,n} = Q_n S_{VC,wat}\left(T_{HPE,I,n} - T_{AQ,ABS,n}\right)$$

$$\phi_{cool-2stage,n} = min\{Q_n S_{VC,wat}\left(T_{AQ,INJ,n} - T_{HPE,O,n}\right); \phi_{cool,n} - \phi_{cool-1stage,n}\}$$

$$\phi_{cool,n} = \phi_{cool-1stage,n} + \phi_{cool-2stage,n}$$

The ATES flow is recalculated again in *Iteration step*, taking as new $T_{HPE,O}$ the average of current and previous

value, and if the new Q_n deviates more than a predefined threshold from the previous one (a 5% threshold is adopted), then *Iteration step* is repeated.

Calculation of ATES pumping power demand

The required pumping power [kW] for ATES operation can be calculated in an hourly basis, assuming overall pressure drop in the line $\Delta p = 600$ kPa and standard pumping efficiency $\eta = 0.55$ (Grundfos SP, 2020):

$$P_{ATES,n} = \frac{Q_n \Delta p}{\eta} \quad (4)$$

Calculation of pumping power demand to DH/DC

Similarly, pumping power [kW] to provide DH/DC through GSHP condenser / evaporator respectively can be calculated in an hourly-basis, assuming overall pressure drop between supply and return lines $\Delta p_{DH} = \Delta p_{DC} = 250$ kPa (DH 2008) and standard pumping efficiency $\eta = 0.55$ (Grundfos NB/NBG, 2020), as follows:

$$P_{HPC-DH,n} = \frac{Q_{HPC,n}\Delta p_{DH}}{\eta}; P_{HPE-DC,n} = \frac{Q_{HPE,n}\Delta p_{DC}}{\eta} \quad (5)$$

$$where \; Q_{HPC,n} = \frac{\phi_{supplied-heat,n}}{S_{VC,wat}\left(T_{HPC,S,n} - T_{DH,R,n}\right)}; Q_{HPE,n}$$

$$= \frac{\phi_{cool-1stage,n} + \phi_{cool-2stage,n}}{S_{VC,wat}\left(T_{DC,R,n} - T_{DC,S,n}\right)}$$

The volumetric heat capacity of water $S_{VC,wat}$ used is 4.19 and 4.1 MJ/m³K respectively for cooling and heating.

Calculation of ATES pumping rate using nonlinear optimization techniques

It is possible to solve ATES pumping flow rate Q_n setting up an optimization problem for each hour of operation. Both Q_n and specific energy consumption of GSHP compressor and ATES pumping need to be minimized. Additional nonlinear optimization problem (Scenario 3) is set up for Scenario 2, defined as follows:

$$Objective \; function: min\left(Q_n + \frac{P_{ATES,n} + P_{HPC,n}}{\phi_{heat,n} + \phi_{cool,n}}\right)$$

$$where \; P_{ATES,n} = \frac{Q_n \Delta p}{\eta} \; (eq. 4) \; and \; P_{HPC,n} = \frac{\phi_{heat,n}}{COP_n};$$

$$\phi_{cool,n} = \phi_{cool-1stage,n} + \phi_{cool-2stage,n}$$

$$\phi_{cool-1stage,n} = Q_n S_{VC,wat}\left(T_{HPE,I,n} - T_{AQ,ABS,n}\right)$$

$$\phi_{cool-2stage,n} = min\{Q_n S_{VC,wat}\left(T_{AQ,INJ,n} - T_{HPE,O,n}\right); \phi_{cool,n} - \phi_{cool-1stage,n}\}$$

$$Subject \; to \; constraints: 0.01 \leq Q_n \leq 0.05 \; [m^3/s]$$

$$T_{HPE,O,n} \geq 2 \; ; T_{AQ,INJ,n} \leq T_{DC,R,n} - 2$$

The model is solved for each hour by varying Q_n and using GRG nonlinear solver in MS Excel.

Numerical model and steady state calibration

MODFLOW (Harbaugh et al. 2005) as finite difference code, under ModelMuse environment (ModelMuse, 2019) is used for the groundwater model. The

discretization of the aquifer area is done using 100x100 m square cell grid, covering a physical extension of about 20 km². Available information is used for 15 close-field observation wells and 8 far-field wells, and their long-term statistical data (average head) in order to calibrate the groundwater model for steady state (see *Figure 3*). The average aquifer thickness is estimated as 10 m (Joronen, 2009) and the maximum allowed average pumping rate is 2500 m³/day (Arola et al. 2014).
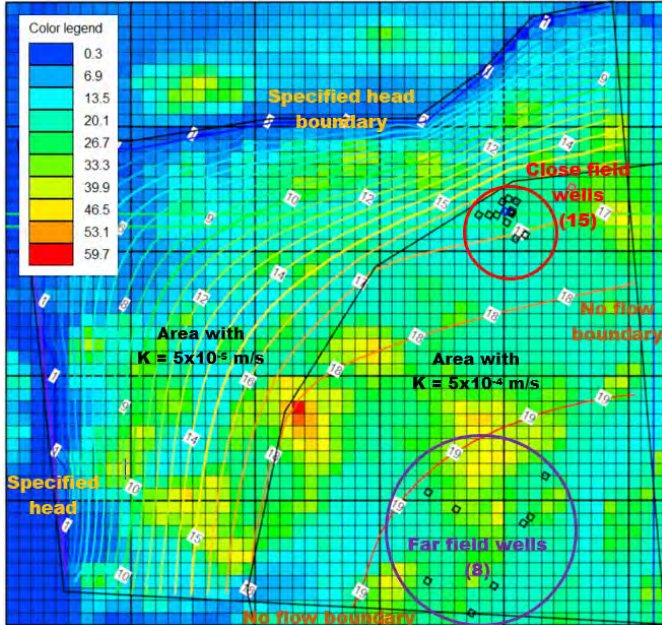
Figure 3. Numerical model and steady state solution

The undisturbed aquifer temperature in Kupittaa area is around 10°C (Arola et al. 2014), quite high due to the subsurface heat island effect (Bayer et al. 2019) observed in high density urban areas like Kupittaa, composed mostly by educational and healthcare buildings, sport facilities and dwellings. North-west and south-west are set as specified head boundaries, while south-east and north-east borders are assumed as no-flow boundaries

Groundwater model calibration for steady state is done according to the procedure developed by Todorov et al. (2020a), and results with RMSE for close- and far-field areas are presented in *Figure 4*, where bubbles´ diameter is the standard deviation of the measured values. A steady state solution is shown in *Figure 3*, where iso-lines are hydraulic heads while color legend represents elevations (in meters above sea level).

A typical horizontal hydraulic conductivity for sand/gravel aquifer is selected: K=5x10^{-5} m/s (Luoma 2018), and during model calibration is adjusted to 5x10^{-4} m/s for the area containing the observation wells. Vertical hydraulic conductivity K_z is assigned equal to *0.1K*. Typical values are also utilized for storativity (S=1x10^{-5} m/s), porosity (*n = 0.25*) and recharge rate of *R*=1.3x10^{-8} m/s (Luoma 2018).
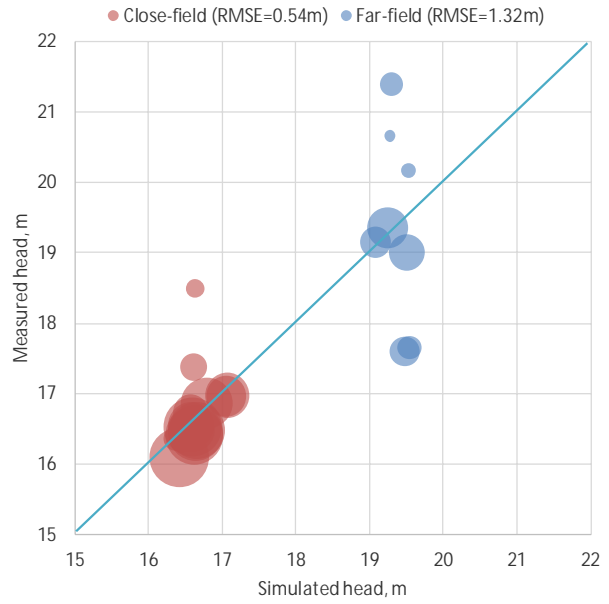
Figure 4. Groundwater model calibration

Technoeconomic evaluation of GSHP-ATES

Based on hourly calculations, different technical variables are computed, like the annual energy demand for heating, cooling and electricity as well as the average daily ATES pumping rate. Cost database regarding various energy generation technologies is used (after Nielsen et al. 2013; DAE 2020), as well as prices for ATES well drilling, heat exchangers and piping (Drenkelfort et al. 2015) for estimating the investment cost. Based on the annuity method, energy generation cost is calculated, assigning annual investment payments (annuity) and assuming 20 years investment's lifetime (Nielsen et al., 2013) / interest rate of 5%. O&M costs (1% of overall investment cost) and electricity cost for GSHP and pumping, given electricity price of 100€/MWh (with taxes, transfer and distribution fees, Nordpool 2020), are also included within the overall annual cost. The economic evaluation is done after Todorov et al. (2020b), and it comprises the calculation of the following variables shown in *Table 2*.

Table 2. Variables for economic evaluation

Variable	Units	Comments
Overall investment cost	€	Geological survey, GSHP, exchangers, drilling and piping
Annuity factor	-	Computed for 20 years lifetime and 5% interest rate
Investment cost (annuity)	€	Overall investment cost times the annuity factor
O&M costs	€	1% of overall investment cost
Annual electricity cost	€	Cost of electricity demand (GSHP and pumping)
Overall annual cost	€	Annuity + O&M costs + energy cost
Specific energy cost	€/ MWh	Overall annual cost per total thermal energy generation

Results and discussion

Technoeconomic analysis

The main technical variables of ATES-GSHP operation for all studied scenarios are presented in *Table 3*. It can be seen, that even with 5-6% of peak heat power respectively for Scenario 1-2/3, the GSHP coverage ratio is 18-21% of the annual heating demand. Moreover, an important advantage of Scenario 2/3 is shown when comparing a cooling demand covered by GSHP. The scheme with two cooling exchangers in Scenario 2 allows to cover 78% of DC demand annually (compared to 67% in Scenario 1), from which the 1st stage cooling accounts for roughly 1/6. The investment cost estimation of ATES-GSHP system as well as the cost of generated thermal energy are presented in *Table 4* and *Table 5* respectively.

Table 3. Technical variables of ATES-GSHP system

Annual results for Scenario 1/2/3	Sc. 1	Sc. 2	Sc. 3
Peak pre-cooling/heating/cooling power, MW	-/1.43/1	0.3/1.67/1.2	
Avg. ATES pumping rate, m³/day	2478	2487	2393
Avg. abstraction temperature, ºC	10.0	10.0	
Avg. injection temperature, ºC	10.0	10.0	
Avg. temperature before GSHP, ºC	10.0	11.5	
Avg. temperature after GSHP, ºC	2.1	2.4	2.0
Avg. HP supply temperature, ºC	65.4	66.7	
Avg. DH return temperature, ºC	40.9	40.9	
Avg. GSHP COP (heating mode)	3.14	3.15	
Heating demand (DH), MWh	67,971		
Heat demand covered, MWh	12,315	14,189	
Heat demand covered by GSHP, %	18 %	21 %	
Cooling demand (DC), MWh	12,382		
1st stage cooling covered, MWh	-	1,604	1,548
2nd stage cooling covered, MWh	8,323	8,031	8,031
Total cooling demand, MWh	8,323	9,635	9,578
Total cooling demand covered, %	67 %	78 %	77 %
Electricity demand (GSHP), MWh	3,934.2	4,509.3	4,509.3
Elec. demand (ATES), MWh	274.1	275.0	264.7
Elec. demand (HP- DH), MWh	57.7	63.0	63.0
Elec. demand (HP- DC), MWh	130.6	150.9	150.0
Total electricity demand, MWh	4,396.6	4,998.2	4,987.0

Table 4. Investment cost of ATES-GSHP system

Investment cost	Price	Total Sc. 1	Total Sc. 2/3
Subsurface study, geological report and pumping tests, €	30,000	30,000	
GS heat pump, €/kW	300	429,000	501,000
Heat exchangers, €/kW	35	85,050	110,950
Pumping well (including equipment and pump), €/u	170,000	1,360,000	
PEHD connection pipes, €/m	250	325,000	
Overall investment cost, €		2,229,050	2,326,950

The resulted thermal energy production cost in Scenario 2 and 3 is slightly below 30 €/MWh. Overall investment cost is around 2.3 million €; 26% of the investment account for GSHP / exchangers and 72% is related to the underground components (connection pipes and wells), figures close to similar ATES realization in Germany (Schüppler et al. 2019).

The optimized Scenario 3 has slightly higher energy production cost (+0.1%) compared to Scenario 2 (*Table 5*), however, there is an important -4% reduction of the average ATES pumping rate (*Table 3*). The average COP is not significantly improved from Scenario 1 to Scenario 2/3, even though evaporator's entering temperature is 1.5 ºC higher on average. This is due to the higher heat fraction which increases the average HP production temperature from 65 to 67 ºC on average.

Table 5. Energy production cost

Annuity method	Sc.1	Sc.2	Sc.3
Annuity factor (5% / 20 years)	0.0802		
Annual investment cost, €	178,865	186,720	186,720
Annual fixed O&M cost, €	22,291	23,270	23,270
Annual energy cost (elec.), €	439,663	499,819	498,699
Total annual cost, €	640,818	709,809	708,689
Cost per MWh of energy, €	31.05	29.79	29.82

GSHP operation is based on energy conversion using electricity to co-generate heating and cooling in a single process. GSHP is the main electricity consumer accounting for 90% of the annual demand, followed by ATES pumping (6%) as well as pumping needed to inject HP´s supply energy to DH/DC networks – respectively 1% / 3%. This is important to be acknowledged since total electricity demand (some 5 GWh/a in Scenario 2 and 3) has a significant impact on the annual cost and, consequently on the specific cost of generated heating and cooling energy, as can be seen in *Table 5*.

ATES system is well balanced, as seen from the average injection and abstraction temperatures equal both to aquifer´s undisturbed temperature of 10 ºC. Moreover, the system is balanced in terms of energy, as shown in *Table 3*, since the annual heat demand covered is equal to cooling demand covered plus GSHP power demand (around 12.3 and 14.2 GWh in Scenario 1 and 2/3 respectively).

The annual variation of all temperatures along ATES flow path in Scenario 2: abstraction, after 1st stage cooling, after GSHP evaporator and finally injection, is shown in *Figure 5*.
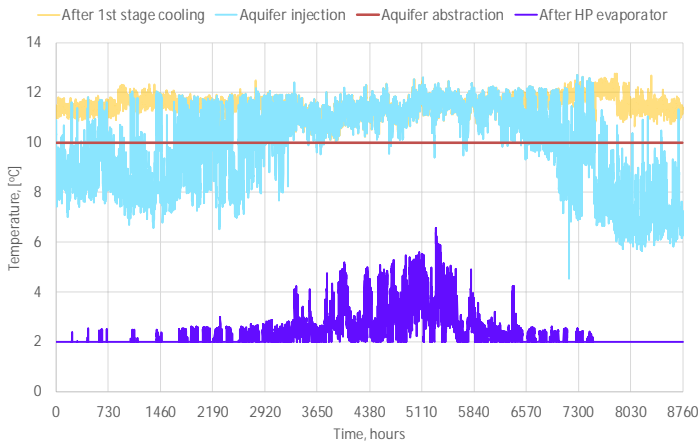
Figure 5. Annual evolution of ATES temperatures (Sc.2)

Impact on groundwater areas

Although the undisturbed aquifer temperature is as high as 10 ºC, first stage cooling can be used 8736 out of 8760 hours annually, and it represents 17% of the cooling demand covered by GSHP (some 1,6 out of 9.6 GWh). This configuration also increases the temperature before GSHP evaporator by 1.5 ºC on average, which improves the COP and enhances heat pump´s capacity in the evaporator as well. The average injection temperature lays in a narrow range of roughly 10 ± 1 ºC, which justifies a one-way ATES operation and consequently, the thermal impact on the aquifer remains very limited.
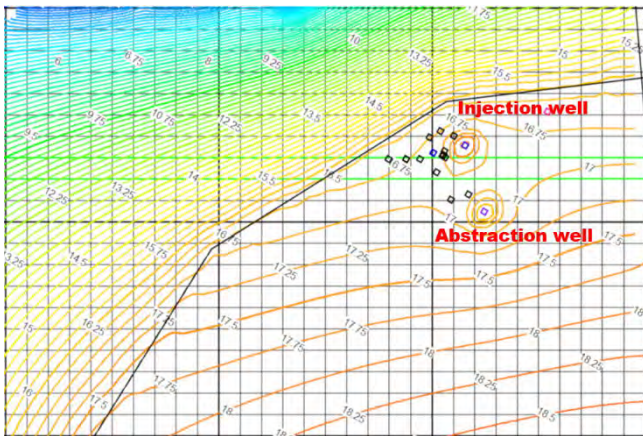
Figure 6. Hydraulic impact after 20 years (Sc. 2)

The long-term hydraulic impact is simulated in ModelMuse and the result after 20 years of one-way operation is presented in Figure 6, where hydraulic head is represented by the iso-lines with resolution of 0.25m. In order to mitigate the hydraulic impact of ATES pumping, the injection well is placed downstream while abstraction well is located upstream (*Figure 6*). The maximum simulated drawdown is 1.25 m, which corresponds to 4.9 m inside the pumping well. The overall impact of ATES pumping vanishes in about 500 m from each well, thus it is not affecting in significant way the surrounding groundwater areas.

Conclusion

The presented case study was successful in demonstrating and developing a mathematical model for system's management: calculation of GSHP recirculation flow, estimation of heat pump COP, as well as an algorithm for computation of ATES pumping flow rate based on the capacity to cover heating and cooling demand in a single process. Additionally, system's technoeconomic feasibility, efficiency and the impact of GSHP-ATES operation on the nearby aquifer were evaluated. Groundwater model was developed and calibrated, utilizing different available data sources like the National Land Survey of Finland, Finnish Environment Institute and Geological Survey of Finland, as well as computational and modelling tools like MS Excel, QGIS and ModelMuse (MODFLOW).

The dispatch of combined heating and cooling loads using annual data of existing Finnish urban district was used in tandem with GSHP-ATES model. It presented attractive economic outcome – competitive energy production cost around 30 €/MWh, far below 79.11 €/MWh, which is the weighted average DH price in Finland (DH, 2018), as well as very limited long-term impact on the nearby aquifer. The maximum drawdown within the pumping well was estimated as 4.9 m after 20 years of operation, and the overall hydraulic impact is limited to 500 m around the wells. Injection temperature deviates from undisturbed aquifer temperature by roughly ±1ºC on average, fulfilling the International legislation regarding groundwater temperature thresholds (Haehnlein et al. 2010). The future transition to low district heating networks (Guzzini et al. 2020) by the introduction of GSHP, can eventually benefit from the proposed mathematical methodology due to its capability to find a trade-off between the energy production cost, ATES pumping flow rate and the temperature drop introduced by the heat pump in DH supply line. Moreover, a sensitivity analysis of system's operation has been performed by Todorov et al. (2020b), showing how exponent parameter *p* influences the energy production cost, the induced temperature drop in DH supply as well as the overall performance of GSHP (COP).

Overall, ATES-GSHP tandem results to be a sustainable and effective alternative to the conventional thermal energy generation primarily based on fossil fuels. It is acknowledged the efficiency of ATES-GSHP systems due to their ability to recycle heating & cooling loads, using the subsurface as thermal storage within integrated district energy networks, especially in urban areas. Last but not least: air pollution in cities, responsible for many chronic & acute illness and premature deaths, can be effectively mitigated by the introduction of greener energy technologies and gradually eliminating the utilization of fossil fuels.

Acknowledgments

Nomenclature

$\varPhi$	[W]	Heating/cooling loads
h	[m]	Hydraulic head
K	[m/s]	Hydraulic conductivity
k	[-]	Power fraction HP/demanded DH load
P	[W]	Power demand (pumping)
p	[-]	Exponent parameter
Q	[m^3/s]	Pumping flow rate
R	[m/s]	Aquifer recharge
S	[-]	Aquifer storativity
$S_{VC,wat}$	[J/m^{3}K]	Water volumetric heat capacity
$T_{DH,S}$	[ºC]	DH supply temperature
$T_{DH,R}$	[ºC]	DH return temperature
$T_{DC,S}$	[ºC]	DC supply temperature
$T_{DC,R}$	[ºC]	DC return temperature
$T_{HPC,S}$	[ºC]	HP condenser supply temperature
$T_{HPC,R}$	[ºC]	HP condenser return temperature
$T_{HPE,I}$	[ºC]	HP evaporator inlet temperature
$T_{HPE,O}$	[ºC]	HP evaporator outlet temperature
$T_{lm,H}$	[ºC]	Sink logarithmic mean temperature
$T_{lm,L}$	[ºC]	Source logarithmic mean temperature
$\varDelta T_{DH}$	[ºC]	DH supply / return temp. difference
$\varDelta T_{HPC}$	[ºC]	Temperature difference HP condenser
$\varDelta T_{DHS}$	[ºC]	Temp. drop in DH supply after HP

References

Arola, T. & Korkka-Niemi, K. (2014). The effect of urban heat islands on geothermal potential: Examples from Quaternary aquifers in Finland. Hydrogeology Journal, 22(8), pp. 1953-1967. https://doi:10.1007/s10040-014-1174-5

Bayer, P., Attard, G., Blum, P., & Menberg, K. (2019). The geothermal potential of cities. Renewable and Sustainable Energy Reviews. https://doi.org/10.1016/j.rser.2019.02.019

DAE 2020, Danish Energy Agency, Technology Data for Generation of Electricity and District Heating (accessed 17.2.2020) https://ens.dk/en/our-services/projections-and-models/technology-data/technology-data-generation-electricity-and

DH 2008, Guidelines for District Heating Substations, Approved by the Euroheat & Power Board, Prepared by Task Force Customer Installations (accessed 12.2.2020): https://www.euroheat.org/wp-content/uploads/2008/04/Euroheat-Power-Guidelines-District-Heating-Substations-2008.pdf

DH 2018. Finnish Energy, District Heating in Finland 2018. Available online (accessed 22.7.2020): https://energia.fi/files/4092/District_heating_in_Finland_2018.pdf

Drenkelfort, G., Kieseler, S., Pasemann, A., & Behrendt, F. (2015). Aquifer thermal energy storages as a cooling option for German data centers. Energy Efficiency, pp. 385–402. https://doi.org/10.1007/s12053-014-9295-1

Eurostat 2020: Renewable energy for heating and cooling (accessed 21.2.2020)

https://ec.europa.eu/eurostat/web/products-eurostat-news/-/DDN-20200211-1?inheritRedirect=true&redirect=%2Feurostat%2F

Fleuchaus, P., Godschalk, B., Stober, I., & Blum, P. (2018). Worldwide application of aquifer thermal energy storage – A review. Renewable and Sustainable Energy Reviews, pp. 861-876. https://doi.org/10.1016/j.rser.2018.06.057

Fleuchaus, P. et al. (2020) Performance analysis of Aquifer Thermal Energy Storage (ATES), Renewable Energy, Volume 146, Pages 1536-1548, ISSN 0960-1481, https://doi.org/10.1016/j.renene.2019.07.030

Greenpeace 2020: Toxic air: The price of fossil fuels, February 2020, (accessed 4.5.2020): https://www.greenpeace.org/usa/wp-content/uploads/2020/02/The-Price-of-Fossil-Fuels-media-briefing.pdf

Grundfos NB/NBG centrifugal pumps:

https://www.grundfos.com/products/find-product/nb-nbg-nbe-nbge.html (accessed 17.2.2020)

Grundfos SP submersible pumps: https://www.grundfos.com/products/find-product/sp.html (accessed 17.2.2020)

Guzzini, Alessandro & Pellegrini, Marco & Pelliconi, Edoardo & Saccani, and. (2020). Low Temperature District Heating: An Expert Opinion Survey. Energies. https://doi.org/10.3390/en13040810

Haehnlein, S., Bayer, P., & Blum, P. (2010). International legal status of the use of shallow geothermal energy. Renewable and Sustainable Energy Reviews, pp. 2611-2625. https://doi.org/10.1016/j.rser.2010.07.069

Harbaugh, Arlen, W. (2005). MODFLOW-2005 , The U . S . Geological Survey Modular Ground-Water Model — the Ground-Water Flow Process. U.S. Geological Survey Techniques and Methods 6-A15. https://doi.org/10.3133/tm6A16

Joronen, L. (2009) Groundwater protection plan for Turku, Kaarina and Rusko orig. title "Turun, Kaarinan ja Ruskon pohjavesialueiden suojelusuunnitelma":

https://www.turku.fi/sites/default/files/atoms/files/2010-turun_kaarinan_ja_ruskon_pohjavesialueiden_suojelusuunnitelma.pdf (accessed 10.2.2020)

Luoma, S. (2018) Groundwater flow models of the shallow aquifer in Hanko (accessed 10.2.2020) http://tupa.gtk.fi/raportti/arkisto/95_2018.pdf

ModelMuse: A Graphical User Interface for Groundwater Models: https://www.usgs.gov/software/modelmuse-a-graphical-user-interface-groundwater-models (accessed 13.3.2020)

Nielsen, S., & Möller, B. (2013). GIS based analysis of future district heating potential in Denmark. *Energy, pp.* 458-468. https://doi.org/10.1016/j.energy.2013.05.041

Nordpool Finnish monthly prices 2006-2020 (accessed 12.3.2020): https://www.nordpoolgroup.com/Market-data1/Dayahead/Area-Prices/FI/Monthly/?dd=FI&view=table

Paiho, S., Saastamoinen, H., Hakkarainen, E., Similä, L., Pasonen, R., Ikäheimo, J., Horsmanheimo, S. (2018). Increasing flexibility of Finnish energy systems—A review of potential technologies and means. Sustainable Cities and Society. https://doi.org/10.1016/j.scs.2018.09.015

Pellegrini, M., Bloemendal, M., Hoekstra, N., Spaak, G., Andreu Gallego, A., Rodriguez Comins, J., Steeman, H. (2019). Low carbon heating and cooling by combining various technologies with Aquifer Thermal Energy Storage. *Science of the Total Environment, 665*, pp. 1-10. https://doi.org/10.1016/j.scitotenv.2019.01.135

Popovski, E., Aydemir, A., Fleiter, T., Bellstädt, D., Büchele, R. & Steinbach, J. (2019). The role and costs of large-scale heat pumps in decarbonising existing district heating networks – A case study for the city of Herten in Germany. *Energy, 180*, pp. 918-933. https://doi.org/10.1016/j.energy.2019.05.122

QGIS - A Free and Open Source Geographic Information System: https://www.qgis.org/en/site/ (accessed 13.3.2020)

Reinholdt, L., Kristófersson, J., Zühlsdorf, B., Elmegaard, B., Jensen, J., Ommen, T. & Jørgensen, P. (2018). Heat pump COP, part 1: Generalized method for screening of system integration potentials. *Refrigeration Science and Technology, 2018*-, pp. 1207-1213. https://doi.org/10.18462/iir.gl.2018.1380

Schmidt, T., Pauschinger, T., Sørensen, P.A., Snijders, A., Thornton, J. (2018) Design Aspects for Large-scale Pit and Aquifer Thermal Energy Storage for District Heating and Cooling. Energy Procedia, Volume 149, September 2018, Pages 585-594. https://doi.org/10.1016/j.egypro.2018.08.223

Schüppler, S., Fleuchaus, P., & Blum, P. (2019). Techno-economic and environmental analysis of an Aquifer Thermal Energy Storage (ATES) in Germany.

Geothermal Energy. https://doi.org/10.1186/s40517-019-0127-6

Soltani, M., M. Kashkooli, F., Dehghani-Sanij, A., Kazemi, A., Bordbar, N., Farshchi, M., . . . B. Dusseault, M. (2019). A comprehensive study of geothermal heating and cooling systems. *Sustainable Cities and Society, 44*, pp. 793-818. https://doi.org/10.1016/j.scs.2018.09.036

Todorov, O., Alanne, K., Virtanen, M. & Kosonen, R. (2020a). A method and analysis of aquifer thermal energy storage (ATES) system for district heating and cooling: A case study in Finland. *Sustainable Cities and Society, 53*. https://doi.org/10.1016/j.scs.2019.101977

Todorov, O., Alanne, K., Virtanen, M. & Kosonen, R. (2020b). Aquifer Thermal Energy Storage (ATES) for District Heating and Cooling: A Novel Modeling Approach Applied in a Case Study of a Finnish Urban District. Energies, 13(10), p. 2478. https://doi:10.3390/en13102478

Wu, X., Nethery, R. C., Sabath, B. M., Braun, D., & Dominici, F. (2020). Exposure to air pollution and COVID-19 mortality in the United States. MedRxiv. https://doi.org/10.1101/2020.04.05.20054502

Airflows and Computational Fluid Dynamics (CFD)

Calculation of airflow rate with displacement ventilation in dynamic conditions

Natalia Lastovets[1*], Risto Kosonen[1,2], Juha Jokisalo[1]
[1] Aalto University, Espoo, Finland
[2] Nanjing Tech University, Nanjing, China
* corresponding author: natalia.lastovets@aalto.fi

Abstract

Design of displacement ventilation (DV) is usually based on a heat balance method when overheating is the primary indoor climate concern. Various models for calculating airflow rate have been developed for several decades. Commonly used models are based only on steady-state models. However, in practical applications, the performance of DV depends on potentially dynamic parameters, such as strength, type and location of heat gains and changing heat gain schedule. Besides, thermal mass affects dynamically changing room air temperature. The paper presents case studies of dynamic DV design in a lecture room. The difference in the designed airflow rate was studied with various models in both dynamic and steady-state conditions. The presented dynamic DV model demonstrated a capability to take into account the combination of dynamic parameters in typical applications of DV. In the case analysed, the airflow rate calculated with the dynamic model is significantly lower than the one calculated with the steady-state models.

Keywords: Displacement ventilation design, airflow rate, temperature gradient, dynamic model.

Introduction

Displacement ventilation (DV) has been first applied in industrial buildings and since the 1980s in non-industrial applications. The basic principle of displacement ventilation is that the cool air is supplied into the occupied zone of the room at low velocity and then rises upwards from the heat sources by the vertical convection currents. As a result, room air with DV has both stratified and mixed zone with different temperature profiles. The design of displacement ventilation is usually based on controlling the desired air temperature in the occupant zone. Thus, the estimation of the vertical temperature gradient is essential in displacement ventilation design.

The temperature gradient in DV systems is usually calculated with the nodal approach, which is suitable for design and system sizing since it provides a rapid solution. Nodal models apply the electrical analogy to represent a heat balance of the room air as an idealised network of nodes connected with airflow paths. Unlike zonal models, nodal models do not predict mass transfer in a room, so that prior knowledge of the airflow patterns is needed in order to specify mass flow in the thermal network (Griffith 2004). Until recently design guidelines from various researchers for displacement ventilation have applied two-nodal models (Mundt 1996, Li et al.

1992, Arens 2000) that predict the linear slope between the air nodes above the floor and exhaust terminal, which is assumed to be always at the ceiling.

Other design guidelines assume a constant vertical air temperature gradient between the head and feet (2°C/m) from the temperature above the floor (Skistad 1994). Since only the heat entering the occupied zone needs to be considered in displacement ventilation systems, later studies proposed fractional coefficient methods to calculate the reduced heat gains in the occupied zone (Yuan et al. 1999, Cheng et al. 2012, Liang et al. 2018, Zhang et al. 2019). In this method, total room space heat gains are artificially divided into occupied and unoccupied fractions. The part of the heat gains in the occupied zone is calculated from the total heat gains with fraction coefficients. These coefficients are estimated empirically or derived from statistical methods based on a database of CFD simulation cases (Lau and Niu 2003).

The multi-nodal models introduce a temperature profile composed by variable slopes between the nodes. The models with a different number of nodes, heat gain configuration and mixing height consideration can be found in the literature (Nielsen 2003, Mateus and da Graça 2015, Lastovets et al. 2020). These models calculate mixing height with plume theory depending on types and number of convective heat sources. The multi-nodal models provide a promising method for the temperature gradient prediction (Kosonen et al., 2016).

However, all models mentioned above have been developed for steady conditions. At the same time, air stratification created by plumes depends on the potentially dynamic parameters, such as strength, type and location of heat gains, ventilation airflow rate and supply air temperature. Besides, since DV is usually applied in non-residential buildings that are not occupied continuously, the thermal mass effect, varied internal and solar heat gains significantly reflect the room air temperatures. It means that in practical applications, current steady-state models cannot accurately predict the room air temperature gradient in dynamic conditions. Thus, an accurate calculation of the vertical temperature gradient in dynamic conditions is required for DV design.

Nodal models implemented in building energy simulation software is an accessible option for design. Some of the two- and multi-nodal models are applied in DV design and available in thermal energy simulation tools. The most frequently used Mundt's model (Mundt 1996) is

implemented in IDA-ICE (Shalin 2003) and EnergyPlus (Crawley et al., 2004). The multi-nodal DV model implemented in Energy Plus (Mateus and da Graça 2015), together with the calculation methods of mixing height was validated in dynamic conditions with the measurements in classrooms (Mateus et al. 2016) and large rooms (Mateus and da Graça 2017).

Simplified building energy models are still practical for pre-design and system sizing in typical applications due to their user-friendliness and straightforward calculation (Kramer 2012). Among the simplified models, the most common are the resistance-capacitance (RC) models of a building zone that imply thermal-electrical analogy based on the similarity between electric current and heat flux. In this approach, an RC-network of a building zone represent every element of the building construction elements and room air with thermal capacities and conductances (Parnis 2012).

The present study applies a simplified dynamic DV model to calculate the vertical temperature gradient (Lastovets et al., 2019) that integrates with the multi-nodal DV model (Lastovets et al., 2020) and two-capacity building energy model (Sirén 2016, ISO 13790: 2008). The thermal capacities and conductances of the dynamic multi-nodal model are calibrated against the results taken from the dynamic building simulation model IDA-ICE (Shalin 2003) and validated in a lecture room. The validated dynamic is further used in to calculate design airflow rates of the steady-state and dynamic models are compared. The novelty of his paper is to study the difference between the selected state-state and dynamic displacement model in dynamic conditions. The paper gives an insight into the investment savings potential when dynamic displacement model is introduced.

Methods

This section introduces the methods to evaluate the feasibility of different models in displacement ventilation (DV) design. This section presents steady-state and dynamic design models of DV. The models are first validated with measurements in a lecture hall. Then design airflow rate is analysed in the validated case room with steady-state and dynamic models.

Design models of DV

The studied design DV methods represent the analytical energy balance approach with lumped parameters. These models threat the building room air as an idealised network of air temperature nodes connected with airflow convection conductances (Griffith 2004). In these nodal models, the room surface temperatures are coupled convectively to air temperatures and long-wave radiatively to each other. The transmission heat transfer through the room structures is calculated with RC (Resistance-Capacitance) method (Parnis 2012).

Two steady-state nodal models with different numbers of nodes and heat gain configuration were chosen for the present analysis. The Mundt (Mundt 1996) model

estimates linear vertical temperature gradient over the room height (H) between the air temperature along the floor at the height 0.1m ($T_{0.1}$) and the exhaust temperature (T_{ex}) (Figure 1a).

The multi-nodal DV model (Lastovets et al. 2020) calculates the temperature profile composed by variable slopes between the nodes (Figure 1b). This model calculates the height of air temperature stratification (h_{mx}) with the vertical heat gain breakdown. The mixing height is the transition level between a mixed upper layer and stratified layer, which is related to the height where the supply airflow rate matches the airflow induced by the thermal plumes in the occupied zone.
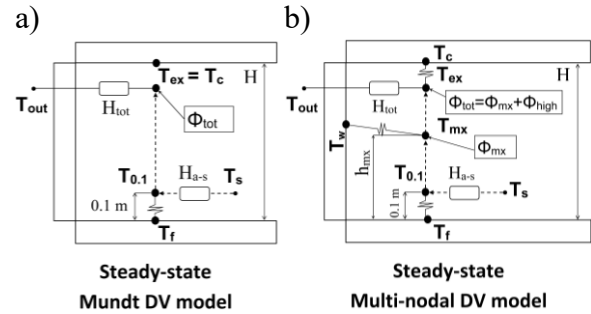
Figure 1: Steady-state displacement ventilation design models.

In the Mundt model, the convective heat flux at the floor is the same as the air temperature increase near the floor from the supply air temperature (T_{sup}) to air temperature at 0.1 height ($T_{0.1}$) (Eq.1). The model assumes that all radiant heat transfer happens only between the floor surface temperature (T_f) and the ceiling surface (T_c). The exhaust air temperature (T_{ex}) is assumed to be the same than ceiling temperature (Eq. 2)

$$H_{a\text{-}s} \cdot (T_{0.1} - T_s) = \alpha_{c,f} \cdot A_f \cdot (T_f - T_{0.1}) \quad (1)$$

$$\alpha_{r,f} \cdot A_f \cdot (T_{ex} - T_f) = \alpha_{c,f} \cdot A_f \cdot (T_f - T_{0.1}) \quad (2)$$

where: $H_{a\text{-}s}$ is the heat conductance of ventilation (W/K); $\alpha_{c,f}$ is the convective heat transfer coefficient at the floor surface ($\alpha_{c,f} = 3$ W/(m²K)); $\alpha_{r,f}$ is the radiative heat transfer coefficient at the floor surface ($\alpha_{r,f} = 5.5$ W/(m²K)); A_f is the floor area (m²).

The heat conductance of ventilation ($H_{a\text{-}s}$) is calculated from the room air properties and supply airflow rate:

$$H_{a\text{-}s} = \rho \cdot c_p \cdot q_v \quad (3)$$

where ρ is the air density (kg/m³), q_v is the supply airflow rate, (m³/s) and c_p is the specific heat of the air (W/(kg·K)).

The exhaust air temperature is calculated from the room air heat balance:

$$H_{a\text{-}s} \cdot (T_{ex} - T_s) + H_{tot} \cdot (T_{ex} - T_{out}) = \Phi_{tot} \quad (4)$$

where Φ_{tot} is the total heat gains (W); H_{tot} is the total conductance of building structures (W/K); T_{out} is the outside air temperature (°C).

The total heat conductance (H_{tot}) determines transmission heat transfer through room structures as follows:

$$H_{tot} = U_{tot} \cdot A_{tot} \quad (5)$$

where U_{tot} is the total U-value of the room structures (W/(m²·K) and A_{tot} is the total area of room surfaces (m²).

The steady-state multi-nodal model calculates three air temperatures at the height of 0.1 m, at the height of the mixed layer (h_{mx}) and the height of the exhaust air temperature that is equal to the room height. The mixing height is calculated with the point source model of plume theory (Kosonen et al. 2017):

$$h_{mx}=\left(k_q^p\right)^{-\frac{3}{5}}\cdot\left(\frac{q_v}{n}\right)^{\frac{3}{5}}\cdot\Phi_c^{\frac{1}{5}}+h_0^{ver} \tag{6}$$

where: h_{mx} is the mixing height (m); q_v is a supply airflow rate (m³/s), Φ_c is a convective heat gain of the vertical buoyancy source (W), n is the number of thermal plumes, h_0^{ver} is a virtual origin height (m), k_q^p is an entrainment coefficient for a point source plume ($k_q^p = 0.005$).

The present study applies the conical correlation with the "minimum" approach (Kosonen et al. 2017) to calculate the virtual origin height above the vertical heat source:

$$h_0^{ver} = H_s - 1.47 \cdot D \tag{7}$$

where H_s is the height of the heat source (1.1 m) and D is the diameter of the heat source (0.4 m).

Heat gain distribution determines the convection heat transfer connection between the wall surfaces and air nodes. The model consists of the set of three convection and three radiation heat balance equations assuming 50% split between the convective and radiative heat gains. The energy conservation equations for the three model air temperatures are the following (Lastovets et al. 2020):

$$H_{a-s}\cdot(T_{0.1} - T_s) = \alpha_{c,f}\cdot A_f\cdot(T_f - T_{0.1}) \tag{8}$$

$$H_{a-s}\cdot(T_{mx} - T_{0.1}) = \alpha_{c,w}\cdot A_w\cdot(T_w - T_{mx}) + \Phi_{mx} \tag{9}$$

$$H_{a-s}\cdot(T_{ex} - T_{mx}) = \alpha_{c,c}\cdot A_c\cdot(T_c - T_{ex}) + \Phi_{high} \tag{10}$$

where $\alpha_{c,c}$, $\alpha_{c,f}$ and $\alpha_{c,w}$ (W/(m²·°C)) are the convective heat transfer coefficients of the room surfaces: ceiling, floor and wall surfaces; Φ_{mx} are the convective heat gains under in the occupied zone (W), Φ_{high} are the convective heat gains over the occupied zone (W); T_w is the average temperature of the walls (°C).

The total heat gain (Φ_{tot}) calculated consists of gains located in the occupied zone of the room (Φ_{mx}) and near the ceiling (Φ_{high}):

$$\Phi_{tot} = \Phi_{mx} + \Phi_{high} \tag{11}$$

The occupied zone heat gains (Φ_{mx}) are usually caused by solar radiation through low or high located windows on the floor, people and office equipment. The gains near the ceiling (Φ_{high}) could be from light fittings, warm high-located windows or solar radiation through windows.

Heat transfer from internal surfaces influences the temperatures of air nodes which are in direct contact with the surfaces. The long-wave radiation between the surfaces is calculated with the mean radiation temperature method (Davies 1990).

The dynamic DV model (Lastovets et al. 2019) represents a hybrid of the room air multi-nodal DV model (Lastovets et al. 2020) and 2-capacity model of building structures (Sirén 2016).

The model calculates dynamic energy balance where the thermal mass of building structures and air capacities are taken into account. The structure of the dynamic DV model (Figure 2) includes thermal capacities of room air (C_a) and building thermal mass (C_m). C_a considers the room air and furniture, while C_m is related to the thermal mass of the building structures (walls, floor and ceiling). In this model, the transmission heat transfer includes the window heat conductance (H_{a-out}) with negligible thermal mass and the total conductance of remaining opaque surfaces (H_{tot}) that is divided into the conductances at both sides of the thermal mass node (H_{a-m} and H_{m-out}). Both thermal conductances include heat conduction in the solid wall material as well as convection on the surfaces.
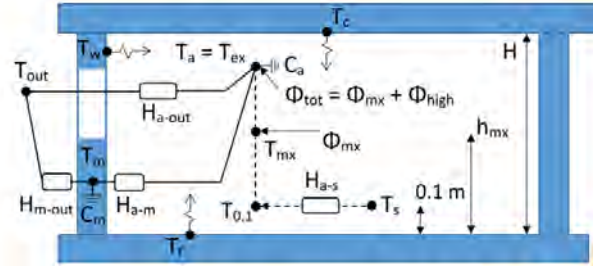
Figure 2: Dynamic design model for displacement ventilation.

The dynamic DV model represents six first-order differential equations to calculate three air and three mass temperatures for the vertical temperature profile (Lastovets et al., 2020). The differential equations can be solved numerically with the explicit Euler method since there is no tendency for numerical oscillations.

Measurements for validation of design DV models

The lecture hall (Lastovets et al. 2020) with the floor area 108 m² is located at Aalto University (Espoo, Finland). The room does not have any outdoor walls since it is located in the central part of the second floor of the building. The air is supplied through 50 diffusers located under the seats and extracted from five exhaust grilles. The exhaust grilles are located near the ceiling height (3 m) along the corridor walls (Figure 3).

For measuring air temperatures at different heights from floor to ceiling, the measuring mast was assembled with 20 TinyTag loggers (Gemini Data Loggers 2018). Seventeen TinyTags were located at ten centimetres distance, starting from 0.1 m to 1.7 m, followed by three more loggers at 2 m, 2.5 m and 3 m, respectively.
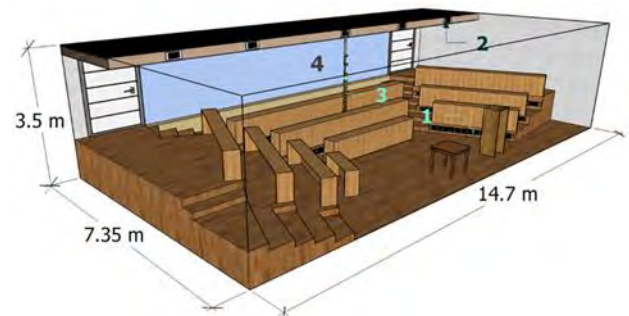
The lecture hall construction includes internal glazing and remaining heavy concrete opaque surfaces. The internal thermal mass takes into account the furniture in the studied room.

Results

Validation of design DV models

This section presents the validation of the DV design models (Figures 1 and 2) with measurements in the lecture hall (Figure 3) to estimate the capability of the DV models to calculate the occupied zone temperature. The simulation models of both validation spaces were modelled in the building simulation software IDA-ICE to calibrate the thermal capacities C_a and C_m and conductances H_{m-out} and H_{a-m} of the dynamic multi-nodal DV model. The calibration method is presented in detail in (Lastovets et al. 2020) publication. The calibration is conducted for fully-mixed conditions, and thus, the air temperature is the same as the exhaust air temperature. The calibration method consists of two phases where steady-state and dynamic set response parameters are separately calibrated. In the calibration, the total conductance H_{tot} is defined in the steady-state parameter identification. The division of this conductance to H_{m-out} and H_{a-m} and two capacities C_a and C_m are determined in the dynamic parameter identification.

In the studied cases, the internal heat gains, supply air temperatures, outdoor air temperatures and airflow rates were constant. The total heat gains in both validation cases consisted of the heat gains from occupants and lighting.

The lecture hall had heavyweight concrete building structures and relatively high internal thermal mass (Table 1). The heat gains of sitting people were estimated to be 100 W per person, and the lighting heat gains were 2.5 kW. During the measurements in all cases, the air temperature of neighbouring rooms was constant 21 °C. In all cases, the operation schedule of fans with the design airflow rate was as follows: mechanical cooling with constant supply airflow rate 0.6 m³/s between 07:30 – 00:50 and the fans were off between 00:50 – 07:30. Table 1 presents the validation cases in the lecture hall.

Table 1: The description of the validation cases in the lecture hall.

Case	Occ. period		№ of occ.	Internal heat gains, kW			T_s °C
	№	time		occ.	light.	tot.	
1	1	1 h 50 min	65	6.5	2.5	9.0	18
	2	1 h 50 min	32	3.2	2.5	5.7	18
2	1	1h 50 min	65	6.5	2.5	9.0	18
	2	50 min	65	6.5	2.5	9.0	18
	3	1h 10 min	58	5.8	2.5	8.3	20

Table 2 presents the calibrated total conductance H_{tot}, conductances H_{a-out}, H_{a-m} and H_{m-out} and thermal capacities C_a and C_m of the multi-nodal DV model for the lecture hall.

Table 2: The calibrated parameters of the dynamic DV model in the lecture hall.

H_{tot} (W/K)	H_{a-m} (W/K)	H_{m-out} (W/K)	H_{a-out} (W/K)	C_a (kJ/K)	C_m (kJ/K)
102	1431	110	45	1636	48701

Figure 4 shows the measured and simulated vertical temperature gradients during the validation period. In Figure 4, the heights of the temperatures modelled at $T_{0.1}$, T_{mx} and T_{ex} are marked with dotted lines. Even though multi-nodal modal is more accurate than the linearised Mundt's model in steady-state conditions (Kosonen et al. 2016), in dynamic conditions, both models overestimate the predicted temperature gradient in rooms with DV. It reveals the importance to take into account the dynamic behaviour of the thermal mass in the modelling.

The temperature gradient below 1m height calculated with the Mundt's model was closer to the measurements than the gradient calculated with the steady-state multi-nodal model. However, the dynamic multi-nodal model provided an accurate prediction of the evolution of the vertical air temperature profile at all heights (T_{ex}; T_{mx} and $T_{0.1}$). Also, the room air temperature modelling as a function of time was close to the measured values.
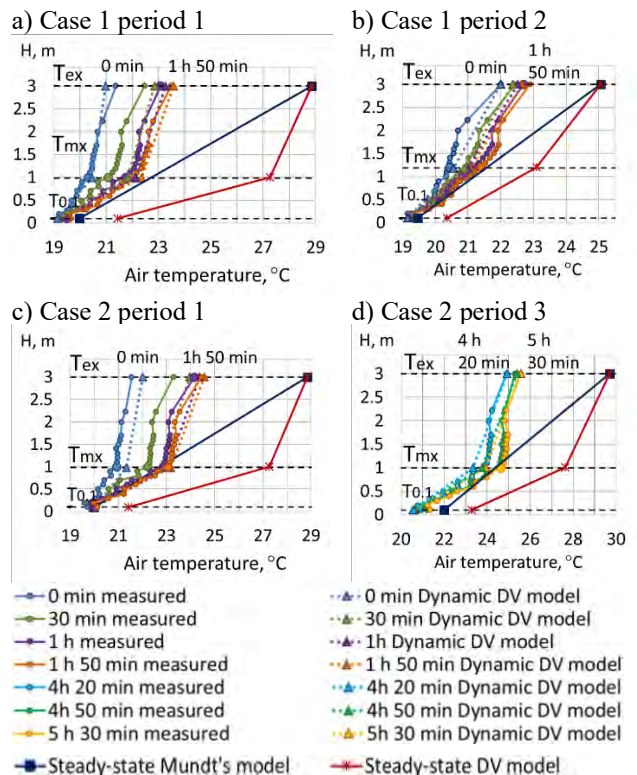
Figure 4: Vertical air temperature gradients measured and calculated with the design DV models

Calculation of the airflow rate with different design DV models

The design airflow rates are calculated with the selected DV models (Figures 1 and 2) for the validated case (Figure 3). In the dynamic DV model, the airflow rate was obtained to fulfil the set of the maximum target room air temperature (25 °C) during the occupied hours (Figure 5).

Since Mundt's model does not take into account the usage profile and thermal mass, it led the same airflow rate of 0.45 m³/s in the case analysed (Table 3). The steady-state multi-nodal DV model taking into account the heat gain breakdown calculates the airflow rate of 0.77 m³/s. Thus, the linear Mundt's model provided a 41% lower design airflow rate than a more detailed steady-state multi-nodal model. However, it should be emphasised that the Mundt's model underestimates the airflow rate required in steady-state conditions, and the target room air temperature cannot be achieved at the occupied zone. In those steady-state conditions, the multi-nodal model is more accurate than Mundt's model (Kosonen et al., 2016). In addition to considering the heat gain breakdown, the dynamic multi-nodal DV model provided different values of airflow rates depending on the effects of thermal mass and varied heat loads during operation time. The dynamic multi-nodal DV model calculated the lowest airflow rate of 0.34 m³/s, quarter lower than with Mundt's model and almost twice lower than the steady-state multi-nodal model calculated (Table 3). It indicates that the thermal mass and dynamic usage profile are playing a significant role in the determination of the design airflow rate.

Table 3: Design airflow rates of three different calculation models.

Case	Airflow rate with different DV design models, m³/s		
	Steady-state Mundt's model	**Steady-state multi-nodal model**	**Dynamic DV model**
Case 1 period 1	0.45	0.77	0.34
Case 2 period 3	0.57	0.95	0.43

Figure 5 presents the dynamic changes in air temperature in the occupied zone in the calculation of the designed airflow rate. In the steady-state models, the design occupied zone temperature remains the same. In Case 1 (Figure 5a), the first occupied period with higher heat gains is determining in the airflow rate calculations. In Case 2 with more extended occupancy period, the highest temperature is at the end of the occupied period.

a)

b)
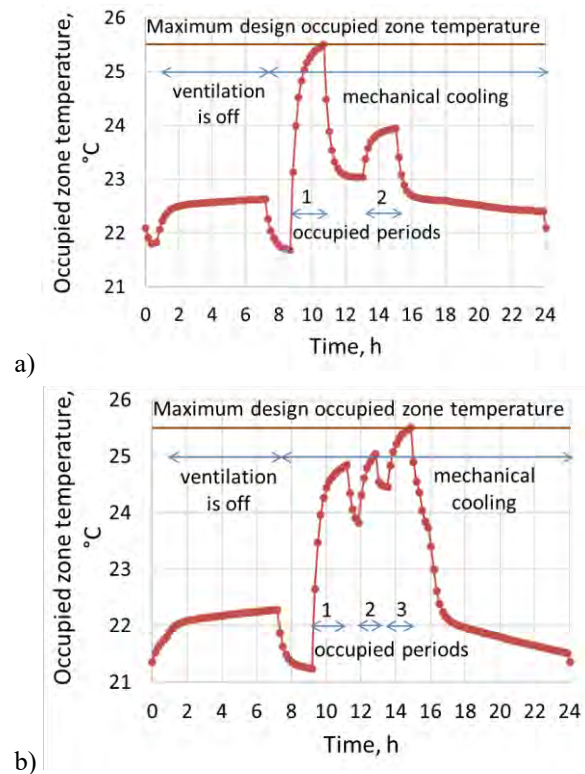
Figure 5: Room air temperatures at the occupied zone with the dynamic DV multi-nodal model for Case 1 (a) and Case 2 (b).

Discussion

In the existing DV design practice, the supply airflow rate is calculated with either the heat balance method or air quality-based methods (Kosonen et al. 2017). The air quality-based design by applying thermal plume theory is only used in industrial types of applications where high exit contaminant loads. In non-industrial premises, e.g. in theatres, design practice it is based on the minimum airflow rate per person of local building codes (e.g. 6 l/s). Heat balance method as the most method in DV design is applied in rooms where room air temperature in the occupied zone is the primary design criterion. In this case, the airflow rate is usually calculated with steady-state models. In some cases, the steady-state heat balance method overestimates the design airflow rate (Lastovets et al., 2020).

Even though some building energy simulation software (e.g., EnergyPlus and IDA ICE) include the model of the thermal environment with displacement ventilation, they are limited to the specific system configuration (Citherlet et al. 2001). In addition, the utilisation of those models requires prior knowledge of both the indoor thermal environment simulation and building energy simulation, which could be a challenge to a building energy engineer.

The commonly used models to design displacement ventilation are based on steady-state temperature gradient calculation with simplified nodal models, among which the multi-nodal models are the most accurate (Kosonen et

al. 2016 and Lastovets et al. 2019). However, for accurate design, these models are insufficient in the estimation of room air temperatures due to the missing effect of thermal mass and varied heat loads during operation time. Steady-state approach and neglecting the dynamic behaviour of heat loads and thermal mass could lead to significant overestimation of the required airflow rate. Thus, the dynamic approach is appreciated in the DV system design.

The presented dynamic DV model predicts the dynamic behaviour of the thermal mass and room air vertical temperature gradient with a proper level of accuracy. However, this model has certain limitations. Since all internal mass, such as floors, walls and furniture, are presented in the model as one entity, it is not able to take into account different thermal properties of individual structures. On the other hand, it could be assumed that in a typical application, it would not significantly affect the thermal behaviour. The dynamic DV model is able to predict within reasonable accuracy the thermal behaviour of typical buildings where the only relatively small active thickness of the structure interacts with the regularly varied heat gains.

In steady-state conditions, Mundt's linearised model underestimates occupied zone air temperature by up to 3 °C and provides unrealistic vertical air temperature profile (Kosonen et al. 2016). However, in the cases with significant lighting heat loads and short occupied period, Mundt's model calculates close airflow rate to the dynamic DV model.

Since the premises with DV are usually not occupied continuously, the dynamic model of room air vertical temperature gradient is appreciated in DV design. The possible application of the presented dynamic DV model is in the rooms where different dynamic factors, such as heat gain variation, location and type of heat gains and building thermal mass have a different effect on indoor thermal conditions. Typical applications are in concert halls that are occupied for a short time and in lobbies that are influenced by highly varied internal heat loads and solar radiation.

Conclusion

The estimation of the vertical temperature gradient reflects airflow rate calculation and thermal comfort estimation in rooms with displacement ventilation (DV). At the moment, it is common to use a steady-state model that is not taken into account occupancy profiles and thermal mass. In this study, two steady-state and one dynamic DV model were validated with measurements in terms of accuracy and dynamics of room air temperature changes in different vertical levels in the lecture hall. Besides, the design airflow rate was calculated with different models in both dynamic and steady-state conditions in the validated case. In the case analysed, the airflow rate calculated with the dynamic DV model is

significantly lower than the airflow rate calculated with the steady-state DV models.

The dynamic model can significantly decrease the design airflow rate of DV, which can result in a reduction of investment costs and electrical consumption of fans. The presented calibrated multi-nodal dynamic DV model is able to take into account varied heat loads and the effect of building thermal mass within good accuracy. The dynamic DV model can be applied in DV design with various applications where heat gains varied, and thermal mass is playing a significant role. The model has good robustness to predict thermal performance under different operation conditions.

Acknowledgement

References

Arens, A.D. (2000). Evaluation of displacement ventilation for use in high-ceiling facilities. Master thesis, Massachusetts Institute of Technology (USA) Available at https://dspace.mit.edu/handle/1721.1/9305. Accessed 05 May 2020.

Cheng, Y., Niu, J., Gao, N. (2012). Stratified air distribution systems in a large lecture theatre: A numerical method to optimise thermal comfort and maximise energy saving. *Energy and Buildings 55*, 515–525.

Citherlet, S., Clarke, J.A., Hand, J. (2001). Integration in building physics simulation. *Energy and Buildings, 33*, 445-461.

da Graça, G.C.C. (2003). *Simplified models for heat transfer in rooms*. Doctoral dissertation, University of California, San Diego.

Davies, M.G. (1990). Room heat needs in relation to comfort temperature: Simplified calculation methods. *Building Services Engineering Research and Technology 11*, 129–139.

Griffith, B., Chen, Q.Y. (2004). Framework for coupling room air models to heat balance model load and energy calculations (RP-1222). *Hvac&R Research 10*, 91–111.

Kosonen, R., Lastovets, N., Mustakallio, P., da Graça, G. C., Mateus, N. M., Rosenqvist, M. (2016). The effect of typical buoyant flow elements and heat load combinations on room air temperature profile with displacement ventilation. *Building and Environment 108*, 207–219.

Kosonen, R., Melikov, A., Mundt, E., Mustakallio, P., Nielsen PV (2017). *Displacement Ventilation, REHVA Guidebook No 23*. Forssa: Federation of European Heating and Air-Conditioning Associations.

Lastovets N, Kosonen R, Jokisalo J, Kilpeläinen S (2019). Dynamic design model of displacement ventilation. Proceedings from *CLIMA 2019*. Bucharest (Romania), 26-29 May.

Lastovets N, Kosonen R, Mustakallio P, Jokisalo J, Li A (2020). Modelling of room air temperature profile with displacement ventilation. *International Journal of Ventilation 19*, 112–126.

Lau, J. and Niu, J.L. (2003). Measurement and CFD simulation of the temperature stratification in an atrium using a floor level air supply method. *Indoor and Built Environment 12*, 265–280.

Li, Y., Sandberg, M., Fuchs, L. (1992). Vertical temperature profiles in rooms ventilated by displacement: Full-scale measurement and nodal modelling. *Indoor Air 2*, 225–243.

Liang. C., Shao, X., Melikov, A.K., Li, X. (2018). Cooling load for the design of air terminals in a general non-uniform indoor environment oriented to local requirements. *Energy and Buildings 174*, 603–618.

Mateus, N.M. and da Graça, G.C. (2015). A validated three-node model for displacement ventilation. *Building and Environment 84*, 50–59.

Mateus, N.M. and da Graça, G.C. (2017). Simulated and measured performance of displacement ventilation systems in large rooms. *Building and Environment 114*, 470–482.

Mateus, N.M., Simoes, G.N., Lúcio, C., da Graca, G.C. (2016). Comparison of measured and simulated performance of natural displacement ventilation systems for classrooms. *Energy and Buildings 133*, 185–196.

Mundt, E. (1995). Displacement ventilation systems – Convection flows and temperature gradients. *Building and Environment 22*, 129–133.

Nielsen, P.V. (2003). Temperature and air velocity distribution in rooms ventilated by Displacement ventilation. *Proceedings from the 7th International Symposium on Ventilation for Contaminant Control (Ventilation 2003)*. Sapporo (Japan), 5 – 8 August.

Parnis, G. (2012). *Building Thermal Modelling Using Electric Circuit Simulation*. Ph.D thesis, University of New South Wales. Sydney (Australia).

Shalin, P. (2003). On the effects of decoupling air flow and heat balance in building simulation models. *ASHRAE Transactions 109*, 788–800.

Sirén, K. (2016). *Course material: A simple model for the dynamic computation of building heating and cooling demand*. Espoo (Finland): Aalto University (2016) Available at: https://mycourses.aalto.fi/pluginfile.php/317972/mod_resource/content/1/Building%20energy%20calculation_Sep_2016.pdf. Assessed 30.03.2020.

Skistad, H. (1994). *Displacement Ventilation*. Somerset, England: Research Studies Press Ltd.

International Organisation for Standardisation (2008). *Energy Performance of Buildings-Calculation of Energy Use for Space Heating and Cooling* (ISO 13790: 2008). ISO Central Secretariat: Geneva, Switzerland.

Yuan, X., Chen, Q., Glicksman, L.R. (1999). Models for prediction of temperature difference and ventilation effectiveness with displacement ventilation. *ASHRAE Transactions 105*, 353–367.

Yang L. and Li, Y. (2008). Cooling load reduction by using thermal mass and night ventilation. *Energy and buildings 40*, 2052–2058.

Zhai, Z., Chen, Q.Y. (2003). Solution characters of iterative coupling between energy simulation and CFD programs. *Energy and buildings 35*, 493–505.

Zhang S., Cheng, Y., Huan, C., Lin Z. (2018). Heat removal efficiency based multi-node model for both stratum ventilation and displacement ventilation. *Building and Environment 143*, 24–35.

Zhang, S., Cheng, Y., Huan, C., Lin Z. (2019). Equivalent room air temperature based cooling load estimation method for stratum ventilation and displacement ventilation. *Building and Environment 148*, 67–81.

POD-interpolation based prediction of indoor airflows

Mats Kluftødegård, Arnab Chaudhuri
Department of Civil Engineering and Energy Technology
OsloMet — Oslo Metropolitan University, Oslo, Norway.

Abstract

This work reports a proper orthogonal decomposition (POD)-interpolation based prediction of indoor airflows related to displacement ventilation. Steady-state computational fluid dynamics (CFD) solution snapshots with varying relevant non-dimensional number are used to estimate the dominant POD coefficients/modal amplitudes and POD modes. A cubic spline interpolation of the POD coefficients is used to compute the solution for desired value of the non-dimensional number of interests. The verification and validation of this data-driven procedure is performed considering a 2D mixed convection problem involving a horizontal channel with cavity heated from below for a range of Richardson numbers. On the other hand, CFD solutions for a standard displacement ventilation configuration is used to decompose the flow field variables in terms of Archimedes number dependent POD coefficients and associated space dependent POD bases. A detailed analysis of the CFD and POD-interpolated predicted flow-field variables for displacement ventilation cases, error estimates and the spatial structures of the POD modes are presented.

Introduction

Fundamentally, air flow, heat and mass transfer phenomena govern the indoor air quality, thermal comfort and energy usage in buildings. Air change rate, pollutant removal, heat removal, exposure and air distribution are the key features to assess the performance of a heating, ventilating and air-conditioning (HVAC) system. Ventilation systems can be classified into various types depending upon the concentration distribution, location of the air supply/exhaust device and the use of natural and mechanical forces (Cao et al. (2014)). For several decades, a substantial scientific research focus has prevailed achieving design of energy efficient, effective airflow distribution and thermal comfort in buildings.

Displacement ventilation (DV) is potentially a very good ventilation strategy among the other types of air distribution principles where the contaminant air is removed from the ceiling level of a room. The exhaust temperature is higher than the occupied zone and a fresh air being supplied at the floor level (Nielsen (1988), Davidson (1989), Nielsen (2000)). A well de-signed DV system can be energy efficient to regulate room temperature and air velocity for thermal comfort and good air quality utilising natural convection currents (Cehlin and Moshfegh (2010)). Several key parameters for such systems are ventilation rate, location of the air terminal device, type of the diffuser and the supply air temperature (Yuan et al. (1998), Nordtest (2003)). Nevertheless, a DV configuration involves complex flow physics like gravity current, radiation effect and thermal stratification. Challenging issues related to thermal characterisation including radiation effects, draft discomfort, etc. are investigated by several researchers (Li et al. (1992), Causone et al. (2010), Magnier et al. (2012), Gilani et al. (2016)). The recent studies with DV systems addresses interesting aspects considering e.g., severe odor problems in hospital environments (Choi et al. (2019)), adaptive climate building with heat source/smart windows (Javad and Navid (2019)) and highly polluted indoor environment with dense oil mist in a machining plant (Wei et al. (2020)). Optimal design and modeling aspects of DV systems in diverse contexts are therefore important active research areas for HVAC scientists and engineers.

Apart from the advanced experimental measurements, CFD is widely used as a reliable numerical tool to predict a wide range of ventilation problems with detailed spatio-temporal distributions of flow-field variables. In CFD, the governing non-linear coupled partial differential equations are solved with a suitable discretization and solution procedure. However, high-fidelity CFD-simulations for design and optimization is indeed costly both in terms of necessary computer resource and CPU time. In this regard, POD based interpolation can be used, exploiting the CFD results with varying one or many parameters (e.g. relevant non-dimensional numbers involved in the governing phenomena) of interest to produce desired predictions in an efficient and cost effective manner. For example, considering a set of steady-state CFD solutions as "snapshots" the dominant POD coefficients/modal amplitudes and POD modes have to be estimated first. These intern can be used with a suitable interpolation of the coefficients to generate desired solution(s) for particular values of the parameter(s) of interest without performing costly CFD simulations. Some of the previous studies used steady state CFD solutions as snapshots for POD e.g., in in-

door airflow application (Elhadidi and Khalifa (2005) and for coupling between CFD and lumped parameter flow network zonal (FNZ) models Khalifa et al. (2007)).

This work aims to predict complex flow physics for a DV configuration of indoor environments using CFD snapshots and POD-interpolation method. CFD results are generated using the commercial computer program StarCCM+. We solved 2D/3D compressible Navier-Stokes equation (without Boussinesq approximation) together with mass and energy equations. Additionally, two-equation turbulence models are employed to account turbulent flow cases. The paper is organized as follows. In section **Method**, we present the governing equations and the overall POD methodology. The validation cases are presented thereafter. Subsequently, the problem setup of the displacement ventilation is given. The flow analysis given in the section **Results and discussion**. Finally, the conclusions are drawn at the end.

Method

Governing equations

In this study, we solve the compressible steady Navier-Stokes equations together with the mass and the energy conservation equations. The general transport equation for any conserved property $(\rho\phi)$ can be expressed as in the following standard form, $\boldsymbol{\nabla}\cdot\rho\phi\mathbf{v} = \boldsymbol{\nabla}\cdot\Gamma\boldsymbol{\nabla}\phi + S_\phi$. Here ρ is the fluid density, $\mathbf{v}$ is the velocity vector and Γ is the diffusion coefficient. The governing equation involves advection term in left hand side and the terms on the right hand side signify the diffusion term and the generation term respectively. The gravity source term in the momentum equations is treated directly without Boussinesq approximation. Formulation of RANS (Reynolds averaged Navier Stokes) system of equations considering two equation SST (Menter) $\kappa-\omega$ turbulence model is used for turbulent flow cases. The choice of SST $\kappa-\omega$ model is based on the findings of Gilani et al. (2016), where the authors reported the superiority of the SST $\kappa-\omega$ model and the standard $\kappa-\omega$ model in predicting thermal plume and thermal stratification in a DV setup. Constitutive relation of Newtonian fluid and equation of state ideal gas close the system of equations with appropriate boundary conditions. We used the finite volume method (FVM) based commercial computer program StarCCM+ to solve the above mentioned governing equations. Second order implicit segregated/coupled flow solvers equipped with Roe schemes for convection, hybrid Gauss least-squared gradient method based 2nd order schemes for diffusion and Venkatakrisnan limiter function are chosen. Algebraic Multi-Grid (AMG) techniques are also invoked with the setup mentioned above.

POD snapshot method

Proper orthogonal decomposition (POD) method can be realized in several forms such as Karhunen-Loève decomposition (KLD), principal component analysis (PCA), and singular value decomposition (SVD) having wide spectrum of applications in scientific and engineering field. The key dominant characteristics/features in a data set can be recognized by a POD technique via low-dimensional descriptions for multidimensional systems. Originally, POD was introduced in the framework of fluid mechanics applications in late sixties. This was followed by the "snapshot POD" methodology by Sirovich and Kirby (1987) and the procedure is essentially a simple data-driven procedure closely related to principal component analysis (PCA), one of the fundamental algorithm of applied statistics and machine learning (Brunton et al. (2020)). In this work, the steady-state CFD solutions "snapshots" are used to decompose a non-dimensional flow variable $\phi^*(\Pi, \vec{x})$, where Π is a governing non-dimensional number of the flow physics under consideration. The decomposition essentially leads to the determination of a finite number of POD coefficients, $a_k(\Pi)$ and space dependent POD modes, $\psi_k(\vec{x})$ as,

$$\phi^*(\Pi, \vec{x}) \approx \sum_{k=1}^{m} a_k(\Pi)\psi_k(\vec{x}). \qquad (1)$$

where, m is the number of snapshots for set of values of $\Pi_i \in [\Pi_{min}, \Pi_{max}], \forall \ i = 1, \ldots, m$. Once, the desired POD coefficients and POD modes are available, a suitable interpolation can be used to construct the flow field variables for any intermediate Π_{int}. The POD-interpolated prediction can be given by

$$\phi^*(\Pi_{int}, \vec{x}) \approx \sum_{k=1}^{N} a_k(\Pi_{int})\psi_k(\vec{x}). \qquad (2)$$

where $N \leq m$. We used a cubic spline interpolation to estimate $a_k(\Pi_{int})$ from $a_k(\Pi_i)$'s.

A brief methodology to determine the POD coefficients and the POD modes is given below (see Meyer et al. (2007), Selimefendigil (2013) for detail). First, the m number of CFD solution of ϕ^* on n mesh points can be arranged in a data set matrix $\boldsymbol{\Phi}^* = [\phi^{*1}\phi^{*2}\ldots\phi^{*m}]$ as,

$$\boldsymbol{\Phi}^* = \begin{bmatrix} \phi_1^{*1} & \phi_1^{*2} & \phi_1^{*3} & \cdots & \phi_1^{*m} \\ \phi_2^{*1} & \phi_2^{*2} & \phi_2^{*3} & \cdots & \phi_2^{*m} \\ \vdots & \vdots & \vdots & \vdots & \vdots \\ \phi_n^{*1} & \phi_n^{*2} & \phi_n^{*3} & \cdots & \phi_n^{*m} \end{bmatrix}. \qquad (3)$$

Then the auto covariance matrix is created. This matrix represents the covariance of the value with it self at some point. Where covariance is a measure

of the linear dependency of two values. This can be defined as:

$$\mathbf{C} = \frac{1}{m} \boldsymbol{\Phi}^{*\intercal} \boldsymbol{\Phi}^{*}. \qquad (4)$$

The following eigenvalue problem then has to be solved:

$$\mathbf{C}\mathbf{X}^i = \lambda^i \mathbf{X}^i, \quad i = 1, 2, ..., m. \qquad (5)$$

Where $\mathbf{X}$ is the eigenvector, and λ is the eigenvalues. This eigenvalue problem was solved using SVD. The solutions are ordered according to the size of the eigenvalues from highest to lowest. The eigenvectors, $\mathbf{X}^i$, in equation (5) forms a basis for making the POD modes, $\boldsymbol{\psi}^i$:

$$\boldsymbol{\psi}^i = \frac{\sum_{j=1}^{m} X_j^i \boldsymbol{\phi}^{*j}}{\left\| \sum_{j=1}^{m} X_j^i \boldsymbol{\phi}^{*j} \right\|}, \quad i = 1, 2, ..., m. \qquad (6)$$

Where X_j^i is the j'th component of the eigenvector corresponding to the eigenvalue λ^i, and $\|\cdot\|$ is the second norm of any vector $\boldsymbol{\xi}$, given as:

$$\|\boldsymbol{\xi}\| = \sqrt{(\xi_1)^2 + (\xi_2)^2 + ... + (\xi_n)^2} \qquad (7)$$

The POD coefficient can be determined by projecting ϕ^{*m} onto the POD modes:

$$\mathbf{a}^m = \boldsymbol{\Psi} \phi^{*m} \qquad (8)$$

Where $\boldsymbol{\Psi} = [\boldsymbol{\psi}^1 \boldsymbol{\psi}^2 \ldots \boldsymbol{\psi}^m]$ The snapshot ϕ^{*m} can then be reconstructed by:

$$\phi^{*m} = \boldsymbol{\Psi}^{\intercal} \mathbf{a}^m \qquad (9)$$

The above methodology has been implemented via Python programming scripts and the data visualisation is performed by MATLAB programming scripts.

Validation

We first solved a 2D benchmark test case of laminar compressible flow through a horizontal channel with an open rectangular cavity in which a discrete hot surface is placed at the bottom wall of the cavity. The setup of this case is similar to that presented in Aminossadati and Ghasemi (2009) as well as in Selimefendigil (2013). The choice of this test case is very much relevant with respect to the indoor ventilation flow physics involving both heat transfer and fluid flow with the active gravity source term. A suitable 2D computational domain consisting of 5175 computational cells is used to simulate a case with Richardson number $Ri = 100$ where, $Ri = \frac{g\beta(T_h - T_c)L}{u_{in}^2}$.

Here, g is the acceleration due to gravity, β is thermal expansion coefficient, T_h is the temperature of the hot
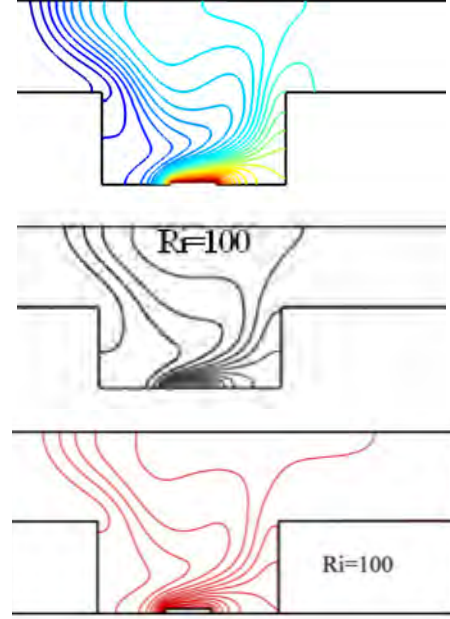
Figure 1: Comparison of numerical solutions, temperature contours for $Ri = 100$. top: present study, middle: Selimefendigil (2013), bottom: Aminossadati and Ghasemi (2009).

surface, T_c is the temperature at the inlet, L is the characteristic length (depth of the cavity) and u_{in} is the inlet velocity. Laminar compressible segregated flow solver setup as mentioned before is used for CFD predictions. Converged solution is extracted once the residuals for all equations drops below 10^{-7}. Figure 1 shows a very good agreement of the present solution with the previous studies reported by Aminossadati and Ghasemi (2009) as well as Selimefendigil (2013) using Boussinesq approximation.

To verify the implementation of the overall POD methodology, steady state CFD solutions are performed with varying Ri, for a fixed value of Grashof number $Gr = 10^4$. The eight CFD solutions obtained via the same aforementioned convergence criteria for $Ri = 40, 50, 60, 70, 80, 90, 100$ and 110 are used as snapshots input data for the POD technique. Evidently with the increase of Ri the naturaal convection effects becomes dominant. The POD-interpolated solution for $Ri = 75$ is constructed and compared with the actual CFD solution for verification and validation. The contours of the non-dimensional temperature $\theta(Ri, \vec{x}) = (T - T_c)/(T_h - T_c)$ and the absolute error estimates (see Figure 2) clearly shows the reliability of the implementation. The spatial structures of the POD modes are shown in Figure 3. The relative energy of the POD modes can be estimated from the eigenvalues as $E_r = \lambda^i / \sum_{i=1}^{m} \lambda^i$. The energy associated with the first POD mode is found to be 99.99999% and the rest of the modes assume values of the order of 10^{-7}% or less. This reveals that the most of the energy contained within the first POD mode.
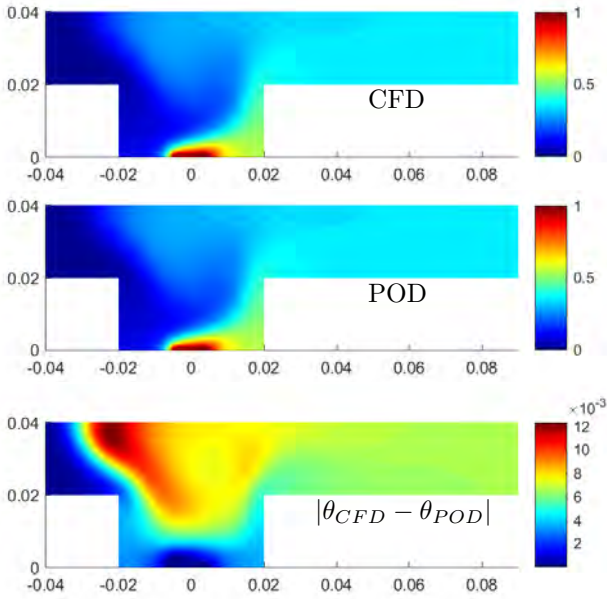
Figure 2: Comparison of CFD and POD predictions, contours of θ and error estimates for Ri=75.

Problem setup

In a DV system, the contaminated hot air from a room is displaced through ceiling level with fresh cold air supply at or near the floor level with a low velocity (typically < 0.5 m/s). This, usually create vertical gradients of air velocity, temperature and contaminant concentration (Cao et al. (2014)). The characteristics of the flow field depends on the type of air terminal device (DV unit) and the distribution of heat sources. To study the indoor airflows in DV configuration, a 3D computational domain of 7.5m(length) by 5.6m(width) by 2.8m(height) is taken (see Figure 4) as a standard room. The dimensions and the overall ventilation strategy with air supply diffuser and exhaust are set essentially following the guideline of the Nordtest method (Nordtest (2003)). A wall mounted displacement ventilation diffuser is placed at the floor level with an area of $0.24m^2$ having height, $h = 0.3m$. The air exhaust is placed on the opposite wall of the diffuser having the same dimensions. The heat loads are provided by heating wire around the room walls except the wall with the air supply. This is placed at $0.7m$ above the floor with a thickness of $0.05m$. Figure 4 also shows the mesh arrangements within the computational domain. Surface mesh and volume mesh controls are invoked to ascertain sufficient mesh resolution in the main interaction zone around air supply diffuser, exhaust and wall boundaries. A total of ≈ 1.06 million computational cells are used for the simulations. The near wall mesh resolution ensures $0.02 < y^+ < 17.06$ for all considered cases. Note that the resolution near ceiling is $0.3 < y^+ < 6.4$ and near floor is $0.08 < y^+ < 6.2$. The boundary conditions are mentioned in Figure 4. Desired mass flow is specified at the diffuser inlet boundary with a constant supply temperature, $T_{in} = 17°C$

and inlet density, $\rho_{in} = 1.216\ kg/m^3$. The exhaust conditions are set as flow outlet with same mass flow value at the inlet with appropriate sign to ensure the global mass conservation. All vertical walls and the floor are set as adiabatic wall boundaries, while a heat loss of 1 W/m^2 is specified on the roof as recommended in the Nordtest method. The internal load in the room is provided via a heat source of 40 W in each wall, giving rise to a total value of 120 W as shown in the Figure 4. This value has been set to mimic the effect of one human occupant. A turbulent intensity of 4% and a length scale of 10% of the inlet diffuser height h are chosen to assign the Dirichlet boundary conditions for κ and ω at the inlet boundary. Zero gradient condition at the outlet and all y^+ wall treatment of the solver is invoked for the remaining no-slip walls regarding these parameters. Converged solutions for all cases are extracted once the residual for mass conservation and energy conservation stabilises $\approx 8 \times 10^{-4}$ and residuals for all remaining equations drops below 4×10^{-5}.

Results and discussion

The flow physics involved in the present ventilation setup is governed by the Archimedes number (analogous to Richardson number) and this can be defined as $Ar = \dfrac{g\beta}{\rho_{in}c_p}\dfrac{q_t L}{u_{in}^3 A_s}$ (Brandan (2012)), where c_p is the heat capacity at constant pressure, q_t is the total heat gain in the room, A_s is the diffuser area of the inlet and L is the characteristic length that can be defined as the difference between the room height and height of the diffuser. Eight different test cases are simulated having $Ar = 2, 6, 10, 14, 18, 22, 26$ and 30 as variable parameter leading to the following functional form for any non-dimensional flow variable, $\phi^*(Ar, \vec{x})$. The following analysis is based on the non-dimensional variables: $\rho^* = \dfrac{\rho}{\rho_{in}}$, $U^* = \dfrac{u}{u_{in}}$ and $T^* = \dfrac{(T - T_{in})\ \rho_{in}c_p\dot{V}_{in}}{q_t}$, where $\dot{V}_{in}$ is the volumetric flow rate at the inlet. We first present the CFD solutions for different Ar. Subsequently, the analysis of POD-interpolated solution for $Ar = 15$ is presented.

DV characteristics and CFD snapshots

The Ar is varied essentially setting different inlet air supply velocity with fixed supply T_{in} and ρ_{in} and heat loads as mentioned before. Figure 5 shows the distribution of U^* on a $x - y$ plane at z=0.1m. The typical air flow pattern for low air velocity diffuser in DV configuration involving the acceleration region (near field) and the velocity decay region (far field) can be clearly realised from the U^* contours. With increasing Ar, the maximum value occurs at further upstream (x-coordinate) locations. Evidently, the acceleration zone is larger for low Ar. Figure 6 shows the effective thermal stratification on a $z - x$ plane at the middle of the room ($y = 2.8m$) for all cases which
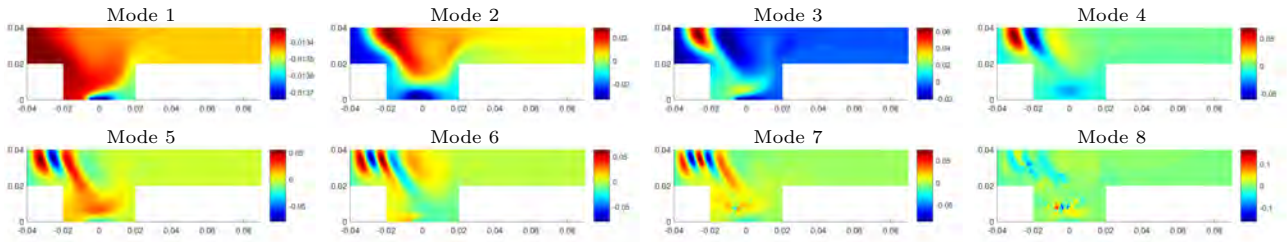
Figure 3: Spatial structures of the POD modes for θ.
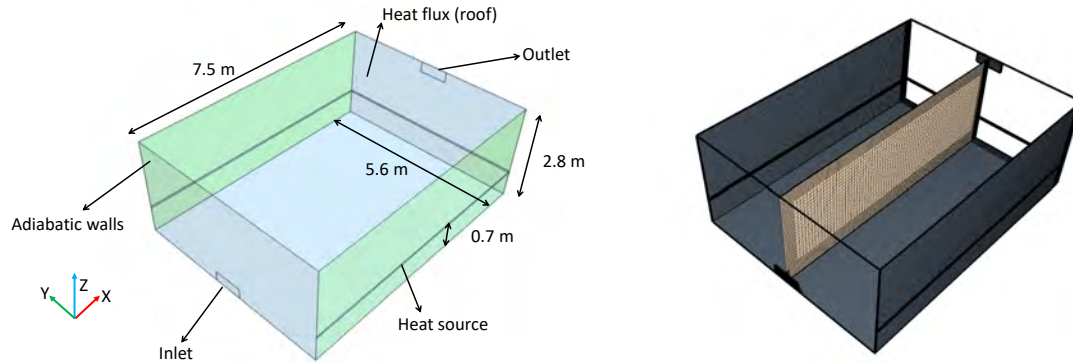
Figure 4: Computational setup of the indoor airflow study, left: domain specification and boundary conditions, right: mesh on some sample planes.
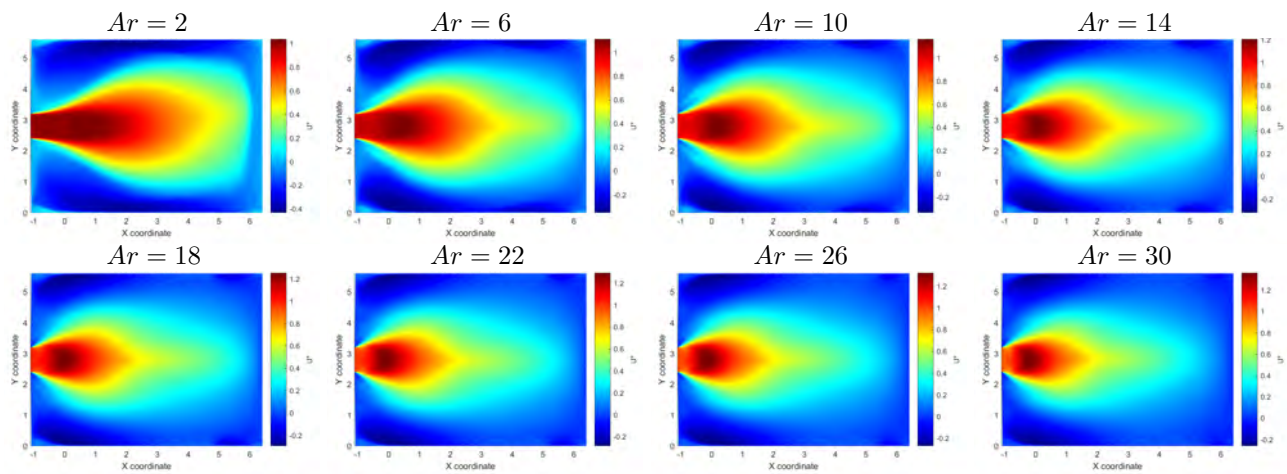
Figure 5: Contours of u-component of the velocity on a horizontal plane at 0.1 m above the floor for different Ar.
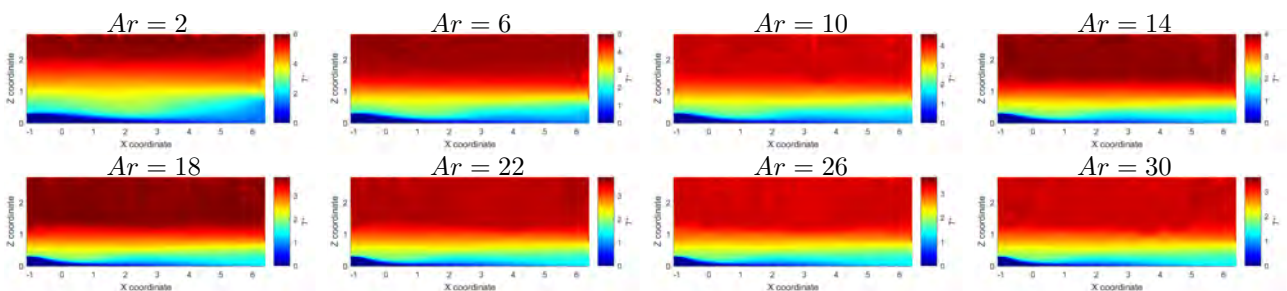
Figure 6: Contours of temperature on a vertical plane in the middle of the room at $y = 2.8m$ for different Ar.
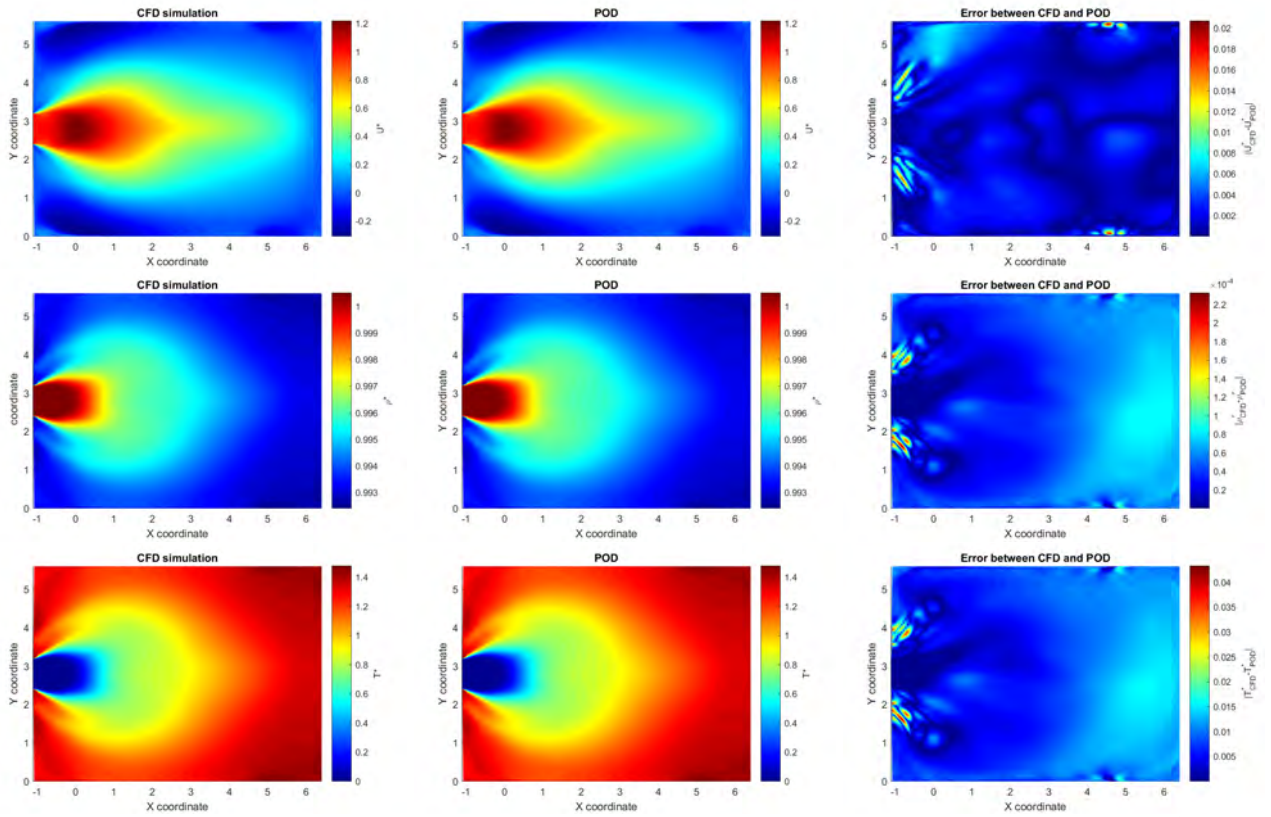
Figure 7: Velocity, density and temperature distributions on horizontal plane at 0.1 m above floor for Ar = 15.
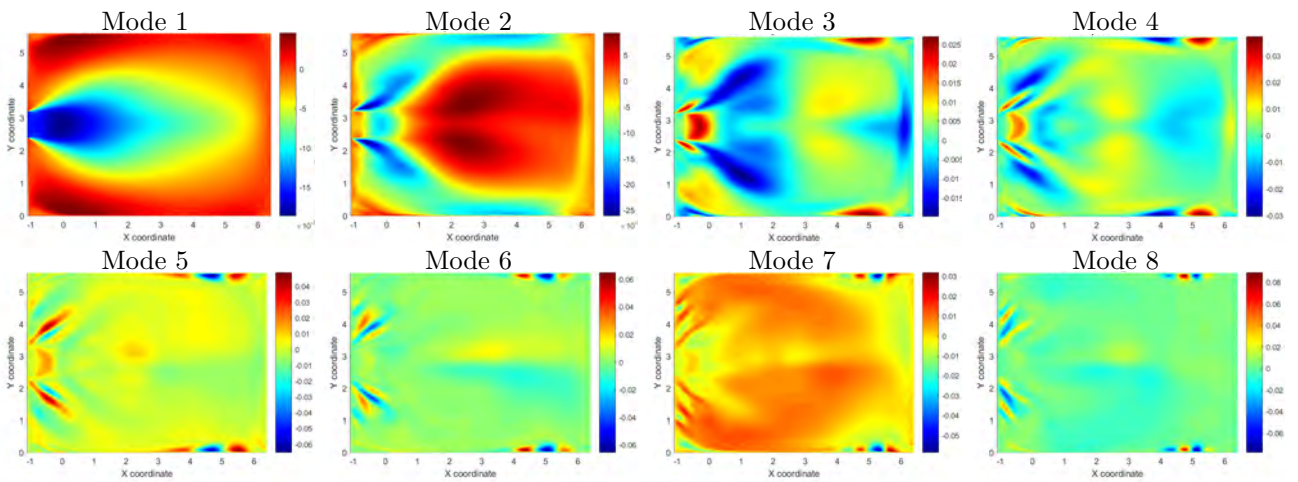
Figure 8: Spatial structures of the POD modes for u-component of the velocity field.
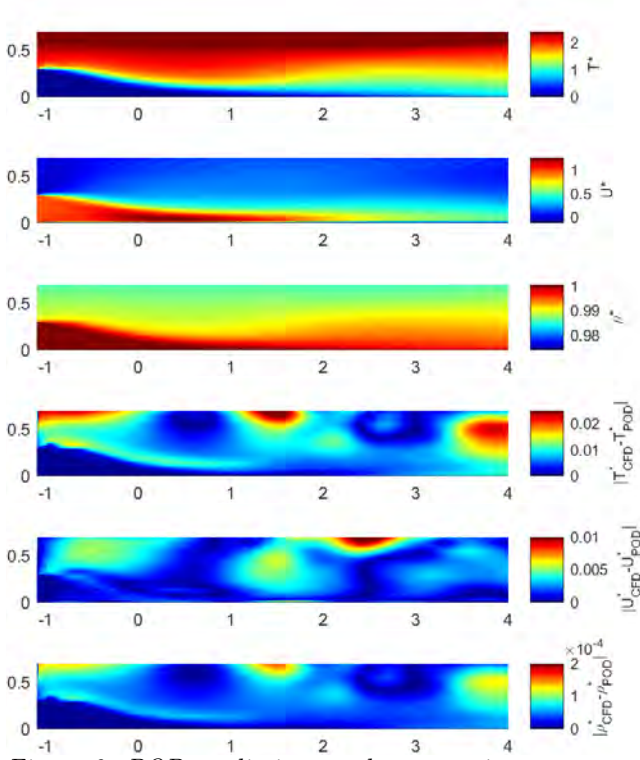
Figure 9: POD predictions and error estimates on a vertical plane at $y = 2.8$ for $Ar = 15$.

Figure 10: Spatial structures of the POD modes for u-component of the velocity field.

is the key aspect of achieving the good air quality for a DV system.

Analysis of POD-interpolated prediction

The steady state CFD snapshots of 8 different cases are used for the POD. We estimate the flow parameters for $Ar = 15$ via POD-interpolated methodology on two different planes (as discussed above). The predicted contours of U^*, T^* and ρ^* at $x - y$ plane are compared with the actual CFD (see Figure 7) results. It can be seen that the absolute error estimates are sufficiently low and the POD-interpolated predictions are in excellent agreement with the CFD counterpart. The spatial structures of the POD modes of the U^* are shown in Figure 8. Here, we found that the most of the energy contained within the first two POD modes. The energy associated with 8 POD modes are 98.01%, 1.76%, 0.19%, 0.00024%, 10^{-5}%, 10^{-5}%, 10^{-5}%, and 10^{-6}% respectively. A similar trend is observed for the predictions on mid $z - x$ plane (see Figure 9). It is evident that the error estimates for this plane appears relatively higher above the diffuser height levels having relatively coarser mesh. Nevertheless, the errors are sufficiently low in the main interaction zone near and below the diffuser height level. The acceleration and velocity decay regions are predicted very well. The spatial structures of the POD modes are shown in Figure 10. As expected, the first two modes are the most dominant modes among all.

Conclusion

In this work, we have presented a POD-interpolation based methodology in resolving complex indoor airflow patterns and thermal stratification related to a DV system. A 2D thermal convection benchmark problem on a cavity geometry has been solved to verify and validate the overall implementation. The guideline of the Nordtest method is adopted to build the case studies associate with a DV configuration for a standard room. Steady-state CFD snapshots with a varying Archimedes number are used to estimate the dominant POD coefficients/modal amplitudes and POD modes. The flow field variables are decomposed in terms of Archimedes number dependent POD coefficients and associated space dependent POD bases. A cubic spline interpolation of the POD coefficients is used to predict the solution for intermediate value of Archimedes number. The analysis reveals that for the u-component of the velocity field the first two POD modes are the most dominant modes accounting the associated energy $\approx 99.8\%$.

The present study clearly shows the capability of CFD snapshot based POD-interpolated fast and reliable predictions of DV configuration involving a wall mounted linear air terminal device. A future study with the different types of air terminal devices could be undertaken and this fast prediction approach is potentially advantageous to carry out further parametric variations without performing a large number

of physical experiments and validate existing semi-empirical models of DV systems.

Acknowledgment

References

Aminossadati, S. M. and B. Ghasemi (2009). A numerical study of mixed convection in a horizontal channel with a discrete heat source in an open cavity. *European Journal of Mechanics-B/Fluids 28*(4), 590–598.

Brandan, M. (2012). *Study of airflow and thermal stratification in naturally ventilated rooms.* Ph. D. thesis, Massachusetts Institute of Technology.

Brunton, S. L., B. R. Noack, and P. Koumoutsakos (2020). Machine learning for fluid mechanics. *Annual Review of Fluid Mechanics 52*, 477–508.

Cao, G., H. Awbi, R. Yao, Y. Fan, K. Sirén, R. Kosonen, and J. J. Zhang (2014). A review of the performance of different ventilation and airflow distribution systems in buildings. *Building and environment 73*, 171–186.

Causone, F., F. Baldin, B. W. Olesen, and S. P. Corgnati (2010). Floor heating and cooling combined with displacement ventilation: Possibilities and limitations. *Energy and Buildings 42*(12), 2338–2352.

Cehlin, M. and B. Moshfegh (2010). Numerical modeling of a complex diffuser in a room with displacement ventilation. *Building and Environment 45*(10), 2240–2252.

Choi, N., T. Yamanaka, K. Sagara, Y. Momoi, and T. Suzuki (2019). Displacement ventilation with radiant panel for hospital wards: Measurement and prediction of the temperature and contaminant concentration profiles. *Building and Environment 160*, 106197.

Davidson, L. (1989). Ventilation by displacement in a three-dimensional room—a numerical study. *Building and environment 24*(4), 363–372.

Elhadidi, B. and H. E. Khalifa (2005). Application of proper orthogonal decomposition to indoor airflows. *Ashrae Transactions 111*(1).

Gilani, S., H. Montazeri, and B. Blocken (2016). Cfd simulation of stratified indoor environment in displacement ventilation: Validation and sensitivity analysis. *Building and Environment 95*, 299–313.

Javad, K. and G. Navid (2019). Thermal comfort investigation of stratified indoor environment in displacement ventilation: Climate-adaptive building with smart windows. *Sustainable Cities and Society 46*, 101354.

Khalifa, H. E., B. Elhadidi, and J. F. Dannenhoffer III (2007). Efficient coupling of multizone and cfd indoor flow models through proper orthogonal decomposition. *ASHRAE Transactions 113*(2).

Li, Y., M. Sandberg, and L. Fuchs (1992). Vertical temperature profiles in rooms ventilated by displacement: Full-scale measurement and nodal modelling. *Indoor Air 2*(4), 225–243.

Magnier, L., R. Zmeureanu, and D. Derome (2012). Experimental assessment of the velocity and temperature distribution in an indoor displacement ventilation jet. *Building and Environment 47*, 150–160.

Meyer, K. E., J. M. Pedersen, and O. Özcan (2007). A turbulent jet in crossflow analysed with proper orthogonal decomposition. *Journal of Fluid Mechanics 583*, 199–227.

Nielsen, P. V. (1988). Displacement ventilation in a room with low-level diffusers.

Nielsen, P. V. (2000). Velocity distribution in a room ventilated by displacement ventilation and wall-mounted air terminal devices. *Energy and Buildings 31*(3), 179–187.

Nordtest (2003). Air terminal devices: Aerodynamic testing and rating at low velocity (NT VVS 083).

Selimefendigil, F. (2013). Numerical analysis and pod based interpolation of mixed convection heat transfer in horizontal channel with cavity heated from below. *Engineering Applications of Computational Fluid Mechanics 7*(2), 261–271.

Sirovich, L. and M. Kirby (1987). Low-dimensional procedure for the characterization of human faces. *Josa a 4*(3), 519–524.

Wei, G., B. Chen, D. Lai, and Q. Chen (2020). An improved displacement ventilation system for a machining plant. *Atmospheric Environment*, 117419.

Yuan, X., Q. Chen, and L. R. Glicksman (1998). A critical review of displacement ventilation. *ASHRAE Transactions-American Society of Heating Refrigerating Airconditioning Engin 104*(1), 78–90.

Analysis of the interfacial mixing in the gravity-driven counterflow through a large vertical opening using Large Eddy Simulation

Elyas Larkermani [1*], Laurent Georges [1]

[1] Department of Energy and Process Engineering, Norwegian University of Science and Technology, NTNU, Trondheim, Norway

* corresponding author: elyas.larkermani@ntnu.no

Abstract

The study of natural convection flows in multizone enclosures is a topic of great importance due to its direct influence on room air circulation patterns, distribution of indoor air contaminants, and thermal comfort inside buildings. In this research, ANSYS Fluent is used to investigate the density-driven bidirectional flow through a large vertical opening connecting two isothermal reservoirs, the so-called bulk flow regime. Many research works on the natural convection flow through a large vertical opening between two enclosures have been done. However, they paid less attention to the unsteady flow structures generated by the sophisticated bidirectional flow, especially in the middle of the doorway. Large Eddy Simulation (LES) results show the development of unsteady flow structures in the middle of the doorway, a phenomenon called "interfacial mixing". This phenomenon has been hardly documented in the literature, only using experiments. Even though unsteady flow structures develop, they do not significantly affect bulk quantities such as the discharge coefficient (C_d).

Introduction

The behavior of natural convection in confined spaces has attracted a lot of attention originating from its application in buildings air conditioning, contaminant spread and electronic equipment cooling. The vast majority of these spaces include internal partitions that the flow can traverse partially. In most situations, the presence of internal partitions with an opening lead to an intrinsically three-dimensional and transient flow field. The characteristics of such complicated flow are of strong interest to many communities and researchers. Several parameters can have an important role in driving this flow such as temperature differences, door motion, occupant motion or wind dynamic pressure. In past investigations, Computational Fluid Dynamics (CFD) simulations of the natural convection flow through a large vertical opening between two enclosures have been performed, but mostly using RANS, and/or two-dimensional assumption, and/or what can be considered today as very coarse grids. This made the unsteady flow structures impossible to be captured by these CFD simulations. From the experimental side, several past studies reported on the flows in differently heated enclosures separated by a partition wall. While these studies analyzed the flow inside these enclosures, the flow within the doorway itself was measured for a limited number of locations. However, the CFD standards of today enable to better investigate the unsteady nature of the bidirectional flow inside large vertical openings.

Two separate mechanisms for natural convection flow between a hot and a cold zone were investigated in the experimental study of Scott et al. [1]: the *boundary layer* regime and the *bulk density-driven* regime. The transition between both regimes was established as a function of the aperture size located in the middle of the partition wall. In another similar work, the effect of internal partitions on the convective heat transfer across an enclosure was described by Neymark et al. [2]. They developed a Nusselt-Rayleigh correlation using the aperture width and a resistance model. Georges et al. [3] conducted RANS simulations using the RNG $k - \varepsilon$ model and ANSYS Fluent for two rooms with an open door in the partition wall. They proved that the thermal radiation could affect the transition between the two aforementioned regimes and opposed to previous reports claiming that the aperture size was the main driving parameter causing such transition.

Favarolo and Manz [4] employed the LVEL $k - \varepsilon$ turbulence model [5] in the FLOVENT commercial CFD software to analyze the influence of different parameters such as temperature difference between indoor and outdoor air on the airflow rate through a large open window. The vertical position and the horizontal distance of the opening from the wall were diagnosed to have the greatest and minor impact on the discharge coefficient (C_d), respectively. Based on their literature review, the value of C_d varies between 0.3 and 0.8, and the origin of these large variations is not clear to the authors. Allard and Utsumi [6] mentioned that this phenomenological coefficient takes into consideration the contraction of the flow while it passes through the opening. They concluded that the definition of C_d is still ambiguous and requires more precision. Pelletret et al. [7] investigate various approaches to determine the C_d as a function of opening height or temperature difference. They also show the difficulty in determining the C_d and point out that a variety of definitions for this coefficient has been introduced in the literature. Hence, despite the significant amount of numerical and experimental studies conducted to date, no clear conclusion can be drawn from previous studies.

The standard model to evaluate the airflow in a doorway, extensively used in building performance simulation (BPS), assumes two isothermal reservoirs and a one-dimensional inviscid steady-state flow. Both assumptions lead to a simple model based on the Bernoulli equation which is defined here as the theoretical model [8]. The resulting theoretical flow is then corrected using the C_d to match the actual airflow in the doorway. Uncertainties related to this modeling framework remain unknown. In particular, the effect of the unsteady flow regime on the value of the discharge coefficient needs to be elucidated.

When both reservoirs are isothermal and the room air temperature is in thermal equilibrium with the wall temperature surrounding it, the airflow in the doorway is in the bulk flow regime. The air temperature difference (ΔT) between both zones and the aperture geometry are the only physical parameters needed to define the flow. The temperature difference between the two zones leads to different bulk air densities and, consequently, different hydrostatic pressure fields. Due to the conservation of mass, both hydrostatic pressure fields are equal at the neutral plane (NP) located near the middle of the doorway. The difference of hydrostatic pressure above and below the NP generates a counterflowing stream of warm and cold air. A schematic of the velocity profile of this bidirectional flow in the vertical centerline of the doorway is shown in Fig. 1. Assuming an inviscid flow, the velocity profile shows a sharp gradient at the level of the NP (i.e. dashed lines in Fig. 1). With a viscous flow, three related phenomena can occur. Firstly, the two airstreams going in opposite directions create a shear layer. Secondly, Wilson and Kiel [9] reported some interfacial mixing due to re-entrainment effects. According to these authors, the resulting velocity and temperature profiles show a smoother transition at the level of the neutral plane (i.e. solid line in Fig. 1). Thirdly, a similar study by Lefauve et al. [10] using two reservoirs connected by a long channel demonstrated that a sustained stratified shear flow could generate large unsteady flow structures. Consequently, the mass and heat flows exchanged through the doorway will be reduced compared to the inviscid flow (i.e., the assumption used in the standard model).
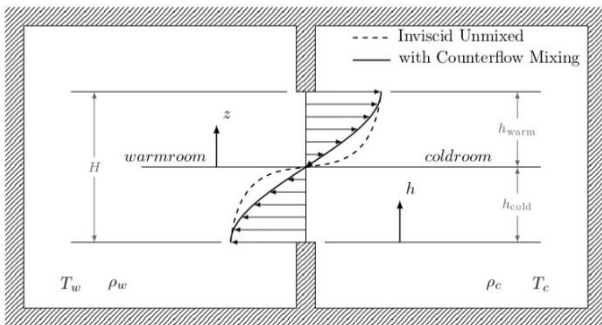
Figure 1: Inviscid and actual profiles of the streamwise velocity for the bidirectional flow in a doorway.

The present work investigates viscous effects and the resulting unsteady flow in the middle of the doorway using Large Eddy Simulation (LES). Two large reservoirs are created by connecting two large isothermal volumes of equal size by a vertical solid partition. The single rectangular aperture located in the middle of the vertical partition enables the air to flow between the two zones. The primary objective of the present study is the interfacial mixing, meaning to characterize the mixing process (i.e. shear, re-entrainment and unsteady flow structures) and its influence on the volume airflow rate and heat transfer across the opening.

Numerical Method

Multizone enclosure description

The bidirectional airflow is generated at the aperture of height $h = 2m$ and width $w = 1m$. Each zone has the same length $L_0 = 16m$ in all spatial directions and is filled with air with constant thermodynamic properties. Figure 2 illustrates the geometry of the three-dimensional multizone enclosure.
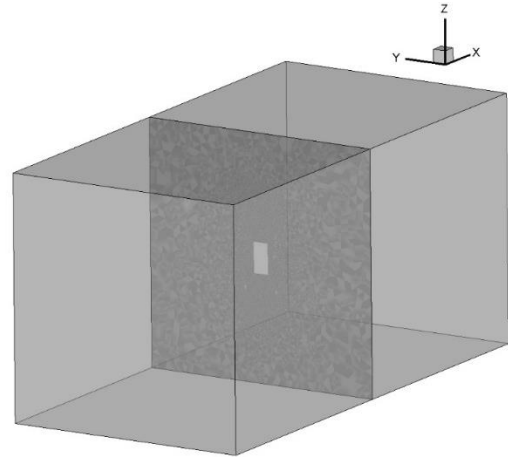
Figure 2: Three-dimensional multizone enclosure configuration.

Governing equations

After applying an implicit filtering operator and considering the Boussinesq approximation, the filtered incompressible Navier-Stokes equations can be expressed as:

$$\frac{\partial \bar{u}_i}{\partial x_i} = 0 \qquad (1)$$

$$\frac{\partial \bar{u}_i}{\partial t} + \frac{\partial \bar{u}_i \bar{u}_j}{\partial x_j} = -\frac{1}{\rho}\frac{\partial \bar{p}}{\partial x_i} + \frac{\partial}{\partial x_j}\left[2 v \bar{S}_{ij}\right] - \frac{\partial \tau_{ij}}{\partial x_j} \\ - g_i[1 - \beta(\bar{T} - T_0)] \qquad (2)$$

$$\frac{\partial \bar{T}}{\partial t} + \frac{\partial \bar{u}_j \bar{T}}{\partial x_j} = \frac{\partial}{\partial x_j}\left[\alpha \frac{\partial \bar{T}}{\partial x_j}\right] - \frac{\partial \tau_{jT}}{\partial x_j} \qquad (3)$$

Where the $\bar{\Delta} = \sqrt[3]{\Delta x \Delta y \Delta z}$ was chosen as the effective filter width. x_i denotes the ith coordinate direction. $\bar{u}_i$ represents the filtered velocity field in the x_i direction, t the time, $\bar{p}$ the modified filtered pressure, and $\bar{T}$ the filtered temperature. The last term in Equation (2) is the buoyancy term where β is thermal expansion of the fluid and g_i the gravitational acceleration. The parameters v, α

indicate the kinematic viscosity and thermal diffusivity, respectively. The subgrid scale (SGS) stress tensor and the scalar SGS thermal flux vector is included, respectively, in the momentum and energy equations above via the unresolved terms $\tau_{ij} = \overline{u_i u_j} - \bar{u}_i \bar{u}_j$ and $\tau_{jT} = \overline{u_j T} - \bar{u}_j \bar{T}$.

Modeling of unresolved turbulent scales

The closure of the Navier–Stokes equations can be achieved by utilizing the Wall-Adapting Local Eddy-viscosity (WALE) turbulence model for calculating the SGS kinematic viscosity, v_{SGS}, based on the invariants of the velocity gradient tensor;

$$\tau_{ij} = \overline{u_i u_j} - \bar{u}_i \bar{u}_j = -2v_{SGS}\bar{S}_{ij} + \frac{2}{3}k_{SGS}\delta_{ij} \qquad (4)$$

$$v_{SGS} = \bar{\Delta}^2 C_w^2 \frac{\left(\bar{S}_{ij}^*\bar{S}_{ij}^*\right)^{3/2}}{\left(\bar{S}_{ij}\bar{S}_{ij}\right)^{5/2} + \left(\bar{S}_{ij}^*\bar{S}_{ij}^*\right)^{5/4}} \qquad (5)$$

$$\bar{S}_{ij}^* = \frac{1}{2}\left(\bar{g}_{ij}^2 + \bar{g}_{ji}^2\right) - \frac{1}{3}\bar{g}_{kk}^2\delta_{ij} \qquad (6)$$

$$\bar{g}_{ij}^2 = \bar{g}_{ik}\bar{g}_{kj} = \frac{\partial \bar{u}_i}{\partial x_k}\frac{\partial \bar{u}_k}{\partial x_j} \qquad (7)$$

Where C_w is the model coefficient, here taken at a constant value equal to 0.325 [11]. k_{SGS} and $\bar{S}_{ij}$ are the SGS kinetic energy and resolved scale strain rate tensor.

$$\bar{S}_{ij} = \frac{1}{2}\left(\frac{\partial \bar{u}_i}{\partial x_j} + \frac{\partial \bar{u}_j}{\partial x_i}\right) \qquad (8)$$

By analogy to the SGS stress tensor modeling, the scalar SGS thermal flux vector, τ_{jT}, can be approximated by the following expression [12];

$$\tau_{jT} = \overline{u_j T} - \bar{u}_j \bar{T} = -\frac{v_{SGS}}{Pr_{SGS}}\frac{\partial \bar{T}}{\partial x_j} \qquad (9)$$

Where Pr_{SGS} denotes the SGS Prandtl number and is fixed at 0.85 in the simulations presented below. The WALE turbulence model is able to reproduce the near-wall behavior correctly. Thus, opposed to most eddy viscosity turbulence models that require wall-damping functions near the wall region, the turbulent viscosity obtained by WALE formulation approaches zero at the wall. The model also generates zero turbulent viscosity in case of a pure shear; hence it can capture the transitional flow from laminar to turbulent [13].

Computational grid and boundary conditions

To achieve high resolution using minimum number of mesh elements, the mesh has been refined in four zones with different grid sizes. The finest elements of the structured mesh concentrates predominantly in a region around the middle of the door to properly resolve 3-D interfacial mixing, re-entrainment phenomena, and other fluctuation structures. An unstructured mesh with a combination of tetrahedra and pyramid cells was employed in the other three refinement zones. A smooth transition between the cell of different sizes is performed.

In total, nearly 25 million elements have been spread all over the multizone enclosure. The computational grid is shown in Fig. 3.
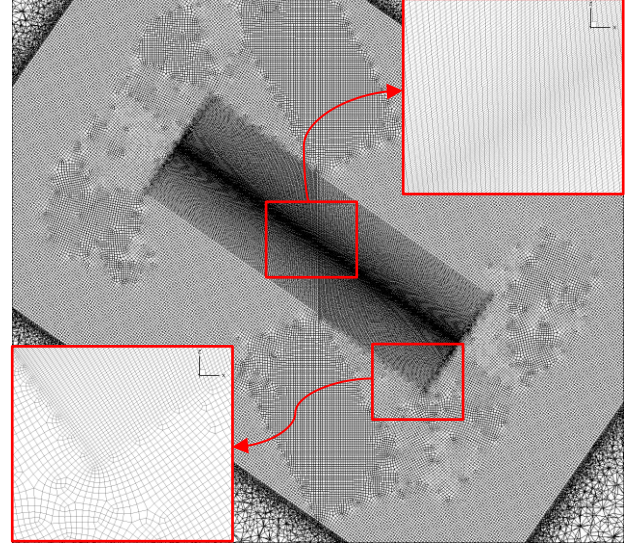
Figure 3: Computational grid.

Uniform initial temperature of $T_c = 293.15K$ and $T_H = 298.15K$ is imposed in the cold and warm reservoirs, respectively ($\Delta T = 5K$). The reference temperature (T_{ref}) is the arithmetic average of these two temperatures. The Prandtl number, $Pr = 0.73$, kinematic viscosity, $v = 1.538 \times 10^{-5}\ m^2/s$, and thermal expansion coefficient of the air, $\beta = 1/T_{ref} = 0.00335$, were applied. The enclosure is initialized with zero velocity, which would guarantee that natural convection would evolve. External walls of the enclosure are adiabatic and with a no-slip boundary condition.

During the first step of the simulation, an adaptive time step has been considered until the start-up fluctuations disappeared. Afterward, a constant time step of $\Delta t = 0.01$ is maintained to keep the Courant number value below 1.0 in order to achieve temporal accuracy and numerical stability. Note that a pseudo-stationary condition is reached after about 60 seconds when the airflow has fully established throughout the enclosure and the transition to turbulent mixing is settled. In this pseudo-steady state regime, the statistical data of time-averaged flow variables is collected for 80 seconds in order to reach full-converged statistics. During this period, the volume-averaged air temperature of both reservoirs remains almost constant.

Numerical Methodology

The non-linear governing equations are discretized using the second-order cell-centered finite volume method (FVM) implemented in the ANSYS Fluent commercial CFD package. The algorithm of Semi-Implicit Method for Pressure Linked Equations (SIMPLE) is employed for decoupling of velocity and pressure in the Navier–Stokes equations. The time derivatives are advanced in time using the Second Order Implicit scheme. The Bounded Central Differencing scheme is adopted for the treatment

of the convective term in the momentum equation. The diffusion terms are central-differenced, while the pressure interpolation is provided by the Body Force Weighted scheme.

ANSYS Fluent is capable of running on distributed processors and uses the public domain openMPI implementation of the standard message passing interface (MPI) to conduct inter-processor communication. The present LES simulation was carried out on the Idun cluster [14], containing Intel Xeon processor nodes with 40 cores and a minimum of 128GB of RAM.

Results and discussion

Interfacial Mixing

The counterflowing streams start setting up once the aperture opens and creates an opening between cold and warm zones. As expected, both warm and cold airflows are initially laminar and after a few seconds, they become turbulent. The low-density warm air descends in the heated plate side of the partition wall and is discharged into the adjacent cold zone by bending rapidly over the upper part of the opening and rise as a buoyant plume due to Archimedes force. Since the dimensions of the two reservoirs are considerable compared to the aperture area, temperature changes in each reservoir will be negligible.

Both air streams will meet at some distance from the bottom and up edges of the opening, where this interface is called the neutral plane. At the position of the neutral plane, the velocity would be zero and the pressure in both rooms are equal; hence there will be no airflow. When the flow is inviscid, there is no mixing or heat transfer between the two opposite airstreams close to and within the aperture. With viscous effects, instantaneous results provided by LES in Fig. 4 show unsteady flow structures developing in the middle of the doorway.
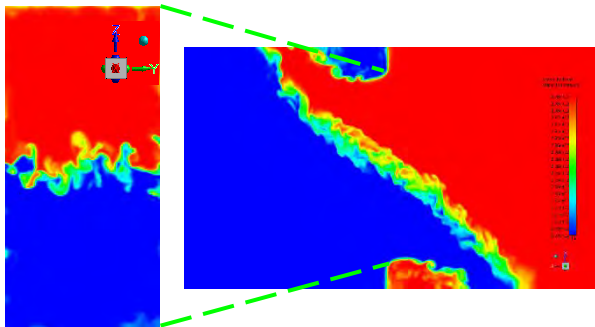
Figure 4: Instantaneous temperature in the door (left) and in a lateral view at the middle of the door in the y-direction (right).

The neutral plane (NP) is clearly visible in the left figure which shows front views of the door. This plane is not straight, and its position fluctuates slightly in space and time. To the authors' best knowledge, this effect has never been reported in the literature. The flow can also be visualized in a plane perpendicular to the door (right figure).

A snapshot of the mean temperature contours on a vertical plane in the middle of the enclosure are presented in Fig. 5. The counterflow develops from the NP with an angle of approximately 35 degrees with the horizontal. Unlike the standard theory assuming the flow to be horizontal at the doorway level, the CFD is strongly three-dimensional. Compared to inviscid flow (i.e. Euler simulation), the interfacial mixing induces a smoother transition of the temperature between both airstreams for viscous flow.
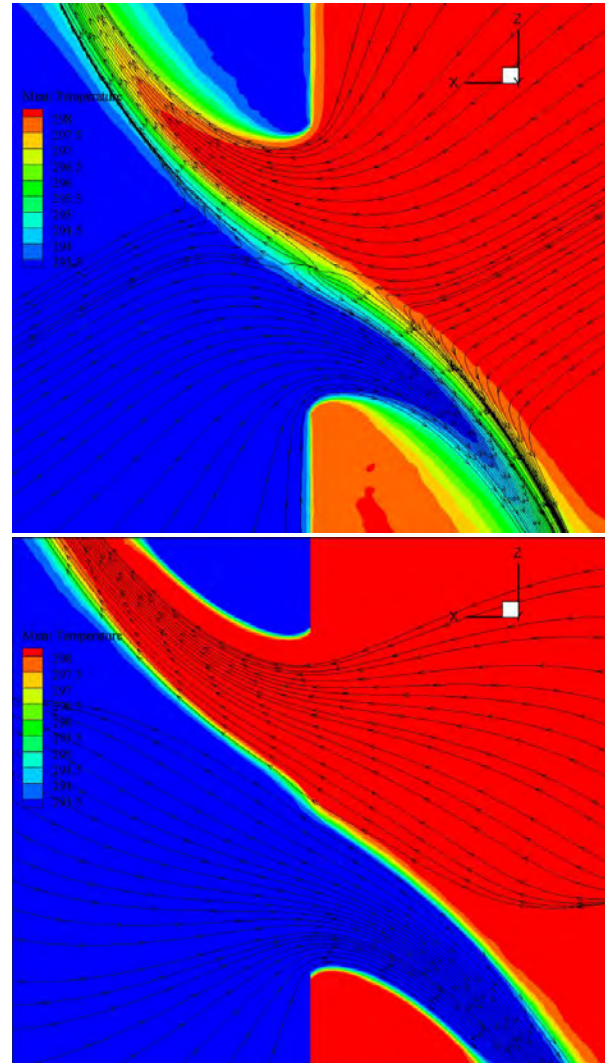
Figure 5: Mean temperature contours with streamlines, (LES above and Euler below).

The streamlines in viscous flow reveal that interfacial mixing causes a fraction of the warm airflow to be brought back into the warm zone, entrained by the cold airstream. This re-entrainment is similar for the cold airflow. However, no re-entrainment happened when the viscosity is switched off (Euler). The sharp edges of the aperture cause flow separation. At a section slightly downstream of the opening where the streamlines get almost horizontal, the maximum flow contraction takes place. In this section, the effective cross-section area for the airflow passage is minimum leading to the maximum velocity magnitude. This narrowest flow region is known as *vena contracta* and can occur when streamlines are unable to

follow sharp angles of openings. This area is shown by the streamlines passing through the aperture in Fig. 5, while it is not predicted by the theoretical model. The contraction will affect the airflow rate (or C_d) and heat exchange through the aperture.

Profiles of the time-averaged streamwise velocity and air temperature along a line in the middle of the doorway are shown in Fig. 6. The simulation results are also compared with those obtained by Euler simulation. For the theory, the velocity is scaled by a C_d calibrated by the LES (see next subsection). The first figure shows that the streamwise velocity is very similar between the LES, Euler simulation and the theory (denoted by Bernoulli) away from the middle of the door where the mixing takes place. The theory is able to successfully reproduce the streamwise velocity over a large part of the doorway. This can explain why this theory has been widely used in practice when an estimate of C_d is available. In the middle of the doorway, the Euler simulation and the theory also show similar results.
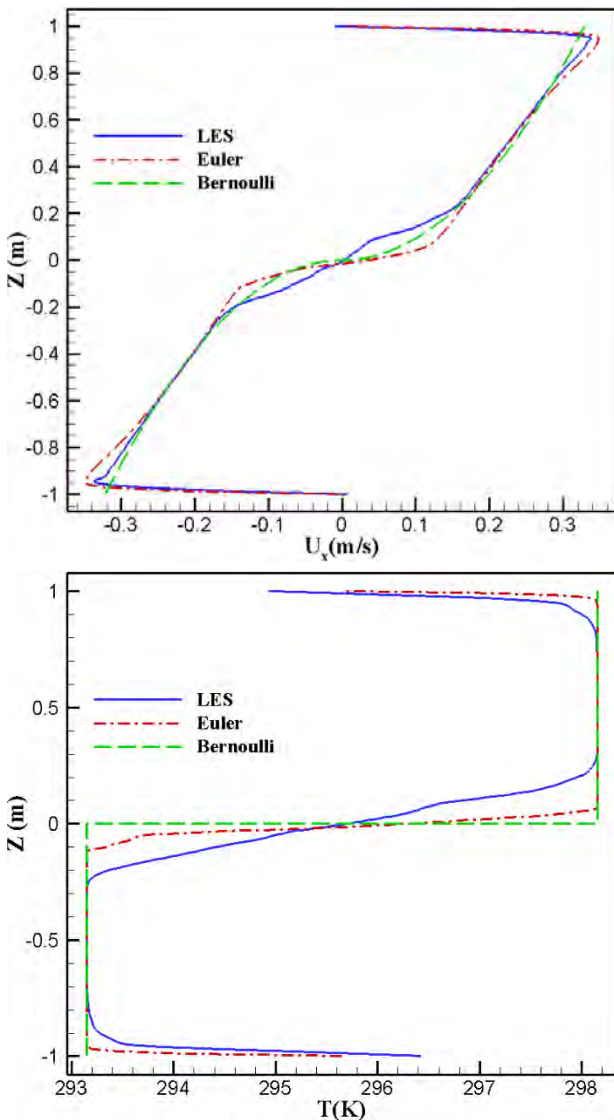
Figure 6: Time-averaged streamwise velocity and temperature profiles in the middle of the doorway.

It is only by introducing viscous effects and the resulting mixing that the velocity field shows a smoother transition. This transition zone has a length of 0.2 H, centered on the NP.

The mean temperature profiles confirm these conclusions. The LES and Euler simulation give similar results over a large fraction of the door. In the middle of the doorway, the Euler temperature profile is close to a step function of 5K as assumed by the theory. On the contrary, the LES has a smoother transition.

Bulk Quantities

Considering the Bernoulli equation for an inviscid horizontal airflow passing through the aperture, the maximum theoretical volume flow rate (Q_{max}) can be evaluated as [9]:

$$Q_{max} = \frac{A}{3}\sqrt{g'H} \qquad (10)$$

$$g' = g\frac{\Delta\rho}{\rho_e} \qquad (11)$$

$$\rho_e = \rho_w \frac{\left(1 + (\rho_c/\rho_w)^{1/3}\right)^3}{8} \qquad (12)$$

$$Q = C_d Q_{max} \qquad (13)$$

Where A and H are the aperture area and height, respectively. g' is defined as the effective acceleration of gravity. For low temperature differences until $40K$ the effective density, ρ_e, can be replaced with the average density [9]. The value of C_d is computed by dividing the actual volume flow rate (Q) by the maximum theoretical volume flow rate from the theory (Q_{max}). The time histories of the total volume flow rate, volume flow rate of each air stream, heat transfer, and doorway orifice coefficient are shown in Fig. 7.

The total volume flow rate of the warm and cold airflows respects the conservation of mass. In other words, the mass flow entering the sealing room must equal the mass flow leaving the room. As both reservoirs are adiabatic, energy is also conserved and the convective heat flow (Qc) of both airstreams has the same magnitude but opposite signs.

Besides the existence of small fluctuations in Fig 4., LES and Euler approaches produce nearly the same values of each bulk quantity (i.e. volume flow rate, C_d and heat transfer). Hence it can be concluded that bulk quantities will not be affected significantly by unsteady flow structures developing along the counterflow interface.

Conclusions

The characteristics of the three-dimensional bulk flow through a large vertical opening induced by the temperature difference of two isothermal reservoirs have been extensively studied in the literature. However, factors influencing the flow (or the discharge coefficient, C_d), such as unsteady flow phenomena should still be studied. ANSYS Fluent was used to investigate this effect. LES using the WALE subgrid scale model was

adopted to predict the unsteady turbulent behaviour of the counterflowing airstreams. Results were compared to
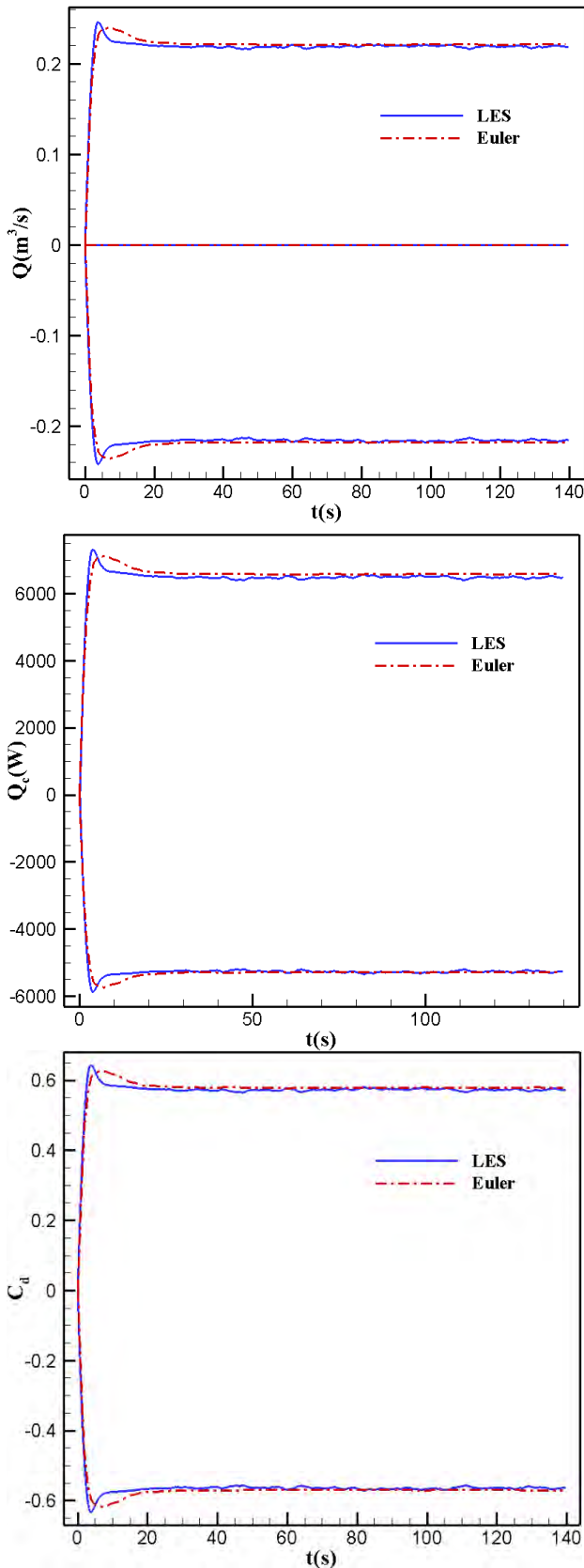
Figure 7: Time histories of mass flow rate, heat transfer, and doorway orifice coefficient.

Euler simulation. The inviscid flow showed no mixing or heat transfer between the opposite airflows close to and within the aperture. On the contrary, unsteady flow structures near the neutral plane were predicted by LES and generate interfacial mixing. Three phenomena resulted from the two counterflowing warm and cold airstreams (i.e. shear layer, re-entrainment effects and unsteady flow structures) and led to a reduction of the mass flow and heat exchange through the doorway. The theory was able to fairly reproduce the streamwise velocity and air temperature over a large fraction of the doorway. However, significant differences between viscous (i.e. LES) and inviscid flows (i.e. Euler and theoretical model) were present in the middle of the doorway ($|z| < 0.2$ H) due to mixing. Even though unsteady flow structures were present in the middle of the doorway, bulk quantities such as C_d were not affected significantly. The values of C_d calibrated by the LES and Euler simulation were very similar.

References

[1] D. Scott, R. Anderson, and R. Figliola, "Blockage of natural convection boundary layer flow in a multizone enclosure," *International journal of heat and fluid flow,* vol. 9, no. 2, pp. 208-214, 1988.

[2] J. Neymark, C. R. Boardman III, A. Kirkpatrick, and R. Anderson, "High Rayleigh number natural convection in partially divided air and water filled enclosures," *International Journal of Heat and Mass Transfer,* vol. 32, no. 9, pp. 1671-1679, 1989.

[3] L. Georges, G. Cao, and H. M. Mathisen, "Further Investigation of the Convective Heat Transfer between Rooms through Open Doorways," in *the 12th REHVA World Congress: volume 5. Aalborg: Aalborg University, Department of Civil Engineering.*, 2016.

[4] P. Favarolo and H. Manz, "Temperature-driven single-sided ventilation through a large rectangular opening," *Building and Environment,* vol. 40, no. 5, pp. 689-699, 2005.

[5] D. Agonafer, L. Gan-Li, and D. B. Spalding, "The LVEL turbulence model for conjugate heat transfer at low Reynolds numbers," *Application of CAE/CAD Electronic Systems, ASME,* vol. 18, pp. 23-26, 1996.

[6] F. Allard and Y. Utsumi, "Airflow through large openings," *Energy and Buildings,* vol. 18, no. 2, pp. 133-145, 1992.

[7] R. Pelletret, G. Liebecq, F. Allard, J. Van der Maas, and F. Haghighat, "Modelling of large openings," in *12th AIVC Conference: Air Movement and Ventilation Control Within Buildings*, 1991.

[8] F. Allard *et al.*, "Airflow through large openings in buildings," *Annex 20: Air flow patterns within Buildings,* 1992.

[9] D. Wilson and D. Kiel, "Gravity driven counterflow through an open door in a sealed room," *Building and Environment,* vol. 25, no. 4, pp. 379-388, 1990.

[10] A. Lefauve, J. Partridge, and P. Linden, "Regime transitions and energetics of sustained stratified shear

flows," *Journal of Fluid Mechanics,* vol. 875, pp. 657-698, 2019.

[11] F. Nicoud and F. Ducros, "Subgrid-scale stress modelling based on the square of the velocity gradient tensor," *Flow, turbulence and Combustion,* vol. 62, no. 3, pp. 183-200, 1999.

[12] A. Leonard, "Energy cascade in large-eddy simulations of turbulent fluid flows," *Adv. Geophys. A,* vol. 18, no. A, pp. 237-248, 1974.

[13] A. Yuen, G. Yeoh, V. Timchenko, S. Cheung, and T. Chen, "Study of three LES subgrid-scale turbulence models for predictions of heat and mass transfer in large-scale compartment fires," *Numerical Heat Transfer, Part A: Applications,* vol. 69, no. 11, pp. 1223-1241, 2016.

[14] M. Själander, M. Jahre, G. Tufte, and N. Reissmann, "EPIC: An energy-efficient, high-performance GPGPU computing research infrastructure," *arXiv preprint arXiv:1912.05848,* 2019.

Simulation Study on the Influence of the Urban Street Intersection Greening on Ventilation Performance

Xin Guo, Zhi Gao[*]

School of architecture and urban planning, Nanjing University, Nanjing, China

* corresponding author: zhgao@nju.edu.cn

Nomenclature

PFR(purging flow rate)

NEV(net escape velocity)

LOR(Land occupation rate)

GC(Green coverage)

GVR(Greening volume ratio)

Abstract

This article hopes to explore the impact of single-row shrubs, single-row trees, and double-row trees on the ventilation performance of street intersections. By simplifying the shape of intersections, ideal models can be built. Use the model and numerical simulation software FLUENT of the cross street intersection to simulate the airflow and pollutant distribution of the intersection, the wind direction is 0 ° and 45 °. Mainly analyzed the pollutant cloud maps of the three height parts (0.5 m, 1.5 m and 5 m), and compared the average speed, average concentration and maximum concentration of the vertical height intersection area, and studied the streets in different directions of green intersections under different wind directions Impact. According to the simulation results of wind speed and pollutant distribution, find the internal flow field and pollutant diffusion law at the intersection of the intersection, and use the ventilation index to compare the greening layout of the intersection and the intersection, especially the ventilation effect of the pedestrian activity space at the bottom. This article hopes to obtain a greening form based on street intersections that focus on urban ventilation and are beneficial to the diffusion of pollutants.

Introduction

At present, many studies have shown that the intersections of urban streets are the most polluted areas of automobile exhaust (Ahmad K, Khare M, Chaudhry K K, 2005). The air quality in this area is poor, and the air index is easily exceeded, especially the high CO content, which seriously harms human health (Hlavinka M W, 1988). The impact of greening on street air quality is controversial. On the one hand, people think that the greening of street canyons is usually a part of the urban landscape strategy, which has an aesthetic value of appreciation, but also has the functions of evaporative cooling, adjusting humidity, improving local microclimate, and avoiding direct sunlight (Chen et al., 2014; Gago, Roldan, Pacheco-Torres, & Ordóñez, 2013; GILL, HANDLEY, ENNOS, & PAULEIT, 2007; Rui, Buccolieri, Gao, Ding, & Shen, 2018; Rui, Buccolieri, Gao, Gatto, & Ding, 2019). On the other hand, more and more studies have found that plants have the ability to remove pollutants, and plants have the ability to purify air by filtering pollutants. Plant leaves absorb gaseous pollutants through stomata, while particulate matter is removed from the air by depositing on leaves and branches (Bealey et al., 2007; McDonald et al., 2007; NowakCrane & Stevens, 2006; Tallis, Taylor, Sinnett, & Freer-Smith, 2011).

Methods

Urban street intersections usually take many forms according to the structure, traffic and commercial building forms of urban streets. According to the number of branches, there are different types of three-way, four-way intersections, roundabouts, etc. The research object selected in this paper is a typical four-way intersection. Figure 1a shows a sketch of four-way in the city of Nanjing (China); based on this, idealized intersection is established (Figure 1b).
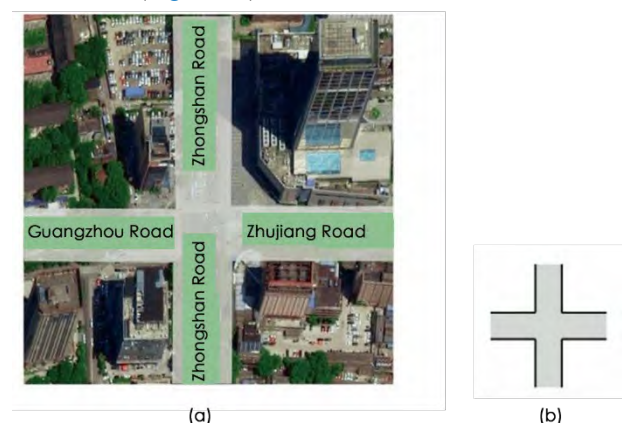
Figure 1. a) Sketch of the types of four-way intersection in Nanjing, China; b) idealized intersection chosen as study case.

In summary, this article sets up three groups of single greening cases. As shown in Figure 2, a single row of shrubs is arranged in the center of the street, two rows of shrubs are arranged on both sides of the street, and two rows of trees are arranged in the street. The green layout and green indicators in this example are shown in Table

1. Table 1 details the green form and related green indicators used in this article. Occupancy rate represents the area of street land occupied by greening. Since trees only occupy a part of the trunk, this part of the area is negligible.
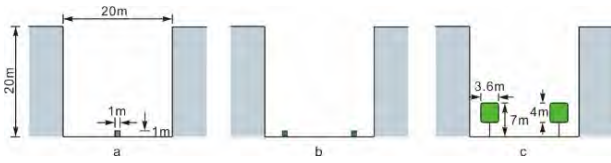
Figure2. Shrub and tree layout Case

Table 1. Greening layout and greening index

	Plant type	Greening pattern	LOR (%)	GC (%)	GVR (%)
a	Shrub[a]	A row of bushes lined up in the middle of the street	3.9	3.9	0.2
b	Shrub	Double rows of shrubs on both sides of the street between motorized and non-motorized lanes	7.8	7.8	0.4
c	Arbor[b]	Double row arbors, arranged on both sides of the street, between motor vehicles and non motor vehicles	0.0	28	5.6

Note: a). In this paper, the height of shrub is 1m, and the density of leaf area is $2m^2/m^3$. b). In this paper, the height of arbor is 7m, the height of crown is 3-7m, and the density of leaf area is $1m^2/m^3$.

The overall model is 460 m long and 460 m wide (Figure 3). The main body of the model (indicated as Case in the figure) is composed of 40 m x 40 m building blocks. In the case of a street canyon with an aspect ratio (W / H) of 1, the street width is 20 m and the building height is 20 m. To consider the influence of surrounding buildings, two rows of buildings are added at the intersection.
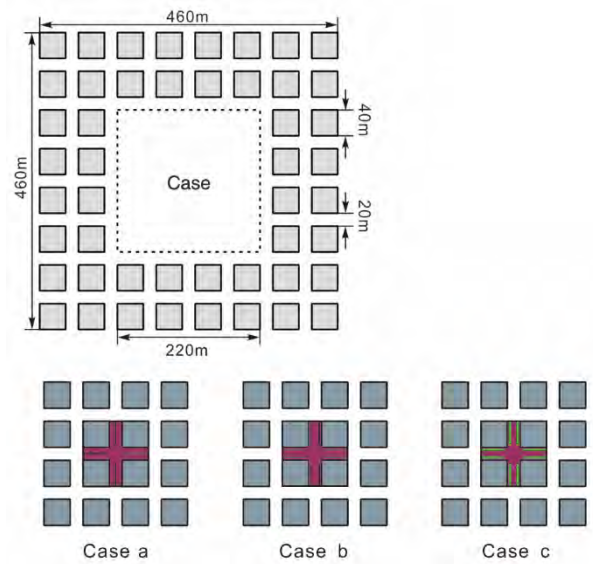
Figure3. Sketch of the model considered in the CFD simulations

In the case simulation, the wind direction is 0 ° and 45 °. In Figure 4, taking 0 ° as an example, the calculation domain and boundary conditions used in the CFD simulation are shown.
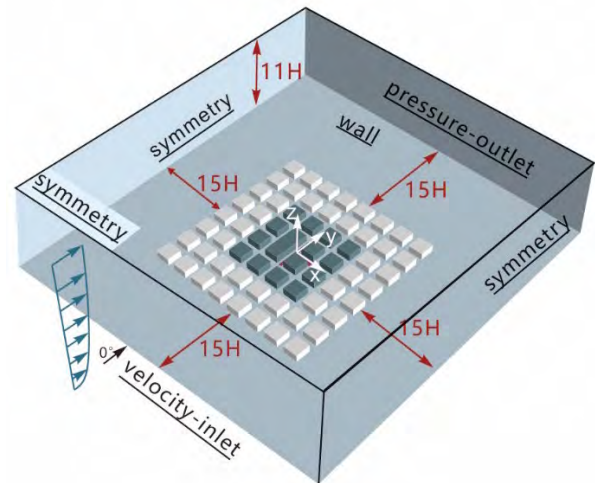
Figure4. Computational domain and boundary conditions used in CFD simulations for 0°

These simulations were performed using ANSYS fluent 16.0. And we choose a standard k-ε model to close the turbulence equation. At present, many scholars have adopted the k-ε standard to study the ventilation and pollutant diffusion of urban streets, and the results are within the acceptable range.

In all the cases considered, the convergence criteria were met after about 3500 iterations using a mesh size of approximately 2460000 cells. The mesh size were selected based on the results of the mesh independent tests. The minimum grid in the intersection area is 0.025 h, i.e. 0.4 m.

The case simulation condition setting in this article has been compared with the urban wind environment simulation and the porous plant simulation, and is

compared with the case of the Japanese Architecture Society (AIJ). Relevant wind tunnel test models and experimental data can be obtained on the official website of the Architectural Society of Japan (AIJ Guideline for Practical Applications of CFD to Pedestriau Wind Environment around Buildings).

This article uses the purging flow rate (PFR) and net escape velocity (NEV). PFR is one of the most important indicators for determining the effectiveness of local ventilation. It can be considered as an indicator for studying the efficiency of local ventilation and refers to the air flow required to effectively remove air pollutants outside the area (KatoIto & Murakami, 2003).

Results

The concentration of pollutants at intersections with height of 0.5 m, 1.5 m and 5 m is shown in Figure 5 when there are no plants（Case NA） and Case a, b and c with plants. At 0.5 m, 1.5 m and 5 m sections, the concentration of pollutants decreased sequentially. Case NA-0 pollutant concentration is mainly concentrated on the downstream of the Y-axis street and the downwind side of the X-axis street. The flow velocity and pollutant concentration distribution of each height of a-0 are relatively symmetrical. The concentration of pollutants in the streets in the Y-axis direction has been significantly increased, especially at the entrance of the downstream streets, the accumulated pollutants in the upstream are blocked by the downstream shrubs. So that the concentration of pollutants in this area is obviously increased. The high concentration of pollution in this area may have an adverse effect on human health. It is noteworthy that the highest concentrations at 0.5 m, 1.5 m, and 5 m can reach respectively, 0.95 g/m^3, 0.81 g/m^3 and 0.57 g/m^3. The average concentration and distribution of Case b-0 are basically the same as Case a-0, and there is no obvious change. Due to the barrier effect of the forest canopy on ventilation, the concentration of Case c-0 pollutants at all heights increased significantly, especially on both sides of the Y-axis street and the center of the intersection. The average concentration of each section can reach 0.46 g/m^3, 0.41 g/m^3 and 0.26 g/m^3, and the maximum concentration can reach 2.30 g/m^3, 1.99 g/m^3 and 0.83 g/m^3, respectively.

(a)

(b)

CO concentration[g/m³]

0.0 0.1 0.2 0.3 0.4 0.5 0.6 0.7 0.8 0.9 1.0
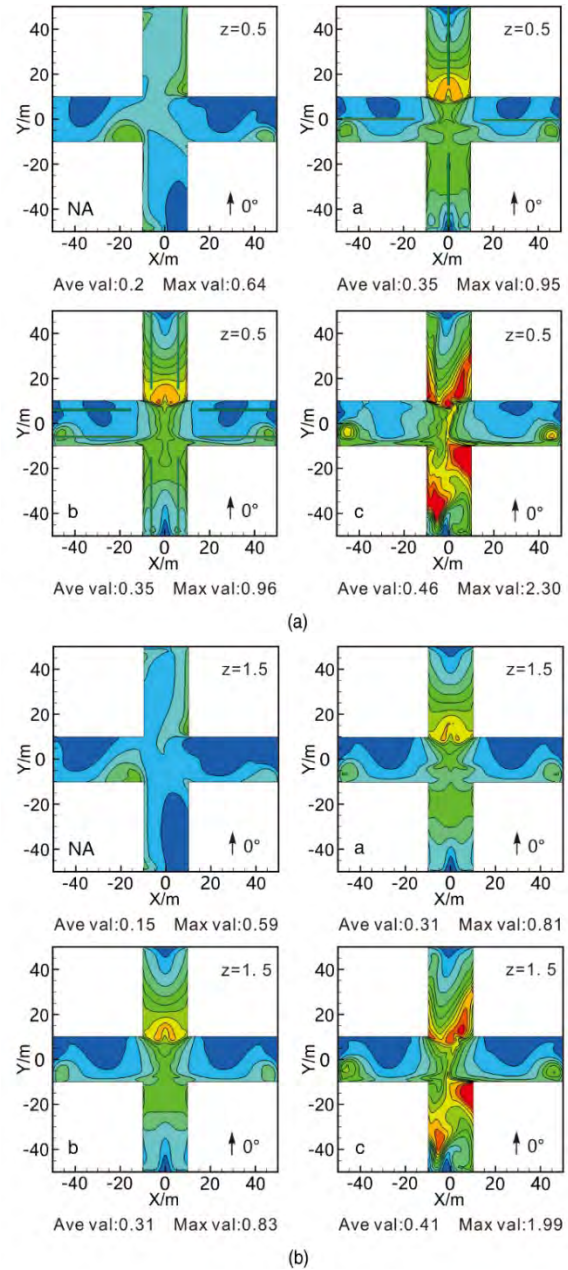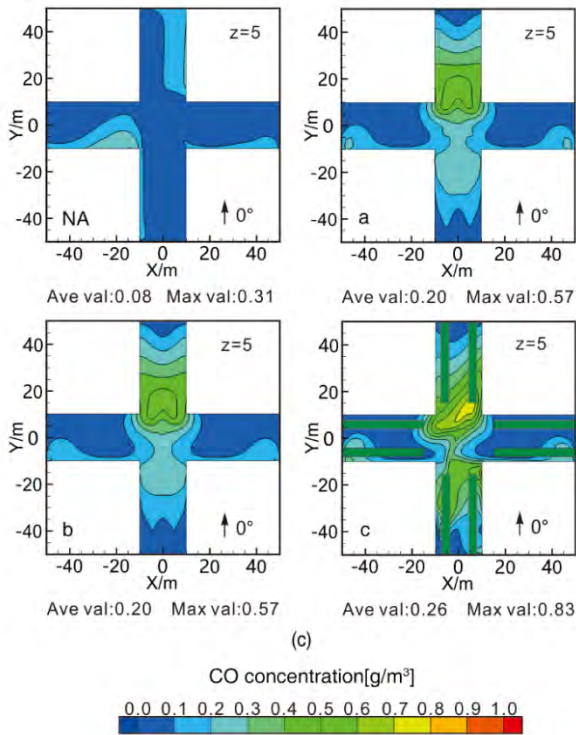
Figure 5. Case NA-0, a-0, b-0, c-0 central intersection at the height of 0.5m, 1.5m, 5m

When the wind direction is 45 °, the pollutant concentration drops sequentially at heights of 0.5 m, 1.5 m, and 5 m, as shown in Figure 6. The concentration at 45 ° is slightly higher than that at 0 °. Case NA-45 pollutant concentration is mainly concentrated on the leeward side and corner of the building. At heights of 0.5 m, 1.5 m and 5 m, the maximum concentrations can reach 0.66 g/m^3, 0.58 g/m^3 and 0.35 g/m^3, respectively. The average concentration and maximum concentration of pollutants in each height section of Case a-45 decreased slightly. At 0.5 m, due to the effect of shrubs, the horizontal diffusion of pollutants was blocked, the vertical diffusion capacity of pollutants was increased, and the concentration of pollutants on the windward and leeward surfaces decreased. In the direction of the Y-axis, the concentration of street pollutants increased significantly, especially at the entrance of downstream streets, where the pollutants accumulated upstream and were blocked by the downstream bushes, which significantly increased the concentration of pollutants in the area, and adverse health effects. The two rows of shrubs in Case b-45 can improve the air quality at the intersection, and reduce the average concentration and maximum concentration at each height. The maximum pollutant concentration is mainly distributed around the two rows of shrubs, unlike Case a-45. The concentration of pollutants in the center is low. Due to the influence of the canopy, the pollutant concentration of Case c-45 increased, especially the local pollutant concentration of the two streets in the downstream wind direction and the leeward side of the building in the lower right corner of the figure. The average pollutant concentration at each height was 0.32

g/m^3, 0.27 g/m^3 and 0.12 g/m^3, and the maximum concentration was 0.98 g/m^3, 0.92 g/m^3 and 0.66 g/m^3, respectively.
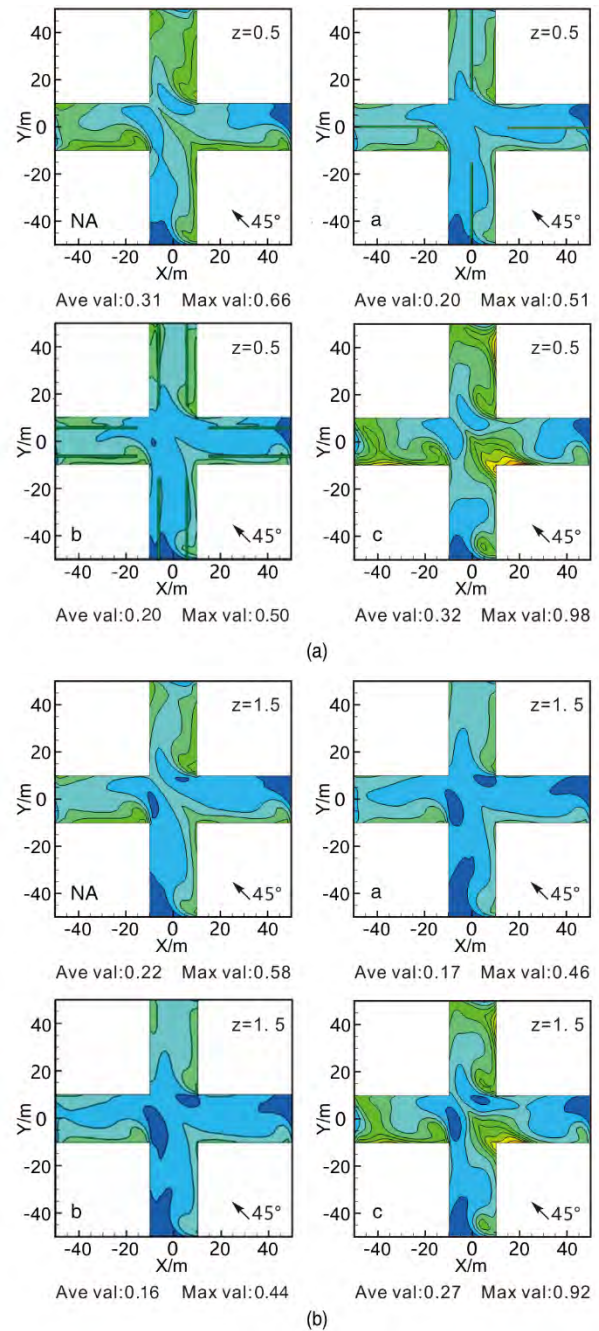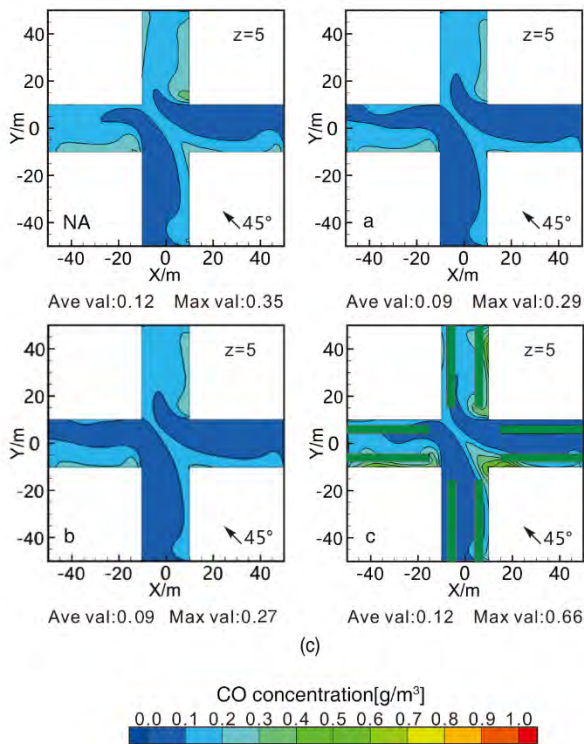
Figure 6. Case NA-45, a-45, b-45, c45 central
intersection at the height of 0.5m, 1.5m, 5m

Discussion

As shown in Figure 7, the light histogram shows the average wind speed in Case NA-45 without greening, and the dark histogram shows the average speed in the intersection after different greening is arranged. The average speed of the intersections with plants at different heights is changed. Figure 7a is the comparison of the average wind speed in the height direction of the center intersection Case a-0, Case a-45 and Case NA-0, Case NA-45. Figure 7b comparison of the average wind speed in the height direction of the central intersection of Cases b-0, Cases b-45 and Cases NA-0, Cases NA-45. Figure 7c shows the comparison of the average wind speed in the height direction of the central intersection of Case c-0, Case c-45 and Case NA- 0, Case NA-45. At 0 ° wind direction, compared with Case NA-0, the average wind speed of each height section of each intersection with greening has a significant decrease, especially the section of 1.5 m to 10 m, the average speed drop More than half of them, the speed change is very obvious. At 45 ° wind direction, it can be found that the average velocity in the sections Case a-45 and Case b-45 is increased compared to the case without greening, but the impact of greening is relatively small. Case c-45 due to the effect of greening, the average speed of each height section has been reduced. In addition, it was also found that the average speed and wind speed of the headspace had a very significant drop, which means that the condition of the two rows of trees has a certain effect on the air exchange at the top of the intersection building.
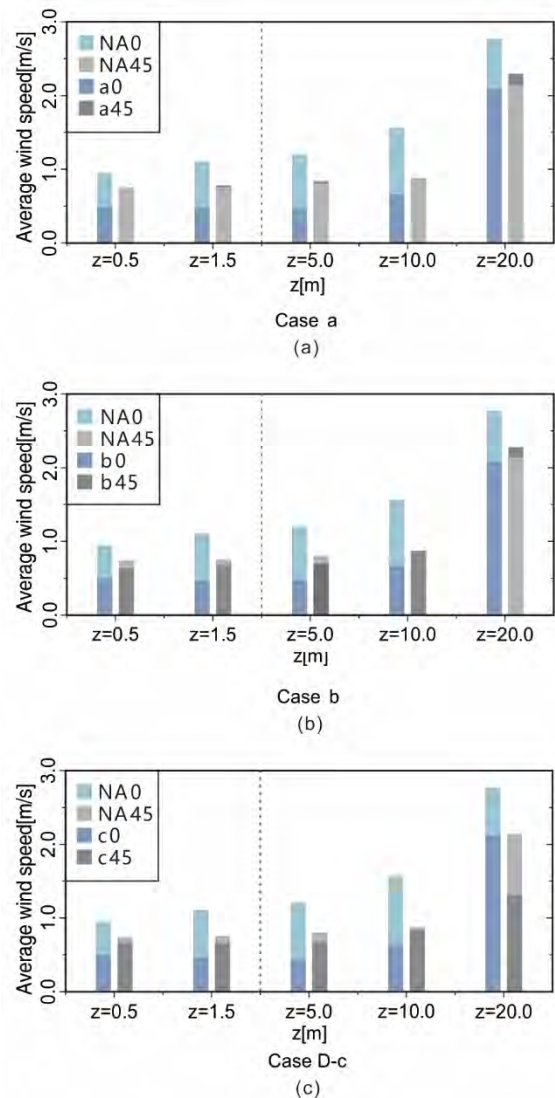
Figure 7. a) Comparison of the average wind speed in the height direction of the central intersection between Case a-0, a-45 and Case NA-0, NA-45; b) comparison of average wind speed in the height direction of Case b-0, b-45 and Case NA-0, NA-45; c) Comparison of average wind speed in the height direction of Case c-0, c-45 and Case NA-0, NA-45

As shown in Figure 8, the light-colored histogram represents the average concentration in Case NA-45 without greening, the light-colored dots represent the maximum concentration, and the dark-colored histogram represents the average in the intersection after different greenings concentration, dark-colored circles indicate the maximum concentration. This series of graphs quantifies the average concentration and the degree of change of the maximum concentration at different heights of intersections containing greenery. Figure 8a is the comparison of the average concentration and the maximum concentration in the height direction of the center intersection Case a-0, Case a-45 and Case NA-0, Case NA-45, Figure 8b shows comparison of the average concentration and the maximum concentration in the height direction of the Case b-0, Case b-45, and Case NA-

0, Case NA-45. Figure 8c shows the comparison of the average concentration and the maximum concentration in the height direction of the central intersections of Case c-0, Case c-45 and Case NA-0, Case NA-45. At 0 ° wind direction, the average concentration of each height section of each intersection containing plants has a significant increase compared to Case NA-0, especially in Case c-0, the average concentration of each section has been increased. More than half, the concentration change is very obvious. At 45 ° wind direction, it can be found that Case a-45 and Case b-45 have improved the average concentration in the cut surface, and the degree of decrease is most obvious at the cut surface of 0.5 m, which is reduced by nearly 0.3 g/m^3. In Case c-45, due to the action of plants, the average concentration of the bottom of the cut surface has increased, and it has little effect on the central and top areas. On the contrary, the average concentration of Case c-45 decreased slightly at the section of 5 m and 10 m, which was due to the role of the tree canopy to block some upward diffusion pollutants. At 0 ° wind direction, the average concentration of each section of each case increased, especially in Case c-0, which is three times as much as the original, the maximum pollutant concentration at the bottom 0.5 m and 1.5 m reached 2.3 g/m^3 and 1.99 g/m^3, respectively. At 45 ° wind direction, the single-row shrub arrangement in Case a-45 and the double-row shrub arrangement in Case b-45 both reduced the maximum pollutant concentration and had an improved effect on the air quality in the intersection. For Case c-45, greening has a significant impact on the maximum concentration of pollutants in the street, greatly increasing the maximum concentration of pollutants at various heights, especially at 0.5 m and 1.5 m, the maximum concentration of pollutants can reach 2.3 g/m^3 and 1.99 g/m^3.
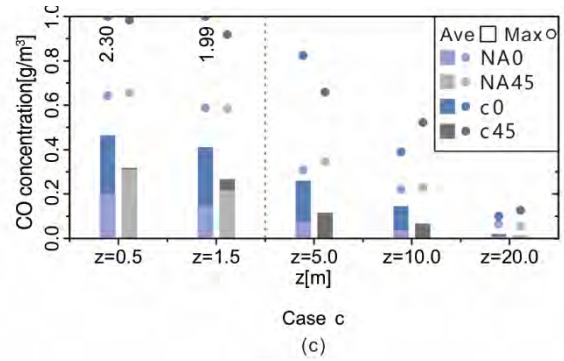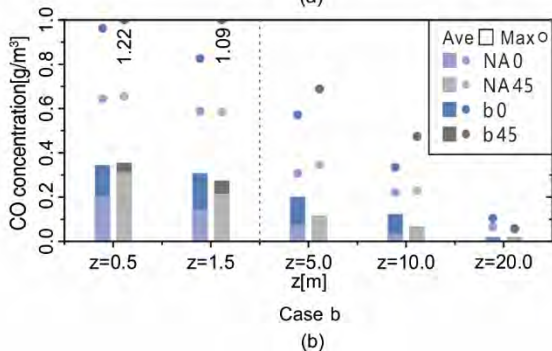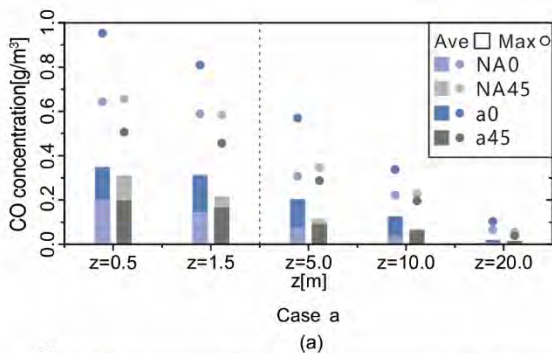
Figure 8. a) Comparison of average concentration and maximum concentration in the height direction of Case a-0, a-45 and Case NA-0, NA-45; b) Comparison of average concentration and maximum concentration in the height direction of Case b-0, b-45 and Case NA-0, NA-45; c) Comparison of average concentration and maximum concentration in the height direction of Case c0, c45 and Case NA-0, NA-45

Figure 9 is based on the Case NA-0 and Case NA-45 without greening, analyzes the extent to which the average speed and average concentration of different areas at the pedestrian height in the intersection are affected by plants. As seen from the velocity and pollutant clouds above, at 0° wind direction, the velocity and pollutant clouds are symmetrically distributed along the Y-axis coordinate, and the velocity in the downstream area is small and the concentration of pollutants is large. At 45° wind direction, the velocity and pollutant clouds are distributed symmetrically along the Y = -X-axis.

It can be found from Figure 9a that when the wind direction is 0 °, the average wind speed in the areas A and B of each case has decreased by at least 25%. In particular, the area A is greatly affected by plants, at least a 60% drop. The difference between the forms of single-row shrubs, double-row shrubs, and double-row trees are small. Shrubs have a relatively large impact on area A, and area B is greatly affected by double-row trees. At 45 ° wind direction, it can be found that area A in Case a-45 and Case b-45 is affected by plants, and the average wind speed has increased. The average wind speed in each area of the remaining cases has decreased, and the highest can be reduced by nearly 40%. When the wind direction is 45 °, the wind speed decreases more obviously in area B due to the influence of plants, especially in the case of double-row trees; the average wind speed in area A is relatively less affected by plants, especially in case a, double-row trees can reduce The average wind speed of nearly 20%.

From Figure 9b, we can find that when the wind direction is 0 °, the plants have a greater influence on the average concentration in the A and B areas. In particular, the average concentration in area A has at least doubled. Relatively speaking, the effect of plant morphological arrangement on concentration is not very obvious. Double-row trees will increase the average pollutant concentration in the area by more than 125%. Due to the effect of shrubs in area B, the average concentration of

pollutants increased by about 50%; the effect of double-row trees was more obvious, causing the average concentration of pollutants in the area to increase by about 80%. When the wind direction is 45 °, it can be found that the concentration of pollutants in areas A and B of Cases a-45 and b-45 has decreased, and the air quality in this area of the shrub structure has an improving effect. Both rows of trees increased the average pollutant concentration in areas A and B. The average concentration in area B was relatively significantly affected by plants. Due to the accumulation of more pollutants in the local area near the ground, a larger concentration of pollutants was produced.
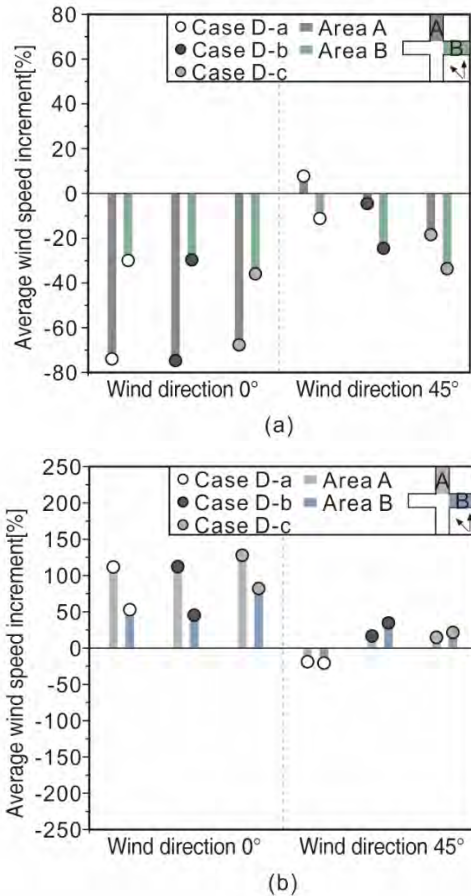
Figure 9. a) Effects of plants on average street speed at different intersections; b) Effects of plants on the average concentration of streets at different intersections.

The ventilation indexes PFR and NEV of Case a, Case b, Case c, and Case NA are shown in Figure 10. When the wind direction is 0 °, in the absence of greening, the ventilation performance below 2 m is good, the ventilation index PFR exceeds 430 m^3/s, and the ventilation index NEV exceeds 0.1 m/s; The ventilation indexes PFR and NEV of Case a-0, Case b-0, Case c-0 have decreased significantly, which means that the ventilation performance of the space area has gradually deteriorated. The PFR of Case a-0 and Case b-0 exceeds 200 m^3/s; The PFR of case C-0 is relatively lower, in contrast, the ventilation performance is poor. From here,

we can find that the presence of greening has a greater impact on the ventilation performance of spaces below 2 m at 0 ° wind direction: in the presence of plants, the ventilation performance will be significantly reduced; The effect of the performance is close, and the effect of double-row trees is relatively large. When the wind direction is 45 °, compared with the Case NA-0, the ventilation performance of the Case NA-45 without greening has decreased, the ventilation index PFR is only 280 m^3/s, and the NEV is 0.07 m/s. It can be seen from the figure that when there is a 45 ° wind direction, the ventilation indicators of the Case a-45, Case b-45 and Case c-45 with plants exist are not significantly different from those at 0° wind direction. At 45 ° wind direction, the ventilation indexes PFR and NEV of Case a-45 and Case b-45 are slightly higher than that of Case NA-45, while the ventilation indexes PFR and NEV of Case c-45 are slightly lower than that of Case NA-45. Generally speaking, the influence of plants is relatively small on the intersection with 45 ° wind direction. Single row shrub and double row shrub structure have the ability to improve the ventilation performance, while a double row tree structure will have a negative impact on the space below 2 m in this area.
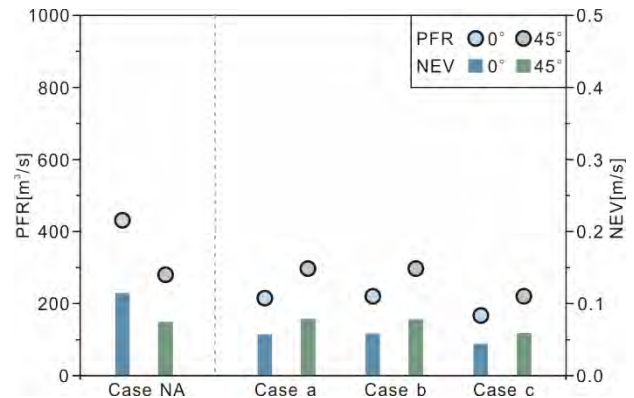
Figure 10. Ventilation index value of Case a, Case b, Case c

Conclusion

This paper focuses on the research task of the influence of greening on the ventilation performance of the cross street intersection, simplifies the shape of the cross street intersection, establishes an ideal intersection model, studies the basic air flow mode and pollutant diffusion situation in the intersection through the numerical simulation method, and compares the ventilation situation of each case through the ventilation index. For the ventilation performance of the pedestrian space area at the bottom of the intersection, the presence of plants has a great impact on the ventilation performance. In the presence of plants, the ventilation performance will be significantly reduced. The impact of single row and double row shrubs on the ventilation performance is similar, especially the impact of double row trees. When the wind direction is 45 °, the influence of plants on the ventilation in the cross street intersection is relatively small, among which the single row and double row shrub

structures have the ability to improve the ventilation performance, while the double row tree structure will have a negative impact on the space below 2 m in the area.

References

Ahmad K, Khare M, Chaudhry K K. Wind tunnel simulation studies on dispersion at urban street canyons and intersections - A review[J]. Journal of Wind Engineering & Industrial Aerodynamics, 2005, 93(9):697-717.

AIJ Guideline for Practical Applications of CFD to Pedestriau Wind Environment around Buildings. AIJ Guideline for Practical Applications of CFD to Pedestriau Wind Environment around Buildings.

Bealey, W. J., McDonald, A. G., Nemitz, E., Donovan, R., Dragosits, U., & Duffy, T. R., et al. (2007). Estimating the reduction of urban PM10 concentrations by trees within an environmental information system for planners. *Journal of Environmental Management, 85*(1), 44-58. Chen, D., Wang, X., Thatcher, M., Barnett, G., Kachenko, A., & Prince, R. (2014). Urban vegetation for reducing heat related mortality. *Environmental Pollution, 192*, 275-284.

Gago, E. J., Roldan, J., Pacheco-Torres, R., & Ordóñez, J. (2013). The city and urban heat islands: A review of strategies to mitigate adverse effects. *Renewable and Sustainable Energy Reviews, 25*, 749-758.

GILL, S. E., HANDLEY, J. F., ENNOS, A. R., & PAULEIT, S. (2007). Adapting Cities for Climate Change: The Role of the Green Infrastructure. *Built Environment (1978-), 33*(1), 115-133.

Hlavinka M W, B. J. A. (1988). Validation of Mobile Source Emission Estimates Using Mass Balance Techniques. *Air Repair, 38*(8), 1035-1039.

Kato, S., Ito, K., & Murakami, S. (2003). Analysis of visitation frequency through particle tracking method based on LES and model experiment. *INDOOR AIR, 13*(2), 182-193.

McDonald, A. G., Bealey, W. J., Fowler, D., Dragosits, U., Skiba, U., & Smith, R. I., et al. (2007). Quantifying the effect of urban tree planting on concentrations and depositions of PM10 in two UK conurbations. *Atmospheric Environment, 41*(38), 8455-8467.

Nowak, D. J., Crane, D. E., & Stevens, J. C. (2006). Air pollution removal by urban trees and shrubs in the United States. *Urban Forestry & Urban Greening, 4*(3-4), 115-123.

Rui, L., Buccolieri, R., Gao, Z., Ding, W., & Shen, J. (2018). The Impact of Green Space Layouts on Microclimate and Air Quality in Residential Districts of Nanjing, China. *Forests, 9*(4), 224.

Rui, L., Buccolieri, R., Gao, Z., Gatto, E., & Ding, W. (2019). Study of the effect of green quantity and structure on thermal comfort and air quality in an urban-like residential district by ENVI-met modelling. *Building Simulation, 12*(2), 183-194.

Tallis, M., Taylor, G., Sinnett, D., & Freer-Smith, P. (2011). Estimating the removal of atmospheric particulate pollution by the urban tree canopy of London, under current and future environments. *Landscape and Urban Planning, 103*(2), 129-138.

CFD Simulation Delivered as SaaS for Building and HVAC Design Testing

Jon Wilde

VP Customer Success

SimScale GmbH, Munich, Germany

Abstract

This paper discusses the application of cloud-based simulation in the early stages of an HVAC and building design process. Its goal is to show the benefits of the technology through a thermal comfort case study. The simulation was run in a standard web browser, using the cloud-based simulation platform, SimScale. Its results demonstrate the value that SaaS-based simulation has in the architecture, engineering, and construction (AEC) industry.

Introduction

With increasingly high demands for indoor air quality, thermal comfort, and energy efficiency, engineers and architects have a multitude of factors to account for in the building design process. Furthermore, in complying with industry standards, such as ASHRAE 55 [1], ISO 7730 [2], and EN 16798-1:2019 [3], all should be assessed long before construction.

Facilitated by the emergence of cloud computing, computer-aided engineering (CAE) technology is now being delivered by different providers in the form of SaaS solutions. This increases the technology's accessibility and ease of use. Online CAE or engineering simulation has become part of the design testing process, as engineers virtually test indoor climates, measure air quality, ensure thermal comfort, and assess energy efficiency in industrial, residential, and commercial buildings.

This paper will illustrate how a particular type of simulation, computational fluid dynamics (CFD), can be used to understand how thermal comfort is impacted in different design scenarios. The research assesses the capability and value of CFD simulation for preliminary design studies and how it might impact the design of high-performance buildings.

The investigation is supported by a case study that simulates a multi-storey residential building, which was tested with the goal of achieving excellent thermal comfort and energy efficiency.

CFD Simulation and the Emergence of SaaS Solutions

Today, around 1 out of 20 engineers who could benefit from simulation in their product development process have access to simulation tools. The low numbers are tied to large upfront hardware and software investments and steep learning curves.

The expertise that users need in order to operate most simulation software packages is significant. Consequently, proving the added value of traditional simulation tools might take several months. That is where the so-called on-demand software model, more commonly known as "SaaS", comes into play.

SaaS stands for "Software as a service" and is a cost-effective and simple concept. Instead of purchasing a license for a software package—as is the standard for traditional tools—users can rent a product (usually via a monthly or yearly subscription). In SimScale's case, for example, which is a SaaS application for engineering simulation, the platform is hosted on Amazon Web Services (AWS).

Through leveraging high-performance computing (HPC), rather than classical local and on-site hardware, one can scale the number of processing

units for a specific problem to both drastically reduce the simulation time as well as parallelise different simulations to help engineers make design decisions.

It is also necessary to have a way to visualize results, which is decoupled from the hardware and allows engineers and designers to make decisions in real-time.

Through the democratization of CAE, there is now a broader range of professionals using simulation, from hobbyists to simulation experts. This democratization has made simulation accessible to a far wider audience than in the days of traditional CFD.

One thing stays the same, however; that is the process of how CFD works "behind the scenes".

1. Creating the CAD model
2. Assigning known inputs
3. Solving/Simulating
4. Post-processing (where the results are visualized)

Often, based on the simulation results, the CAD model is then altered and the design is improved, forming an iterative design process.
For the largest impact, simulation should be utilised in the concept and design phase of a product development cycle.

SaaS solutions fill this growing need for on-demand CFD simulation capabilities by leveraging the performance as well as scalability of HPC systems and eliminating high upfront costs and software licensing. For solutions like SimScale, everything is compactly embedded into a web browser to run sophisticated simulations without compromising on simulation performance or security.

Challenges in Building Design and HVAC Design

Along with the standard concerns for structural integrity, aesthetics, and wind effects, every design project has to meet certain requirements. Residential and commercial buildings need to ensure proper thermal comfort while optimizing for energy

consumption, hospitals require high standards of indoor air quality and very specific airflow patterns, factories need measures for contaminant control and underground parking lots must be prepared for fire safety and smoke management.
All of these projects and their challenges have one thing in common; they rely on a well-designed heating, ventilation and air conditioning (HVAC) system.

The process of planning the HVAC system for a building takes into account multiple factors; from the macro, such as the building's position, wind exposure or entrance locations to micro, such as positioning of supplies and returns, windows, heaters, type of insulation, room dimensions, the capacity of the HVAC system, as well as the number of occupants or even positioning of furniture.

All of these elements should be considered in the design phase, and this cannot be done without a proper testing procedure. While standard calculations and data do part of the work, they are often insufficient in assessing a building's performance, especially when regulations need to be met.

Case Study: CFD Analysis of a Multi-Storey Residential Building

One of the main tasks for an HVAC engineer is to design a highly energy efficient system that guarantees indoor air quality and thermal comfort that ensures the safety and wellbeing of its occupants. This is no easy process as a large number of variables need to be taken into consideration. Among these factors are the building materials and layout, the number of occupants, the sources of heat and/or the supply/extract of air to name a few. There are multiple ways an HVAC engineer can tackle the challenge that this task comes with. One effective solution, when dealing with large and complex systems, comes through the use of CFD simulation as a numerical prediction tool. CFD allows the engineer to gain insights into the performance of the HVAC design.
In this project, created online with SimScale, a three-story residential building was simulated in order to validate the effectiveness of the HVAC system, the

indoor air quality, and the thermal comfort in typical summer and winter conditions.

As per ASHRAE 55, the thermal comfort of humans can be determined with two variables; the predicted mean vote (PMV) and the predicted percentage dissatisfied (PPD). ASHRAE 55 states that the PMV is "an index that determines the mean value of votes of a group of occupants on a seven-point thermal sensation scale". The different thermal sensations are shown in the legend below.
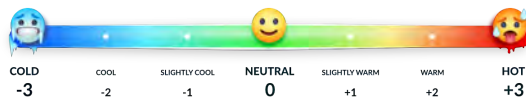
Figure 1: PMV seven-point thermal sensation scale

The PMV value uses six different factors;
1. The predicted occupant metabolic rate
2. Clothing insulation
3. Relative humidity
4. Airspeed
5. Air temperature
6. Mean radiant temperature

In addition to the PMV, the PPD shows the likeliness of local discomfort by the occupants. Amongst the main factors that adversely impact the comfort of occupants are, on one end of the spectrum, too much air movement (this can feel like strong drafts) and on the other end, too little airflow (feels like warm, stale air). In the simulated scenario, all the factors described above will be taken into consideration and PMV will be used to assess thermal comfort.

Model of the Building and Its Environment

The CAD model to be simulated is a three-story apartment building in the city of Munich, with one apartment at each level. The ground floor is made of a 46m² apartment and a 12.6m² office, the first floor apartment is 58.5 m² with a TV room, and on the second floor, there is a 55m² apartment with a 3.2m² balcony. Below the office floor, there is a garage,

which is not included in the CAD model. This section is assumed as an unheated space. There is a hallway on the north side of the building. This part is also not included in the CAD model. In each apartment, two occupants are represented, along with furniture, kitchen countertops, wardrobes, tables, and chairs. In the office, one person is modeled, also with simplified furniture shapes. Supplies and extracts are included and without any of the associated duct work. The level of detail of such a model is minimised to ensure a reasonable computational time while maintaining a good level of accuracy.
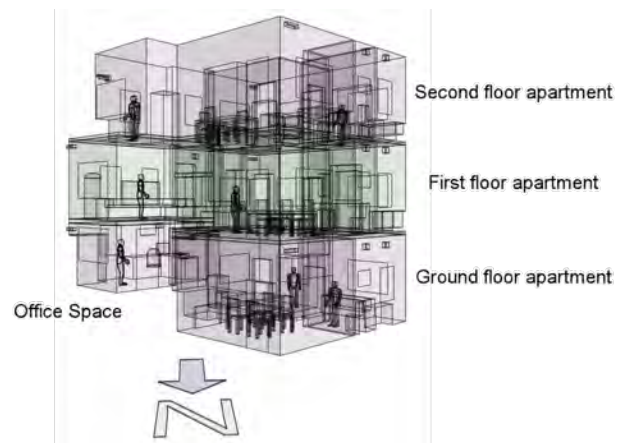
Figure 2: Model of the multi-storey residential building tested in this project

The analysis includes airflow distribution throughout the three apartments and the office. The concrete slabs between the apartments would allow the heat to be transferred through thermal conduction (this model is assuming there are no air gaps or thermal bridging).

Both summer (34°C) and winter (-16°C) scenarios will be considered, with an ambient humidity of 50%.

Direct Normal Irradiance (DNI) for summer and winter seasons are selected based on the coldest and warmest days of the seasons, although both were simulated around midday so the winter scenario is not worst-case.

Within the specified time range, average DNI loads for winter and summer seasons are calculated as 168W/m² and 417 W/m² respectively. The solar load is added only on the windows facing South-East and

South-West. Only 75% of the DNI is assumed to pass through the windows, to account for reflectivity and the frames.

All heat transfer coefficients and conductance used in this project have been determined according to EN ISO 6946 [4] and EN ISO 10077 [5]. An external heat transfer coefficient of 25 W/(K.m²) is applied on all external walls, doors, and windows. The floor of the building is assigned a high heat transfer coefficient with the ground at 4.5°C for winter and 29.25°C for summer.

According to ISO 6946, an unheated space can be considered as an additional layer with a specific thermal resistance. The transfer coefficient between the office space and garage ceiling is applied as 4.21 W/(K.m²). The apartment entrances are connected to an unheated hallway, therefore a heat transfer coefficient of 2.08 W/(K.m²) is applied to doors and hallway walls. The heat transfer between the air and internal walls is calculated by the solver, based on the local air velocity and temperature.

The apartment block is considered to be equipped with highly insulative components. This project uses thermal conductance as a measure of the thermal insulation. This measure is described in the EN ISO 6946 and EN ISO 10077 standards as the rate of heat transfer through a material. This is usually a composite and the value represents the real-world performance of the materials.

In this project, the thermal conductance through the frame and sash of door and windows was omitted for simplification purposes. The following table shows the conductance values of the building components.

Component	Thermal conductance (W/(K.m²))
Walls	0.32
Double Glazed Windows	2.2
Door	2.55
Roof	0.13
Office Floor (above garage)	0.13
Floor	0.13

Table 1: Typical thermal conductance values [6] [7]

Indoor Air Quality

With any modern building, indoor air quality (IAQ) is of huge importance. This focuses on Ventilation Effectiveness (pollutants, CO2 and other particulates) and Air Change Effectiveness (age of air and fresh air rates).

In this project, to fully control thermal comfort, the constant renewal of air is guaranteed through continuous mechanical ventilation. The outdoor air supplied to the rooms is distributed through hidden ductwork.

Winter Heating Strategy

For the winter scenario, the heating strategy utilizes radiators placed throughout the rooms of the apartments. These devices are usually placed under windows. The windows' thermal transmittance is higher than the walls' and therefore their surfaces would generally be colder. By placing the heaters directly under the windows, the hot air generated would rise and act as an air shield, preventing the cold air from penetrating further towards the center of the rooms.

The power required for the radiators to maintain an average temperature of 21°C was estimated with a hand calculation. This gives a good starting point for a CFD calculation. While the details of the calculations are not presented in this study, the results for the heating requirements for each apartment and office are shown in the table below.

Level	Heating Requirement (W)
Office	105
Ground Floor	431
First Floor	745
Second Floor	702

Table 2: Heating requirement for each floor to reach an average of 21°C – simple hand calculation

It should be noted that the thermal mass of the building has not been considered, nor was any thermal bridging; this is merely a starting point.

For the winter scenario, the total ventilation rate Q_{tot}, per apartment is specified in Table 4.1b of the ASHRAE 62.2 [8] standard. For the $47.3m^2$, $60.4m^2$, and $58m^2$ apartment units occupied by two people, the standard recommends a 21 l/s total ventilation rate.

As there are three extraction units per apartment, the baseline design will equally distribute the outdoor air rate at 7 l/s (or 8.3g/s) among these inlets.

The outdoor air rate V_{bz} for the office falls under the ASHRAE 62.1 [8] standard calculation since it is not considered a residential space and is determined with the following formula:

$$V_{bz} = R_P \cdot P_z + R_a \cdot A_z$$

With:
V_{bz} = Outdoor air rate (l/s)
A_z = Zone floor area (m^2)
P_z = Zone population
R_p = Outdoor airflow rate required per person (l/s.person)
R_a = Outdoor airflow rate required per unit area (l/s.m²)

For a $12.6m^2$ office space occupied by one person, R_p= 2.5 l/s and R_a =0.3 l/s.m²
V_{bz} = 6.56 l/s (or 7g/s).

In this design, mechanical ventilation is considered to be operated by a mechanical ventilation heat recovery system (MVHR). This system has been widely used over the last decade in order to maximize the energy efficiency of buildings. With this installation, the outdoor air is heated up by the exhaust air through a heat exchanger before being introduced into the dwellings. High-performance, double-flow controlled mechanical ventilation units can reach up to 93% efficiency, which means that the -16°C outdoor air is heated to around 1°C by the 21°C air that was just extracted. An auxiliary heating unit then raises the temperature to the desired supply temperature. For the purposes of this project, the building is considered airtight, although leakage paths could be modelled.

Summer Cooling Strategy

For the summer scenario, cool air is supplied into the rooms. In this scenario, the ideal internal room temperature is around 24.5°C, as per ASHRAE 55. Inlet air temperature and speeds must be carefully controlled, in order to avoid any condensation inside the ducting, as well as minimising noise or high pressure losses. Finally, flow rate and temperature should be adjusted carefully, controlling the room temperature while keeping the peak velocity below 0.8m/s. This will ensure that the design remains within the targeted thermal comfort (PMV) range.

Thermal Comfort and Predicted Mean Vote (PMV)

As discussed in the first part of this study, PMV is calculated through six parameters; three of these are taken directly from the CFD results (surface temperature, velocity, and air temperature), the others are manually input (metabolic rate, humidity, and clothing coefficient).
The values for clothing coefficient and metabolic rate are provided by ASHRAE 55:

- For the winter scenario, a metabolic rate of 1.2 (cooking/cleaning) and a winter clothing coefficient of 1 (winter indoor clothing) were chosen.
- For the summer scenario, a metabolic rate of 1.2 (cooking/cleaning) and a winter clothing coefficient of 0.6 (trousers, long-sleeve shirt) were chosen.
- A humidity value of 50% was set as input for the calculation of PMV.

Figures 3, 4 and 5 describe the simulation boundary conditions (known input variables) for the winter simulation, including inlet flow rates, temperature, and internal heat loads.
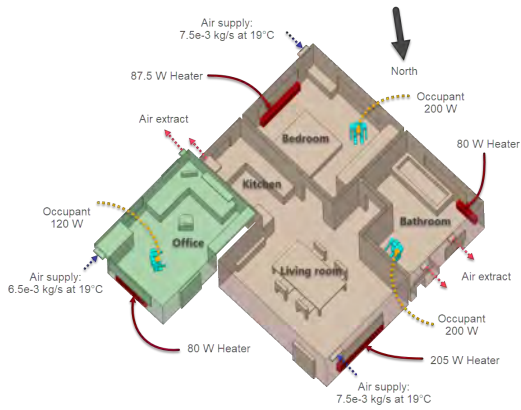
Figure 3: Simulation setup for the ground floor apartment and office

Figure 6: Simulation setup for the ground floor apartment and office
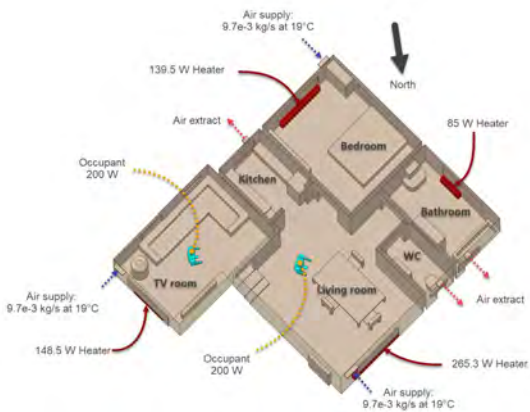
Figure 4: Simulation setup for the first floor apartment

Figure 7: Simulation setup for the first-floor apartment
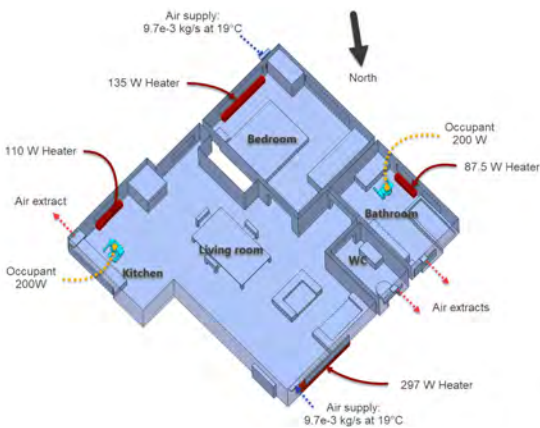
Figure 5: Simulation setup for the second floor apartment

Figure 8: Simulation setup for the second-floor apartment

Figures 6, 7 and 8 describe the simulation boundary conditions for the summer simulation, including inlet flow rates, temperature, and internal heat loads.

CFD Simulation Results – Winter

The CFD results obtained with SimScale show an accurate heat map throughout the rooms, highlighting hot spots and colder areas. In the pictures below, representing the temperature distribution at 1.5m, one can easily identify hot spots at the heaters and occupants. There are colder zones at the windows and some walls with no heater nearby.

For the ground floor apartment and the office, the temperature remains relatively evenly distributed, with locally low temperatures close to the windows, as expected. The average temperature in the ground-level apartment is 21.3°C and in the office space is 21.1°C. Note that the presence of an occupant in such a small office space (12.6m²) producing 120W of heat, contributes greatly to the heating of the space, the heater in this room producing only 105W.
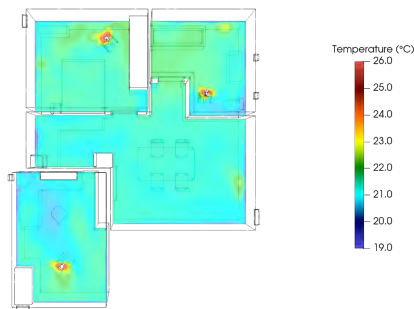
Figure 9: Heat map of the office and ground floor apartment at a height of 1.5m

The first-floor apartment average temperature is 21.7°C and the heat map at 1.5m shows stable throughout the rooms. The warm areas are located at the heaters.
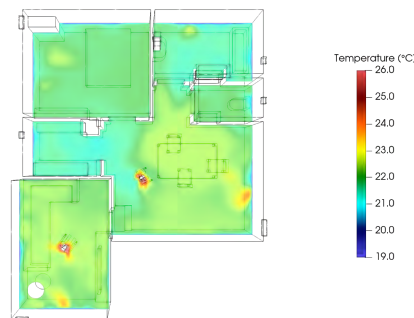
Figure 10: Heat map of the first-floor apartment at a height of 1.5m

The second-floor apartment shows the highest average temperature of all floors, with 21.8°C.
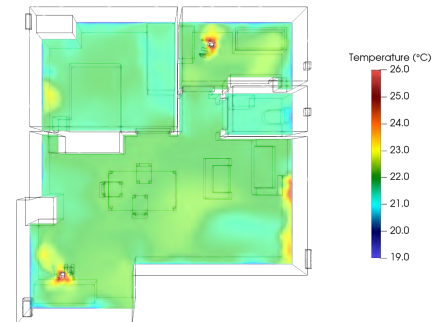
Figure 11: Heat map of the second-floor apartment at a height of 1.5m

The temperature distribution over the entire building reveals the location of the building components with the lower insulation values (or higher conductance); doors and windows are low-temperature faces. It is through these faces that most heat loss occurs and therefore the insulation is essential for energy saving.
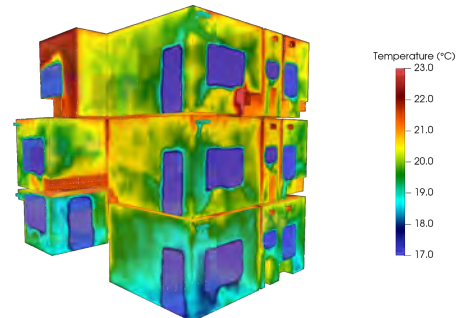
Figure 12: Temperature distribution on the external surfaces

The thermal comfort parameters (PMV) are within an acceptable range as per ASHRAE 55 and so the occupants are likely to feel comfortable. The average temperature in each room is very close to the temperature goal of 21°C (max 0.8°C difference)
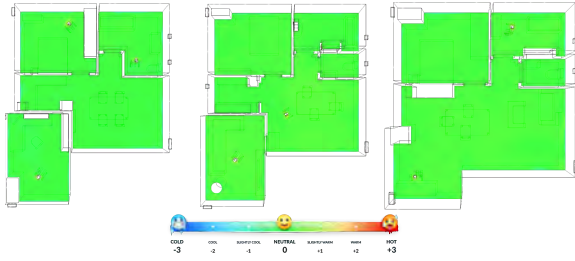
Figure 13: PMV map at a height of 1.5m in each apartment and the office (ground/office, first floor, second floor)

The air velocity results show very low values (below 0.2m/s) throughout the apartments and office, and are considered insignificant to impact PMV results.

The airflow pattern, however, highlights phenomena participating in the thermal comfort results. The heater's hot air shield effect can easily be observed in the pictures below, where the foreground slice shows that the rise of the warm air blocks a cold air pocket against the cold window surfaces. The importance of the phenomenon is clearly visible in the background where cold air is falling downwards and towards the center of the room and over the bed.
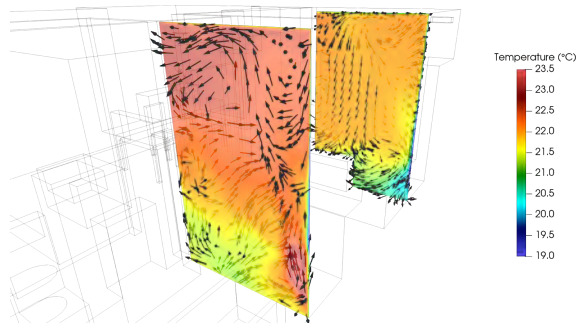
Figure 14: Temperature vertical slices in the second-floor apartment

The thermal comfort results are highly impacted by each heater placement.

CFD Simulation Results – Summer

As with the winter results, heat maps for the summer conditions are shown at 1.5m.

The ground floor apartment is 20.9C on average and the office space is 21.6°C.
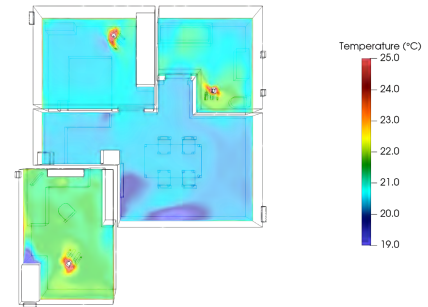
Figure 15: Heat map of the office and ground floor apartment at a height of 1.5m

The first-floor apartment is 21.2°C on average and the 1.5m high heat map, shown below, indicates a very small variance throughout the apartment temperature.
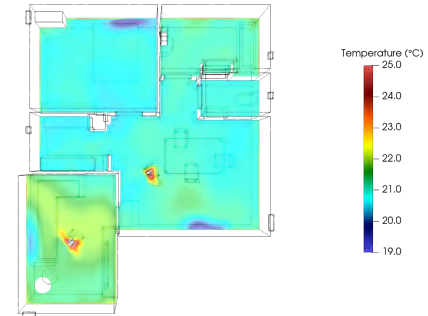
Figure 16: Heat map of the first-floor apartment at a height of 1.5m

The second-floor apartment is 21.4°C on average.

Figure 17 shows that the second-floor apartment bathroom is warmer than the rest of the apartment. This is due to the smaller space and the presence of an occupant contributing an additional 200W.
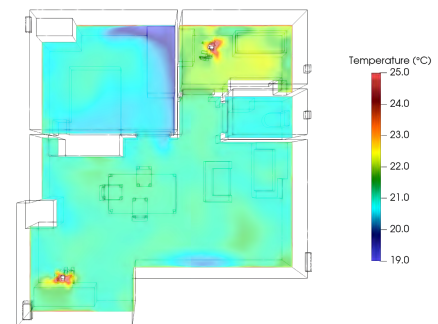
Figure 17: Heat map of the second-floor apartment at a height of 1.5m

On average, the indoor temperature is 21.4°C under summer conditions. The cooling estimation was therefore overestimated since the temperature goal was 24.5°C.

As for the winter scenario the surface temperature results, shown in Figure 18, highlight locations where most heat is transferred between internal and external environments. The windows and doors are warmer on average than the indoor temperature and therefore play a significant role in the apartments' heat gain. Solar radiation also plays a large role in adding heat to the southerly rooms.
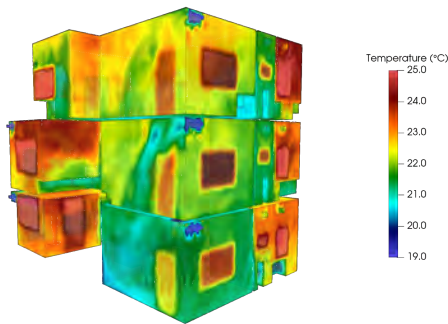
Figure 18: Temperature distribution on the external surfaces

As warm air rises, the air is warmer closer to the ceilings and the upper apartments are warmer overall. The picture below shows a sliced heat map through the row of inlets in the living rooms. Cold air enters the room and falls towards the ground due to its higher density and mild stratification is visible in each room. Visualising the air distribution helps to position the diffusers of the ventilation system appropriately and also to size them in order to ensure the appropriate air velocity and temperature as specified in ASHRAE 55.
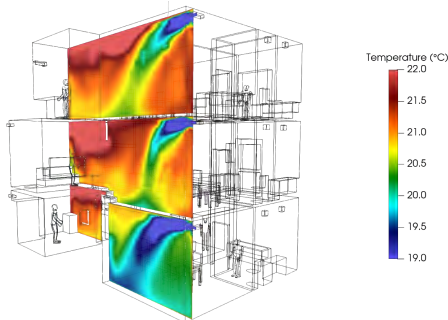
Figure 19: Vertical slice heat map showing the temperature distribution in the living rooms

The thermal comfort results are mainly satisfactory, with PMV values within the recommended range (between -0.5 and 0.5) as per ASHRAE 55. Occupants are expected to feel comfortable in this space.
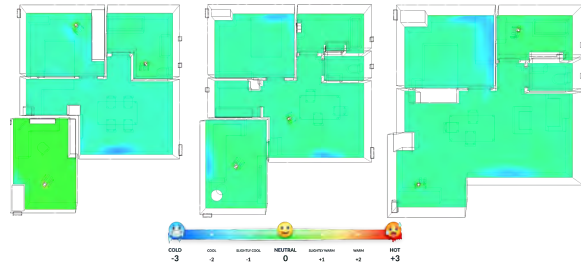
Figure 20: PMV map at a height of 1.5m in the apartments and the office (from left to right, ground/office, first floor, second floor)

Conclusion

When it comes to ensuring thermal comfort, indoor air quality and maximizing energy efficiency, CFD simulation is a convenient tool for HVAC engineers. The visualization of flow distribution can be particularly useful in solving thermal comfort issues. If used early in the design phase, it can deliver valuable information to optimise the HVAC strategy.

Energy calculations can be useful but they are not able to capture the small details. CFD provides additional insights that can significantly impact thermal comfort.

As stated above, in both summer and winter scenarios the thermal comfort is mainly within a satisfactory range and the occupants are expected to feel comfortable in this space. Some regions are outside of the recommended limits, although they are closer to the walls and rarely occupied.

To optimise this design, as the overall air speed is well below the maximum allowable 0.8 m/s, we could look to save energy through a higher supply velocity. This would mean we could spend less energy on cooling the air, which should produce a more efficient system overall. The advantage of using SaaS based CFD is that various experiments can be run in parallel. This means it is possible to assess a range of proposed designs in the time it takes to produce results for one.

References

1. Standard 55-2017 -- Thermal Environmental Conditions for Human Occupancy (ANSI/ASHRAE Approved), https://www.techstreet.com/ashrae/standards/ashrae-55-2017?product_id=1994974

2. ISO 7730:2005 Ergonomics of the thermal environment https://www.iso.org/standard/39155.html

3. EN 16798-1:2019 Energy performance of buildings. Ventilation for buildings. https://shop.bsigroup.com/ProductDetail?pid=000000000030297474

4. ISO 6946:2017, Building components and building elements; Thermal resistance and thermal transmittance; Calculation methods, https://www.iso.org/standard/65708.html

5. EN ISO 10077 Thermal performance of windows, doors and shutters https://www.iso.org/standard/64995.html

6. Designing Buildings Wiki, U-values, https://www.designingbuildings.co.uk/wiki/U-values

7. ENSTO, U-values, http://www2.amk.fi/Ensto/www.amk.fi/opintojaksot/0705016/1204287624126/1240556832300/1240557351157/1240563573560.html

8. Standard 62.1-2019 -- Ventilation for Acceptable Indoor Air Quality (ANSI Approved) https://www.ashrae.org/technical-resources/bookstore/standards-62-1-62-2

Application of Coupling of CFD and Human and Clothing Thermal Response in Ceiling Mounted Localized Air Distribution Systems in Winter Conditions

Eusébio Z. E. Conceição[1*], Mª Inês L. Conceição[2], Mª Manuela J. R. Lúcio[1]
and Hazim B. Awbi[3]

[1]FCT - University of Algarve, Campus de Gambelas, 8005-139 Faro, Portugal
[2]Instituto Superior Técnico, Av. Rovisco Pais, 1049-001 Lisboa, Portugal
[3]School of Construction Management & Engineering, University of Reading, Reading, RG6, 6AW,
United Kingdom
* corresponding author: econcei@ualg.pt

Abstract

This work presents and applies a numerical model, developed by the authors in the last years, that considers the coupling of the CFD (Computational Fluids Dynamics) and HCTR (Human and Clothing Thermal Response). The coupling system, itself, generates the external occupants' surfaces and the surrounding surfaces and transfers the inputs/outputs between the CFD and HCTS numerical models.

The input of the compartment, using the CAD (Computational Aid Design), the location of the occupants and the external environmental variables are introduced in the software, while the occupants' geometry is generated by empirical equations, based in height and weight.

The study is made in a virtual chamber occupied by twelve virtual manikins, six desks and twelve seats and equipped with a new ceiling mounted localized air distribution system. The ventilated system is equipped with an inlet system, built with two horizontal ducts, and an extraction system, built with six ducts. The inlet horizontal ducts consider twelve jets located above the head and in front to the occupants' level and twelve jets located above the desk area.

In the present study the thermal comfort level, the air quality level and the ADI (Air Distribution Index) are calculated, for an inlet air velocity of 1, 3 and 5 m/s, in winter conditions. The ADI index is highest for highest inlet air velocities.

Introduction

This work is a continuation of ceiling mounted localized air distribution systems presented in Conceição et al. (2017). In this work the inlet is made above the head level and the extraction is placed in the ceiling level. Similar works about the ceiling mounted were developed by other authors, such as Yang et al. (2010) and Yang et al. (2009).

To develop a HVAC (Heating, Ventilating and Air-Conditioning) system, a numerical software is used to calculate the thermal comfort, the DR (Draught Risk) and the indoor air quality levels. However, in order to evaluate the performance of the HVAC system, namely the effectiveness for heat removal and the effectiveness for contaminant removal, it is also important to evaluate the ADI.

The DR, that considers the air temperature, air velocity and air turbulence intensity, was developed in Fanger et al. (1988). Some applications can be seen, as example, in Conceição et al. (2008).

The detailed presentation of the ADI can be seen in the works of Awbi (2004) and Conceição et al. (2013), respectively, for uniform and non-uniform environments.

In the HCTR numerical model the PMV (Predicted Mean Vote) and PPD (Predicted Percentage of Dissatisfied people) indexes, are applied in the thermal comfort level determination in a conditioned space. These indexes were developed by Fanger (1970) and adopted by international standards like ISO (2005). This standard defines three comfort categories accordingly to the occupied spaces thermal comfort requirements.

To evaluate the indoor air quality, using the CFD numerical model, the indoor carbon dioxide (CO_2) concentrations are used. ASHRAE (2016) presents values which can be considered to guarantee acceptable indoor air quality (CO_2 concentration below 1800 mg/m^3). Some applications, using the airflow rate, can be seen in Conceição et al. (1997).

The numerical software, developed by the authors, and applied in this work, considers the coupling of CFD and HCTR numerical models. Some application of the coupling methodology were presented in Conceição and Lúcio (2011) and Conceição and Lúcio (2010a).

The surrounding surfaces, used by the coupling software, used a third software that evaluates the Building Dynamic Software. This numerical model, is used to evaluate the temperature, concentration and energy in a building or vehicles. See as example, Conceição et al. (2000), Conceição et al. (2008) and Conceição et al. (2000).

These numerical software develop a new HVAC system based in a ceiling mounted localized air distribution systems. The study is made in winter typical day conditions. The thermal comfort, the indoor air quality, the DR, the effectiveness for heat removal, the effectiveness for contaminant removal and the ADI are evaluated.

The motivation of this work is to develop a new ceiling mounted localized air distribution systems with the objective to guarantee best indoor air quality and thermal comfort levels. The main idea of the system is to consider an inlet system, placed above the head level and in the occupation area, and an extraction system, also placed above the head level but in the not occupied area. The two systems are placed in the same level to facilitate the extraction of the CO_2 concentration. The inlet system considers one jet located above the head level and another jet located above the desk level, while the extraction considers six vertical ducts. The jet located above the desk level is used to improve the airflow around the occupant seated in this table and the occupant seated in front.

Numerical Model

The Human and Clothing Thermal Response numerical model (Conceição 2000), (Conceição 1999), (Conceição and Lúcio 2001) and (Conceição et al. 2010), is built by sub-models of:

- human body thermal system;
- thermoregulatory system;
- clothing system;
- thermal comfort.

This software, that simulates simultaneously a group of people, in the human body thermal system and in thermoregulatory system, evaluates:

- Human body temperature;
- Blood flow in the human body;
- Water transpiration flow;
- Blood (arterial and venous) temperature.

The HCTR numerical model works in transient conditions and in steady-state conditions. In this work, for each CFD thermal condition, the steady-state conditions were obtained.

The clothing system calculates:

- Temperature of the clothing;
- Water flow through the clothing.

Finally, the thermal comfort sub-model, that uses the PPD and PMV indexes, developed by Fanger (1970), is used to evaluate the thermal comfort level, considering all heat fluxes verified in the human body.

More details about the validation of the HCTR numerical model can be seen in Conceição (1999), in the study of

evaluation of thermal comfort and simulation of HCTR numerical model and in Conceição and Lúcio (2001), in a numerical and subjective responses of human thermal sensation.

The CFD numerical model presented in Conceição et al. (2008) that works in steady-state conditions, evaluates the:

- air temperature;
- air velocity;
- carbon dioxide (CO_2) concentration;
- turbulent kinetic energy;
- turbulent energy dissipation;
- indoor air quality level;
- DR level.

In the partial differential equations discretization, used in the CFD numerical model developed by the authors and applied in this work, the finite volume method is used. The hybrid scheme is used in the convective/diffusive fluxes. The SIMPLE (Semi-Implicit Method for Pressure-Linked Equations) algorithm is used in the velocity and pressure equations. The non-uniform methodology is used in the grid generation. The iterative TDMA (Tri-Diagonal Matrix Algorithm) method is used in the equations system resolution. The RNG turbulence model, for high Reynolds number, is used in the turbulence simulation. In the wall boundary the surface proximity is used.

The CFD numerical model simulates:

- isothermal thermal conditions (Conceição et al., 2008);
- non-isothermal thermal conditions (Conceição and Lúcio, 2016) using the k-epsilon turbulence model and (Conceição and Lúcio, 2016) using the RNG turbulence model.

The development and validation were made in Conceição et al. (2008), in a study of airflow inside office compartments with moderate environments.

In the validation, of the coupling software with the Building Dynamic model (Conceição and Lúcio, 2016), the experimental and numerical values of the chamber surface temperature, the air temperature, the air velocity, the air turbulence intensity and the DR around the occupants are compared.

The Building Dynamic numerical model (Conceição and Lúcio, 2010b), used in the study in the evaluation of surrounding surfaces, was validated in Conceição et al. (2004), in winter condition, and Conceição and Lúcio (2006), in summer conditions.

The ADI, developed in Awbi (2004) for uniform environments and adapted in Conceição et al. (2013) to non-uniform environments, uses the thermal comfort number and the air quality number. The first one considers the effectiveness for heat removal and the PPD, while the second one considers the effectiveness for

contaminant removal and the percentage of dissatisfied associated to the indoor air quality.

Numerical Methodology

The new ceiling mounted localized air distribution systems consider an inlet system, placed above the head level and in the occupation area, and an extraction system, also placed above the head level but in the not occupied area. This not occupied area, is located between the two occupation areas.

The inlet system considers one jet located above the head level and another jet located above the desk level, while the extraction considers six vertical ducts. This numerical study is made in a virtual chamber. The chamber is occupied by twelve occupants and equipped with six desks and twelve seats.

The virtual chamber, equal to an existing experimental chamber, which simulates a virtual office, with $4.5 \times 2.55 \times 2.5$ m³. The real experimental chamber is built by a wood structure equipped with an isolation material with a thickness of 3 cm.

The ventilated system is equipped with:

- an inlet system built with two horizontal rectangular ducts. Each inlet horizontal rectangular duct considers twelve jets located above the head level and in front to the occupants and twelve jets located above the desk area (see figures 1 to 4);
- an extraction system, built with six vertical extraction ducts. Each extraction duct is divided in a vertical duct, connected to a horizontal duct (see figures 1 to 4).

In the numerical simulation, made in winter conditions, the inlet air velocity is 1 (0.064 m³/s), 3 (0.19 m³/s) and 5 (0.32 m³/s) m/s.

In figure 1 is presented the scheme of the virtual chamber, equipped with ceiling mounted localized air distribution systems, using in the CFD. The figure a) represents the occupants, desks, seats and ventilation system, while b) represents only the occupants, desks and seats.

The scheme of the virtual chamber, equipped with ceiling mounted localized air distribution system, used in the HCTR is depicted in Figure 2. The Figure a) represents the occupants, desks, seats and ventilated system, while b) represents only the occupants, desks and seats. The Figure a) also includes the surrounding surfaces. The grid presented in these Figures is used in the calculation of the heat exchanges by radiation (1) between the occupants and (2) between the occupants and the surrounding surfaces of the desk and ventilation system. This Figure is used by the HCTR numerical model, but is generated in the CFD numerical model.

Figure 3 shows the location of the occupants and the identification of the number of the occupants seated in the experimental chamber.

This numerical work, that simulates a small classroom, considers four rows of students, namely, two located in the corridor side and two located in the window or wall side.
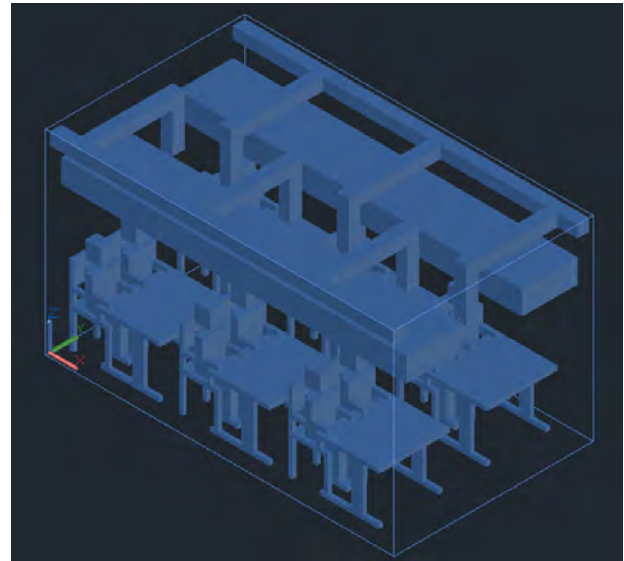
a) occupants, desks, seats and ventilated system.
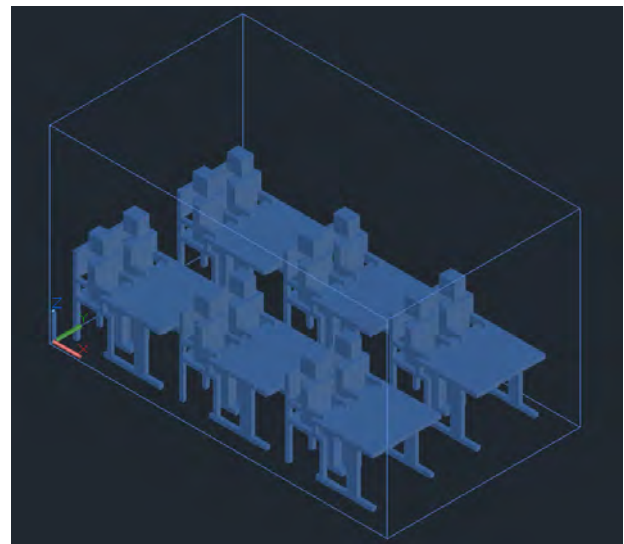
b) only the occupants, desks, seats.

Figure 1. Scheme of the virtual chamber, equipped with ceiling mounted localized air distribution systems, used in the CFD.

The students 1, 2, 7 and 8 are located in the beginning of the rows, while the students 5, 6, 11 and 12 are located in the end of the rows. In the beginning of the rows the students are only subjected to a jet located in front to the occupant, while the students located in the middle or in the final of the rows are subjected to a jet located in front and another jet located behind them.

The inlet airflow location used in the CFD numerical simulation is depicted in Figure 4. The inlet and also the outlet, are located 1.8 m above the floor level.

a) occupants, desks, seats and ventilated system.

Figure 3. Location of the occupants and identification of the number of the occupants.

b) only the occupants, desks, seats.

Figure 2. Scheme of the virtual chamber, equipped with ceiling mounted localized air distribution systems, used in the HCTR.

The occupants' clothing level, used in the HCTR numerical model, in winter conditions, is 1 clo and the activity level is 1.2 met. The clothing level, considered in this work is formed by long sleeved shirt, dust, pants, shoes and normal underwear.

a)
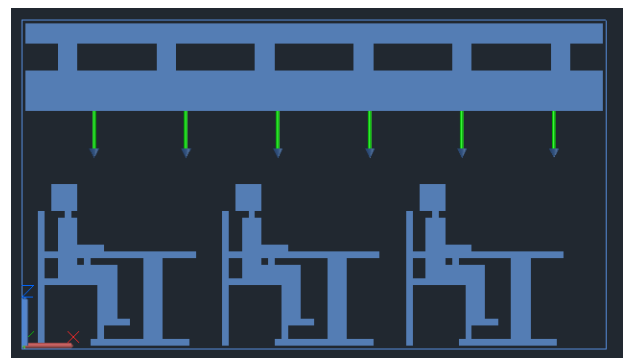
b)

Figure 4. Inlet airflow location used in the numerical simulation. a) front and b) side view.

Results and Discussions

In this section the air velocity, the air temperature, the DR and the ADI are presented.

Figures 5, 6 and 7 show, respectively, the air velocity, air temperature and DR around the occupants. Figures (a), (b) and (c) are associated to, respectively, inlet air velocity of 1, 3 and 5 m/s.

The mean values of air velocity, air temperature and DR are calculated using all values around each of the 25 occupants' sections.

The air velocity around the occupant section increases when the inlet air velocity increases and the air velocity around the occupant is relatively uniform. However, the occupants located in the corridor side, present a highest air velocity in the upper member located in the corridor side.

The air temperature around the occupants' section decreases when the inlet air velocity increases and the air temperature around the occupant sections are relatively uniform. However, the air temperature around the hands presents the lowest value, mainly when the inlet air velocity is 3 and 5 m/s.

The DR around the occupant section increases when the inlet air velocity increases. In general, the DR around the occupant is uniform. However, the occupants located in the corridor side, present a highest DR in the upper member located in the corridor side. This highest DR values are associated to highest air velocities values. The DR level is acceptable in accordance with the category C (30% of dissatisfied people) of the ISO (2005).

The obtained ADI value is showed in Tables 1, 2 and 3, respectively, when the inlet air velocity is 1, 3 and 5 m/s. In these Tables are also presented the values of effectiveness for heat removal, thermal comfort level, thermal comfort number, CO_2 concentration in the respiration area, effectiveness for contaminant removal and air quality number.

The effectiveness for heat removal decreases when the inlet air velocity increases. The effectiveness for heat removal is relatively uniform for all occupants.

The thermal comfort level, evaluated by the PPD index, increases when the inlet air velocity increases. For an inlet air velocity of 5 m/s the thermal comfort level is acceptable in accordance with the international standards ISO (2005). The thermal comfort level, mainly for higher inlet air velocities, is better for occupants seated in the corridor side.

The thermal comfort number is evaluated by the quotient of the effectiveness for heat removal and the PPD index. The thermal comfort number increases when the inlet air velocity increases. This parameter, mainly for higher inlet air velocities, is better for occupants seated in the corridor side.

The CO_2 concentration in the respiration area, decreases when the inlet air velocity increases. In accord to the international standards (ASHRAE, 2016), the internal air quality is acceptable in all simulations. However, the air quality level is better for higher inlet air velocities, than for lower inlet air velocities.

The effectiveness for contaminant removal decreases slightly, when the inlet air velocity increases and is relatively lower for occupants located in the beginning of the row (subjected only to one air jet) than the others.
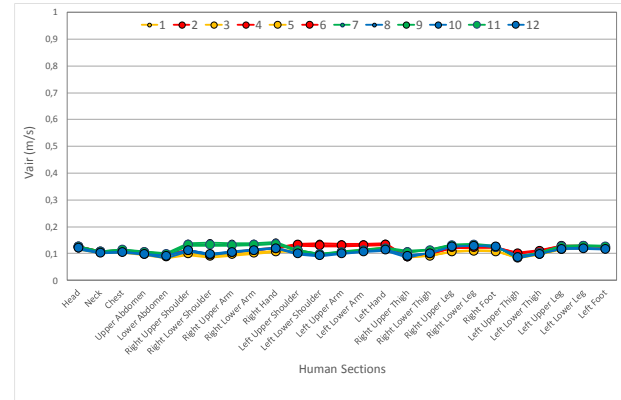
a)
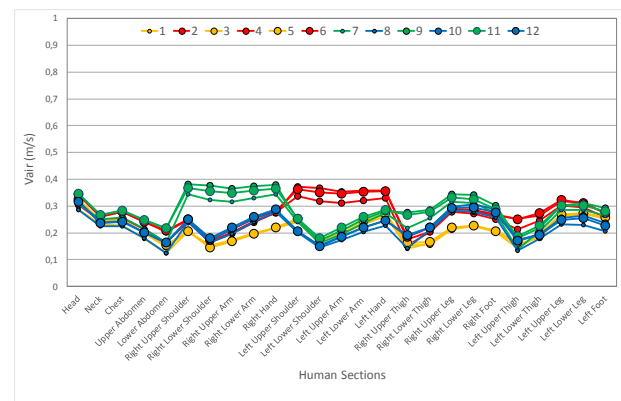
b)
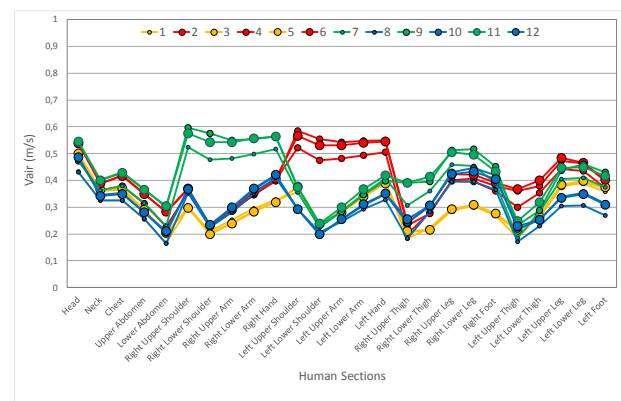
c)

Figure 5. Air velocity around the occupants, when the inlet air velocity is 1 (a), 3 (b) and 5 (c) m/s.

The air quality number increases when the inlet air velocity increases and is relatively lower for occupant located in the beginning of the row.

Finally, the ADI increases when the inlet air velocity increases. The ADI, in general, is higher when the occupants are subjected simultaneously to jets located in front and behind them than when the occupants are subjected only to jets located in front and is higher when the occupants are located in the corridor side than the occupants are located in the wall side.
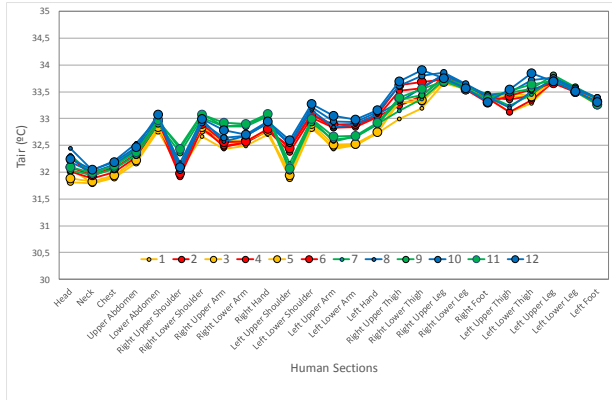
a)
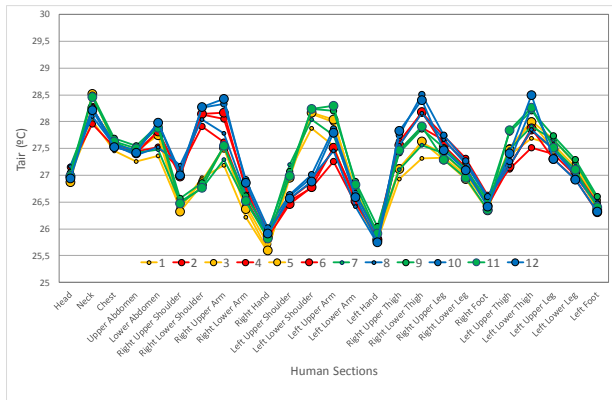
b)
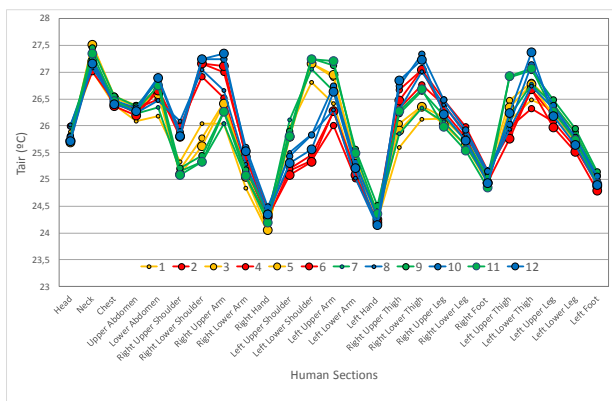
c)

Figure 6. Air temperature around the occupants, when the inlet air velocity is 1 (a), 3 (b) and 5 (c) m/s.
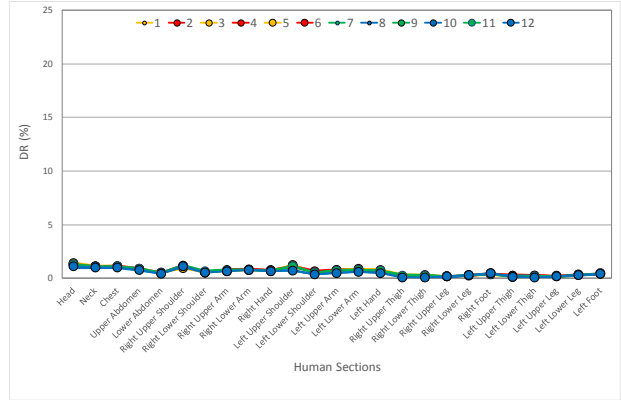
a)
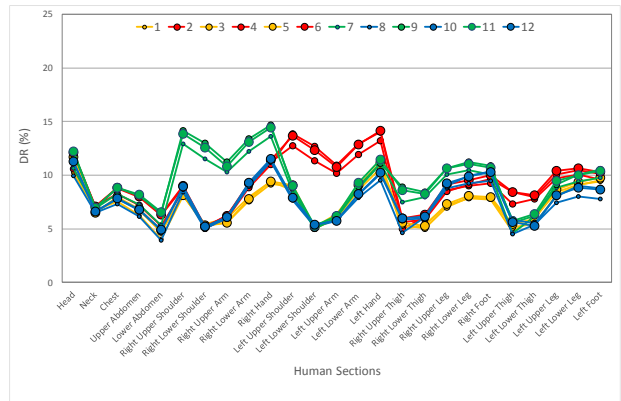
b)
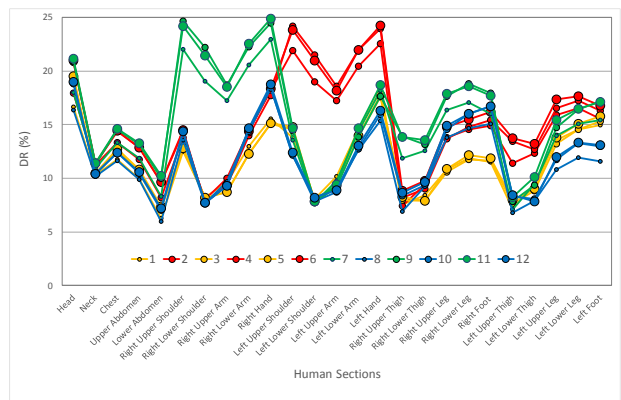
c)

Figure 7. Draught Risk around the occupants, when the inlet air velocity is 1 (a), 3 (b) and 5 (c) m/s.

Table 1. Obtained ADI values, when the inlet air velocity is 1 m/s.

Occupant number	1	2	3	4	5	6	7	8	9	10	11	12	Mean
Inlet Temperature (ºC)	20,0	20,0	20,0	20,0	20,0	20,0	20,0	20,0	20,0	20,0	20,0	20,0	20,0
Outlet Temperature (ºC)	32,4	32,4	32,4	32,4	32,4	32,4	32,4	32,4	32,4	32,4	32,4	32,4	32,4
Body Mean Temperature (ºC)	32,6	32,7	32,6	32,7	32,6	32,8	32,8	32,8	32,7	32,8	32,8	32,9	32,7
Effectiveness For Heat Removal (%)	98,6	97,4	98,4	97,6	98,2	97,3	97,1	96,7	97,4	96,7	97,1	96,4	97,4
PPD (%)	67,4	68,2	67,9	68,0	67,9	68,2	68,3	68,5	68,1	68,5	68,2	68,6	68,1
Thermal Comfort Number	1,5	1,4	1,5	1,4	1,4	1,4	1,4	1,4	1,4	1,4	1,4	1,4	1,4
Inlet CO2 Concentration (mg/m3)	500	500	500	500	500	500	500	500	500	500	500	500	500
Outlet CO2 Concentration (mg/m3)	1210	1210	1210	1210	1210	1210	1210	1210	1210	1210	1210	1210	1210
CO2 in the Respiration Area (mg/m3)	1569	1652	1504	1569	1425	1501	1659	1851	1582	1805	1503	1708	1611
Effectiveness Contaminant Removal (%)	66,4	61,7	70,7	66,4	76,8	71,0	61,3	52,6	65,6	54,4	70,8	58,8	64,7
Ventilating Rate (l/s/Olf)	5,3	5,3	5,3	5,3	5,3	5,3	5,3	5,3	5,3	5,3	5,3	5,3	5,3
PD with Indoor Air Quality (%)	24,5	24,5	24,5	24,5	24,5	24,5	24,5	24,5	24,5	24,5	24,5	24,5	24,5
Air Quality Number	2,7	2,5	2,9	2,7	3,1	2,9	2,5	2,1	2,7	2,2	2,9	2,4	2,6
Air Distribution Index(ADI)	2,0	1,9	2,0	2,0	2,1	2,0	1,9	1,7	2,0	1,8	2,0	1,8	1,9

Table 2. Obtained ADI values, when the inlet air velocity is 3 m/s.

Occupant number	1	2	3	4	5	6	7	8	9	10	11	12	Mean
Inlet Temperature (ºC)	20,0	20,0	20,0	20,0	20,0	20,0	20,0	20,0	20,0	20,0	20,0	20,0	20,0
Outlet Temperature (ºC)	24,9	24,9	24,9	24,9	24,9	24,9	24,9	24,9	24,9	24,9	24,9	24,9	24,9
Body Mean Temperature (ºC)	27,2	27,3	27,4	27,4	27,3	27,3	27,3	27,4	27,5	27,5	27,4	27,4	27,4
Effectiveness For Heat Removal (%)	67,7	66,8	66,4	66,0	66,7	66,5	66,6	66,3	65,2	65,3	65,8	65,7	66,2
PPD (%)	18,3	17,7	18,5	17,5	18,2	17,1	17,8	19,0	17,5	18,7	17,3	18,5	18,0
Thermal Comfort Number	3,7	3,8	3,6	3,8	3,7	3,9	3,7	3,5	3,7	3,5	3,8	3,5	3,7
Inlet CO2 Concentration (mg/m3)	500	500	500	500	500	500	500	500	500	500	500	500	500
Outlet CO2 Concentration (mg/m3)	733	733	733	733	733	733	733	733	733	733	733	733	733
CO2 in the Respiration Area (mg/m3)	892	902	844	858	819	837	903	962	863	927	840	896	879
Effectiveness Contaminant Removal (%)	59,5	57,9	67,8	65,1	73,0	69,1	57,8	50,4	64,1	54,5	68,5	58,8	62,2
Ventilating Rate (l/s/Olf)	16,0	16,0	16,0	16,0	16,0	16,0	16,0	16,0	16,0	16,0	16,0	16,0	16,0
PD with Indoor Air Quality (%)	10,2	10,2	10,2	10,2	10,2	10,2	10,2	10,2	10,2	10,2	10,2	10,2	10,2
Air Quality Number	5,8	5,7	6,7	6,4	7,2	6,8	5,7	5,0	6,3	5,4	6,7	5,8	6,1
Air Distribution Index(ADI)	4,7	4,6	4,9	4,9	5,1	5,1	4,6	4,2	4,8	4,3	5,1	4,5	4,7

Table 3. Obtained ADI values, when the inlet air velocity is 5 m/s.

Occupant number	1	2	3	4	5	6	7	8	9	10	11	12	Mean
Inlet Temperature (ºC)	20,0	20,0	20,0	20,0	20,0	20,0	20,0	20,0	20,0	20,0	20,0	20,0	20,0
Outlet Temperature (ºC)	23,2	23,2	23,2	23,2	23,2	23,2	23,2	23,2	23,2	23,2	23,2	23,2	23,2
Body Mean Temperature (ºC)	26,0	26,1	26,2	26,2	26,1	26,1	26,1	26,2	26,3	26,3	26,2	26,2	26,2
Effectiveness For Heat Removal (%)	53,4	52,6	51,9	52,1	52,6	52,8	52,6	52,0	51,4	51,1	52,1	51,7	52,2
PPD (%)	7,7	7,2	7,7	6,9	7,5	6,7	7,2	8,1	6,9	7,9	6,7	7,7	7,4
Thermal Comfort Number	6,9	7,3	6,7	7,5	7,0	7,9	7,4	6,4	7,4	6,5	7,7	6,7	7,1
Inlet CO2 Concentration (mg/m3)	500	500	500	500	500	500	500	500	500	500	500	500	500
Outlet CO2 Concentration (mg/m3)	646	646	646	646	646	646	646	646	646	646	646	646	646
CO2 in the Respiration Area (mg/m3)	749	759	714	724	699	713	756	789	726	766	712	747	738
Effectiveness Contaminant Removal (%)	58,5	56,3	68,0	64,9	73,1	68,5	56,8	50,4	64,5	54,7	68,6	58,9	61,9
Ventilating Rate (l/s/Olf)	26,6	26,6	26,6	26,6	26,6	26,6	26,6	26,6	26,6	26,6	26,6	26,6	26,6
PD with Indoor Air Quality (%)	6,2	6,2	6,2	6,2	6,2	6,2	6,2	6,2	6,2	6,2	6,2	6,2	6,2
Air Quality Number	9,5	9,1	11,0	10,5	11,8	11,1	9,2	8,1	10,4	8,8	11,1	9,5	10,0
Air Distribution Index(ADI)	8,1	8,2	8,6	8,9	9,1	9,3	8,2	7,2	8,8	7,6	9,3	8,0	8,4

Conclusions

This numerical study develops a HVAC system based in a ceiling mounted localized air distribution systems. The study is made in winter typical day conditions. The thermal comfort, the indoor air quality, the DR, the effectiveness for heat removal, the effectiveness for contaminant removal and the ADI, are evaluated.

When the inlet air velocity increases the DR around the occupants increases. The DR is acceptable in accordance to the international standards.

The thermal comfort level increases when the inlet air velocity increases and is acceptable for highest inlet air velocities in accordance with the international standards.

The indoor air quality level increases when the inlet air velocity increases and is acceptable, in accordance with the international standards for all simulations.

Finally, the ADI increases when the inlet airflow increases. The ADI is highest when the occupants are subjected simultaneously to jets located in front and behind and is highest for occupants located in the corridor side.

Acknowledgement

References

ASHRAE. 2016. "Ventilation for Acceptable Indoor Air Quality." *Journal of Physics A: Mathematical and Theoretical*.

Awbi, H. B. 2004. *Ventilation of Buildings*.

Conceição, E., A. Silva, and Lúcio M. M. J. R. 2004. "Numerical Study of Thermal Response of School Buildings in Winter Conditions." Pp. 5–8 in *Proceedings of the 9th Conference on Air Distribution in Rooms (Roomvent 2004), Coimbra, Portugal*.

Conceição, E. Z. E. 1999. "Avaliação de Condições de Conforto Térmico: Simulação Numérica Do Sistema Térmico Do Corpo Humano e Do Vestuário." *Proceedings of the CIAR*.

Conceição, E. Z. E. 2000. "Evaluation of Thermal Comfort and Local Discomfort Conditions Using the Numerical Modelling of the Human and Clothing Thermal System." Pp. 131–36 in *RoomVent'2000-7th International Conference on Air Distribution in Rooms*.

Conceição, E. Z. E. and Lúcio, M. M. J. R. 2006. "Numerical Study of Thermal Response of School Buildings in Summer Conditions." in *HB 2006 - Healthy Buildings: Creating a Healthy Indoor Environment for People, Proceedings*. Vol. 3.

Conceição, E. Z. E., and Lúcio, M. M. J. R.. 2010a. "Evaluation of Thermal Comfort Conditions in a Localized Radiant System Placed in Front and behind Two Students Seated Nearby Warmed Curtains." *Building and Environment* 45(10).

Conceição, E. Z. E., and Lúcio, M. M. J. R.. 2010b. "Numerical Simulation of Passive and Active Solar Strategies in Buildings with Complex Topology." *Building Simulation* 3(3).

Conceição, E. Z. E., and Lúcio, M. M. J. R. 2011. "Evaluation of Thermal Comfort Conditions in a Classroom Equipped with Radiant Cooling Systems and Subjected to Uniform Convective Environment." *Applied Mathematical Modelling* 35(3).

Conceição, E. Z. E., and Lúcio, M. M. J. R. 2016. "Numerical Simulation of the Application of Solar Radiant Systems, Internal Airflow and Occupants' Presence in the Improvement of Comfort in Winter Conditions." *Buildings* 6(3).

Conceição, E. Z. E., Lúcio, M. M. J. R., and H. B. Awbi. 2013. "Comfort and Airflow Evaluation in Spaces Equipped with Mixing Ventilation and Cold Radiant Floor." *Building Simulation* 6(1).

Conceição, E. Z. E., Lúcio, M. M. J. R., and M. C. Lopes. 2008. "Application of an Indoor Greenhouse in the Energy and Thermal Comfort Performance in a Kindergarten School Building in the South of Portugal in Winter Conditions." *WSEAS*

Transactions on Environment and Development 4(8).

Conceição, E. Z. E., Lúcio M. M. J. R., V. D. S. R. Vicente, and V. C. T. Rosão. 2008. "Evaluation of Local Thermal Discomfort in a Classroom Equipped with Cross Flow Ventilation." *International Journal of Ventilation* 7(3).

Conceição, E. Z. E., and Lúcio, M. M. J. R. 2001. "Numerical and Subjective Responses of Human Thermal Sensation." *Proceedings of the BioEng*.

Conceição, E. Z. E., Rosa, S. P., Custódio, A. L. V., Andrade, R. L., Meira, M. J. P. A. and Lúcio, M. M. J. R.. 2010. "Study of Airflow around Occupants Seated in Desks Equipped with Upper and Lower Air Terminal Devices for Slightly Warm Environments." *HVAC and R Research* 16(4).

Conceição, E. Z. E., Santiago, C. I. M., and Awbi, H. B.. 2017. "Numerical Study of Different Ceiling-Mounted Air Distribution Systems for a Virtual Classroom Environment." *Indoor and Built Environment* 26(10).

Conceicao, E. Z. E., Silva, M. C. G., Andre, J. C. S. and Viega, D. X. 2000. "Thermal Behaviour Simulation of the Passenger Compartment of Vehicles." *International Journal of Vehicle Design* 24(4):372–87.

Conceição, E. Z. E., Silva, M. C. G. and Viegas, D. X.. 1997. "Air Quality inside the Passenger Compartment of a Bus." *Journal of Exposure Analysis and Environmental Epidemiology* 7(4).

Conceição, E. Z. E., Vicente, V. D. S. R. and. Lúcio M. M. J. R. 2008. "Airflow inside School Building Office Compartments with Moderate Environments." *HVAC and R Research* 14(2).

Fanger, P. O., A. K. Melikov, H. Hanzawa, and J. Ring. 1988. "Air Turbulence and Sensation of Draught." *Energy and Buildings*.

Fanger, P. O. P. 1970. "Thermal Comfort. Analysis and Applications in Environmental Engineering." *Copenhagen: Danish Technical Press*.

ISO. 2005. "ISO 7730: Ergonomics of the Thermal Environment Analytical Determination and Interpretation of Thermal Comfort Using Calculation of the PMV and PPD Indices and Local Thermal Comfort Criteria." *Management*.

Yang, Bin, Arsen Melikov, and Chandra Sekhar. 2009. "Performance Evaluation of Ceiling Mounted Personalized Ventilation System." in *ASHRAE Transactions*.

Yang, Bin, Chandra Sekhar, and Arsen K. Melikov. 2010. "Ceiling Mounted Personalized Ventilation System in Hot and Humid Climate - An Energy Analysis." *Energy and Buildings*.

Energy Flexibility, Control and Energy Storage

A coordinated control to improve energy performance for a building cluster with energy storage, EVs, and energy sharing

Pei Huang[1*], Xingxing Zhang[1], Chris Bales[1], Tomas Persson[1]
[1]Energy Technology, Dalarna University, Borlänge, 79188, Sweden
*corresponding author: phn@du.se

Abstract

Existing studies have developed some advanced controls for energy storage system charging/discharging in a building cluster (enabling PV power sharing among different buildings), which can effectively improve the aggregated performances. However, in the existing controls, the flexible demand shifting ability of electric vehicles (EVs) are rarely considered, leading to limited performance improvements at building cluster level. Thus, this study proposes a coordinated control of building cluster with both energy sharing and the EV charging considered, with the purpose of improving the cluster-level performance. The simulation results show that in a typical summer week in Sweden, the developed control can increase the cluster-level daily renewable self-consumption by 40% and meanwhile reduce the electricity bills by as much as 20% compared with conventional controls for a summer week in Ludvika, Sweden.

1. Introduction

The integration of distributed energy systems has promoted the transformation of buildings' role from energy consumers to energy prosumers, i.e. energy consumers who produce energy for their own consumption using distributed energy technologies (Huang, Copertaro et al. 2020). The transformation of buildings' role into energy prosumers provides opportunities for collaborations among buildings to improve the overall cluster-level performances. When multiple building prosumers are in a building cluster, they can share their excessive renewables with others in shortage (Fan, Huang et al. 2018). Such energy sharing can help improve the building-cluster-level renewable self-consumption rates and thus reduce the grid power usage (due to an increased share of renewable energy utilization). A study conducted by Luthander *et al.* (2016) shows that that even a simple energy sharing (i.e. aggregate electricity demand and supply) among 21 houses in Sweden can easily improve the PV power self-consumption by over 15%. While when there is shared energy storage, the improvement in PV power self-consumption can even reach 29%.

To achieve energy sharing among buildings, existing studies have developed a number of advanced controls. For example, Odonkor *et al.* (2015) proposed a control method of zero energy buildings (ZEBs) using genetic algorithm and Pareto decision making based on an adaptive bi-level decision model (with a facilitator agent at cluster level and local systems at single NZEB level) (Odonkor and Lewis, 2015). Fan *et al.* (2018) proposed a collaborative demand response control of zero energy buildings for enhancing the building-cluster-level performances. In their method, the control of each building was conducted in sequence, and the optimization of one building's operation was based on the previously optimized buildings' operation (Fan *et al.,* 2018). Prasad and Dusparic developed a Deep Reinforcement Learning based method for ZEB community (Prasad and Dusparic 2019). The abovementioned controls optimize the building cluster performance in a bottom-up way, and they merely perform very limited collaborations among buildings. With the purpose of maximizing the energy sharing within a building cluster, researchers have developed controls that directly use the building-cluster-level performances as the optimization targets. For instance, Huang et al. developed a top-down control for a cluster of building prosumers equipped with electrical energy storage system (Huang, Wu et al. 2018). In their study, the optimal performances that can be achieved are first searched by using an advanced searching algorithm. Then the optimal performances at the top-level are divided into separate goals for each individual building at the bottom-level. Similarly, in a three-step demand response control algorithm is developed considering the dynamic pricing. Taking into account of the demand prediction uncertainty, in a robust collaborative control is developed.

These existing controls can effectively improve the performances at building cluster level. However, electric vehicles (EV), which also play an important role in the building cluster scale energy systems, are usually considered as non-scheduled electrical loads (such as lighting) and their flexible demand shifting ability is rarely used (Taşcıkaraoğlu, 2018; Huang, *et al.*, 2019). As a result, the flexible demand shifting ability of EVs are rarely considered together with the building control, leading to limited performance improvements at building cluster level (Barone *et al.*, 2019; Dallinger *et al.*, 2013). For instance, in practice the EV charging will start once they are plugged into charging stations. However, in such charging period the renewable generation may be insufficient to cover the EV charging load, leading to grid electricity imports. On the other hand, when there is surplus renewable generation, the EVs cannot be used as electricity storage if they have already been fully charged,

leading to the surplus renewable energy exports. As a result, the overall building-cluster-level performance is not fully optimized.

By properly scheduling the EV charging loads, the batteries in EVs can be used as flexible energy storage to help regulate the electricity demands in the power grid. Existing studies have also developed some advanced controls for EVs. For instance, Geth et al. developed a coordinated charging control for a number of EVs (Geth, Willekens et al. 2010). In their control, a vehicle owner first indicates the point in time when the batteries should be fully charged. Then, the aggregator collects this information and calculates when each EV can start charging, based on two rules: (i) charging is most economically when the total demand (including the residential, industrial and EV consumption) is low, and (ii) the EVs can be charged during working hour in the working places. Similarly, Usman et al. proposed an automated coordinated control of EV fleets, which can plan the charging strategy at the cheaper moments while keeping the vehicle charged enough to complete its scheduled trips (Usman, Knapen et al. 2016). Their control uses a grid agent to grant tokens to the EVs in idle state based on the grid electricity prices. By shifting charging loads to low electricity price period (usually with low aggregated electricity demands in the power grid), this control can effectively increase the match between the available power and the consumed power. The abovementioned studies can effectively improve the economic performances of EV or EV fleets. However, these studies typically consider EVs as a separate role in the urban energy system and thus neglect their integration with the building controls.

To sum up, the existing studies have developed some advanced building side controls, which enables renewable energy sharing and aims at optimizing building-cluster-level performance via regulating the energy storage charging/discharging. However, the flexible demand shifting capability of EVs is not considered in the cluster-level controls. Therefore, this study proposes a coordinated control of building cluster with both energy sharing and the EV charging considered, with the purpose of improving the cluster-level performance by taking advantage of energy sharing and storage capability of electricity batteries in both buildings and EVs.

2. Methodology

This section introduces the developed coordinated control. Fig. 1 presents the flowchart of the developed control optimization method. The aim of the coordinated control is to coordinate the operation of energy storage (installed in each single building) and the EVs, to achieve the optimal cluster-level performances. The coordinated control consists of four steps. In Step 1, all the buildings in the building group are considered as a 'representative' building, and the electrical demand, renewable energy generation and load shifting capacity of the 'representative' building are predicted, i.e. its electrical

demand/renewable generation/demand shifting capacity equals the aggregated demand/ generation/capacity of all buildings inside the cluster. In Step 2, the operation of the 'representative' building and the EV charging rates are optimized using genetic algorithm (GA). The performance of the 'representative' building, obtained by simultaneous optimization of the building and EV operation, is considered to be the best performances that the building group can achieve (Shen, Li et al. 2016). In Step 3, the operation of each single building inside the building group is coordinated using non-linear programming (NLP) based on the 'representative' building's operation obtained from Step 2. In Step 4, the performances of the proposed coordinated control are compared with two existing controls, including a conventional individual control (Scenario 1 (Shen, Li et al. 2016)), which does not enable renewable sharing and charge the EVs immediately after being parked, and an existing coordinated control (Scenario 2 (Gao and Sun 2016)), which enables full renewable energy sharing but also charges the EVs immediately after being parked. The details of each step are introduced below.
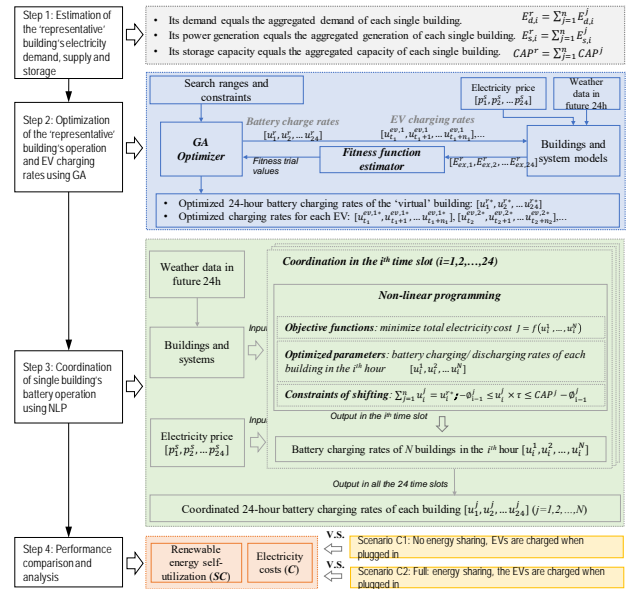
Figure 1 Flowchart of the coordinated control

Step 1: *Estimation of the 'representative' building's demand and storage*

In this step, all the buildings inside the cluster are considered as a 'virtual' building. Its hourly electricity demand ($E_{d,i}^r$ (kW·h)) equals the aggregated hourly electricity demand (including the household electricity, and electricity for heating or heat pumps) of each single building ($E_{d,i}^j$ (kW·h)) (i indicates time with a unit of hour), its hourly renewable generation ($E_{s,i}^r$ (kW·h)) equals the aggregated hourly renewable generation of each single building ($E_{s,i}^j$ (kW·h)) and its load shifting capacity (CAP^r (kW·h), i.e. battery capacity) is the aggregated load shifting capacity of each single building (CAP^j (kW·h)).

Step 2: *Optimization of the 'representative' building's operation using GA*

The GA algorithm searches the optimal charging/discharging rates of both the battery and EVs that can minimize the electricity costs of the 'representative' building. For example, the EVs can be scheduled to be charged in periods with sufficient renewable generations while not charged in periods with insufficient generations. In the GA simulation, the inputs mainly include the battery charging/discharging rates (to be optimized), the EV charging rates (to be optimized), the EV parking periods, the future 24-hour weather data, building parameters, and battery parameters. The EVs are different from the building integrated electricity storage system, as they are not constantly connected into the buildings. This study uses four parameters to characterize an EV (e.g. the kth EV): arrival time to the charging port (t^k), parking periods in the charging port (n^k), initial state of charge (SOC_0^k), and the required state of charge when the car departs from the charging port (SOC_1^k). These parameters are considered known and will be used as inputs in the optimization.

In each generation of GA, trials of 24-hour thermal storage hourly charging/discharging rates (i.e., $[u_1^v, u_2^v, \dots u_{24}^v]$ kW) and charging rates of each EV (i.e. $[u_{t_k}^{ev,k}, u_{t_k+1}^{ev,k}, \dots u_{t_k+n_k}^{ev,k}]$ kW) are generated by the GA optimizer. The representative building's hourly power demand ($E_{d,i}^r$ kW) and hourly renewable power generation ($E_{r,i}^r$ kW) in the future 24 hours is then predicted using the building and system models. The charging/discharging rates of the electrical battery should meet the following two constraints:

(i) The battery charging amount could not exceed the remaining battery storage capacity.

(ii) The battery discharging amount could not exceed the stored electricity in the battery. These two constraints are expressed by Eqn. (4) (Lu, Wang et al. 2015),

$$0 \leq \emptyset_0^r + (u_1^r + u_2^r + \dots + u_i^r) \times \tau \leq CAP^r \quad \text{where i=1,2,...,24} \quad (1)$$

where $\emptyset_0^v$ (kW·h) is the amount of electricity energy initially stored in the electrical energy storage system, τ is the duration of battery charging/discharging (i.e., 1 hour in this study).

Similarly, the charging rates of the kth EV should meet these two constraints, as expressed by Eqn. (2). $SOC_{0,k}$ is the initial state of charge when the kth EV arrives at the charging port. CAP_k^{ev} (kW·h) is the capacity of the kth EV battery. t_k is the arrival time of the kth EV at the charging port, and n_k is the parking duration.

$$0 \leq SOC_{0,k} \times CAP_k^{ev} + (u_{t_k}^{ev,k} + u_{t_k+1}^{ev,k} + u_{t_k+i}^{ev,k}) \times \tau \leq CAP_k^{ev}$$
$$\text{where i=1,2,...,} n_k \quad (2)$$

In addition, the EV battery should be charged to a user-specified level ($SOC_{1,k}$) before they depart the charging port. This constraint is expressed by Eqn. (3). When $SOC_{1,k}$ equals 1, it represents the EV users require the EV

battery to be fully charged before they depart the charging port.

$$SOC_{0,k} \times CAP_k^{ev} + (u_{t_k}^{ev,k} + u_{t_k+1}^{ev,k} + \dots + u_{t_k+n_k}^{ev,k}) \times \tau \geq SOC_{1,k} \times CAP_k^{ev} \quad (3)$$

This study considers the strategy to minimize daily electricity cost of the building group. Following this control goal, a fitness function is determined, as expressed by Eqn. (4) (Salom, Widén et al. 2011).

$$J_{grid} = \min (Cost) \quad (4)$$

$$Cost = \sum_{i=1}^{24} E_{ex,i}^r \times \tau \times \chi_i, \begin{cases} \chi_i = \chi_{buy}, if\ E_{ex,i}^r > 0 \\ \chi_i = \chi_{sell}, if\ E_{ex,i}^r \leq 0 \end{cases} \quad (5)$$

where χ_i (kr/(kW·h)) is the electricity price in the ith time slot. χ_{buy} (kr/(kW·h)) is the price of purchasing electricity from the power grid, and χ_{sell} (kr/(kW·h)) is the feed-in-tariff. The outputs of the GA search are the 'representative' building's battery charging/discharging rates ($[u_1^{r*}, u_2^{r*}, \dots u_3^{r*}]$ kW) in the next 24 hours and the charging rates of each individual EV ($[u_{t_1}^{ev,1*}, u_{t_k+1}^{ev,k*}, \dots, u_{t_k+n_k}^{ev,k*}]$, ... kW). The optimized battery charging/ discharging rates of the 'representative' building are used in Step 3.

Step 3: *Coordination of single building's operation using NLP*

In this step, the single building's battery charging/discharging rates (i.e. u_i^j is the jth building in the ith hour) are coordinated using NLP based on the 'representative' building's operation (Zhao, Lu et al. 2015). The NLP is conducted in each hour and will be repeated 24 times for obtaining the building's daily operation. The fitness function of the NLP is expressed by Eqns. (6) and (7), which aims at minimizing the electricity costs of the building group.

$$J_{NLP} = \min(Cost_{all,i}) \quad (6)$$

$$Cost_{all,i} = \sum_{j=1}^{n} (E_{d,i}^j \times \chi_i)^2 \quad (7)$$

In order to reduce the uneven allocation of the battery charging/discharging rates (otherwise only a few buildings take benefits from the demand response), the square of each building's operational cost is used in the fitness function. $E_{d,i}^j$ (kW·h) is the energy demand of the jth building in the ith hour after applying the u_i^j (kW) amount of battery charging/discharging, which is calculated by the models presented in Section 3. χ_i (HKD/(kW·h)) is the electricity price in the ith hour. In the ith hour, the optimized parameters in the NLP are the hourly battery charging/discharging rates of all the buildings inside the building group, i.e., $[u_i^1, u_i^2, \dots, u_i^N]$ (kW), where N indicates the number of buildings in the building group. The battery charging/discharging rates in each hour should follow the constraints below.

(i) The sum of battery charging/discharging rates of each building (u_i^j (kW)) should equal the battery charging/discharging of the 'representative' building (u_i^{r*} (kW)) (obtained from Step 2).

$$\sum_{j=1}^{N} u_i^j = u_i^{r*} \quad (8)$$

(ii) For each single building, the electricity charging amount must be smaller than the remaining storage capacity of the battery, and the electricity discharging amount must be smaller than the amount of electricity stored in the battery. There are 2N inequality constraints for N buildings.

$$-\emptyset_{i-1}^j \leq u_i^j \times \tau \leq CAP^j - \emptyset_{i-1}^j \quad \text{(j=1,2,...N, respectively)} \quad (9)$$

where τ is the charging duration (i.e., 1 hour), CAP^j (kWh) is the battery capacity of the jth building, $\emptyset_{i-1}^j$ (kW·h) is the electricity energy stored in the jth building's battery. $\emptyset_{i-1}^j$ (kW·h) is calculated by Eqn. (10).

$$\emptyset_{i-1}^j = (u_1^j + u_2^j + \cdots + u_{i-1}^j) \times \tau \quad (10)$$

Step 4: *Performance comparison and analysis*

In this step, the performances of the proposed coordinated control are compared with two existing controls in aspects of renewable energy self-consumption improvements and economic cost savings. The two existing controls include a conventional individual control (Scenario 1 (Shen, Li et al. 2016) (Gao and Sun 2016)), which does not enable renewable sharing and charge the EVs immediately after connecting them, and an existing coordinated control (Scenario 2 (Huang, Wu et al. 2018)), which enables full renewable energy sharing in the building cluster but charges the EVs immediately after connecting them. In both the two comparative studies, the EVs demand are first computed and then added to the building electricity demand, which will then be used as inputs for battery charging/discharging controls. In Scenario 1 (i.e. an existing individual control) (Shen *et al.* 2016), GA was used for searching the optimal battery charging/discharging rates in each building, which is similar to the control optimization of the 'representative' building (see Step 2 in Fig. 2 without EV related variables). After obtaining the individual buildings' optimal operation, their electrical demands were aggregated for evaluating the building-cluster-level performances. In Scenario 2 (i.e. an existing coordinated control) (Gao and Sun, 2016), the battery charging/discharging rates of all the three buildings are optimized simultaneously using GA, and the minimization of the building-cluster-level performance was used as the fitness function.

Table 1 Configuration of the three scenarios

Scenario	EV control?	Energy sharing?
1	Charged immediately when plugged in	No
2	Charged immediately when plugged in	Full sharing
3	Charged at any time when parked	Full sharing

3. Buildings and system modelling

This section introduces the building information and system modelling. Each building is installed with a renewable energy system (i.e., PV panels), an electricity storage system (i.e., battery), as well as an EV.

3.1 Building modelling

This study considered a real building cluster located in Ludvika, Dalarna region, Sweden. This building cluster consists of three separate buildings, as shown in Fig. 2. These buildings will be improved by a series of renovation plans including installation of PV, battery storage, direct current (DC) micro grid, and EV charging station. It is assumed the heating is provided by district heating system. So, the PV panels will only need to provide power supply to the domestic electricity demand (e.g. lighting, TVs, dish wash).

Figure 2 Bird view of the case building cluster located in Ludvika, Sweden

3.2 Renewable energy system modeling

The power generation from the PV panel P_{PV} (kW) is calculated by Eqn. (14) (Klein *et al*., 2004),

$$P_{PV} = \tau \times I_{AM} \times I_T \times \eta \times CAP_{PV} \quad (11)$$

where τ is the transmittance-absorptance product of the PV cover for solar radiation at a normal incidence angle, ranging from 0 to 1; I_{AM} is the combined incidence angle modifier for the PV cover material, ranging from 0 to 1; I_T (W/m^2) is the total amount of solar radiation incident on the PV collect surface; η is the overall efficiency of the PV array; CAP_{PV} (m^2) is the PV surface area. The local weather data in Ludivika was used as inputs with a time resolution of 1 hour.

3.3 Electrical battery and EV battery modeling

This study used simplified electrical battery and EV battery models. The electricity stored in the battery is calculated using a simplified model, as expressed by Eqns. (4) and (5). It is estimated from the hourly charging rates (Sun, Huang et al. 2018). This study considers three EVs. Table 2 summarizes the capacity, maximum charging rates as well as the parking periods of each EV. EV 1, EV 2 and EV 3 are assumed to be charged in Building A, B and C, respectively. To consider the various EV usage, these three EVs are assumed to have different parking periods. EV 1 is assumed to be owned by a resident living in the building, and thus it is parked at night from 18:00 to 07:00 in the next day. EV 2 and EV 3 are assumed to be owned by some working staff in the building estate, and they are parked during daytime (i.e. one from 08:00~16:00 and the other from 09:00~17:00). The EV battery capacity and maximum charging rates are referred from the available EV models in the market in (Ustun, Zayegh et al. 2013).

Table 2 Capacity, charging limits and parking periods of the three different EVs, data obtained from (Ustun, Zayegh et al. 2013)

ID	Battery capacity (kW·h)	Maximum charging rates (kW)	Parking period
EV 1	22	4	18:00~07:00
EV 2	27	5	08:00~16:00
EV 3	53	10	09:00~17:00

In all the three scenarios, the EVs are required to be fully charged before they leave the charging station (Note that the time of departure is considered as a known parameter set by the EV owners). When the EVs arrive in a charging station in the home, a random SOC parameter (between 0 and 1) is assumed to represent the remaining storage in the EV battery.

4. Case studies and results analysis

In the case studies, a typical summer week was selected to validate the developed coordinated controls. The weather data of Ludvika was used for modelling the local renewable generations. This section first presents the individual building's electricity demand and renewable generation information. Then, the detailed EV charging and battery charging results obtained from the two scenarios (see Step 4 in Section 2) and the developed control are compared and analyzed. Finally, the overall economic and energy performances are compared.

Table 3 summarizes the input parameters used in the case studies. According to the building dimension, 100 m², 200 m² and 300 m² roof areas are planned for installing PV panels in the three buildings, respectively. It was assumed each building is installed with an electrical battery with capacity of 20 kW·h and maximum charging/ discharging rates of 6 kW. The price of purchasing electricity from the power grid was set as 0.16 € /(kW·h). Considering the negative impacts on the grid stability and safety, the feed-in-tariff was set as 0.05 € /(kW·h), which is lower than price of electricity purchase (Huang, Lovati et al. 2019). The price of electricity trading in the building cluster was set as 0.1 € /(kW·h). Such price setting will provide incentives for energy sharing within the building cluster, i.e. the building owners can earn more by selling their excessive renewable energy to the building cluster than sell to the power grid, and vice versa.

Table 3 System configuration and electricity prices

Input parameter	Value
Area of PV panel in Building A (m²)	100
Area of PV panel in Building B (m²)	200
Area of PV panel in Building C (m2)	300
Battery capacity (kW·h)	20
Battery maximum charging/discharging rates (kW)	6
Price of electricity sold to the grid (€ /(kW·h))	0.05
Price of grid electricity purchased (€ /(kW·h))	0.16
Price of electricity trading in building cluster (€)	0.1

4.1 Electricity demand, supply and mismatch

Fig. 3 displays the hourly electricity demand, hourly PV generation, and the hourly electricity mismatch of the three buildings in the selected week. Note that the heating needs of the three buildings are assumed to be met by the district heating system. Thus, the electricity demand only includes the domestic electricity loads (i.e. lighting, washing machine, TV, etc.). The trends of PV power production of the three buildings are similar, since the solar irradiation is nearly the same for the three buildings which are located in the same location. As Building C has the largest roof area, more PV panels can be installed on its roof. Thus, it has the largest average PV production.

Power mismatch of each building is calculated as the deviation between its hourly power demand and the hourly renewable generation. The diversity between the power mismatch provides good opportunities for the buildings to collaborative with each other in aspects of energy sharing. For instance, at noon (i.e. 11:00~16:00) in the first day of the selected summer week, Building A has insufficient renewable generations (i.e. 7.6 kW·h more demand), while Buildings B and C have excessive renewable generations (i.e. 24.7 kW·h and 55.8 kW·h more supply, respectively). Buildings B and C can share their surplus renewable generation with Building A to avoid grid power imports (for Building A) and power exports to the grid (for Buildings B and C), and thus help improve the overall performance at the building-cluster-level.
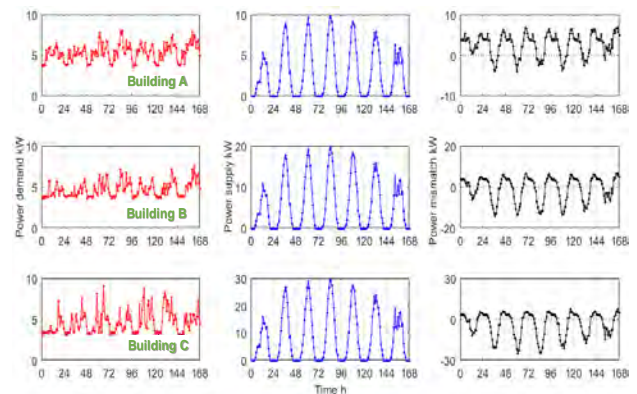
Figure 3 The hourly power demand (red), renewable generation (blue) and power mismatch (black) of the three buildings in the selected summer week

4.2 Detailed battery control and energy flow

To have a close look at the charging of EVs and battery storage, as well as the energy flow in the system, the detailed operation in the first day of the selected week is presented and analyzed in this section. Note that the EV charging loads are exactly the same for the three scenarios. The initial SOCs when EVs arrive at the charging stations are the same for three scenarios. The initial SOCs upon arrival for the three EVs are 0.29, 0.61 and 0.62, respectively. All the EVs are required to be fully charged when they depart the charging stations, i.e. SOC

equals 1. Fig. 4 presents the State of Charge (SOC) of the three EVs' battery and the aggregated battery in the first day of the selected week. For Scenarios 1 and 2, since the EVs are charged at their maximum charging rates (i.e. 4 kW, 5 kW and 10 kW for the three EVs, respectively) immediately after being plugged into the charging ports, there is a stable increase in the SOCs for all the three EVs in the beginning of parking periods. In the developed control, the EVs are charged flexibly in the parking period. In some timeslots, they are charged at a high rate; while in some timeslots, they are charged at a low rate (or even zero). Despite the different charging patterns, all the EV batteries are fully charged (as specified in the case study, see Section 3.3) before they depart the charging ports in the three scenarios.
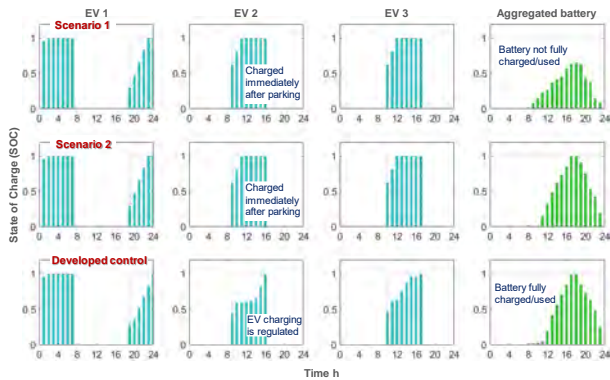
Figure 4 State of Charge (SOC) of the three EVs and the aggregated battery in the first day of selected week

Regarding the battery storage usage, the aggregated battery has not been fully charged (and thus not fully utilized) in Scenario 1, while it has been fully charged (and thus fully utilized) in Scenario 2 and the developed control. This is because in Scenario 1 the collaboration (i.e. renewable energy sharing) is not allowed among the buildings, while in Scenario 2 and the developed control, collaboration is enabled (see Fig. 6 for detailed energy sharing). The collaboration enables buildings to store their surplus renewables in other building's battery, thereby helping to increase the overall battery utilization. Such increased battery utilization can help the building cluster keep more renewable energy onsite instead of exporting to the power grid, and thus contribute to increased renewable energy self-consumption rates.

Fig. 5 depicts the electricity energy flow of the building cluster (i.e. electricity demand), aggregated PV production, power grid, aggregated battery and three EVs in the first day of the selected week for the three different scenarios. The aggregated energy exchanges within the building cluster become zero in the aggregated level, since the amount of purchased electricity from the building cluster compensates with the amount of electricity sold to the building cluster. In the period 9:00~12:00, for Scenario 1 and Scenario 2, large electricity demand occurs, as EV 2 and EV 3 are charged immediately after being plugged in. Unfortunately, the renewable energy generation is not sufficient in this

period to meet the large demands. As a result, a large amount of grid electricity is purchased by the building cluster, i.e. 48.7 kW·h and 52 kW·h for Scenarios 1 and 2, respectively. In Scenario 3 (developed control), as EV 2 and EV 3 can be flexibly charged in any timeslot during the parking period, the controllers set relatively small EV charging rates in this period. Consequently, the amount of grid power purchase is significantly reduced in the developed control, i.e. 14.6 kW·h. In the period 14:00~17:00, for Scenario 1, since there is no collaboration among buildings, only a small part of the surplus renewable energy is kept onsite, while a large part of the surplus renewables (i.e. 28.5 kW·h) is exported to the power grid at a low price. In Scenario 2, contributed by the energy sharing within building cluster, more renewable energy can be stored in the battery. After the batteries in the building cluster all being fully charged, only a small amount of surplus renewable energy (i.e. 14.1 kW·h, which is only half of the amount of exported electricity in Scenario 1) is still exported to the power grid. Scenario 2 has better performance compared with Scenario 1. Since the batteries of EV 2 and EV 3 have already been fully charged in the period 9:00~12:00, there is no energy flow for them in the period 14:00~17:00. In the developed control, considering the large renewable energy production in this period, the controller shifts the charging load of EV 2 and EV 3 to this period. Part of the surplus renewable generation is stored in the building battery and part of the surplus renewables is used to supply the EV load. As a result, exporting renewable energy to the power grid is completely avoided. This can effectively improve the renewable energy self-consumption rate of the building cluster.
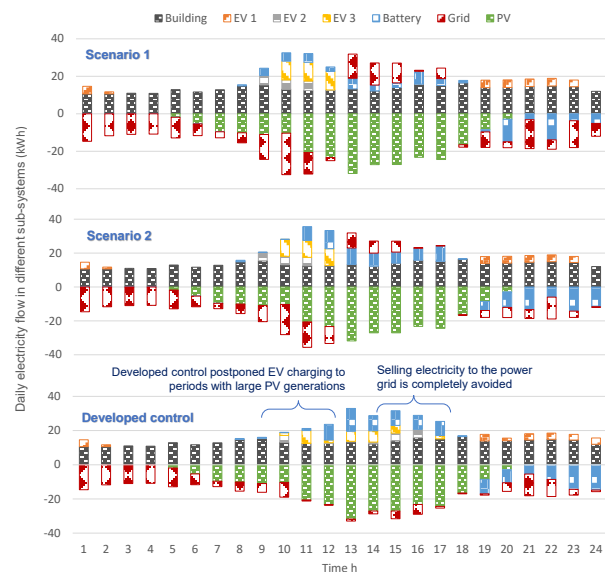
Figure 5 Detailed energy flow (of building, PV systems, battery and three EVs) in the building cluster in each scenario in the first day of the selected week

To sum up, in Scenario 1, the building cluster exported 41.3 kW·h electricity to the grid and imported 177.0 kW·h electricity from the grid. In Scenario 2, the building

cluster exported 23.0 kW·h electricity to the grid and imported 159 kW·h electricity from the grid. Scenario 2 performs better than Scenario 1 (i.e. with reduced energy imports/exports) as energy sharing enables the building cluster to keep more renewable energy on-site. While using the developed control, the building cluster exported 0 kW·h electricity to the grid and imported 135.6 kW·h electricity from the grid. Scenario 3 performs even better than Scenario 2 (i.e. with reduced energy imports/exports), as the controller shifts EV charging loads to periods with large renewable production (and thus help keep more renewable energy used onsite in case the batteries have been fully charged).

4.3 Economic and energy performance comparison

This section compares the overall economic and energy performance of different controls. Table 4 summarizes the building-cluster-level daily electricity costs and renewable energy self-consumption rates. in different scenarios. Fig. 6(a) compares the daily renewable energy self-consumption rates of the three scenarios in the selected week. The relative performances improvements of Scenario 2 and the developed control compared with Scenario 1 are also depicted. Compared with Scenario 1, Scenario 2 improved the renewable energy self-consumption by 5%~24%. This is because the collaboration enables buildings to share their surplus renewable energy with other buildings with insufficient supply and thus help reduce the electricity exports to the power grid (i.e. keep more renewable energy onsite). Compared with Scenario 2, the developed control further improves the renewable self-consumption rates by 2% to 12%. This is because the developed control makes use of the flexible charging ability of EVs. By shifting the EV charging load to periods with large renewable generation periods, more renewable energy can be used onsite, especially when the electrical battery storages are fully charged.
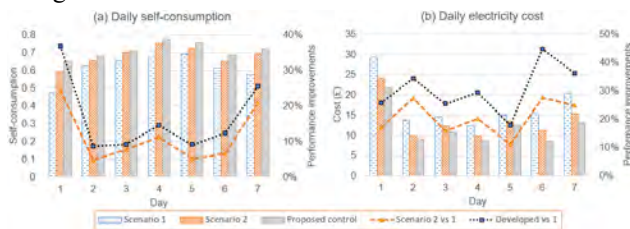
Figure 6 Comparison of the daily renewable energy self-consumption rates and electricity costs of the three scenarios

Fig. 6(b) compares the daily electricity costs of the three scenarios in the selected week. Due to increased renewable energy self-consumption rates and thus less grid power purchase, Scenario 2 achieves 11%~28% cost saving compared with Scenario 1, and the developed control achieves 7%~17% more cost saving compared with Scenario 2 (see Table 4). The relative improvements in economic performance is much larger than the relative improvements in daily self-consumption rates. This is because the building cluster purchase electricity from the

power grid at a high price (i.e. 0.16 €/(kW·h)) but sell electricity at a much lower price (i.e. 0.05 €/(kW·h)). When the building cluster exports more renewables to the power grid (i.e. in Scenario 1), they will need to buy more electricity from the grid at a high price, as the aggregated daily electricity demand is fixed.

5. Conclusion

This study has proposed a coordinated control of building clusters for improving the cluster-level performance, with both energy sharing and EV charging considered. The developed coordinated control first uses a 'representative' building to represent the whole building cluster and optimizes its energy storage operation as well as the EV charging using genetic algorithm. The optimized performance of the building cluster is considered to be the optimal one that maximizes the energy sharing within the building cluster by coordinating individual building's operation. Then, non-linear programming is used to coordinate the operation of each individual building. For validation, the developed control has been tested using the energy demand and supply data on a real buildings cluster (with three EVs considered) in Ludvika, Sweden, and its detailed energy performance (i.e. renewable self-consumption rate) and economic performance (i.e. electricity cost) have been compared with two scenarios (i.e. one does not enable energy sharing and one allows full energy sharing, both do not have EV charging controls). The major findings are summarized as follows:

- The developed coordinated control provides a mechanism to coordinate each single building's operation and EV charging demands for improved building cluster performances.
- In aspect of renewable utilization, the coordinated control improved the daily self-consumption rates by as much as 37% compared with Scenario 1 and as much as 12% compared with Scenario 2. This is because the developed control shifts the EV charging load to periods with large renewable generation periods, and thus more renewable energy are used onsite, especially when the electrical battery storages are fully charged. Note that the time of departure is an important factor affecting the EV charging control and is considered as a known input in this study decided by the EV owner. In return, EV owner can be charged less for the electricity usage.
- In aspect of economic costs, the coordinated control reduced the daily electricity costs by as much as 36% compared with Scenario and as much as 17% compared with Scenario 2. This is because the developed control reduces the amount of high-price grid electricity imports.

In this study, the detailed driving patterns of EVs are not considered, and the SOC when they arrive the charging ports are determined by some random values. Future work will take account of the predictive EV driving patterns in the optimization to achieve better performances.

Meanwhile, the uncertainty in demand and renewable prediction is not considered in this study. Future work will try to develop more robust controls.

Acknowledgments

References

Barone, G., A. Buonomano, F. Calise, C. Forzano and A. Palombo (2019). "Building to vehicle to building concept toward a novel zero energy paradigm: Modelling and case studies." Renewable and Sustainable Energy Reviews **101**: 625-648.

Dallinger, D., S. Gerda and M. Wietschel (2013). "Integration of intermittent renewable power supply using grid-connected vehicles – A 2030 case study for California and Germany." Applied Energy **104**: 666-682.

Fan, C., G. Huang and Y. Sun (2018). "A collaborative control optimization of grid-connected net zero energy buildings for performance improvements at building group level." Energy **164**: 536-549.

Gao, D.-c. and Y. Sun (2016). "A GA-based coordinated demand response control for building group level peak demand limiting with benefits to grid power balance." Energy and Buildings **110**: 31-40.

Geth, F., K. Willekens, K. Clement, J. Driesen and S. D. Breucker (2010). Impact-analysis of the charging of plug-in hybrid vehicles on the production park in Belgium. Melecon 2010 - 2010 15th IEEE Mediterranean Electrotechnical Conference.

Huang, P., B. Copertaro, X. Zhang, J. Shen, I. Löfgren, M. Rönnelid, J. Fahlen, D. Andersson and M. Svanfeldt (2020). "A review of data centers as prosumers in district energy systems: Renewable energy integration and waste heat reuse for district heating." Applied Energy **258**: 114109.

Huang, P., M. Lovati, X. Zhang, C. Bales, S. Hallbeck, A. Becker, H. Bergqvist, J. Hedberg and L. Maturi (2019). "Transforming a residential building cluster into electricity prosumers in Sweden: Optimal design of a coupled PV-heat pump-thermal storage-electric vehicle system." Applied Energy **255**: 113864.

Huang, P., H. Wu, G. Huang and Y. Sun (2018). "A top-down control method of nZEBs for performance optimization at nZEB-cluster-level." Energy **159**: 891-904.

Klein, S., W. Beckman, J. Mitchell, J. Duffie, N. Duffie, T. Freeman, J. Mitchell, J. Braun, B. Evans and J. Kummer (2004). "TRNSYS 16–A TRaNsient system simulation program, user manual." Solar Energy Laboratory. Madison: University of Wisconsin-Madison.

Lu, Y., S. Wang, Y. Sun and C. Yan (2015). "Optimal scheduling of buildings with energy generation and thermal energy storage under dynamic electricity pricing using mixed-integer nonlinear programming." Applied Energy **147**: 49-58.

Luthander, R., J. Widén, J. Munkhammar and D. Lingfors (2016). "Self-consumption enhancement and peak shaving of residential photovoltaics using storage and curtailment." Energy **112**: 221-231.

Odonkor, P. and K. Lewis (2015). Adaptive Operation Decisions in Net Zero Building Clusters.

Prasad, A. and I. Dusparic (2019). Multi-agent Deep Reinforcement Learning for Zero Energy Communities.

Salom, J., J. Widén, J. Candanedo, I. Sartori, K. Voss and A. Marszal (2011). Understanding net zero energy buildings: evaluation of load matching and grid interaction indicators. proceedings of building simulation.

Shen, L., Z. Li and Y. Sun (2016). "Performance evaluation of conventional demand response at building-group-level under different electricity pricings." Energy and Buildings **128**: 143-154.

Sun, Y., G. Huang, X. Xu and A. C.-K. Lai (2018). "Building-group-level performance evaluations of net zero energy buildings with non-collaborative controls." Applied Energy **212**: 565-576.

Taşçıkaraoğlu, A. (2018). "Economic and operational benefits of energy storage sharing for a neighborhood of prosumers in a dynamic pricing environment." Sustainable Cities and Society **38**: 219-229.

Usman, M., L. Knapen, A.-U.-H. Yasar, Y. Vanrompay, T. Bellemans, D. Janssens and G. Wets (2016). "A coordinated Framework for Optimized Charging of EV Fleet in Smart Grid." Procedia Computer Science **94**: 332-339.

Ustun, T. S., A. Zayegh and C. Ozansoy (2013). "Electric Vehicle Potential in Australia Its Impact on Smart Grids." Industrial Electronics Magazine, IEEE **7**: 15-25.

Zhao, Y., Y. Lu, C. Yan and S. Wang (2015). "MPC-based optimal scheduling of grid-connected low energy buildings with thermal energy storages." Energy and Buildings **86**: 415-426.

Digital twin of the Live-In Lab Testbed KTH: development and calibration

Marco Molinari[1], Davide Rolando[1*],

[1]KTH – Royal Institute of Technology, Stockholm, Sweden

* corresponding author: drolando@kth.se

Abstract

In the last decade, the development of Information and Communication Technology (ICT) has enabled unprecedented possibilities to tackle worldwide ambitious sustainability targets. Demonstration facilities like the KTH Live-In Lab are fundamental for the adoption of ICT solutions for energy efficiency and sustainability in buildings. The Live-In Lab monitoring infrastructure enables the creation of a digital-twin, which facilitates a cost effective development, testing and implementation of advanced control and fault detection strategies.

The paper proposes a calibration methodology for the thermal model (energy and comfort) of the Live-In Lab, developed in IDA-ICE, to be deployed as a digital twin. The methodology first screens the parameters with most impact on energy use and then calibrates the model minimizing the error in both indoor comfort and energy use with a weighting parameter β. Calibration results are then validated against the measured data.

The results of this paper will be instrumental to the improvement of control systems and it will facilitate the study of behavioral aspects of the energy use.

Introduction

The recent development of ICT has originated an exceptional potential for cost-effective improvement of energy efficiency in buildings, providing tools for more advanced building monitoring and building data analysis, more advanced control architectures and fault detection.

Nevertheless, large scale implementation of ICT-related solutions in buildings need to be well proven and smart building demonstrators are required. Emerging tools to gain better and more realistic insights on the potential of ICT in buildings are virtual testbeds and digital twins.

According to the CIRP Encyclopedia of Production Engineering (Stark and Damerau 2019) the definition of a digital twin can be given as:

"A digital twin is a digital representation of an active unique product (real device, object, machine, service, or intangible asset) or unique product-service system (a system consisting of a product and a related service) that comprises its selected characteristics, properties, conditions, and behaviors by means of models,

information, and data within a single or even across multiple life cycle phases."

In a recent review, (Jones et al. 2020) identify 13 characteristics common to digital twins; according to (Jones et al. 2020) all digital twins share, among other characteristics, a physical entity (e.g., a building), the virtual entity or twin (e.g., the building model of the building), a physical and virtual environment (e.g. the weather and the weather monitored data), a physical-to-virtual connection and twinning, i.e., the act of synchronizing virtual and physical states. An interesting example of implementation of a digital twin for buildings can be found in (Lydon et al. 2019); they present a coupled simulation for the thermal design of a space heating and cooling integrated in a lightweight roof structure to support design improvements.

In building design and operation, digital twins can serve as an invaluable tool to test the effectiveness of advanced control architectures in reducing energy use and providing improved comfort, to test cost-efficient fault detection schemes, to generate realistic data for benchmarking of algorithms and to investigate potential privacy risks related to the increasing sensing and monitoring capabilities.

The KTH Live-In Lab ("KTH Live-In Lab"), whose monitored data will be used as benchmark in this paper, has evolved from a single building (now Testbed KTH) to a set of demonstration buildings with the goal of testing and demonstrating the impact of ICT-based solutions in the building to facilitate innovation in the building industry. The testbed KTH is configured as a smart building; a key element to foster research is the creation of its energy digital twin. The first step in the creation of the digital twin is the implementation and the calibration of an energy model: this paper deals with the process of calibration and introduces a methodology considered particularly suitable to the specific requirements of a digital twin.

The capability to accurately predict energy use and temperature is crucial. Prediction discrepancies in building simulation models typically arise from uncertainties in input data relative to the building enclosure, like for instance geometry, air-tightness and wall insulation, to the HVAC system, control setting, e.g. temperature setpoints, and to the building usage, i.e.

internal gains from people, light and equipment. The issue of reliable data retrieval for simulations may be even more problematic for older buildings, where such information may not be available at all – thus relying on an assessment based on expert knowledge. In addition, the monitoring of certain environmental conditions, like solar radiation, can be impracticable, expensive or not commonly available; similarly, certain variables like occupancy estimation in time may not be accurate. All these uncertainties are likely to result in a relevant mismatch between the building and the building model it represents. Building models calibration against measured data has proven an effective way to improve the prediction accuracy of the models. Important contributions in the literature on thermal model calibration will be briefly summarized in this section.

The calibration of a building energy model can be used as a first step towards the evaluation of energy savings measures: examples can be found in (Ascione et al. 2019) that perform a calibration for the whole building model – a university building- on the available monthly energy data (gas and electricity) after a preliminary investigation on the prevalent indoor conditions, with errors after calibration below recommended thresholds.

(Coakley, Raftery, and Keane 2014) provide an exhaustive overview of challenges, software tools, procedures and methods in matching building energy simulation models to measured data. Building energy performance simulation calibration approaches are grouped in analytical tools, mathematical and statistical techniques, manual calibration approaches and automated calibration approaches, which include optimization-based techniques and Bayesian techniques. The application of optimization techniques to building simulations is object of the review by (Nguyen, Reiter, and Rigo 2014), who stress the growing number of publications and illustrate the main challenges related to the topic.

Bayesian approach for building model calibration and parameter ranking is used by (Yuan et al. 2017) in an existing building in Singapore, based on monthly electricity data. Other successful examples of Bayesian calibration are found in (Chong et al. 2017), who apply it to two building cooling plants, in (Kristensen, Choudhary, and Petersen 2017), who investigate the effect of aggregation of smart meter data on the calibration of a building energy model and in (Zhu et al. 2020), who propose a new Bayesian calibration approach combined with machine learning. Finally, guidelines for the implementation of Bayesian calibration are provided by (Chong and Menberg 2018) to ease general users from its complexity and need of specific information due to its statistic formulation, which make it non-trivial for building designers and consultants.

Compared to Bayesian approaches, optimization-based calibration methodologies have the advantage of a being more intuitive and have been widely used in literature.

(Asadi et al. 2019) deal with the calibration of the cooling energy of a building in a temperate zone (Doha), with hourly electricity monitoring, using a Harmony search optimization algorithm. (Mustafaraj et al. 2014) perform a two-step calibration of the model of a large university building in Ireland to evaluate potential energy savings measures; two steps are required due the complexity of the model and satisfactory results are reached after the second step of the calibration.

(Yang et al. 2016) applies a calibration method based on sensitivity analysis and Particle Swarm Optimization to a building in Shanghai to improve the prediction accuracy of the model. The model is developed using eQUEST and the calibration, which is performed on monthly energy data on HVAC, lighting and equipment, manages errors below the recommended thresholds.

(Chaudhary et al. 2016) propose an "Autotune" calibration methodology and test it on a deliberately de-tuned building model and on a manual calibration approach, yielding accurate results and time efficient operation.

(Monetti et al. 2015) perform a calibration of a test building model of approximately built around a climatic room. Given the limited dimensions (160 m^2) of the building, a thermal zone was defined for each of the rooms, for a total of seven thermal zones. Most calibration parameters are given a variation range of 25%. The hybrid generalized pattern search with Particle Swarm Optimization was used in a two steps calibration: first with time-varying parameters (like equipment and infiltrations) and then building envelope parameters, for a total of 11.

A slightly different approach is used by (Allesina et al. 2018), who opt to calibrate a building model, a 3600 m^2 retail store building from the 70's in Italy. The calibration is based on the energy signature of the whole building and data recovered from gas bills; instead of using heuristics, they create a mesh of 176 configurations of the building model, built with EnergyPlus.

As model calibration may involve numerous parameters in the optimization process, refined methods include a screening analysis before the calibration process. (Zuhaib, Hajdukiewicz, and Goggins 2019), for instance, perform a Morris analysis to isolate parameters with significant impact on the model thermal dynamics, and then perform a two steps optimization. Similarly, (Li et al. 2018), use Morris analysis to reduce the number of parameters in the optimization from 15 to 6; after calibration, the discrepancy between monitored and predicted energy (CV) in the validation period decreases from 84% down to 16%. Sensitivity analysis is used also by (Ascione et al. 2020) to validate the model of an industrial building in Southern Italy and evaluate different retrofit measures with a Pareto frontier.

Calibration processes can also be extended to aggregated set of buildings: (Taylor et al. 2019), for instance, propose a method to calibrate an aggregate energy demand model.

(Li et al. 2018) stress that current calibration practice is mostly carried out on monthly data with fewer studies with hourly calibration. In building energy models to be deployed as digital twins, calibrations with higher time resolutions are preferable, but there is a trade-off between effort and calibration resolution. The necessary data may not be available, it may be costly to obtain or it may come with high uncertainty. It is often challenging to get data with the desired time resolution and spatial resolution; a temperature sensor may be available for only a room in a large space or set of rooms.

It is commonly found in literature that uncertainty is related to occupancy related dynamics, including gains from occupants, equipment and lighting, and energy flows from demand-controlled ventilation. In this work, high resolution data from the Live-in Lab Testbed KTH enables the evaluation of a calibration methodology with a detailed model, with a zone for each room, and hourly resolution. The testbed monitoring platform includes motion sensors; such data is used to estimate occupancy patterns and evaluate the impact of occupancy in the calibration of the model; furthermore, the calibration methodology introduces a weight factor β to enable the evaluation of the errors of both energy and indoor environment in the cost function of the calibration.

The following paragraphs of the paper include a methodological section, with a description of the building to be calibrated and the methodology proposed, based on a screening analysis and an optimization algorithm based on sequential search technique; the results of the calibration are then presented. The discussion of the results follows and a conclusion section ends the paper.

Method

The building energy model and the measurements refer to the Live-In Lab Testbed KTH (Figure 1). The Testbed KTH is a residential building for students located in the KTH Main Campus. The Testbed KTH premises feature total of 305 square meters distributed over approximately 120 square meters of living space, split into four apartments; each apartment is divided into a living room, a kitchen and a bathroom. The remaining space is used as technical space and an office. The testbed is designed to be energetically independent, with dedicated electricity generation systems through PV panels, a heat generation system (ground source heat pumps), and energy storage (electricity and heat). Sensors are extensively used to improve energy efficiency and indoor comfort, study user behaviour and to improve control and fault detection strategies. Indoor environmental quality is continuously monitored via multiple temperature, relative humidity, CO_2 and VOC sensors in each room. Additional sensors include, for instance, occupancy detectors and magnetic sensors to detect the opening of windows. Space heating energy is distributed through the ventilation system and both ventilation and energy are continuously monitored at the apartment level; in addition, electricity consumption is also logged per apartment.

A building model, to be used as a digital twin has been created in the IDA-ICE 4.8 simulation environment ("IDA ICE - Simulation Software | EQUA"). The IDA-ICE release 4 has been validated according to EN 15255-2007 and performs within given error boundaries (0,5 Kelvin for operative temperature and 5 % for maximum and average cooling power) in all but one test cases; validation scores according to EN 15265 are A in most of the heating cases (Equa Simulation AB and Equa Simulation Finland Oy 2010). To enhance the model accuracy, the simulation model features a zone per each room of the apartments; all apartments share the same layout with a living room, a kitchen/entrance and a bathroom.

Figure 1: Computer generated view of the Testbed KTH building [source: property developer Einar Mattsson] and the building model generated in IDA-ICE.

The methodology for calibration discussed in this paper pivots around two crucial steps: a screening analysis and the actual calibration.

The screening analysis is a fundamental step to evaluate the impact that the parameters have on the thermal dynamics, i.e. indoor temperature and energy demand, of the model. The impact of each single parameter can differ significantly from building model to building model.

The ranking of the parameters is primarily intended to limit the calibration process to a more restricted subset; this is two-fold beneficial, speeding up the calibration process and avoiding that a too large set of parameters to calibrate might become intractable. In this screening analysis each parameter is varied one at a time with respect to the initial configuration of the building model. Each parameter is varied only between a given minimum and maximum value. A performance indicator, the Sensitivity Index S.I. (Heiselberg et al. 2009), is defined by:

$$S.I.(\%) = \frac{E_{max} - E_{min}}{E_{min}} \qquad (1)$$

where E_{max} and E_{min} represent the energy demand relative to the maximum and minimum parameter value.

Upon completion of the screening process, the selected parameters are used in the calibration process, which is essentially an optimization problem.

The software architecture is displayed in Figure 2, where the monitored building (blue box) constitutes the basis for calibration. A simulation manager, based on an ad-hoc code developed in Python, launches the simulation model (yellow box) and evaluates the outputs of the IDA-ICE simulation model against the monitored building; the difference between the simulated results and the monitored data is the error, i.e. the cost function to minimize.

To maximize model fidelity, a climate file derived from the weather station installed in the monitored building is used as input for the simulation model; similarly, internal loads and occupancy schedules are reconstructed based on metered electricity consumption and motion detector sensors.
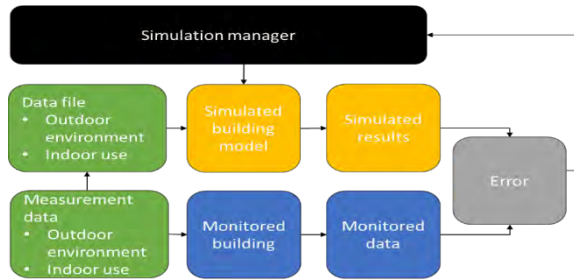
Figure 2: illustration of the simulation conditions and workflow.

The algorithm used for optimization is the one proposed by Box in (Box 1965); the algorithm is capable to escape global maximum of a multivariable non-linear function subject to non-linear constraints. The optimization algorithm is based on a sequential search technique, proven effective in solving problems with non-linear objective functions and without requiring the calculation of derivatives. The optimization procedure is initialized with a set of K points randomly scattered throughout the feasible region of the N independent variables (Box 1966). The required dimension of the set of points is K≥N+1, while the dimension of the points is N.

Common performance indicators for calibration accuracy used in literature are the Mean Biased Error, MBE, and the Coefficient of Variation (Root Mean Square Error), CV(RMSE), defined in (2) and (3), (Ruiz and Bandera 2017)

$$MBE(\%) = \frac{\sum_{i=1}^{N_p} (m_i - s_i)}{\sum_{i=1}^{N_p} (m_i)} \quad (2)$$

$$CV(RMSE)(\%) = \frac{\sqrt{\sum_{i=1}^{N_p} (m_i - s_i)^2 / N_p}}{\bar{m}} \cdot 100 \quad (3)$$

m_i and s_i denote respectively the measurement m_i and the simulated output s_i at the same timestep i, which is sampled on an hourly basis; N_p is the number of samples in the considered sampling interval. Recommended maximum errors for calibration depend on whether calibration is carried out hourly or monthly and are given in Table 1.

Table 1 Suggested values for maximum error for calibrated models according to different sources, from (Ruiz and Bandera 2017).

Guideline	Hourly (%)		Monthly (%)	
	MBE	CV(RMSE)	MBE	CV(RMSE)
ASHRAE	±10	30	±5	15
IPMMVP	±5	20	±20	
FEMP	±10	30	±5	15

The proposed calibration approach aims at the minimization of the error of energy and room indoor temperature the overall error to minimize in the cost function is reduced to a scalar through the weight factor β, introduced in equation (eq. 4) and set prior to the calibration run. For β=0 the cost function is evaluated through the error on energy only; for increasing values of β, the weight of the temperature error in the cost function grows.

$$Weighted\ CV(RMSE) = CV(RMSE)(T) \cdot (\beta) + CV(RMSE)(En) \cdot (1-\beta) \quad (4)$$

Results

To speed up the optimization problem, a screening analysis has first been carried out to identify and rank the variables with the largest impact on the building thermal dynamics and to rule out the parameters with marginal impact on the model calibration. Since the calibration process considered in this work only focuses on thermo-physical properties of the building envelope, set-points and parameters of the heating and ventilation system and internal gains, the building geometry has been excluded from the calibration process; the rationale for this decision is building geometry can usually be estimated with good accuracy either through building drawings or with in-situ measurements. Table 2 shows the list of the variables and the resulting ranking. The large impact of the efficiency of the heat recovery system is largely due to the large airflows required by the full-air heating system. Similarly, the transmittance of the windows has a large impact because of the high windows-to-walls ratio. On the opposite, the impact of the cooling setpoint is due to the simulation period, March. Windows G-value and insulation on external walls show a similar S.I.; insulation was chosen for the calibration due to less reliable information available. Occupant gains in kitchen and bathroom result in no impact due to the spaces being barely used. Living rooms feature variable ventilation between minimum and maximum airflows; in the screening analysis the values minimum and maximum

airflows are varied. Kitchens and bathrooms instead use a constant ventilation strategy, i.e the ventilation flow is kept constant within a simulation; in the screening analysis the value of the ventilation flow is varied. The S.I. of kitchen and bathroom heating setpoints is due to constant ventilation flow scheme. Heat capacity of the thermal envelope, which has been dealt varying the thickness of the external walls, resulted in a limited impact in the screening analysis.

To showcase the method, parameters have been divided into three groups: building envelope (*BENV*), HVAC system (*HVAC*), and building occupancy and behaviour (*BEHV*). Two parameters per group have been chosen, for a total of six parameters; insulation thickness and windows U-value for the building envelope; heat recovery system and airflows for the HVAC, and occupancy gains and temperature set-points for the third group.

Table 2: Results from the screening analysis; selected parameters for calibration are highlighted.

Type	Parameter	S.I.	Selected
HVAC	Heat recovery efficiency	117.2%	Y
BENV	Windows U-value	14.9%	Y
HVAC	Living room minimum airflow	11.9%	N
HVAC	Living room maximum airflow	9.3%	Y
BENV	Windows G-value	8.7%	N
BENV	Insulation thickness	8.3%	Y
HVAC	Kitchen airflows (constant)	8.3%	N
BEHV	Living room heating setpoint	5.7%	Y
HVAC	Bathroom airflows (constant)	5.7%	N
BENV	Infiltrations	4.7%	N
BEHV	Living room occupant gains	4.4%	Y
BEHV	Living room equipment gains	0.8%	N
BEHV	Living room light gains	0.8%	N
BEHV	Bathroom light gains	0.8%	N
BEHV	Kitchen light gains	0.7%	N
BEHV	Bathroom equipment gains	0.7%	N
BEHV	Kitchen equipment gains	0.7%	N
BEHV	Living room cooling setpoint	0.6%	N
BENV	Building envelope heat capacity	0.2%	N
BEHV	Kitchen occupant gains	0.0%	N
BEHV	Bathroom occupant gains	0.0%	N
HVAC	Bathroom cooling setpoint	0.0%	N
HVAC	Bathroom heating setpoint	0.0%	N
HVAC	Kitchen cooling setpoint	0.0%	N
HVAC	Kitchen heating setpoint	0.0%	N

The calibration algorithm has been tested to benchmark its optimization performance. Arbitrarily de-tuned simulation building model building configuration have

been used as initial values for optimization, which used a reference building configuration as a "ground truth". Starting from the initial configuration, the optimization algorithm efficiently converged to the target –benchmark-configuration even with several parameters, without getting stuck in local minima.

Table 3 shows the cumulated errors on energy and temperature after calibrations for different values of the weight parameter β. Weighted CV(RMSE) is the overall error; the lowest weighted CV(RMSE) after calibration is equal to 6% and is found for β=0.75; this value is below the recommended values found in literature and summarized in Table 1, and it ensures that the calibration is satisfactory for both energy and indoor environment.

Table 3: Coefficient of variation for energy and temperature mapped for different values of the parameter β.

β	0.25	0.5	0.75
MBE Energy [%]	-8%	-3%	-2
MBE Temperature [%]	2%	-2%	-2
CV(RMSE) Energy [%]	16%	14%	13%
CV(RMSE) Temperature [%]	3%	3%	3%
Weighted CV(RMSE) [%]	13%	9%	6%

Figure 3 shows measured and simulated trends for averaged temperature and overall energy in the apartments in the initial configuration; these results, before calibration, are for the period between 07-03-19 and 11-03-19. Although the temperature trends almost overlap, the time series illustrates clear discrepancies energy; the CV(RMSE) Temperature is 2%, the CV(RMSE) Energy is 46% and the Weighted CV(RMSE) is 13%.
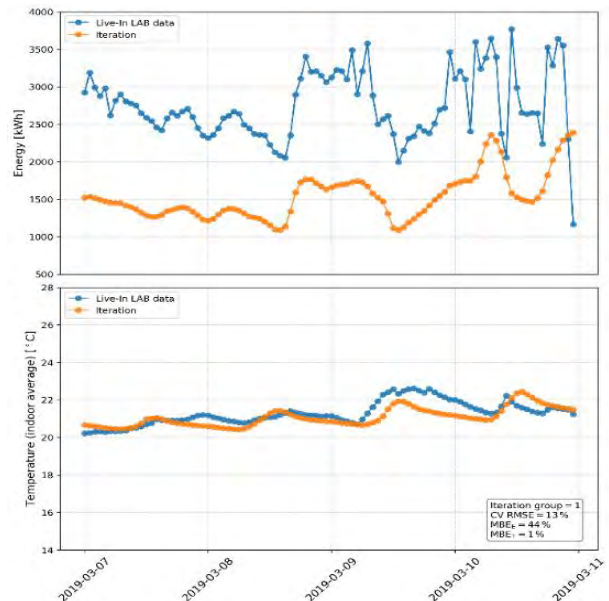
Figure 3: Comparison of energy use (top) and average indoor temperature (below) with hourly resolution in the period between 07-03-19 and 11-03-19 before calibration. Energy and temperature measured are plotted against the actual monitored values.

Figure 4 shows measured and simulated trends for averaged temperature and overall energy in the apartments for the same period after calibration for β=0.75. The Weighted CV (RMSE) is 6% and the time series shows almost overlapping trends for both.
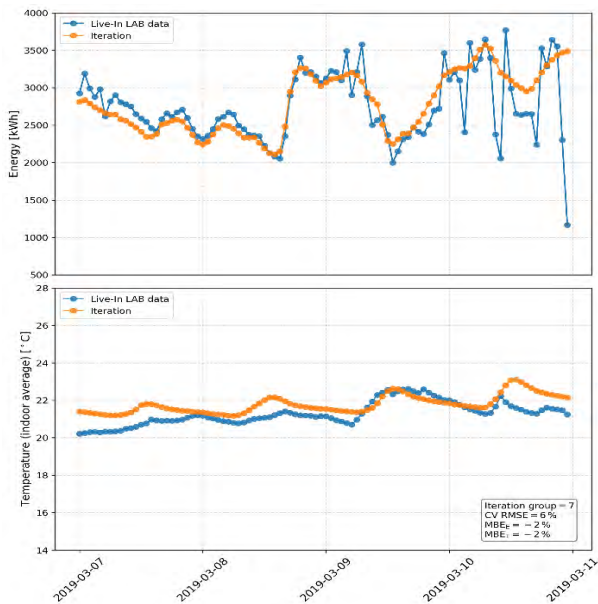
Figure 4: Comparison of energy use and average indoor temperature with hourly resolution in the period between 07-03-19 and 11-03-19 after calibration.

Table 4 summarizes the values of the parameters included in the calibration process for the initial and calibrated configuration for β=0.75.

Table 4: Initial and optimized values for the considered variables.

Parameter	Initial value	Calibrated value
External walls insulation [m]	0.05	0.10
Windows U-value [-]	1.4	1.87
Living room maximum airflow [l/sm^2]	2.0	2.0
Air heat recovery efficiency [%]	0.85	0.60
Heating set-point [ºC]	22	18
Occupants gain [n$_{people}$]	1.0	1.5

Discussion

The screening analysis has a two-fold importance. First, selecting only the parameters with the most impact on the thermal dynamics, it reduces the number of variables to optimize for; this speeds up the overall simulation time and reduces the risk of local minima. Furthermore, including parameters with low impact in the calibration is likely to result higher uncertainty in such calibrated parameters, due to the limited sensitivity that they have in the cost functions. Although the selection of the parameters to calibrate can – and usually is – be done based on expert knowledge of the impact that each parameter has on thermal dynamics and the uncertainty that exists on that parameter, the impact of each parameter on a building model can vary significantly in building and

important parameters may be overlooked and excluded from the validation; the sensitivity analysis mitigates this risk.

The simple screening approach used still has a degree of subjectivity, based on expert knowledge, in the choice of minimum and maximum values of the parameters, which in turn influences the sensitivity index. Another limitation of the chosen screening approach is that, given that it is a local sensitivity analysis approach, the initial configuration has an impact on the results of the screening analysis. A global sensitivity analysis, like the Morris method, can be a more accurate tool the problem but at a cost of a higher computational burden.

Upon completion of the calibration, the implemented methodology has been shown to decrease significantly the discrepancy between measured and simulated data for both energy and temperature. The initial value of CV (RMSE) was 2% for the temperature and 46% for energy with an overall error, CV (RMSE), of 13%; this error has decreased down to 6%, CV (RMSE), with 2% and 13% respectively for a value of the weighting factor β of 0.75. These calibrated values are below the suggested thresholds found in literature and are satisfactory for the chosen hour time resolution.

The introduction of the weighting factor β is considered central in the context of digital twins. Calibration procedures may disregard to quantify the error in the indoor conditions. Qualitative assumptions on indoor temperatures may be sufficient for calibrations for models used for energy auditing or the evaluation of renovation measures. Instead, for digital twins the capability to fine tune the model accounting for both energy and temperatures is expected to deliver a superior model to generate synthetic data to support a better understanding of the behaviour dynamics in relation to advanced control and fault detection schemes, calibrated models are needed for both energy use and indoor environment. In this context, detailed calibrated models with hourly time resolution can be an optimal trade-off between prediction accuracy and the cost to produce them. More refined time resolution calibrations require higher resolution datasets that are often not available, e.g., outdoor data from existing weather stations, prone to errors, like motion detectors sensors or more costly to manage, like indoor data with higher resolution.

Advanced monitoring platforms, like the one of the Testbed KTH, that includes the continuous measurement of indoor environmental variables, occupancy and internal gains from detailed electricity readings, are powerful tools for model calibration and advance the implementation of models for building digital twins. Sensors with low sampling time, occupancy detectors and electricity monitoring can provide useful information to reconstruct the occupancy patterns and estimate internal gains.

An immediate practical extension of the use of the calibrated parameters is to support fault detection and

predictive maintenance; for instance, significant discrepancies in a parameter like external wall transmittance above the design values can pinpoint a problem with the building envelope insulation characteristics, and trigger further investigation.

However, caution should be used, as results presented here are only preliminary; in this case, for instance, parameters are calibrated only on a limited time series to show the viability of the proposed approach and the advantages of calibrating a model with both temperature and energy in the cost function. Given the observation window, the calibrated parameters – though realistic- may change in a calibration carried out over different seasons.

Conclusion

This paper has showcased an innovative calibration procedure for the calibration of building energy models, validated against preliminary data from the Live-In Lab, a recently built residential building testbed in the KTH Main Campus in Stockholm. A detailed building energy model has been created in IDA-ICE and has been calibrated with hourly sampling, which is the current state-of-the-art resolution.

The calibration methodology consists in a screening analysis to select a subset of parameters to optimize and subsequently an optimization process. The implemented calibration minimizes the error between the model and the monitored data with a multi-objective cost function based on the discrepancy between indoor temperature and the energy demand. In the calibration process the user can set a parameter β to weigh the relative importance of the temperature and energy error.

The calibration process has proved to be straightforward and after calibration the overall error has been reduced from 13% to 6%, while guaranteeing that both errors on energy and indoor temperature trends are minimal. For optimized configurations, the proposed procedure has managed to yield a calibration error below the recommended thresholds in the literature.

Although the monitored dataset is currently limited in extension, the observed dynamics in the model follow closely the monitored temperature and energy trends, which is a key feature for the adoption of the model as digital twin.

The sensor platform of the Testbed KTH, which includes the continuous monitoring of indoor comfort conditions, occupancy and internal gains from detailed electricity readings, has proved an invaluable tool to provide the necessary data for calibration and in the evaluation of the impact of user activities.

Future development of this work will include a calibration with extended datasets to study seasonal effects.

Acknowledgements

References

Allesina, G., E. Mussatti, F. Ferrari, and A. Muscio. 2018. "A Calibration Methodology for Building Dynamic Models Based on Data Collected through Survey and Billings." *Energy and Buildings* 158 (January): 406–16. https://doi.org/10.1016/j.enbuild.2017.09.089.

Asadi, Somayeh, Ehsan Mostavi, Djamel Boussaa, and Madhavi Indaganti. 2019. "Building Energy Model Calibration Using Automated Optimization-Based Algorithm." *Energy and Buildings* 198 (September): 106–14. https://doi.org/10.1016/j.enbuild.2019.06.001.

Ascione, Fabrizio, Nicola Bianco, Teresa Iovane, Gerardo Maria Mauro, Davide Ferdinando Napolitano, Antonio Ruggiano, and Lucio Viscido. 2020. "A Real Industrial Building: Modeling, Calibration and Pareto Optimization of Energy Retrofit." *Journal of Building Engineering* 29 (May): 101186. https://doi.org/10.1016/j.jobe.2020.101186.

Ascione, Fabrizio, Martina Borrelli, Rosa Francesca De Masi, Filippo de' Rossi, and Giuseppe Peter Vanoli. 2019. "Energy Refurbishment of a University Building in Cold Italian Backcountry. Part 1: Audit and Calibration of the Numerical Model." *Energy Procedia*, Renewable Energy Integration with Mini/Microgrid, 159 (February): 2–9. https://doi.org/10.1016/j.egypro.2018.12.009.

Box, M. J. 1965. "A New Method of Constrained Optimization and a Comparison With Other Methods." *The Computer Journal* 8 (1): 42–52. https://doi.org/10.1093/comjnl/8.1.42.

———. 1966. "A Comparison of Several Current Optimization Methods, and the Use of Transformations in Constrained Problems." *The Computer Journal* 9 (1): 67–77. https://doi.org/10.1093/comjnl/9.1.67.

Chaudhary, Gaurav, Joshua New, Jibonananda Sanyal, Piljae Im, Zheng O'Neill, and Vishal Garg. 2016. "Evaluation of 'Autotune' Calibration against Manual Calibration of Building Energy Models." *Applied Energy* 182 (November): 115–34. https://doi.org/10.1016/j.apenergy.2016.08.073.

Chong, Adrian, Khee Poh Lam, Matteo Pozzi, and Junjing Yang. 2017. "Bayesian Calibration of Building Energy Models with Large Datasets." *Energy and Buildings* 154 (November): 343–55. https://doi.org/10.1016/j.enbuild.2017.08.069.

Chong, Adrian, and Kathrin Menberg. 2018. "Guidelines for the Bayesian Calibration of Building Energy Models." *Energy and Buildings* 174 (September):

527–47.
https://doi.org/10.1016/j.enbuild.2018.06.028.

Coakley, Daniel, Paul Raftery, and Marcus Keane. 2014. "A Review of Methods to Match Building Energy Simulation Models to Measured Data." *Renewable and Sustainable Energy Reviews* 37 (September): 123–41. https://doi.org/10.1016/j.rser.2014.05.007.

Equa Simulation AB, and Equa Simulation Finland Oy. 2010. "Validation of IDA Indoor Climate and Energy 4.0 with Respect to CEN Standards EN 15255-2007 and EN 15265-2007." http://www.equaonline.com/iceuser/validation/CEN_VALIDATION_EN_15255_AND_15265.pdf.

Heiselberg, Per, Henrik Brohus, Allan Hesselholt, Henrik Rasmussen, Erkki Seinre, and Sara Thomas. 2009. "Application of Sensitivity Analysis in Design of Sustainable Buildings." *Renewable Energy* 34 (9): 2030–36. https://doi.org/10.1016/j.renene.2009.02.016.

"IDA ICE - Simulation Software | EQUA." n.d. Accessed April 27, 2020. https://www.equa.se/en/ida-ice.

Jones, David, Chris Snider, Aydin Nassehi, Jason Yon, and Ben Hicks. 2020. "Characterising the Digital Twin: A Systematic Literature Review." *CIRP Journal of Manufacturing Science and Technology*, March. https://doi.org/10.1016/j.cirpj.2020.02.002.

Kristensen, Martin Heine, Ruchi Choudhary, and Steffen Petersen. 2017. "Bayesian Calibration of Building Energy Models: Comparison of Predictive Accuracy Using Metered Utility Data of Different Temporal Resolution." *Energy Procedia*, CISBAT 2017 International ConferenceFuture Buildings & Districts – Energy Efficiency from Nano to Urban Scale, 122 (September): 277–82. https://doi.org/10.1016/j.egypro.2017.07.322.

"KTH Live-In Lab." n.d. KTH. Accessed May 15, 2020. https://www.liveinlab.kth.se/en.

Li, Wancheng, Zhe Tian, Yakai Lu, and Fawei Fu. 2018. "Stepwise Calibration for Residential Building Thermal Performance Model Using Hourly Heat Consumption Data." *Energy and Buildings* 181 (December): 10–25. https://doi.org/10.1016/j.enbuild.2018.10.001.

Lydon, G.P., S. Caranovic, I. Hischier, and A. Schlueter. 2019. "Coupled Simulation of Thermally Active Building Systems to Support a Digital Twin." *Energy and Buildings* 202 (November): 109298. https://doi.org/10.1016/j.enbuild.2019.07.015.

Monetti, Valentina, Elisabeth Davin, Enrico Fabrizio, Philippe André, and Marco Filippi. 2015. "Calibration of Building Energy Simulation Models Based on Optimization: A Case Study." *Energy Procedia*, 6th International Building Physics Conference, IBPC 2015, 78 (November): 2971–76. https://doi.org/10.1016/j.egypro.2015.11.693.

Mustafaraj, Giorgio, Dashamir Marini, Andrea Costa, and Marcus Keane. 2014. "Model Calibration for Building Energy Efficiency Simulation." *Applied Energy* 130

(October): 72–85. https://doi.org/10.1016/j.apenergy.2014.05.019.

Nguyen, Anh-Tuan, Sigrid Reiter, and Philippe Rigo. 2014. "A Review on Simulation-Based Optimization Methods Applied to Building Performance Analysis." *Applied Energy* 113 (January): 1043–58. https://doi.org/10.1016/j.apenergy.2013.08.061.

Ruiz, Germán, and Carlos Bandera. 2017. "Validation of Calibrated Energy Models: Common Errors." *Energies* 10 (10): 1587. https://doi.org/10.3390/en10101587.

Stark, Rainer, and Thomas Damerau. 2019. "Digital Twin." In *CIRP Encyclopedia of Production Engineering*, edited by The International Academy for Production Engineering, Sami Chatti, and Tullio Tolio, 1–8. Berlin, Heidelberg: Springer Berlin Heidelberg. https://doi.org/10.1007/978-3-642-35950-7_16870-1.

Taylor, Z. Todd, Yulong Xie, Casey D. Burleyson, Nathalie Voisin, and Ian Kraucunas. 2019. "A Multi-Scale Calibration Approach for Process-Oriented Aggregated Building Energy Demand Models." *Energy and Buildings* 191 (May): 82–94. https://doi.org/10.1016/j.enbuild.2019.02.018.

Yuan, Jun, Victor Nian, Bin Su, and Qun Meng. 2017. "A Simultaneous Calibration and Parameter Ranking Method for Building Energy Models." *Applied Energy* 206 (November): 657–66. https://doi.org/10.1016/j.apenergy.2017.08.220.

Zhu, Chuanqi, Wei Tian, Baoquan Yin, Zhanyong Li, and Jiaxin Shi. 2020. "Uncertainty Calibration of Building Energy Models by Combining Approximate Bayesian Computation and Machine Learning Algorithms." *Applied Energy* 268 (June): 115025. https://doi.org/10.1016/j.apenergy.2020.115025.

Zuhaib, Sheikh, Magdalena Hajdukiewicz, and Jamie Goggins. 2019. "Application of a Staged Automated Calibration Methodology to a Partially-Retrofitted University Building Energy Model." *Journal of Building Engineering* 26 (November): 100866. https://doi.org/10.1016/j.jobe.2019.100866.

Influence of space heating distribution systems on the energy flexibility of Norwegian residential buildings

Christoph Nickl[1,3,*], John Clauß[2,3], Laurent Georges[3]

1 Team für Technik GmbH, Munich, Germany
2 SINTEF Community, Trondheim, Norway
3 Norwegian University of Science and Technology, Trondheim, Norway
* *nickl@tftgmbh.de*

Abstract

This work evaluates the influence of the heating distribution system on the energy flexibility of highly insulated single-family residential buildings. The behavior of three different systems (air heating, radiator heating, and floor heating) is assessed for schedule-based and price-based rule-based control of the heating system aiming at peak shaving and cost reduction. Dynamic building performance simulations are performed in the software tool IDA ICE.

The investigated controls activate the thermal mass and water storage tanks. When activating only the thermal mass, the energy use during peak hours decreases by nearly 10% in the radiator heating cases, in the air heating cases the effect is less pronounced and shows little to no shifting potential. In the floor heating cases, a slight decrease in energy use is found for the price-based control, whereas a slight increase is observed with a schedule-based control.

In contrast, when domestic hot water and space heating tank set points are adjusted, the energy use during peak hours decreases in all versions. The schedule-based control achieve reductions between 20% to 30% among the different heat emission systems. The price-based control however, is less effective, leading to lower reductions in energy use. The total energy use and operational costs increase in each case, most pronounced with the schedule-based set point variations for the domestic hot water and space heating tank.

It is found that a good demand response measure is not only dependent on a correct selection of the set point at the supervisory control level, but also a good implementation of the local controller that considers the thermal dynamics of the heating system is required.

Introduction

In the current electricity supply structure, power generation follows demand. The ongoing integration of intermittent renewable energy sources into the power grid in Europe is a challenge for grid stability. The control of the demand side to match the instantaneous production may be one key to solve this problem (Lund *et al.*, 2015). This is usually done by shifting loads using storages. For example, the thermal masses of buildings can be considered storages, which enable postponing active cooling and heating without violating thermal comfort (Arteconi *et al.*, 2012). The storage potential is largely depending on the type of construction, the heat distribution system and user specific comfort criteria. In combination with electricity-based heating, buildings can therefore offer different services for the grid by applying demand side management (DSM) and load control strategies (IEA DSM, 2016). In general, DSM describes the change of use in magnitude and/or time. Flexibility can also be obtained by using storage tanks, or in different form, by managing onsite generation and batteries. This work focuses on the influence of the space heating (SH) distribution system on the energy flexibility of residential buildings.

Many studies on energy flexible buildings have been carried out under the framework of IEA Annex 67, which defines "energy flexibility" as "*the ability to manage [a building's] demand and generation according to local climate conditions, user needs, and energy network requirements*" (Jensen et al., 2017).

Even though heating flexibility of buildings plays an important role for district heating, most studies on building energy flexibility focus on all-electric buildings. Naturally, the focus is on power generation from photovoltaic or combined heat and power and the main consumers, which typically are white goods, cooling appliances, air handling units and in case of electrified heating, heat pumps or resistance heaters. Heat pump systems with thermal storages are seen as an attractive heating system in cold climates. Most related studies focus on floor heating as a heat distribution system. However, radiator systems were studied in (Baetens *et al.*, 2010; Le Dréau and Heiselberg, 2016; Reynders *et al.*, 2013; Wolisz *et al.*, 2013).

Heat distribution system

Besides building-specific and time-varying external parameters, the heat distribution system is expected to have significant influence on the energy flexibility potential, as floor heating (FH), air heating (AH), and radiator (RAD) heating show different dynamics.

Air heating is very dynamic and reacts directly to the heat demand needed in the room. The heat transfer can be considered completely convective. For radiator systems,

the heat transfer is usually (around 70%) convective. The air volume is heated directly without considerable delay, where the heat-up time is in the range of a few minutes. The warmer air then activates all surrounding surfaces in the room. The amount of heat that can be stored is largely depending on the material properties of the outermost layer of the construction. Regarding water-based FH, several system specifications are possible. In general, pipes containing water or other media are embedded in the construction. A distinction is made between dry systems, usually using a panel of dry screed above the pipes and wet systems, with pipes completely covered by concrete. In case heating is needed, the slab or the construction is heated and heat is conducted to the floor covering. The warmer surface then heats up the air, and the other surfaces via radiation. As all the layers have different properties, the dynamic behavior is strongly dependent on the chosen system. Capillary systems can heat up almost as fast as radiator systems when parquet flooring is chosen but cool down more slowly. For conventional systems, the heat-up and cool down times are in the range of several hours.

Research question

This work evaluates the influence of the SH distribution system on the energy flexibility of highly insulated single-family residential buildings by investigating AH, RAD heating and FH. Compared to previous studies in literature, this work provides detailed information on the design procedure of the investigated heat emission systems. In this work, heat distribution system refers to the emission, distribution and control system for each of the three systems studied.

Methods

To evaluate the influence of the SH distribution system on the energy flexibility, detailed dynamic simulations are carried out. The modelling procedure applied in this work is presented in Figure 1.

Simulation procedure

Building performance simulations are performed using the software IDA ICE 4.7.1. The building is modelled with the previously mentioned heat distribution systems. The sizing of these systems is done according to NS-EN 12831-1:2007. Four rule-based control strategies are implemented, which aim to activate the thermal mass in the rooms only or additionally also the SH and DHW tanks. Results are evaluated based on the key performance indicators energy use, operational costs, and load shifting.

Case study description

The case study building is the Living Laboratory at the Gløshaugen Campus of the Norwegian University of Science and Technology (NTNU). It is a single-family residential building, which comprises of two bedrooms, a bathroom and a combined area for cooking and living. The building has a total heated floor area of 105 m². A floor plan of the building is presented in Figure 2. As the building is designed as a Zero Emission Building (ZEB),

the building envelope is highly insulated and airtight, almost in accordance with the Norwegian passive house standard NS 3700:2013 (Standard Norge). The building has a lightweight wooden construction.
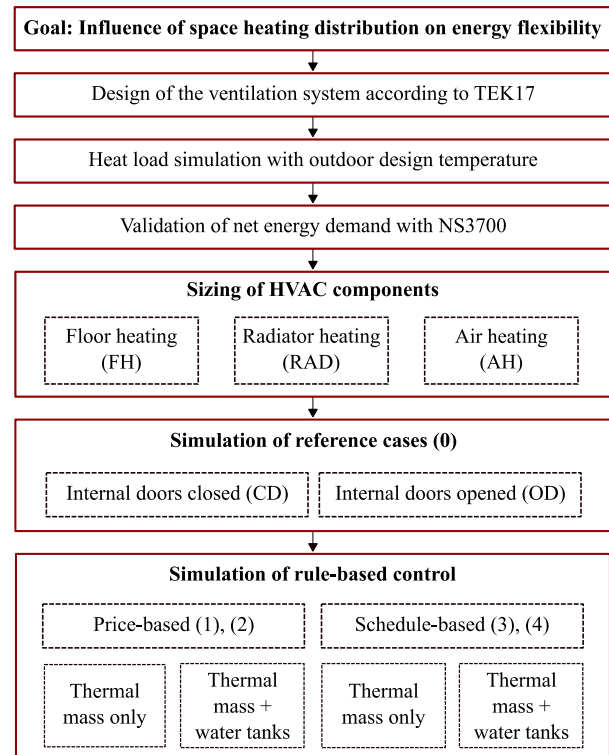
Figure 1. Overview of the modelling procedure.

Climate and location

For improved coherence of weather and spot prices, measured weather data of the year 2015 are used, retrieved from shinyweatherdata (Lukas Lundström).

Internal heat gains

As it is a highly insulated building, the hourly profiles for internal gains from lighting, electric appliances and occupants have a great impact on the thermal demand of the building. In this study, schedules for occupancy and lighting follow hourly profiles for the ISO/FDIS 17772-1 standard developed by (Ahmed *et al.*, 2017). The number of occupants and the nominal power of the light bulbs are adjusted to fit the yearly specific use of 13.1 kWh/m² and 11.4 kWh/m² for occupants and lighting given in NS/TS 3031:2016 (Standard Norge, 2016). The hourly schedule and heat gains from appliances are in accordance with NS/TS 3031:2016. All internal gains are assumed equally distributed within the building. Windows and outer doors are closed at all times.

Ventilation system

The ventilation system is designed according to the installed system in the case building, and the current building regulation TEK17. The ventilation system comprises of a central air handling unit with heat recovery (efficiency 85%) and an electrical heating coil with a nominal power of 1200 W in the FH and RAD heating

cases. In the AH cases the electrical heating coil is replaced by a water-based coil. The specific fan power is set to 1.5 kW/(m³/s) for both fans. The efficiency of the fans is set to 0.7. The air flow rates are determined by using the pre-accepted minimum values according to TEK17, leading to a total ventilation rate of 154 m³/h.

In heating mode for the FH and RAD cases, the supply air temperature is constant at 19°C, and since there is no cooling coil, the supply air temperature is close to the outdoor air temperature for ambient temperatures above 19 °C. Further details for the air heating cases are discussed in the next section.

Heat generation system

The core of the heating setup of the Living Lab is a water storage tank which consists of two tanks in one shell. The upper part consists of the domestic hot water (DHW) tank and the lower part is for SH. In the SH tank there are two heat exchangers, one for the solar thermal circuit and one for pre-heating DHW. This way the solar thermal panels mounted on the south facade of the building can support both SH and DHW. Primarily, the heat demand is covered by a ground source heat pump (GSHP) which is connected to a horizontal surface collector. The geothermal collector supplies the SH tank directly whereas it is connected to the DHW tank via a heat exchanger. Both tanks can also be heated with electric resistance heaters, with a power of 3 kW (DHW) and 9 kW (SH) respectively. To reach the ZEB balance, the building is equipped with a 12 kWp photovoltaic system.

Sizing and implementation in IDA ICE

It is a common approach to design heating systems by calculating the overall heat loss of a building at design outdoor temperature (DOT). Regardless of the operation mode, the size of the heat pump is therefore always dependent on the thermal properties of the building and the climate (Le Dréau and Heiselberg, 2016). Water storage tank volumes are dependent on the nominal power of the heat pump. Fischer et al. (Fischer *et al.*, 2016) showed that current sizing practices already lead to sufficiently large tanks for the use of DSM.

A heat load calculation is carried out in accordance to NS:EN 12831-1:2017 (Standard Norge, 2017). The proposed internal design temperature is constant at 24°C for the bathroom and 20°C for all other rooms. The DOT is -22 °C for Trondheim (Sintef Byggforsk). Solar radiation and internal heat gains are neglected for the heat load calculation. The ventilation system has a constant supply air temperature set point of 19°C. The calculation is done using an ideal heater in each room. These room units have no mass and react directly to the heat power need. The required zone heating is 3.58 kW.

Heat generation system

Heat pump

The operating mode of the heat pump was chosen monovalent/mono-energetic. The chosen GSHP, a "Calorex WW3500", has a nominal power of 3.5 kW and a COP of 4.0 at rating conditions 0/35°C. For higher temperatures, e.g. a RAD or AH system, the available power will decrease to 2.6 kW at 0/55°C. The maximum supply temperature for DHW is 65°C. The compressor power can modulate between 30% and 100% of the nominal capacity.

Space heating tank

The recommendations for sizing the SH-tank vary widely and are depended on blocking times, the chosen heat emission system and the used heat pump. According to manufacturer data, 20-25 l/kW are used to optimize the duration of heat pump cycles, whereas 30-60 l/kW are advised when blocking hours are considered (Viessmann Deutschland GmbH, 2011). Other references also distinguish between FH and RAD heating. The advised volume is doubled for radiators, due to the smaller inertia of the system and smaller amount of water in the circuits (Stiebel Eltron, 2017). As the heat generation setup should be similar for all versions, a volume of 200 l was chosen corresponding to 57 l/kW.

Domestic hot water tank

The tapping profile for DHW is decisive for sizing the DHW tank. In the model, the profile from NS/TS 3031:2016 for small houses is implemented. The hourly peak demand is 1.442 kWh and the daily consumption is 7.2 kWh. Assuming cold water at 10 °C and a desired DHW temperature of 60 °C, this leads to a volume of 124 liter. For the model, a 160 l DHW tank was chosen. For the implementation in IDA ICE dimensions of a commercially available storage tank are used. That way, physical heights of tank-pipe connections are already defined. The volumes of the internal heat exchangers are calculated according to the given pipe diameter and surface area.

Water storage tanks are described in IDA ICE as a piled number of horizontal layers. For each layer the mass and heat balances are computed. Both tank parts consist of six layers with heights of 0.195 m (SH) and 0.181 m (DHW). The DHW tank is equipped with two temperature sensors, which are in the upper part (TM 4) and in the lower part of the tank (TM 3). The charging of the tank begins when the temperature of TM 4 is below 55°C and stops when the measurement from TM 3 is above this set point temperature. The auxiliary heater (AUX 2) switches on/off with a dead band of 0.8 K when the temperature of the upper sensor is 1 K under the threshold. The charging of the SH tank is rather similar; there are also two sensors at different heights (TM1 & TM2). If the measurements of the upper sensor fall short of the value of the outdoor temperature compensation curve (OTCC) of the chosen heat distribution system, the tank is charged until the temperature at the lower sensor is 5 K above the current value of the OTCC. This also ensures a reasonable run time of the heat pump. The auxiliary heater (AUX 1) is switched on when TM2 is 2 K below the current value of

the OTCC. A dead band of 6 K was applied here, because of its high nominal power of 9 kW the run time would otherwise be shorter than two minutes. A detailed description of the charging principle is presented in (Clauß and Georges, 2019).

The heat pump has a SH and a DHW operation mode. The charging of the DHW tank has priority. In DHW mode, a P-controller adjusts the mass flow through the condenser to achieve a temperature of 60°C. The heat pump is then operating at full capacity. In SH-mode, the mass flow is constant and the compressor power is adjusted continuously between 30%-100%.

Water-based radiator

Sizing

A single radiator is placed in the middle of the house. Similar simplified heat distribution systems were assessed in studies with focus on thermal zoning in passive houses (Georges *et al.*, 2016; Georges *et al.*, 2017). The radiator model is based on the commercially available product "Lygnson MC33 2300x900". The power at design conditions (75/65/20°C) is 7590 W. These temperatures are too high to be operated with a heat pump system. At operation conditions (50/45/20°C) the power is 3569 W.

Implementation in IDA ICE

The radiator is placed next to the wall between *Floor* and *Kitchen*. The unweighted average of the mean air temperatures in both rooms is chosen as the input signal. The mass flow is controlled by a PI-controller. The maximum mass flow is calculated by the software automatically based on the design power and exponent (Lygnson: 1.28). It is worth mentioning here that the inertia of a radiator is not represented by this IDA ICE model. In the simulations the surface temperature of the radiator-wall- part drops according to the instantaneous delivered power.
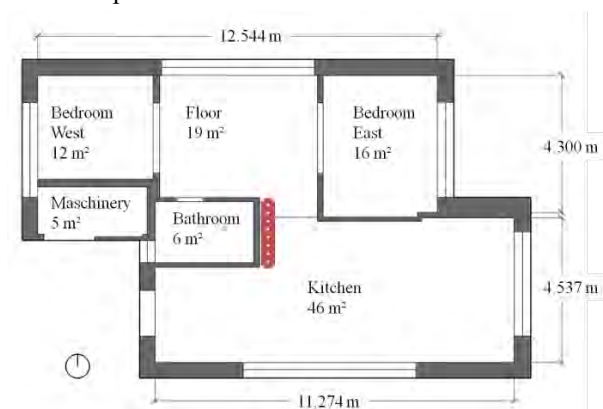
Figure 2. Floor plan and location of the radiator.

Water-based floor heating

Sizing

The FH is implemented as a dry screed system, "Roth Clima Comfort TBS" is used for design and calculation according to EN 1264-3:2009 (European Commitee for Standardization, 2009). The construction on top of the

pipes consists of parquet flooring (22 mm) and dry screed tiles (25mm), underneath there is a wooden frame construction with a U-value of 0.1 W/(m²K). The system can be considered as fast reacting compared to conventional wet systems.

From a practical point of view, the supply temperature is chosen for a distance of 15 cm between pipes and a desired temperature difference of 5 K for the zone with the highest specific heat load (except Bathroom). The supply temperature for all zones is given as 38.2 °C. Based on the FH system of that room, suitable distances between the pipes and thus temperature differences and mass flows are calculated for all other rooms. However, with this system the required heating power for the bathroom cannot be reached. Even with a temperature difference in the flow of 3 K, there is still a margin of around 100 W. For calculating the total mass flow in the circuits at design conditions, the downward heat flux density is approximated to 4.37 W/m², originating from the heat resistance of the construction below the circuits (ca 0.332 m with 0.036 W/(mK)) and a temperature difference of 42 K (difference between DOT and indoor air temperature). The total nominal heating power to the zones is 3445 W, which is 136 W lower than the total heat load in the zones.

Implementation in IDA ICE

FH systems are implemented as a heat exchanger immersed in one layer of the floor construction with uniform layer temperature. The structural component is divided into two parts, with layers above and beneath the floor heating pipes. The maximum mass flow is calculated automatically in IDA ICE based on the given power and temperature difference at design conditions. The heat transfer coefficient between the pipes and the layer they are located in is assumed to be 10 W/m²K. The mass flow in the circuits are controlled by a P-controller which uses a sensor for mean air temperature.

Air heating

Sizing

The third considered heat distribution system is AH. AH uses a temperature control to adjust the emitted power while the RAD and FH use a weather compensation heating curve in combination with mass flow control. Nevertheless, hygienic ventilation rates are not sufficient for times of high heating demand as the maximum inlet air temperature is defined at 55 °C, which is the temperature of dust carbonization and in line with (Georges *et al.*, 2014). Consequently, with the volume rates according to TEK17, only 1.8 kW of heat can be supplied. To cover the heat load of 3.5 kW, the total volume rate has to be increased from 153.7 m³/h to 298 m³/h, which is equivalent to 0.9 ACH

Implementation in IDA ICE

The air is heated by a water-based heating coil, which is implemented as a fixed-size heating coil model with mass flow control. The heat transfer is calculated according to

the NTU method. The heating coil is configured according to manufacturer data from "system air VBC 200-3".

In general, all the discussed AH versions show high temperatures in the Bedrooms, and colder temperatures in the living room. This is conflicting with findings of several studies interviewing occupants of super-insulated building in cold climates. The desired temperatures ranged from 22-24 °C in the living room whereas 16 °C was desired in bedrooms (Georges *et al.*, 2017; Georges *et al.*, 2014). Due to this, the pre-accepted ventilation rates according to TEK 17 (Kommunal- og moderniseringsdepartementet, 2017) might not be suitable for a centralized air heating concept.

Differences between the heat distribution systems

To summarize, all three distribution systems are connected to a water storage tank and thus are dependent on the heat pump operation. For AH, the air is heated up in a water-based heating battery. The two other distribution systems are directly connected to the water storage tank.

All three heat emission systems have a limited thermal inertia. Even the floor heating is relatively fast reacting as it is a lightweight construction: nevertheless, the investigated RAD and AH systems have a shorter reaction time and reach a desired room temperature faster than the FH system. This is due to i) the direct heating of the air for AH, ii) short heat-up times for the surface of the radiator, but iii) a delay of reaching a required surface temperature and thus heating the air for the FH system due to mainly radiative heating.

As shown, there are slight differences among the three heat emission systems regarding their nominal power: 3500 W for AH, 3445 W for FH and 3569 W for RAD.

Differences in the thermal behavior of the heat distribution system can be attributed to the differences in thermal inertia of each of the systems as well as differences in the system-specific control.

Controls for energy flexibility

Price-based control

Predictive price-based control 1

In this control approach, the set points in the zones are changed according to a price signal. This control is aiming at reducing operational costs by reducing the energy use during hours with high spot prices, based on the principle presented in (Clauß *et al.*, 2019). The spot price evolution is divided into three segments: low, medium and high. The upper threshold is 75% of the maximum spot price in the next 24 h and the lower threshold is 25% of the maximum spot price. When the current value is between the thresholds, temperature set points are kept. If the current hourly spot price is considered high, the set point will be decreased by 2 K; if it is low, the set point will be increased by 2 K. The comparison is done for each hour and its respective succeeding 24 hours. The analysis is

based on data from 2015 for the Trondheim bidding area at Nordpool market (Nordpool).

Predictive price-based control 2

The price-based control 1 is extended to the DHW and SH tanks. These set points in the tanks are raised or lowered by 3 K depending on the price signal.

Schedule-based control

Peak-shaving control 3

Based on a typical energy use profile for Norwegian households (Bergesen *et al.*, 2013), the heating set points in the zones are adjusted depending on a schedule. The schedule aims to reduce the electricity need in peak hours 7–9a.m. and 5–7p.m. Consequently, the set point is decreased from 21°C to 19°C in these hours. In the time from 5–7a.m. and 4–5p.m. the SH set-points are increased to 23°C. The remaining hours of the day, the set point is 21°C.

Peak-shaving control 4

Control approach 3 is expanded to the DHW and the SH tank. These set points are increased by 3 K in the hours before the peak and decreased by 3 K during the peak hours.

Results

Results are evaluated based on the following performance indicators:

- *Heating use for DHW and SH:*
  The sum of energy delivered to the heat distribution system or used for DHW.

- *Electricity delivered in peak hours*
  The hourly values of total electricity use (heating and other electricity consumers) in peak hours 7-9a.m. and 5-7p.m. are summed up and presented in kWh/m²a.

- *Energy costs during operation without feed-in*
  For each hour, total electricity use is multiplied with the current spot prices used in the controls above. In average, these are 0.189 NOK/kWh, a constant grid fee incl. tax of 0.493 NOK/kWh and taxes for electricity use of 0.139 NOK/kWh were added. Consequently, the total average electricity price is 0.817 NOK/kWh. The hourly values are then summed up and presented.

- *Energy costs during operation with feed-in*
  The surplus electricity generated by the building integrated PV is multiplied by the current spot price and subtracted from the current costs due to consumption. This is also done with hourly resolution. Prices are similar for imported and exported electricity.

Evaluation reference scenarios

As shown in Figure 1, there are two separate reference scenarios for the open doors and closed doors cases respectively. Both reference scenarios have constant heating temperature set-points of 21 °C for all three heat distribution systems.

The annual heating needs for SH and DHW is 73.0 kWh/m², 84.1 kWh/m² and 72.5 kWh/m² for the open door (OD) cases for AH, FH and RAD heating, respectively. The FH versions stand out, because of higher transmission losses caused by the tempered slab. Nevertheless, the corresponding electricity use is lowest for FH, as the maximum supply water temperature is in general lower (38.2°C) compared to air heating (58°C) and radiator heating (50°C). FH also leads to the highest COP of the heat pump.

The closed door (CD) cases of FH and AH show only small deviations in heating energy use from the OD versions as each zone is provided with the needed amount of heat.

The RAD cases clearly show that closed doors significantly reduce the transport of heat to the zones without heating device. Similar findings are presented in (Johnsen *et al.*, 2019). For the closed door RAD cases, the room temperature set-point of 21°C is reached faster. In contrast, the closed-door AH version has a slightly higher heating demand, as the heat supplied in the bedrooms is prevented from direct exchange with the other zones. AH with closed doors leads to higher volume-averaged indoor temperatures to enable the right temperature in the living areas.

The amount of electricity delivered during peak hours in the OD versions is highest in the AH case followed by RAD and FH with 15.9, 15.8 and 13.8 kWh/(m²a), respectively. Again, electricity use of domestic appliances is dominant with 8.6 kWh/(m²a) in all versions.

Consequently, the amount of electricity delivered during peak hours for heating only differs strongly for the different heat emission systems. In the FH cases it is only 5.2 kWh/(m²a) representing ca 24% of the annual heating energy use. In the RAD and AH cases this share is between 33 and 34%, thus leading to a higher shiftable load. This difference is due to the higher supply water temperatures for AH and RAD heating leading to a lower COP of the heat pump and higher average temperatures in the tank.

Evaluation control strategies open door cases

Figure 3 shows a comparison of the heating energy use for the open door cases for the different control strategies.

The implementation of price-based control 1, e.g. the change of the heating set point in the zones, resulted in higher electricity use for each of the heat distribution systems. Compared to the reference cases, energy use rises 8%, 3% and 4% for AH_1_OD, FH_1_OD and RAD_1_OD respectively.

Peak hour energy use for heating only was reduced by 17% in the RAD version, by 7% for AH and by 27% for FH. Nevertheless, this control approach also resulted in higher operational costs, as the increased temperature set point is kept for long low-price periods, which could not be balanced by cost savings due to lower prices.

The price-based control 2 also includes the DHW and the SH tank. The total annual electricity use and operational costs increase compsared to the reference case and price-based control 1.
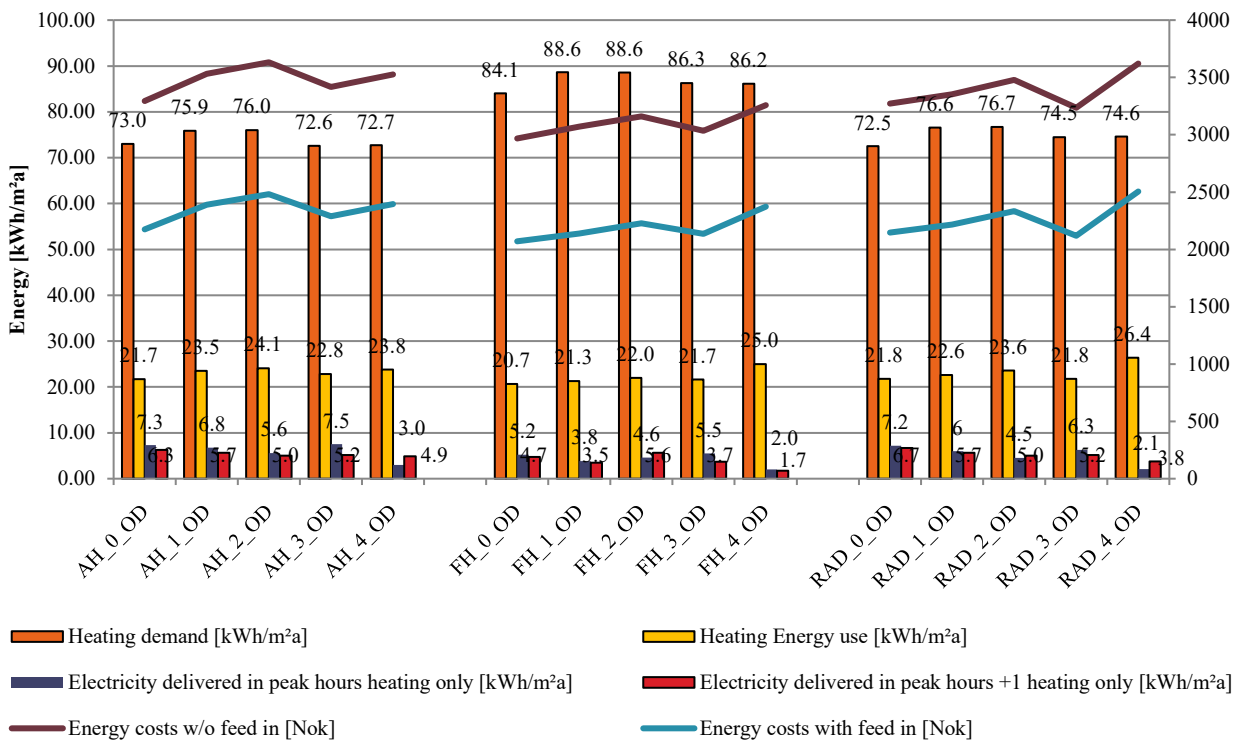
Figure 3. Comparison of the heating energy use for the open door cases for the different control strategies (AH and RAD with PI-controller, FH with P-Controller).

The is due to extensive periods with high temperature set-points, leading to higher heating losses from the tank as well as to prolonged periods of DHW heating by the heat pump. Due to the DHW prioritization of the heat pump, a more frequent use of the electric auxiliary heater in the SH tank is required. The reduction of consumption in peak hours is best for the radiator system (38%), followed by the air heating system (23%). In the floor heating case however, consumption decreased by 12%.

The schedule-based control 3 is able to reduce the energy use during peak hours for the RAD versions. Control 3 does not lead to a reduction of electricity use in peak hours for the FH version, which can be attributed to the combination of four phenomena: i) in the case of control strategy FH_3_OD the heat pump continues running for some time after the zone heating setpoint has been reduced due to the charging strategy of the SH tank. It has been shown that the same control was able to shift energy use, if the period from 8-10a.m. (-22%) instead of 7-9a.m. (+5%) was considered as peak period. The choice of local controller may delay the stop of the heat pump; ii) as stated previously, FH has its own thermal mass and has a higher share of radiant heating, iii) the heating systems use air temperature, not the operative temperature as control signal, and iv) the tuning of the PI-controller parameters of the heat pump control. The chosen PI-controller parameters may lead to integral windup problems that cause an extended heat pump operation until the integral error has come back to 0, especially after set points have been reduced.

When also considering adjusting the set-points for DHW and SH on the heat generation side (control 4), the reduction of peak hour consumption (59% for AH, 61% for FH and 71% for RAD) is the most pronounced, but at the expense of higher costs and total consumption.

Influence door opening

Door opening has little to no influence when the heat distribution is planned according to heat demand of each zone. Consequently, the air heating and floor heating results do not deviate much from the respective open door versions. On the contrary, the simplified heat distribution with one radiator in the floor and kitchen is naturally largely depending on the balancing effects of airflow through internal openings.

Discussion

This work is aiming at evaluating the influence of the heat distribution system on the energy flexibility of residential buildings. However, the case study building only represents a small percentage of the actual building stock. Studies (Reynders *et al.*, 2017; Le Dréau and Heiselberg, 2016) showed that differences between RAD and FH change with the age of the building.

It should be noted that the case study building is not suitable for AH. The heat loss of the envelope constructions can be considered too high. The ventilation rates have to be increased significantly (up to 0.9 ACH)

in times of cold outdoor temperatures to ensure thermal comfort. Due to the needed supply air temperatures up to 50 °C the indoor air would be very dry, and humidification would be required to ensure comfortable surroundings. However, local discomfort may occur.

A general concern is the variation of the supply temperature for the heating systems, as this temperature is a trade-off between available power and system losses due to higher temperatures as a function of the outdoor temperature. In the current work, these temperatures are calculated in relation to the needed heat load for an indoor temperature of 23°C as this is the maximum temperature set point for SH in the investigated versions. That means, at any outdoor temperature, there should be enough power to heat up the building to 23°C. Nevertheless, if the heating is supposed to happen in a short period of time, more power may be required. Furthermore, the schedule-based controls only use heat-up and cool-down periods of two hours, whereas longer periods would also be feasible.

The heating system layout, especially pre-heating of DHW in the SH tank, can be seen critically. Whenever DHW is needed the SH tank is cooled down and the heat pump heats the DHW tank first. This causes an increased use of the backup heater in the SH tank. The capacity of the auxiliary heaters could also be reduced. The auxiliary heaters are active for only a short time but lead to significant peaks in energy use. Furthermore, the internal heat exchanger for DHW pre-heating causes problems for the evaluation of the operation of the water-based heat distribution systems:

- i) As soon as SH is required, heat is taken from the tank without operating the heat pump,
- ii) Afterwards, heat is taken from the tank while the heat pump is operating to keep the temperature set point in the SH tank,
- iii) The heat pump continues its operation to charge the SH tank even though no more heating is required in the zones due to three issues:
  - a) DHW is drawn and the internal heat exchanger in the SH tank cools down the SH tank.
  - b) The PI controller has to react to the cool down of the tank that comes from the cold water flow through the heat exchanger.
  - c) Integral windup of the PI controller as it tries to compensate for the positive error from the heating period until the temperature set point is reached.

The RAD system has a lower heating demand (see Figure 3) as it mainly supplies heat to the *floor* and *kitchen*, whereas the bedrooms are mainly heated by the ventilation system. A temperature set point of 21 °C is not sufficient for the RAD system, if also the other rooms are supposed to reach 21 °C.

Conclusion

Several cases were set up to evaluate the influence of the space heating distribution on energy flexibility. Four rule-

based controls were introduced and their effects on energy use and costs evaluated.

All systems have been sized to have a similar nominal power. The performance of the three emission systems is rather similar. The performance is mostly influenced by the quality of the control rather than the properties of the heat emission system. The small differences come from specific aspects for each of the heat emitters and the way they are modelled.

- The floor heating system shows the highest increase in heating energy use and costs. That is especially the case for the schedule-based controls.
  Floor heating has a lower temperature level which leads to higher COP but it has some additional heat losses through the floor. Among the three systems evaluated, it is the most flexible for temperature zoning as there is at least one FH circuit per room. It is found that the proposed schedule-based control is not suitable for the proposed FH system configuration. It is essential to consider the time constant of the heating system when designing proper control strategies, meaning that change in air temperature set point and the heating hysteresis in the SH tank have to be coordinated Furthermore, it is found that a good demand response measure is not only dependent on a correct selection of the set point at the supervisory control level (like with MPC or RBC), but also a good implementation of the local controllers. This effect is often ignored. Usually, studies on demand response focus on the supervisory control level and do not consider the local controller, which here has proven to be responsible for a delay of the stopping of the heat pump leading to a deteriorated performance with regards to shifting energy use in a defined period.
  Both price-based controls are not able to decrease operational costs. Due to low hourly fluctuations in electricity prices in Norway in combination with the control not always loading the building at the right time makes both controls not very efficient. Furthermore, the heating set points are increased for extended periods.

- The air-heating is not suited for this building as the building nominal heating power is too high. In the air heating versions, the control strategies focus on charging the thermal mass and show little to no effect. In general, the problem of air heating is the temperature zoning with closed internal doors (also shown in (Georges *et al.*, 2014). The average temperature in the building has to increase significantly to ensure the right temperature level in the living room. It is also difficult to get cold bedrooms with warm living areas.

- The radiator system shows the best performance in terms of shifting loads without significantly increasing cost and energy use. The simplified space-heating using one radiator is working well, but ensuring high temperatures in bedrooms with closed internal doors

can be challenging as the thermal mass in other rooms cannot directly be activated. In that regard, thermal zoning is a disadvantage. This has also been concluded by (Johnsen *et al.*, 2019).

- Comparing FH and RAD heating for the time period from 8a.m. to 10a.m., the controls show a similar behavior and energy use is in the same order of magnitude for controls 3 and 4. In IDA ICE, the FH has a thermal inertia, and is therefore effected by the delay of stopping the heat pump operation.

- It is shown that a lightweight FH system does not behave very differently from a radiator system, except from a small delay. This is an important conclusion as most residential buildings in Norway can be considered as lightweight.

- Regarding the different control strategies, the rule-based controls show a better performance when also activating the DHW storage as the storage efficiency of the tank is higher than the heat storage efficiency of the thermal mass of the building construction.

For future research, the influence of the sizing of the heat distribution components and the role of the outdoor compensation curve should be further investigated. It should also be tested how the systems behave for longer activation times and periods. Advanced controls like model predictive control (MPC) or model-free soft (or intelligent) control can be tested to operate each system in a better way (i.e. closer to optimal control).

References

Ahmed, K., Akhondzada, A., Kurnitski, J. and Olesen, B. (2017), "Occupancy schedules for energy simulation in new prEN16798-1 and ISO/FDIS 17772-1 standards", *Sustainable Cities and Society*, Vol. 35, pp. 134–144.

Arteconi, A., Hewitt, N.J. and Polonara, F. (2012), "State of the art of thermal storage for demand-side management", *Applied Energy*, Vol. 93, pp. 371–389.

Baetens, R., Coninck, R. de, Helsen, L. and Saelens D. (2010), "The impact of the heat emission system on the grid-interaction of building integrated photovoltaics in low-energy dwellings".

Bergesen, B., Henden Groth, L., Langseth, B., Magnussen, I.H., Spilde, D. and Wiik Toutain, J.E. (2013), *Energy consumption 2012: Household energy consumption*, Oslo.

Clauß, J. and Georges, L. (2019), "Model complexity of heat pump systems to investigate the building energy flexibility and guidelines for model implementation", *Applied Energy*, Vol. 255, p. 113847.

Clauß, J., Stinner, S., Sartori, I. and Georges, L. (2019), "Predictive rule-based control to activate the energy flexibility of Norwegian residential buildings. Case of an air-source heat pump and direct electric heating", *Applied Energy*, Vol. 237, pp. 500–518.

European Commitee for Standardization (2009), *Water based surface embedded heating and cooling systems -*

Part 3: Dimensioning, Vol. 91.140.10 No. EN 1264-3:2009.

Fischer, D., Lindberg, K.B., Madani, H. and Wittwer, C. (2016), "Impact of PV and variable prices on optimal system sizing for heat pumps and thermal storage", *Energy and Buildings*, Vol. 128, pp. 723–733.

Georges, L., Berner, M. and Mathisen, H.M. (2014), "Air heating of passive houses in cold climates. Investigation using detailed dynamic simulations", *Building and Environment*, Vol. 74, pp. 1–12.

Georges, L., Håheim, F. and Alonso, M.J. (2017), "Simplified Space-Heating Distribution using Radiators in Super-Insulated Terraced Houses", *Energy Procedia*, Vol. 132, pp. 604–609.

Georges, L., Wen, K., Alonso, M.J., Berge, M., Thomsen, J. and Wang, R. (2016), "Simplified Space-heating Distribution Using Radiators in Super-insulated Apartment Buildings", *Energy Procedia*, Vol. 96, pp. 455–466.

IEA DSM (Ed.) (2016), *IEA DSM Task 17 - Conclusions and Recommendations: Demand Flexibility in Households and Buildings*, United Nations, New York, Geneva.

Jensen, S.Ø., Marszal-Pomianowska, A., Lollini, R., Pasut, W., Knotzer, A., Engelmann, P., Stafford, A. and Reynders, G. (2017), "IEA EBC Annex 67 Energy Flexible Buildings", *Energy and Buildings*, Vol. 155, pp. 25–34.

Johnsen, T., Taksdal, K., Clauß, J., Yu, X. and Georges, L. (2019), "Influence of thermal zoning and electric radiator control on the energy flexibility potential of Norwegian detached houses", *CLIMA 2019 Congress*, Vol. 111.

Kommunal- og moderniseringsdepartementet (2017), *Forskrift om tekniske krav til byggverk (Byggteknisk forskrift): TEK17.*

Le Dréau, J. and Heiselberg, P. (2016), "Energy flexibility of residential buildings using short term heat storage in the thermal mass", *Energy*, Vol. 111, pp. 991–1002.

Lukas Lundström, *shinyweatherdata*.

Lund, P.D., Lindgren, J., Mikkola, J. and Salpakari, J. (2015), "Review of energy system flexibility measures to enable high levels of variable renewable electricity", *Renewable and Sustainable Energy Reviews*, Vol. 45, pp. 785–807.

Luthander, R., Widén, J., Nilsson, D. and Palm, J. (2015), "Photovoltaic self-consumption in buildings. A review", *Applied Energy*, Vol. 142, pp. 80–94.

Nordpool, "Historical market data", available at: https://www.nordpoolgroup.com/historical-market-data/ (accessed 4 May 2020).

Reynders, G., Nuytten, T. and Saelens, D. (2013), "Potential of structural thermal mass for demand-side management in dwellings", *Building and Environment*, Vol. 64, pp. 187–199.

Salom, J., Marszal, A.J., Widén, J., Candanedo, J. and Lindberg, K.B. (2014), "Analysis of load match and grid interaction indicators in net zero energy buildings with simulated and monitored data", *Applied Energy*, Vol. 136, pp. 119–131.

Sintef Byggforsk, "Byggforskserien: 451.021 Klimadata for termisk dimensjonering og frostsikring." (accessed 31 January 2018).

Standard Norge, *Kriterier for passivhus og lavenergibygninger boligbygninger* No. NS 3700:2013 (accessed 31 January 2018).

Standard Norge (2016), *Bygningers energiytelse - Beregning av energibehov og energiforsyning* No. SN/TS 3031:2016, available at: http://www.standard.no/en/webshop/ProductCatalog/ProductPresentation/?ProductID=859500.

Standard Norge (2017), *Energy performance of buildings - Method for calculation of the design heat load - Part 1: Space heating load, Module M3-3* No. NS-EN 12831-1:2017, available at: http://www.standard.no/no/Nettbutikk/produktkatalogen/Produktpresentasjon/?ProductID=941524.

Stiebel Eltron (2017), "Planung und Installation Wärmepumpen".

Verein Deutscher Ingenieure (2010), *VDI heat atlas: With 539 tables, VDI-Buch,* 2. ed., Springer, Berlin, Heidelberg.

Viessmann Deutschland GmbH (2011), "Planungshandbuch Wärmepumpen".

Wolisz, H., Constantin, A., Streblow, R. and Müller, D. (2013), "Performance assessment of heat distribution systems for sensible heat storage in building thermal mass".

Model predictive control of District Heating substations for flexible heating of buildings

Harald Taxt Walnum[1*], Igor Sartori[1], Marius Bagle[1]
[1]SINTEF Community, Oslo, Norway

corresponding author: harald.walnum@sintef.no

Abstract

The potential in cost and energy savings by replacing a feed forward weather compensated control (WCC) controlled radiator system with a linear MPC controller is investigated in a Modelica-Python setup. It is shown that if the MPC is optimized for minimum energy consumption it can reduce the energy consumption by up to 12 %. It is also demonstrated how variable price signal can influence the heat demand profile, and thereby shift energy consumption away from peak hours. By introducing a peak load tariff, it is also possible to reduce the rapid changes and large peaks often caused by optimization-based controllers

Introduction

The Clean Energy Package of the European union highlights the importance of utilising end-user flexibility to support the decarbonisation of the energy system (European Commission 2018). A significant part of Europe's energy demand for heating and domestic hot water is covered by district heating systems. District heating can exploit several sources of energy, thus serving as a source of flexibility for the electric grid (Sandberg et al. 2019). Heat supply usually consists of several production units, from base to peak load units, with different sources and operational costs. Their operation is prioritized to minimize the total system cost. Heat demand is mainly dependent on outdoor temperature, although factors related to user behaviour also influence the demand. Due to increased DHW demand in the morning and evening, and the use of night setback controls, significant peaks can often be observed during these hours (Kensby, Trüschel, and Dalenbäck 2015). To minimize the total production cost and related emissions, it is usually desirable to minimize the peaks in demand. Reducing peak demands, can also remove bottle necks in the distribution grid and allow for increased heat delivery. Several studies have shown that utilisation of the building thermal inertia has a large potential for peak reduction (Kensby, Trüschel, and Dalenbäck 2015; Romanchenko et al. 2018).

A common way of controlling buildings with district heating is through an outdoor temperature compensation curve, that decreases the supply temperature to the radiators as the outdoor temperature gets milder than the design conditions. This is called weather compensated control (WCC) (Hou, Li, and Nord 2019). In many buildings, especially older ones, the radiators are only equipped with manually adjustable valves, so that WCC is the only automated control for the heat supply and works as a feed-forward controller. Thus, the indoor temperatures fluctuate somewhat in the various rooms, given that occupants only marginally adjust the radiator valves. In other words, WCC relies on the users' tolerance, presuming – without feedback knowledge – that indoor temperatures fluctuate within a limited and still comfortable range. Such buildings present an opportunity for simple and cost-efficient introduction of Smart controllers for the heating system. Model predictive controls (MPC) is one approach, with the potential to improve indoor climate, and reduce both energy consumption and peak loads (Halvgaard et al. 2012).

In MPC, a model representation of the real system is used to optimize a sequence of control signals for a finite control horizon (Nc) subject to predictions of future disturbances (e.g. weather and internal gains), constraints (e.g. allowed indoor temperatures) and external signals (e.g. energy price). The objective function is typically to minimize energy consumption or energy cost. The first control signal (u_k) is then applied to the system. At the next time step (k+1), measurements are returned to the control model and the optimization is re-run and a new control signal applied. This iterative process is also called receding horizon control.

In this work we demonstrate the potential for how replacement of WCC controllers at DH substations with MPC can reduce energy consumption and energy cost as well as respond to other external signals, such as minimizing consumption in peak hours.

Method

To evaluate the performance of the model predictive controller with different cost functions a test setup with a substation emulator in Modelica (Mattsson and Elmqvist 1997) has been created. The BOPTEST framework (Blum et al. 2019) is used to enable co-simulation between the emulator and the controller model. A basic schematic of the simulation setup is shown in Figure 1 and the main components are described in subsections below. The emulator model is compiled as a Functional Mock-up Unit (FMU) and kept within the BOPTEST docker container together with times series data for disturbances

(internal gains, outdoor temperature and solar radiation) and constraints (indoor temperature band). Measurements from the emulator and forecast for the constraints are sent to the controller model (in the MPC formulation) for each control step and new setpoints are returned.
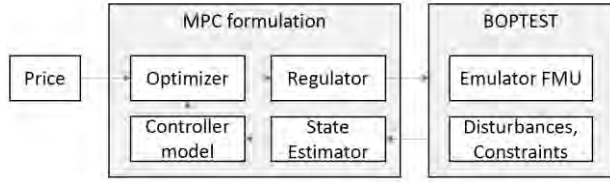
Figure 1: Schematic of simulation setup

Emulator

The Modelica substation model is a modified version of the substation model presented by Kauko et al. (2018). The main components are based on the library presented by Rohde et al. (2018). Models from the Buildings Library (Wetter et al. 2014) are used for weather data, internal gains and communication with the BOPTEST framework. The principal layout of the substation model is shown in Figure 2. The baseline controller is WCC, with a predefined linear supply temperature curve based on current outdoor temperature. The prescribed supply temperature can be overwritten by the external controller model. In this work, the DHW system is not included in the evaluation.
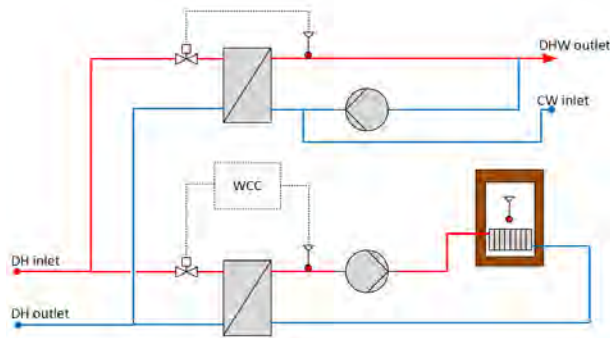
Figure 2: Principal layout of emulator substation model

The building envelope is modelled with a 2R2C network as shown in Figure 3. However, with the inclusion of the thermal mass and resistance in the radiator, the model becomes a 3R3C system. *Cw* and *Ci* represent the heat capacity of the building envelope and interior respectively. *Rw* is the resistance between the ambient and the envelope and *Ri* is the thermal resistance between the envelope and the interior. The radiator is modelled according to EN 442-2 (CEN 2014). *weaBus* is the connection to the external weather data and feeds the solar radiation (φ_s) and the ambient temperature (*Ta*) to the model. Aw denotes the effective window area, so that the solar gains into the interior is *Aw**φ_s. The heat from the ventilation (φ_v) is calculated as:

$$\varphi_v = \dot{V}_v \times \rho_a \times c_a(T_a - T_i) \qquad (1)$$

Where V_v is the ventilation flow rate, ρ_a is the air density and c_a is the air heat capacity. The internal gains (φ_{int}) are defined by a user occupancy, lighting, and other electric equipment schedule.
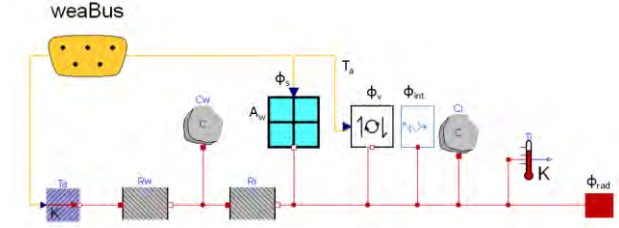
Figure 3: Schematic of building envelope emulator model

MPC formulation

The MPC formulation consists of a state estimator, a controller model, an optimization algorithm and a regulator. The whole MPC formulation is programmed in Python and communicates with BOPTEST via the request API.

The controller model is a linear and time invariant state space formulation of the 2R2C model shown in Figure 4. The general form of the state space formulation is given in equation (2) and (3).

$$dX(t) = A(\Theta)X(t) + B(\Theta)U(t) + E(\Theta)D(t) \quad (2a)$$
$$Y(t) = CX(t) \qquad (2b)$$

where X(t) is the state vector, which in building energy modelling usually represents internal temperatures. U(t) is the vector of controllable inputs (heat from radiator ϕ_h). D(t) are disturbances (solar radiation ϕ_s, internal heat gains ϕ_{ig}). A and B are matrices whose elements are functions of the parameters Θ, while C describes the relation between the model's states (predicted temperatures) and the measured outputs Y(t) (measured temperatures).
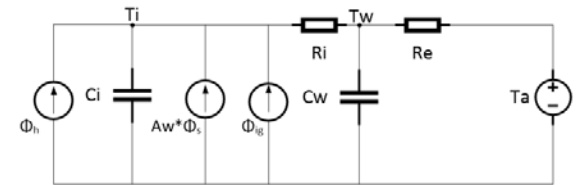
Figure 4: RC network of controller model (2R2C).

An advantage with the linear and time invariant state space model is that it can be reformulated directly into a linear programming (LP) optimization problem (Halvgaard et al. 2012).

A set of constraints are applied to the problem. The DH heat exchanger is only able to reach a fixed maximum supply temperature. This is reformulated into a maximum heat emission ($\overline{u}$). In addition, a constraint on the indoor temperature is added to define a thermal comfort band between maximum($\overline{y}$) and minimum ($\underline{y}$). Since there is a risk that the only valid solution to the problem is outside the allowed temperature range (e.g. during warm periods), the temperature constraint is formulated as a soft

constraint. The violation of the temperature constraint (δ) is included in the objective function with a penalty factor (ρ). This yields the following optimization problem:

$$\min\left[\sum_{k=1}^{N_c}(c_k^{var}u_k + \rho\delta_k)\,\Delta t\right] \quad (3a)$$

$$s.t. \quad x_{k+1} = Ax_k + Bu_k + Ed_k \quad (3b)$$

$$y_k = Cx_k \quad (3c)$$

$$\underline{y}_k - \delta_k \le y_k \le \overline{y}_k + \delta_k \quad (3d)$$

$$\underline{u}_k \le u_k \le \overline{u}_k \quad (3e)$$

$$\delta_k \ge 0 \quad (3f)$$

where c_k^{var} is the energy cost for each timestep k. The problem is formulated in python using the optimization package pyomo (Hart et al. 2017) and the GLPK optimization algorithm(GLPK 2018).

The results from the optimization yields a sequence of optimum heat emissions from the radiator. This is passed to the regulator to transform it to radiator supply temperatures. The regulator includes the same equations for the radiator as the emulator model, except that it does not take the thermal mass into account (i.e. the radiator model is steady-state in the regulator).

As described above, the controller model has two states. However, as for a real implementation, the internal state (T_w) of the building envelope cannot be measured. To estimate this state at each control update step, while filtering out measurement and process noise (not included in this study), a Kalman filter is applied as state estimator, using the FilterPy library (Labbe 2018).

Testcase and objective functions

To evaluate the potential for the MPC to both improve the energy efficiency and to respond to external signals, a one-week testcase has been specified. The testcase is designed to emulate an energy efficient residential building of 1 000 m^2.

Model parameters

The main model parameters for the emulator model are shown in Table 1. The properties of the building envelope is based on the identified parameters in (Walnum, Lindberg, and Sartori 2019), but scaled up to a 1 000 m^2 building. The heating system is dimensioned according to the building demand from simulation, with a supply temperature of 60 °C at design winter temperature.

Table 1: Model parameters

Building	
Area [m^2]	1 000
Ci [J/kgK]	3.6 E7
Cw [J/kgK]	1.4 E8
Ri [k/W]	1.2 E-3
Rw [K/W]	1.2 E-2
Aw [m^2]	20

Ventilation rate [m^3/h]	1440
Heating system	
Q$_{dim}$ [kW]	35
ΔT$_{rad,nom}$[K]	30
n$_{rad}$	1.3
T$_{sup,design}$ [°C]	60

Disturbances, forecasts and constraints

The weather data and internal gains used in the emulator model are shown in Figure 5. The weather data is taken from the first week of January in the TMYx dataset for Oslo, Blindern (climate.onebuilding.org 2020).

The internal gains schedule is defined in accordance with the national standard for building energy simulations SN/TS 3031:2016 (Standard Norge 2016).
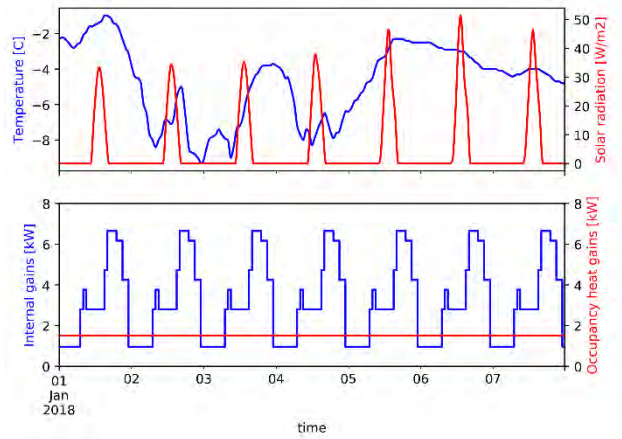
Figure 5: Weather data and internal heat gains for testcase.

The weather data is transferred to the MPC directly, so that it operates with perfect forecast. However, as the internal gains are more difficult to predict, the forecast sent to the MPC is a constant value equal to the daily average.

The upper indoor temperature constraint ($\overline{y}$) is fixed to 22 °C and the lower indoor temperature constraint is set to 18 °C at night (23:00 to 08:00) and to 21 °C during daytime (08:00 to 23:00).

Simulated cases

To evaluate the performance and potential for the MPC, several cases have been defined. The baseline case is the WCC, which has a supply temperature directly linked to the outdoor temperature. The applied curve is shown in Figure 6. The curve has been manually tuned to minimize the time outside the thermal comfort band of 21-22 °C through a full year simulation.
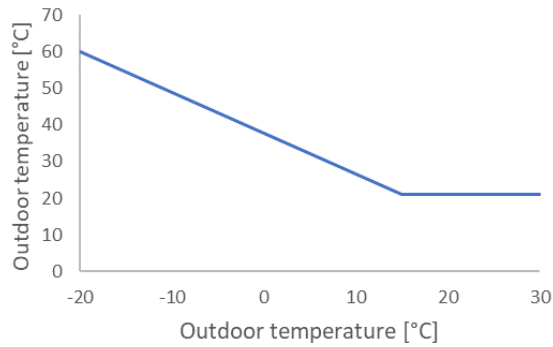
Figure 6: WCC temperature compensation curve

To evaluate how the MPC can respond to different price signals, artificial price signals with a fixed daily profile have been generated. The price signal is split into three categories and six periods:

- Low price(c_{low}): 00:00-06:00 and 22:00- 00:00
- High price (c_{high}): 07:00-10:00 and 17:00- 20:00
- Middle price (c_{mid}): 06:00-07:00, 10:00-17:00 and 20:00-22:00

The price signal is defined by the % deviation of c_{high} from c_{mid}, so that c_{mid} and the daily average price is always equal to 0.5 NOK/kWh. Four different price signals are generated with 0 % (constant price), 10 %, 20 % and 30 % deviation, respectively.

In addition, the constant price signal applied together with a daily peak power (hourly peak) tariff equal to 2.25 NOK/(kWh/h) is tested. This corresponds to one of the new grid tariff structures proposed by the Norwegian Energy Regulatory Authority for the electricity grid (Eriksen et al. 2020).

Results

In the following graphs this terminology is used to refer to the different type of controllers and different price signals:

Different controllers:

- WCC = WCC controller, the baseline
- MPC-Energy = MPC with min. energy objective function
- MPC-Cost = MPC with min. cost objective function

Different tariffs:

- 0, 10, 20, 30 % = level of price variability (min. & max. deviation from daily average)
- Daily peak = tariff with constant energy price & additional daily peak power.

Figure 7 shows the resulting energy cost for each case, while Figure 8 shows total energy consumption and Figure 9 the energy consumption during peak hours.

Note that MPC-Energy and MPC-Cost give identical results at 0% price variability, and this is used as a reference for comparison with the other price signals

when discussing the charts below. First of all, it is worth comparing the behaviour of the two reference controllers: WCC and MPC-Energy (or MPC-Cost) at 0 % price variability, by looking at Figure 10 (at the end), before returning to comment on Figure 7 to Figure 9.
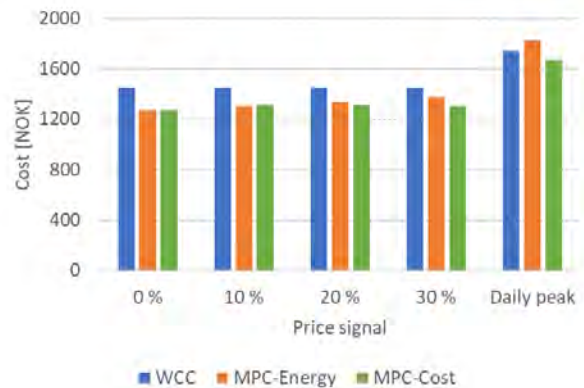
Figure 7: Resulting energy cost in NOK
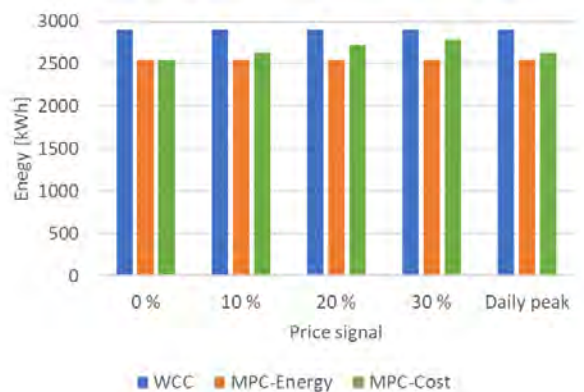
Figure 8: Resulting energy consumption in kWh
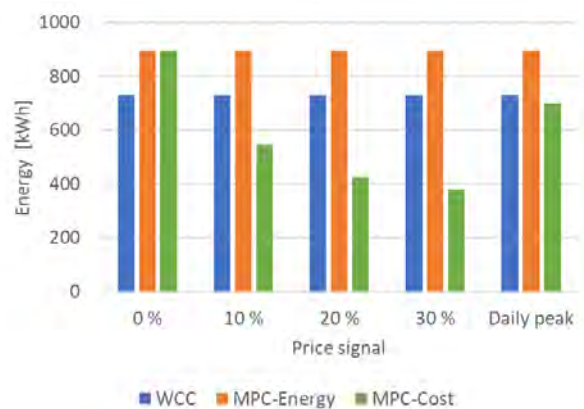
Figure 9: Energy consumption during peak hours

Figure 10 compares the indoor temperatures, the radiator supply temperatures, and the supplied heat for the WCC and the MPC controllers, respectively, when minimum energy is the objective function. One can see that the WCC controller holds a relatively constant supply temperature, according to the outdoor temperature compensation curve, while the corresponding indoor temperature fluctuates due to changes in internal gains and solar radiation. The MPC on the other hand imposes

large variations in the supply temperature, to exploit the allowed night setback, and thereby save energy. However, this results in very high peak loads in the morning, to increase the temperature back up to the daytime temperature setpoint. This peak will normally coincide with the period with the highest strain on the DH network. The hourly energy peak is increased by 72 % compared to the WCC.

From Figure 7 and Figure 8 we can see that the MPC reduces both the energy cost and the energy consumption with about 12 % compared to the WCC with the constant price signal.

We can see that, as the price variation increases (from 10 % to 30 %), the MPC-Cost results in increased total energy consumption compared to MPC-Energy. Nevertheless, the total cost is reduced. This is because the MPC algorithm chooses, to some extent, to overheat the building when energy is cheaper (therefore increasing thermal losses) in order to limit the consumption when energy is more expensive. At the 30% deviation case, MPC-Cost results in about 5% lover energy costs than MPC-Energy (compare green and orange bars in Figure 7 while it has about 10 % higher energy consumption (compare green and orange bars in Figure 8).

The difference between MCP-Cost and MPC-Energy is significant when we look at the energy consumed in the peak hours only, as it is shown in Figure 9. However, to understand what is happening we need to look at Figure 11 and Figure 12.

Figure 11 compares the indoor temperatures, the supply temperatures, and the supplied heat for the MPC-Energy and all price signals for two selected days. The variable price signal (30 % variation) is shown as a grey background to emphasise the relation to the price. As the deviation in the price increases, we can see that the controller applies less night setback, but instead preheats the building during night, to allow reduced energy consumption during the morning hours with peak energy prices. The fact that it holds the indoor temperature at the upper constraint, shows that it also utilizes the building envelope as thermal storage, in addition to the indoor air. The variation in total energy consumption and cost are relatively small for the different cases. However, the energy consumption shifted away from the peak hours is significant, as it is clearly shown in Figure 9. Compared to the WCC, the MPC-Cost reduces the energy consumption during peak hours by 25 %, 42 % and 48 % for the price signals with 10 %, 20 % and 30 % deviation, respectively. On the contrary, the MPC-Energy increases the energy consumption with 18 % in peak hours, compared to the WCC.

When looking at the results for the Daily peak tariff, the cost data cannot be directly compared with the other cases, as it adds an extra cost. However, in comparison with the WCC, the MPC-Energy results in 5% higher cost despite having a 12 % lower energy consumption. On the other hand, the MPC-Cost yields 4 % lower cost and 9 % lower energy consumption.

Figure 12 compares the indoor temperatures, the supply temperatures, and the supplied heat for the three controllers. It shows that the MPC-Cost applies some night setback but compared to the MPC-Energy it starts reheating much earlier, to avoid high peak energy demands.

Discussion

The results from the controller tests shows a significant potential to reduce the energy cost and energy consumption by replacing legacy WCC controllers with MPC. It also demonstrates how an MPC controller can respond to different price signals and thereby shift heat loads in time. However, there are several obstacles for achieving similar results in a real-life application.

The test setup is very ideal. The controller model is almost equal to the emulator model, and except for the internal gains and the ventilation, the controller model works with perfect forecast. The dynamics of a real building cannot be perfectly described by a three-state model (as done with the emulator in this paper), and therefore the controller model will be less accurate in reality, and the results less optimal.

Controlling the heat supply of a large building by a single average indoor temperature is also suboptimal. However, compared to the existing WCC, which is a pure feed-forward controller it is an improvement. Implementing individual room controllers in such buildings would require replacement of all the radiator valves and installation of a large set of indoor temperature sensor, which would significantly increase the required investment cost. An important challenge for implementing the proposed MPC would therefore be to describe a representative indoor air temperature with minimum number of sensors.

The results also demonstrate how optimized controllers can be sub-optimal for the grid operation, by creating large changes is the heat demand, either during changes is control constraints (night setback temperatures) or during changes is the price signal. This shows that as more buildings apply smart controllers, developing smart pricing schemes becomes more important. The daily peak tariff, for example, shows benefit for both the building and the energy system.

Conclusion

In this work we have demonstrated the potential in energy and cost savings with replacement of an existing WCC controller with MPC in buildings with district heating and manual radiator valves. It is also shown how an MPC can respond to different prising signals and thereby also shift loads in time.

There are several barriers for implementing such controllers in real buildings. However, it is an interesting option due to the low installation cost.

In further work with this approach it is planned to test this on a real building. However, first we will increase the

complexity of the emulator model, by developing a Modelica model of the planned demonstration building.

Acknowledgement

References

Blum, David et al. 2019. "Prototyping the BOPTEST Framework for Simulation-Based Testing of Advanced Control Strategies in Buildings." In *Proceedings of the International Building Performance Simulation Association*, Rome: IBPSA.

CEN. 2014. *EN 442-2*. Brussels, Belgium.

"Climate.Onebuilding.Org." 2020. http://climate.onebuilding.org/ (March 20, 2020).

Eriksen, Andreas Bjelland et al. 2020. "RME Høringsdokument Nr 01/2020 - Endringer i Nettleiestrukturen." : 84. http://publikasjoner.nve.no/rme_hoeringsdokumen t/2020/rme_hoeringsdokument2020_01.pdf.

European Commission. 2018. "Clean Energy for All Europeans - The Winter Package." https://ec.europa.eu/energy/en/topics/energy-strategy-and-energy-union/clean-energy-all-europeans (November 26, 2018).

GLPK. 2018. "GNU Linear Programming Kit, Version 4.65." http://www.gnu.org/software/glpk/glpk.html.

Halvgaard, Rasmus, Niels Kjølstad Poulsen, Henrik Madsen, and John Bagterp Jørgensen. 2012. "Economic Model Predictive Control for Building Climate Control in a Smart Grid." In *2012 IEEE PES Innovative Smart Grid Technologies, ISGT 2012*,.

Hart, William E et al. 2017. 67 *Pyomo--Optimization Modeling in Python*. Second. Springer Science & Business Media.

Hou, Juan, Haoran Li, and Natasa Nord. 2019. "Optimal Control of Secondary Side Supply Water Temperature for Substation in District Heating Systems." *E3S Web of Conferences* 111(201 9): 06015.

Kauko, Hanne et al. 2018. "Dynamic Modeling of Local District Heating Grids with Prosumers: A Case Study for Norway." *Energy* 151: 261–71.

Kensby, Johan, Anders Trüschel, and Jan-Olof Dalenbäck. 2015. "Potential of Residential Buildings as Thermal Energy Storage in District Heating Systems – Results from a Pilot Test." *Applied Energy* 137: 773–81. https://www.sciencedirect.com/science/article/pii/ S0306261914007077 (January 3, 2019).

Labbe, Roger R. 2018. "Kalman and Bayesian Filters in Python." *GitHub repository*: 504. https://github.com/rlabbe/Kalman-and-Bayesian-Filters-in-Python.

Mattsson, Sven Erik, and Hilding Elmqvist. 1997. "MODELICA | AN INTERNATIONAL EFFORT TO DESIGN THE NEXT GENERATION MODELING LANGUAGE." In *7th IFAC Symp. on Computer Aided Control Systems Design, CACSD'97*, Gent, Belgium.

Rohde, Daniel, Trond Andresen, and Natasa Nord. 2018. "Analysis of an Integrated Heating and Cooling System for a Building Complex with Focus on Long–Term Thermal Storage." *Applied Thermal Engineering* 145: 791–803.

Romanchenko, Dmytro, Johan Kensby, Mikael Odenberger, and Filip Johnsson. 2018. "Thermal Energy Storage in District Heating: Centralised Storage vs. Storage in Thermal Inertia of Buildings." *Energy Conversion and Management* 162: 26–38. https://www.sciencedirect.com/science/article/pii/ S0196890418300803?via%3Dihub (January 3, 2019).

Sandberg, Eli, Jon Gustav Kirkerud, Erik Trømborg, and Torjus Folsland Bolkesjø. 2019. "Energy System Impacts of Grid Tariff Structures for Flexible Power-to-District Heat." *Energy* 168: 772–81.

Standard Norge. 2016. "SN/TS 3031." : 168. http://www.standard.no/no/Nettbutikk/produktkata logen/Produktpresentasjon/?ProductID=859500.

Walnum, Harald Taxt, Karen Byskov Lindberg, and Igor Sartori. 2019. "Influence of Inputs Knowledge on Grey-Box Models for Demand Response in Buildings." In *Proceedings of the International Building Performance Simulation Association*, Rome: IBPSA.

Wetter, Michael, Wangda Zuo, Thierry S. Nouidui, and Xiufeng Pang. 2014. "Modelica Buildings Library." *Journal of Building Performance Simulation* 7(4): 253–70. http://www.tandfonline.com/doi/abs/10.1080/1940 1493.2013.765506 (March 13, 2020).

.
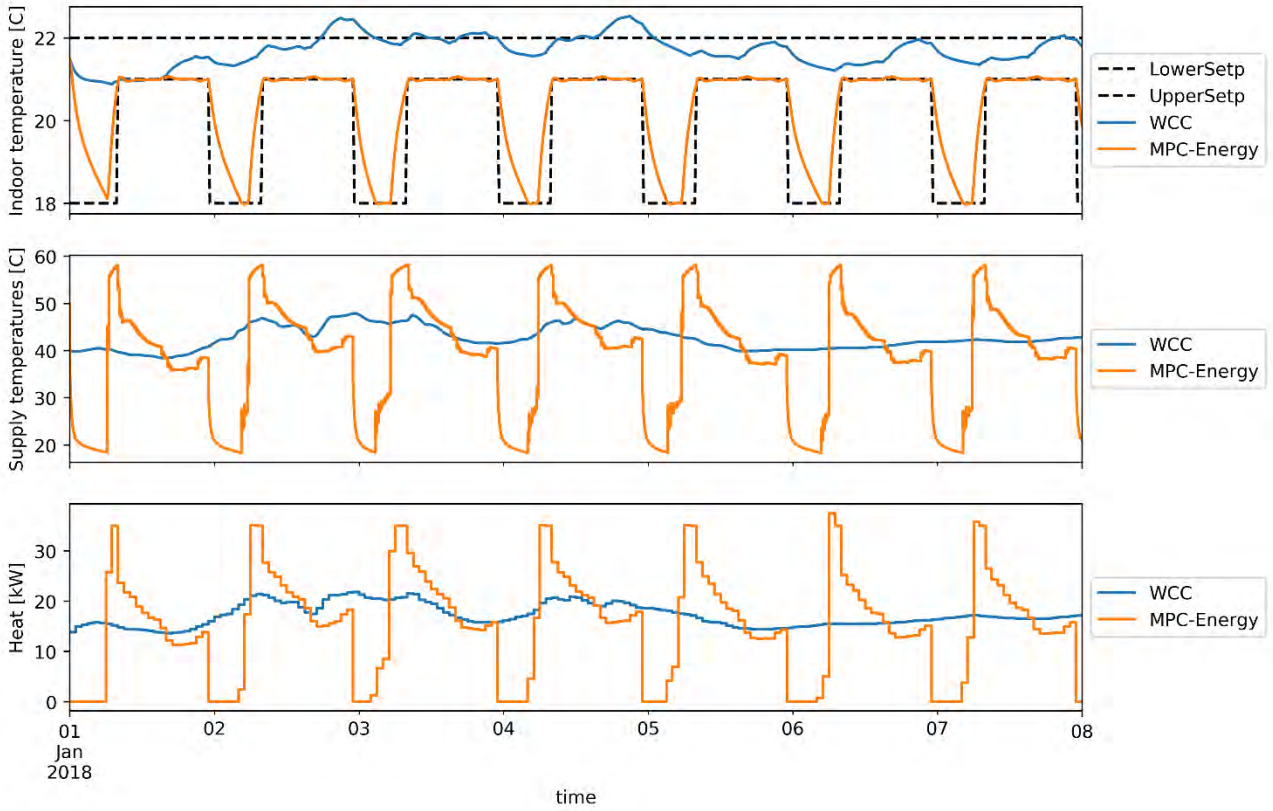
Figure 10: Baseline WCC control vs MPC with minimum energy objective function
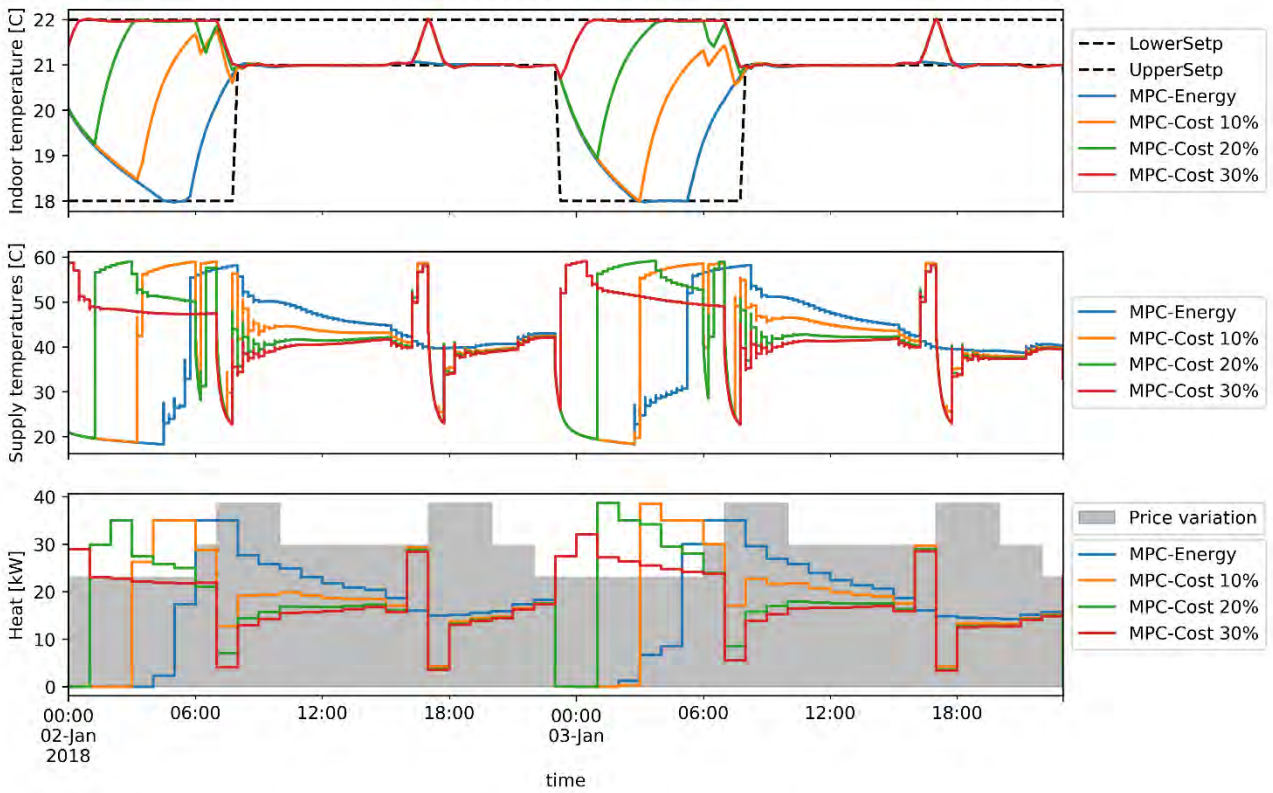
Figure 11: Comparison of MPC controller results with different variable prices
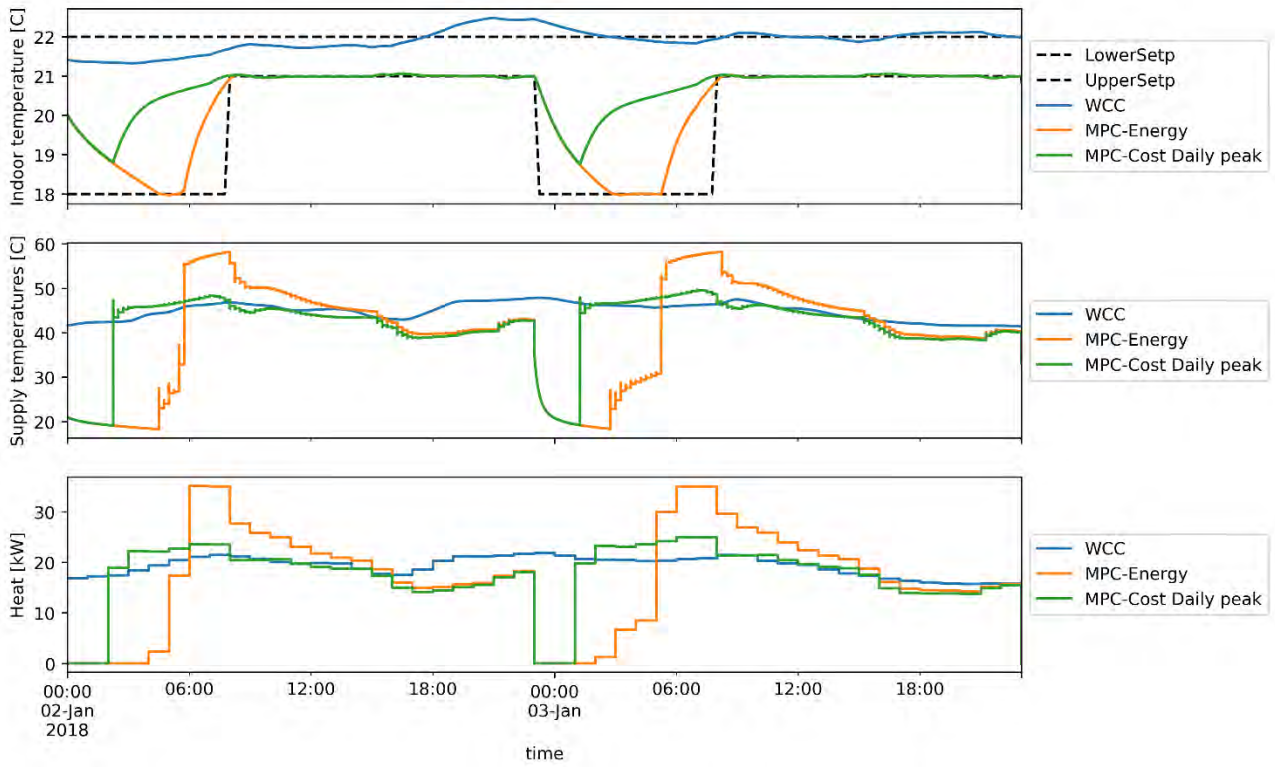
Figure 12: Comparison of WCC and MPC controllers with peak power tariff

Analyses of thermal storage capacity and smart grid flexibility in Danish single-family houses

Kim B. Wittchen[1*], Ole Michael Jensen[1], Jaume Palmer[2], Henrik Madsen[2]

[1] Aalborg University, Copenhagen, Denmark

[2] Danish Technical University, Lyngby, Denmark.

corresponding author: kiwi@build.aau.dk

Abstract

This paper describes theoretical analyses of typical detached Danish single family houses' ability to provide thermal capacity and thus flexibility, in an electricity grid, if they were heated by individual heat pumps.

A set of archetype house models have been set up for analyses of their ability for moving energy use in time by dynamic simulations in BSim (Wittchen et al., 2000-2019). The archetypes was established in order to analyse single-family houses constructed in different periods, usually related to shifts in building regulations or building traditions.

Finally, results from archetype modelling are scaled to the total number of Danish single-family houses located outside district heating areas to estimate the future thermal capacity in these houses. Analyses showed that up to 99 % of the energy demand for space heating within peak hours can be moved outside peak hours, with acceptable influence on the indoor temperature.

The paper describes the simulation approach and the results for different archetype houses as well as upscaling to nation-wide thermal storage potential. Moreover, the paper describes flexibility studies on selected houses based on both peak response and price signal response.

Introduction

In the near future, where fluctuating renewable energy, e.g. from wind turbines dominates the electricity grid, flexibility will be essential for a stable electricity grid and maximum utilization of the renewable energy resources (Ministry of Climate, Energy and Buildings, 2013). One source for this flexibility is buildings heated by heat pumps (Dréau and Heiselberg, 2016). Around 50 % of Danish detached single family houses are located outside district heating grids (Statistics Denmark, 2020) and will, in the near future equipped with heat pumps (Danish Ministry of Climate, energy and Utilities, 2020).

This transformation towards electric heating of single family houses using heat pumps is the perspective of this study. Put otherwise, we presuppose that Danish single family houses were heated by heat pumps and on this background estimate thermal capacity and flexibility in an electric grid (Hedegaard and Balyk, 2013). A simple

approach for the energy flexibility potential has been used (Reyndres et al. 2018) to evaluate the houses' ability to move heating energy use away from peak periods, utilising the houses' thermal storage capacity (Reynders et al. 2017). The houses thermal capacity has been simulated with the current energy performance level and heating system capacity.

Six archetype models, representing Danish single-family houses, have been set up to analyse the thermal storage potential The archetypes represents differences in building tradition and historical changes in energy requirements stated in shifting Danish Building regulations (Wittchen et al., 2016), covering the following age categories:

- 1850-1930
- 1931-1950
- 1951-1960
- 1961-1972
- 1973-1978
- 1979-1998

These age categories are typically constructed of heavy building materials, have reasonable insulation levels due to carried out renovation and are reasonable air-tightness (Danish Energy Agency, 2020). These are all parameters that support the houses in maintaining an acceptable indoor temperature during periods without heat supply.

The reasoning for not analysing houses older than 1850 is that these houses are normally poorly insulated, leaky (Danish Energy Agency, 2020) and represent a very small share of the total housing stock (Statistics Denmark, 2020). Houses constructed after 1998 have also been excluded as these houses are normally made of light constructions (little thermal energy storage possibility) and are highly insulated and airtight (Wittchen et al., 2016). They do thus not offer a large thermal energy storage potential.

The analyses did not aim at exploring the potential CO_2 emission reduction by utilising the thermal capacity of single family houses in an electric grid. The aim was solely a simple quantification of the amount of energy and in second hand electricity that can be moved away from daily peak periods (breakfast and cooking peaks).

Extrapolation to total energy flexibility is limited to Danish single-family houses located outside district

heating areas constructed in 1850-1998, assuming they will be heated by individual heat pumps in the future.

In parallel, existing, high frequency measurements of energy consumption and indoor temperatures from 140 detached single-family houses in a night setback experiment (Jensen, 2016) were used to validate if the archetype models performed as expected (Palmer et al. 2020). Data from this experiment can be used to characterise the houses' dynamic behaviour as any change in the heat supply for a house will result in a dynamic response. Measurements of the indoor and outdoor temperatures can be used to estimate the time-constants of the house. Time constants are one of the key parameters to understand the dynamic thermal behaviour of a system (house) and thus its potential flexibility (Jakobsen and Kolarik, 2018). The measurements were used to estimate time constants for houses corresponding to each archetype and compared to time constants estimated from simulation results of the archetype models (Palmer et al., 2020).

Model set-up

Archetype models were set up in the building simulation tool BSim (Wittchen et al., 2000-2019). To meet the special needs for this study, BSim was extended with a "parasite" that controls the program and among others makes it possible to extract simulation results on sub-hourly level rather than the normal hourly output (Jensen et al., 2020).

Archetype models were defined with focus on accurate modelling of the thermal mass, window-to-floor ratio, thermal performance of the building envelope, and size of heating system. Ventilation was estimated based on experiences form measurements in multiple Danish single-family houses (Bergsøe, 1996) and internal loads (persons, lighting and auxiliary electricity) was estimated using national standards (Aggerholm, 2018) for energy certification of buildings. The heated floor area and the heating supply of the archetype houses is extracted form information in the Danish Building and Dwelling stock Register (BBR).

The focus was on simulation of existing houses in in their current stage in terms of energy performance and heating system installation in order to evaluate the thermal storage potential of the existing housing stock.

Due to the simplifications in ventilation rates and internal loads, all archetype houses only had one zone, except for those archetypes that has two floors. All internal walls however, are modelled in order to maintain the correct thermal capacity of the house.

The building model do not take into account thermal storage capacity in the technical building systems and therefore neither a potential water tank. Inclusion of a water tank will potentially be able to increase the total thermal storage capacity of the house. Heating systems in all archetypes are adjusted to match the actual power of the representative example houses.

Figure 1 show a wireframe drawing and a photo of an example archetype house with 180 m² gross heated floor area representing the construction period 1961-1972.

Due to the daily routines of Danes, there are normally two daily peak periods (Figure 2): two hours in the morning (breakfast peak) and three hours in the evening (cooking peak).
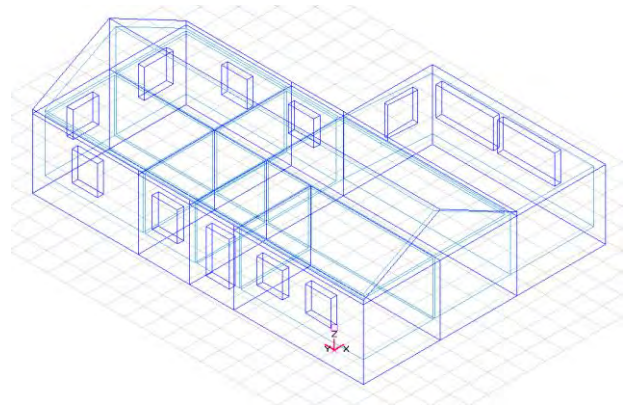
Figure 1. Wire-frame drawing of 1961-1972 archetype house in simulation tool and photo of corresponding example house (1966).

The idea behind the simulation experiment, was to move as much energy demand for space heating away from the peak-periods, still maintaining an acceptable indoor temperature (20-22 °C). This is done by three different control strategies.

1. Fixed indoor temperature of 22 °C (reference).
2. Turn off heating at the start of the peak-periods and let the indoor temperature drop towards 20 °C, i.e. 2 degree temperature setback.
3. Pre-heating or charging of the thermal mass to 23 °C the house 1 and 2 hours in advance of the peak-periods with temperature setback to 20 °C during peak-periods.

The first control strategy (2) is almost the same as a traditional night set-back strategy aiming at reducing the energy use, but carried out over a shorter periods (2 and 3 hours) and during daytime. In the time after the set-back period there is an increase in power uptake compared to

the control with a fixed indoor temperature. The second demand control strategy (3) may result in an annual increased energy use. This control strategy is, in contrast to Knudsen and Petersen (2016), a simple strategy, which do not aim at minimising the CO_2 emissions, but only move energy uptake away from peak periods. Fluctuating wind result in fluctuations in the CO_2 emission from the Danish electricity production and these fluctuations are thus not synchronous with the fixed peak periods (Clauß et al., 2019) used in this study. Analyses of the potential for moving energy use away from peak hours is an example on how thermal storage capacity in Danish single-family houses can be utilised as flexibility. This capacity is studied for, but not limited to, peak-periods. Both strategies (2 and 3) may be able to decrease the total CO_2 emissions as a result for less fossil-fuel based energy in the energy mix during peak periods or other periods with a large share of fossil fuels in in the energy mix.

Pre-heating demand control strategy (3) takes advantage of the houses' ability to act as a thermal storage for electricity grid. The storage capacity of houses will be able to increase the grid's resilience towards fluctuations as wind power delivers an increasing share of the total electricity production.
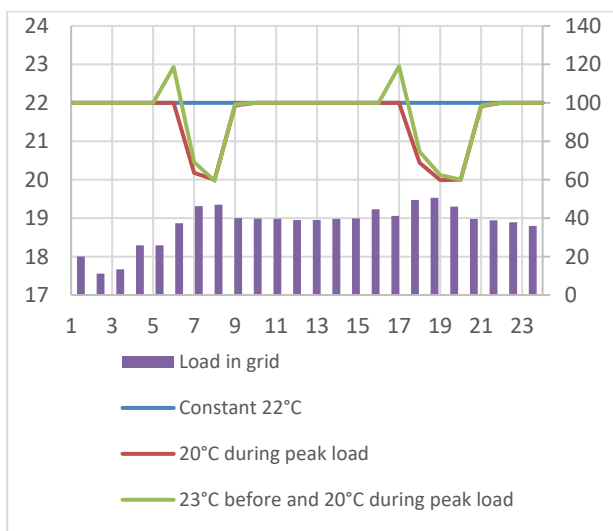
Figure 2. Example indoor temperature in a house that offers flexibility to the grid.

Example 1966 house

Measurements in the Middelfart dataset (Jensen, 2016) include high frequency (between 1 and 5 minute intervals over 2 years) measurements of indoor and outdoor temperatures as well as energy consumption in 140 Danish detached single-family houses in a night setback experiment.

Within the archetype period 1960-1972 is data from one single-family house from 1966 in the Middelfart dataset of good quality, i.e. data is of sufficient granularity and with enough un-interrupted sampling periods. This makes it possible to use the data for statistical studies of cooling characteristics, i.e. time-constants, of the house.

Even though this house is heated by district heating, data from night setback cool-down periods can be used as representative for such houses' dynamic behaviour. Use of data from a house with district heating are equally valid for use in the statistical analyses and estimation of time-constants as data from a house with another heat source.

The selected house was renovated in 2006 with addition of cavity insulation in the brickwork walls and replacement of windows. The heat capacity of the house is maintained during this operation as the internal leaf of the brick walls are unchanged. This kind of post insulation work is common in Denmark. Due to the low price of this work, compared to the energy savings, the intervention is widespread for this age of houses. This kind of renovation works are typical for houses from this period (Danish Energy Agency, 2020), thus the house is considered typical for the period. The house is thus assumed to be representative for the archetype of this period.

Estimating time-constants

Night indoor temperature curves for this house shows that a typical setback is about 2.5 degree. The night temperature is decreasing until about 18 °C and towards 8 AM the temperature increases to a little above 20 °C. In this house there is not much difference between weekdays and weekends. Figure 3 depict the night setback as measured indoor temperature for a selected period.
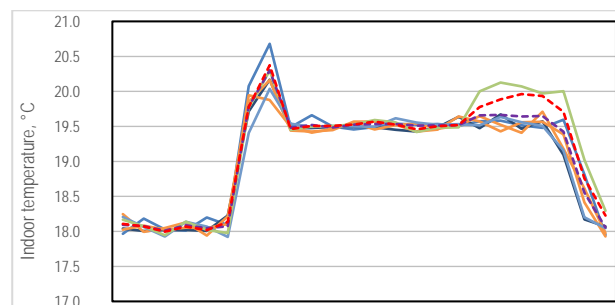
Figure 3. Examples of temperature 24h curves for night set-back in house from 1966. Red dotted line indicates the average for weekdays while the blue dotted line is the average for weekends.

Based on measurements of the indoor temperature during periods with night set-back in a house, it is possible to estimate the time-constant for using a first order auto-regressive model (Bacher & Madsen, 2011). In Figure 4, time-constants for all analysed archetype representatives are shown.

The 1966 house show the longest time-constant, 50.8 hours, which indicates a thermally heavy house with good insulation level and air-tightness. This matches the expectations for a house constructed from heavy building materials (brickwork) that has been insulated in the cavity walls and with new windows.
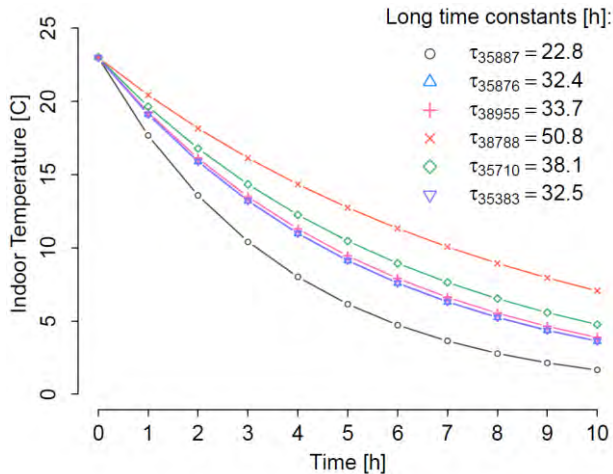
Figure 4. Estimated cooling curves for six selected houses (the six archetype categories) in the Middelfart dataset. The 1966 example house has a time-constant of 50.8 (red curve marked with x).

Simulating peak periods' flexibility

The annual simulated net heating demand with a constant indoor temperature at 22 °C is 26 729 kWh with a maximum power demand of 10.7 kW (Table 1). By cutting off heating during peak periods (control strategy 2) and letting the indoor temperature float towards 20 °C, the annual net heating demand decreases to 26 140 kWh but at the same time the maximum power demand increases to 14.4 kW. If the house is pre-heated to 23 °C one hour in advance of the peak-period (control strategy 3), the annual net heating demand becomes 26 322 kWh and maintaining the maximum power demand at 14.4 kW. Preheating 2 hours before peak-periods increases the annual heat demand to 26 633 kWh.

Table 1. Annual net space heating demand and max power demand for 1960-1972 archetype simulations.

	Heat kWh	Power kW
Constant indoor temperature 22 °C (reference)	26 729	10.7
Maximum 2 degree set-back during peak-periods	26 140	14.4
Pre-heating 1 hour before peak-periods to max 23 °C and 2 degree set-back during peak-periods	26 322	14.4
Pre-heating 2 hours before peak-periods to max 23 °C and 2 degree set-back during peak-periods	26 633	14.4

Summarising the hours that are within the peak-periods the annual net heating demand becomes as shown in Table 2. It is clear that the relative reduction in annual net heating demand within the peak-periods is significantly higher than for the whole year. In this way, it is possible

to move up to 99 % (5 480 kWh) of the net heating demand away from the peak-periods.

Table 2. Annual heating demand within peak-periods for archetype 1960-1972 simulations.

	Heating kWh	Reduction %
Constant indoor temperature 22 °C (reference)	5 514	-
Maximum 2 degree set-back during peak-periods	86	98
Pre-heating 1 hour before peak-periods to max 23 °C and 2 degree set-back during peak-periods	34	99
Pre-heating 2 hours before peak-periods to max 23 °C and 2 degree set-back during peak-periods	34	99

Indoor temperature during peak periods

The internal loads is set to increase during peak-periods with a factor 3 e.g. due to cooking. This increase reflects the increased activity in the house during peak-periods.

Even with a control strategy aiming at a constant indoor temperature of 22 °C, there are some hours with indoor temperature in the living area below the set-point (Figure 5 and Table 1). This points to a slightly undersized heating system. That is a normal situation in houses constructed in this period as the heating system is laid out for a constant indoor temperature of 20 °C when the outdoor temperature is -12 °C. In the Danish reference year used in the simulations, the outdoor temperature reaches -15 °C at the depth of winter (Wang et al., 2013). Introducing periods with heating cut-off will naturally challenge the power of the heating system, but the situation is realistic for existing houses where such dynamic control strategy are introduced.

Figure 5 show the number of hours with indoor temperature below 22 °C.

The number of low indoor temperature hours increases dramatically when the set-point is decreased during peak-periods. Therefore, the influence of pre-heating to 23 °C two hours in advance of the peak-periods was analysed for this archetype. A two hour pre-heating strategy proved to have limited influence on the overall heating demand and maximum power demand (Table 1 and Table 2), but significant influence on the number of hours with indoor temperatures below 22 °C (Table 3).
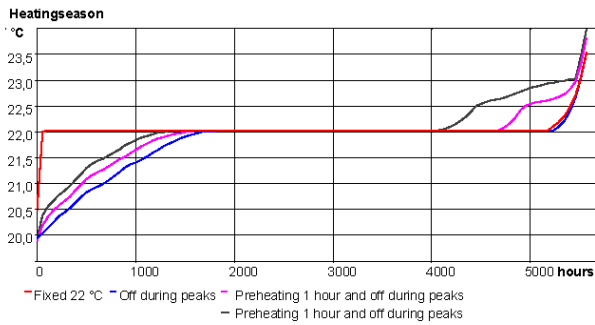
Figure 5. Distribution curve for the indoor temperature during the heating season in the four simulated cases.

In all control strategies, the number of hours during the heating season with an indoor temperature below 20 °C is limited.

In Wittchen et al. (2020) results from simulations and time-constant estimates of all archetypes are described.

Table 3. Number of hours during the heating season with indoor temperature below 20 and 22 °C respectively in the living area for four simulated control strategies.

Number of hours	<20°C	<22°C
Constant indoor temperature, 22 °C (reference)	0	50
Maximum 2 degree set-back during peak-periods	14	2 677
Pre-heating 1 hour before peak-periods to max 23 °C and 2 degree set-back during peak-periods	9	2 321
Pre-heating 2 hours before peak-periods to max 23 °C and 2 degree set-back during peak-periods	2	1 903

Storage capacity on national level

Based on BSim simulations and the accompanying calculations of the heating demand in widespread Danish single-family houses, it has been possible to estimate the potential for thermal energy storage capacity (flexibility).

If Danish single-family houses outside district heating areas, are equipped with heat pumps and a control favouring flexibility, the total flexibility potential can be estimated. This was done by a simple conversion from thermal energy to electricity in heat pumps using an annual COP of 3

Table 4 shows an upscaling of the total annual flexibility for Danish single-family houses located outside district heating areas, if they were heated by heat pumps. The total flexibility (conversion from thermal storage capacity) in these houses sum to a total of 544 GWh, for the fixed (morning and evening) peak-periods only.

Table 4. Flexibility in archetype houses and upscaling to Danish houses outside district heating areas, assuming they are heated by heat-pumps (COP=3).

	Flexibility per. house kWh	Houses in BBR -	Total flexibility GWh
1850-1930	487	110 596	53.82
1931-1950	1 266	68 739	87.00
1951-1960	851	50 356	42.87
1961-1972	1 827	142 275	259.89
1973-1978	933	73 940	68.96
1979-1998	489	65 402	31.98
Total			544.53

If energy use is being moved away from peak periods, then there will be a new, but smaller peak just after the traditional peak period. The simulations are carried out for single houses, but in reality these are almost 0.5 million individual houses all with their own individual use and dynamic behaviour. The new peak period will therefore be scattered over the hours after the traditional peak. Not considering the wind dependent CO_2 emission over time, this have the potential of resulting in a smaller demand for supplemental fossil fuel for electricity production.

When houses are being renovated, the time-constant and hence the potential for flexibility will increase. A house that are being renovated will typically have unchanged thermal capacity (except for internal insulation), but lower transmission and ventilation losses due to added insulation and potentially implementation of mechanical ventilation with heat recovery.

The total electricity production in Denmark in 2018 from wind turbines was 13 915 GWh, equal to 45 % of the total Danish electricity consumption (Danish Energy Agency, 2019). The potential for flexibility in Danish single family houses in 2018 would have been 4 % of the total electricity production from wind turbines in Denmark.

Utilization of buildings' energy flexibility may result in increased annual energy demand (Déreau and Heiselberg, 2016). In most European countries, a building's energy performance is judged on its annual primary energy demand. This may be a hindrance for utilizing buildings' energy flexibility, unless some kind of "discount" is allocated to buildings offering flexibility to the grid (Edelenbos et al., 2015). This is especially important for new buildings, where a building's energy performance below a certain threshold is one prerequisite for obtaining a building permit. But also in refurbishment of existing buildings, thresholds for the energy demand is of importance.

Discussion

Dérau and Heiselberg (2016) finds a storage capacity almost 2.5 as high as in this study. Their analyses covers simulation of 365 individual days, i.e. no thermal history from previous charging/discharge cycle, each cycle with a maximum period of 6 hours charging and discharging.

Given this differences in experiment setup, results are judged as comparable.

The nature of the set-back control strategies during hours of occupation (not sleeping) will naturally compromise the thermal indoor climate. The temperature drops from the desired 22 °C towards 20 °C during the peak-periods. This is however not considered a real problem as 20-22 °C is within the comfort band for residential buildings during the heating season (DS/EN 15251:2007). Additionally, almost no hours (Table 3) are in comfort category III for all control strategies.

The indoor temperature are challenged during reheating after peak-hours when introducing a dynamic control strategy in existing houses due to slightly undersized heating systems. But replacement of existing heating systems with heat pumps offers the opportunity of increasing the installed power and in that way reduce the reheating period.

The undersized heating system simulated results in a slightly longer reheating period after peak-period set-back. This affects the indoor temperature and consequently slightly the annual energy use due to the lower average indoor temperature.

Analyses of the five remaining archetypes show similar results, however the selected example show the largest individual annual potential for thermal storage (Table 4). This archetype also have the largest time-constant (Figure 4) and the archetype is representing 27.8 % of the existing Danish single-family housing stock.

In a fluctuating electricity energy grid, primarily based on production from wind-turbines, there may be more periods with need for flexibility, hence the real flexibility from Danish single family houses could potentially be higher.

Increased flexibility

Post insulation of existing houses will increase the time-constant for the house, but the level of flexibility depends on where the insulation is placed in relation to the thermal mass. Internal insulation will decouple the thermal mass from the indoor temperature, and the amount of energy stored in the house for flexibility will decrease. External or cavity-wall insulation however, will increase the time-constant and maintain the contact between the thermal mass and the indoor temperature.

Increased air-tightness of the house, and even better combined with installation of mechanical ventilation with heat recovery, will increase the time-constant of the house. This solution maintain the amount of energy that can be stored in the thermal mass.

Adding thermal mass in the constructions of an existing house is not simple, but the request for floor-heating in combination with renovation works may open for the possibility. To utilize the storage capacity of a thermally heavy floor with floor-heating requires that the control is similar to the room temperature control, i.e. with heat supply cut off during peak periods. On the other hand, pre-

heating of a floor with floor-heating installed, and compared to other constructions, more of the thermal mass in the floor can be activated.

Most existing Danish single-family houses have a water tank for domestic hot water and have a water-based heating system. This systems are in most cases reused when converting to a heat-pump heating system, e.g. air-to-water or water/soil-to-water heat-pumps. This water tank can be used as storage for the heating system if reconfigured or replaced at the end of its service life.

Price signal response

Parallel to the analyses of houses' thermal storage capacity, the measured data were used to analyse their flexibility using a price response signal. If the context of flexibility is not only peak response but price signal response all over the day, all year round, the potential of flexibility of single family can be even larger. This will be the case in near future when fluctuating renewable energy, e.g. from wind turbines dominates the electricity grid. A simulation (Palmer et al., 2020) of such a situation was made on three single family houses (Figure 6), H1, H2 and H3 represent three different houses with different characteristics.
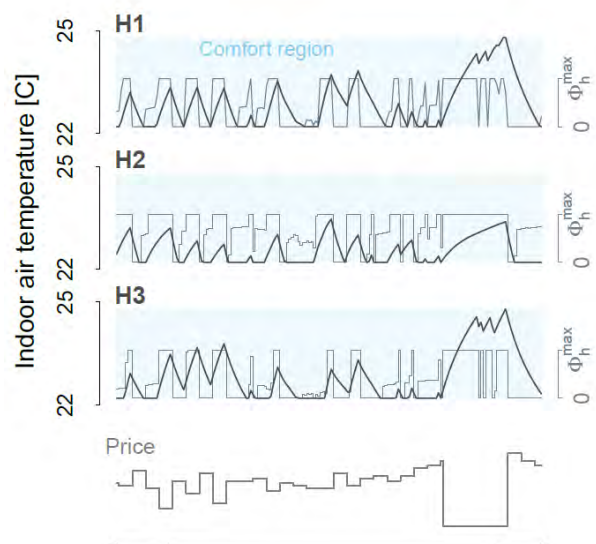
Figure 6. Grey-box simulation of the flexible control scenario for the representative houses (Palmer et al., 2020). Indoor temperature follows the schedule of heat supply, which is controlled by a price signal at the bottom of the plot.

It can be seen that when the price is low, the heating is switched on and when the price increases the heating is turned off until the temperature approaches the lower boundary. It can be noticed that the heating in H3, due to its high thermal resistance and capacity, is able to keep indoor temperature within the comfort region with the heating system running for a shorter time comparing to the other two houses. <put otherwise the heating could be

turned off for a longer time due to the building's higher time constants. The indoor air temperature in building H2 never reached the upper boundary of the comfort region due to higher heat losses.

So, in addition to the two daily peak-periods in the electricity grid, there will also be periods with insufficient electricity in a wind dominated grid. Flexibility from houses can also help shifting electricity demand from these periods. Periods with overproduction of electricity will occasionally happen during the daily peak-periods and activating houses' flexibility thus call upon some kind of signals from the grid.

Conclusions

In this study (Wittchen et al., 2020), the potential for thermal storage capacity in Danish detached single-family houses located outside district heating areas (approx. 50 % of the houses) was analysed. Analyses were carried out both statistically - based on existing measurements from night set-back experiments in 140 houses - and by simulations of archetype house models. Statistical estimates of time-constants on the simulated results were used to calibrate the archetype models.

In the future, it is assumed that all these houses will be heated by heat pumps and therefore the thermal storage capacity can be converted to flexibility (by demand side control) in the electricity grid. The energy use for houses located outside district heating areas will thus be fully electrical. If the amount of renewable electricity is insufficient during peak-periods, it must be supplemented by fossil fuel generated electricity. Shifting energy use away from peak-periods (or electricity exchange with other electricity grids) is thus needed to reduce the annual CO_2 emissions.

Six archetype models were set up, representing Danish single family houses constructed between 1850 and 1998, which covers approx. 90 % of the Danish detached single-family housing stock. Houses constructed after 1998 are excluded from the study as they are traditionally constructed from lightweight materials and have a good insulation standard. Even though these houses have long time-constants, their total energy demand is low and their individual potential for providing flexibility is limited.

Simulations of archetypes with decreased set-point for indoor temperature during peak periods give an indication of the houses' annual possibility to shift energy demand from these periods. Peak periods are defined as 2 daily periods, 2 hours in the morning and 3 hours in the evening – the latter often denoted cooking peak. Simulations also analysed the effect of pre-heating the houses 1-2 hours in advance of the peak-periods. This control strategy may potentially increase the total energy demand in some houses. This happen if the amount of stored energy during pre-heating exceeds the energy demand for maintaining a constant indoor temperature during peak-periods. Some of the stored energy will be transmitted to the outdoors

because of increased temperature of the constructions in the thermal envelope instead of keeping the indoor temperature above the set-point during peak-periods. But as energy use is moved away from peak-periods it may at the same time reduce the total CO_2 emission from the electricity production as the peaks will be lower. Lowering the peaks will reduce the risk for activating fossil fuel power plants to supplement the renewable energy in a wind energy dominated electricity grid.

On this background it can be concluded that almost all Danish single family houses erected before 1998 can contribute to the grid with flexibility. This flexibility is significant and if extrapolated to all single-family houses outside district heating areas it summarises to an annual flexibility of 544 GWh, or 4% or the total Danish electricity production from wind turbines in 2018 (45% of the total Danish electricity use).

Moreover, this flexibility can be increased by simple building renovation like external or cavity wall insulation as well as replacement of windows to new ones with better insulation and air-tightness. Additionally, mechanical ventilation with heat recovery will increase the houses' time-constant and thus flexibility. More exotic, it is possible to increase the house flexibility if domestic hot water tanks are reconfigured or replaced to act as storage for the heating system.

Thus an overall conclusion is that future building renovation should be seen in the perspective of flexibility. Put otherwise energy retrofit of the existing building stock must be seen in quite another perspective than energy performance only.

Future work

The next step in the development of BSim and analyses of energy flexibility of buildings, will be implementation of a model for predictive control of a building's energy systems. The model for predictive control will enable simulating the control of heating systems and indoor climate based on the availability of wind- and/or solar-power in the grid. The control can either be based on price signals or forecasts of the weather and thus an advance simulation of the indoor climate and the availability of renewable energy in the grid.

Acknowledgements

References

Aggerholm, S. (2018). Buildings' energy demand (In Danish: Bygningers energibehov). SBi Direction 213. Danish Building Research Institute, Aalborg University, Copenhagen.

Bergsøe, N.C. (1996). Natural Ventilation in single-family houses (In Danish: Naturlig ventilation i enfamiliehuse). Danish Building Research Institute, Hørsholm, Denmark.

Bacher, P & H. Madsen (2011): Identifying suitable models for the heat dynamics of buildings. Energy and Buildings, 43:1511–1522, 2011.

Clauß J, Stinner J, Solli C, Lindberg KB, Madsen H and Georges L (2019). Evaluation Method for the Hourly Average CO2eq. Intensity of the Electricity Mix and Its Application to the Demand Response of Residential Heating. Energies 2019, 12, 1345.

Danish Energy Agency (2020). Online statistics from the Danish energy performance certification scheme: sparenergi.dk/forbruger/vaerktoejer/find-dit-energimaerke (located: 2020.07.02).

Danish Energy Agency (2019). Energy statistics (In Danish: Energistatistik 2018). Copenhagen, Denmark.

Danish Ministry of Climate, energy and Utilities, 2020. Climate agreement for energy and industry etc. (In Danish: Klimaaftale for energi og industri mv. 2020). https://kefm.dk/media/13163/aftaletekst-klimaaftale-energi-og-industri.pdf (located 10 June 2020).

Dréau J. Le, and Heiselberg, P. Energy flexibility of residential buildings using short term heat storage in the thermal mass. Energy 111 (2016) pp 991-1002.

DS/EN 15251:2007. Indoor environmental input parameters for design and assessment of energy performance of buildings addressing indoor air quality, thermal environment, lighting and acoustics. Danish Standard, Charlottenlund, Denmark.

Edelenbos E. Tokeby M. and Wittchen K.B. (2015). Implementation of Demand Side Flexibility from the perspective of Europe's Energy Directives. Found at: www.ea-energianalyse.dk/reports/. (14. May 2020).

Hedegaard K. and Balyk O. Energy system investment model incorporating heat pumps with thermal storage in buildings and buffer tanks. Energy 63 (2013) pp 356-365.

Jakobsen A and Kolarik J. – ed. (2018). Chapter: Building dynamics (Christensen, JE) in Technical disciplines and knowledge in relation to energy and indoor climate in building management. (in Danish).

Jensen, O.M. Wittchen K.B. Sørensen C.G. Sørensen K.G. Rose J. & Svane N.D. (2020). Update of a living building-simulation tool. Submitted to BuildSim Nordic 2020.

Jensen, O.M. (2016). Smart energy in home. Evaluation of test with intelligent temperature control in single-family houses (In Danish: Smart energi i hjemmet. Evaluering af forsøg med intelligent temperatur-regulering i enfamiliehuse). SBi 2016:15. Danish Building Research Institute, Aalborg University, Copenhagen.

Knudsen M.D. and Petersen S (2016). Demand response potential of model predictive control of space heating based on price and carbon dioxide intensity signals. Energy and Buildings 125 (2016) pp 196–204.

Ministry of Climate, Energy and Buildings (2013). Smart grid strategy – the intelligent energy system of the future (In Danish: Smart Grid-Strategi - fremtidens intelligente energisystem). Copenhagen, Denmark.

Palmer J. Rasmussen C. Leerbecka K. Li R, Jensen O.M. Wittchen K.B. & Madsen H. (2020): Scalable strategies for characterizing the dynamics of the flexibility potential of residential buildings. Submitted to Journal of Energy and Buildings.

Reynders G. Diriken J. and Saelens D. Generic characterization method for energy flexibility: Applied to structural thermal storage in residential buildings. Applied Energy 198 (2017) pp 192–202.

Reynders G. Lopes R.A. Marszal-Pomianowska A. Aelenei D. Martins J. and Saelens D. Energy flexible buildings: An evaluation of definitions and quanti-fication methodologies applied to thermal storage. Energy & Buildings 166 (2018) pp 372–390.

Statistics Denmark (2020). Online table "BYGB40: Bygninger og deres opvarmede areal efter område, enhed, opvarmingsform, anvendelse og opførelsesår": statistikbanken.dk/statbank5a/default.asp?w=1920 (located 2020.07.02).

Wang P.G. Scharling M. Nielsen K.P. Wittchen K.B. and Kern-Hansen C. (2013). 2001–2010 Danish Design Reference Year - Reference Climate Dataset for Technical Dimensioning in Building, Construction and other Sectors. Technical Report TR13-19. Danish Meteorological Institute, Copenhagen.

Wittchen K.B. & Jensen O.M. (2020). Buildings as energy storage in a smart grid (In Danish: Bygninger som eneregilager i et smart-grid). SBi 2020:14. Depar-tment of the Built Environment, Aalborg University, Copenhagen.

Wittchen, K.B., Johnsen, K. & Grau, K. (2000-2019). BSim – User's Guide. Danish Building Research Institute, Aalborg University, Copenhagen.

Wittchen, K.B, Kragh, J & Aggerholm, S. (2016) Potential heat savings during ongoing renovations of buildings until 2050. SBi 2016:04. Danish Building Research Institute, Aalborg University, Copenhagen.

Insight on a local energy community:
Agent based model of a peer to peer (P2P) interaction for a group of prosumers

Marco Lovati[1*], Carl Olsmats[1], Xingxing Zhang[1]

[1]Dalarna University, Falun, Sweden

corresponding author: mlov@du.se

Abstract

Energy communities are becoming a promising opportunity for distributed energy systems in positive energy districts (PED), in which the electric energy is bought and sold in a neighborhood through a shared local infrastructure. The paper considers the complexity of the set-up using of ABM (Agent Based Modelling) as a mean to investigate how such communities work. The results of an ABM simulation regarding techno-economic matters in a small energy community (48 households) are reported and discussed. Different ownership structures and price schemes are tested and evaluated. The research result thus tend to discover 'latent opportunities' that were previously unknown and provide guidance to optimize the market design and its variables for the best performance, towards energy surplus, efficiency and climate neutrality in PEDs.

Introduction

Positive energy districts (PED) are defined as energy-efficient and energy-flexible building areas with surplus renewable energy production and net zero greenhouse gas emissions by the IEA in annex 83. Solar photovoltaic (PV) is becoming one of most significant renewable sources in PEDs. The distributed systems are dominating the Swedish PV markets. The installed capacity of PV systems in Sweden is expected to continuously soar in the future, mainly contributed by homeowners and private or public companies at relatively small or medium scales (Swedish Energy Agency, 2016) according to its particular market setup and subsidy (e.g. SOLROT deduction, tax reduction, etc).

However, relying on subsidy is not sustainable for PV deployment. At the moment, there is still limited access to capital and appropriate financing mechanisms, resulting in a slow uptake of PV under traditional business models (i.e. power purchase agreements and net-metering mechanism), which are not applicable anymore for small PV systems (Huijben & Verbong, 2013). The existing business models cannot map the full potentials of both energy supply and demand, as well as energy sharing. So if there is no subsidy in the future, the prosumers (i.e. small PV owners) can only sell their excess production at market price back to grid, which is not only less profitable to PV owners, but also reduces reliability and stability of grid.

Fortunately, the regulation is changing positively in Sweden, which starts to allow the local sharing of PV electricity in a positive energy community under § 22 (a) of the IKN Regulation 2007:215 (Sveriges Riksdag,

2007). This can be an opportunity for a new business model development within energy sector, e.g. Peer-to-Peer (P2P) trading. In such business model, consumers and prosumers form up energy communities, in which the excess production could be sold to other members (Parag & Sovacool, 2016). The benefits are threefold as the prosumers could make an additional margin on their sale, consumers could buy electricity at a more advantageous price and grid could be more stable and reliable. This can be a potential solution to promoting PV in a sustainable way, while reducing the dependency on subsidies.

In order to support new regulations, careful design and optimal modelling of P2P business models for PV penetration is necessary by analysing current scenarios and proposing future ways of exchanging energy. (Huijben & Verbong, 2013) summarized three possible ownerships of PV systems, such as Customer-Owned (single ownership), Community Shares (multiple ownership) and Third Party ownership. Based on these possibilities (Schwabeneder et al.) further described three different system boundaries of a PV prosumer business concept: "Group (1)" single direct use (one consumer directly uses the generated PV electricity on site), "Group (2)" local collective use of PV in one building (several consumers share the generated PV electricity with or without the public grid), and "Group (3)" district power model (PVs are installed in several buildings, where those prosumers directly consume locally generated PV and the PV electricity is further shared using public or private micro grid). It is possible to have different ownerships in each category of these boundary conditions, resulting in a large number of possibilities and uncertainties in the practical business operation. So learning and mapping (i.e. testing) a wide array of these possible designs and combinations is necessary, especially for different energy communities within diverse contexts.

This paper thus aims to propose and simulates a series of P2P business models for 48 individual building prosumers with PV in a 'virtual' Swedish community. It considers the electricity/financial flows, ownerships, and trading rules in a local electricity market, using simulated load and generation profiles. Three different local electricity markets (single, multi PV ownerships and free market) are designed and studied using agent-based modelling, with different energy demands, cost-benefit schemes and financial hypotheses for performance evaluation.

Methodology

Agent-Based Model (ABM)

Because of the complexity of the interactions between prosumers in a micro-grid in the introduction, an ABM simulation was developed to get an insight on the energy and economic fluxes exchanged between the different actors in the local grid. Usually every agent of the simulation represents one household in the local grid (i.e. a consumer or a prosumers), but producers are not excluded. Example of producers are energy providers, i.e. companies or investor that interact with the local grid without necessarily being served by it, or the parent grid, i.e. the larger grid on which the local grid is embedded. The local grid could be a micro-grid but also a secondary network where the prosumers are allowed to a certain level of control of the network.

In an ABM, each agent can interact with all the other agents by trading energy, thus it can send energy in exchange for money or vice-versa. The movement of energy in the micro-grid is an emergent behaviour which results from the interaction of a number of independent actors, this is opposed to a control algorithm where the behaviour is set by a series of rules or conditions. Naturally the freedom of the agents can be limited by the introduction of rules, for example a producer could be forced to prioritize the sale of renewable electricity to those consumers that have used the least of it in a given period. If the rules become tighter the freedom of each individual agent is reduced, if the rules are as tight as to completely limit any possibility of choice for the agents the ABM degenerates into a control algorithm.

In the present study, the behaviour of the agents is extremely simplified: the consumers prioritize the purchase of electricity from the cheapest source available at any given time, on the other end the producers have the ability to set the price, and they do so according to the case as explained in the following section (i.e. ownership structures and business models).

Figure 1 presents the possible ownership structures arranged in three main families, these are slightly different from those from (Huijben & Verbong, 2013) for the purpose of this study:

- Local Energy Provider (LEP) (a in Figure 1): It occurs when a single agent owns the totality of the production or storage capacity of the entire local network and the other agents are strictly consumers. The owner of the plant can be either a producer or a prosumers .
- Local Energy Community (LEC) (b in Figure 1): Is the case in which a communal plant is shared among all or a group of agents, the shares could be equally distributed or according to other principles such as energy used from the plant or share of the initial investment.
- Local Energy Market (LEM) (c in Figure 1): Is the most complex and free-form of all the structures, it is

characterized by the presence of multiple producers, consumers and prosumers , in this arrangement the interaction between agents can reach significant complexity and the agents could achieve higher earnings by engaging in intelligent behaviours.
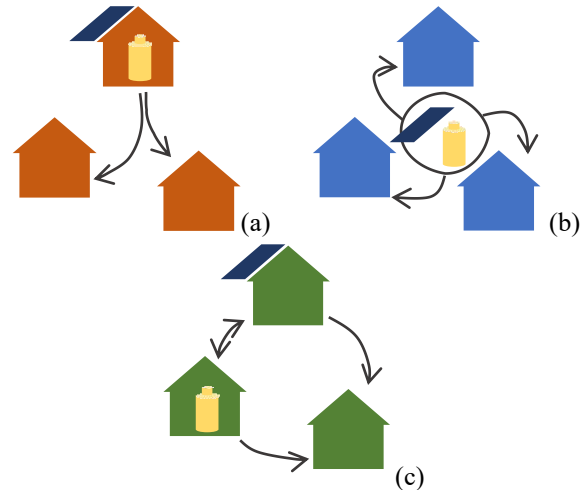
Figure 1: possible ownership structures organized in three main families: Local Energy Provider (LEP)(a), Local Energy Community (LEC)(b) and Local Energy Market (c).

Ownership structures and business models

In the case study examined (see case study section) a communal PV plant is shared among the different households in the building, this allow for two of the three basic ownership structures from Figure 1 (i.e. LEP and LEC). The ownership structure is intertwined with the business model and the rules of the market, in the following studies the same communal PV plant is shared between the households in the local grid in three different scenarios:

- **LEC gratis:** in this arrangement the electricity from the communal PV plant is given for free when available, all the households participate in the initial investment and in the Operation & Maintenance (O&M) costs of the plant according to equal shares.
- **LEC LCOE:** in this arrangement the electricity from the communal PV is given at production cost (i.e. without profit) and the revenues are divided among the shareholders. Although variable shares are possible, in this study all the households are equal sharers in the LEC (i.e. initial investment and O&M costs, and revenues are shared equally).
- **LEP n%:** This arrangement is a pure form of LEP, thus the production plant is owned by a single provider who can set the price at its own will. Obviously, the provider cannot set the price higher than that of the parent grid (i.e. the average price for Swedish household consumer as assumed in the section "The case study") as the consumers retain the right to purchase electricity from the cheapest source. In this study the provider sets the price as half-way between the minimum of the local LCOE and the

maximum of the consumer price from the parent grid. More precisely, the provider sets a price at a percentage n so that n = 0 is the LCOE, n = 100 is the price offered by the parent grid and n = 50 is exactly half-way.

In all the arrangements the consumer is programmed to buy electricity from the cheapest source, but by having a single source in the local grid the choice is only between the local source and the parent grid. This implies that the price of electricity in the local grid must be at any time below the Swedish consumer price, and that if the local production is absent or insufficient (i.e. local consumption > local production) the demand shall be covered partially or totally by the parent grid. If the local production is not sufficient, in a given point in time, to cover entirely the demand, all the households will be served equally in terms of percentage of their demand as shown in the system of relations in (1).

$$\begin{cases} E_{local} = \eta \cdot D_{local} \\ E_{house} = \eta \cdot D_{house} \quad \forall house \\ D_{local} = \sum D_{house} \end{cases}$$
(1)

In (1):

- E_{local} and E_{house} are the electricity available in a given time for the aggregated local grid and for a specific household respectively.
- η is the self-sufficiency: a number between 0 and 1 that represent the share of the demand that is covered by locally produced electricity, note that is the same globally and for each household.
- D_{local} and D_{house} represent the aggregated demand and the demand of each single household respectively.

The equations in (1) implies that having a larger consumption when the local electricity production is scarce guarantees access to a larger amount of local energy, albeit equal in percentage.

Another consequence of the relation in (1) involves the price of the electricity for each household: the price results from the weighted average (weighted on energy) of the prices from the different sources of electricity purchased. In the specific case of this study the price can be calculated with the relation (2):

$$P_{house} = P_{local} \cdot \eta + P_{parent} \cdot (1 - \eta), \tag{2}$$

Where:

- P_{house}, P_{local} and P_{parent} represent the electricity price for the individual household, the price for the energy produced locally and the price for the energy bought from the parent grid respectively.
- η is the self-sufficiency coefficient as defined for (1).

Considering that η is the same for every household in the local grid as shown in (1), (2) implies that at any given time there is a unique price of the electricity within the local grid which depends on the relation between the aggregated energy demand D_{local} and the aggregate energy production E_{local}, thus that the price for the

electricity is solely function of the Hour Of the Year (HOY) and not of any given household.

The case study

Figure 2: bird's eye picture of the small district in the case study. The picture is taken from (Huang et al. 2019).

The agent based model is tested on a digital representation of a moderate size residential district (see Figure 2) equipped with a shared PV system + DC micro-grid as described in (Huang et al., 2019). The group of three buildings on three stories is located in Sunnansjö, Ludvika, Dalarna region, Sweden. The common PV system is formed by the arrays shown in Table 1, in total there are 3 arrays on the roof and one on the southern façade (totalling 65.5 kWp).

Table 1: characteristics of the shared PV system

block	facing	Tilt [Deg]	Capacity [kW$_p$]	Production [MWh]
B	South	18	28.4	22
C	East	18	15.9	10.4
A	West	18	15.9	10.3
A	South	90	5.3	3.4

The system capacity and the position of the arrays over the building resulted from an optimization process, presented in (Huang et al., 2019), to maximize the self-sufficiency while maintaining a positive NPV over the lifetime. In this system no electric storage was installed. The LCOE (Levelized Cost of Electricity) of the system was calculated to be ca. 0.83 SEK/kWh (0.077 €/ kWh) under the following assumptions:

- initial price of the turn-key system without taxation: 10000 SEK/kWp (935 €/kWp)
- price of the inverter: 2500 SEK/kWp (234 €/kWp) (changed 2 times over the lifetime). The number of changes was retrieved as the expected value assuming a lifetime of the inverter between 12 and 15 years
- planned lifetime of the system: 30 years
- maintenance costs for the system (substitutions, cleaning and inspection): 5109 SEK/year (477 €/year). This value is calculated as the expected value out of 100 stochastic simulations.
- degradation of the performance of the system: ca. -1.15% /year

The weather file and the production of the diverse arrays of PV have been calculated from PVGIS (Huld et al., 2005). The load profile of the 48 households could not

be published for privacy concerns, thus the study is presented using data generated by the LPG (Load Profile Generator) software (Pflugradt, 2016). The parent grid (i.e. the Swedish national grid) has been assumed to offer electricity for 1.8 SEK /kWh (0.17 €/kWh) from October to March and 1.2 SEK/kWh (0.11 €/kWh) from March to October. These prices have been assumed as a reasonable price for each single households at the annual cumulative level of consumption observed. According to (Eurostat, 2007-2019), the average price for household electricity in 2019 was 1.39 SEK/kWh (0.1297 €/kWh) for electricity transmission, system services, distribution and other necessary services. If VAT and levies are added the average price would reach 2.2 SEK/kWh (0.2058 €/kWh) (Eurostat, 2007-2019). It is not clear what taxes can be avoided consuming locally produced electricity, but it is reasonable to believe that VAT can be avoided in both the LEC cases explored as the electricity is offered for free or at a price equal to production cost. Conversely it is not possible to estimate how much of the base 1.39 SEK can be reduced thanks to the aggregation of the loads. The price of the electricity is not static but is projected to grow linearly over the next 30 years at a rate of +1%/year, this under the assumption that the national grid will need liquidity to invest in the energy transition. Conversely, the revenues for the energy sold to the grid are set to be worth 0.3 SEK/kWh (0.028 €/kWh) but are assumed to shrink by 1.67%/year under the assumption that the increase in installation of PV will gradually discount the energy during sunny hours.

Results and discussion

The results section begins with a discussion about the self-sufficiency of the different households in the local network, then proceeds with a techno-economic analysis of each arrangement to establish its features and its behaviour (i.e. distribution of risk and profit among stakeholders). Given that the local PV plant is unique, the movement of energy in the network is the same in all the arrangements, thus the self-sufficiency is a static figure throughout the arrangements.

Self-sufficiency of the households

The system, as it is designed, allows to cover an estimated 20.2% of the annual cumulative demand of the district, this result is satisfactory for a system without any electric storage: for a reference, according to (IEA PVPS, 2020), the country with the most electricity production from PV (i.e. Honduras), has an estimate PV self-sufficiency of 14.8% with the EU on average having 4.9%. It has been calculated in (Lovati et al. 2019) and (Huang et al. 2019) that the economically optimal self-sufficiency of a conveniently aggregated system, even in absence of electric storage, is comfortably above any penetration level we see today (i.e. often above 20%). The economically optimal self-sufficiency sets a conservative limit of hosting capacity in an electrical system in a regime of self-sufficiency. The P_{50}

household has a self-sufficiency of 18.5% as shown in Figure 2 (a): this value is below the value of the aggregated district because the slope of the increase is higher to the right of P50 (see Figure 2 (a)). The P_{50} household has a relatively low self-sufficiency also because there is a positive correlation between annual cumulative demand and self-sufficiency (see discussion about Figure 3). In general, the variability in self-sufficiency between the households in the micro-grid is high, the most self-sufficient household possesses in fact a value double of the lesser one (14.1% to 28.4%). This strong variability suggests that, even without any deliberate attempt for demand control, some households show habits, or a way of life, that can take out the most from the available PV energy.

(a)

(b)

(c)
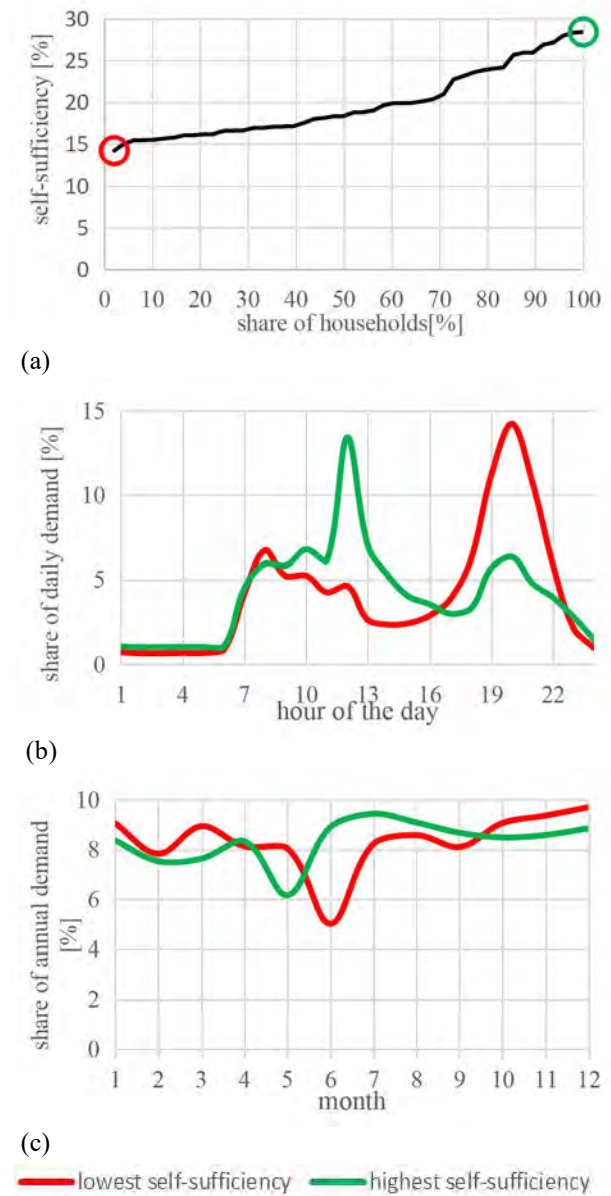
Figure 3: self-sufficiency of the apartments in the local grid. (a) is the distribution of self-sufficiencies across the 48 households,(b) shows the hourly average of the extreme households,(c) shows the monthly average consumption of the extreme households.

Figure 2 (b) and (c) shows the share of the annual demand in different hours of the day or month of the year respectively: which is to say how much of the total annual demand is concentrated during a specific hour of every day or month along the year.

In the household with the highest self-sufficiency the electricity demand around 12:00 is particularly prevalent (see Figure 2 (b)), it indicates that its inhabitants use to cook at home for lunch. On the other end, the evening peak of the most self-sufficient household is way less prominent than in the lowest one. Looking at the prevalence throughout the months of the year (Figure 2 (c)), the difference is less marked compared to the daily average: both the households present a steep drop in sunny months which seems to indicate an absence due to summer holidays.

The most self-sufficient household appears to have had an absence for holidays during May instead of June (Figure 2 (c)), this might be advantageous as it allow to use more PV electricity when the overall electricity demand of the district is lower and the radiation from the sun is higher. It should be noted that, in general, the best performing household presents a smaller dip in demand for the summer holidays, it is unknown whether it is due to a shorter holiday or at the presence of some household's components at home.
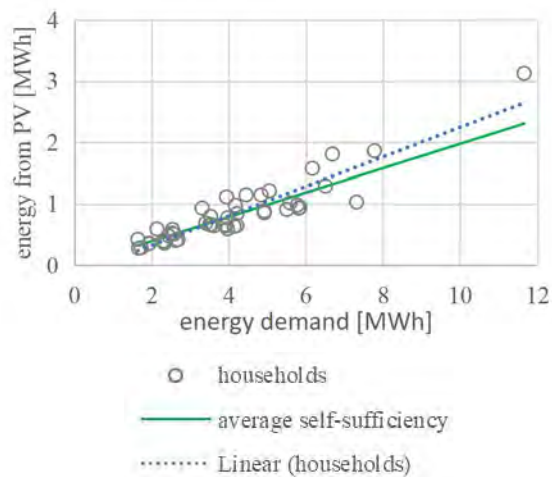
Figure 4: annual cumulative energy demand and annual cumulative energy used from the PV system for every household in the local grid.

Figure 3 Shows the relation between the annual cumulative demand and the annual cumulative energy received from the shared PV system. These two variables are strongly correlated (R > 0.9), thus the quantity of energy consumed from the PV system can be assumed with good confidence from the annual cumulative demand alone (i.e. regardless of the self-sufficiency). This aspect, although counter-intuitive, is a consequence of the highest variability in annual cumulative demand compared to the variability in self-sufficiency: if in fact the highest self-sufficiency is two times the lowest one, the highest cumulative demand is

almost 5 times the lowest one (excluding the highest value as an outlier, otherwise is more than 7 times). The strong prominence in variability of cumulative demand compared to self-sufficiency reduces the variation in self-sufficiency as a mere noise compared to the other variable (as visible in Figure 3). Furthermore, as self-sufficiency is a share of the demand, does not have much importance in absolute terms when applied to households with low cumulative demand. This fact represents somewhat a hindrance as it implies that increasing overall consumption works better than improving self-sufficiency to seize larger quantities of scarce local renewable resources. Nevertheless, it is not clear what power has an individual household to change its cumulative energy demand. Further investigation on the aspects that influence the cumulative energy demand (e.g. number of people in the household, cooking habits, holiday habits etc..) is needed to assess whether it is something that the inhabitants can change. If each household has significant power on the cumulative energy consumption it is reasonable to fear a sharp increase in the overall consumption after the installation of the communal PV system. It should be acknowledged that the lack of data with respect to other households might focus the attention of the inhabitants on their own energy demand advising them to increase the self-sufficiency. Another interesting aspect shown in Figure 3 is that the linear interpolation of the household data points has a steeper slope than the average self-sufficiency of the 48 households: this means that the household with highest annual cumulative consumption have also, on average, a highest self-sufficiency. A correlation analysis between annual cumulative consumption and self-sufficiency found a positive, albeit weak, correlation (R ≈ 0.2). Although weak, thus uncertain, the correlation suggests that highly consuming households might have more contemporaneity with the production from PV: this might be due to larger households having some components who stay at home during daytime, or to electric consumption of people who spend daytime at home being larger overall.

LEC gratis

In this arrangement the households in the district are shareholders of the system and thus, when available, can use the electricity produced by the system for free. In this study the shares of the PV system are equal, each household will therefore have to pay 13646 SEK (1275 €) of initial investment plus ca. 342 SEK/year (32 €/year) for maintenance and substitution of the inverter. Different ownership structures are possible, but the business model should be modified to avoid loopholes in the risk-benefit balance. For example, equal shares could be distributed to a sub-group of the households (i.e. there are consumers who do not hold shares). In this case a price of the electricity for non-owners should be established (see section LEP n%).

Figure 5 shows the difference in price between the energy offered by the parent grid and the energy available within the local system. The chart shows monthly values, these refer to the average cost of the electricity that month in the grid. We know from the section "Ownership structures and business models" that at any given time the price of the electricity is unique within the micro-grid and depends from the relationship between production of PV and demand (see equation 1 and 2). The bars in Figure 5 are the average of all the electricity prices of the respective month weighted by the aggregated electric consumption in that month. Obviously, since the energy not met by the local production is bought from the parent-grid, the external price has an influence on the internal one. In simpler terms, the internal price of the electric energy in one month, because of the Equation 2 with $P_{local} = 0$, is proportional to the residual demand. Notice that, due to the higher external price, the drop in cost of electricity during the months of March (month 3) is similar to that in April (month 4) despite a lower self-sufficiency.

Figure 5: monthly difference in price between the energy offered by the parent grid and the average paid by the shareholders in a LEC gratis arrangement.

Even if the price of the electricity is the same within the micro grid at any given point in time , the average price paid by each household varies according to the time patterns of consumption. An household which consumed a large share of its annual consumption at times when the electricity was free (or at least cheaper) will enjoy a lower average price. This is to say that a higher self-sufficiency will lower the average price. However, in terms of gross economic benefit (i.e. the sum that can be saved) it is not the average price that matter, but the cumulative energy received for free. In this sense, the conclusion from Figure 4 is troublesome as the earnings are not due to the ability to obtain a higher self-sufficiency, but simply to the sheer cumulative consumption. In Figure 6 The households in the micro-grid are divided in 3 groups of 16 elements each according to their annual cumulative consumption. As in Figure 4 the correlation of the KPI with annual cumulative consumption is evident. In fact, the lifetime economic balance is determined solely by the savings, thus by the sheer quantity of energy that is received by each household. From Figure 6 it is visible how being in the upper third of the cumulative consumption charts

guarantees substantial earnings (IRR from 1.9% to 6%) given the initial investment of about 13646 SEK (1275 €/household). Conversely, the low-consumption households are doomed to economic losses, which means they are unable to recover the investment itself.
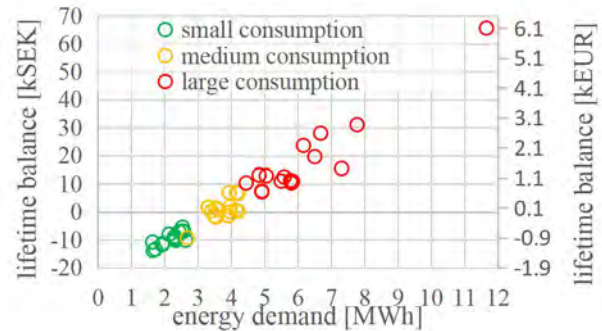
Figure 6: cumulative balance over the lifetime of the system against the annual energy demand (energy given free to the shareholders). The households have been divided in 3 groups, each of 16 specimens, according to their cumulative consumption.

If the relation between annual cumulative consumption and lifetime earnings would become known by the households in the local grid, there is a risk that there would be a considerable increase of the cumulative demand after the installation of the communal system. This fact, although potentially reducing the risk for those investing in the system (especially in a LEP case) would counteract the purpose of reducing consumption of electricity from the grid.

LEC LCOE

If instead of being given for free the energy is sold at production cost (LCOE), the difference in lifetime balance from the different households are greatly reduced, but they persist. In this case the advantage associated with the use of energy from the system is influenced by the stake of ownership of the system. In general it can be noted that the lifetime earnings (i.e. Figure 6 and Figure 7) follow a linear transformation from the extreme inequality (as in Figure 6), to a situation of complete equality of earnings (if a LEC grid-price is hypnotized) where no benefit is obtained by the use of in-situ electricity. In the hypothesis that a benefit for self-consumed electricity would spur increased self-sufficiency, a balance should be found between risk for the low consumption households and reward for the consumption of local renewable energy.
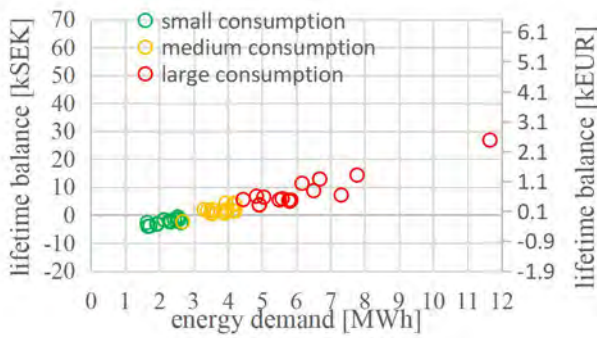
Figure 7: cumulative balance over the lifetime of the system against the annual energy demand (energy given at production cost to the shareholders). The households have been divided in 3 groups, each of 16 specimens, according to their cumulative consumption.

LEP n%

In this arrangement the PV system is owned by a single provider who has the right to set the price. Obviously, since the parent grid has the ability to supply 100% of the demand of the district, the owner cannot set the price higher than the electric grid lest being completely outbidded (i.e. no household would use the owner's energy).In this study the provider sets the price as half-way between the minimum of the local LCOE and the maximum of the consumer price from the parent grid. More precisely, the provider sets a price at a percentage n so that n = 0 is the LCOE, n = 100 is the price offered by the parent grid and n = 50 is exactly half-way.

Table 2 shows how the annual revenues, the balance over the lifetime and the real IRR (Internal Rate of Return) change according to the price at which the electricity is sold.

Table 2: annual revenues, lifetime balance and Internal Rate of Return (real) of the investment by different prices set by the owner.

n [%]	revenues [SEK]	balance [SEK]	balance [€]	IRR [%]
0	34'553	-94'058	-8'790	-0.5
9.43	37'689	0	0	0.0
25	42'864	155'247	14'509	0.7
50	51'174	404'553	37'809	1.6
75	59'484	653'859	61'108	2.3
100	67'794	903'165	84'408	2.9

Notice how with n = 0 % (i.e. the electricity sold at production cost of 0.83 SEK/kWh) the balance, thus the IRR result negative. This is due to the fact that the self-consumption of the system is not 100% (it is in fact ca.85%). In other words, not all the energy produced by the PV system is consumed by the households in the local grid, therefore part of the production is sold to the grid below LCOE and results in a moderate loss over the lifetime. The existence of this loss justifies the use of a LCOE adjusted for self-consumption as described in

(Huang et al., 2019). This loss also explains why, under LEC LCOE arrangement, some households experience economic losses over the lifetime when the electricity by the communal system is given at price of cost (see Figure 7). When the electricity is sold at LCOE, the IRR of the PV system is negative, thus holding its shares leads to a loss unless the benefit for cheaper energy outweighs the costs.

Applying an n = 9.43% does not result in any loss or gain over the lifetime of the system, it can be argued that no investor would like to take any risk to have an expected NPV (Net Present Value) of 0 at the end of the lifetime with a discount rate of 0. Nevertheless, there are potential business models for large homeowners such as general contractors or municipalities who could substitute part of the roof and façade cladding with BIPV thus avoiding the cost of an alternative material. Furthermore, this price tag is extremely interesting as price of sale from LEC. It in fact presents the advantage of forecasting the expected lifetime economic balance in positive ground for each household.

A good business opportunity is finally offered by the n = 100%. This price, while suggesting a real IRR around 3% for the LEP, offers the occupants the opportunity to largely increase their share of renewable energy use without having to pay any upfront cost. In this case the households have no economic benefit in installing the PV, but they have no risk nor upfront investment and could receive information about their own self-sufficiency by the provider, for example with a monthly email.

Conclusion

In the study, a newly developed Agent Based Model was tested on a shared PV system serving a small district comprising 48 apartments. 2 different ownership structures were tried: LEC (Local Energy Community) and LEP (Local Energy Provider). The LEC arrangement was tried both with the electricity given for free to all the equal shareholders or given at a price (in the study the LCOE). For the LEP, because the free offering would make no sense, an array of different prices was tried (see Table 2). In the local grid , if the renewable energy is not enough to cover the electric demand during a specific hour, the aggregated self-sufficiency is assigned to each household regardless of its demand (see Equations 1 and 2). A large difference in terms of self-sufficiency has been observed within the 48 households, with the individual self-sufficiencies spanning from ca. 14% to more than 28% (see Figure 3 a). Considering the absence of active strategies to increase the self-sufficiency in the cluster, such large differences can be attributed only to socio-cultural factors and spontaneous lifestyle choices. From Figure 3 (b) it appears that the most self-sufficient household has on average the peak of energy consumption at noon (possibly due to home cooking), while the least self-sufficient one has usually its peak consumption at 8 P.M.

Differences are visible also over the different months of the year but their effect is not as clear as in the hours of the day. The large differences observed in self-sufficiency, having no active engagement or use of demand-shifting technologies, invites a deeper analysis and understanding of the existing electric demand and the factors which affect self-sufficiency. Despite the large variation in self-sufficiency, it has been observed that the sheer amount of energy used from the system is mainly determined by the annual cumulative demand (see Figure 4). This phenomenon, albeit counter-intuitive, is due to the fact that the variability of cumulative demand far outweighs the variability in self-sufficiency (the largest being 5 or even 7 times the smallest one). In other words, the fraction self-consumed is not significant when applied to a group of households whose entire demand is hardly significant compared to others. This fact is problematic because the energy savings (i.e. the main earning mechanism of the investment) come from the amount of PV energy consumed, and not from the self-sufficiency reached. The relation between annual cumulative consumption and cumulative energy from PV is in fact transposed in the relation between energy consumption and lifetime balance (see Figure 6). The balance in a LEC gratis arrangement (Figure 6) is almost completely determined by the cumulative consumption, with the self-sufficiency being reduced to a noise in the linear relation. Even more telling is that, if the households are divided in 3 groups according to their cumulative consumption, the biggest consumers all have positive balance and the smallest consumers all have a negative one. This aspect suggests that, if the communal PV system is installed under a LEC gratis arrangement, the shareholders might increase their electric demand in a bid to outdo each other's energy consumption. This behaviour would possibly defeat the purpose of installing on-site renewables in the first place. It should be also considered that, due to privacy laws and standard practice, each individual household is likely only aware of its own electric demand and self-sufficiency. This lack of data might drive each household to work on improving self-sufficiency instead of annual cumulative demand. It should also be remembered that the earnings are savings, thus increasing the cumulative demand would anyway lead to an increase in the energy bill. In this sense, the increased exploitation of the common electricity through increased cumulative demand would happen only if increased consumption is perceived as a value, for example through the purchase or increased use of energy hungry appliances for cooking or DIY (Do It Yourself) purposes. The difficulty to change self-sufficiency compared to cumulative demand should also be considered to assess the likelihood of one scenario over the other. For example, cumulative demand might be strongly constrained by working schedule or number of household members. These aspects reiterate the need for a deeper study on the aspect of demand that influence self-sufficiency. From the perspective of the investment in PV, both the changes in behaviour envisioned would increase self-consumption, hence earning potential.

Assuming that the shared PV system is owned by a single entity in a LEP (Local Energy Provider) arrangement, this entity enjoys freedom in setting the price for the sale of electricity. This freedom is nevertheless constrained by the LCOE of the PV system and by the price offered by the parent grid. If the LEP sells electricity at a higher price than the parent-grid, because the grid has the capacity to satisfy 100% of the demand at any time, it will have no purchaser among the households. For this reason, a coefficient "n" has been devised so that: n=0 is the LCOE of the local system and n= 100 is the sale of energy at exactly the same price as from the parent grid. It has been shown that at n = 0, despite selling at production cost, the lifetime balance is < 0. This is due to the self-consumption being below 100% (i.e. ca 85%), hence ca. 15% of the energy produced being sold at spot price (i.e. 0.3 to 0.15 SEK/kWh or 3 to 1.5 €cent/kWh). This loss also explains why in the LEC LCOE arrangement some households still have a negative lifetime balance (see Figure 7). Selling energy at the price of the parent grid (n = 100) could be an interesting investment as it guarantees the LEP with a real IRR of around 3%, it provides no economic benefits for the household consumers but it gives them the ability to boost their reliance on renewable without any upfront cost nor risk. Furthermore, the possibility for the households to buy voluntarily sized shares of the LEP could kickstart a set of tantalizing business opportunities.

Acknowledgement

References

Swedish Energy Agency (2016). Förslag till strategi för ökad användning av solel. ET 2016:16, ISSN 1404-3343

Huijben, J. C., & Verbong, G. P. (2013). Breakthrough without subsidies? PV business model experiments in the Netherlands. Energy Policy, 56, 362-370.

Sveriges Riksdag, Infrastrukturdepartementet (2007). Förordning (2007:215) om undantag från kravet på nätkoncession enligt ellagen (1997:857)

Schwabeneder, D., Dallinger, B., & Moisl, F. EXISTING AND FUTURE PV PROSUMER CONCEPTS.

Parag, Y., & Sovacool, B. K. (2016). Electricity market design for the prosumer era. Nature energy, 1(4), 1-6.

Huang, P., Lovati, M., Zhang, X., Bales, C., Hallbeck, S., Becker, A., ... & Maturi, L. (2019). Transforming a residential building cluster into electricity prosumers

in Sweden: Optimal design of a coupled PV-heat pump-thermal storage-electric vehicle system. Applied Energy, 255, 113864.

Huld, T., Šúri, M., Dunlop, E., Albuisson, M., Wald, L., (2005). Integration of HelioClim-1 database into PVGIS to estimate solar electricity potential in Africa. Proceedings from 20th European Photovoltaic Solar Energy Conference and Exhibition, 6-10 June 2005, Barcelona, Spain, http://re.jrc.ec.europa.eu/pvgis/.

Pflugradt, N. D. (2016). Modellierung von wasser und energieverbräuchen in haushalten.

Eurostat, Electricity prices for household consumers - bi-annual data (2007-2019)

Building Envelope, Daylighting and Thermal design

Experimental and numerical studies on thermal performance of an office cubicle having gypsum boards coated with PCM-enhanced spackling

Tor Arvid Vik[1*], Habtamu Bayera Madessa[1], Arnab Chaudhuri[1], Andreas Aamodt[1], Chakkrit Phengphan[1], Ebenezer Twumasi Afriyie[2]

[1]OsloMet, Oslo, Norway
[2]Saint-Gobain Sweden AB, Bålsta, Sweden
* corresponding author: torvik@oslomet.no

Abstract

PCM enhanced wallboards on internal surfaces of building spaces is an attractive solution for improvement of thermal performance in buildings. This work deals with using a novel spackling compound as a primer coating material, from Gyproc Saint-Gobain, Sweden AB, in the inner walls of building envelopes for passive cooling and thermal comfort management. The spackling compound contains fillers, rheological additives and binding agents together with micro-encapsulated PCM. Experimental measurements and numerical simulations are performed for an office cubicle having 14 m^2 floor area with and without PCM enhanced spackling material. PCM enhanced spackling has been applied on the internal walls and ceiling surface. The results show that a significant cooling effect could be achieved when covering walls and ceiling with PCM enhanced spackling directly exposed to the occupied zone. Furthermore, a parametric study shows that the PCM's thickness, and the nighttime ventilation airflow rate and supply air temperature have considerable impact on the cooling performance.

Introduction

In recent years, the construction industry gained a worldwide attention towards improvement of energy efficiency and innovation. The global challenges for construction engineering encompass research areas in all phases of the building process, starting from planning to final disposal of the building (Casini (2016)). Progress in material science and technology can provide innovative, sustainable, and environmentally friendly solutions to meet such global challenges. Incorporation of phase change materials (PCMs) in building elements essentially increases the thermal mass and are used in latent thermal energy storage systems and thermal management systems (Madessa (2014), Vik et al. (2017)). PCMs are widely used in construction materials e.g. HVAC systems, floors, ceilings, roofs, concrete, drywalls, coating plasters blends etc. Among these, PCM enhanced wallboard in the interior side of the building envelope is the most common solution for implementing PCM into building elements (Kalnæs and Jelle (2015)). Microencapsulation is the most effective way to integrate PCM into building materials. Several researchers have studied the benefit of PCM incorporated gypsum boards (Feldman et al. (1991), Athienitis et al. (1997), Neeper (2000), Zhang et al.

(2012), Borreguero et al. (2010)) in the interior. Nevertheless, dependencies of the thermo-physical properties and overall energy performance on different wt% of PCM incorporated in a composite material are the most important aspects toward the optimal and cost effective PCM loading. The key challenges are to improve the overall lower thermal conductivity and latent heat of a PCM incorporated composite as well as to meet the fire safety requirements.

However, bulk production of microencapsulated PCM (MPCM) incorporated gypsum boards incurs a high production cost. An interesting cost effective alternative is to make a suitable spackling mixture incorporated with MPCM. This work is motivated by the recent novel spackling compound produced by Scanspac (Saint-Gobain Sweden AB, 2020) as a primer coating material in the inner walls of building envelope (walls/ceilings about 1-3 mm thickness) toward efficient thermal management by passive cooling/heating. The coating could be applied on gypsum boards, plaster boards, concrete or bricks. It is to be noted that, spackling compounds are often used in the interior surface of building envelope to repair defects of the surfaces. These compounds are typically made of (Kurp (2003)) binders, clay, lubricant, stabilizer, thickeners etc. Spackling materials could be of different application types and densities. For example, "lightweight" spackling is suitable for minor repairs. On the other hand, "heavy duty" spackling is relatively denser and more suitable for covering nails, drywall screw holes, filling significant depressions and holes of wall board (Foster and Bonifas (2010)). US patent (Gozum and LaFleur III (2016)) reported the self-priming spackling compound which yields consistent and uniform appearance when painted. The spackling compound used in this study contains fillers, MPCM, rheological additives and binding agents. To the best of our knowledge, there is no literature about the MPCM enhanced spackling material and its usage for thermal management in building applications. In this work, we present an experimental and numerical analysis of the aforementioned novel spackling material towards efficient thermal performance in buildings. The work is organised as follows. In section Methodology, we first present the overall experimental setup followed by the numerical setup for the present work. The analysis is

presented in sections Results and Discussions. Finally, conclusions are drawn at the end.

Methodology

The impact of the PCM spackling material on the operative temperature of an office cubicle is measured in a full-scale test room. The measurements are also used to validate a numerical model of the lab experiment in IDA ICE. Measurements of temperature in the test room were performed with and without PCM spackling on wall and ceiling surfaces.

Experimental setup

The test room is located inside an indoor climate laboratory at OsloMet. The test room is separated from the laboratory room by roof, floor and walls. On one of the walls, there is a (1 x 2) m^2 door and a (2 x 2) m^2 window towards the laboratory room. The floor area of the test room is 14 m^2 and the room height is 2.34 m. The room height of an office cubicle is normally higher than in the test room, usually around 2.7 m. Due to stratification it can be assumed that the measured air temperatures in the occupied zone were slightly higher than what would have been in a room with a higher ceiling. Figure 1 shows sketches and a photo of the test room and the test setup. Table 1 shows the internal heat loads of the office cubicle, together with important design data. There is also some heat gain from measurement devices and electronic control equipment, amounting to approximately 40W.

The floor, ceiling and walls of the test room are made of sandwich elements consisting of 100 mm thick polyurethane foam covered with thin metal plates on both sides. Inside of ceiling and walls there is an uninsulated wood frame (between 48 and 73 mm thick) and 13 mm thick gypsum boards. The gypsum boards were covered with approximately 1.8 mm thick PCM spackling and a layer of white painting. The floor consists of a wood parquet on top of the polyurethane foam element.

The test room is equipped with a mechanical balanced ventilation system, a diffuser for supply air in the ceiling and exhaust at ceiling level on the wall.

Internal heat loads for the cubicle are listed in Table 1. Lighting load was provided by two fluorescent lamps. Occupants and equipment corresponds to two persons. As illustrated in Figure 1, heat load from occupants and equipment was provided by vertical cylindrical ventilation ducts with heating elements inside and matt black outside surface. Solar heat load corresponds to a south facing window of (2 x 2) m^2, with automatically controlled external solar shading, at midsummer at Oslo airport Gardermoen. A simplification is made by distributing the diurnal solar heating energy as a constant load of 200 W within the business hours of the office.
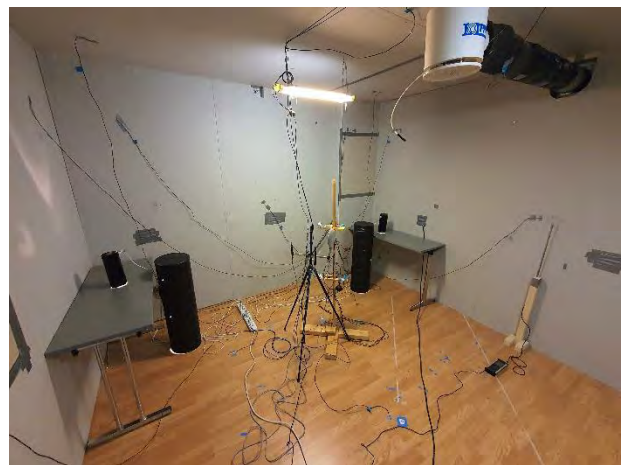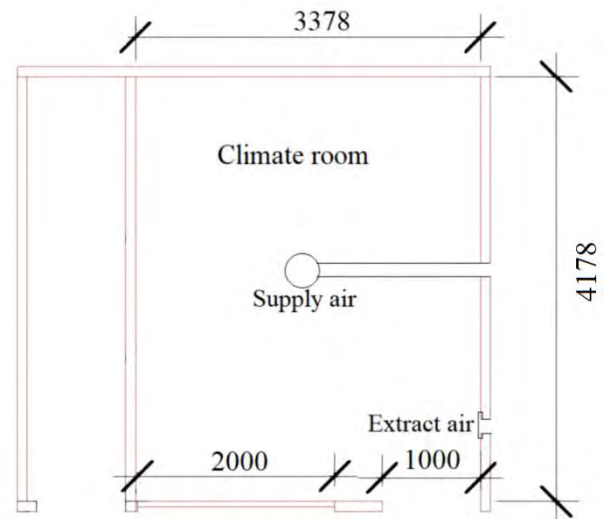
Figure 1: sketch (above) and a photo (below) of test room and setup (dimensions are in mm).

Table 1: Input data of the office cubicle

Parameter	Value
Supply air temperature for business hours [°C]	19
Supply air temperature for non-business hours [°C]	14
Supply airflow for business hours [m^3/h]	135 (3 l/sm^2)
Supply airflow for non-business hours [m^3/h]	230 (5 l/sm^2)
Heat gain from computers [W/m^2]	9
Heat gain from occupants [W/m^2]	13
Heat gain from lights [W/m^2]	4
Heat gain from sun [W/m^2]	14
Schedule business hours	08:00-18:00
Schedule non- business hours	18:00-08:00
Infiltration [ACH] @ 50 Pa	3.4
U-value (door/window) [W/(m^{2}K)]	0.6/0.8
U-value (wall/ceiling/floor) [W/(m^{2}K)]	0.20/0.20/0.21

This heat load was provided by an electric heating foil placed on the inside of the window. The window pane was covered with aluminium foil in order to reduce radiation heat loss from the heating foil through the window.

The PCM spackling consists of an ordinary spackling to which encapsulated micro size PCM spheres is added. Key data of PCM and spackling are listed in Table 2.

During the test, air temperature was measured in the supply air duct, and in the middle of the test room at 0.6 m above the floor. The test room's internal wall surface temperatures, as well as the top surface of the PCM in the suspended ceiling and the surface of the PCM in the wall were also measured. Both the air and surface temperatures were measured by T-type thermocouples, having +/- 1.5 °C uncertainty. The thermocouples were logged by an Intab PC-logger 3100i which was operated by Intab EasyView software version 5.6. Most of the measurement points are shown in Figure 2.
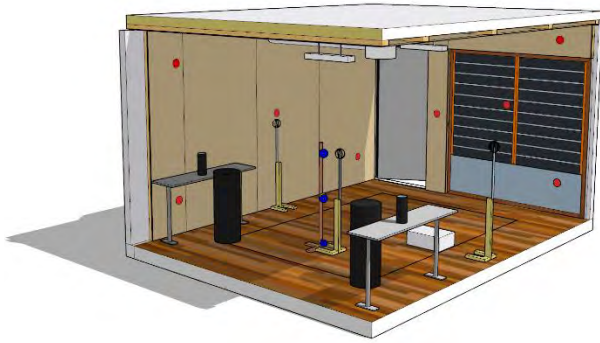
Figure 2: Measurement points (red and blue circles).

The air velocity during the experiment was measured lower than 0.2 m/s. Thus, the operative temperature can be calculated as an average of the calculated mean radiation temperature and the measured values of air temperature at 0.6 m above floor level. The mean radiation temperature is calculated from measured surface temperatures and view factors of the surfaces exposed to a person sitting in the middle of the room:

$$\overline{T_r^4} = T_1^4 F_{p-1} + T_2^4 F_{p-2} + \cdots T_N^4 F_{p-N} \qquad (1)$$

Where $\overline{T}_r$ is the mean radiation temperature (K), T_N is the surface temperature of surface N (K), and F_{p-N} is the view factor between a person and surface N (Standard Norge, 2001).

Numerical simulation

In the numerical analysis, IDA Indoor Climate and Energy 4.8 (IDA ICE) software (Equa, 2020) was used to study the performance of the PCM enhanced spackling. First, the PCM wall extension in IDA ICE was validated against measurement data. Then, parametric analysis was conducted in order to study the effect of different design parameters on the spackling performance.

PCM wall model validation

The measured average indoor air temperature of the office cubicle was used to validate the PCM wall model behaviour in IDA ICE. The PCM wall model has been developed for years and is now available in the Expert edition of IDA ICE. The wall model uses an enthalpy formulation method, considering the temperature dependence of the enthalpy of a PCM during melting and solidifying phases, and solves the heat transfer equation using the finite difference method.

The cubicle was considered as a single thermal zone, as shown in Figure 3, and all the design parameters used in the experimental test, including air flow rate, ventilation schedule and supply air temperatures, and internal heat loads were employed as input data for the validation. Since the cubicle is placed inside a laboratory room, the surrounding conditions are represented by the temperature of the laboratory room. This varied between 22.2 °C to 22.6 °C.

In the simulation, the heating mat that approximate the solar heat load was replicated by placing an electric radiator of the same surface area as the heating mat. Moreover, in our numerical analysis we approximated the internal heat load from measuring devices to 3 W/m².

Figure 3: Office cubicle designed in IDA ICE

Consistent to the PCM layer implemented in the experimental test, 2.10 mm and 1.75 mm PCM layer thickness was applied on the ceiling and the wall surfaces respectively. Variation of specific heat capacity of the PCM with temperature, as shown in Figure 4, was also employed in the PCM wall model. The model uses discrete points to approximate the temperature dependency of the specific heat capacity curve within the temperature range of the curve. Other thermo-physical properties of the PCM are shown in Table 2.
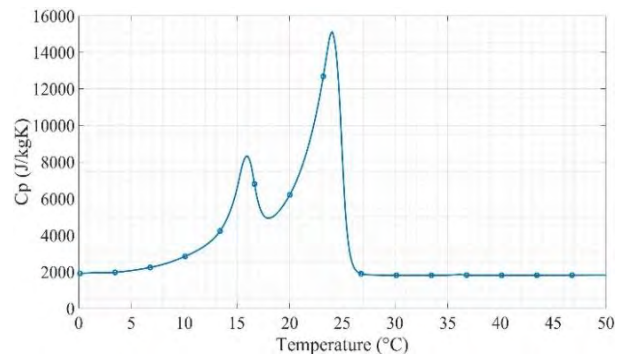
Figure 4: Specific heat capacity vs temperature of the PCM spackling measured using differential scanning calorimetry test (Saint-Gobain Sweden AB, 2020).

For validation purpose, a simulation was run for three days and the result was compared with the measurement as shown in Figure 5. The result showed that the simulated mean air temperature corresponds well with the measured mean air temperature, and the maximum relative error is about 6.6 % around at 19:00. It is important to note that the measured mean air temperature represents the average air temperature of the air temperatures measured at different heights of the cubicle.

Table 2: Thermo-physical properties of the PCM spackling (Saint-Gobain Sweden AB, 2020)

Property	Value
Density [kg/m^3]	970
Total heat storage capacity[KJ/kg]	88.4
Thermal conductivity, solid[W/m K]	0.08
Thermal conductivity, liquid [W/m K]	0.08
Onset melting point [°C]	20
Peak melting point [°C]	24
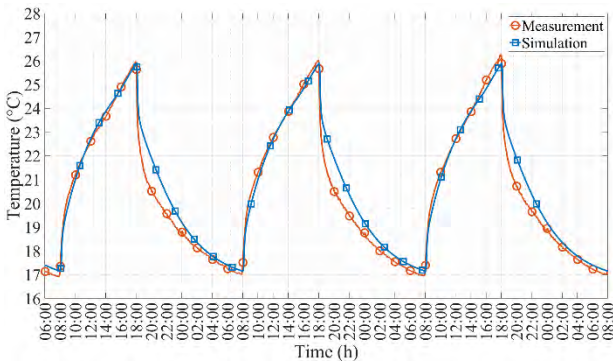
Figure 5: Comparison of measured and simulated data

Figure 5 shows a qualitative comparison of the measured and simulated values of the mean air temperature of the cubicle. An R^2 value of 0.976 implying that the variation in simulated temperature strongly corresponds with the measured temperature.
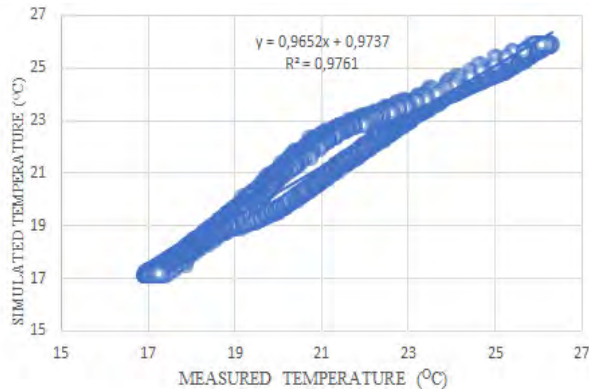
Figure 6: Scatter plot of measured and simulated indoor air temperature

Moreover, Coefficient of Variation of the Root Mean Square Error (CV$_{RMSE}$) approach using Equation 2 is adopted to check the deviation of the measured data from the simulated result. The CV$_{RMSE}$ showed a 1.12 % error, which also indicates good accuracy of the model.

$$CV_{RMSE} = \frac{1}{y_m} \sqrt{\left(\sum_{i=1}^{n} \frac{(\hat{y}_i - y_i)^2}{n}\right)} \qquad (2)$$

Where y_i is the simulated/predicted value, $\hat{y}_i$ is the actual/measured value, y_m is the mean of measured values, and n is the number of data points.

The validation results revealed that the PCM wall extension in IDA ICE replicates the measured data and it can also be used for further investigation of PCMs performances. However, it is important to note that the validation process investigated conditions typical for the summer season, and the validity of the model under other conditions is not guaranteed by this validation process. Future study should be devoted to extend the validation of the model.

Parametric design analysis

In order to study the effect of the spackling layer thickness, supply air temperatures, and the air flow rate on the performance of the spackling PCM, a parametric analysis was conducted for the same office cubicle designed for experimental test. In the analysis, only one of the design parameters was varied while the other design parameters were kept constant. Hence, in the first scenario, three PCM layers, with thicknesses of 2 mm, 3 mm and 4 mm were considered when the PCM was applied on internal walls and ceiling surfaces. The supply air temperatures and air flow rate for both business hours and non-business hours, schedules, and internal heat loads mentioned in Table 1 were used as input data.

In the second case, the thickness of the PCM layer was set to 3 mm and the supply air temperature for the non-business hours was varied between 14°C and 17°C, while the other design parameters were held constant.

The third scenario investigate the effect of the ventilation air flow rate during the non-business hours. The air flow rates were set to 135 m^3/h, 180 m^3/h, 225 m^3/h and 270 m^3/h. Again, a 3 mm PCM layer thickness was chosen, and all the other design parameters were kept constant.

All the three scenarios were identical in terms of construction materials, dimensions and configuration, and the parametric analysis focused on the temperature reduction potential of the PCM enhanced spackling compared to a reference case without PCM enhanced spackling.

Results and discussion

Experimental results

The experimental study was focused on the performance of the PCM enhanced spackling, in terms of reduction of operative and surface temperatures of the office cubicle.

Operative temperature

The operative temperature which is calculated from the measurements is depicted in Figure 7. The result revealed that adding the PCM spackling to the ceiling and wall surfaces reduced the operative temperature with 0.9-1.1°C, e.g. from 27.0°C to 25.9°C at day 1. The temperature reduction seems to be relatively constant between 14 and 16:00. It is also interesting to observe that the cooling impact of the PCM seems to start around 9:00 in the morning, at an operative temperature of about 20°C. The operative temperature during non-business hours is almost equal with and without PCM spackling. This indicates that the ventilation airflow rate during non-business hours is abundant in order to remove heat released from the PCM when the temperature in the cubicle drops.
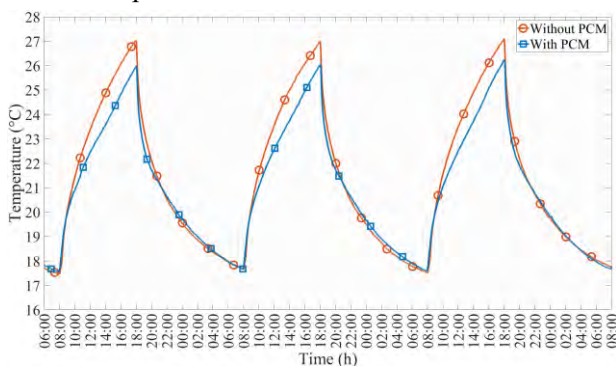
Figure 7: Operative temperature.

Surface temperature

Surface temperatures with and without PCM, in the ceiling and at the walls, are shown in Figure 8.
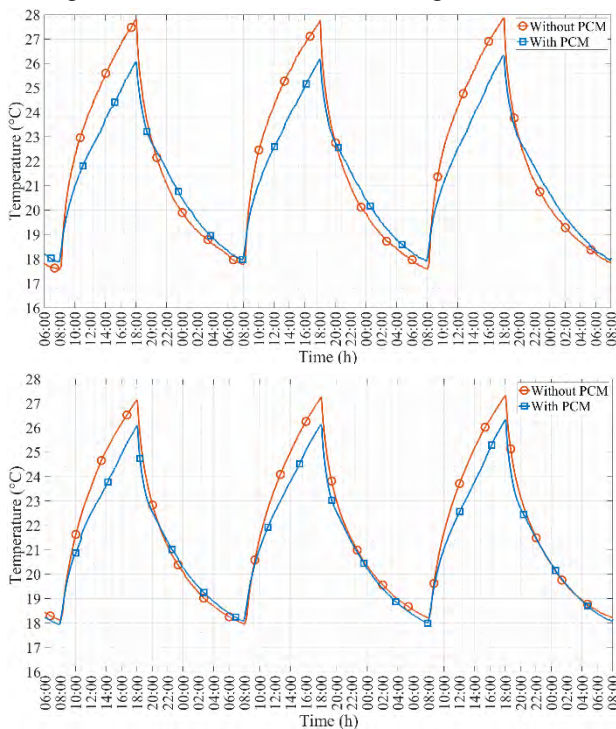
Figure 8: Surface temperature of ceiling (upper) and walls (lower).

The surfaces with PCM reached peak temperatures of between 26.0°C and 26.4°C, which is around the upper end of the transition area of the PCM, as shown in Figure 4. The impact of the PCM is significantly stronger in the ceiling than at the walls; the PCM reduces the surface temperature with about 1.6°C in the ceiling compared with about 1.0°C at the walls. This means that more of the cooling potential in the PCM in the ceiling has been utilized. The lowest temperatures in the morning varied between 17.8°C and 18.1°C. This is close to the lower end of the transition area of the PCM (see Figure 4). At the walls the temperatures measured with and without PCM are almost similar. In the ceiling, however, the temperatures measured with PCM are 0.2-0.3°C higher than without PCM. It is also interesting to observe that the cooling impact of the PCM seems to start around 8:30 in the morning, at a surface temperature of about 19°C. This corresponds well with the start of the transition period (see Figure 4).

Numerical results

The effect of the PCM layer thickness

Figure 9 shows compared results of the simulation run for a reference case without PCM and with three different spackling PCM layers applied on the ceiling and wall surfaces. The simulation is run for summer climate conditions in Oslo. The mean air temperatures of the cubicle increases from 08:00 until 18:00 following activation of internal heat gains. At about 09:00, the PCM starts to melt when the air temperature is 20°C, initiating a drop in the mean air temperature compared to the reference case. It is important to note that the maximum drop in mean air temperature happened at different hours for different PCM layer thicknesses. For the 4 mm thickness, the maximum temperature drop happened at 18:00, while for 2 mm PCM layer it happened at 14:00.

It has also been observed that the number of hours for the mean air temperature above 26°C is zero for 3 mm and 4 mm layer PCM, while it was 4 hours for the reference case. This indicates that the PCM enhanced spackling has demonstrated the capability to sink peak indoor temperature.

In the non-business hours, it was also observed that the mean air temperature drop is more sluggish for the cases with PCM than for the reference case without PCM. This indicates that the PCM releases the absorbed latent heat to the surrounding by radiation and convection heat transfer.

This also indicates that the spackling layer thickness play an important role for the dampening effect of the temperature fluctuation, reduction of the cooling energy load of buildings and thermal comfort of occupants.
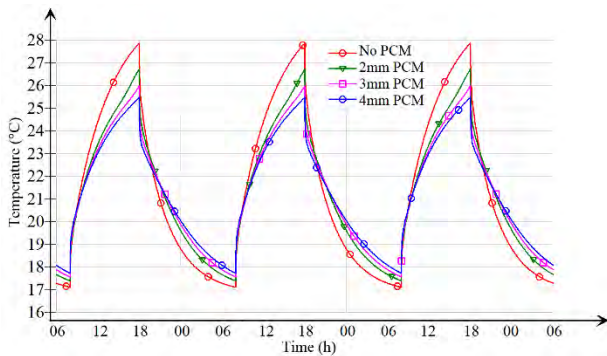
Figure 9: Air temperature variation with PCM layer thickness.
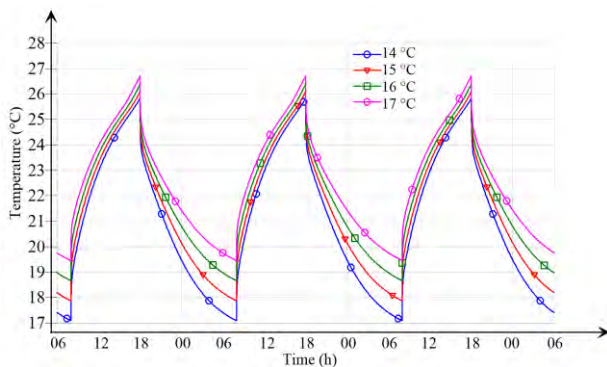
Figure 10: Air temperature variation with supply air set point.

The effect of the supply air temperature set point

The second scenario was to investigate the effect of the ventilation supply air temperature set point during the non-business hours. In this study, the air flow rate during the night was maintained at 230 m³/h, while the supply temperature varied from 14°C to 17°C. It should be noted that 14 °C as a supply temperature is somewhat lower than what could be expected when applying night ventilation on a hot summer day.The result in Figure 10 depicts that having a lower supply air temperature assists the PCM to perform better. PCM loses heat and solidifies between 00:00 and 08:00.

During the daytime, 08:00-18:00, the PCM spackling absorb the heat available inside the cubicle, store it as latent heat and release it later in night to be ready to absorb heat on the next day. By doing so, the PCM can help to keep the room at a comfortable temperature.

The effect of the air flow rate during the night

In this scenario, the effect of the air flow rate of 135 m³/h, 180 m³/h, 225 m³/h and 270 m³/h were investigated for the non-businesses hour ventilation. As expected, Figure 11 shows that an increase in the airflow rate has assisted the PCM to reduce the air temperature during the day. This is, actually, due to an increase in the convective heat transfer coefficient between the exposed surfaces and the circulating air. The non-business hours or night time ventilation is important to remove the heat from the PCM, in order to make the PCM active for the next day operation.

It is evident that the parametric study showed that the PCM enhanced spackling has an effect on cooling energy saving during summer season. Therefore, for the PCM to have a better performance, it is vital to optimize its design parameters. For instance, an increase in the PCM layer thickness, does not necessarily reduce the air temperature accordingly. The amount of PCM applied on the walls and ceiling should be designed properly so that all the PCM can melt during the business hours and solidify during the night.
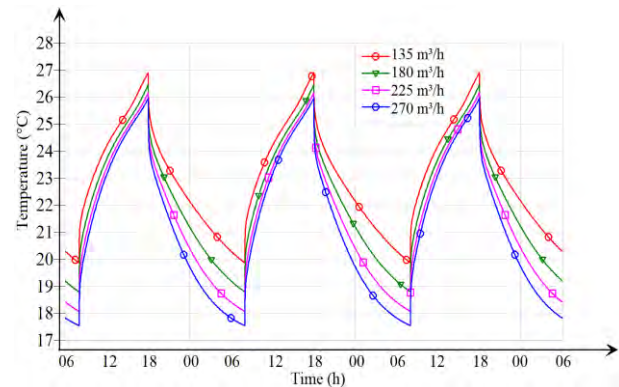
Figure 11: Air temperature variation with air flow rate.

Conclusion

In this study, experimental and numerical simulations were adopted to study the cooling potential of a PCM enhanced spackling manufactured by Scanspac. The spackling was applied on internal ceiling and wall surfaces of an office cubicle (14 m² floor area) exposed to Oslo summer climate. Initially, the PCM performance was tested in a full scale test room, then the measurement data were used for validating a simulation model in IDA ICE. Finally, a parametric study was conducted by varying the PCM's thickness as well as the nighttime ventilation airflow rate and supply air temperature. The following is a brief account of the findings:

- The results of the experiments showed that the PCM enhanced spackling has a significant potential for cooling.
- The experiment also showed that the cooling impact starts when the temperature of the spackling surface reaches 19°C.
- The simulation model works well and can be used to study performance of PCMs.
- The parametric study revealed that the PCM layer thickness, as well as the nighttime ventilation airflow rate and supply air temperature, play important roles for the positive impact of the PCM. This indicates that further research with multi-objective optimization is important.

Acknowledgement

mention for his skilful work on building the walls and ceiling, and spackling and painting the surfaces. The authors would also like to thank Mr. Øystein Anderson (Senior Engineer) and Mr. Ernst Erik Hempel (Staff Engineer) of OsloMet for their support during the experimental work.

References

Athienitis, A., C. Liu, D. Hawes, D. Banu, and D. Feldman (1997). Investigation of the thermal performance of a passive solar test-room with wall latent heat storage. *Building and environment 32* (5), 405-410.

Borreguero, A. M., M. Carmona, M. L. Sanchez, J. L. Valverde, and J. F. Rodriguez (2010). Improvement of the thermal behaviour of gypsum blocks by the incorporation of microcapsules containing pcms obtained by suspension polymerization with an optimal core/coating mass ratio. *Applied Thermal Engineering 30* (10), 1164-1169.

Casini, M. (2016). *Smart buildings: Advanced materials and nanotechnology to improve energy efficiency and environmental performance*. Wood-head Publishing.

IDA Indoor Climate and Energy, Version 4.9 (2020). Available from https://www.equa.se/en/ida-ice (accessed 05.04.2020)

Feldman, D., D. Banu, D. Hawes, and E. Ghanbari (1991). Obtaining an energy storing building material by direct incorporation of an organic phase change material in gypsum wallboard. *Solar energy materials 22* (2-3), 231-242.

Foster, V. R. and A. P. Bonifas (2010, September 7). Spackling composition containing polyaramid fibers and ceramic microparticles, and methods of repair and attachment. US Patent 7,790,796.

Gozum, J. E. and H. A. LaFleur III (2016, April 19). Self priming spackling compound. US Patent 9,315,643.

Kalnæs, S. E. and B. P. Jelle (2015). Phase change materials and products for building applications: A state-of-the-art review and future research opportunities. *Energy and Buildings 94*, 150-176.

Kurp, R. D. (2003, March 11). Ready to use spackle/-repair product containing dryness indicator. US Patent 6,531,528.

Madessa, H. B. (2014). A review of the performance of buildings integrated with phase change material: Opportunities for application in cold climate.

Neeper, D. (2000). Thermal dynamics of wallboard with latent heat storage. *Solar energy 68* (5), 393-403.

Saint-Gobain, Sweden AB (2020) https://www.gyproc.se/

Standard Norge (2001). Ergonomics of the thermal environment - Instruments for measuring physical quantities. NS-EN ISO 7726:2001.

Vik, T. A., H. B. Madessa, P. Aslaksrud, E. Folkedal, and O. S. Øvrevik (2017). Thermal performance of an office cubicle integrated with a bio-based PCM: experimental analyses.

Zhang, H., Q. Xu, Z. Zhao, J. Zhang, Y. Sun, L. Sun, F. Xu, and Y. Sawada (2012). Preparation and thermal performance of gypsum boards incorporated with microencapsulated phase change materials for thermal regulation. *Solar Energy Materials and Solar Cells 102*, 93-102.

Visualizing user perception of daylighting: a comparison between VR and reality

Muhammad Hegazy[1*], Ken Ichiriyama[1], Kensuke Yasufuku[2], Hirokazu Abe[2]

[1]Graduate School of Engineering, Osaka University, Suita, Japan

[2]Cybermedia Center, Osaka University, Suita, Japan

* Corresponding author: hegazy_muhammad@arch.eng.osaka-u.ac.jp

Abstract

This study introduces a novel method to investigate human perception of daylight in an interactive and immersive way, using game-engine and virtual reality (VR). The proposed method produces highly realistic renderings in real time of which users can explore freely and report daylight brightness perception using rated snapshots. Perceptions on daylighting in the virtual environment were found consistent with that in the physical one. The proposed approach can overcome some of the challenges facing current light simulation tools, regarding rendering speed and interactivity. It also encourages more validation studies to light simulation in game-engines.

Introduction

Evaluation of the qualitative attributes of daylight is challenging in different aspects, whether the assessed is a real or a virtual environment. The dynamic and variable essence of daylight, on the one hand, borders an obstacle to a completely manageable test environment (Gherri, 2014; Rockcastle & Andersen, 2013). In addition, as daylight efficiency is related to key design features (e.g., building orientation, opening sizes and walls), improving daylight after construction is typically an asset-intensive solution(Ma et al., 2012). On the other hand, simulating daylight correctly in a virtual environment (VE) needs consideration of various parameters to generate persuasive conditions for users to deliver relevant feedback (Bhavani & Khan, 2011).

In virtual reality, immersion and interaction principles are described as two key aspects of a credible user experience of the simulated space (Alshaer et al., 2017; Bishop & Rohrmann, 2003; Slater et al., 1996). Through applying these two aspects more rigorously, interactive virtual environments (IVEs) can offer an alternative to real environments in light-perception research (Kynthia Chamilothori et al., 2018). Various studies have employed IVEs to investigate subjective aspects of daylighting within a human-centric approach. For example, (Kynthia Chamilothori et al., 2016) investigated the impact of the perceived spatial ambiance of daylight patterns through the use of physically based renderings in VR. Using a similar method, (Rockcastle et al., 2017) assessed the visual perception of daylighting in virtual environments. While the previous studies provided basic immersion and interaction in their proposed frameworks, they have also shown limitations with respect to the environment customizability and interactive feedback.

The objectives of this study are twofold; firstly, to introduce a novel, real time approach for subjective evaluation of daylighting in virtual reality. Secondly, to investigate the perceptual validity of the introduced system through comparing perceptions in virtual and physical environments. The proposed approach offers a highly interactive daylight experience that allows users to explore in real time and collect their perception of brightness through 4-point ranked snapshots. Using the developed system at similar spatial and temporal contexts, this approach is validated by an experiment comparing input from subjects in a real daylit environment and its simulated mock-up. The proposed method has the potential to address some of the difficulties confronting traditional light simulation platforms with respect to speed and user engagement. It also accentuates further verification research on game-engines as light simulation tools. The novelty of this study lies in its employment of game engine as a light simulator rather than the benchmark tools (e.g. Radiance), to overcome some of the limitations in previous research regarding the immersiveness (by including head and body movement) and interactivity (using questionnaire-free evaluation system) in the virtual environment. Moreover, to the authors' knowledge, this is the first study to evaluate perceptual accuracy of light simulation in game engines through comparing perceptions in physical and virtual environments.

Background

Persky and McBride (Persky & McBride, 2009) define immersive virtual environments as a collection of hardware and software intended to immerse users in an artificially created virtual environment so that they can perceive their inclusion and interaction into the environment in real-time. Numerous studies have addressed virtual environments as a representative and evaluative tool for daylighting in built-environment, and as an architect-user communication tool. Chamilothori et al. (Kynthia Chamilothori et al., 2018) investigated the reliability of immersive virtual reality in measuring the perception of daylit spaces. The study examined five perceptual aspects: perceived pleasantness, interest, excitement, complexity, and satisfaction. Users' perception in respect with these aspects were collected in

a daylit room and compared to that in a virtual replica through a Head Mounted Display (HMD). The study showed consistency between perceptions in real or virtual environments. Similarly, Rockcastle et al. (Rockcastle et al., 2017) employed VR and HMD, along with head-tracking, to collect visual interest ratings of 8 different spaces under different sky conditions, and compared it to results predicted by an image-based algorithm. The study showed consistency between results of users' feedback and predictive algorithms.

In another study by Rockcastle and Andersen (Rockcastle & Andersen, 2015), they compared subjective ratings of (contrast, uniformity, complexity, variation, stimulation, and excitement) for nine virtual architectural spaces in different sky conditions to local and global contrast metrics. The study found that ratings of (excitement and stimulation) were consistent with quantitative contrast measurements more than that of (contrast) itself, of which those quantitative measurements were developed for, suggesting more investigation on user comprehension of the term 'contrast'. Furthermore, other studies integrated both subjective and physiological responses to daylighting in IVE; In a study by Chamilothori et al. (K. Chamilothori et al., 2019), the impact of sunlight pattern geometry on occupants was investigated through measuring skin conductivity and heart rate while in IVE, along with a verbal questionnaire. The experiment showed that spaces with irregular sunlight patterns were perceived as more exciting and more interesting on the subjective side and caused cardiac deceleration on the physiological side.

Other experiments expanded IVE's application in lighting study by creating digital tools for daylight modelling and visualization. For example, Heydarian et al. (Heydarian et al., 2017) analysed consumer lighting habits in IVE by configuring the settings of window shutters and artificial light intensity while executing a reading function. The study showed that the participants favoured full daylighting and in this situation performed better. Similarly, Carneiro et al. (Carneiro et al., 2019) proposed an IVE-based input system to direct the lighting needs of the occupants as to light intensity and energy usage. The system showed efficiency in guiding subjects to rethink their lighting preferences, especially those relating to energy. In a different application, (Kreutzberg, 2019) captured 360° panoramas from scale model interiors to enable a 1:1 experience of daylighting effects virtual reality. The introduced approach aimed to guide students through the conceptual design phase with scale models, by offering a more engaging experience to the space and its different lighting scenarios.

In lighting evaluation research, consistency of photometric values between simulation and reality (i.e. illuminance and luminance) is necessary (Merghani & Bahloul, 2016). In this regard, one of the main benchmark tools in daylight simulation is Radiance, which uses sky model data and backwards ray tracing to simulate light

behaviour accurately, offering an acceptable error range compared to reality (Ward, 1994). However, producing high quality renders in Radiance and similar applications is often a time consuming process, which limits the ability of users to explore wide range of scenarios in short time (Jones, 2019). As a result, various ongoing studies have explored methods to speed up the rendering process in Radiance (Jones & Reinhart, 2017a, 2019, 2017b). In this regard, game engines are known for their ability to render lighting in real-time through several techniques, one of which is light mass, which "bake" direct and indirect light effects on the model surfaces and thus enable to move inside the environment without the need to re-render each scene (Sheng et al., 2013). Recently, the introduction of real-time ray tracing in game engines enabled even faster, physically-based results (Liu et al., 2019). However, one of the significant barriers of adopting such tools in light evaluation research is the lack of validation studies regarding photometric accuracy. A few researchers have explored the suitability of various game engines for non-gaming applications, such as lighting simulation (Christopoulou & Xinogalos, 2017; Petridis et al., 2012, 2010). Moreover, Natephra et al. (Natephra et al., 2017) have used Unreal Engine to develop an immersive VR light modelling framework to provide realistic simulation of daylight as well as artificial illumination. The system offered a range of interactive tools including shifting and revolving fixtures and adjusting lighting levels.

In this study, Unreal Engine 4 (UE4) was used to create the immersive framework to simulate daylight. UE4 was preferred over other engines because of different factors; firstly, UE4 uses a range of physically dependent lighting units (Epic Games, 2018a). Secondly, Lighting algorithms in UE4 are based on real light physics, in which the actual relationship between light and surfaces is correctly represented as per the inverse square law (Walker, 2014) and Material attributes imitate the behavior in the physical world (Epic Games, 2018b; Karis, 2013). For daylight, UE4 is based on the Bruneton sky model (Bruneton, 2016), which can simulate the dynamics of daylight, including Rayleigh and Mie multiple light scattering (Bruneton & Neyret, 2008). Furthermore, the photometric accuracy of UE4 compared to field measurements and Radiance was verified in a study by Natephra et al. (Natephra et al., 2017). The error percentage of UE4 regarding illuminance estimation was found below 10% as recommended by Fisher (Fisher, 1992).

Methodology

This section describes the methodology of creating the virtual reality system, perceptual evaluation, and analysis of the subjects' feedback in reality and VR. Firstly, the selected indoor environment is modelled in detail and exported to the game engine software, where physically based materials are added to the surfaces, and the interaction controls in VR are setup. Daylighting

simulation is ran in the game engine using a physical sun object for direct sun light and a physical sky model for ambient daylighting. The spatiotemporal settings are set in accordance to experimental settings in the real environment. In both VR and the physical environments, subjects are given a tour to the accessible areas of the building, then verbally instructed to explore these areas freely and report daylight intensity in their scenes of choice on a 4-point nominal scale, using VR controllers or smart phone camera. To analyse daylight perception in both environments, snapshots reported by the subjects are recreated as camera objects in the 3D modelling software to replicate position, target scene and daylight rating. In each area, the number and rating distribution of snapshots in VR and reality are compared.

Test Environment

A multipurpose office hall was selected as the test environment in this investigation (**Error! Reference source not found.**). It features an open floor plan space daylit by a courtyard of 7.0m x7.0m dimensions. The investigated space hosts open areas, meeting rooms, canteen corner, and an open meeting hall (Figure 2). A 3D model of the test area was created in 3Ds Max software, based on the building's blueprints and field work scans. Furthermore, in Unreal Game-Engine 4 (UE4), the 3D model was imported to build physical materials, light rendering and Virtual reality interface functions.

Figure 1: Main area in the investigated environment

The developed IVE system aimed to enable more immersion and interaction of users while collecting daylight-related feedback. To offer 6 degrees of freedom in exploring the virtual environment, the head-mounted display was used to track the user's head movement (looking around), while two tracking stations were used to track body movements (physical movement). Furtherly, several interaction controls were programmed to dual motion controllers using the Blueprint scripting tool in UE4. Users could use the controller's buttons to move in all directions horizontally, jump, and take a snapshot of what they see. The later control was added as a self-expressive approach to enable users to report their

brightness perception of various scenes in VR without the need for questionnaires. Moreover, the IVE system was equipped with environment customization controls such as changing daytime in VR. Finally, a similar keyboard and mouse controls were added in case researchers needed to intervene.
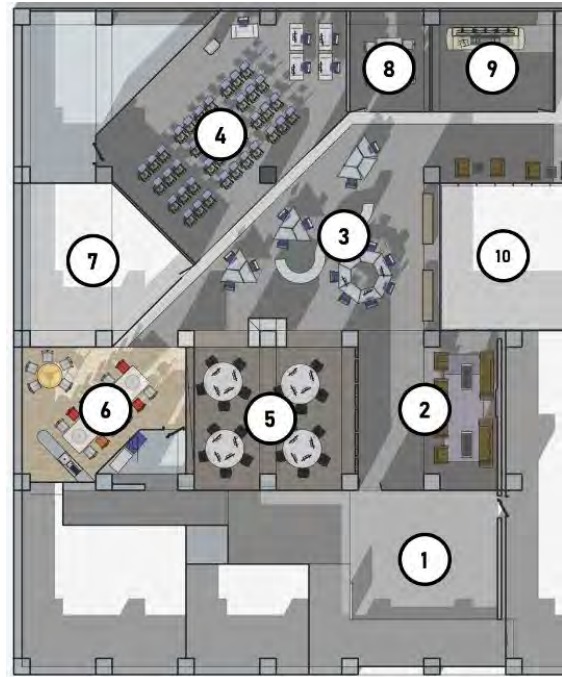
Figure 2: Accessible areas in the investigated space: 1) entrance lobby, 2) court corner, 3) open office, 4) open meeting hall, 5) computer room, 6) canteen, 7) lab room, 8) meeting room 1, 9) meeting room 2, 10) courtyard.

Experiment procedures

Thirty six subjects were enrolled (20 males, 16 females) to provide their opinions on daylighting in the test room. The number of subjects needed were identified as illustrated by several related studies (Abd-Alhamid et al., 2019; Cauwerts & Bodart, 2011; Cha et al., 2019; Kynthia Chamilothori et al., 2018; Franz et al., 2005; Heydarian et al., 2014). To alleviate the presentation-order bias that can arise while viewing physical and VR environments (Kynthia Chamilothori et al., 2018; Charness et al., 2012) subjects were randomly separated into two groups, each exposed to either actual or virtual environment. Furthermore, to estimate the effect size that can be acquired with this number of participants, we conducted a priori power analysis using G*Power software (Faul et al., 2007). At a statistical power of 0.8, our sample size was found adequate to detect large effects (Cohen, 1992), with an effect size (Cohen's d) of 0.97.

The experiment was carried out under a condition of overcast sky. The researchers instructed subjects about the purpose of the study and a description of the necessary tasks. To start the experiment, subjects were advised to wander freely around various locations within the test area, and to use their smartphones to snapshot places that

they consider as bright or dark on a 4-point scale. The verbal order used was as follows: "please explore different areas freely with daylighting in mind, snapshot the areas/scenes of which you perceive brightness as one of the following: very dark, dark, bright, or very bright". At each snapshot, subjects were asked to explain what they meant to look at, as well as their snapshot brightness rating. Experiment time was limited to 20 minutes, during which researchers didn't interact with subjects (Figure 3 upper). Afterwards, subjects were told to upload their snapshots to a specific web-based database, along with ranking for each shot.

In the virtual model, time and sky conditions were configured as to that during the experiment in the real environment. Subjects were provided with a computer-based overview on the intent and procedures of the study. They were then introduced to a motion controls demonstration to know what and how they should control inside the IVE. Eventually, an explanation was given about the tasks to be performed during the experiment. Prior to wearing the VR headset, subjects spent a total adaptation period of 10 minutes in the testing room.

After the subject got comfortable with the IVE system, the simulated model was loaded starting at the entrance lobby. The subjects were asked to assess their experience of brightness in freely chosen scenes utilizing the same verbal order as demonstrated in physical environments. Subjects were able to take as many screenshots as they liked and move between various areas of the virtual model (Figure 3 lower). Any time a subject took a snapshot, he / she was asked to verbally disclose what they intended to look at, as well as their perceived brightness of that snapshot the 4-point scale.
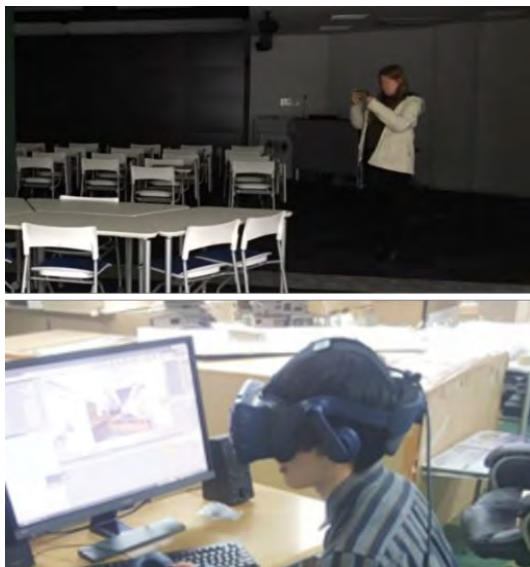
Figure 3 Subjects in real (upper) and virtual spaces (lower).

Results and analysis

During the tests in actual and simulated environments, subjects were expected to travel freely around various areas and record their experience of brightness by taking a screenshot of the scenes they interpret as one of the following: very dark, dark, bright or very bright (Figure 4). Table 1 illustrates subjects' feedback in actual and simulated environments and their respective ratings. With 345 and 330 snapshots respectively, subjects marginally submitted more scenes in real environment than in VR. Likewise, the average ratings of all shots in both reality and VR were fairly similar, with an average of 2.26 and 2.47 respectively, reflecting an average ranking varying from dark to bright in both environments. In real-environment snapshots, though, a consistent distribution of snapshot ratings could be observed compared to a significant difference in snapshot rankings in simulated environments, at an SD value of 3.40 and 15.26 respectively.

Table 1 Overview of reported snapshot rankings in real and virtual environments

Responses	Reality	VR
Total snapshots	345	330
"very dark" shots	89	65
"dark" shots	89	87
"bright" shots	85	101
"very bright" shots	82	77
Mean value of all shots (1=very dark, 4= very bright)	2.26	2.47
SD value	3.40	15.26

Figure 5 shows a description of the region and related classification of the recorded snapshots. Observational assessment shows a general consistency in the total snapshots recorded in both reality and VR in separate locations, with the exception of the canteen area, where a higher rate of snapshots was captured in reality than in VR (29, 17 snapshots respectively). In both, subjects largely recorded in the open office area, while the least recorded was in the lab room.

Distributed by brightness ratings, the snapshotted "very bright" scenes were shown mostly in the open office area, suggesting a shared perception of it among subjects as the brightest in both real and VR environments. Though, significantly more snapshots were submitted in the open area in reality than in VR (54, 38 snapshots respectively). In addition, a steady outcome in both environments could be shown in case of "bright" scenes, where the open office area had the most reported bright shots in both cases (40, 49 snapshots in reality and VR respectively).
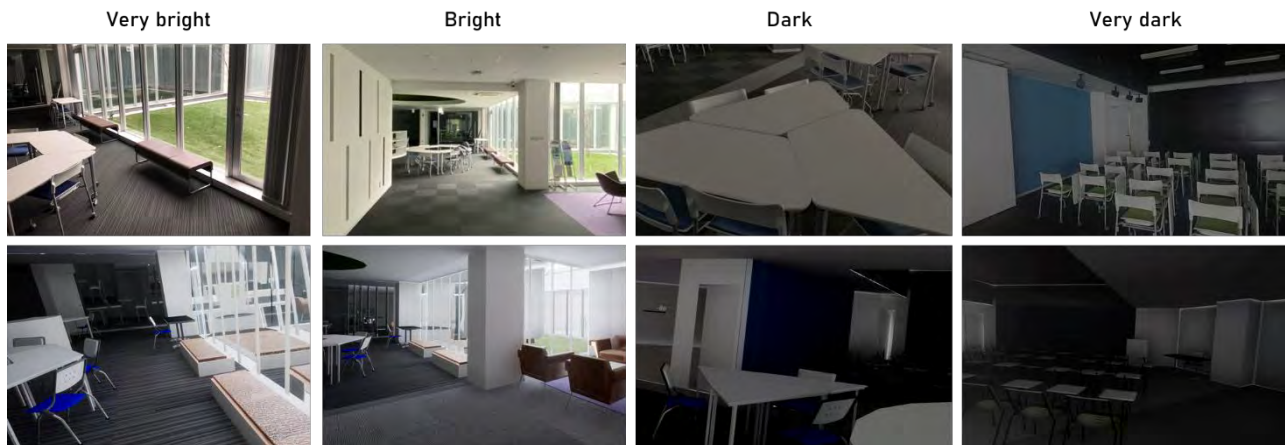
Figure 4: Subjects' snapshots in reality (upper row) and VR (lower row) showing different brightness ratings.
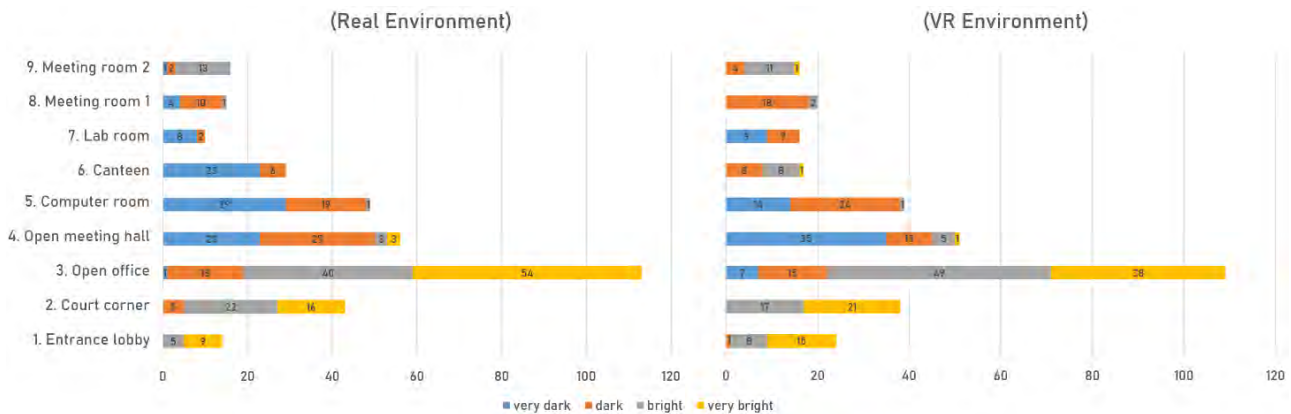
Figure 5: Snapshot distribution by area and ranking in real (left) and virtual environments (right).

In case of "dark" snapshots, similarly, the open meeting hall (27 shots) and computer room (24 shots) produced the highest number of snapshots in reality and VR respectively. In case of "very dark" scenes, subjects reported the most at the open meeting hall (23 shots) and the computer room (35 shots) in VR and reality respectively.

Discussion

The VR system introduced in this article suggested a strategy for incorporating game engines into IVEs used in subjective light evaluations. Within this regard, a game engine was used as a rendering element to simulate daylight and create an interactive method of feedback. Although the introduced method requires additional research about its potentialities and limitations, it enables a broad variety of applications to address existing drawbacks of current IVE strategies. This potential is demonstrated through the enhancement the proposed system brought in the interactivity and simulation speed in the virtual environment. Furthermore, the interactive method of ranked snapshots has provided a more personalized output and consequently a higher variety of responses from a small number of subjects. It also gave empirical insights on subjects' contextual settings when they provided their perceptual feedback (e.g. standing

point and target scene). Comparative analysis between the subjective responses in reality and VR reveals a sensible agreement between the numbers of reported scenes in the two environments. This consistent allocation was also noticeable among the majority of the investigated areas, where subjects in VR perceived brightness in a similar way to those in the physical environment.

While the representation accuracy of the developed IVE was validated by comparing brightness perception in VR and physical environment, including quantitative human comfort indicators (e.g. glare, and productivity) could shed more light on the limitations of the proposed system. Moreover, in this study, daylight intensity was subjectively identified through the subjects' perceptions. In a further ongoing study, a quantification methodology will be developed in order to validate the photometric accuracy of the game engine renderings in terms of physical lighting measurements, mainly illuminance (in lux) and luminance (in Cd/m^2).

Conclusions

In this study, a game engine was employed as light simulation tool in an immersive real-time daylighting environment using a self-expressive assessment approach. The developed system provided a real time simulation of daylighting as well as facilitated an

interactive method to report light perception within the virtual environment. To investigate the adequacy of the proposed method, thirty-six subjects distributed across two groups explored a daylit physical environment and its virtual replica in the developed system. In the two environments, subjects snapshotted and rated brightness of various areas within the test environment on a 4-point scale (very dark, dark, bright, and very bright). Subjects reported a fairly similar number of scenes in the two environments, where the most reported bright scenes were found around the courtyard and entrance lobby, and the most reported dark scenes inside semi-closed areas with a high volume of furniture. In both physical environment and VR, there were no significant discrepancies were found between subjects' brightness perceptions. The findings of this study illustrate the potentials of game engines as tools to simulate daylight accurately and improve user interactivity with VR systems in light perception studies. It also encourages further research to validate the photometric and luminous accuracy of such engines against the well-established physically based rendering tools.

References

Abd-Alhamid, F., Kent, M., Bennett, C., Calautit, J., & Wu, Y. (2019). Developing an Innovative Method for Visual Perception Evaluation in a Physical-Based Virtual Environment. *Building and Environment*, *162*, 106278. https://doi.org/10.1016/j.buildenv.2019.106278

Alshaer, A., Regenbrecht, H., & O'Hare, D. (2017). Immersion factors affecting perception and behaviour in a virtual reality power wheelchair simulator. *Applied Ergonomics*, *58*, 1–12.

Bhavani, R. G., & Khan, M. A. (2011). Advanced lighting simulation tools for daylighting purpose: Powerful features and related issues. *Trends in Applied Sciences Research*, *6*(4), 345–363.

Bishop, I. D., & Rohrmann, B. (2003). Subjective responses to simulated and real environments: A comparison. *Landscape and Urban Planning*, *65*(4), 261–277. https://doi.org/10.1016/S0169-2046(03)00070-7

Bruneton, E. (2016). A qualitative and quantitative evaluation of 8 clear sky models. *IEEE Transactions on Visualization and Computer Graphics*, *23*(12), 2641–2655.

Bruneton, E., & Neyret, F. (2008). Precomputed atmospheric scattering. *Computer Graphics Forum*, *27*, 1079–1086.

Carneiro, J. P., Aryal, A., & Becerik-Gerber, B. (2019). Influencing occupant's choices by using spatiotemporal information visualization in Immersive Virtual Environments. *Building and Environment*, *150*, 330–338. https://doi.org/10.1016/j.buildenv.2019.01.024

Cauwerts, C., & Bodart, M. (2011). Investigation of 3D projection for qualitative evaluation of daylit spaces.

Proceedings of PLEA 2011 "Architecture and Sustainable Development".

Cha, S. H., Koo, C., Kim, T. W., & Hong, T. (2019). Spatial perception of ceiling height and type variation in immersive virtual environments. *Building and Environment*, *163*, 106285. https://doi.org/10.1016/j.buildenv.2019.106285

Chamilothori, K., Chinazzo, G., Rodrigues, J., Dan-Glauser, E. S., Wienold, J., & Andersen, M. (2019). Subjective and physiological responses to façade and sunlight pattern geometry in virtual reality. *Building and Environment*, *150*, 144–155. https://doi.org/10.1016/j.buildenv.2019.01.009

Chamilothori, Kynthia, Wienold, J., & Andersen, M. (2016). Daylight patterns as a means to influence the spatial ambience: A preliminary study. *Proceedings of the 3rd International Congress on Ambiances*.

Chamilothori, Kynthia, Wienold, J., & Andersen, M. (2018). Adequacy of Immersive Virtual Reality for the Perception of Daylit Spaces: Comparison of Real and Virtual Environments. *LEUKOS*, *0*(0), 1–24. https://doi.org/10.1080/15502724.2017.1404918

Charness, G., Gneezy, U., & Kuhn, M. A. (2012). Experimental methods: Between-subject and within-subject design. *Journal of Economic Behavior & Organization*, *81*(1), 1–8. https://doi.org/10.1016/j.jebo.2011.08.009

Christopoulou, E., & Xinogalos, S. (2017). Overview and Comparative Analysis of Game Engines for Desktop and Mobile Devices. *International Journal of Serious Games*, *4*(4), Article 4. https://doi.org/10.17083/ijsg.v4i4.194

Cohen, J. (1992). Statistical Power Analysis: *Current Directions in Psychological Science*, *1*(3). https://journals.sagepub.com/doi/10.1111/1467-8721.ep10768783

Epic Games. (2018a). *Physical Lighting Units*. https://docs.unrealengine.com/en-US/Engine/Rendering/LightingAndShadows/PhysicalLightUnits/index.html

Epic Games. (2018b). *Physically Based Materials*. https://docs.unrealengine.com/en-US/Engine/Rendering/Materials/PhysicallyBased/index.html

Faul, F., Erdfelder, E., Lang, A.-G., & Buchner, A. (2007). G*Power 3: A flexible statistical power analysis program for the social, behavioral, and biomedical sciences. *Behavior Research Methods*, *39*(2), 175–191. https://doi.org/10.3758/BF03193146

Fisher, A. (1992). Tolerances in lighting design. *Proceedings of the CIE Seminar on Computer Programs for Light and Lighting*.

Franz, G., von der Heyde, M., & Bülthoff, H. H. (2005). An empirical approach to the experience of architectural space in virtual reality—Exploring relations between features and affective appraisals of rectangular indoor

spaces. *Automation in Construction*, *14*(2), 165–172. https://doi.org/10.1016/j.autcon.2004.07.009

Gherri, B. (2014). An Extensive Daylight Assessment Through Quantitative Appraisal and Qualitative Analysis. *Proceedings Experiencing Light 2014: International Conference on the Effects of Light on Wellbeing, Eindhoven, The Netherlands,* 62.

Heydarian, A., Carneiro, J., Gerber, D., & Becerik-Gerber, B. (2014, July 8). *Towards Measuring the Impact of Personal Control on Energy Use through the Use of Immersive Virtual Environments*. 31st International Symposium on Automation and Robotics in Construction, Sydney, Australia. https://doi.org/10.22260/ISARC2014/0073

Heydarian, A., Pantazis, E., Wang, A., Gerber, D., & Becerik-Gerber, B. (2017). Towards user centered building design: Identifying end-user lighting preferences via immersive virtual environments. *Automation in Construction*, *81*, 56–66. https://doi.org/10.1016/j.autcon.2017.05.003

Jones, N. L. (2019). Fast Climate-Based Glare Analysis and Spatial Mapping. *Proceedings of Building Simulation 2019: 16th Conference of IBPSA*.

Jones, N. L., & Reinhart, C. F. (2017a). Experimental validation of ray tracing as a means of image-based visual discomfort prediction. *Building and Environment*, *113*, 131–150. https://doi.org/10.1016/j.buildenv.2016.08.023

Jones, N. L., & Reinhart, C. F. (2019). Effects of real-time simulation feedback on design for visual comfort. *Journal of Building Performance Simulation*, *12*(3), 343–361. https://doi.org/10.1080/19401493.2018.1449889

Jones, N. L., & Reinhart, C. F. (2017b). Speedup potential of climate-based daylight modelling on GPUs. *Building Simulation Conference*, 1438–1447.

Karis, B. (2013). Real Shading in Unreal Engine 4. *Proceedings of SIGGRAPH*.

Kreutzberg, A. (2019). Establishing daylight studies inside architectural scale models with 360° panoramas viewed in VR. *Ecaade Ris 2019. Virtually Real. Immersing Into the Unbuilt*, 81–88.

Liu, E., Llamas, I., Cañada, J., & Kelly, P. (2019). Cinematic Rendering in UE4 with Real-Time Ray Tracing and Denoising. In E. Haines & T. Akenine-Möller (Eds.), *Ray Tracing Gems: High-Quality and Real-Time Rendering with DXR and Other APIs* (pp. 289–319). Apress. https://doi.org/10.1007/978-1-4842-4427-2_19

Ma, Z., Cooper, P., Daly, D., & Ledo, L. (2012). Existing building retrofits: Methodology and state-of-the-art. *Energy and Buildings*, *55*, 889–902. https://doi.org/10.1016/j.enbuild.2012.08.018

Merghani, A. H., & Bahloul, S. A. (2016). Comparison between Radiance Daylight Simulation Software Results andMeasured on-Site Data. *Journal of Building and Road Research*, *20*(0), Article 0.

http://onlinejournals.uofk.edu/index.php/JBRR/article/view/2395

Natephra, W., Motamedi, A., Fukuda, T., & Yabuki, N. (2017). Integrating building information modeling and virtual reality development engines for building indoor lighting design. *Visualization in Engineering*, *5*(1), 19. https://doi.org/10.1186/s40327-017-0058-x

Persky, S., & McBride, C. M. (2009). Immersive Virtual Environment Technology: A Promising Tool for Future Social and Behavioral Genomics Research and Practice. *Health Communication*, *24*(8), 677–682. https://doi.org/10.1080/10410230903263982

Petridis, P., Dunwell, I., De Freitas, S., & Panzoli, D. (2010). An engine selection methodology for high fidelity serious games. *Proceeding of Second International Conference on Games and Virtual Worlds for Serious Applications*, 27–34.

Petridis, P., Dunwell, I., Panzoli, D., Arnab, S., Protopsaltis, A., Hendrix, M., & de Freitas, S. (2012). Game engines selection framework for high-fidelity serious applications. *International Journal of Interactive Worlds*, Article ID 418638.

Rockcastle, S., & Andersen, M. (2013, September 17). Celebrating Contrast and Daylight Variability in Contemporary Architectural Design: A Typological Approach. *Proceedings of LUX EUROPA*.

Rockcastle, S., & Andersen, M. (2015). Human Perceptions of Daylight Composition in Architecture: A Preliminary Study to Compare Quantitative Contrast Measures with Subjective User Assessments in HDR Renderings. *Proceedings of 14th Conference of International Building Performance Simulation Association*.

Rockcastle, S., Chamilothori, K., & Andersen, M. (2017). An Experiment in Virtual Reality to Measure Daylight-Driven Interest in Rendered Architectural Scenes. *Proceedings of Building Simulation*.

Sheng, W., Nakata, S., Tanaka, S., Tanaka, H. H., & Tsukamoto, A. (2013). Modeling High-Quality and Game-Like Virtual Space of a Court Noble House by Using 3D Game Engine. *2013 International Conference on Culture and Computing*, 212–213.

Slater, M., Linakis, V., Usoh, M., & Kooper, R. (1996). Immersion, presence and performance in virtual environments: An experiment with tri-dimensional chess. *Proceedings of the ACM Symposium on Virtual Reality Software and Technology*, 163–172.

Walker, J. (2014). *Physically Based Shading In UE4*. https://www.unrealengine.com/en-US/blog/physically-based-shading-in-ue4?sessionInvalidated=true

Ward, G. J. (1994). The RADIANCE lighting simulation and rendering system. *Proceedings of the 21st Annual Conference on Computer Graphics and Interactive Techniques - SIGGRAPH '94*, 459–472. https://doi.org/10.1145/192161.192286

The Potential of the Multi-Angled Facade System in Improving Natural Ventilation

Loay Hannoudi[1*], Noha Saleeb[2]
[1]Middlesex University, London, United Kingdom
[2]Middlesex University, London, United Kingdom
*corresponding author: Loayahann@gmail.com

Abstract

This paper is part of a research study focusing on highlighting the potential of using Multi-Angled Facade systems in improving natural ventilation inside an office room. The multi-angled façade is a three-dimensional façade with two different window orientations. The design of the intake and outtake depends on formulae from SBi Directive 202. The calculations of the consumed energy and the evaluation of indoor climate are made using the software packages IDA ICE and Autodesk CFD. The results show that the two oriented facade parts will help to improve air penetration, with heat removal upto 31% higher than for a flat façade, thus leading to a better indoor climate in the office room.

Introduction

The research study focuses on the potentials of the Multi-Angled facade in improving natural ventilation inside the office room and providing an acceptable indoor climate.

The design concept of the Multi-Angled facade is a three-dimensional façade that extends outwards from, and is connected at its sides to, the original building flat façade. The design concept targets the use of two different orientations of windows in each façade (see Figure 1) to optimize the use of solar radiation and daylight through the façades, depending on the appropriate window properties and the solar shading control system (Hannoudi et al., 2016b) A considerable advantage would be that, while having the solar shading shut on one part of the room façade due to direct solar radiation, another part of the façade may have no shading, thus continuing to provide daylight and views to the outside on sunny days.

Global climate change is posing increasingly severe threats to ecosystems, human health, and the economy. Climate change is caused by the release of large amounts of greenhouse gases into the atmosphere as a result of human activities worldwide, especially the burning of fossil fuels for electricity generation, heating, and transport (The European Environment Agency (EEA), 2020). Buildings account for approximately 40% of energy consumption and 36% of CO2 emissions in the EU. Buildings are therefore the single largest energy consumer in Europe (European Commission, 2020).

The aim of this research is therefore to minimize these negative environmental impacts, by integrating a natural ventilation system into the design of buildings. Many office and commercial buildings worldwide have implemented this strategy such as Red Kite House and Bloomberg European HQ in Great Britain and Industriens Hus in Denmark. The previously mentioned building has used a double-skin facade with natural ventilation, while this research presents the potential of the Multi-angled facade System as a new facade concept that is not used or researched before to improve natural ventilation inside the building.
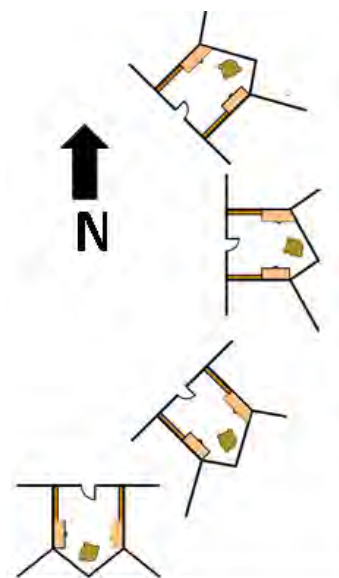
Figure 1 Different orientations for an office room that show the use of two different orientations of windows in each room façade, where the large part is oriented more to the North and the small part is more to the South (Hannoudi et al., 2017b)

Background

All buildings need a ventilation system (mechanical, hybrid, or natural) to achieve an acceptable indoor climate and good air quality. In winter, the ventilation system maintains good air quality and removes CO_2 when it exceeds the acceptable limit, whereas in summer it maintains an acceptable thermal indoor climate.

The air that penetrates through room openings depends on two main factors: the thermal driving force and wind pressure. The thermal driving force depends on thermal buoyancy and the temperature difference between the inside and outside of the building. Usually, the difference

between indoor and outdoor temperatures during the summer season in Denmark, as an example case study used in this research is between 3 °C and 4 °C (State Building Research Institute, 2000).

Natural ventilation depends also on the wind pressure. For example, in Denmark the annual mean wind speed is approx. 4 m /s inland and approx. 5.5 m /s to the coast. Generally, the prevailing wind direction is from the west–southwest; on warm summer days and from the east–southeast. On some winter days, the wind direction is from the north (Technical University of Denmark, 2009).

Using the information above regarding wind speed and temperature difference between inside and outside will help carrying out calculations for the natural ventilation design. There are several natural ventilation principles that can be implemented in the design of an office building, such as one-side ventilation, cross ventilation, and thermal buoyancy ventilation. Many office rooms in Europe, specifically Denmark, are single rooms with a door that opens to the corridor. Thus, one-side ventilation can be adopted when designing natural ventilation inside a room. This research will concentrate on natural ventilation in offices by implementing the first principle, i.e. one-side ventilation. Since the office room is a part of a building, there are some periods when the door is opened, which might create a kind of cross ventilation. But the assumed scenario in this research is while the door of the room is closed, which most often happens.

A healthy and accepted indoor climate can be ensured in the office rooms by implementing an automatic control of the opening of façade windows. The size of the window openings and the frequency of opening are based on the pre-defined values of the operating parameters for temperature, CO_2 level and humidity, both for the indoor and the outdoor climate. These values are pre-defined in a control system made by the producing company

Methods

This study starts with a literature review on the potential of natural ventilation in buildings, including the principles, design methods, and control systems of natural ventilation. The review was combined with communications with some experts in this field, such as consultants from Window Master International A/S, as the best company in Denmark for the design of natural ventilation and one of the providers of natural ventilation solutions in northern Europe.

The method for investigating the potential of the multi-angled facade system in improving natural ventilation consists of three main steps:

1. The intake and outtake areas are designed depending on formulae from the (SBi) directive 202 (State Building Research Institute, 2002).
2. The results of number of overheating hours, relative humidity (RH), CO2 evaluations, and energy consumption are calculated by the software IDA ICE (IDA Indoor Climate and Energy, 2019).

3. The simulations of airflow through the office room facade (both the flat and Multi-angled façade) and inside it, along with the room temperature and air velocity are conducted by the Autodesk software CFD 2019

Input data for the calculations and simulations

Calculations for the window opening area

The window opening areas that allow sufficient natural ventilation were calculated for different outdoor climate parameters, as listed in Table 1 and in Table 2 that completes Table 1. This is in accordance with the procedure in SBi directive 202, which is based on differences in solar radiation, external and internal operative temperature in different periods of the year to calculate the necessary opening area for natural ventilation. The typical values for outdoor temp. and solar radiations in the Danish climate are represented by middle values (average values) and critical values are represented by maximum values. The values are either hourly-based values or whole day values. (State Building Research Institute, 2002). The input data for the main parameters for the calculations are presented in the next section.

Table 1 The parameters used for the calculations of window opening areas based on the temperature and solar radiations intensity.

The Season	The month	The period	Temperature °C	Solar radiation
Winter	January	middle day	middle	middle
Summer	July & August	middle day	middle	middle
		maximum day	middle	middle
		maximum hour	maximum temperature	maximum hour value
Autumn & Spring	April October	middle day	middle	middle
		maximum day	middle	middle

Table 2 The parameters used for the calculations of window opening areas, which are based, in addition to the above parameters, on wind velocity, and wind direction. 1.for day with t_{max}>20 °C. 2. for day with t_{max} >25 °C. 3. for hours with t>25 °C. 4. For the whole year

The Season	The month	Wind velocity	Wind direction
Winter	January	no wind	
Summer	July & August	25%-quantile[1]	south east
		25%-quantile[2]	south east
		25%-quantile[3]	south east
Autumn & Spring	April October	25%-quantile[4]	south west
		25%-quantile[4]	south west

The calculations were divided into six scenarios for an office room with a flat façade. The calculations for the scenario with the most critical climate data were made for an office room with a flat facade in addition to a room with a Multi-Angled façade where the demand for natural ventilation is highest in both facade types and the calculated opening area is the largest compared to the other scenarios. The six scenarios represented the best possibilities in defining the necessary climate data for the different seasons of the year. In the winter situation, the wind speed is low when the outdoor temperature is below 0°C. Therefore, calculations were based on thermal buoyancy of the air inside the room. One scenario is made for this season due to the lower demand for natural ventilation compared to the other seasons. In the summer situation, calculations were carried out for the middle and maximum temperature respectively in the summer months where the heat load is greatest (July and August). In the spring and Autumn situation, calculations were carried out for the middle and maximum temperature respectively in the April and October. The input data for the main parameters for the calculations are shown below.

Scenario 1: Ventilation based on heat removal

- July and August
- Time period (middle day)
- Middle temperature 16 °C
- middle solar radiation 2850 Wh/m² day
- Wind from south east 1 m/s

Scenario 2: Ventilation based on heat removal

- July and August
- Time period (Maximum day)
- Middle temperature 21°C
- middle solar radiation 4404 Wh/m² day
- Wind from south east 1,3 m/s

Scenario 3: Ventilation based on heat removal

- July and August
- Time period (Maximum hour)
- Maximum temperature 29 °C
- Solar radiation maximun hour 7236 Wh/m² day
- Wind from south east 4,6 m/s

Scenario 3-1 (Multi-angled facade): Ventilation based on heat removal

- July and August
- Time period (Maximum hour)
- Maximum temperature 29 °C
- Solar radiation maximun hour 7020 & 5130 Wh/m² day
- Wind from south east 4,6 m/s

Scenario 4: Ventilation based on CO_2 removal

- January
- Time perio(Middle day)
- Middle temperature -1°C
- Middle solar radiation 372 Wh/m² day
- No wind

Scenario 5: Ventilation based on CO_2 removal

- April or October

- Time period (middle day)
- Middle temperature 7,4 °C
- middle solar radiation 1674 Wh/m² day
- Wind from south west 1 m/s

Scenario 6: Ventilation based on CO_2 removal

- April or October
- Time period (Maximum day)
- Middle temperature 12,45 °C
- middle solar radiation 3270 Wh/m² day
- Wind from south west 1 m/s

The window opening areas for both facade types were calculated through the following steps:

1. Defining the placement of the intake and outtake points. The greater the distance between them the better, as this increases the stack effect, where the air moves into and out of the room resulting from air buoyancy. Buoyancy occurs due to a difference in air density resulting from temperature. There are multiple ways to achieve this. One solution is to have an opening close to the floor level, and another higher up at the ceiling level (Roth, 2020). This solution will be used in the calculations, and the distance between the centre of intake and outtake is 2.4 m (Figure 2). This is by assuming that the height of the openings (both intake and outtake) is 0.2 m and the intake is 0.3 m higher than the floor The only disadvantage of this solution is that the lower opening (intake) can be affected by snow, leaves, etc. Because of the near distance to the ground.
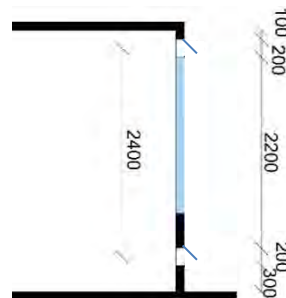
Figure 2 The placement and the distance between the intake and outtake in the room facade

2. The calculation of the required opening areas for heat removal by natural ventilation starts by calculating the required air change for heat removal from solar radiation and the internal heat gain inside the office room. This calculation also considers the specific heat loss transmission through the external facade envelope, and the specific ventilation heat loss. The next step is to calculate the pressure difference between the inside and outside, where thermal buoyancy and wind work. Finally, the required area of the opening is calculated according to the pressure difference in the opening and the necessary air change for heat removal.

3. The calculation of the required opening area for CO_2 removal by natural ventilation is divided into two types: with wind pressure on the façade and without wind pressure. For the first type of calculation, the first step is calculating the required air change for CO_2 removal inside the room. The next step is calculating the pressure difference between the inside and outside, which takes into consideration the internal pressure inside the room and the wind pressure. The internal pressure calculation depends on the wind pressure coefficient and the opening area in addition to the room volume and the air density. The pressure difference depends on the difference between the pressure caused by the wind and stack effect in the room on one hand and the internal pressure on the other hand. Finally, the required opening area is calculated according to the pressure difference in the opening and the necessary air change for CO_2 removal inside the room. For the second type of calculation, the first step is calculating the required air change for CO_2 removal inside the room which takes into consideration the CO_2 concentration outside and inside the room in addition to the emission of CO_2 per person. Then, the required area of the opening is calculated according to the pressure difference in the opening due to temperature difference, and the necessary air change for CO_2 removal inside the room.

Simulation in IDA ICE

The input data for the simulations in IDA ICE were based on Danish Building Regulations, Danish and European standards, site visits and interviews. The input data are:

- A model for a room with inner dimensions 5 x 4.5 x 3 m (L x W x H) . These dimensions were based on site-visits and a case study for a large number of office buildings in Copenhagen. The model of the room had adjacent rooms above, below and on each side. The model of the room is simulated with two types of external facades, a flat facade and a multi-angled façade, where the large part is oriented more to the North and the small part is more to the South.as per Figure 3. The optimized dimensions and the angles of this facade are the results of a number of simulations carried on this facade concept. The room external facade is directed toward the west, where the optimal usage of this facade concept is either towards the West or the East.

- The building is located in Copenhagen, Denmark: Latitude 55.633 N, Longitude 12.667 E.

- It is assumed that two occupants are working in the room (activity level 1.2 met (European Committee for Standardization, 2006). An average occupancy of 80% is expected for the two occupants with two computers (40 W/PC) .

- The electrical lighting is in use during the occupancy hours and is assumed to be energy efficient lighting
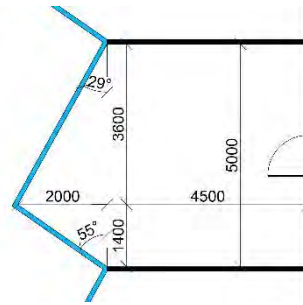
Figure 3 A plan for an office room with a multi-angled façade system

that provides 500 Lux for the working area of the office room (European Committee for Standardization, 2006) (which is assumed to be 2/3 of the room area). The electrical lighting has a total lighting power of 110 W with luminous efficacy of 80 lm/W. Energy-efficient fluorescent lighting is used as the source of electrical lighting.

- For the naturally ventilated office room, the opening's area is calculated according to the scenario for the period "Maximum hour," both for the flat façade and the Multi-Angled Façade. This scenario is with the most critical climate data that provides the data for window maximum openings area. The size of the opening's area is adjusted and optimized in the flat façade to improve the indoor climate in the office room. This optimized opening area is divided into two parts and used on the two sides of the Multi-Angled Façade. The window starts to open in the following two cases:
  1. The operative temperature doesn't fulfil the criteria in summer for building category (B) 24.5+-1.5 °C (European Committee for Standardization, 2006). Category (B) is used because it is a normal office building and
  2. CO_2 concentration doesn't fulfil the criteria for building category (B) 500 PPM above the outdoor level (European Committee for Standardization, 2006) so the concentration is between (min. 700 PPM. and max. 1100 PPM). relative humidity is kept between 30% and 70% (European Committee for Standardization, 2001)

- For the office room mechanically ventilated, the mechanical ventilation system is Variable Air Volume VAV during working hours (08:00–17:00). The control of the ventilation system depends on room temperature and CO_2 concentration. The heat exchanger efficiency is 80%. Fan efficiency (electricity to air) is 0.8. The ventilation system have a normal pressure drop of about 800 Pa. The SFP of the ventilation system is 1000 J/m³ (Hvlid, 2014).

- It is assumed that the heating system consists of water-based radiators. Heating set point is 21°C during working hours (07:00–17:00) (European Committee for Standardization, 2006) and 16°C outside working hours. It is assumed that the energy source for heating

the building and for the domestic hot water is district heating.

- The parapet under the window consists of a concrete panel (thickness is 0.1 m) and insulation from the outer side (thickness is 0.245 m) with facade covering materials of wood. U-value for the parapets is 0.125 W/m²K, which is accepted in the Building Regulation 2015.
- External shading devices are used with a shading factor of 0.2. For the office room with multi-angled facade, the shading system of the small window more towards the south depends on the operative temperature (closes at 24°C). The shading system of the large window more towards the north depends on solar radiation intensity (closes at 250 W/m² (solar radiation intensity measured externally)), which is recommended in Denmark.
- The air change through leaks in the building envelope does not exceed 1.00 l/s per m² heated floor area by pressure test with 50 Pa" according to BR15 (Building and housing agency, 2019).
- The window of the flat facade is a three-layer glass window (U_g is 0.53 W/m² K, LT_g 0.72, g_g 0.5, U_f 1.56 W/m²K) (Secretariat of the energy labeling scheme for vertical windows, 2020). This window is also used for the large part of the multi-angled facade, while the smaller part has the window (U_g is 0.62 W/m² K, LT_g 0.74, g_g 0.63, U_f 1.56 W/m²K) (Secretariat of the energy labeling scheme for vertical windows, 2020). The lower window frame is at a height of 0.9m from the floor and the upper window frame is at a height of 2.85m from the floor for the flat facade and 3m for the multi-angled facade. The window area below 0.9m doesn't provide daylight to the working area inside the room and it increases the heat loss at the same time.The ratio between the glass area to the window area is almost 0.82.

Simulation in Autodesk CFD

The input data for the simulations in Autodesk CFD are as follows:

- The input data for the model of the office rooms are the same as those used in the IDA ICE simulations (explained subsequently) in terms of the dimensions, internal heat gain, and material properties.
- The input data for the solar radiation on the room's external facade and the airflow through the intake and outtake of the rooms were taken from the results of the simulations with IDA ICE mentioned in the last section. The solar radiation values were the average values in July.
- The external and internal operative temperatures were assumed to be 20 °C and 25 °C, respectively, which are average values in the summer in Denmark.

Three main horizontal levels for the results 0.1m, 1.1m, 1.7m (ankle, head of a sitting person, head of a standing person), will be focused on in addition to a vertical plane through the openings.

Results

Calculations for the window opening area

The results of the calculations for the window opening areas in the six scenarios are summarized in Table 3.

The maximum intake and outtake areas in Table 3 can be used for the design and dimensioning the window while the other areas in Table 3 represent the opening area for this window in different periods through the year. The penetration length is the depth that the air penetrating through the opening area inside the room, reaches.

Table 3 The result of the calculations for the window opening areas in the six scenarios according to the parameters mentioned in table 1and 2

Scenario nr.	Intake (m²)	outtake (m²)	penetration length (m)
1	0.010	0.010	2.450
2	0.025	0.025	3.210
3	0.078	0.078	3.980
3-1	0.107	0.107	3.640
4	0.004	0.004	2.460
5	0.006	0.006	2.340
6	0.007	0.007	1.970

IDA ICE simulation results

The results of the simulations of the energy consumed inside the office room with a flat façade and multi-angled façade, for both mechanical and natural ventilation scenarios, in addition to the results of the simulation of the indoor climate are listed in Table 4 and 5 (these results will be discussed in detail subsequently).

Table 4 The results of the simulation of primary energy consumption for lighting, HVAC Aux, heating, and the total primary energy consumption for the flat and multi-angled façade, for both mechanical ventilation (MV) and natural ventilation (NV) scenarios, according to BR15

	Flat facade		Multi-angled facade	
	MV.	NV.	MV.	NV.
The room area (m²)	22.5	22.5	27.5	27.5
Lighting (kWh/(m²·year))	5.7	5.7	4.3	4
HVAC Aux (fans & pumps). (kWh/(m²·year))	13.5	0	10.5	0
Heating (kWh/(m²·year))	26.9	32.1	25.0	29.6
Total (kWh/(m²·year))	46.0	37.9	39.8	33.6

Table 5 The results of the simulation of the indoor climate of office rooms with the flat and multi-angled façade (MAF) (both naturally ventilated)

		Flat facade (nr. of hours)	MAF (nr. of hours)
Overheating hours	above 26°C	88	38
	above 27°C	24	6
CO_2 level (ppm)	1100 - 700	1720	1410
	700 - 400	890	1200
Relative humidity (%)	70%- 80%	11	7
	lower than 20%	28	46

To compare the amount of heat removed by natural ventilation through the outtakes of both rooms with a flat facade and multi-angled facade, Table 6 lists the average values of heat removed by natural ventilation in Watt through the outtake in the flat facade **FF**, and the outtake in both parts of the multi-angled facade **MAF1**. The table also presents the results of two other simulations of heat removal by natural ventilation through the multi-angled façade. In the simulation of **MAF2**, there was an intake in one part of the multi-angled façade that was double in size, while the intake on the other part was removed. In the simulation of **MAF3** there were two intakes in one part of the multi-angled façade, while the intake on the other part was removed.

Table 6 The average amount of heat removed by natural ventilation in Watt through the outtakes of both rooms with a flat facade (FF) and multi-angled facade (MAF)

	FF (W)	MAF 1 (W)		MAF 2 (W)	MAF 3 (W)	
Intake		P1	P2	P1	P1.1	P1.2
Area (m²)	0.2	0.1	0.1	0.2	0.1	0.1
Jan	58	14	33	49	24	25
Apr	98	66	90	79	38	39
Jul	230	165	135	225	107	110
Oct	60	35	50	41	19	21

The results of Table 6 will be discussed in detail subsequently

Results for Simulation in Autodesk CFD

The results of the simulations with Autodesk CFD for the temperature distribution in naturally ventilated office rooms with a flat facade and multi-angled facade at three levels are shown in Figures 4-6. The three levels from the ground (0.1 m, 1.1 m, 1.7 m) (ankle, head of a sitting person, head of a standing person. The results of the simulations with CFD software for the air velocity in the naturally ventilated office rooms with a flat facade and multi-angled facade at horizontal and vertical planes are shown in Figures 7-10. The results in the Figures 4-10 will be discussed in detail subsequently.
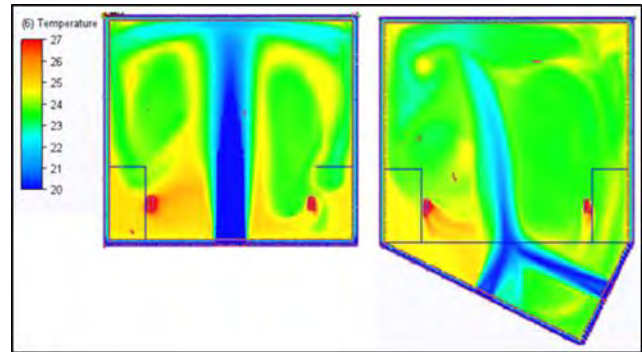
Figure 4 Temperature distribution (°C) in the naturally ventilated office rooms with a flat and a multi-angled facade at a horizontal plane with 0.1 m from the ground.
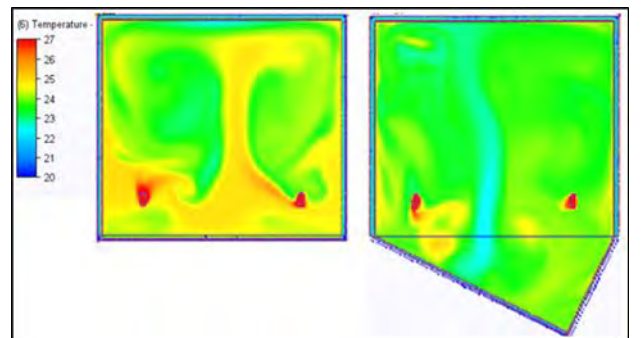
Figure 5 Temperature distribution (°C) in the naturally ventilated office rooms with a flat and a multi-angled facade at a horizontal plane 1.1m from the ground.
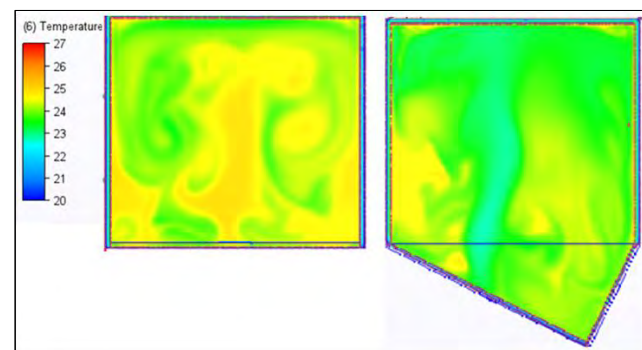
Figure 6 Temperature distribution(°C) in the naturally ventilated office rooms with a flat and a multi-angled facade at a horizontal plane 1.7 m from the ground.
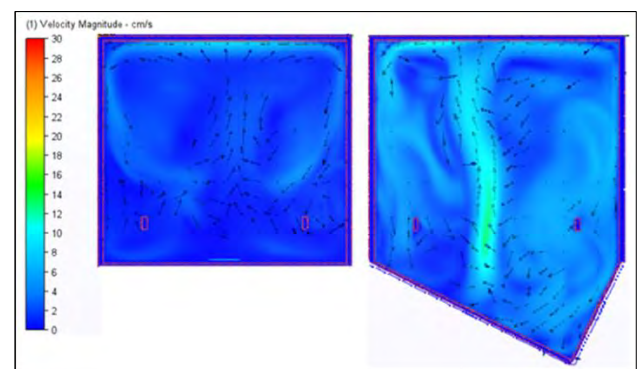
Figure 7 Air velocity (cm/s) in the naturally ventilated office rooms with a flat and a multi-angled facade at a horizontal plane with a height of 1.1 m from the ground.
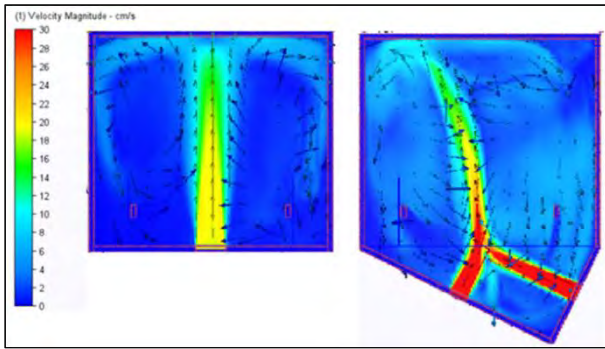
Figure 8 Air velocity (cm/s) in the naturally ventilated office rooms with a flat and a multi-angled facade at a horizontal plane with a height of 0.1 m from the ground
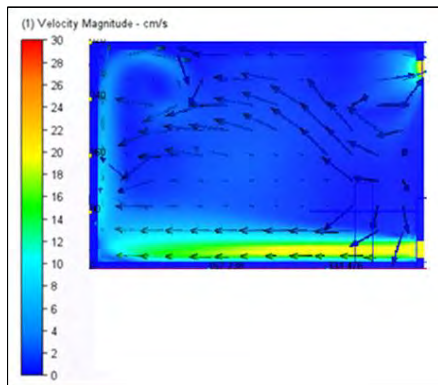
Figure 9 Air velocity in the naturally ventilated office rooms at a vertical plane with a distance of 2.5 m from the sidewall and through the ventilation opening.
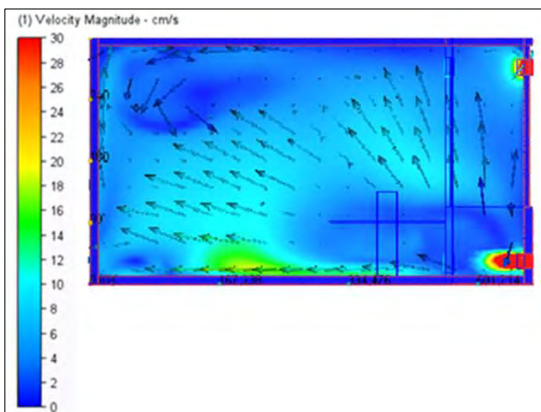
Figure 10 Air velocity in the naturally ventilated office rooms with a multi-angled facade at a vertical plane with a distance of 2.0 m from the sidewall where it comes through the ventilation opening.

Discussion

Natural ventilation is one of several solutions that can be implemented in buildings to reduce the total energy consumption by saving the energy required for mechanical ventilation. The area-weighted primary energy consumption (energy consumption/room area) for mechanical ventilation of the office room, as simulated and presented in this research, is about 25% of the total area-weighted primary energy consumption, and this saving is economically significant in the long term.

The calculations for the intake and outtake areas were based on several equations from SBi Directive 202. In general, the calculation results are very close to similar results for a number of models presented in the SBi Directive 202, Which gives them credibility. The results of the calculations made by these equations for the opening areas were used in the simulations in the IDA ICE software and the opening area chosen was from the third scenario (Maximum hour), which is the largest opening area due to the high solar radiation intensity on the facade. There was a need to adjust the size of the openings taken from Table 3 for the simulations in IDA ICE to achieve an acceptable indoor climate. This was due to the difference between the results of calculations based on fixed values in Table 3 and those from dynamic simulations by IDA ICE.

The simulations in IDA ICE provided results in three main areas: the energy consumption, indoor climate, and amount of heat removed by the air. Regarding the first type of results for a room with a Multi-angled facade, there is a saving of about 16% of the total area-weighted consumed energy, when it is naturally ventilated, as shown in Table 4. Using the design concept of multi-angled façade also has its impact on the consumed energy when it is naturally ventilated, compared to a naturally ventilated flat facade room. A naturally ventilated multi-angled façade room saves about 12% of the total area-weighted consumed energy compared with a naturally ventilated flat façade room, as shown in Table 4. There is an increase in the energy consumed for heating for a naturally ventilated multi-angled facade room of about 18% compared to the energy consumed for heating a mechanically ventilated multi-angled facade room, as shown in Table 4. This is because of the impact of eliminating the heat exchanger that was used in mechanical ventilation. The design concept of a Multi-Angled Façade also has an impact on the indoor climate, which is much better for a naturally ventilated Multi-Angled Facade room compared with a naturally ventilated flat façade room. The number of overheating hours above 26°C and 27°C are much lower for a naturally ventilated multi-angled facade room compared to a flat façade room, as shown in Table 5. The same is true for the CO_2 concentration, which is lower for the naturally ventilated Multi-Angled Façade room, as shown in Table 5.

The multi-angled facade design concept affects the amount of heat removed under natural ventilation. In July, the average amount of heat removed inside a multi-angled facade room by natural ventilation is approximately 31% higher than the heat removed by natural ventilation inside a flat facade room, as shown in Table 6. The ventilation openings with two different orientations in a multi-angled façade improves the natural ventilation and increases heat removal. This can be attributed to the different wind directions on the two sides of the multi-angled façade, which can drive the natural ventilation inside the room. The average amount of heat removed by natural

ventilation in July inside a Multi-Angled Façade room with two openings, each on one section of the two multi-angled facade parts, is about 39% higher than the heat removed by natural ventilation inside a Multi-Angled Façade room with two openings on only one part of the multi-angled facade, and about 34% higher than the heat removed by natural ventilation inside a multi-angled facade room with one double-sized opening on only one part of the Multi-Angled Façade, as shown in Table 6. This demonstrates the positive impact of having two differently oriented openings on the natural ventilation inside the room.

The simulations with the CFD software yielded two types of results: the room temperature and air velocity. The room temperature was higher in the naturally ventilated flat façade room compared with the multi-angled façade room. The average temperature at three levels from the ground (0.1 m, 1.1 m, 1.7 m) (ankle, head of a sitting person, head of a standing person) ranged between 23.5 °C and 25 °C in the flat facade room, and between 23 °C and 24 °C in the multi-angled façade room. The temperature was more uniformly distributed at the three levels in the multi-angled facade room than in the flat façade room, as shown in Figures 4-6.

The air velocity was higher in the naturally ventilated room with multi-angled facade than with the flat facade. At the level 0.1 m from the ground, the average velocity was 10 cm/s in the multi-angled façade room, and approximately 4 cm/s in the flat façade room. These values cover most of the areas at this level except the path of the air draught from the openings, where the air velocity was approximately 22 cm/s and 30 cm/s in the flat facade and multi-angled façade room, respectively. At higher levels (1.1 m and 1.7 m), the average velocity ranged between 12 cm/s and 8 cm/s in the multi-angled façade room, and between 4 cm/s and 8 cm/s in the flat façade room, shown in Figures 7-10. In general, the air velocity at the three levels, except for the lowest level in the path of the air draught, was within the permissible mean velocity of category A according to the CEN report (Ventilation for buildings - Design criteria for the indoor environment) (CR 1752).

Conclusion

The results of the study show that the multi-angle design concept has the potential of improving natural ventilation inside an office room compared with a flat facade. Furthermore, the average amount of heat removed by natural ventilation inside the multi-angled facade room was approximately 31% higher than the heat removed by natural ventilation inside the flat facade room. There were also reductions in the total energy consumed by the building owing to savings in the consumed energy for mechanical ventilation. There is a saving of about 16% of the total area-weighted consumed energy, when a room with a Multi-angled facade is naturally ventilated. The naturally ventilated office rooms with multi-angled facade can provide an acceptable indoor climate in terms of room temperature, where the number of overheating hours above 26 °C and 27 °C were much lower compared with a naturally ventilated flat façade room. Moreover, the CO_2 level was acceptable and there were no draught problems in the working area inside naturally ventilated office rooms with multi-angled façade.

References

Building and housing agency. (2019). Retrieved from Danish Building regulation : http://bygningsreglementet.dk/

European Commission. (2020, April). *Energy performance of buildings directive*. Retrieved from https://ec.europa.eu/

European Committee for Standardization. (2001). *(CR 1752) Ventilation for buildings- Design criteria for the indoor environment.* Technical Committee CEN/TC.

European Committee for Standardization. (2006). *DS/ EN 15251 Indoor environment input parameters for design and assesment of energy performance of buildings.* CEN Technical Secretariat.

Hannoudi, L., Lauring, M., & Christensen, J. E. (2016 b). *Multi-angled facade system for office building renovation.* Bern: GmbH. ISBN: 978-3-98120539-8.

Hannoudi, L., Lauring, M., & Christensen, J. E. (2017 b). *Evaluating architectural solutions such as multi-angled façades in specific urban contexts.* London: London South Bank University, UCL Press, proceeding 9, PP.161-173. ISSN 2398-9467.

Hvlid, C. (2014). *Design of Ventilation.* Lyngby: DTU.

IDA Indoor Climate and Energy. (2019). IDA ICE version 4.8 (Software). Stockholm: EQUA, Sweden, Available from: URL: www.equa.se.

Roth, J. K. (2020, March). Head of Building Performance Engineering/ Window master. (L. A. Hannoudi, Interviewer)

Secretariat of the energy labeling scheme for vertical windows. (2020). Retrieved from Energy windows: http://energivinduer.dk

State Building Research Institute. (2000). *SBI directive 196 (Indoorclimate handbook).* Copenhagen: 2nd edition.

State Building Research Institute. (2002). *SBi Directive 202 (Natural ventilation in commercial buildings).* Copenhagen: 1st edition.

Technical University of Denmark. (2009). *Basic indoor climate, installations and energy design.* Lyngby: DTU.

The European Environment Agency (EEA). (2020, April). *Energy and climate change*. Retrieved from https://www.eea.europa.eu/

Adapting to future climate change by integration of Phase Change Materials (PCMs) into the building envelope: a case study in Stockholm, Sweden

Benedetta Copertaro[1], Jingchun Shen[1], Lorenzo Sangelantoni[2], Pei Huang[1], Xingxing Zhang[*1]
[1] Department of Energy and Building Communities, Dalarna University, Falun, Sweden
[2] CETEMPS, Center of Excellence, Department of Physical and Chemical Sciences, University of L'Aquila, L'Aquila, Italy
* corresponding author: xza@du.se

Abstract

This paper presents a numerical investigation on the effectiveness of phase change materials (PCMs) wall implementation as building refurbishment solution, under both historical and future climate conditions. Specifically, the paper aims at proofing the PCM capability of being an effective refurbishment strategy. The study is based on dynamic building simulations carried out by IDA ICE on a typical residential single zone house in Stockholm city (Sweden). Specifically, two key performance indices have been considered: total energy demand and indoor thermal comfort. The results of the simulations highlight that in lightweight building envelope, PCM can contribute to a reduction of cooling demand and improve the indoor thermal comfort under both historical and future climate. PCM results slight effectiveness in reducing heating loads. However, the annual energy saving resulted between -1.5% and -2.4% for the historical period and between -1.9% and -5.7% for the future one.

Introduction

In Sweden, a large part of the housing stock is more than 50 years (Mangold et al., 2016), which means that it is presumably energy inefficient and with a limited capability to adapt to the future climate conditions. In this regard, it is noteworthy that the envelope optimization represents a straightforward strategy for a building to adapt to climate change (Shen et al., 2020). In fact, optimizing the building envelope allow less energy dependence on heating and cooling, while still maintaining the desired indoor thermal comfort conditions (Shen et al. 2020). Latent Thermal Energy Storage (LTES) is considered an effective way to temporary store energy in terms of latent heat, which is beneficial to enhance the building energy efficiency by increasing the lightweight envelope heat capacity. Accordingly, Phase Change Materials (PCMs) offer a great solution in energy storage due to their high latent heat capacity, which allow them to store and release a huge amount of energy in a small temperature interval (de Gracia and Cabeza, 2015). Specifically, when PCM is applied as a passive component, it is able to produce a sort of extra thermal capacity to the building envelope. Owning to this, the indoor temperature swings are smoothed as well as the heating and cooling demand

reduced. PCMs and their passive applications in building envelope have been under study by many researchers around the world for over 30 years, showing remarkable results in terms of reduced heating and cooling energy consumption, peak load shaving and indoor thermal comfort improvement. Among them, PCM melting temperature, thickness, position and their interaction with the climatic conditions of a specific geographic location has been deeply addressed. It has been found that PCM as a passive component should be designed for each building type and climatic conditions. Moreover, considering that the lifetime of a building (50-100 years) (Constantinos et al. 2007) and PCM (30-80 years) (Panayiotou et al. 2016) corresponds to a period over which substantial changes in climate conditions are expected, it becomes important to have a valuable information on the PCM building refurbishment strategy viability not only in the present period but also into the future. To the best of the Authors knowledge, only Gassar and Yun (2017) assessed the effect of future climate on the performance of PCM applied in a new office building in humid and warm temperate climate (East Asia). They found that adding a PCM layer on the building envelope can increase the building energy performance during both heating and cooling seasons, also under future climate conditions. The **study motivation** lies on deepening findings from a previous paper published by the Authors Shen et al. (2020), where climate adaptive designs of multi-family building in a typical Scandinavian city were explored. The study highlighted that high thermal mass building envelope represents a good building adaptation strategy to climate change. This is especially true in Scandinavian Countries where the use of lightweight wood-based building envelopes is the most prevalent. In fact, a low thermal inertia envelope, even if characterised by high thermal resistance, could lead to overheating risks when irradiated by the sun with a consequent increase in the indoor temperature, energy consumption and occupants' thermal discomfort. Based on this, the **aim of the study** is to assess the building performance of a residential single zone house (in Stockholm city, Sweden), which lightweight envelope has been fully refurbished with PCM. The single zone house performance will be studied under both historical and future climate conditions, with the purpose of evaluating the effectiveness of this

refurbishment solution also in the future. Hence, **the objectives of the study** are to: 1) define the climate change impacts on thermal comfort and heating/cooling demand of a residential single zone house in Sweden; 2) investigate the passive potential of PCM addition into conventional construction material and specify the optimal PCM thickness and melting temperature for both historical and future climate conditions. Even though there is a limited number (in Scandinavian regions) of residential buildings equipped with a unit cooler, overheating in summer can lead the occupants to adopt air-conditioning increasing the energy consumption of the building. Therefore, it seems wise to investigate the PCM cooling load reduction potential also in Scandinavian Countries.

Methods

Energy simulation

In this study, the IDA ICE (Indoor Climate and Energy) software has been used in order to perform the dynamic energy simulations of a single zone-house. The PCM layer is an IDA ICE module that calculates the amount of latent heat absorbed and released by the PCM. It uses the enthalpy method to define the relation between temperature and enthalpy (h-T curves) during PCM melting and solidification phase.

Building model description

A residential single zone house (day zone, including living room, kitchen and dining area) has been defined as reference model for Stockholm city. The reference model is a rectangular single-zone house (2.44 wide × 6.09 length × 2.6 height) with no internal portions (Figure 1).

Internal Floor Area
14.86 m²
External Envelope
Area 44.19 m²
Roof Area 14.86 m²
Total Volume 38.49 m³
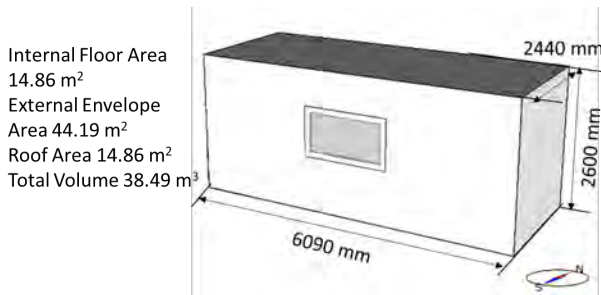
Figure 1: Residential single zone model

The main glazed façade is oriented to the south with a window to floor ratio of 10%, which can be considered typical among the single zone house with similar purposes (BREEAM-Health and Wellbeing). Window properties are shown in Table 1. No internal and external sun screening have been considered at this stage.

Table 1: Window properties of the single zone model

Two-layer panel window	Values
Solar heat gain coefficient (g)	0.60
Solar transmittance (t)	0.7
U (W/m²K)	2.9
Internal emissivity	0.837

External emissivity	0.837
Visible transmittance	0.81

The construction materials are defined based on a survey about the existing building stock in Sweden (TABULA project, https://episcope.eu/welcome/) Table 2– 4. In Table 6 the U-transmittance values are set based on the existing requirements (https://www.eurima.org/). This will allow to focus only on the building envelope refurbishment in terms of increasing thermal mass.

Table 2: Wall construction of the single zone model

Material	Thickness (m)	K (W/mK)	Density (kg/m³)	Cp (J/kg K)
Gypsum	0.026	0.22	970	1090
Frames cc 600+ insulation	0.25	0.130	56	1720
Air in 20 mm vertical air gap	0.02	0.160	1.2	1006
Wood cladding	0.025	0.14	500	2300

Table 3: Roof construction of the single zone model

Material	Thickness (m)	K (W/mK)	Density (kg/m³)	Cp (J/kg K)
Roof material	0.02	0.58	1500	840
Frames cc 600 + insulation	0.25	0.130	56	1720
Gypsum	0.013	0.22	970	1090

Table 4: Floor construction of the single zone model

Material	Thickness (m)	K (W/mK)	Density (kg/m³)	Cp (J/kg K)
Wood flooring	0.025	0.14	500	2300
Mineral Wool 0.037	0.25	0.037	20	750
Concrete medium density	0.2	1.42	2000	1000

RUBITHERM® RT organic PCMs (RT 21, RT 21 HC, RT 24 and RT 26) with three different thickness (1 cm, 2 cm and 3 cm) and three different melting temperature (21 °C, 24 °C and 26 °C) are investigated on the vertical walls of the reference single zone house. The RT 21 HC has been also included in order to test its higher heat storage capacity (20-30% higher than classic RT) and ability to melt in a narrower temperature range. Specifically, a melting temperature range between 21 °C and 26 °C will be explored, as belonging to the maximum and minimum thermal comfort temperature range during winter and summer period in Stockholm city (Climate Consultant v6.0) (Saffari et al. 2016). The thickness will vary between 1 cm and 3 cm as any further increase means that not all the thickness can be involved in the phase change

process (Copertaro et al. 2016). The PCM added wall construction specification is given in Table 5.

Table 5: Refurbished wall construction with PCM

Material	Thickness (m)	K (W/mK)	Density (kg/m³)	Cp (J/kg K)
Gypsum	0.026	0.22	970	1090
Rubitherm PCM	0.03 0.02 0.01	0.20	880	2000
Frames cc 600 + insulation	0.25	0.130	56	1720
Air in 20 mm vertical air gap	0.02	0.160	1.2	1006
Wood cladding	0.025	0.14	500	2300

A mechanical ventilation system providing a constant and fixed rate of 0.4 air change per hour (ACH) is used. The latter is based on comfort and health criteria and defined according with the required ventilation for pollution from occupants and building components under EN 15251. Moreover, it is expected to increase the amount of heat discharged by PCMs, which improves their efficiency. During the occupancy period (not at home from 8:00 to 17:00 during the weekdays), internal gains are due to people (one, which has been assumed reading 108 W), lighting (2 W/m²) and other electrical equipment (2.4 W/m²) based on ASHRAE Fundamentals. The summary of the main simulation parameters is given in Table 6.

Table 6: Simulation parameters

Vertical walls U-value	0.18 (W/m²K)
Vertical PCM added walls U-values	0.18 (W/m²K), PCM 3 cm 0.18 (W/m²K) PCM 2 cm 0.18 (W/m²K) PCM 1cm
Roof U-value	0.17 (W/m²K)
Floor U-value	0.14 (W/m²K)
Window g-value	0.60
Ventilation rate always on	0.4 ACH
Occupancy time	From 17:00 to 8:00 from Monday to Friday. Always at home from Saturday to Sunday.
Number of people	1
People sensible heat load	108 (W)
Artificial light load	2 (W/m²)
Electric equipment load	2.4 (W/m²)
RT21 and RT21HC melting temperature peak	21 °C
RT24 melting temperature peak	24 °C
RT26 melting temperature peak	26 °C

Future climate data

Stockholm city, in Sweden (Lat: 59.350N, Long: 18.067E) is considered as reference site in the present study. According to Köppen-Geiger climate classification

Stockholm is classified as Dfb (temperate continental climate/humid continental climate) as representative of typical maritime northern European cities climate. In order to assess the single zone house performance under future climate scenarios, an hourly dependent climate dataset is necessary for a dynamic simulation. In this regard, the future climate data 2080s (2071-2100) have been generated by using a morphing approach based on the UK Met Office Hadley Centre general circulation model (GCM) predictions for a 'medium-high' emissions scenario (A2). The historical year is derived by the average period of 1971-2000 (Jentsch et al. 2008).

Heating and cooling system

The sensible cooling and heating needs are evaluated by using built-in IDA ICE function "ideal heater and cooler" with an infinite capacity to satisfy heating and cooling loads. This choice will help to keep the results independent from a specific mechanical system performance. The indoor comfort set point temperatures are 26 °C during summertime and 21 °C during wintertime.

Thermal comfort assessment

The ANSI/ASHRAE Standard 55-2013 defines the thermal comfort as a condition in which the human mind express satisfaction with the thermal environment. The latter is strongly dependent on indoor air temperature and to mean radiant temperature, which can be combined through the definition of the operative temperature (Eq.1).

$$t_0 = \frac{h_r t_{mr} + h_c t_a}{h_r + h_c} \qquad (1)$$

Where h_r is the radiative heat transfer coefficient, h_c is the convective heat transfer coefficient, t_a is the air temperature and t_{mr} is the mean radiant temperature. Specifically, in cases where the air temperature and the mean radiant temperature are similar to each other and the air speed is less than 0.1 m/s the air temperature itself can be a reasonable indicator of thermal comfort. However, in cases in which the surfaces have a significant thermal mass due to e.g. PCM addition, it is strongly recommended to take into account the operative temperature in assessing thermal comfort. In fact, PCM thank to their capability of melting at a constant temperature range, can keep the surface temperatures more stable, and allow for better thermal comfort.

Analytical approach of the parametric study

The total 26 simulated scenarios are categorized based on the climate typology (i.e. historical and future) and location (Stockholm). For each of them, a parametric analysis with different PCM melting temperature and thickness is performed. A summary of the analytical approach for the simulated scenarios is provided in Figure 2.

Figure 2: Analytical approach of simulated scenarios

For sake of simplicity, the simulations are classified and discussed in the Results and Discussion Section as reported in Figure 3.

Figure 3: Parametric study analysis

Results and Discussion

Climate change impact on the reference single zone house without PCM

This section assesses the climate change impact on the indoor thermal comfort of the reference single zone house. Figure 4 shows the historical and future trends in a year, of the monthly average operative temperatures and operative temperatures in the reference single zone house (without PCM). Moreover, the monthly average outdoor temperature for the historical and future period is presented. As it can be observed the highest difference (between historical and future) can be found in the intermediate (spring and autumn) and summer seasons. Specifically, during winter months (January, February, November and December), there is an outdoor temperature increase between 2.7 °C and 4.6 °C, which becomes more significant during the summer months (June, July, August and September) with an increase until 5.7 °C in August. This outdoor temperature increase clearly affects the indoor operative temperatures. Specifically, the indoor operative temperature is showing a limited variation in winter, while the climate change influence is more visible in summer, determining an increase of 2-3 °C in the future climate. Accordingly with the Swedish Guidelines for the Specification of Indoor Climate Requirements released by SWEDVAC, the operative temperature target value of a residential building are equal to 20.0-24.0 ºC and 23.0-26.0 ºC during winter and summer season respectively. While in winter, the operative temperature values fall into the required target also in the future, in months like July and August it exceeds the maximum value, increasing thermal discomfort risks. The following section further evaluated the climate change impact on the heating and cooling demands of the reference single zone house. Table 7 shows a clear influence of climate change over the heating and cooling demand. Specifically, in 2080s it is expected

a decrease of the heating demand by about -25 kWh/m^2, while the cooling one is likely to increase of +24.2 kWh/m^2. These results are in accordance with the main findings highlighted by the Authors (Shen et al. 2020). In fact, the 21st century climate trends will be characterized by a significant increase of winter-season temperature over the Scandinavian region, driven also by the positive feedback deriving from loss of snow-cover and related decrease of albedo. On the other hand, in summer season, higher environmental temperature and extreme events (like heat waves) are also expected in the next decade climate.
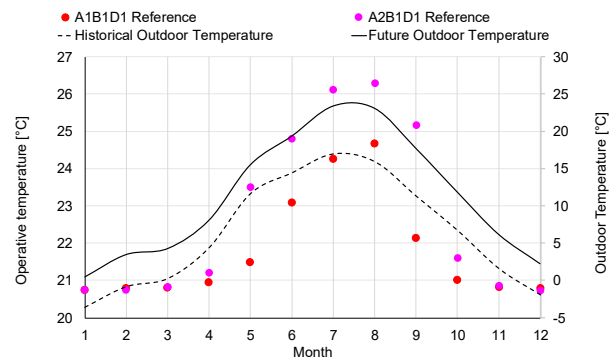
Figure 4: Monthly outdoor and resulted operative temperature variations under historical and future cases without PCM

Table 7: Annual heating and cooling demand for the historical and future climate cases without PCM

	A1B1D1 Reference (kWh/m^2)	A2B1D1 Reference (kWh/m^2)
Heating	105	80
Cooling	1.8	26

Figure 5 shows the total wall conduction heat transfer across the reference single zone house walls during heating, cooling and the rest of time. In IDA ICE, the average conduction heat transfer across the external walls results from the average of the inside face heat conduction and outside face heat conduction. Therefore, positive values indicate resultant heat flowing to the internal space, while the negative one defines the resultant heat released to the external environment. As it can be appreciated, in 2080s, due to the outdoor temperature increase during the winter season, less energy is released to external environment and then delivered to the space. During the summer season the relation is the reversed. In this case, the high thermal resistance value offered by the insulation layer coupled with higher future outdoor temperature presumably increased the indoor temperature, determining a slight increase of the heat flowing to the external environment.

Effect of PCM on the indoor environment for the historical period

The PCM influence on the indoor thermal environment of the single zone house is studied in the historical period. Figure 6 shows the comparison of the average operative

temperature throughout the year in the A1B1 group. As it can be appreciated the highest variations between the A1B1D1 reference case and the PCM variants occur in summer (i.e. June, July and August) and middle season months (i.e. May and September). Overall, it can be stated that the building refurbishment with PCM application successfully yields a reduction in the average indoor operative temperature during the summer months, due to the latent heat storage of PCM.
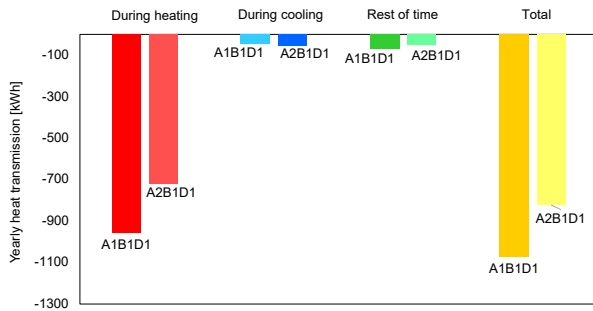
Figure 5: Annual wall conduction for the historical and future climate cases without PCM

Specifically, among all studied variants, the maximum mean operative temperature deviation (– 0.43 °C) from the A1B1D1 reference case has been found for A1B1D4 group which refers to the thickest PCM layer (PCM 3 cm). Then it follows A1B1D3 group (PCM 2 cm), with a maximum operative temperature deviation of – 0.26 °C from the A1B1D1 reference case. Finally, A1B1D2 group (PCM 1 cm) with a maximum operative temperature deviation of – 0.13 °C from the reference case. The reason can be related to the fact that a large amount of incoming heat can be stored in the PCM layer, keeping the indoor surface temperature lower for a longer period. However, during the August month, the walls with the highest PCM melting temperature (D4, 26 °C) showed a slight increase of the average operative temperature (+ 0.26 °C A1B1D2, + 0.37 °C A1B1D3, + 0.34 °C A1B1D4), compared with the reference case. The reason of this reduced PCM potential is owing to the reduced cool storage capacity of PCM during warm nights. In fact, high night temperature could cause the PCM surface to be around or beyond the solidification, remaining liquid during the night and just exploiting the sensible heat capacity the following day. High variations between the all studied variants and the A1B1D1 reference case can be found in September, where the PCM helped to maintain a higher operative temperature, providing a better thermal environment in a month characterized by low external temperature.

Table 8 is showing the annual number of hours with the operative temperature above 26 °C. Generally, the implementation of PCM demonstrated a successful reduction in overheating risks from 215 hours (A1B1D2 base case) to 31 hours (A1B1D3E4) in one year. More in detail, the number of hours when the operative temperature goes over 26 °C is lower when the thickest PCM layer is applied, whichever the phase transition temperature. For example, the number of hours with the

operative temperature higher than 26 °C were reduced from 144 h to 79 h when the thickness of PCM increased from 1 cm to 3 cm for PCMs with a melting temperature of 21 °C and 24 °C. However, as the melting temperature increased to 26 °C, there is a significant reduction (31 h) of the number of hours with operative temperature higher than 26 °C. This result has been obtained for the PCM layer with 3 cm thickness.
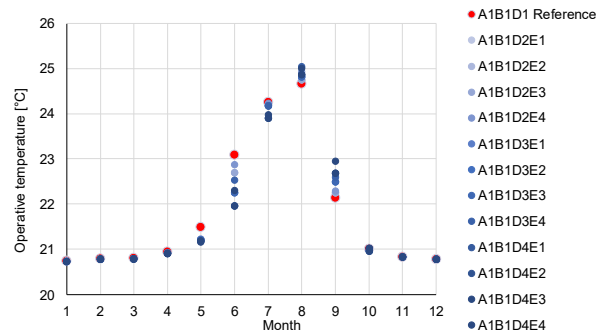
Figure 6: Annual average operative temperature comparison in A1B1 group.

Table 8: Annual number of hours with operative temperature above 26 °C

A1B1 group	Number of hour
A1B1D1 Reference	215
A1B1D2E1/2/3	≈144
A1B1D2E4	91
A1B1D3E1/2/3	≈96
A2B1D3E4	60
A1B1D4E1/2/3	≈79
A2B1D4E4	31

Effect of PCM on the heating and cooling demand for the historical period

In addition, the PCM influence on the heating and cooling demands of the single zone house is investigated in the historical period (Table 9). Overall, the heating demand resulted the predominant one and nearly no influences on all the PCM studied variants, with respect to the A1B1D1 reference case. The reasons for this reduced PCM potential can be related to the fact that an insufficient amount of solar heat gains passed through the limited window area or that a limited amount of sensible heat has been generated by internal load sources. In this regard, is assumed that during the wintertime the PCM could not undergo as many melting and solidification cycles as possible. By this way the PCM remained solid for most of the time, and so utilizing its sensible heat capacity. Conversely, a cooling demand reduction can be observed when PCM is applied. Specifically, the cooling demand is lower when the thickest PCM is applied, whichever the phase transition temperature. As an example, the cooling demand is reduced from -33% to -60% when the PCM thickness is increased from 1 cm to 3 cm for PCMs with a melting temperature of 21 °C and 24 °C. However, as RT26 (3 cm thick) is applied, a significant reduction of the cooling demand (i.e. -57% A1B1D2E4; -77%

A1B1D3E4 and -88% A1B1D4E4) has been obtained. Therefore, it can be stated that a PCM with a melting temperature of 26 °C and 3 cm thick is appropriate for reducing the cooling load and thus providing significant benefit in cooling season. Overall, the total energy demand savings varied from -1.5% to -2.4%, at the increase of PCM melting temperature and thickness, compared with the reference case.

Table 9: Annual heating and cooling demands comparison in A1B1 group (Unit: kWh/m²)

	A1B1D1 Reference	A1B1D2E1/2/3	A1B1D2E4
Heating	105	104	104
Cooling	1.8	1.2	0.78
	A1B1D1 Reference	A1B1D3E1/2/3	A1B1D3E4
Heating	105	104	104
Cooling	1.8	0.83	0.42
	A1B1D1 Reference	A1B1D4E1/2/3	A1B1D4E4
Heating	105	103	104
Cooling	1.8	0.72	0.22

Table 10 shows the total wall conduction across the PCM added walls of single zone house during heating, cooling and the rest of time. As it can be appreciated during the heating season, the variants A1B1D4E1/2/3 had the best performance in retaining more useful heat gain inside. Firstly because the A1B1D4 variants belong to the largest PCM thickness in this study, which determines a highest thermal mass value. Secondly because E1, E2, E3 belong to the PCMs with melting temperature between 21 °C (E1 and E2) and 24 °C (E3), which determines a reduced temperature difference between the internal and external surfaces. In this regard, most of the heat which has been stored during the daytime is re-radiate back to the indoor environment throughout the night, reducing the heat transfer to the outside. Obviously, when the PCM RT 26 °C is applied, less useful heat gains can be retained. Anyway, the heat transmission value decreased at the increase of the PCM RT26 thickness, due to the increased wall´s thermal mass. During the cooling season, A1B1D3E4 and A1B1D4E4 helped in dissipating more undesirable heat gain outside, compared with the other PCM variants. This result is because of fact that during the summer a significant temperature variation between night-time and daytime can occur. In fact, during the daytime the PCM absorbs the heat at a constant temperature equal to 26 °C and re-radiate it at night due to the reduced outdoor temperature. Obviously, the higher is the indoor surface temperature, the higher is the heat dissipated through the wall.

Table 10: Annual heat transmission summary through external walls in A1B1 group (Unit: kWh)

	A1B1D1 Reference	A1B1D2E1/2/3	A1B1D2E4
Heating	-959.2	-938.6	-938.6
Cooling	-44	-35.6	-35.6
Rest of time	-71.4	-92.9	-92.9
Total	-1074.6	-1067.1	-1067.1
	A1B1D1 Reference	A1B1D3E1/2/3	A1B1D3E4
Heating	-959.2	-925.6	-935.8
Cooling	-44	-35	-50
Rest of time	-71.4	-102.3	-78.2
Total	-1074.6	-1062.9	-1064
	A1B1D1 Reference	A1B1D4E1/2/3	A1B1D4E4
Heating	-959.2	-913.1	-923.1
Cooling	-44	-36.2	-53.1
Rest of time	-71.4	-108.7	-83.9
Total	-1074.6	-1058	-1060.1

Effect of PCM on the indoor environment for the future period (2080s)

The PCM influence in the indoor thermal environment of the single zone house under is simulated under future climate conditions. Figure 7 shows the average operative temperature comparison in the A2B1 group. It is observed that the highest variation between A2B1 reference case and all the PCM variants occurs during middle season, while during summer season it is greatly reduced. Overall, the building refurbishment with PCM application perform worse under future climate, compared with the historical one. In fact, during the summer season is not possible to appreciate any considerable mean operative temperature reduction compared with the reference case. The maximum mean operative temperature deviation of –0.08 °C has been found for the A1B1D4 group which belong to the thickest PCM layer (3 cm). As for the historical period, this result is related to the fact that more heat can be stored in the PCM layer at constant temperature. Generally, the climate change negatively affected the PCM effectiveness of reducing the mean operative temperature during the summer period, increasing thermal discomfort risks. This result might be related to the fact that the increased environmental temperature, expected in 2080s, cannot match the different melting temperatures selected (21 °C, 24 °C and 26 °C) determining only a partial exploitation of the PCM latent heat storage capacity. In this regard when the transition temperature is lower than the expected operating temperature the PCM remains mainly in the liquid state, providing nearly no or reduced influence on the operative temperature reduction. The obtained results can be confirmed by the annual number of hours with indoor air temperature above 26 °C, which are shown in Table 11. In short, the number of hours with the operative air temperature above 26 °C is significantly increased compared with the historical period. PCM implementation showed a reduction of overheating risks from 1420 hours (A2B1D1 reference

case) to a maximum of 1220 hours (A2B1D4E4) in one year.
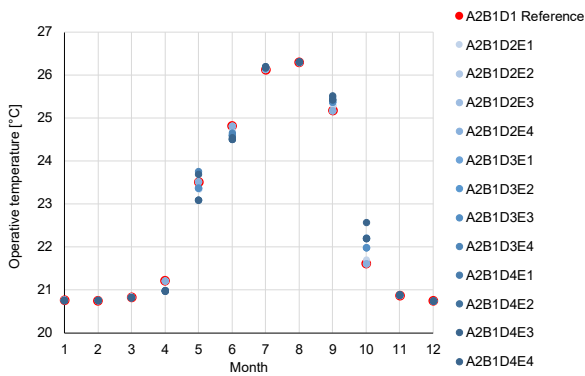
Figure 7: Annual average operative temperature comparison in A2B1 group.

The number of hours for the operative temperature over 26 °C is still lower when the thickest PCM layer is applied, whichever the phase transition temperature. For instance, the number of hours with indoor air temperature above 26 °C where reduced from 1370 h to 1298 h when the PCM thickness increased from 1 cm to 3 cm. This result is related to PCMs with a melting temperature of 21 °C and 24 °C. Specifically, the best performance has been shown by the A2B1D4 group which belongs to the thickest PCM with a successful reduction ratio between 8.6% and 14.1%. PCM RT 26 °C, resulting in the best performance also under future climate conditions.

Table 11: Annual number of hours with operative temperature above 26 °C.

A2B1D1 group	Number of hour
A2B1D1 Reference	1420
A2B1D2E1/2/3	≈1370
A2B1D2E4	1317
A2B1D3E1/2/3	≈1317
A2B1D3E4	1248
A2B1D4E1/2/3	≈1298
A2B1D4E4	1220

Effect of PCM on the heating and cooling demand for the future period (2080s)

Moreover, the PCM impact on the heating and cooling demands of the single zone house is depicted as following (Table 12). Both heating and cooling demand are varying slightly among the all PCM variants with respect to the reference case. As in the historical period, the heating demand is the most prominent and nearly constant for all the PCM studied variants, with respect to the A1B1D1 reference case. Conversely, a slight decrease in cooling demand can be observed when PCM RT26 is applied. Specifically, whichever the thickness, a cooling demand reduction of 15% is observed. The total heating and cooling demand savings varied between 1.9% and 5.7%, increasing along the PCM thickness and melting temperature. In this regard PCM RT26 is still able to reduce the cooling loads and thus providing significant

benefits in cooling seasons also under future climate. As for the historical period, no significant variations in the heating demand have been found. The total energy demand savings vary from -1.9% to -5.7% with the increase of PCM melting temperature and thickness, compared with the reference case.

Table 12: Heating and cooling demands comparison in A2B1 group (Unit: kWh/m²)

	A2B1D1 Reference	A2B1D2E1/2/3	A2B1D2E4
Heating	80	79	78
Cooling	26	25	22
	A2B1D1 Reference	**A2B1D3E1/2/3**	**A2B1D3E4**
Heating	80	78	78
Cooling	26	24	22
	A2B1D1 Reference	**A2B1D4E1/2/3**	**A2B1D4E4**
Heating	80	78	78
Cooling	26	23	22

Table 13 illustrates the total wall conduction across the PCM added walls of single zone house walls during heating, cooling and the rest of time. During the heating season in the future, the variants A1B1D4E1/2/3 are still showing the best performance in retaining the highest useful gains inside. The main reason relies on the increased thermal mass value and to reduced temperature difference between internal and external surface, which can be achieved by using the thickest PCM layer with melting temperature ranging between 21°C and 24 °C. During the cooling season, all the PCM variants enhances the dissipating undesirable heat gain outside, if compared with the historical period. However, RT26 with 3 cm thickness, still showed the best performance.

Table 13: Heat transmission summary through external walls in A2B1 group (Unit: kWh)

	A2B1D1 Reference	A2B1D2E1/2/3	A2B1D2E4
Heating	-719.7	-691.4	-698.3
Cooling	-53.9	-57.2	-76.3
Rest of time	-50.2	-71.8	-47.5
Total	-823.8	-820.4	-822.1
	A2B1D1 Reference	**A2B1D3E1/2/3**	**A2B1D3E4**
Cooling	-53.9	-65.4	-87.4
Rest of time	-50.2	-83.2	-58
Total	-823.8	-820	-822.9
	A2B1D1 Reference	**A2B1D4E1/2/3**	**A2B1D4E4**
Heating	-719.7	-659.4	-669.4
Cooling	-53.9	-64.4	-91.6
Rest of time	-50.2	-94.6	-62
Total	-823.8	-818.4	-823

Study limitations

In the present study, the performance of a residential single zone house (in Stockholm city, Sweden) fully refurbished with PCM has been assessed by IDA-ICE modelling. However, it presents some study limitations which should be pointed out:

1) The numerical simulations are not taking into account the macroencapsulation of the PCM, which might be considered when coming to a real application for numerical model validation purposes. This can be done only by applying the PCM as separate component as sheet of macro-encapsulated PCM pouches that are generally installed in walls behind the gypsum boards (ENERG Blanket https://phasechange.com/)

2) More methodological advancement (such as optimization and advanced controls) in the study of PCM effects must be considered in future studies.

Conclusions

The results of this study indicated that the incorporation of a PCM layer in the building envelope, with a correctly selected melting temperature and thickness, could reduce heating and cooling demand, while still maintaining the indoor thermal comfort. Specifically, the PCM RT26 (3 cm thick, with a melting temperature of 26 °C) has the highest annual energy saving for historical (-2.4%) and future climate (-5.7%) conditions, when assuming an all-day around HVAC operation. Most of the energy saving derives from the cooling season (-88% for historical and -15% for future climate), as the RT26 melting temperature is equal to the cooling-set point. The limited energy saving in the heating season, for future and historical climate, could be attributable to the reduced amount of solar heat gains passed through the window. In this regard, it can be assumed that whichever the melting temperature, PCM failed in undergoing as many melting and solidification cycles as possible. This can be improved from either a large window to wall ratio or additional heat gains from internal loads. Finally, PCMs with the largest thickness (3 cm), whichever the melting temperature, has the highest reduction in terms of average operative temperature during summer months for historical (-0.43 °C) and future climate (-0.08 °C). This result is related to the fact that a large amount of heat can be stored in PCM layer, keeping the indoor surface temperature low for a longer period. Specifically, PCM RT26 (3 cm thick) has the best performance in terms of reduced number of hours with an operative temperature higher than 26 °C for both historical (-184h up to 215h of reference case) and future climate conditions (-200h up to 1420h of reference case). In general, the future climate negatively affected the PCM capability in reducing the mean operative temperature during the summer period.

Acknowledgment

References

Copertaro, B., Principi, P., Fioretti, R. (2016). Thermal performance analysis of PCM in refrigerated container envelopes in the Italian context – Numerical modeling and validation. Applied Thermal Engineering 102,873-881.

Constantinos A. Balaras, Athina G. et al. (2007). European residential buildings and empirical assessment of the Hellenic building stock, energy consumption, emissions and potential energy savings. Building and Environment, 42, 1298-1314.

de Gracia, A., Cabeza, L.F., (2015). Phase change materials and thermal energy storage for buildings. Energy and Buildings. 103, 414-419.

Gassar, AAA, Yun. GY. (2017). Energy Saving Potential of PCMs in Buildings under Future Climate Conditions. Appl. Sci. 7(12), 1219.

Jentsch, M. F., Bahaj, A. S., James, P.A.B. (2008). Climate change future proofing of buildings—Generation and assessment of building simulation weather files. Energy and Buildings. 40(12), 2148-2168.

Mangold, M., Österbring, M., Wallbaum, Holger., Thuvander, l., Femenias, P. (2016). Socio-economic impact of renovation and energy retrofitting of the Gothenburg building stock. Energy and Buildings. 123, 41-49.

Panayiotou G.P., Kalogirou S.A., Tassou S.A. (2016) Evaluation of the application of Phase Change Materials (PCM) on the envelope of a typical dwelling in the Mediterranean region, Renewable Energy. 97, 24-32.

Saffari, M., de Gracia, A., Ushak, S., Cabeza, L.F. (2016). Economic impact of integrating PCM as passive system in buildings using Fanger comfort model. Energy and Buildings. 112, 159-172.

Shen, J., Copertaro, B., Sangelantoni, L., Zhang, X., Suo, H., Guan, X. (2020). An early-stage analysis of climate-adaptive designs for multi-family buildings under future climate scenario: Case studies in Rome, Italy and Stockholm, Sweden. Journal of Building Engineering. 27,100972.

Shen, J., Copertaro, B., Zhang, X., Koke, J., Kaufmann, P., Krause, S. (2020). Exploring the Potential of Climate-Adaptive Container Building Design under Future Climates Scenarios in Three Different Climate Zones. Sustainability. 12, 108.

The Effect of Local Climate Data and Climate Change Scenarios on the Thermal Design of Office Buildings in Denmark

Steffen Petersen[1*]

[1] Aarhus University Department of Engineering, Aarhus, Denmark

corresponding author: stp@eng.au.dk

Abstract

The effect of climate change on Danish office building energy performance was investigated. Local mean weather data and national design reference year are morphed into future weather files, and the output from a total of 313,000 EnergyPlus simulations was analysed. The results indicate that the current Danish building design practice is not appropriate if buildings designed today are to be resilient to climate change.

Introduction

Thermal building performance simulation (T-BPS) can be used during the design phase to make reliable predictions of the thermal indoor climate and energy performance of proposed building designs under the weather conditions of the building site. In terms of weather conditions for simulation, the decade-long practice in Denmark is to use a so-called Design Reference Year (DRY) for any building no matter its geographical location. DRY is an artificial hourly dataset constructed according to a specific procedure described by Lund (1995). The result of the procedure is a dataset that expresses the mean weather conditions of the past years of actual weather used to construct the DRY. The first version of DRY from 1995 (Jensen and Lund, 1995) also included 'an appropriately representative sample of extreme values from the 15-year datasets'. The second – and current – DRY from 2013 (Wang et al., 2013a; Wang et al., 2013b) is also a 'mean year' that seems to have been constructed like the former DRY1995 but it is not clear from the documentation.

It is mandatory to use DRY2013 when documenting the annual energy and thermal indoor climate performance according to the Danish building code (BR18, 2018). The use of a 'mean year' can be regarded as an expression of mean expected energy and thermal indoor climate performance of a building design over a range of years. This could be informative to designers and building owners as long as they realise that it is a mean value, i.e. that the performance can be better or worse depending on the weather data of a specific year. In other words, designing a building to marginally comply with BR2018 using DRY correspond to designing a building to perform *better* than the demands in BR2018 for 50% of its lifetime years but that the building can also be expected to perform *worse* than the demands in BR2018 for 50% of its lifetime years. Realising this, the use of DRY for building design seems like a risky approach to avoid overheating. The Danish tradition is – for various reasons, see e.g. (Petersen and Knudsen, 2017) – to allow the building design to have a certain amount of hours above a summer comfort threshold. For example, a maximum of 100 hours above 26 °C and 25 hours above 27 °C for office buildings. This means that when using DRY for assessing compliance with this criterion will lead to building designs that can be expected to be additionally overheated every 2nd year on average.

The use of a 'mean year' as a boundary condition for T-BPS seems to have some limitations that building designers should be aware of. However, using a 'mean year' like DRY is just one of many ways of representing weather conditions; several studies have described and contrasted the these, see e.g. Barnaby and Crawley (2011), Al-Mofeez et al. (2012), Herrera et al. (2017), Ramon et al. (2018), and Yassaghi and Hoque (2019) to mention a few. Overall, there seem to be two strategies for setting up weather data files for T-BPS, namely 1) use of past weather data or 2) use of future weather. Within these strategies, different types of weather data files are regarded to serve different purposes in building design. The following two sections provide a brief overview of the two strategies and their different categories of weather files. The last section of this introduction outlines the contribution of this paper.

Past weather

The use of past weather for T-BPS can be divided into the following three categories[1]: 1) 'Multi-Year', 2) 'Typical Year', and 3) 'Extreme Year'. The weather data in these categories may originate from observed weather recordings, climate models, or climate generators. Using past weather data for building design implies the expectation that the data also represents future weather conditions. The following subsections contain a short description and purpose of the weather data in each category.

Multi-year

The 'Multi-Year' approach for T-BPS can be defined as the use of annual weather data for a consecutive number of past years for a specific location. A multi-year weather

---

[1] Ramon et al. (2018) suggests a fourth category named 'Representative Datasets' where a set is a 'typcial year' and an extreme cold and warm year for a specific location.

dataset should consist of 30 annual files (preferably for a period spanning from the current year minus 1 and 30 years back in time) as the World Meteorological Organization considers that climate statistics converge over 30 years (Brisson et al., 2015). Past weather data for building simulation can be obtained from observations, climate models e.g. from NCAR (NCAR, 2020) (see the webpage www.vejrdatafiler.dk (Broholt and Petersen, 2020) for an application example) or MESAN (MESAN, 2020) (see Shiny Weather Data (Lundström, 2020)), or climate generators (Eames et al., 2011).

Thermal simulations using 'Multi-Year' weather data provides insights into the variability of the building performance due to long-term variation in weather conditions. This variability is also useful for determining the risk profile for HVAC sizing. However, a multi-year simulation comes with a relatively long simulation time.

Typical Year

The 'Typical Year' approach for T-BPS can be defined as the use of a single-year dataset that represents the average weather conditions recorded for a consecutive number of past years at a specific location – hence considered to be 'typical' ('Average Year' or 'Representative Year' could be alternative names for this category). There are several methods to construct or select this type of weather data leading to different weather data files such as the Test Reference Year (TRY) (Levermore et al., 2006), Typical Meteorological Year (TMY, TMY2, TMY3) (Renné, 2016), Design Reference Year[2] (Lund, 1995), International Weather year for Energy Calculations (IWEC) (Thevenard and Brunger, 2002), Weather Year for Energy Calculations (WYEC, WYEC2) (Crow, 1981). The past weather data used for generating these files are most often observed data but could also be generated using climate models as in the Typical Downscaled Year (TDY) (Nik, 2016) or the probabilistic Test Reference Year (pTRY) (Liu et al. 2019).

This single-year approach is more computationally efficient than a 'Multi-Year' approach but only provides the average performance of a building over its lifetime as the data of a 'Typical Year' is essentially at the 50th percentile of the full distribution of possibilities; i.e. the probability that a data value within the dataset will be exceeded is 50% (Renné, 2006). The dataset does not contain extreme events and is therefore not suitable for 'stress tests' or HVAC sizing. A 'Multi-Year' or 'Extreme Year' approach should be applied for this purpose.

Extreme Year

The 'Extreme Year' approach for T-BPS can be defined as the use of a single-year dataset that is selected or constructed to contain extreme or near-extreme weather conditions for a specific location. There are several ways to select or construct an extreme year leading to different weather data files such as Design Summer Year (DSY) (Hacker et al., 2014), Hot Summer Year (HSY) (Liu et al., 2016), Extreme Warm Year (EWY) and Extreme Cold Year (ECY) (Nik, 2016), hot and cold extreme reference years (ERY_h and ERY_c) (Pernigotto et al., 2019), Typical Hot Year (THY) (Guo et al., 2019) or combinations of both like the Extreme Meteorological Year (XMY) (Ferrari, 2008)[3], Untypical Meteorological Year (UMY) (Narowski et al., 2013), the Design Reference Year[2] (DRY) (Watkins et al. 2013), or P10/P90 Extreme Year (Remund et al., 2018).

Thermal simulations using files from the category 'Extreme Year' are useful for 'stress test' of the building design and to size HVAC systems – like the 'Multi-Year' simulation; however, it is less time-consuming than a 'Multi-Year' simulation. The 'Extreme Year' approach cannot be used for assessing average expected performance or distribution of annual performance. A 'Typical Year' and 'Multi-Year' approach, respectively, should be applied for this purpose.

Future weather

All climate change scenarios published by the International Panel on Climate Change (ICPP) are anticipating an increase in the global outdoor temperature (Moss et al, 2008). This has been the main motivation for recent studies that seek to develop weather data files for T-BPS that considers climate change scenarios. One approach is the 'analog scenario method' that seeks to identify weather files from a location that currently has the climate conditions that are expected to be the future conditions at the current building location (Belcher et al., 2005). A similar approach, seen used in practice, is to identify a year from the past for the specific location that is warmer than normal. Limitations of these approaches are discussed briefly by Ramon et al. (2018). Another approach downscales data from General Circulation Models that take future climate scenarios into account from a spatial resolution of 150-600 km, see e.g. IPCC (2013), to a relevant spatial resolution for building simulations, e.g. by using dynamic downscaling, interpolation, stochastic weather generators or morphing (Wilby and Wigley, 1997; Belcher et al., 2005). The pros and cons of these downscaling methods are discussed by Ramon et al. (2018). The downscaling approach can be used to generate future weather files for T-BPS for both multi-year, typical, extreme years (see the section 'Past weather' of this paper for details on these definitions).

Contribution of this paper

Research on the consequence of future climate on thermal building performance in the Danish context is very rare. This paper presents the outcome of a simulation-based analysis of how climate change affects the thermal

---

[2] There are two different definitions of DRY. The first definition of DRY (Lund, 1995) is an expansion of the month selection method of the TRY and TMY method whereas Watkins et al. (2013) defines DRY as 'a year formed from individual more extreme weather months' and is proposed as a replacement of DSY.

[3] Another 'Extreme Year' definition also called XMY is provided by Crawley and Lawrie (2015).

performance of Danish office buildings. The analysis takes into consideration local differences in weather conditions across Denmark. This may challenge the current decade-long practice concerning T-BPS and building design where only one dataset, namely DRY, is assumed to represent weather conditions for all locations in Denmark. Furthermore, the results from a sensitivity analysis on how various building design parameters affect the variability of the simulation output are presented to investigate whether there is a shift in the ranking of design parameters most important to the simulation output variance due to climate change.

Method

Local TMY data files used for the analysis reported in this paper was downloaded from climate.onebuilding.org (climate.onebuilding, 2019). The TMY files available on this webpage are derived from observed hourly weather data from the US NOAA's Integrated Surface Database (ISD, 2019) using ISO 15927-4 (ISO, 2005). Only TMY files from locations in Denmark where a TMY file named 'TMYx.2003-2017…' are available were used; these files are derived from weather data from the 15 years 2003-2017 (other available files on the site use data from the period 1957-2017). Exceptions from this rule were location 'Aalborg airport' which was omitted due to an abnormal mean temperature of the dataset (9.4 °C) compared to neighbouring datasets, and Bornholm was only represented by one of its three data locations (namely 'Bornholm AP'). Furthermore, one data location in Germany near the Danish border was added ('Leck AP') to have a dataset that represents the most southwestern part of Denmark. This led to a total of 52 TMY locations.

The 52 local TMY dataset was morphed to future climate scenarios (the 2020s, 2050s, and 2080s) using the Climate Change Weather Generator tool (CCWorldWeatherGen, 2013). This tool uses the HadCM3 GCM (Pope et al., 2000) for the SRES A2 emission scenario as the basis for the morphing procedure (Jentsch, 2013). The SRES A2A scenario represents high growth and a global 3.5 °C warming relative to 1990 by 2100 (Nakicenovic et al., 2000). This led to 165 (3x52) TMY files.

A section of a one-story office building for six persons was modelled as one thermal zone in EnergyPlus, and uniform probability density functions (PDFs) of 24 input parameters were defined; see Petersen et al. (2019) for further details. A total of 1000 Latin hypercube samples was generated from the PDFs and implemented in 1000 individual EP models of the office section. These models were simulated for all 208 (4x52) TMY files resulting in a total of 208,000 EP simulations.

As mentioned in the introduction, Wang et al. [18] reported briefly on the construction of the Danish DRY2013 that has to be applied when documenting

fulfillment of the energy performance and overheating criteria in the Danish Building Code (BR18, 2018). The report claims that the dataset is 'representative for the largest possible share of the Danish building stock given the available measurements' but does not contain any further documentation, specifications, or reference to the method used for establishing the DRY2013 dataset. Neither does the other reports about DRYs for Denmark (Wang et al. 2012; Nielsen, 2019). What can be derived from the reports is that the DRY2013 dataset contains one year of hourly weather parameters built from observed weather data for 12 typical months. The observed data comes from three different weather stations located in the eastern part of Denmark, and that only data from one station is used per parameter in the DRY2013 dataset. It is of interest to investigate how representative the use of DRY is for Denmark as a whole when compared to the local TMYs and the morphed local TMYs. The 1000 individual EP models were therefore also simulated using the DRY2013 weather file. The energy need for heating, cooling, and mechanical ventilation was extracted for all of the above-mentioned simulations and are presented in the result section.

The sensitivity analysis on how the 24 input parameters with an ascribed PDF affects the variability of the simulation output was performed by analysing the total-order effects (S_{Ti}) generated using the Sobol' method (Sobol', 1993) the same way as described by Kristensen and Petersen (2016). N=1000 Latin hypercube samples from the PDFs of the 24 input parameters were generated resulting in 26 000 EP models to be simulated. DRY2013 was morphed to the future climate scenarios DRY2020s, DRY2050s, and DRY2080s using CCWorldWeatherGen. The EP models were simulated with DRY2013 and morphed DRYs resulting in 104 000 simulations. The 95% confidence bounds of S_{Ti} for each weather scenarios were derived using 200 bootstrap samples.

Results

Morphed weather data analysis

Figure 1 illustrates the mean outdoor temperature of the morphed local TMYs on a map of Denmark. The grid is generated in Matlab using the interpolation option 'nearest' in the 'grid data' function. The grid size corresponds to approx. 7.5x7.5 km on the map. Figure 1, (top/left) shows that the annual average outdoor temperature for DRY is 8.1 °C while it is 1 °C higher (9.1 °C) for the average of all historical local TMYs. The average annual temperature across the TMY locations varies less than ±1 °C. In the morphed 2020s scenario (Figure 1, top/right), the average of all morphed local TMYs increased by 1.1 °C to 10.2 °C compared to the historical data. The increasing trend continues for the 2050s (Figure 1, bottom/left) with an increase of 1.2 °C
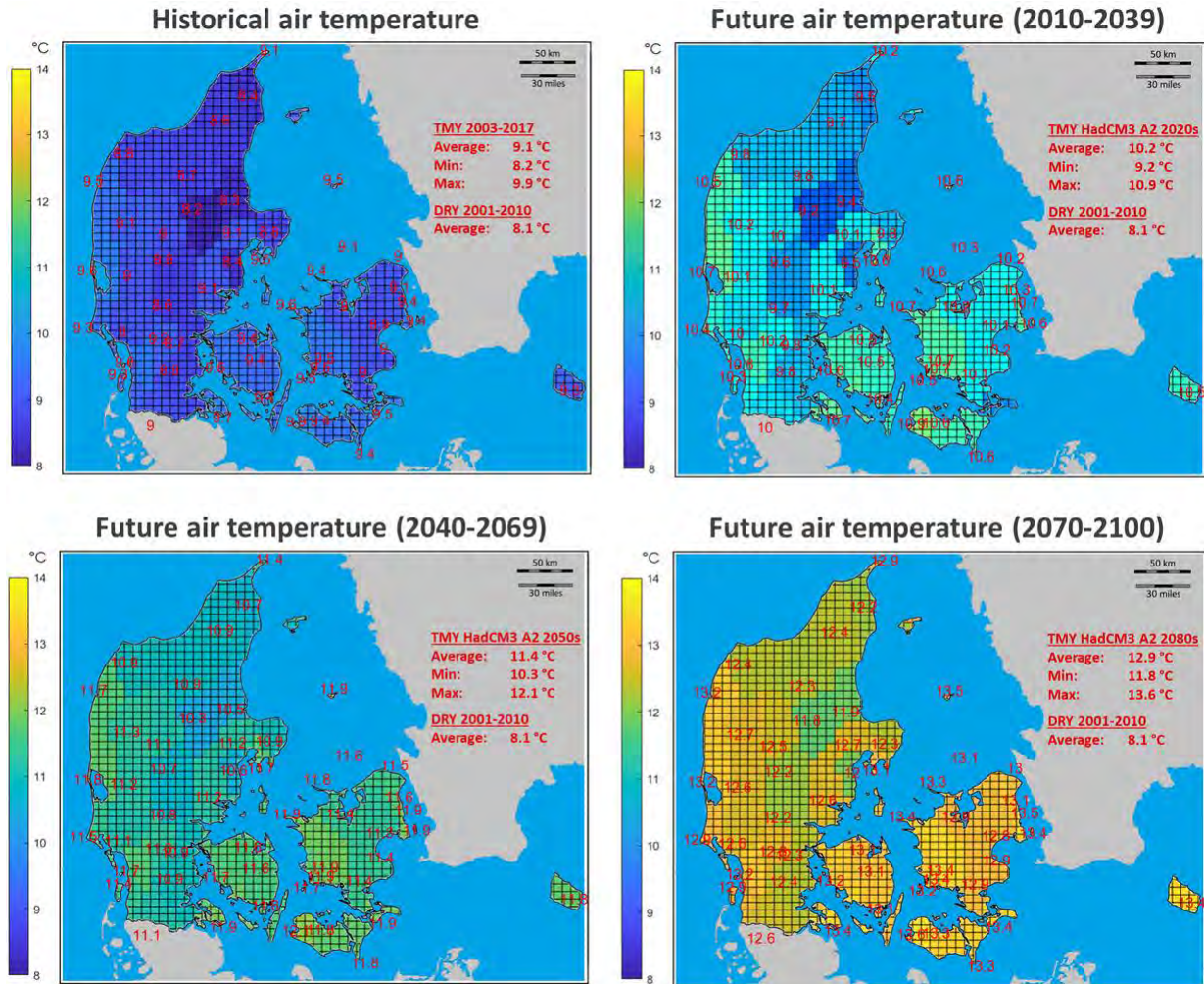
Figure 1: Local outdoor temperature now and in climate change scenarios.

to 11.4 °C, and another 1.5 °C to 12.9 °C for the 2080s (Figure 1, bottom/right). This corresponds to the mean warming of approx. 3.8 °C for Denmark by 2100. The slight deviation from the warming of 3.5 °C could be because that TMY data morphed in this study is not generated from the same 1961–1990 baseline climate data as the HadCM3 model runs. On the other hand, the HadCM3 'morphed' weather data that is based on the 'general circulation model', which is the case for CCWorldWeatherGen, are likely to underestimate future climate impacts under temperate climates with maritime influence (like Denmark) compared to more detailed 'regional climate model' data of the same emissions scenario family (Jentsch, 2013).

Figure 2 (left) illustrates the monthly mean temperatures of the datasets in the analysis including the former Danish DRY from 1995. DRY2013 is, in general, colder in the heating season months Oct-Mar than the TMY datasets; in fact, there are three months where the mean monthly temperature in DRY2013 is lower than the lowest average of all TMYs (Mar, Nov, Dec). Especially March seems unusually low; 3.1 °C lower than the lowest mean in the TMYs. The mean temperatures in the other months of the year are quite alike but DRY2013 is a little warmer in July

and August. It is also noted that there is a rather large difference in mean for the TMYs in each month. The monthly mean temperatures in the climate change scenarios have – with few exceptions the same magnitude of increase as the mean annual temperatures.

Figure 2 (right) illustrates the monthly mean global solar radiation on a horizontal plane. The mean solar radiation for DRY2013 and DRY1995 are much lower in May-July compared to the mean of the TMYs but they are not outside their noticeable large min-max range. The climate change scenarios only result in slightly increased solar radiation in the summer and fall months.
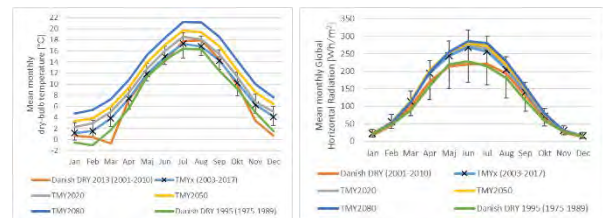
Figure 2: Monthly mean values of weather data.

Building simulation

Figure 3 and 4 illustrates the mean heating and cooling output, respectively, from the 1000 EP simulation for
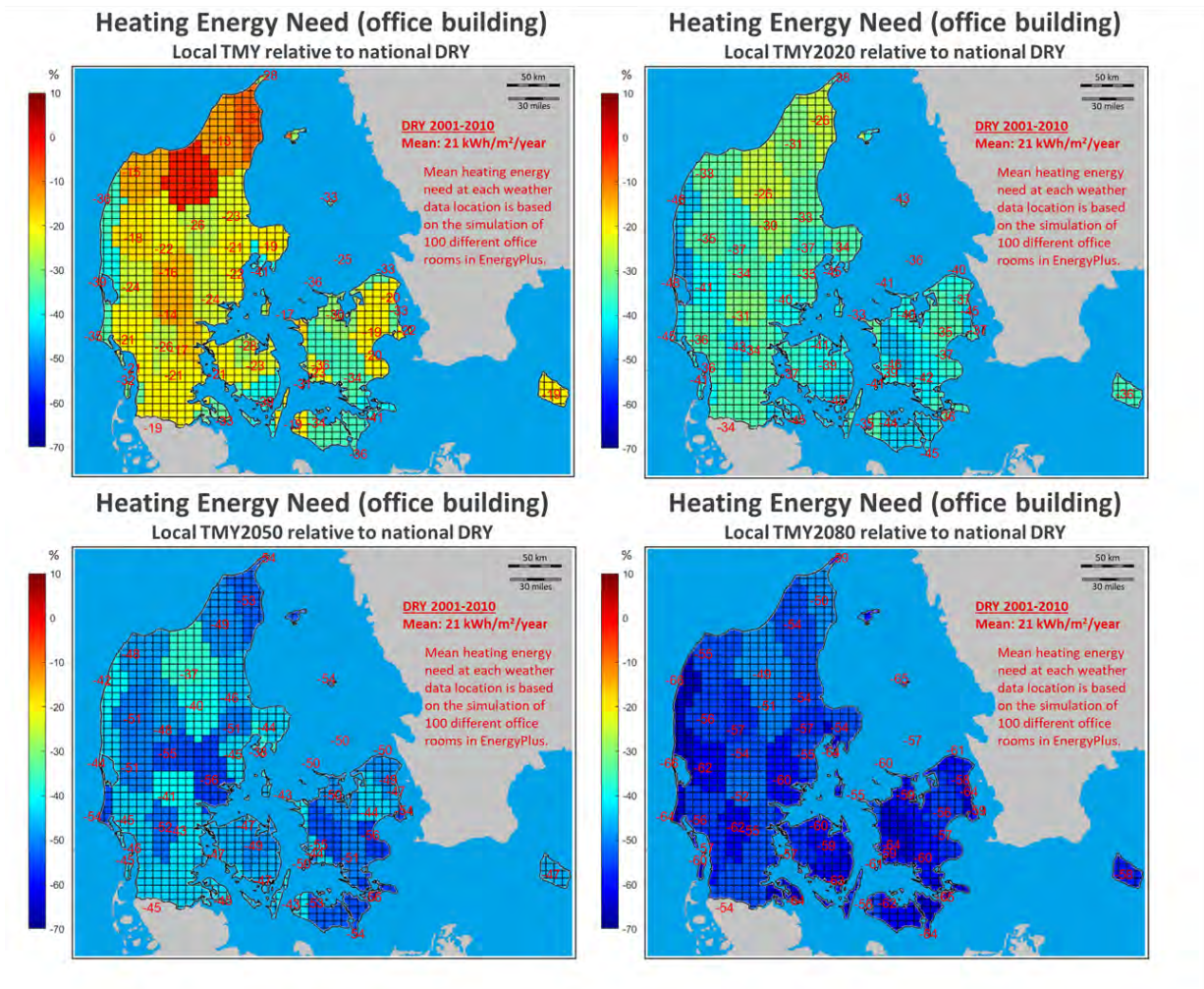
Figure 3: Local heating energy needs now and in climate change scenarios relative to DRY2013.

each TMY location relative to DRY2013. The energy need for heating and cooling for the historical TMYs is, in general, lower than for DRY; in fact, some locations do not have a cooling need according to TMY. Only a few locations have a higher cooling need.

In the 2020s scenario, the heating need is getting lower and the cooling need is getting higher for all TMy locations; more locations exceed the cooling need calculated with DRY2013. This development continues in the 2050s where it is almost only the west coast of Jutland that still has a cooling need lower than DRY2013. In the 2080 scenario, the cooling need is >200% and the heating need is <50% for the vast majority of the country.

Sensitivity analysis

Figure 5 illustrates the simulation outcome from the 1000 EP models for DRY2013 and its three morphed scenarios. The mean heating need drops and the spread is decreased as a function of the scenario time frame; the tendency is opposite for the cooling need.

The results from a sensitivity analysis on how the 24 building design parameters affect the variability of the simulation output using DRY2013 and the climate change scenarios, respectively, are shown in Figure 6. The group

of most important parameters is not changed due to the climate change scenarios but a shift in priority seems to take the form: While the importance of passive means such as window area, solar heat gain coefficient (SHGC), and night ventilation drops slightly as a function of the scenario time frame, the coefficient of performance of the cooling system (COP) is getting increasingly more important. This seems reasonable as it is the outdoor temperature that is affected by climate change; this reduces the potential for night cooling and increases the importance of effectively cooling down the outdoor air before supplying it to the indoors. Consequently, the window variables get less important as they govern solar heat gain which is not affected much by the climate change scenarios.
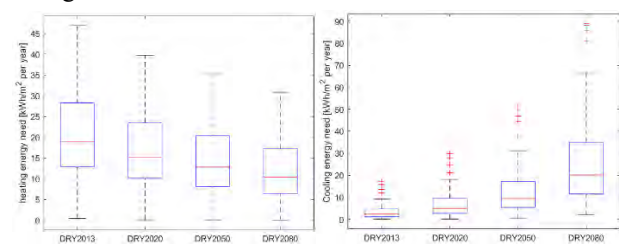
Figure 5: Simulated heating and cooling need now (DR2013) and in climate change scenarios.
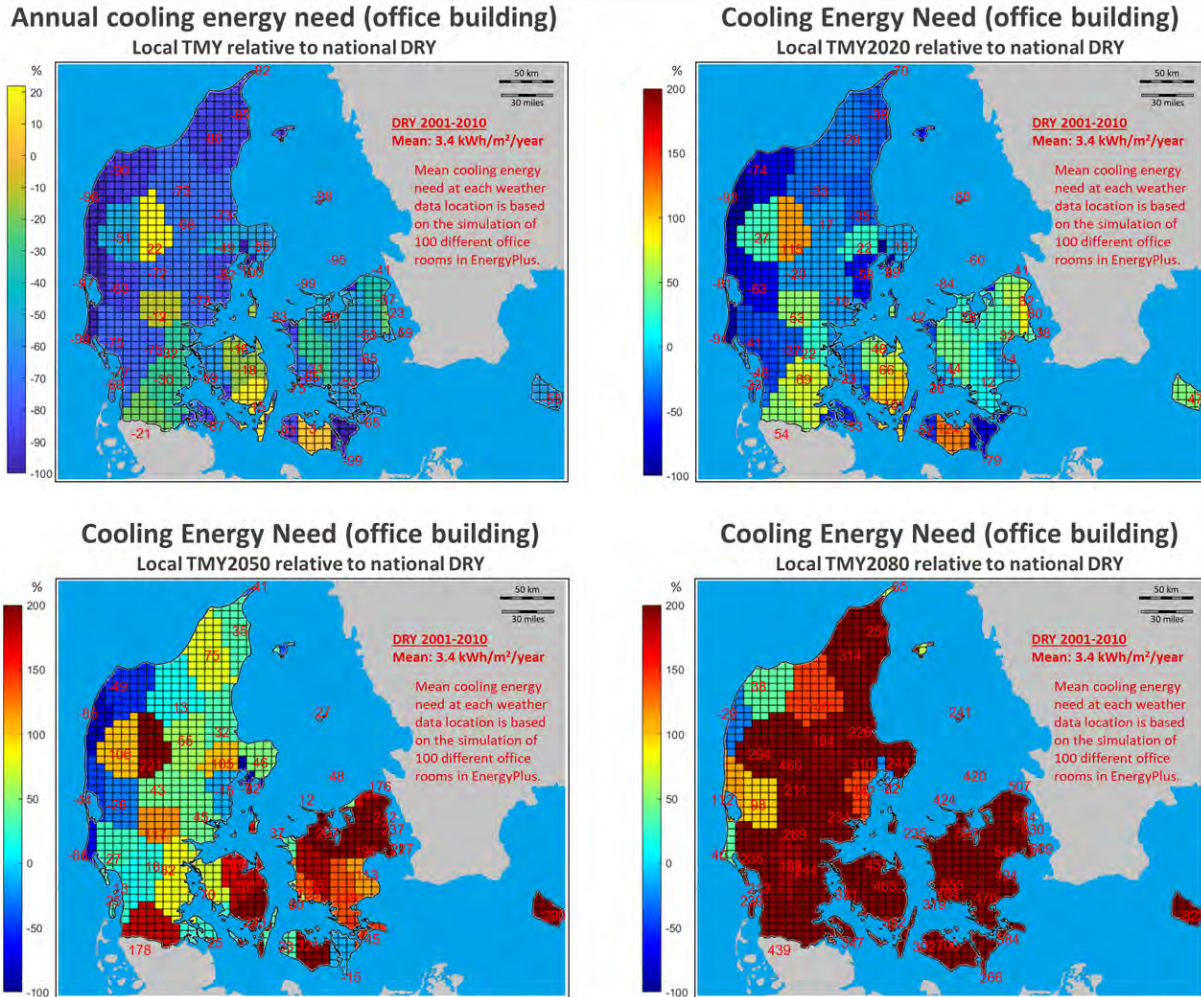
Figure 4: Local cooling energy needs now and in climate change scenarios relative to DRY2013.
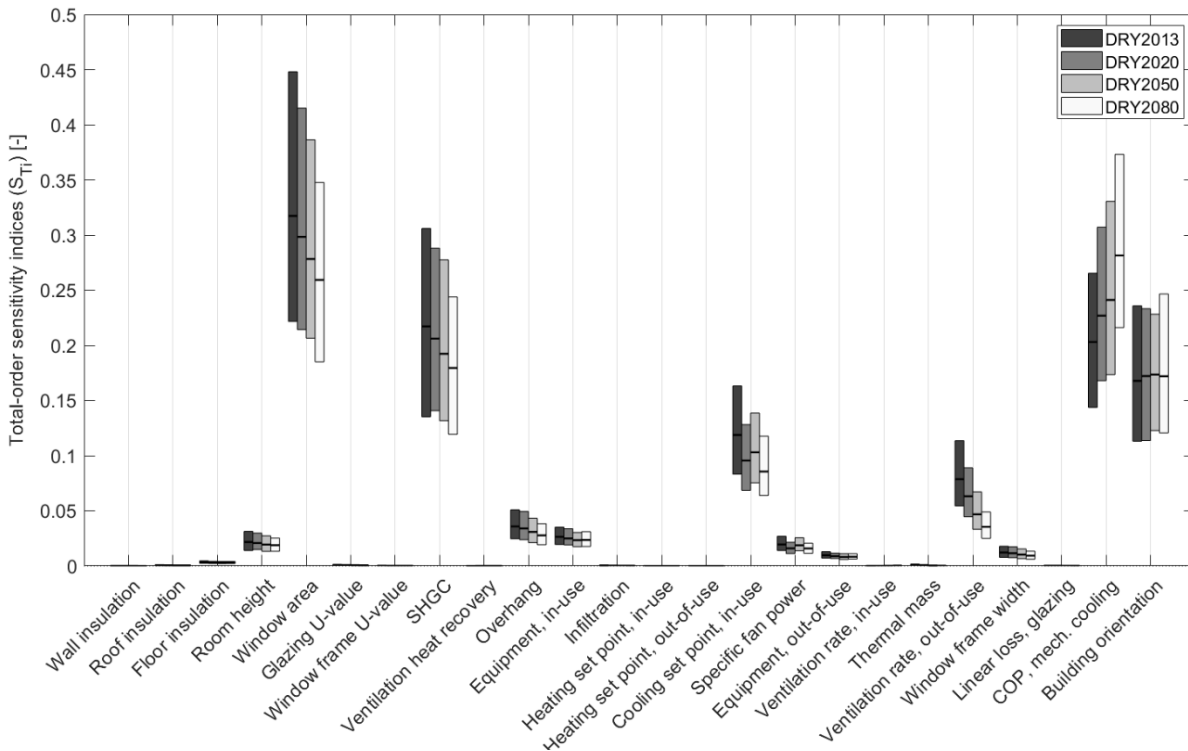
Figure 6: Results from the sensitivity analysis using DRY2013 and the climate change scenario.

Conclusion

The results of the study indicate that the current Danish practice of using mean weather data constructed from historical data for T-BPS for informing design decisions is not appropriate if building designs are to be resilient to climate change. There are several options for integrating considerations about the variability of annual weather conditions and climate change into a more climate change-resilient design practice. This paper provides a comprehensive list and discussion of these options; future research should investigate these in a Danish context carefully as an input to a discussion on changing practice regarding design weather conditions. Furthermore, sensitivity analysis indicates that variability in energy performance is becoming less sensitive to passive design; increasing outdoor temperatures due to climate change makes the energy performance more sensitive to the energy efficiency of mechanical cooling systems. This change of priorities should also be integrated into the design practice of today.

References

Al-Mofeez I.A., M.Y. Numan, K.A. Alshaibani, and F.A. Al-Maziad (2012). Review of typical vs. synthesized energy modeling weather files. *Journal of Renewable and Sustainable Energy 4*, 012702.

Barnaby, C.S., and D.B. Crawley (2011). Weather data for building performance simulation. In Hensen, J.L.M., Lamberts R. *Building Performance Simulation for Design and Operation*. Routledge. London (UK).

Belcher, S., J. Hacker and D. Powell (2005). Constructing design weather data for future climates. *Build. Serv. Eng. Res. Technol. 26*, 49–61.

Brisson E., M. Demuzere, P. Willems and N.P.M. van Lipzig 44 (2015). Assessment of natural climate variability using a weather generator. *Clim. Dyn. 44(1-2)*, 495–508.

BR18 (2018). Danish Transport- Housing- and Construction Authority, Danish Building Code. http://bygningsreglementet.dk/. (Last accessed 2020-05-14)

Broholt, T.H. and S. Petersen (2020). Vejrdatafiler.dk. http://vejrdatafiler.dk/.

CCWorldWeatherGen (2013). The Sustainable Energy Research Group (SERG). University of Southampton. http://www.energy.soton.ac.uk/ccworldweathergen/ (Last accessed: 2020-05-14)

Climate.OneBuilding (2019). Climate.onebuilding.org, http://climate.onebuilding.org. (Last accessed: 2020-05-14)

Crawley D. and L.K. Lawrie. Rethinking the TMY: Is the 'typical' meteorological year best for building performance simulation? *Proceedings of BS2015 14th Conf. Int. Build. Perform. Simul. Assoc.* Hyderabad (IN), 7-9 December 2015.

Crow L.W. (1981). Development of hourly data for weather year for energy calculations (WYEC), *ASHRAE J. 23*, 37–41.

Eames, M., T. Kershaw and D. Coley (2011). On the creation of future probabilistic design weather years from UKCP09. *Build. Serv. Eng. Res. Technol. 32*, 127–142.

Ferrari D. and T. Lee (2008). Beyond TMY: Climate data for specific applications. *Proceedings from ISES-AP 3rd Int. Sol. Energy Soc. Conf. – Asia Pacific Reg. Inc. 46th ANZSES Conf.* Sydney (AUS), 25-28 Nov. 2014.

Guo S., D. Yan, T. Hong, C. Xiao and Y. Cui (2019). A novel approach for selecting typical hot-year (THY) weather data. *Applied Energy 242*, 1634-1648.

Hacker J., S. Belcher and A. White (2014). *Design Summer Years for London (CIBSE report TM49)*. London (UK).

Herrera, M., S. Natarajan, D.A. Coley, T. Kershaw, A.P. Ramallo-González, M. Eames, D. Fosas and M. Wood (2017). A review of current and future weather data for building simulation. *Building Services Engineering Research and Technology 38*(5), 602–627.

International Organisation for Standardisation (2005). *Hygrothermal performance of buildings — Calculation and presentation of climatic data — Part 4: Hourly data for assessing the annual energy use for heating and cooling (ISO 15927-4:2005)*.

IPCC (2013). *Climate Change 2013: The Physical Science Basis. Contribution of Working Group I to the Fifth Assessment Report of the Intergovernmental Panel on Climate Change.* Stocker, T.F., D. Qin, G.-K. Plattner, M. Tignor, S.K. Allen, J. Boschung, A. Nauels, Y. Xia, V. Bex and P.M. Midgley (eds.). Cambridge University Press, Cambridge (UK) and New York City (USA).

ISD (2020). National Oceanic and Atmospheric Administration, Integrated Surface Database. https://www.ncdc.noaa.gov/isd. (Last accessed: 2020-05-14)

Jentsch, M.F., P.A.B. James, L. Bourikas, A.S. Bahaj (2013). Transforming existing weather data for worldwide locations to enable energy and building performance simulation under future climates. *Renew. Energy 55*, 514–524.

Jensen J.M., and H. Lund (1995). *Design reference year – a new Danish reference year (DTU report LFV-281)*. Kgs. Lyngby (DK).

Kristensen M.H. and S. Petersen (2016). Choosing the appropriate sensitivity analysis method for building energy model-based investigations. *Energy Build. 130*, 166–176.

Levermore G.J. and J.B. Parkinson (2006). Analyses and algorithms for new Test Reference Years and Design

Summer Years for the UK. *Build. Serv. Eng. Res. Technol. 27,* 311–325.

Liu, C., W. Chung, F. Cecinati, S. Natarajan and D. Coley (2019). Current and future test reference years at a 5 km resolution. *Building Services Engineering Research and Technology 0*(0), 1-25.

Liu, C., T. Kershaw, M.E. Eames and D.A. Coley (2016). Future probabilistic hot summer years for overheating risk assessments. *Build. Environ. 105*, 56–68.

Lund H. (1995). *The design reference year user's manual (DTU report LFV-274)*. Kgs. Lyngby (DK).

Lundström L. Shiny Weather Data App. https://rokka.shinyapps.io/shinyweatherdata/ (Last accessed: 2020-05-14).Mesan (2020). Swedish Meteorological and Hydrological Institute. https://www.smhi.se (last accessed: 2020-05-14).

Moss, R., M. Babiker, S. Brinkman, E. Calvo, T. Carter, J. Edmonds, I. Elgizouli., S. Emori, L. Erda, K. Hibbard, R. Jones, M. Kainuma., J. Kelleher, J.F. Lamarque, M. Manning, B. Matthews, J. Meehl, L. Meyer, J. Mitchell, N. Nakicenovic, B. O'Neill, R. Pichs, K. Riahi, S. Rose, P. Runci, R. Stouffer, D. van Vuuren, J. Weyant, T. Wilbanks, J.P. van Ypersele, M. Zurek (2008). Towards New Scenarios for Analysis of Emissions, Climate Change, Impacts and Response Strategies. IPCC expert meeting report, 19–21 September. Noordwijkerhout (NL).

Nakicenovic N., J. Alcamo, A. Grubler, K. Riahi, R.A. Roehrl, H-H Rogner and N. Victor (2000). *Special Report on Emissions Scenarios (SRES), A Special Report of Working Group III of the Intergovernmental Panel on Climate Change.* Cambridge University Press. Cambridge (UK).

Narowski P., M. Janicki and D. Heim (2013). Comparison of untypical meteorological years (umy) and their influence on building energy performance simulations. *Proceedings of BS 2013 13th Conf. Int. Build. Perform. Simul. Assoc.*, Chambéry (F), 25-30 Aug. 2013.

National Center for Atmospheric Research, Research Data Archive, (2020). https://rda.ucar.edu/.

Nielsen K.P. (2019). 2001-2010 Danish Design Reference Year. Datasets, Update and supplementary Datasets (DMI TR18-20). Copehnhagen (DK).

Nik V.M. (2016). Making energy simulation easier for future climate – Synthesizing typical and extreme weather data sets out of regional climate models (RCMs). *Appl. Energy 177*, 204–226.

Pernigotto G., A. Prada and A. Gasparella (2020). Extreme reference years for building energy performance simulation. *Journal of Building Performance Simulation 13*(2), 152-166.

Petersen S., M.D. Knudsen (2017). The economic value of indoor climate as design criterion in office building retrofit. *Building and Environment 122*, 15–22.

Petersen S., M.H. Kristensen and M.D. Knudsen (2019). Prerequisites for reliable sensitivity analysis of a high fidelity building energy model. *Energy and Buildings 183*, 1-16.

Pope, V., M.L. Gallani, P.R. Rowntree, R.A. Stratton (2000). The impact of new physical parameterizations in the Hadley Centre climate model: HadAM3. *Clim. Dyn. 16*, 123-146.

Ramon D., K. Allacker, N.P.M. van Lipzig, F. De Troyer and H Wouters (2018). Future Weather Data for Dynamic Building Energy Simulations: Overview of Available Data and Presentation of Newly Derived Data for Belgium. In Agarwal A.K., Pandey A. *Energy Sustainability in Built and Urban Environments*. Springer. New York City (USA).

Remund J., S. Müller, C. Studer, R. Cattin (2018). *Meteonorm Handbook part I: Software (7th ed., Meteotest)*. Bern (CH). http://www.meteonorm.com.

Renné D.S. (2016). Resource assessment and site selection for solar heating and cooling systems. In Wang R.Z., Ge T.S. *Adv. Sol. Heat. Cool.* Woodhead Publishing. Cambridge (UK).

Sobol' I.M. (1993). Sensitivity estimates for nonlinear mathematical models. *Math. Model. Comput. Exp. 1* (4), 407–414.

Thevenard D.J. and A. Brunger (2002). The development of typical weather years for international locations: Part I, algorithms. *ASHRAE Trans. 108*, 376–383.

Wang P.G., M. Scharling and K.P. Nielsen (2012). 2001–2010 Design Reference Year for Denmark. Datasæt til teknisk dimensionering (DMI TR12-17), Copenhagen (DK).

Wang P.G., M. Scharling, C. Kern-Hansen, K.B. and Wittchen (2013a). 2001–2010 Dansk Design Reference Year. Supplerende datasæt (DMI TR13-18). Copenhagen (DK).

Watkins R., G. Levermore and J. Parkinson (2013). The design reference year – a new approach to testing a building in more extreme weather using UKCP09 projections. *Build. Serv. Eng. Res. Technol. 34*, 165–176.

Wang P.G., M. Scharling, K.P. Nielsen, K.B. Wittchen and C. Kern-Hansen (2013b). *2001–2010 Danish Design Reference Year. Reference Climate Dataset for Technical Dimensioning in Building, Construction and other Sectors (TR13-19)*. Copenhagen (DK).

Wilby, R.L., T.M.L. Wigley (1997). Downscaling general circulation model output: a review of methods and limitations. *Prog Phys Geog. 21*, 530–548.

Yassaghi, H. and S. Hoque (2019). An Overview of Climate Change and Building Energy: Performance, Responses and Uncertainties. *Buildings 9*, 166.

Heat Pumps and Air-Conditioning Systems

Simulation and parametric study of a building integrated transpired solar collector heat pump system for a multifamily building cluster in Sweden

Puneet Saini[1,2], Frank Fiedler[1], Emmanouil Psimopoulos[1,2], Benedetta Copertaro[1], Joakim Widén[2], , Xingxing Zhang[1]

[1]Department of Energy and Built Environment, Dalarna University, Sweden
[2]Department of Engineering Sciences, Civil Engineering and Built environment, Uppsala University, Sweden

Abstract

Solar integrated building envelopes represent a significant energy harvesting potential in an era of decentralized building energy systems. This paper aims to simulate an energy system that consists of a transpired air solar collector component for a multifamily building cluster in Sweden. The energy system consists of an unglazed transpired solar collector in conjunction with air ventilation unit and exhaust air heat pump. The hot air from the solar collectors is used to increase the brine temperature at heat pump evaporator inlet to improve its coefficient of performance. The exhaust air heat pump is used to meet space heating and hot water demand for the buildings. The energy system is modelled using TRNSYS simulation program. The associated controls of the energy systems are optimized to increase the seasonal performance factor of the complete system, while maintaining the optimal performance of various subsystems. The quantification of the energetic benefits obtained from the proposed energy system is also presented using various key performance indicators. Furthermore, sensitivity analysis of different collector areas and operating variables such as airflow rate of the collector is conducted. The results show that the seasonal performance of the simulated energy system is 1.43 and the annual collector utilization factor is 0.18. Furthermore, the variation of the collector airflow rate has a positive impact on system performance, with an increase of 2 % in the annual heat pump coefficient of performance.

Introduction

The thermal demand for residential buildings in Nordic climates is characterized by large space heating (SH) loads in the winter and relatively constant domestic hot water (DHW) demand over the year (Chauvet. L,1994). Most of the thermal demand is often met by district heating (DH) networks. Even though DH has a low carbon footprint in Sweden, still the availability of the network is limited by the distance of the consumer from the central heat generation plant (Nilsson.S, 2007) In the non-availability of the DH, heat pumps (HP) are often used to meet the SH and DHW demand in the buildings (Davis.A, 2017). More specifically, air-source heat pump (ASHP) represents the state of the art in the Swedish climates to fulfil heating demand in the residential sector (Poppi.S, 2017). In a typical single-family house, ASHP

is often connected to thermal store which is used to meet SH and DHW loads (Poppi.S, 2017). The performance of the ASHP is negatively affected by a decrease in ambient air temperature, assuming all other influencing parameters (e.g load temperature, operational capacity) remain unchanged. In the past few years, the exhaust air heat pump (EAHP), representing a special ASHP, has evolved as an efficient solution due to the capability a) of recovering the energy from the ventilation air of the building and b) of improving the ASHP performance due to the elevated temperature on the source side of HP (Fehrm.M,1990). However, a major share of the EAHP are installed in newly built single family houses in Sweden, as ventilation system and ducting can be designed to extract the air from the building to a centralised point.

Even though the seasonal performance factor (SPF) for EAHP is usually higher than the typical ASHP given the same boundary conditions, still there exist possibilities to alleviate the system performance by integrating various solar technologies such as PV, solar thermal, and hybrid technology (Wang.X, 2020). For instance, Liu et al. experimentally investigated a solar-driven exhaust air thermoelectric heat pump recovery system. The results showed that the proposed system can obtain higher fresh air supply temperature (12 °C higher than the indoor air temperature) in winter and lower fresh air (6 °C) supply temperature in Summer (Lui.Z, 2019). Psimopoulos et al. develop a techno-economic analysis of control algorithms for an EAHP system coupled to a photovoltaic system with the aim to minimize the building energy usage and maximize self-consumption. The developed method resulted to reduce energy usage by 5–31 % and the annual net cost by 3–26 % (Psimopoulos.E, 2019). Safijahanshahi and Salmanzadeh numerically simulated the performance of an air-to-air HP combined with an unglazed transpired solar collector (TSC). The results showed that the solar assisted heat pump could decrease the electricity consumption and the CO_2 generation up to 10 % with respect to a conventional air-to-air HP (Safijahanshahi.S, 2019). Similarly, Perisoglou et al . presented the performance of a TSC used as a preheater for an air to air HP installed in a demonstration house in Wales, UK. The results showed that the system contributed to 15 % of the heating and cooling demand in one year, which can be translated into £100 to £200

savings per year compared to a conventional heating source (Perisoglou.E, 2017). In their study Januševičius et al. validated a simulation model of a system that combines an unglazed TSC assisted with an ASHP. The results demonstrated good conformity between model and experimental performance (Januševičius.K, 2016). Saini et al. show that the variation in collector air flow rate can increase the savings up to 60 % in an TSC-ASHP system configuration analyzed for Swedish climates (Saini.P, 2019)

Amongst the various available solar technologies, TSCs are specially designed collectors that can easily be integrated with building facades and therefore can be installed potentially in a large area to heat the ambient air to meet the residential energy needs. Unlike state-of-the-art flat plate air collectors, TSC is made of the corrugated metallic sheet with perforation on the top surface to create a pressure difference across the plate while ensuring heat transfer form heated plate surface to the ambient air. The distribution of the holes on the plate surface results in asymptomatic boundary layer thickness leading to almost fixed convection losses, irrespective of the collector width (Kutscher.F, 1993). The distinct advantages of TSCs are related to their simple construction and installation on the building envelope, lack of hydraulic components, and well architectural integration with the building walls and roof.

As it can appreciated from the already mentioned state of the art, there is very limited literature which addresses the integration of TSC in conjunction with EAHP system, especially for Nordic climates, where the sensible parameters for system design and operation stay unclear. Therefore, this paper aims to fill the above-mentioned research gaps by analysing an EAHP system coupled with a TSC (in a series arrangement) for SH and DHW supply to a residential building cluster in Swedish climatic location. The specific objectives of the study are 1) the simulation and the energetic analysis of integrated TSC-EAHP system for multifamily building cluster in Sweden; 2) to perform a sensitivity analysis to identify the effect of the critical parameters, such as collector airflow control strategies and collector area on the proposed TSC-EAHP system performance. The overall structure of this paper is depicted as below: Next section illustrates the research methodology and defines the system input parameters as well as boundary conditions, followed by main results, insights and findings, the conclusion is finally summarized in last section

Research method and boundary Conditions

The study follows a systematic approach starting by the definition of various boundary conditions of the energy system, the selection of the most appropriate simulation tool and the relevant key performance indicators (KPIs) in the context of complete system performance. The data from a residential building cluster located in Sunannsjö,

.
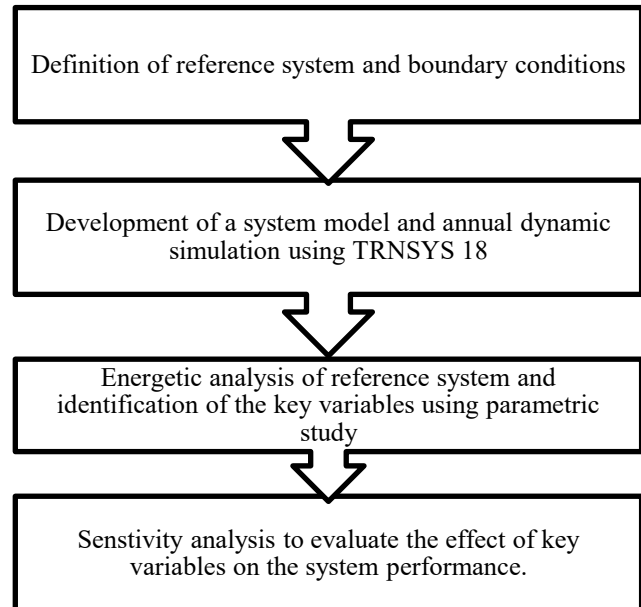
Figure 1 : Methodology used for the analysis

Sweden is used to define a reference energy system. As the focus of the study is on comparative analysis of the various energy systems which may require local programming of control strategies therefore TRNSYS (TRNSYS, 2020) simulation tool is used due to its open source code. TRNSYS also has a wide range of components library for solar heating systems and therefore provides higher flexibility compared to other tools such as Polysun (Polysun, 2020) or IDA-ICE (IDA, 2020). The annual dynamic simulation of the energy system is performed and the results are expressed using standard KPIs (such as seasonal performance factor, coefficient of performance etc.) used in most solar heat pump system analysis. The results are further analysed to identify the most critical system variables, and a sensitivity analysis is carried to study the effect of such variables on the system performance. The methodology used in the paper is summarized in Figure 1.

Reference system and system boundaries

To carry a transparent and reliable performance comparison among different systems, it is imperative to define a reference case and boundaries of the energy system. The following subsections address the building characteristics, energy system description, and meteorological conditions for system under study.

Building and loads characteristics

The system chosen for this paper consists of a multifamily dwelling unit made of three buildings built in 1973. The complex (three buildings) includes 53 apartments over 2 floors and a basement, having a lot size of 4488 m². The envelope is composed by 2146 m² of the total façade area and 1750 m² of the pitched roof. The building walls are insulated with an effective U-value of 0.33 W/(m² · K). The aerial view of the buildings is as shown in Figure 2.

Figure 2: Ariel view of the buildings

The total thermal load of the building consists of SH and DHW load. The total heating load was simulated using a building simulation model in TRNSYS and later calibrated with real measurements within the framework of the project (EnergyMatching, 2020). The annual thermal energy demand for the cluster is 526.7 MWh. The specific SH and DHW demand 109.8 kWh/m² and 26.6 kWh/m² respectively. The monthly variation in the total demand is shown in Figure 3
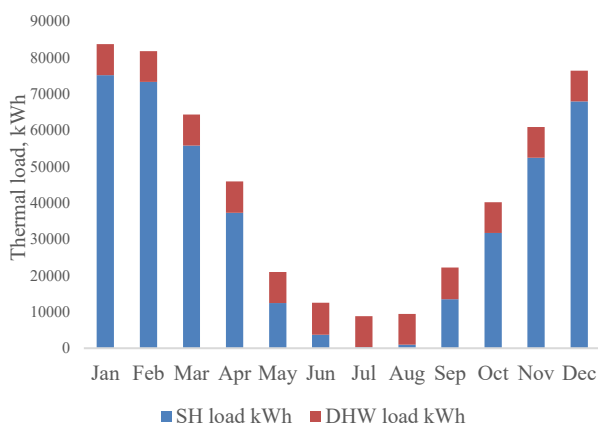
Figure 3 Annual thermal demand of the building cluster

Figure 3 illustrates that up to 80 % of the total demand is for SH and the rest 20 % is due to DHW. The seasonal variation in the SH demand is higher and most of the demand occurs in months with a low ambient temperature. On the contrary, the DHW demand has a small seasonal variation, as the requirement for hot water is consistent over the year.

Reference energy system description

The energy supply system for the buildings consists of a centralised EAHP and an auxiliary pellet boiler. The EAHP is a brine to water type and is designed based on the ventilation air rate of 0.35 l/m² · s available from the various building zones. The EAHP includes a variable speed compressor and has a designed capacity of 45 kW with COP of 4.11 defined at compressor frequency of 90 Hz, and brine (source) & water (load) temperature of 0 °C and 35 °C respectively. The ventilation air at room

temperature from all 3 buildings is extracted and ducted to an air/brine heat exchange unit installed in the attic of each building, which recovers the heat from ventilation air and delivers this heat to HP via a brine circuit. The condenser side of the HP delivers heat either directly to SH circuit, or to a storage tank of 2.5 m³ capacity to meet the DHW load. DHW circuit is designed to supply 55 °C hot water to the user, whereas the maximum allowable heating temperature of HP is 65 °C . The designed supply/return temperatures of SH circuit are 55/45 °C respectively and heat is dissipated using indoor radiator units. The operation mode of HP is determined based on the charging level of the DHW tank, with the priority being the full charging of the DHW tank at maximum HP capacity. A small storage vessel of 0.35 m³ is installed in SH circuit and is used to cater the SH loads when the HP operates in DHW mode. The compressor speed of the HP is varied in SH mode, to achieve the designed radiator inlet temp. If the heat demand of the building exceeds the HP capacity, a pellet boiler is used as a supplementary heat source. TSCs are installed on the south facade with a total collector area of 207.5 m² and tilt of 90°. The hot air from the solar collectors is mixed with extracted building ventilation air and is fed to the air/brine heat exchanger to increase the brine temperature stream and thus the HP performance.

Meteorological parameters

The variation in monthly average global irradiation on the horizontal surface and the vertical South surface is shown in Figure 4. The annual global horizontal irradiation for the location is 971 kWh/m² and has a large seasonal variation. The annual average wind speed and ambient temperature for the location is 3.3 m/s and 4 °C respectively.
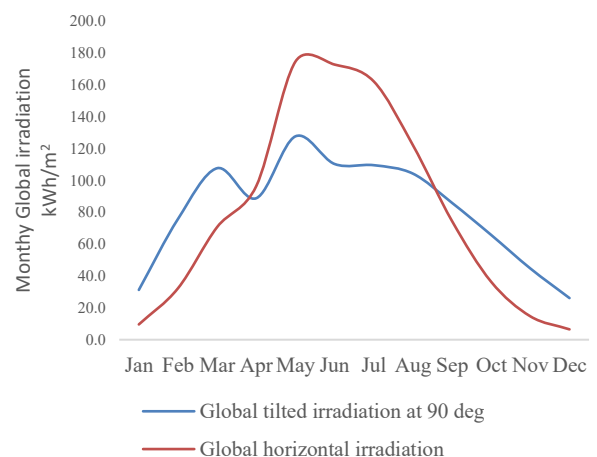
Figure 4 Monthly irradiation variation for project location

TRNSYS model description

The proposed energy system is modelled in TRNSYS 18 using appropriate types available in the components library. A quick overview of components used in the system is given in Table 1 with a brief description.

Table 1 Components overview for the developed model

Key elements	TRNYS type	Description
EAHP	Type 1927	The performance map model uses manufacturer's catalogue data and performance map under wide range of independent variable conditions. A scaling function is used to adapt the HP capacity based on the proposed heating system.
Air brine heat exchanger	Type 508b	This component model the heat transfer from ventilation air to the brine loop of HP.
Storage tanks	Type 158	This type model the DHW storage (2.5 m³) and SH buffer (0.35 m³) using a constant volume storage tank with a vertical configuration.
Auxiliary heater Type	Type 138	This component conditions the existing pellet boiler as a back-up source, with electricity to heat conversion factor of 0.9.
Hydronics	Valves (Type 11)	Control the flow direction in response to the receiving signals.
	Pumps (Type 114 & 742)	Variable speed pumps in SH and DHW circuit and to maintain outlet mass flow and temperature according to set points.
Transpired air solar collector	Type 201	An unglazed transpired plate model developed and validated as part of IEA SHC task 35 (Delisle, V, 2007).
Weather data	Type 15	Ground based weather data of year 2014 for Borlänge location, which is the closest weather station to the project location.
Heating loads	Type 9	One input file for all 3 buildings is used for SH and DHW loads.

System controls

The HP operates in either SH or DHW mode, and is governed by using a differential control (Type 165) to prioritize the DHW tank charging. The HP runs in DHW mode when the water temperature at bottom of DHW tank falls below a set point minus a hysteresis of 6 ℃ . The HP compressor works at full speed in DHW mode to charge the tank as quickly as possible. An external heat exchanger (Type 5) in counterflow mode and a variable speed water pump is used to prepare the hot water. The variation in the inlet DHW temperature is considered based on ambient temperature. When the DHW tank is fully charged, the HP switches to SH mode. The compressor speed is adapted in SH mode using a PID (proportion integration differentiation) controller (Type 22) to reach design supply temp at the radiator inlet. The supply temp to the radiator inlet is varied depending on the ambient temp according to the space heating curve. The mass flow variation in the radiator is obtained using PID controller to generate a control signal based on input parameters and setpoint temperature. The auxiliary electric heater is placed in both SH and DHW circuit and it adapts the capacity to provide heating rate required to reach set points in both circuits. The HP is turned off when the DHW tank is fully charged and SH demand is zero. The solar collector is simulated using Type 201, is mounted vertically on the South facade, and is integrated into a series arrangement with HP where the hot air is indirectly used as the heat source for heat pump evaporator in addition to exhaust ventilation air. The flow rate controls for the TSC are obtained using variable speed fan (Type 147), PID controller and equation blocks to control the fan speed. The fan starts only if the irradiation on the collector plane is more than 100 W/m² and varies the airflow rate to reach an outlet air temperature of more than 21 ℃ , while keeping the minimum collector efficiency limit, and maximum brine temperature limit.

Key performance indicators

The following energetic KPIs are used in this paper for results discussion and system modus operandi.

Component performance figures

Coefficient of performance: The COP of the heat pump is the ratio between heating capacity ($Q_{hp,h}$), and electricity consumption ($P_{el,hp}$), and is given in the Equation 1.

$$COP = \frac{Q_{hp,h}}{P_{el,hp}} \qquad (1)$$

Collector energy utilization ratio: It depicts the performance of solar collector (or field) over a specific period as given in Equation 2, where Q_{coll} is the annual thermal output of solar collector in kWh, G_{coll} is global irradiation on the collector plane in kWh, and A_{coll} is the gross area of the collector in m².

$$\omega_{th} = \frac{Q_{coll}}{\int G_{coll} dt \, A_{coll}} \qquad (2)$$

System performance figures

Total electricity use (P_{el}): It is used to define the electricity used by system components such as HP, auxiliary heater, pumps, and fans, etc. For the given system integrated with the solar collector, total electricity use is described as per Equation 3, where the $P_{el,hp}$, $P_{el,wp}$, $P_{el,aux}$, $P_{el,fan}$ are electricity consumption of HP, water pumps, auxiliary, and fan respectively.

$$P_{el} = P_{el,hp} + P_{el,wp} + P_{el,aux} + P_{el,fan} \qquad (3)$$

In case when the solar collector is not integrated, the power consumption of fans and relevant pumps is not considered.

Seasonal performance factor: SPF is used to express the final energy efficiency of the whole system and is defined as the ratio of total useful thermal energy supplied to the user ($Q_{SH} + Q_{DHW}$) to the total electricity use (P_{el}) of the system. The SPF can be defined as per Equation 4

$$SPF = \frac{Q_{SH} + Q_{DHW}}{P_{el,hp}} \qquad (4)$$

Results

The energy system is simulated with a time step of one minute for a period of one year. The results show that HP supports 51.1 % of total heating load, whereas the rest of the demand is met using the auxiliary heating system. The HP covers all the DHW load and 37 % of the SH load, and the rest of the SH load is covered by Auxiliary (Q_aux_sh) as shown in Figure 5. The annual heat losses from SH (Q_loss_sh) and DHW tank (Q_loss_dhw) are 600 kWh and 4200 kWh respectively.
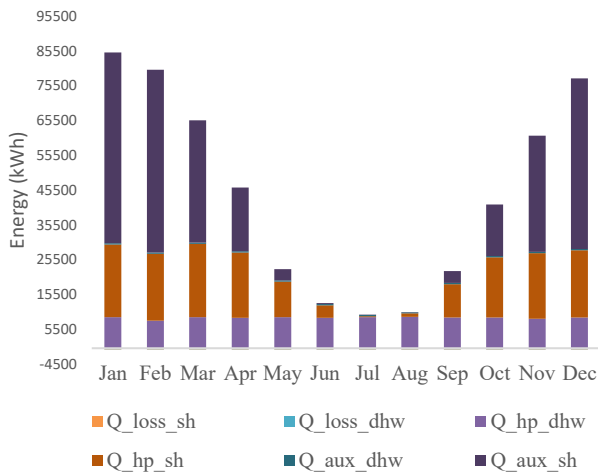
Figure 5 : Energy balance for the proposed system

The total electricity use P_{el} for the system is 368 MWh, and is shown in Figure 6. Over 80 % of electricity is used by the auxiliary heating system, anda 16.8 % is used by HP compressor. Other system components such as fans, and pumps consume 2.1 % of the total electricity. The SPF of the complete system is 1.43. The annual average COP of the heat pump is 4.55 and the monthly variation in HP

COP is shown in Figure 7. The HP performs more efficiently in the winter (November-February) period as it operates majorly in SH mode and thus with a lower water outlet temp. However, in a period from July to August, the SH load is negligible and thus HP operates majorly
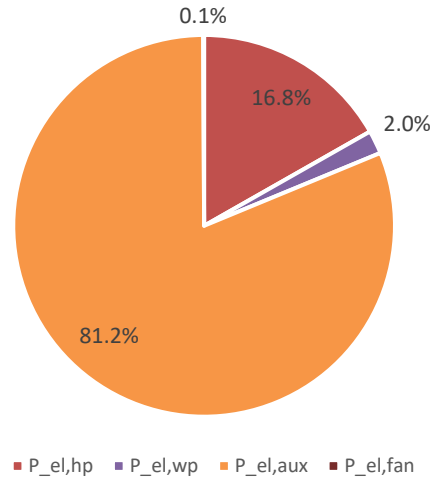
Figure 6 : Electrical consumption % of system components

in DHW mode with a higher designed water temp compared to SH system, which results in a lower COP. The period from April to June and September to October shows a large variation in HP COP, as it operates in almost equally in both DHW and SH mode.
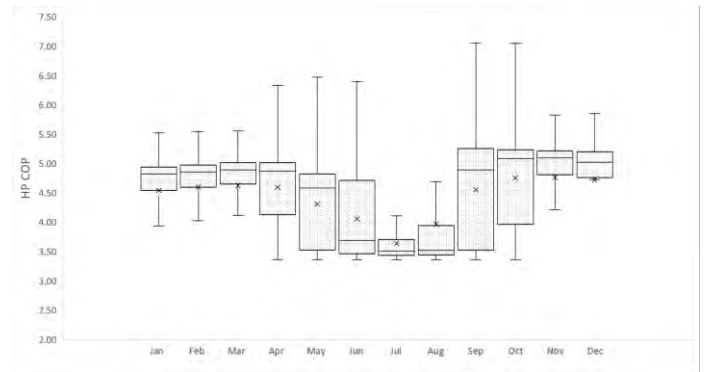
Figure 7 : Monthly variation in HP COP.

The annual thermal output of the solar collector field is 36 MWh, and the annual utilization factor ω_{th} is 0.18. The variation in monthly specific thermal output of the collector is shown in Figure 8.
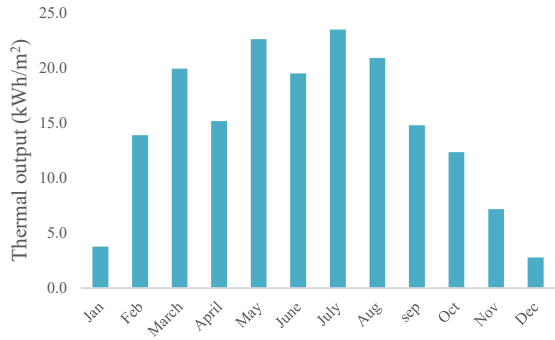
Figure 8 : Thermal output variation for solar collector

Effect of fixed collector flow rate on system performance

In the reference system, the airflow rate behind the collector surface is controlled using a variable speed fan and a PID controller. The fan adjusts the flow rate based on the global irradiation, ambient temperature, and brine temperature to reach a design collector outlet temperature. The minimum and maximum limit of design outlet air temperature is governed by exhaust ventilation air temp and brine temperature into HP respectively. However, in most of the installations, TSCs are installed with fixed design flow, without any fan speed control provision. Therefore, a comparative analysis is carried by simulation of an energy system with a fixed collector flow rate of 60 $kg/(h \cdot m^2)$ as used in most of the real installations. Figure 9 compares the monthly HP COP for reference case (variable flow), and a fixed flow case.
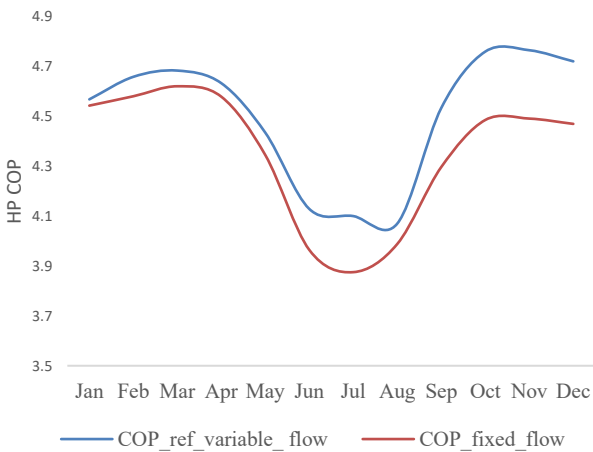
Figure 9 : HP COP variation for various flow conditions

The results show that HP COP is higher with variable airflow, as the variation in airflow allows to leverage the lower irradiation in the winter months to heat the ambient air above the ventilation air temperature, and thus increasing the HP COP. However, in a fixed flow case, the collector outlet air temperature seldom exceeds the ventilation air temperature during winters and thus the HP COP is lower. During summer with high irradiation, the fixed flow control strategy exceeds the maximum limit of design outlet air temperature, and thus the partial volume

of the heated air needs to bypass to keep the HP brine temperature below the maximum limit, and thus the HP COP is lower than variable flow rate case which can provide a higher volume of the air at maximum design temperature. The SPF for the fixed flow case is 0.5 % lower than the reference case.

Effect of collector area on the total electricity use

The effect of TSCs area on the HP performance and total electricity use is investigated. The collector area and fan capacity are varied using a scale factor of 0, 0.5, 0.75, 1.5 in comparison to the reference system. The change in total electricity use (ΔP_{el}) is used as an indicator which is the difference in the total electricity use of the system under study and the of the reference system (P_{el}). The variation in (ΔP_{el}) and SPF for various collector area is shown in Figure 10. The results show that higher collector area results in lower total electricity use, and thus lower ΔP_{el}. A system without any solar collector (scale factor = 0) installation consume nearly 1700 kWh of additional electricity compared to the reference system. Similarly, a small increase in SPF can be seen at higher collector areas.
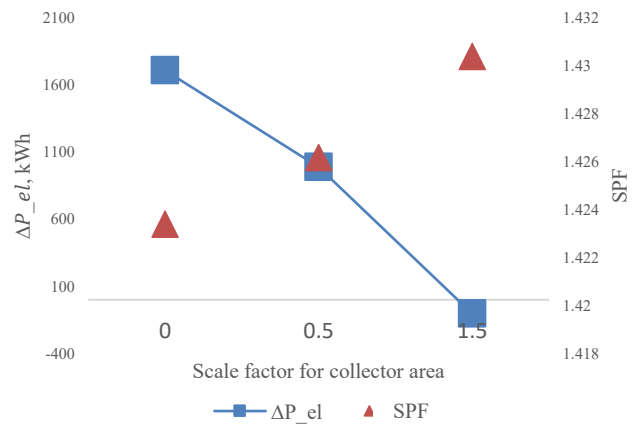
Figure 10 : SPF and electricity variation at various collector area

Conclusions

From the analysis of the results applied to a residential building cluster in Sweden, it can be seen that the integration of TSCs has a small but positive impact on the overall system performance. A system without any solar collector installation consume nearly 1700 kWh of additional electricity compared to the reference system. Furthermore, it can be concluded that the variation of the collector air flow rate can be used as an effective control strategy to increase the annual HP COP and thus the SPF of the overall system to maximize the savings. The result shows that the simulated reference system has SPF of 1.43, and annual collector energy utilization factor of 0.18. The optimization and variation in collector flow rate resulted in a 2 % increase in HP COP and a 0.5 % increase in system SPF in comparison to a fixed flow rate case. Furthermore, the sensitivity analysis shows that an increase in the collector area can result in lower total

electricity use, and thus higher SPF. Compared to the conventional roof-mounted liquid-based solar collector, a transpired solar collector component can be easily mounted on building facades, and does not require any hydronic system. This results in reduction of major space/cost in installation and systems. However, lower irradiation in Nordic climates can be a limiting factor for the annual performance of these collectors, and thus can be a barrier for wide adaption of the technology for the proposed system configuration. The future work includes testing of improved airflow control strategies and system analysis for southern European climates.

Acknowledgment

References

Chauvet, L., Probert, S., & Nevrala, D. (1994). Thermal-energy stores for supplying domestic hot-water and space-heating. Applied Energy, 48(2), 163–190. doi: 10.1016/0306-2619(94)90022-1

Nilsson, S. F., Reidhav, C., Lygnerud, K., & Werner, S. (2008). Sparse district-heating in Sweden. Applied Energy, 85(7), 555–564. doi: 10.1016/j.apenergy.2007.07.011

David, A., Mathiesen, B. V., Averfalk, H., Werner, S., & Lund, H. (2017). Heat Roadmap Europe: Large-Scale Electric Heat Pumps in District Heating Systems. Energies, 10(4), 578. doi: 10.3390/en10040578

Poppi, S. (2017). Solar heat pump systems for heating applications : Analysis of system performance and possible solutions for improving system performance (PhD dissertation). Stockholm. Retrieved from http://urn.kb.se/resolve?urn=urn:nbn:se:du-26498

Poppi, S., Bales, C., Haller, M. Y., & Heinz, A. (2016). Influence of boundary conditions and component size on electricity demand in solar thermal and heat pump combisystems. Applied Energy, 162, 1062–1073. doi: 10.1016/j.apenergy.2015.10.190

Fehrm, M. (1990). Exhaust Air Heat Pump Potential in Europe. Heat Pumps, 733–745. doi: 10.1016/b978-0-08-040193-5.50083-3

Wang, X., Xia, L., Bales, C., Zhang, X., Copertaro, B., Pan, S., & Wu, J. (2020). A systematic review of recent air source heat pump (ASHP) systems assisted by solar thermal, photovoltaic and photovoltaic/thermal sources.

Renewable Energy, 146, 2472–2487. doi: 10.1016/j.renene.2019.08.096

Liu. Z., Li, W., Zhang, L., Wu, Z., & Luo, Y. (2019). Experimental study and performance analysis of solar-driven exhaust air thermoelectric heat pump recovery system. Energy and Buildings, 186, 46–55. doi: 10.1016/j.enbuild.2019.01.017

Psimopoulos, E., Bee, E., Widén, J., & Bales, C. (2019). Techno-economic analysis of control algorithms for an exhaust air heat pump system for detached houses coupled to a photovoltaic system. Applied Energy, 249, 355–367. doi: 10.1016/j.apenergy.2019.04.080

Safijahanshahi, E., & Salmanzadeh, M. (2019). Performance simulation of combined heat pump with unglazed transpired solar collector. Solar Energy, 180, 575–593. doi: 10.1016/j.solener.2019.01.038

Perisoglou.E, Patterson.J, Stevenson.V, Huw .J, (2017) Investigating the application of small scaletranspired solar collectors as air preheaters for residential buildings L,. Cardiff University, Welsh School of Architecture

Januševičius, K., Streckienė, G., Bielskus, J., & Martinaitis, V. (2016). Validation of Unglazed Transpired Solar Collector Assisted Air Source Heat Pump Simulation Model. Energy Procedia, 95, 167–174. doi: 10.1016/j.egypro.2016.09.039

Saini, P. K. (2019). A Preliminary Optimisation and Techno-economic Analysis of Solar Assisted Building Heating System Using Transpired Air Solar Collector and Heat Pump in Sweden (Dissertation). Retrieved from http://urn.kb.se/resolve?urn=urn:nbn:se:du-30537

Kutscher, C. F., Christensen, C. B., & Barker, G. M. (1993). Unglazed Transpired Solar Collectors: Heat Loss Theory. Journal of Solar Energy Engineering, 115(3), 182–188. doi: 10.1115/1.2930047

TRNSYS, University of Wisconsin--Madison. Solar Energy Laboratory. (1975). TRNSYS, a transient simulation program. Madison, Wis. :The Laboratory, (Accessed: May 2020)

POLYSUN: simulation software. http://www.velasolaris.com/espanol/home.html (Accessed: May 2020)

IDA Indoor Climate and Energy . Retrieved from https://www.equa.se/en/ida-ice (Accessed: May 2020)

EnergyMatching, Retrieved from https://www.energymatching.eu/ (Accessed: May 2020)

Delisle, V., Collins, M.R(2007), "PVT Unglazed Corrugated Transpired Solar Collector Model", Canadian Solar Buildings Conference, Calgary, June.

Impact of AC Outdoor Unit Placement on Energy Efficiency

Krishna Patel[1], Rajan Rawal[2]

[1]Faculty of Technology, CEPT University, Ahmedabad, India

[2]Centre for Advanced Research in Building Science and Energy, CEPT University, Ahmedabad, India

corresponding author: rajanrawal@cept.ac.in

Abstract

Growing urbanisation in India has led to the increasing development of high-rise buildings. To maintain the building aesthetics, the outdoor air conditioner (AC) units are stacked withing a recessed space. The heat rejected from these outdoor units (ODU) leads to increase in air temperature of the recessed space. This causes inefficient working of AC units. The paper reports the difference in results when on-site measurement data were compared to CFD simulation results. The on-site measurements were taken for six storeys of an eleven-storey building. The different turbulence models were studied, and it was concluded that the NK turbulence model had the least percentage difference of 8.89% when compared to the site data. Further, NK model was used to study the placement of ODUs in recessed spaces having varying depth and width. When the horizontal distance between the ODUs increased by 1m, maximum condenser on-coil temperatures reduced by 6°C. The studies concluded that, even by allocating lesser area to the recessed space, but by optimizing the depth and width of the space, the temperature increase of the microclimate can be avoided and AC efficiency can be maintained.

Introduction

Currently, India has 6% share in total global primary energy demand which is expected to increase to 11% by 2040. Easy access to electricity and increased prosperity has increased the demand for luxury and better standard of living. As a result, the use of AC has become very common in India. A 40% reduction in electricity demand can be achieved in India if efficient air conditioning systems are adopted (Phadke et al., 2014).

According to the Global cooling report mini-split ACs or Window ACs constitute about 70% of the total AC used (Campbell et al., 2018). Energy used by the Room ACs from 2016 to 2050 is expected to increase five folds in developing countries. Cooling energy demand in India from RACs in 2016 was 94 TWh which is expected to rise to 1890 TWh in 2050. The growth rate of sales of AC unit is 10%-15% in one year. The energy use per-capita for space cooling in India is expected to rise from 72 kWh to 1140 kWh making it one of the world's largest consumer by 2050.

To cater to this, constant efforts are made to increase the efficiency of the AC. Though the system efficiency has been looked upon and improved to a great extent, not much care has been taken in the installation practices. Stacking ODU is one such wrongly implemented practice that results in inefficient working of AC units. The use of split AC has increased due to ease of installation and its cost effectiveness.

Due to growing population and increase in urbanisation, India focuses more on vertical development. As a result, the number of high-rise apartments is constantly increasing. The ODUs in the high-rise apartments are usually stacked vertically one above the other in a recessed space. If they operate simultaneously, they reject heat in the space. Due to buoyancy effect of hot air, it rises upwards. The hot air accumulates near the ODUs at the top. Due to increasing temperatures near the inlet area of the ODUs on top floors, the efficiency of Air Conditioners decreases. As a result, energy consumption increases.

To understand the impact of stack effect due to heat dissipation by the condenser units, number of studies have been done using CFD simulations.

The relation between building height and condenser on-coil temperature was obtained by studying buildings heights of 70m, 98m and 126m. It was concluded that while increasing the height from 70m to 126m, a temperature increase of 2°C was observed (T. T. Chow & Lin, 1999). The on-coil temperatures for a building re-entrant and lightwells were studied. To verify the simulation results, a laboratory experiment was conducted on the model of 1:100 scale. Similar results were obtained by the simulation method and laboratory experiment (Tin Tai Chow et al., 2000). The different shapes i.e. of re-entrants I, L and T were studied (T. T. Chow et al., 2000). The I-shaped, L-shaped and T-shaped re-entrant had maximum temperatures up to 42.5°C, 39.5°C and 37.5°C respectively. Condenser Group Performance Indicator (CGPI) was used to assess the group performance of AC. The impact of depth of recessed space on on-coil temperatures. Depths of the re-entrants were taken to be 6m and 10m and it was observed that in deeper recessed space, mass flow rate reduced by 9% over 16th floor. The studies showed that for inner condenser units deeper recessed space shows a lower rise in temperature compared to shallow space by 42% at 5th storey. For outer

condenser units, the deeper recessed space showed a higher rise in temperature compared to the shallow recessed space by 234% at 5th storey and 53% at the last story (Bojic et al., 2002). As various studies were done for high rise recessed space, the placement configuration of condenser units in a plant room of low-rise residential building were studied. Increment of 1ºC temperature of condenser on-coil temperature, COP of AC unit drops by 3%. The study suggested that the placement of compressors should be such that outlet air should not return to the condenser (T. T. Chow et al., 2002). The impact of building height on the performance of ODUs placed in a plant room with different wind velocity was studied. It was concluded that if condenser on-coil temperatures increases to more than 48°C, the efficiency of AC drops by 9.4% to 25.5% based on entrant area shape and wind velocity (Choi et al., 2005). The impact of louver (angle and spacing) and placement configuration (horizontal-vertical and distance) of ODU, concluded that optimum louver angle and louver spacing was 80° and 50mm respectively. The vertical arrangement proved to be better than horizontal arrangement (Duan et al., 2016).

On-site experiment to understand the horizontal and vertical profile near the outdoor air condenser units was conducted. According to studies, on the 10th and 20th floor, the temperature rose by 10°C and 19°C respectively. Considering the CGPI metric, 18% drop was observed in the performance of AC units (Bruelisauer et al., 2014).

The existing studies are either simulation-based, or experiment-based. The validation of simulation results by on-site experiment data is yet not achieved. This study aims to compare the CFD simulation results with the measurement data collected at site and further optimize the area of recessed space for ODU placement.

Methodology

Data collection on site

The data was collected for 6 storeys of Casa Riva Hotel, Surat. According to The National Building Code of India, Surat has hot and dry climate. The measurements were taken on the outdoor air conditioner units. The ambient air temperature of the outdoor environment was measured using Onset HOBO data loggers at an interval of 5 minutes for 3 hours. The air velocity at the outdoor environment was measured using Velocicalc TSI at 40 minutes interval for 3 hours. For initial conditions, the average values of ambient outdoor air temperature and air velocity were considered. The specifications of the ODU were noted to use them as inputs for modelling.

Table 1: Initial Conditions of Computational Domain

Parameter	Values
Outdoor Ambient Temperature	28.7°C
Wind Velocity	2.2 m/s

Table 2: ODU Specifications for modelling inputs

Parameters	Values
Capacity	3500 Watts (1 Ton)
Dimensions of ODU	0.72m x 0.56m x 0.26m
Inlet air area from Back	0.6m x 0.4m
Inlet air area from Side	0.15m x 0.3m
Area of Outlet Air	0.4m x 0.4m
Volume flow rate at ODU outlet	0.2 m³/s

The condenser on-coil temperature and outlet air temperature were measured at each compressor unit. These temperatures at the ODUs were further compared to the temperatures given by the CFD simulation model.

CFD Simulation Model

Only one façade was taken for simulation. Based on it building dimensions of 5m x 5m were taken. The building height was kept 18m with each floor being 3 meters high. The ODUs were placed at 0.23m from the wall. The depth and the width of window shades were 0.25m and 2.5m respectively. They were placed at 2.1m height from the floor level at each floor. The vertical distance between the ODUs was 3m.
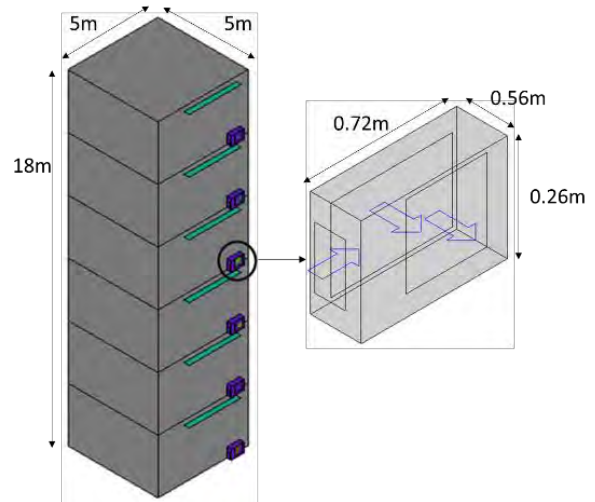
Figure 1: Geometry of the building and ODU

The capacity of the air conditioner was 3.5kW. The measured outlet air flow rate was 0.2 m³/s. The area out outlet and inlet of condensing unit is shown in Figure 2.
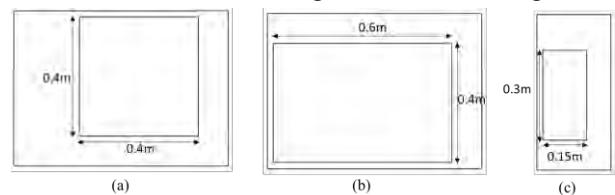
Figure 2: AC outdoor unit dimensions (a) Outlet Area (b) Inlet air (back) (c) Inlet air (side)

Governing Equations:

Mass Conservation Equation:

$$\frac{\partial u_i}{\partial x_i} = 0 \qquad (1)$$

Where,

u_i = Velocity in i direction

x_i = Coordinate

Momentum Conservation Equation:

$$\frac{\partial \rho u_i}{\partial t} + \frac{\partial u_i \rho u_i}{\partial x} = -\frac{\partial p}{\partial x_j} + \frac{\partial}{\partial x_j} \mu \frac{\partial u_i}{\partial x_j} - \rho g_i \beta (T - To) \quad (2)$$

t = time

T = temperature

ρ = density of fluid

p = pressure

μ = viscosity

β = Coefficient of Thermal expansion

T_o = reference temperature

Energy Conservation Equation:

$$\frac{\partial \rho CpT}{\partial t} + \frac{\partial u_j \rho CpT}{\partial x_j} = \frac{\partial}{\partial x_j} K \frac{\partial T}{\partial x_j} + q \quad (3)$$

Cp = specific heat at constant pressure

K = Thermal conductivity

q = Heat source

Turbulence Models used:

To predict the best-suited model, four different mathematical models that are used to analyse the turbulence of the fluid. Turbulence models studied here are: Standard k-ε model, Re-Normalization Group analysis k-ε model (RNG), Modified Production k-ε model (MP), improved LK (Launder-Kato) k-ε model and NK (Nagano and Kim) two-equation heat transfer model.

Standard k-ε model:

$$\frac{\partial \rho k}{\partial t} + \frac{\partial u_i \rho k}{\partial x_i} = \frac{\partial}{\partial x_i}\left(\frac{\mu_t}{\sigma_k}\frac{\partial k}{\partial x_i}\right) + G_s + G_T - \rho \varepsilon \quad (4)$$

$$\frac{\partial \rho \varepsilon}{\partial t} + \frac{\partial u_i \rho \varepsilon}{\partial x_i} = \frac{\partial}{\partial x_i}\left(\frac{\mu_t}{\sigma_\varepsilon}\frac{\partial \varepsilon}{\partial x_i}\right) + C_1 \frac{\varepsilon}{k}(G_s + G_T)\left(1 + C_3 R_f\right) - C_2 \rho \varepsilon^2 \quad (4.1)$$

Where,

$$G_s = \mu_t \left(\frac{\partial u_i}{\partial x_j} + \frac{\partial u_j}{\partial x_i}\right)\frac{\partial u_i}{\partial x_j} \quad (4.2)$$

$$G_T = g_i \beta \frac{\mu_t}{P_{rt}}\left(\frac{\partial T}{\partial x_i}\right) \quad (4.3)$$

$$R_f = -\frac{G_T}{G_s + G_T} \quad (4.4)$$

k = turbulence kinetic energy

ε = turbulence dissipation rate

Re-Normalization Group Analysis (RNG) model: Standard k-ε model consideres the constants based on experimental methods. In the RNG model, the constants have been defined using theoretical methods using Fourier analysis.

Table 3: Constants adopted in RNG model

σ_k	σ_ε	C_1	C_2	C_3	C_μ
0.719	0.719	$C_1(\eta)$	1.68	0	0.085

$$C_1(\eta) = 1.42 - \frac{\eta\left(1 - \frac{\eta}{4.38}\right)}{1 + 0.012\eta^3} \quad (5)$$

$$\eta = \frac{k}{\varepsilon} s \quad (5.1)$$

$$s = \left\{\frac{1}{2}\left(\frac{\partial u_i}{\partial x_j} + \frac{\partial u_j}{\partial x_i}\right)\left(\frac{\partial u_i}{\partial x_j} + \frac{\partial u_j}{\partial x_i}\right)\right\}^{\frac{1}{2}} \quad (5.2)$$

Modified Production (MP) k-ε model: This model is used to compensate the overestimated turbulent kinetic energy, k, near the stagnation point of the standard k-ε model.

Where, $G_s = \rho \check{C}_\mu \frac{k}{\varepsilon} s\Omega \quad (6)$

Where,

$$\check{C}_\mu = \min\left(0.09, \frac{0.3}{1\, 0.35 S^{1.5}}\right) \quad (6.1)$$

$$S = \min\left(20, \frac{k}{\varepsilon} S\right) \quad (6.2)$$

$$s = \left\{\frac{1}{2}\left(\frac{\partial u_i}{\partial x_j} + \frac{\partial u_j}{\partial x_i}\right)\left(\frac{\partial u_i}{\partial x_j} + \frac{\partial u_j}{\partial x_i}\right)\right\}^{\frac{1}{2}} \quad (6.3)$$

$$\Omega = \left\{\frac{1}{2}\left(\frac{\partial u_i}{\partial x_j} - \frac{\partial u_j}{\partial x_i}\right)\left(\frac{\partial u_i}{\partial x_j} - \frac{\partial u_j}{\partial x_i}\right)\right\}^{\frac{1}{2}} \quad (6.4)$$

$$\mu_t = \check{C}_\mu \rho \frac{k^2}{\varepsilon} \quad (6.5)$$

Improved LK (Launder-Kato) k-ε model: The fact that Ω in the above equation gets smaller around the stagnation point is taken into consideration. Based on that G_s is further modified.

$$G_s = \begin{cases} v_t, & \Omega/s \geq 1 \\ v_t S\Omega, & \Omega/s < 1 \end{cases} \quad (7)$$

$$v_t = C_\mu \frac{k^2}{\varepsilon} \quad (7.1)$$

NK model: In the NK turbulence model, instead of Prandtl number and eddy viscosity μ_t, the temperature variance t^2 and its dissipation rate ε_t are used.

Temperature Variance equation:

$$\frac{\partial \rho \overline{t^2}}{\partial t} + \frac{\partial \rho \overline{u_i t^2}}{\partial x_i} = \frac{\partial}{\partial x_j}\left\{\left(\frac{K}{cp} + \frac{\rho \alpha t}{\sigma h}\right)\frac{\partial t^2}{\partial x_j}\right\} + Pt - 2\rho \varepsilon_t + D_t \quad (8)$$

Dissipation rate equation:

$$\frac{\partial \rho \varepsilon_t}{\partial t} + \frac{\partial \rho \overline{u_i}\varepsilon_t}{\partial x_i} = \frac{\partial}{\partial x_j}\left\{\left(\frac{K}{cp} + \frac{\rho \alpha_t}{\sigma_\varphi}\right)\frac{\partial \varepsilon_t}{\partial x_j}\right\} + \frac{\varepsilon_t}{t^2}\left(C_{p1}f_{p1}\frac{P_t}{2} - C_{D1}f_{D1}\rho \varepsilon_t\right) + \frac{\varepsilon_t}{k}\left(C_{P2}f_{P2}G_s - C_{D2}f_{D2}\rho \varepsilon\right) + E_t \quad (8.1)$$

Where: $P_t = -2\rho \overline{u_j t}\partial \overline{T}/\partial x_j$ denotes the production term of the temperature variance, D_t and E_t are additional terms.

$$-\overline{u_j t} = \alpha_t \frac{\partial \overline{T}}{\partial x_j} \qquad (8.2)$$

Table 4: Constants adopted in NK turbulence models

C_{p1}	C_{P2}	C_{D1}	C_{D2}	σ_h	σ_f
1.8	0.72	2.2	0.8	1.0	1.0
f_{p1}	f_{P2}	f_{D1}	f_{D2}	D_t	E_t
1	1	1	1	1	0

The eddy diffusivity for heat is defined as follows:

$$\alpha t = C\lambda\, f\lambda\, k\tau m = C\lambda\, f\lambda\, k\sqrt{\frac{k}{\varepsilon}}\,\sqrt{\frac{t2}{\varepsilon t}} = C\lambda\, f\lambda \frac{k2}{\varepsilon}\sqrt{2R}$$

Where $R = \tau_t/\tau_u = (\overline{t^2}/\varepsilon_t)(k/\varepsilon)$ is the time-scale ratio, and

$\tau_m = \sqrt{k/\varepsilon}\sqrt{\overline{t^2}/\varepsilon_t}$ is the mixed time scale.

The extent of the computational domain was decided based on temperature variations and the required area of analysis. The computational domain extended 4m on the sides, 10m on the front, 3m at the bottom, and 4.5m at the top. Natural outflow conditions were assumed at the five boundaries of the computational domain i.e. top boundary, bottom boundary, X_{min}, Y_{min}, and Y_{max}. On the X_{max} side, that was North of the building according to site data was given fixed velocity condition. The average value of velocity was 2.2m/s from north to south. The ambient temperature of the computational domain was set at 28.7°C based on measurement data on site. Gravitational acceleration of 9.8m/s² was considered. The steady-state analysis was done for the simulation model. Pseudo-time step relaxation was considered for the heat balance equation. Under relaxation was used for advection and diffusion term. Convergence criteria was 10^{-4} for temperature, velocity, turbulent kinetic energy, and turbulent dissipation rate. Mesh independent grid test was done to make the model independent of size of the mesh. The optimum mesh size had 10,38,588 elements. At the building geometry, the element size was 100mm X 100mm.

Staking of ODU in different geometries of recessed space
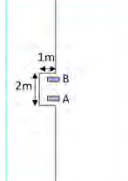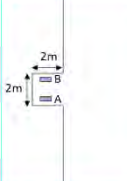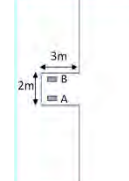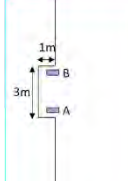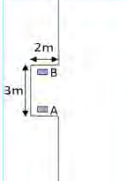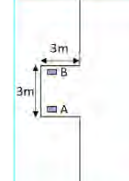
Six different stacking geometries were studied to understand the impact of geometry of the recessed space on performance of AC.

Table 6 represents the depth and width of the recessed space in which the ODUs are placed. 11 storey building was considered. The total height of the building was 33 meters. The ODUs were placed in two columns: Column A and Column B.

Table 5: Placement of ODUs in Recessed Space

Column A	The side inlet area of the ODUs in column A faced the open end of the recessed space
Column B	The side inlet area of the ODUs in column B faced the closed end of the recessed space.

Table 6: Geometries of recessed space

Case	1 (W2xD1)	2 (W2xD2)	3 (W2xD3)
Depth	1m	2m	3m
Width	2m	2m	2m

Case	4 (W3xD1)	5 (W3xD1)	6 (W3xD1)
Depth	1m	2m	3m
Width	3m	3m	3m

The boundaries of the computational domain were set to have natural outflow conditions. As the main area of analysis was recessed space, the domain boundaries coincided with the building geometry on the sides and back. The extent of computational domain was 5 meters at the front and, 3 meters at the top of the recessed space. No-wind condition was assumed. COP was calculated using the given formula (T T Chow et al., 2006).

$$COP = 4.825 - 0.0687 t_o$$

Results

Figure 3 represents the percentage difference of each turbulence model for outlet air temperature, condenser on-coil temperature from the rear, and side of ODU when compared to site data. RMSE (Root Meat Square Error) method was further used to find the mean difference of six floors. NK model shows 8.89% and 4.87% and 3.53% difference for outlet, inlet temperature at back and inlet temperature at side of ODU, respectively.
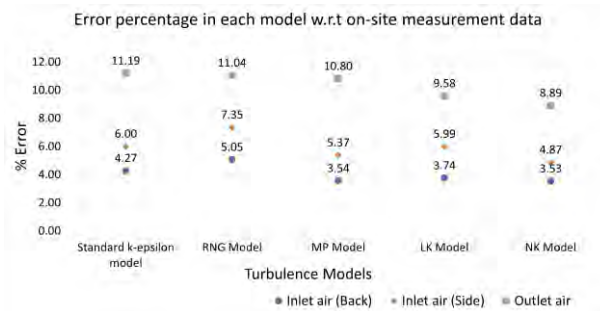
Figure 3: Percentage difference in each model compared to site data

CFD simulations also does not show the effect of stack. Wind velocity is a major reason that stack effect cannot

be seen. The magnitude of velocity ranged from 1.5m/s to 3m/s near the ODUs. Thus, it drove away the heat dissipated from the compressors. The placement of ODUs at an open façade caused faster diffusion of the heat rejected from the ODUs in the atmosphere. As a result, the ODUs located at the top floors are not affected by the heat rejection from the ODUs at the lower floors. Similar temperature profile was observed at site.
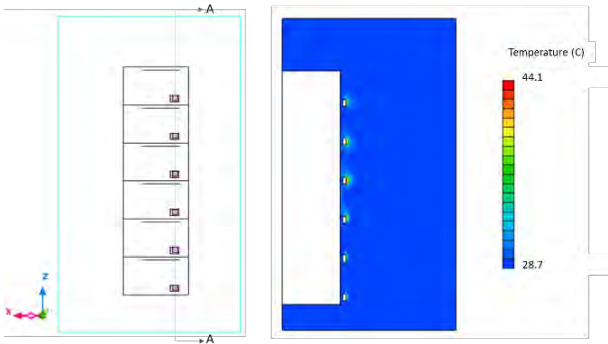
Figure 4: Air temperature variation at section A-A obtained from simulation results

Table 7: CFD simulation results at ODU of Air Conditioner

Floor	Outlet Air Temperature (°C)	Inlet Air Temperature (Back) (°C)	Inlet Air Temperature (Side) (°C)
1	38.73	28.7	28.70
2	41	29.75	28.77
3	41.94	29.8	29.19
4	44.06	30.52	31.97
5	41.45	29.49	31.02
6	39.7	29.22	30.51

Comparison of condenser on-coil temperature at ODUs placed in different geometries of recessed spaces

Condenser on-coil temperatures at back of ODUs placed in Column A increases to 38°C and 34°C for 2m and 3m wide recessed spaces, respectively. The condenser on-coil temperatures at the back of ODUs at Column A does not vary more than 1.5°C.
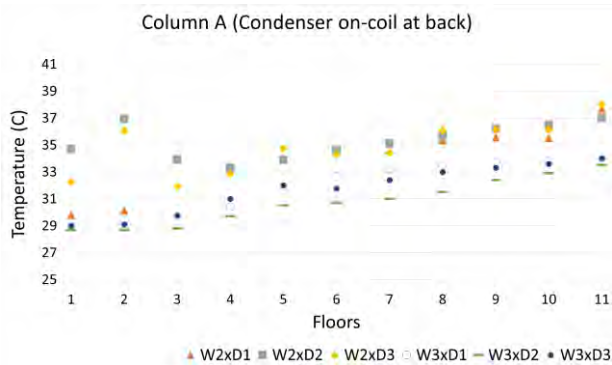
Figure 5: Condenser on-coil temperature at back of ODU placed at Column A for different recessed spaces

For the lower depth of the AC, condenser on-coil temperatures at the sides was minimum. For 2m wide recessed space, the maximum condenser on-coil temperatures were 33.5°C, 35°C and 36.5°C for 1m, 2m and 3m depth, respectively. When the recessed space having width of 3m was considered, the condenser on-coil temperatures further lowered to 31.4°C, 31.6°C and 32.1°C. Thus, for 3m wide space when different depths were considered, the condenser on-coil temperatures did not vary more than 1°C.
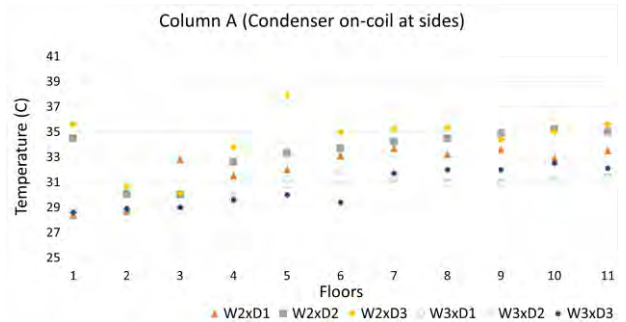
Figure 6: Condenser on-coil temperature at side of ODUs placed at Column A for different recessed space

Figure 7 shows that the condenser on-coil temperatures increase with increasing floor height. At 11th floor, these temperatures increase to 39.5°C and 36°C for 2m and 3m wide recessed space, respectively. The impact of depth of recessed space on condenser on-coil temperatures is seen up to fifth floor. Beyond 5th floor the variation in temperature is mainly caused due to the width of the recessed space rather than depth. From 6th floor to 11th floor, the impact of depth of condenser on coil temperatures at the back of the ODUs at Column B is less 1.5°C and 1°C and for 2m and 3m wide recessed spaces, respectively.
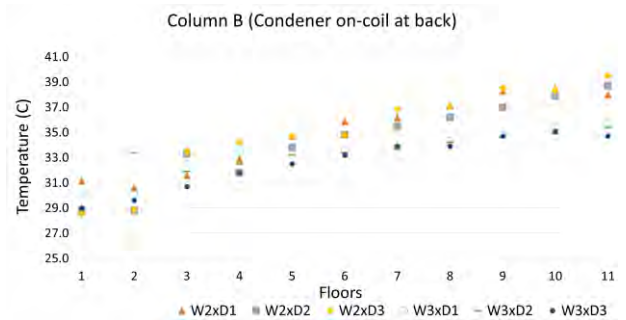
Figure 7: Condenser on-coil temperature at back of ODUs placed at Column B for different recessed spaces

As the side inlet area for Column B lies towards the closed end of the recessed space, the depth does not impact the condenser on-coil temperatures by more than 1°C after 5th floor. Though the width of the recessed space, when increased from 2m to 3m brings down the maximum on-coil temperatures by 3°C. For 2m wide space, the temperature on sides of ODU reaches up to 40°C when the depth is 1m and 3m.
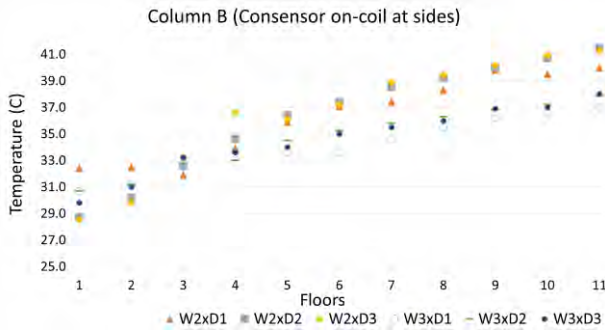
Figure 8: Condenser on-coil temperature at side of ODUs placed at Column B for different recessed space

Figure 9 and Figure 10 shows the temperature profile different cases of recessed space. For no wind conditions, buoyancy drives the motion of fluid. The condenser on-coil temperatures rise by 10°C at last floor for 2m wide recessed space. For 3m wide space, the maximum temperature rises by 5°C at the last floor in the recessed space.
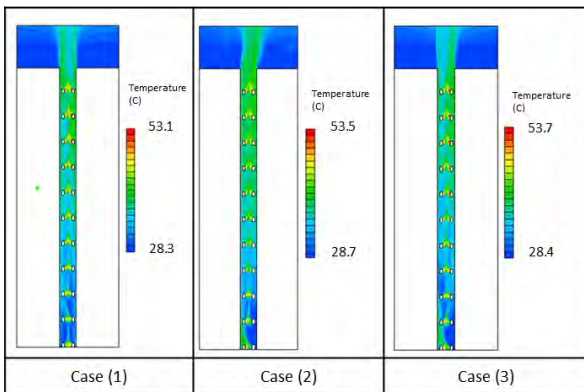
Figure 9: Temperature variation in 2m wide recessed space
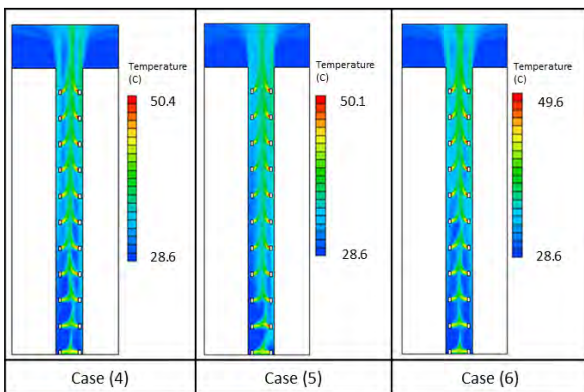
Figure 10: Temperature variation in 3m wide recessed space

Impact on Energy Efficiency of AC

The value of reference COP is taken at ambient temperature of 28.7°C. The calculation for percentage drop of COP is with respect to reference COP value. The maximum drop in COP of AC units was 27% and 22% in Column A and Column B, respectively can be seen in the air conditioner units placed in Case 3. The recessed space having width of 2m shows average 21% and 25% drop in

COP of AC at higher floors placed in Column B and Column A respectively. The average drop in the COP of AC placed in 3m wide recessed space was 11% for ODUs placed in Column A and 17% for ODUs placed in Column B. Minimum drop is observed in the ODU of Column A of 3m wide and 1m deep recessed space.
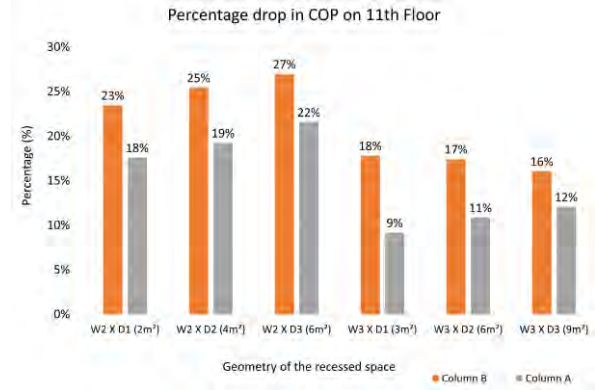
Figure 11: Maximum percentage drop in COP of Air Conditioner units

Discussion

The NK two-equation heat transfer model proves to be the most accurate model when compared to on-site measurement data with minimum difference of 4.58% for condenser on-coil temperatures and 8.89% for outlet air temperature from the ODU.

Wider recessed space is beneficial for reducing the increment in condenser on-coil temperatures. For 2m wide recessed space, the temperature at the 11th floor increased to almost 39.8°C, whereas the condenser on-coil temperatures of ODUs placed in 3m wide recessed space increased to 33.7°C. The condenser on coil temperature at the side inlet area rises as high as 41.3°C for the ODUs placed at Column B. This is because the inlet area at the side of the compressor unit faces the closed end of the recessed space. The heat accumulation is more near the closed space. The condenser on coil temperature at the side inlet area of ODU units placed in Column A rise to 35.5°C. The temperature increment of almost 5-6°C can be avoided by placing the compressor units such that the side inlet area faces the open end of recessed space.

According to the analysis done for the recessed space, the geometry that has 6m2 area of the recessed space which is 2m wide and 3m deep has the most inefficiently working AC. For the same area of recessed which has 3m width and 2m depth can prove to be 10-15% more efficient. When the recessed space with 3m2 area was studied, an average drop of 13.5% was noted in the COP of AC compared to a 25% drop observed for 2m wide recess space.

As the simulations were done for no-wind conditions, the buoyancy was the only factor that caused the motion of fluid. As a result, the depth did not impact the condenser on-coil temperature at the back of ODU but increasing the depth of recessed space did show increment in the

condenser on-coil temperatures at the side of the ODU units for Column A. As the depth of the space was increased, the heat accumulated more at the side inlet area of ODUs in Column A. Average increment of 2°C was observed in condenser on-coil temperatures at the side inlet area of ODUs placed in Column A when the depth was increased from 1m to 3m.

Conclusion

In major Indian cities, urbanisation and increasing population contribute to increasing vertical development. As a result, the cities have many high-rise residential apartments where the outdoor units of Air Conditioners are densely stacked.

This project thus focuses on first comparing the simulation results with on-site measurements and further simulating placements of outdoor units in recessed spaces having varying depth and width. The simulation study was carried out using scSTREAM simulation software.

It was observed that in case 3, the recessed space is the densest, which has 2m width and 3m depth and has 6m² area. The COP drops by 27% for Column B and 22% for Column A. For the recessed space with lesser area in Case IV, where the area is just 3m², minimum drop in COP can be seen. With more width and less depth, only a 9% drop can be seen in the COP of air conditioner at higher floors. Thus, the broader area of the recessed space should be preferred. The width if kept minimum will help in easy dissipation of hot air into the atmosphere rather than accumulating in the space

The study will be beneficial during the pre-design stage to decide the optimum dimensions or recommended ventilation of the recessed space. The study will further help during the installation of ODU to determine the optimum placement of air conditioning units. The building owners, HVAC engineers and installers can decide the optimum placement of ODU units using a defined simulation method. The study will benefit during the pre-design stage to decide the optimum dimensions of the recessed space along with placement of air conditioning units.

Acknowledgment

References

Bojic, M., Lee, M., & Yik, F. (2002). Influence of a depth of a recessed space to flow due to air-conditioner heat rejection. *Energy and Buildings*, *34*(1), 33–43. https://doi.org/10.1016/S0378-7788(01)00078-0

Bruelisauer, M., Meggers, F., Saber, E., Li, C., & Leibundgut, H. (2014). Stuck in a stack - Temperature measurements of the microclimate around split type condensing units in a high rise building in Singapore. *Energy and Buildings*, *71*(March), 28–37. https://doi.org/10.1016/j.enbuild.2013.11.056

Campbell, I., Kalanki, A., & Sachar, S. (2018). *Solving the Global Cooling Challenge: How to Counter the Climate Threat from Room Air Conditioners*. 50.

Choi, S. H., Lee, K. S., & Kim, B. S. (2005). Effects of stacked condensers in a high-rise apartment building. *Energy*, *30*(7), 968–981. https://doi.org/10.1016/j.energy.2004.08.004

Chow, T. T., & Lin, Z. (1999). Prediction of on-coil temperature of condensers installed at tall building re-entrant. *Applied Thermal Engineering*, *19*(2), 117–132. https://doi.org/10.1016/S1359-4311(98)00042-8

Chow, T. T., Lin, Z., & Wang, Q. W. (2000). Effect of building re-entrant shape on performance of air-cooled condensing units. *Energy and Buildings*, *32*(2), 143–152. https://doi.org/10.1016/S0378-7788(99)00048-1

Chow, T. T., Lin, Z., & Yang, X. Y. (2002). Placement of condensing units of split-type air-conditioners at low-rise residences. *Applied Thermal Engineering*, *22*(13), 1431–1444. https://doi.org/10.1016/S1359-4311(02)00068-6

Chow, T T, Lin, Z., Wang, Q. W., Lu, J. W. Z., Avenue, T. C., Tong, K., & Kong, H. (2006). Split-Type Air-Conditioners At Building Re-Entrant Via Computer Simulation. *City University of Hong Kong ENERGY PERFORMNANCE OF SPLIT- CFD SIMULATION WITH k- ε MODEL*, *23*(1), 1–7.

Chow, Tin Tai, Lin, Z., & Wang, Q. W. (2000). Applying CFD Simulation in Analysing Split-type Air-conditioner Performance at Buildings. *Architectural Science Review*, *43*(3), 133–140. https://doi.org/10.1080/00038628.2000.9696896

Duan, R., Wang, X., Song, Y., & Liu, J. (2016). Influence of Air-conditioning Outdoor Unit Arrangement Strategy on Energy Consumption. *Procedia Engineering*, *146*, 350–358. https://doi.org/10.1016/j.proeng.2016.06.409

Phadke, A., Abhyankar, N., & Shah, N. (2014). Avoiding 100 New Power Plants by Increasing Efficiency of Room Air Conditioners in India : Opportunities and Challenges. *Eedal '13*, *June*, 1–14.

Energy Performance of Ground-source Heat Pump and Photovoltaic/thermal (PV/T) in Retrofitted and New Buildings: Two Case Studies Using Simulation and On-site Measurements

Arefeh Hesaraki[*], Hatef Madani

KTH Royal Institute of Technology, Department of Energy Technology, Stockholm, Sweden

* corresponding author: arefeh@kth.se

Abstract

This paper aims to contribute by presenting calculated and measured electricity usage in two single-family case studies during the heating season of 2019-2020 located in Stockholm, Sweden. The electricity usage included consumption by heat pumps' compressor to cover space heating and domestic hot water, auxiliary energy for fans and pumps, and ventilation system. The first case study was built in 1936 with an oil burner, which was renovated to a ground-source heat pump (GSHP) in 2015, and the second case study was a new building built in 2013 with a GSHP. The application of photovoltaic/thermal (PVT) systems in combination with GSHP was theoretically investigated for both case studies. Buildings were modelled using the energy simulation tool IDA Indoor Climate and Energy (ICE), and the model was validated against the measured electrical energy usage. PVT was designed to balance the maximum heat production with domestic hot water consumption during the summer months. Simulation results revealed that combining GSHP with 5 m_2 grid-connected PVT gave 21% and 22% energy savings in case study 1 and case study 2, respectively. Employing a battery storage to store extra electricity production by PVT increased the energy savings to 24 % and 32 % for case study 1 and case study 2, respectively. Moreover, in both cases approximately half of the total annual domestic hot water need was prepared by 5 m_2 PVT.

Introduction

Background

An International Climate Panel forecasted an increase in the Earth's temperature by 6 °C on average by 2050 (National Research Council, 2011). To keep the climate change below 2 °C and to avoid the consequences of global warming, the European Union (EU) has ambition to become climate-neutral by 2050 (European Commission, 2018). In short term, EU has also set several key targets as to decrease the greenhouse gas emissions by 40%, to increase the energy efficiency by 32.5%, and to use at least 32% share of renewable energy by 2030 compared to 1990 levels (European Commission, 2014). In addition, Sweden has its own ambitions to have 50% more efficient energy use by 2030 compared with 2005, to have 100% renewable electricity production by 2040

and to achieve zero net greenhouse gas emissions by 2045 (Baylan I., 2018). In Sweden, the building sector is responsible for almost 40% of the total energy consumption and represents about a third of CO_2 emissions. To achieve the national and international energy policies, it is therefore vital to introduce sustainable and efficient renewable-based energy systems into near-zero energy buildings.

Heat pump has been known as one of the most efficient systems that extracts low-temperature heat from renewable and low-quality energy sources stored in the ambient air, in the ground or in groundwater, and converts it to useful heat of higher temperature to meet the energy demand in buildings. By using a heat pump with coefficient of performance (COP) of 4, at least 75% of total energy requirement in building is covered by renewable sources.

With double-digit growth for the fourth year in a row, the number of installed heat pumps in Europe was increased by 60% between 2014 and 2018 (EHPA, 2019). Raising with the same rate, European Heat Pump Association (EHPA) expects a doubling in the heat pump market by 2024. According to EHPA statistical data, Sweden was the fourth leading country in heat pump market by 2018 among 21 European countries. All these facts show that heat pump is a growing technology, and a further improvement in heat pump's configurations or in the control strategies would result in great energy savings potential and large reduction in greenhouse gas emission.

One enhancement in heat pump's configuration is to combine its compressor with photovoltaic (PV) to supply the required electricity from solar energy. Integrating grid-connected PV, which has been increased by more than 67% in Sweden between 2017 and 2018 (Ebenå G., Berard J., 2019), with heat pump would increase the self-consumption of installed PV and lead to less primary energy usage in building. Another improvement in heat pumps' configuration is to integrate it with a solar collector in series or in parallel (Vega J., Cuevas C., 2020). On parallel configuration, heat pump and solar system work independently to meet the energy demand in building. However, in series connection, heat pump's evaporator is fed by solar renewable energy, exclusively or in addition to other renewable sources, such as ground or air (Lazzarin R. M., 2012). In addition to individual PV and solar collector, a hybrid system, namely photovoltaic/thermal (PVT) can be combined with heat

pump. PVT delivers both electricity and heat simultaneously in one and the same system, which results in higher efficiency compared to the individual system of PV. Previous study by Besgani et al. showed that combining an air-source heat pump with PVT would significantly increase the efficiency of the system by avoiding the defrost cycles (Besagni G., Croci L., Nesa R., Molinaroli L., 2019). Moreover, combining a ground-source heat pump with PVT can be cost effective as it reduces the borehole length and the required field compared to a conventional ground-source heat pump (Sommerfeldt N., Madani H., 2019). In addition, including more renewable sources in heat pump's evaporator through a seasonal thermal energy storage, which stores heat from summer to winter, would increase the efficiency and COP of heat pump (Hesaraki et al. 2015 a, 2015 b)

With respect to thermal efficiency and COP of heat pump, two sides of energy supplier in thermal side and the energy distribution in demand side are highly coupled. It means that less work is required by the compressor of the heat pump as the temperature difference between the renewable source side and the sink side decreases. As a rule of thumb, COP of heat pump improves by 1-2 % for every degree reduction in supply water temperature. Therefore, combining heat pump with low-temperature heat emitter, which works with supply temperature levels of lower than 45 ºC, could be efficient (Boerstra A., Veld P.O., Eijdems H., 2000). During recent years, more buildings have become more energy-efficient by having better thermal insulation, less infiltration and more efficient heating and ventilation systems. Therefore, the low space heating demand in buildings can be met by using a lower supply water. Hesaraki et al. have experimentally investigated the energy performance of low-temperature heat emitter with heat pump in five new buildings (Hesaraki A., Holmberg S., 2013) and in a climate chamber box (Hesaraki A., Bourdakis E., Ploskic A., Holmberg S., 2015)

We have observed that a number of researches have been carried out to investigate the performance of heat pump with solar system in forms of PV, collector, or PVT. However, to our knowledge there is a lack of studies clearly investigate the performance of a ground-source heat pump with PVT connected to low-temperature heating system in single-family houses located in cold climates. This research gap claims the need for more comprehensive study on the development and evaluation of this system in different buildings and to compare its distinctiveness from conventional ground-source heat pump. This paper tends therefore to focus on investigating the energy performance of a PVT-assisted ground-source heat pump in two case studies, including a renovated building with medium-temperature heating system, and a newly built single-family house with low-temperature heating system located in Stockholm, Sweden.

Description of the case study buildings

The first case study was a naturally ventilated two-story single-family house with 140 m_2 floor area, which was built in 1936 with an oil burner. In 2015, the house was renovated by installing a ground-source heat pump with a single 150 m borehole, and the roof was isolated with an additional 400 mm insulation layer. Moreover, all windows with poor U-value of 2.8 W/(m_2·K) were substituted by energy efficient three-pane windows. Two people were living in this house, whom kept the indoor temperature between 19-20 °C. Before renovation, the building used approximately 4 m_3 oil per year, corresponding to 285 kWh/m_2. This high energy usage, however, was decreased to 59 kWh/m_2 after installing a ground-source heat pump and improving the building's envelope.

For the second case study, we chose a one-story 130 m_2 single-family house built in 2013 with a ground-source heat pump connected to a single borehole with 190 m depth. The house was implemented by a mechanical balanced (supply/return) ventilation with a heat recovery system with efficiency of 80%, which supplied ventilation flow rate of 0.4 L/(s·m_2). Moreover, the heat was distributed in the house through low-temperature under-floor heat emitter. In this house with the indoor temperature of 21 °C, two adults and two children were living. The annual measured electrical energy consumption for space heating, domestic hot water, ventilation system, and auxiliary energy was 48 kWh/m_2.

Method

In this study, we used IDA Indoor Climate and Energy (ICE) 4.8 simulation tool to investigate the energy performance of case study buildings. IDA ICE is a dynamic simulation tool initially developed at KTH Royal Institute of Technology, Sweden to investigate energy usage, thermal comfort and indoor climate in buildings. IDA ICE has been validated in several studies with respect to CEN standards (Equa Simulation, 2010 a) (Kropf S., Zweifel G.) and ASHRAE standard (Equa Simulation, 2010 b).

Firstly, we used IDA ICE to model our case study buildings with a ground-source heat pump, and after that we improved our models by integrating PVT in the energy system. To validate our models, we conducted field measurements of electrical energy usage during heating season from 1st October 2019 to 29th February 2020. Measurements included electricity usage for space heating, domestic hot water (DHW), ventilation system, and pumps.

Model description

Two case-study buildings were modelled in ICA ICE according to their geometry, construction materials, heat pump specification, and their heating and ventilation system. To calculate energy usage for case-study buildings, ASHRAE's typical weather data of

International Weather for Energy Calculations (IWEC2) for Stockholm was used. The weather data derived from up to 25 years of avarage weather observations for at least every three hours of wind speed and direction, dry-bulb temperature, dew-point temperature, and global horizontal solar radiation from cloud cover.

In all models, we used a southward-oriented PVT with a slope of 45 degree and efficiency of 24,18% for PV. The efficiency of modelled PVT was taken from product specification of a commercial PVT produced by Samster AB (Samster). To avoid over production of heat, PVT's area was calculated to balance the maximum thermal production and the DHW consumption in summer.

Electricity produced by PVT was used to primarily feed the compressor of the heat pump, and the overproduction of electricity was supposed to either charge the battery or to be sold to the grid. Solar collector of PVT system was supposed to work in parallel with the heat pump for producing domestic hot water, which was then stored in a water tank with a capacity of 500 L, see Fig. 1. Since our measurements were conducted during heating season, we could not separate the energy usage for space heating from the energy usage for domestic hot water. Therefore, we assumed that the DHW consumption was equal for all months, which seems reasonable as hot water usage may not be dependent of weather condition.

To define variables that were dependent to occupants behaviour; such as DHW usage, internal heat gains from occupants, light, and equipment, Sveby Standard (Lindvall S., 2012) was used, see Table 1. Sveby, which stands for Standardize and Verify Energy Performance in Buildings, is a tool to define unpredictable variables from user behaviour in energy performance evaluation. Sveby's materials are in line with Swedish National Board of Housing, Building and Planning (Boverket).

To calculate the efficiency of the energy system, two terms of Energy Savings (ES) and Solar Fraction (SF) were used, see Eqs. (1) & (2). In Eqs. (1) & (2), $E_{PVT,self-consumed}$ refers to the electricity produced by PVT which was used inside the building, either directly by the heat pump or indirectly by charging the battery storage. Moreover, the total annual electricity demand for space heating, DHW preparation and ventilation system by building with GSHP and GSHP+PVT is indicated by $E_{total,GSHP}$ and $E_{total,GSHP+PVT}$, respectively.

$$SF = \frac{E_{PVT,self-consumed}}{E_{total,GSHP+PVT}} *100 \quad (1)$$

$$ES = (1 - \frac{E_{total,GSHP+PVT}-E_{PVT,self-consumed}}{E_{total,GSHP}})*100 \quad (2)$$

Results
Simulation results
- Case study 1

After running a number of simulations, it was revealed that installing a 5 m_2 PVT would match the maximum heat production in May with monthly DHW consumption. The results of energy flows including thermal and electrical production by PVT, DHW usage, and total required electricity in case of GSHP, and GSHP+PVT are given in Fig. 2. As can be seen in Fig. 2, the bars showing excess/required electricity in PVT+GSHP system have both negative and positive values. Positive figures demonstrate required (bought) electricity, and negative values indicate extra produced electricity by solar cells in PVT system, which occurred in summer as DHW need was covered mainly by solar thermal collector of PVT.
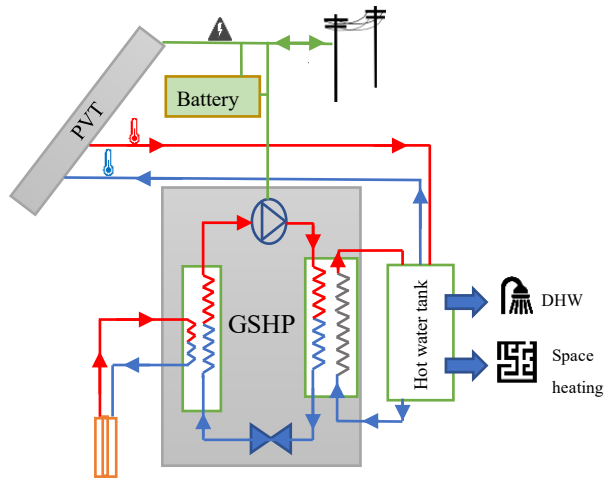
Figure 1 Configuration of the energy system studied

Table 1: Defined variables in IDA ICE based on Sveby Standard, the number of occupants is based on real data **(Lindvall S., 2012)**

Parameter	Amount	Schedule in IDA ICE	Internal heat gain
Occupants	Case 1: 2 people, Case 2: 4 people	Absent from 8:00 to 18:00, and present otherwise	Activity level of 0.8 MET, corresponding to 80 W
Household electricity	$\frac{30}{8.76} * \frac{A_{temp}}{A_{floor}}$ W/m2	Always on	70 % converts to heat
Domestic hot water	20 kWh/m2 with a repeated daily profile	Annual usage	20 % converts to heat

As stated earlier, extra generated electricity by PVT can be either stored in a battery or sold to the grid. In case of grid-connected PVT coupled with ground-source heat pump, the electricity usage for case study 1 was 46 kWh/m2, causing 21% energy savings compared to individual ground-source heat pump with 58 kWh/m2 electrical energy usage, see Fig. 3. Moreover, using Eq.

(1), the solar fraction was calculated as 18% if excess electricity was sold to the grid. On the other hand, storing extra electricity to a battery storage for later usage would increase the self-consumption, which resulted in decreasing the annual electricity demand from 58 kWh/m2 to 44 kWh/m2. Employing a battery storage in case study 1 caused 24% energy savings and a solar fraction of 22%. Additionally, annual simulation revealed that 49% of total domestic hot water need could be covered by 5 m2 PVT.

Moreover, selling extra electricity to the grid in PVT+GSHP system caused 22% energy savings and a solar fraction of 20%, see Fig. 5. As indicated in Fig. 5, storing excess generated electricity to a battery storage decreased the yearly electricity usage from 48 kWh/m2 to 33 kWh/m2. It means that energy savings and solar fraction were 32% and 34%, respectively. Furthermore, our results indicated that installing 5 m2 PVT covered 54% of total DHW requirement in case study 2.

Fig.2: Energy flows in case study 1

Fig.4: Energy flows in case study 2
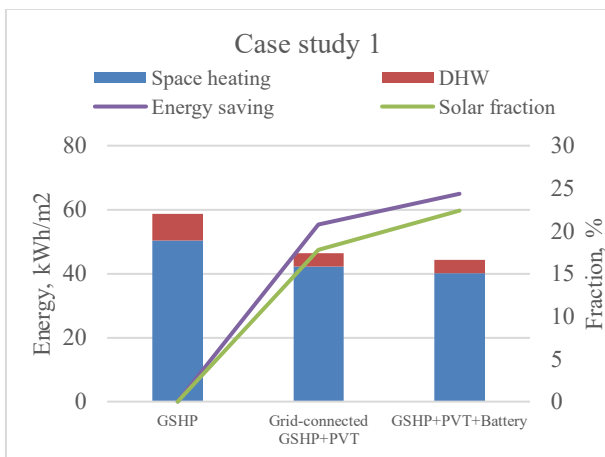
Fig.3: Electricity usage, energy savings, and solar fraction in case study 1
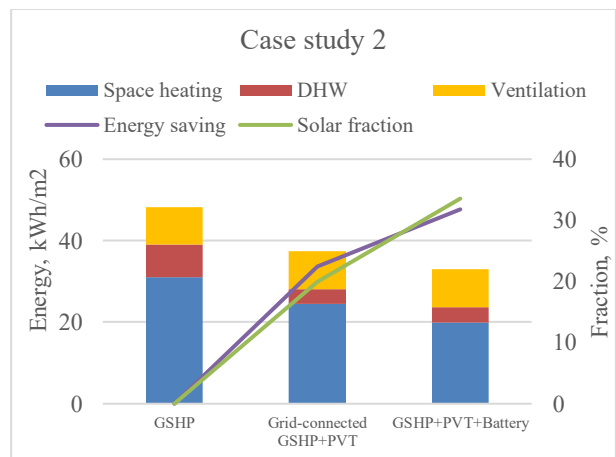
Fig.5: Electricity usage, solar fraction and energy savings in case study 2

- Case study 2

Similar to the first case study, simulations showed that a 5 m2 PVT was needed in case study 2 to create an acceptable balance between the monthly domestic hot water need and the maximum heat production in July, see simulation results in Fig. 4. Our results indicated that combining a ground-source heat pump with the grid-connected PVT would reduce the total electrical energy usage from 48 kWh/m2 to 37 kWh/m2.

Measurement results and model validation

IDA ICE model was experimentally validated against measurements of electricity usage for space heating, domestic hot water, ventilation and auxiliary energy used for fans and pumps during heating season of 2019-2020. Results of validation for case study 1 and case study 2 are presented in Fig. 6 and Fig. 7, respectively. As can be seen in Figs. 6 & 7, the measured electrical energy usage in October for both cases were approximately 30% higher than the simulated values. This large deviation can be

attributed to the difference between standard weather data of IWEC2 used in simulation and actual weather condition in measurements. According to the Swedish Meteorological and Hydrological Institute, October 2019 had the coldest start days during the past 20 years compared to the October's normal temperature, and the winter of 2019 had arrived 1-2 weeks earlier than the normal year during the past 40 years (SMHI, 2019). This unpredictable actual weather conditions in October 2019 caused the underestimation of energy usage in our simulation compared to the reality.

On the other hand, the electricity demand in January was overestimated by simulation compared to the measurement. This deviation could be explained due to unpredictable occupants' behaivior during New year's holiday by for example taking a trip. Despite the fact that occupants' behaviour and actual weather conditions caused underestimation or overestimation of the actual energy usage, in other months of November, December, and February there appeared to be a good agreement between measurements and simulation.
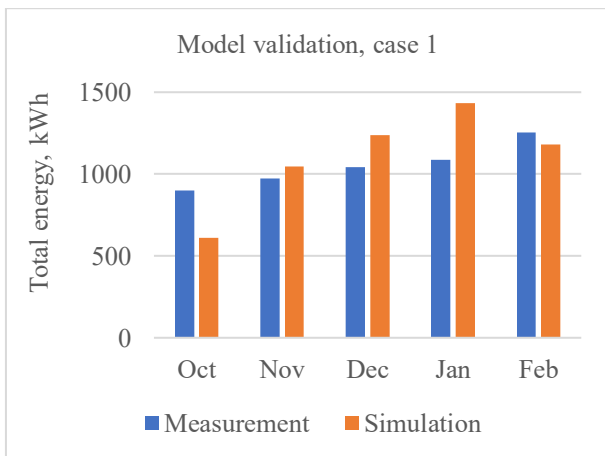
Fig 6. Comparison of measured and calculated electrical energy demand in case study 1
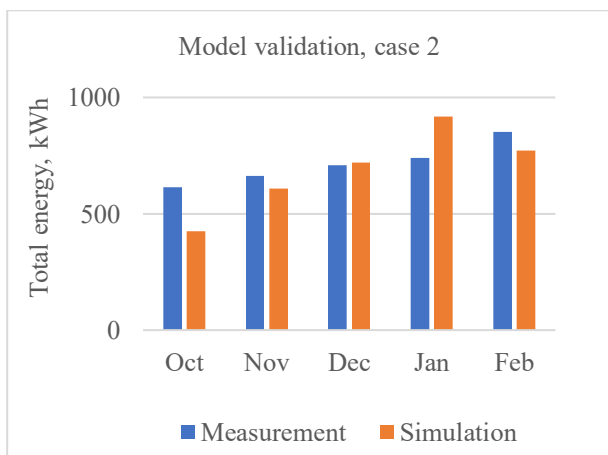
Fig. 7. Comparison of measured and calculated electrical energy demand in case study 2

Discussion

As shown by results, the ratio of self-consumed electricity to the total PVT generation plays a key role in determining two factors of solar fraction and energy savings. Results showed that the self-consumption ratio for case study 1 was considerably larger than that in case study 2; which was 81% for case 1, and 59% in case 2. The greater self-consumption in case 1 can be explained by the fact that some parts of the electricity generation by PVT were used to cover space heating need during summer nights in this old building, which was not required in case 2 as a new building.

To increase the self-consumption ratio, one possibility is to utilize a battery storage, which leads to higher solar fraction and greater energy savings. As shown by results, storing excess electricity to a battery storage in case 2 could significantly improve the solar fraction and energy savings, which were increased by 10-14 % compared to the grid-connected case with no battery storage. On the contrary, in case 1, employing a battery storage had minor impacts on energy savings and solar fraction, as those performance indicators were only increased by 3-4% compared to the grid-connected PVT cases. Therefore, it can be concluded that it would be more beneficial to have a battery storage in new buildings to achieve higher efficiency in energy system.

Moreover, in IDA ICE simulation the typical weather file of ASHRAE's IWEC2 was used, which was different from actual weather condition and resulted in deviation between measurement and simulation. Next step of our project is, however, to use the actual weather file in simulation for validating our model.

Conclusion

The objective of the study was to investigate the application of photovoltaic-thermal (PVT) system combined with ground-source heat pump (GSHP) in new and retrofitted construction. IDA ICE simulation tool was used to calculate total electricity usage of case-study buildings, which was validated against measurements conducted during heating season of 2019-2020. In our model, PVT worked in parallel with ground-source heat pump for covering domestic hot water usage, and the electricity produced by PVT was primarily used to feed the compressor of the heat pump. To evaluate the performance of the energy system two indicators of solar fraction and energy savings were used, which depended on self-consumption electricity and the total electrical energy demand.

Simulation showed that using 5 m_2 PVT for both cases could create a good balance between generating thermal energy by PVT and domestic hot water usage during the summer season, and it covered around half of the annual domestic hot water demand. Moreover, depending on the building type and the existence of a battery storage, solar fraction and energy savings varied between 18-34 % and

21-32%, respectively. The lowest values for both solar fraction and energy savings were achieved for the old building in case study 1 without a battery storage, and the highest values attributed to the new building in case study 2 with a battery storage. As employing a battery storage in energy system is very costly, its benefits should be justified considering building type and self-consumption ratio.

It should be noted, however, that this study was of two dwellings only; future study of other types and greater number of dwellings are needed before it is possible to generalize regarding all houses using PVT-assisted ground-source heat pump.

Acknowledgement

References:

Baylan I. (2018). Energipolitikens inriktning. *Regeringen, 2018*. - 2017:18-228 .

Besagni G. Croci L., Nesa R., Molinaroli L. (2019) Field study of a novel solar-assisted dual-source multifunctional heat pump. *Renewable Energy 132* 1185-1215.

Boerstra A. Veld P.O., Eijdems H. (2000) The health, safety and comfort advantages of low temperature heating systems: a literature review *Proceedings of the 6th International Conference on Healthy Buildings*, Espoo, Finland, August, 2000.

Ebenå G. Berard J. (2019) Nätanslutna solcellsänläggningar 2018, *ER 2019:24 Swedish Energy Aganecy* .

EHPA 2019. European heat pump association market data https://www.ehpa.org/market-data/

Equa Simulation 2010 a. Validation of IDA Indoor Climate and Energy 4.0 with respect to CEN Standards EN 15255-2007 and EN 15265-2007.

Equa Simulation 2010 b. Validation of IDA Indoor Climate and Energy 4.0 build 4 with respect to ANSI/ASHRAE Standard 140-2004

European Commission 2014. Communication from the commission to the European Parliament, the Council, the European economic and social committee and the committee of the regions A policy framework for climate and energy in the period from 2020 to 2030 /* COM/2014/015 final.

European Commission 2018. Communication from the Commission to the European Parliament, the European Council, the European economic and social committee, the committee of the regions and the European investment bank. - Brussels

Hesaraki A. Halilovic A., Holmberg S. (2015 a). Low-temperature heat emission combined with seasonal thermal storage and heat pump. *Solar Energy 119* 122–133.

Hesaraki A. Holmberg S. (2013). Energy performance of low temperature heating systems in five new- built Swedish dwellings: A case study using simulations and on-site measurements. *Building and Environment 64* 85-93.

Hesaraki A. Holmberg S., Haghighat F. (2015 b). Seasonal thermal energy storage with heat pumps and low temperatures in building projects—A comparative review. *Renewable and Sustainable Energy Reviews 43* 1199–1213.

Hesaraki A., Bourdakis E., Ploskic A., Holmberg S. (2015). Experimental study of energy performance in low-temperature hydronic heating system, *Energy and Buildings 109* 108-114

Kropf S. Zweifel G. Validation of the Building Simulation Program IDA-ICE According to CEN 13791 „Thermal Performance of Buildings - Calculation of Internal Temperatures of a Room in Summer Without Mechanical Cooling - General Criteria and Validation Procedures. *Hochschule für Technik+architektur Luzern*.

Lazzarin R. M. (2012). Dual source heat pump systems: Operation and performance. *Energy and Buildings 52* 77–85.

Lindvall S. Levin P. (2012). Brukarindata bostäder Svebyprogrammet

National Research Council (2011). Climate Stabilization Targets: Emissions, Concentrations, and Impacts over Decades to Millennia. *The National Academies Press* Washington, DC, USA

Samster AB, https://www.samster.se/

SMHI 2020, https://www.smhi.se/klimat/klimatet-da-och-nu/manadens-vader-och-vatten-sverige/manadens-vader-i-sverige/oktober-2019-kall-start-gav-ovanligt-tidig-host-i-hela-landet-1.150666.

Sommerfeldt N. Madani H. (2019). In-depth techno-economic analysis of PV/Thermal plus ground source heat pump systems for multi-family houses in a heating dominated climate. *Solar Energy 190* 44-62.

Vega J. Cuevas C. (2020). Parallel vs series configurations in combined solar and heat pump systems: A control system analysis. *Applied Thermal Engineering 166* 114650.

Quasi-Dynamic Modelling of DC Operated Ground-Source Heat Pump

Patrik Ollas[1,2], Caroline Markusson[1], Jörgen Eriksson[3], Huijuan Chen[1],
Markus Lindahl[1] & Torbjörn Thiringer[2]

[1]RISE Research Institutes of Sweden, Borås, Sweden
[2]Chalmers University of Technology, Gothenburg, Sweden
[3]EQUA Solutions, Stockholm, Sweden

Abstract

The performance of a conventional ground-source heat pump (GSHP) has been measured in the laboratory with alternating current (AC) and direct current (DC) operation using the standardised points from EN14511:2018. The results from these measurements have been used to modify a variable speed heat pump model in IDA Indoor Climate and Energy (ICE) and the annual performance of AC and DC operation have been simulated for an entire year's operation at two geographical locations in Sweden. Results show that the energy savings with DC operation from laboratory measurements span between 1.4–5.2% and when simulating the performance for an entire year's operation, the energy savings vary between 2.5–3.4%. Furthermore, the energy savings from the simulations have been compared to the bin method described in EN14825:2018.

Introduction

The recent market developments of solar photovoltaic (PV) and batteries for residential buildings have had an exponential growth the last couple of years (IEA (2019); Ralon et al. (2017)). As PV and batteries, as well as most household appliances are natively operated on DC, DC distribution in buildings has lately gained interest since conversion losses can be avoided compared to traditional AC topologies.

There are many attempts in literature to estimate the energy savings when switching from AC to DC distribution in buildings (Vossos et al. (2014); Glasgo et al. (2016); Seo et al. (2011); Denkenberger et al. (2012); Hofer et al. (2017)), however findings from these studies differ substantially, varying between 1.5–25.0% in saving potential depending on the choice of reference case, types of appliances included (and their efficiency gains), and system studied. Further, findings in literature on DC savings for individual systems/appliances are often taken as a steady-state value without considering the dynamic behaviour of the appliances. Ryu et al. (2015); Lucía et al. (2013); Weiss et al. (2015); Fregosi et al. (2015) and Kakigano et al. (2010), have shown energy savings from DC operation for individual household appliances and HVAC-components in the span 1.5–9%, which is strongly reflected in the final energy savings for the system. Differences in energy savings are evident when studying different types of appliances but suggests that more research is needed to pin-down the savings more precisely. Also, often a constant efficiency saving is assumed without regards to its varying operation.

Conventional heat pumps are operated using DC at the final stage, where the supplied AC is rectified inside the heat pump using an AC/DC conversion step. Since these conversions are subject to losses, it is desirable to minimise these by feeding the heat pump directly with DC. A demonstration of a DC operated heat pump is presented in Huang et al. (2019) for a DC micro grid in Sweden, coupled with direct DC generation from PV, DC storage in a battery and direct DC loads. As this study focuses on the micro grid energy performance, no comparison was made for the DC operated heat pump's performance.

Ollas (2020) and Gerber et al. (2019) have suggested topologies for an AC and DC system respectively and presents the potential energy savings for DC, especially when renewable energy (RE) and battery storage are included. Missing in these studies are however measured energy gains from DC operation of individual appliances.

In this paper the annual performance of an AC and DC operated GSHP for space heating is quantified using laboratory measurements of an AC and DC operated GSHP. The laboratory measurements are done according to the steady-state operating points specified in EN14511:2018 to show the energy gains achieved with direct DC operation. The results from these steady-state points are then used to simulate the annual performance of the GSHP for a nearly-zero energy building (nZEB) at two locations in Sweden. The simulations are done using IDA ICE and a modified model for a variable speed heat pump.

Theory

A heat pump uses electrical input to generate a heating/cooling output through a cycle of evaporation and

condensation of a refrigerant. In this study, a variable speed compressor heat pump is studied. The compressor speed is controlled to give a specific supply temperature of the water in the heat distribution system based on the measured outdoor temperature, i.e. colder outdoor temperatures gives higher supply temperatures. A variable speed heat pump is designed to operate in a specific frequency interval, meaning that at low part loads, the compressor cannot reduce the speed enough and will instead operate in an ON/OFF mode.

Since the heating/cooling[1] output is higher than the required power input, conventional theory about efficiency cannot be applied. Instead, the Coefficient of Performance (COP) is used to evaluate the performance, and it is defined as

$$COP(t) = \frac{Q_{heat}(t)}{W_{power}(t)} \qquad (1)$$

where Q_{heat} and W_{power} are the heat output and power input respectively at time t. The COP is often related to a specific operating point at steady-state conditions. A more relevant performance factor is the Seasonal Coefficient of Performance (SCOP) which describes the average performance over a defined time period, considering only the space heat generation. From time-series data, the SCOP can be found, similar to (1), by analysing the heat generation and power usage over a defined time-period, as

$$SCOP = \sum_{t_1}^{t_2} \frac{Q_{heat}(t)}{W_{power}(t)} \qquad (2)$$

where Q_{heat} and W_{power} are the sum of heat delivered and electrical energy usage over the time period t_1–t_2.

Methodology

In this section, the case study, being a single-family nZEB, is introduced together with the method used for the heat pump steady-state measurements, and finally the heat pump and building models are described, and key performance indexes are defined.

Case Study – nZEB

The single-family nZEB in this study was developed and commissioned within the project "New Energy Efficient Demonstration for Buildings" (NEED4B), and have the specifications given in Table 1. The specified working interval for the GSHP means that the compressor can adjust its speed to deliver 1.5–6 kW of heat output. For a heating demand below 1.5 kW, the compressor will start to work in ON/OFF mode. If the supply temperature of the heating system is too low at maximum compressor speed the backup heater will start to generate more heat to the system, to cover the demand deficit. For the building

in this case study the system is more or less monovalent, and the use of the backup heater is limited. For the modelling of the annual heat pump performance, a nZEB is used and the building model is adopted from Chen and Markusson (2018) and adjusted with a mechanical supply and exhaust ventilation with a heat exchanger. In the referred article, a comparison was made with measured performance from Ylmén and Persson (2017), and the results showed good coherence between simulated and measured performance.

Heat Pump Laboratory Measurements

A conventional GSHP have been tested in a laboratory setup using the standardised operating cycles from EN14511:2018 (CEN (2018a)), at both AC and DC operation, in order to quantify the energy savings from the latter. For the DC measurements, the rectification stage, done inside the heat pump, has been removed and the heat pump is supplied directly with 380 VDC[2].

Measurements are made at four operating frequencies of the compressor, spanning between 30–118 Hz, and at two operating modes of brine and water temperatures (0/35°C and 0/55°C), according to the operating points defined in EN14511-2:2018. Where the former is typically used for low-temperature underfloor space heating and the latter for DHW production or space heating using a radiator system.

Building & Heat Pump Modelling

Using the measured data for the heat pump and data for the building from the case study, the heat pump performance have been simulated for an entire year's operation in an nZEB for two locations in Sweden: Malmö (south) and Luleå (north). Figure 1 shows a duration curve of the outdoor temperatures at the two simulated locations[3].
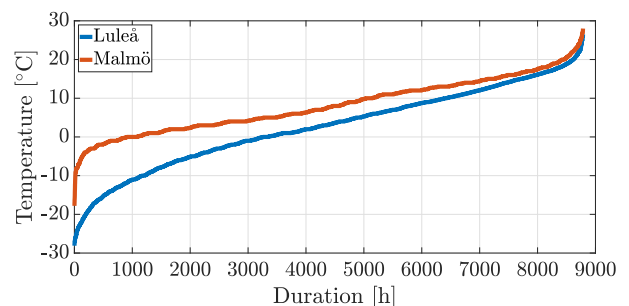
Figure 1: Duration curve of the outdoor temperatures for the two simulated locations: Luleå and Malmö.

A model of the single-family house is created in IDA ICE version 4.8. The house model has a total floor area of 155 m² and is modelled with an occupancy level of two adults and two children to mimic a

---

[1]In this study, only heating is required and thus, cooling is left out from here on out.

[2]The relays where operated on AC, but these power levels remained below 7 W.

[3]The weather data are taken from the ASHRAE IWEC 2 database, available in the IDA ICE program, and are used in the simulation of the building energy usage.

Table 1: Technical specification used in the modelling of the studied single-family nZEB.

Floor area (2 floors)	155 m^2
Average heat transfer coefficient, U$_{avg}$	0.20 W/m^2/K
Heating system	GSHP with a floor heating system
Ventilation	Balanced ventilation system with heat recovery
Ventilation flow rate – supply and exhaust	60 and 66 l/s respectively
Heating demand at –22°C	3.5 kW
GSHP working interval	1.5–6.0 kW
Air tightness	0.2 l/s/m^2 external surface with a pressure difference of 50 pa
Rotatory heat exchanger efficiency	82%

normal-sized Swedish single-family house. Different occupancy schedules are applied to the residents, and the house is divided into 13 zones in the modelling. An internal heat load (i.e., heat generated by lighting and other equipment) of 30 kWh/m^2 is used, suggested by SVEBY (Levin et al. (2009)) as a standard value in Sweden for residential building energy simulations. The weather data files for Malmö and Luleå are available in the IDA software, and are derived from integrated surface hourly weather data, originally archived at the national climate data centre (Equa Simulation Technology AB (1999)).

The energy demand simulated in IDA does not include air-rising losses due to opening of windows and external doors. Instead, only losses due to transmission and ventilation are compensated for. The air-rising losses are assumed to be 4 kwh/m^2 per year according to Levin et al. (2009).

A balanced ventilation system with a rotatory heat exchanger is used, with a supply and exhaust flow rate of 60 and 66 l/s respectively. The efficiency of the heat exchanger is set to 82%, according to the manufacturer's specifications. The house is heated by a floor heating system that is directly connected to the heat pump, which means that no storage tank is used. The water supply temperature in the floor heating system is specified in the range 20–35°C and varies with the outdoor temperature. Figure 2 shows the simulated heating system supply temperature, t_{supply}, as a function of outdoor temperature, $t_{outdoor}$ together with the set-points for the GSHP operation. The house is modelled with the constraint to keep an indoor temperature of at least 21°C.

As the difference between the AC and DC operated heat pump with regards to COP, is small, it is difficult to use an ordinary regression model to capture these differences. Instead, a model based on tables of measurement data is used, where the values are normalised by the Carnot COP, COP_{Carnot}. The output at the condenser, Q_c, is given in a table as a function of the compressor speed (in Hz) for the two tested points 0/35 and 0/55°C. Interpolation between the points is made by assuming a continuous derivative. The COP is handled similarly, but instead of giving
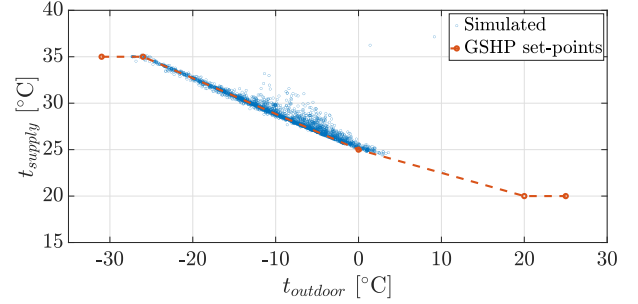
Figure 2: Simulated supply temperature for the heating system, t_{supply}, as a function of outdoor temperature, $t_{outdoor}$ together with the GSHP operating set-points.

the COP in the table, a ratio is calculated as

$$n_c(t) = \frac{COP(t)}{COP_{Carnot}} \qquad (3)$$

The COP used in the simulation, $COP(t)$, is the interpolated value of $n_c(t)$ multiplied by the Carnot COP, COP_{Carnot}. The compressor and evaporator power, $P_c(t)$ and $Q_e(t)$ respectively, are then calculated as

$$P_c(t) = \frac{Q_c(t)}{n_c(t) \cdot COP_{Carnot}} \qquad (4)$$

$$Q_e(t) = Q_c(t) - P_c(t) \qquad (5)$$

Based on discussions with the GSHP manufacturer, the COP value was assumed constant for compressor frequencies below the lowest test point, e.g. 30 Hz.

The heat pump is controlled by a PI-controller. The output is converted to a desired frequency between 18–120 Hz. The floor heating system have a large thermal mass and limits the need for a tank. The PI controller has a tacking time of 30 seconds that limits the wind-up.

Key Performance Indicators

The heating demand for the building is simulated in IDA ICE by setting a desired indoor temperature. The required heat pump electrical energy to maintain that indoor climate is calculated as

$$E_{power} = \int_{t_1}^{t_2} W_{power}(t)dt \qquad (6)$$

where W_{power} is the heat pump input power, and the energy usage is evaluated for an entire year's opera-

tion (t_1-t_2). Similarly, the generated heating energy is calculated as

$$E_{heat} = \int_{t_1}^{t_2} Q_{heat}(t)dt \tag{7}$$

From EN14825:2018 (CEN (2018b)), the SCOP is calculated by dividing the evaluated time period into a number of hours at different outdoor temperatures ("bins") for a specified climate[4], to reflect the variations in the heating period. For each of these bins, a COP value is calculated and is then used to calculate the SCOP value for the annual operation. For the time-series data given from the simulations in IDA ICE, the SCOP calculation is adopted from Zottl et al. (2011) and system boundary "SPF_{H3}" without the inclusion of heat and electricity for domestic hot water production, Q_{W_hp} and E_{HW_hp}, and electrical energy use of the brine/well pump, $E_{S\_fan/pump}$. Thus, the SCOP is given from the IDA simulations as

$$SCOP_3 = \frac{Q_{H\_hp} + Q_{HW\_bu}}{E_{HW\_hp} + E_{HW\_bu}} \tag{8}$$

where Q_{H_hp}, Q_{HW_bu} are the heat energy delivered for space heating from the heat pump and electrical back-up heater respectively, and E_{HW_hp} and E_{HW_bu} the electrical energy usage for the heat pump (for space heating) and electrical back-up heater respectively.

For the SCOP comparison the bin method from EN14825:2018 is applied to the results from the laboratory measurements of the GSHP. The bin-method is based on the calculation method for a low temperature system in a "cold climate" in EN14825:2018, using some modifications. The main modification is the replacement of the cold reference climate, with climate data for Luleå and Malmö[5]. Another modification, compared to the standard, is that the building's energy signature is based on the IDA ICE simulations with a heating demand of 3.5 kW at –22 °C. The heating demand is assumed to decreases linearly down to 0 kW at +6 °C, see Figure 3 for a visualisation of the simulated heating demand as a function of outdoor temperature. Thereby the building simulated has a heating demand to +6°C, instead of +16°C as defined in EN14825:2018.

Results

Here, results are presented first for the laboratory measurements of the AC and DC operated heat pump, using the points specified in EN14511:2018, and then these measured performance sets are incorporated into the heat pump model to model the performances for two geographical locations. The latter

Figure 3: Energy signature for the modelled nearly-zero energy building showing the measured heating demand at difference outdoor temperature, $t_{outdoor}$, and a linearization of the dependency.

to quantify the energy savings from DC operation, also with regards to the GSHP's operating condition. A comparison of the simulated energy savings is also made using the bin method defined in EN14825:2018.

Heat Pump Measurements – AC & DC Operation

Results from the laboratory measurements of AC and DC operation of the heat pump are given in Table 2 for different operating frequencies and modes of operation. Results are shown for heat output (to the system) and input power (electrical). The resulting COP values are also given in Figure 4 at different compressor frequencies and brine/water temperatures. Noteworthy from these results is that the measured COP is higher for all cases with DC operation, due to the eliminated rectification loss, and that the gains are higher for the low-loading, i.e. low operating frequencies.
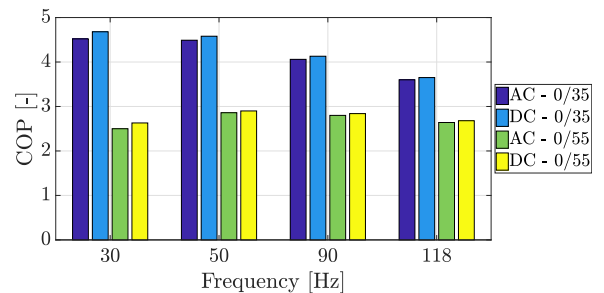
Figure 4: Measured Coefficient of performance (COP) from laboratory measurements at different compressor frequencies and brine/water temperatures (0/35 and 0/55).

Simulated Heat Pump Performance

The measured performance from Table 2 has been incorporated into the heat pump model, described in the methodology section, to simulate one year's operation for the nZEB case study at two geographical locations: Malmö[6] and Luleå[7]. The simulated energy savings, with regards to a reduced energy demand, span between 2.5–3.4% for DC operation in Luleå

---

[4]In EN14825:2018, three reference climates are given – Helsinki ("cold"), Strasbourg ("average") and Athens ("warmer").

[5]The outdoor temperature data is taken from Meteonorm version 6.1.

[6]**Longitude:** 55.609534 — **Latitude:** 13.002925

[7]**Longitude:** 65.588774 — **Latitude:** 22.156974

Table 2: Results from laboratory measurements of an AC and DC operated heat pump according to the operating points defined in EN14511:2018.

| | | Unit | Frequency [Hz] | | | | | | | |
			30		**50**		**90**		**118**	
Common data	Brine in/Water out	°C	0/35	0/55	0/35	0/55	0/35	0/55	0/35	0/55
	Brine out	°C	-3	-3	-3	-3	-3	-3	-3	-3
	Water in	°C	30	47	30	47	30	47	30	47
AC operation	Heat output	W	1796	1389	3063	2632	5961	5305	8057	7444
	Power input	W	397	556	682	921	1470	1895	2241	2825
DC operation	Heat output	W	1810	1426	3053	2616	5964	5283	8029	7379
	Power input	W	387	542	667	902	1443	1857	2198	2755
	COP gain	%	**3.5**	**5.2**	**2.0**	**1.4**	**1.7**	**1.4**	**1.4**	**1.5**

and Malmö respectively. Based on the simulated performance of the heat pumps operation made in IDA ICE, a duration curve of the compressor's frequencies is shown for both locations in Figure 5. Noticeable is that the heat pump is operated at the lower range of its frequency interval during a vast majority of the time and thus in the upper span of the energy savings according to Table 2. Furthermore, the difference between AC and DC operating frequency is small. The heat pump is well oversized for the simulated building and for working in space heating mode only, and thus operates frequently in an ON/OFF stage, especially prominent for the Malmö case.
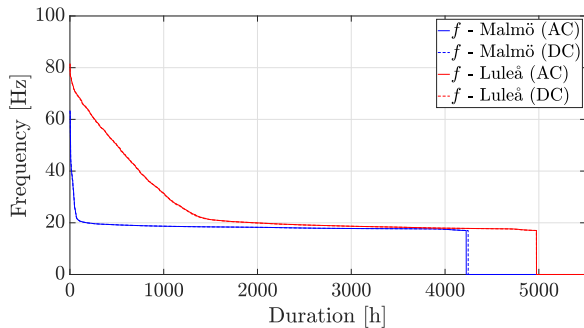
Figure 5: Registered compressor frequencies for AC and DC operated heat pump in Luleå and Malmö from the IDA simulation.

As a comparison, the energy savings for the two locations have also been calculated for AC and DC operation using the bin method described in EN14825:2018 using the outdoor temperature recordings from Meteonorm 6.1 and the measured heat pump performance from Table 2. The resulting SCOP savings are shown in Table 3 together with the modelled results from IDA ICE, which shows good coherence.

Conclusion

Results from laboratory measurements of a GSHP show performance gains with DC operation, in terms of an increased COP, in the range 1.4–5.2% for the measured operating cycles defined in EN14511:2018.

Table 3: Comparison of SCOP savings from IDA simulation and the bin method for the two geographical locations.

Method	Unit	Malmö	Luleå
Energy savings – IDA	%	3.4	2.5
Energy savings – bin	%	3.3	2.8

The energy savings also differ depending on the operation point, with higher gains for the lower operating frequencies. When these results are applied and simulated for an entire year's operation, the energy savings, in terms of a reduced electricity demand, span between 2.5–3.4% for the two simulated locations in Sweden. The energy savings from DC operation are larger for Malmö due to a more frequent operation in the lower frequency interval, where the largest savings are noted from the laboratory measurements.

Furthermore, the energy savings for space heating from the simulated results in IDA ICE and the bin method, according to EN14825:2018, shows good coherence.

Acknowledgment

References

European Committee for Standardization (2018a). *Air conditioners, liquid chilling packages and heat pumps for space heating and cooling and process chillers, with electrically driven compressors – Part 2: Test conditions*.

European Committee for Standardization (2018b). *Air conditioners, liquid chilling packages and heat pumps, with electrically driven compressors, for space heating and cooling - Testing and rating at part load conditions and calculation of seasonal performance*.

Chen, H. and C. Markusson (2018). Demand controlled ventilation in residential buildings. In *Cold Climate HVAC Conference*, pp. 111–122. Springer.

Denkenberger, D., D. Driscoll, E. Lighthiser, P. May-Ostendorp, B. Trimboli, and P. Walters (2012). Dc distribution market, benefits, and opportunities in residential and commercial buildings.

Equa Simulation Technology AB (1999). *Simulation Environment. Version 2.11, Reference manual*.

Fregosi, D., S. Ravula, D. Brhlik, J. Saussele, S. Frank, E. Bonnema, J. Scheib, and E. Wilson (2015). A comparative study of dc and ac microgrids in commercial buildings across different climates and operating profiles. In *2015 IEEE First International Conference on DC Microgrids (ICDCM)*, pp. 159–164. IEEE.

Gerber, D. L., R. Liou, and R. Brown (2019). Energy-saving opportunities of direct-dc loads in buildings. *Applied Energy 248*, 274–287.

Glasgo, B., I. Azevedo, and C. Hendrickson (2016). How much electricity can we save by using direct current circuits in homes? In *Understanding the potential for electricity savings and assessing feasibility of a transition towards DC powered buildings*.

Hofer, J., B. Svetozarevic, and A. Schlueter (2017). Hybrid ac/dc building microgrid for solar pv and battery storage integration. In *2017 IEEE Second International Conference on DC Microgrids (ICDCM)*, pp. 188–191. IEEE.

Huang, P., M. Lovati, X. Zhang, C. Bales, S. Hallbeck, A. Becker, H. Bergqvist, J. Hedberg, and L. Maturi (2019). Transforming a residential building cluster into electricity prosumers in sweden: Optimal design of a coupled pv-heat pump-thermal storage-electric vehicle system. *Applied Energy 255*, 113864.

International Energy Agency Photovoltaic Power Systems Programme (2019). *Trends in photovoltaic applications 2019*.

Kakigano, H., M. Nomura, and T. Ise (2010). Loss evaluation of dc distribution for residential houses compared with ac system. In *The 2010 International Power Electronics Conference-ECCE ASIA-*, pp. 480–486. IEEE.

Levin, P. et al. (2009). Brukarindata för energiberäkningar i bostäder. *SVEBY, Tech. Rep.*.

Lucía, Ó., I. Cvetkovic, H. Sarnago, D. Boroyevich, P. Mattavelli, and F. C. Lee (2013). Design of home appliances for a dc-based nanogrid system: An induction range study case. *IEEE Journal of Emerging and Selected Topics in Power Electronics 1*(4), 315–326.

Ollas, P. (2020). Energy savings using a direct current distribution net-work in a pv and battery equipped residential building.

Ralon, P., M. Taylor, A. Ilas, H. Diaz-Bone, and K. Kairies (2017). Electricity storage and renewables: Costs and markets to 2030. *International Renewable Energy Agency: Abu Dhabi, United Arab Emirates*.

Ryu, M.-H., H.-S. Kim, J.-W. Baek, H.-G. Kim, and J.-H. Jung (2015). Effective test bed of 380-v dc distribution system using isolated power converters. *IEEE transactions on industrial electronics 62*(7), 4525–4536.

Seo, G.-S., J. Baek, K. Choi, H. Bae, and B. Cho (2011). Modeling and analysis of dc distribution systems. In *8th International Conference on Power Electronics-ECCE Asia*, pp. 223–227. IEEE.

Vossos, V., K. Garbesi, and H. Shen (2014). Energy savings from direct-dc in us residential buildings. *Energy and Buildings 68*, 223–231.

Weiss, R., L. Ott, and U. Boeke (2015). Energy efficient low-voltage dc-grids for commercial buildings. In *2015 IEEE First International Conference on DC Microgrids (ICDCM)*, pp. 154–158. IEEE.

Ylmén, P. and J. Persson (2017). Monitoring of pilot sites. deliverable d6.3. wp 6. monitoring and evaluation during the operation phase.

Zottl, A., R. Nordman, M. Miara, and H. Huber (2011). System boundaries for spf calculation. In *Proceedings of the 10th IEA Heat Pump Conference, Tokyo, Japan*, pp. 16–19.

Parametric analysis of ground source heat pump system for heating of office buildings in Nordic climate

Mehrdad Rabani[1,2*], Habtamu Bayera Madessa[1], Jørgen Torgersen[3], Natasa Nord[2]

[1]Department of Civil Engineering and Energy Technology, Oslo Metropolitan University, Oslo, Norway

[2]Department of Energy and Process Engineering, Norwegian University of Science and Technology, Trondheim, Norway

[3]Asplan Viak AS, Norway

* Mehrdad Rabani: Mehrdad.Rabani@oslomet.no

Abstract

This paper presents a sensitivity analysis followed by an optimization to improve the performance of a ground source heat pump (GSHP) system for an office building located in Norway, for Oslo, Stavanger, and Tromsø climatic conditions. The ground source heating model was firstly validated by available measured data. The sensitivity and optimization simulations were conducted by using IDA ICE software and its integration with the GenOpt tool for optimization. The sensitivity results showed that the borehole depth was the most prominent parameter. Therefore, by increasing and decreasing the borehole length by 20%, for example for Tromsø climatic condition, the energy supplied by the top heating reduced by 22% and increased by 31%, respectively.

Introduction

Buildings contribute around 33% to the greenhouse gas emissions. Therefore, reducing the energy use of the building stock may significantly decrease the global CO_2 emissions (Metz et al., Ally et al.). To have a substantial impact, a deep retrofitting is essential. Therefore, in addition to improvements of the building envelope, utilization of renewable energy sources in the energy supply system of buildings should increase. Ground energy source is an example in this point, which is a clean and available renewable energy that has shown a great potential for heating applications, especially in cold climate countries such as Norway (Nord et al. 2016, Nord 2017). Many researchers have investigated different ways to reduce the building energy use by taking advantage of ground energy source.

A ground source heat pump (GSHP) is an efficient method for extracting energy from the ground and use for heating applications. As the earth has a relatively constant temperature at depth, this technology can transfer the stored heat in ground to the building site. Several studies analyzed this system. Madessa et al. conducted a parametric study to assess the performance of the GSHP with vertical bore holes configuration. The results showed that ground depth is an important factor affecting the coefficient of performance (COP) of the GSHP significantly. Further, Wang et al. analyzed the potential

of the GSHP by modelling the energy use of a conventional building under various climatic conditions. They found out that the thermal conductivity of local geological materials could considerably affect the system performance. Integration of the GSHP with other technologies such as solar thermal collectors (Emmi et al., Naranjo-Mendoza et al.), concentrated photovoltaic thermal solar collectors (Chen et al.), and heat recovery and exhaust air heat pump (Nord et al., Zhang et al.) proved to be a robust solution for heating application in cold climate countries.

This study performed a sensitive and optimization analyses on different parameters of a the GSHP system in cold climatic condition in order to identify the influential system parameters and find their best combination set that could result in minimum delivered energy to the building for space heating application.

Theoretical Background

A compression based heat pump is a machine used to transfer heat from a low temperature source to a high temperature sink (application area) by using the compression work. It consists mainly of an evaporator, a compressor, a condenser, and an expansion valve. The heating performance of the heat pump is evaluated using a factor called coefficient of performance (COP) indicating the ratio between the useful heat supplied by the heat pump condenser and the required work input to the compressor.

In a GSHP, a secondary loop system transfers the heat from the heat pump to the building. The ground borehole, which transfers the heat from the circulating fluid to the heat pump loop, could be buried horizontally or vertically. The amount of thermal energy extracted from the ground depends on borehole depth, number of boreholes, and radius of boreholes, mass flow rate of the working fluid as well as the conductivity of ground and filling mass of borehole.

Method

To study the effect of different parameters on the performance efficiency of the GSHP system, IDA-ICE energy simulation software was used. Furthermore, to

optimize the system input parameters for improving the GSHP performance, IDA-ICE was coupled with the GenOpt optimization tool.

Borehole modeling for validation

To validate the borehole extension model in IDA-ICE, numerical results were validated by the available measured data taken from the Powerhouse Kjørbo's ground heating system, located in Bærum, Norway. It should be noted that the borehole extension model in IDA-ICE was also validated by Fadejev and Kurnitski.

The results for the temperature of the brine liquid at the outlet of the borehole and the thermal performance of the soil were compared. This was done by controlling the type of brine liquid, its mass flow rate and pressure, and the brine liquid temperature at the inlet of the borehole. Figure 1 shows the location, configuration, and schematic of the vertical boreholes considered for the validation study.
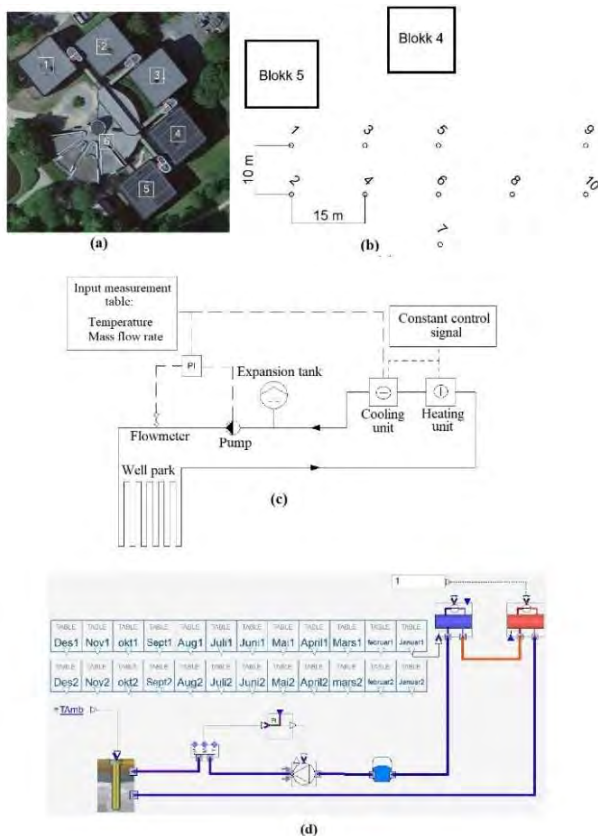
Figure 1. (a) Location and (b) configuration of boreholes, (c) schematic, and (d) simulated model of vertical borehole system

In the simulation model for the borehole system for validation, the heat carrier, from the outlet of the well park, flowed through a heating unit and then passed through a cooling unit and reached the real measured temperature. The real measured temperature was the brine

liquid temperature at the inlet of the borehole, was given as an input table in Figure 1 (c). The cooling and heating units had a constant control signal equal to 1, meaning that they are switched on all the time and they can adjust the brine liquid temperature at the inlet of the borehole to those of measurements. The circulation pump received a control signal from a PI controller to keep the measured mass flow at the set point value. It is worth mentioning that the table values in the simulation (Figure 1 (d)) were averages of all the collected logged values from Kjørbo. The logged values from Kjørbo was collected every other minute.

The borehole temperatures in IDA ICE were modelled by ten nodes, evenly distributed over the borehole length. In addition, the borehole had input value for the outdoor air temperature to calculate the temperature in the ground and at the surface. In the borehole model, the average temperature in the soil as well as a temperature gradient should be stated. These were implemented as explained in Table 1. In addition, other information about the parameters used for validation of borehole model, including borehole properties, are listed in this table

Sensitive analysis and optimization settings

Figure 2(a) shows the floor plan and shape of the reference office building considered for sensitive analysis and optimization study. The office building met the requirements for Norwegian passive house standard according to the NS 3701 standard and had a heated area of 4 903 m^2. Energy calculations for the building were carried out in accordance with the NS 3031 Norwegian standard as described in the Norwegian building code TEK17.

Table 1. Detail of parameter values used for validation of borehole model

Parameter	Value
Borehole depth (m)	219
Borehole radius (m)	0.0575
Borehole casing (m)	6
Number of boreholes	10
Number of collector tubes per borehole	1
Collector pipe radius	0.016
Thickness of the collector tube (m)	0.024
Surface heat capacity (J/(kg·K))	1140
Surface conductivity (W/(m·K))	0.75
Surface density (kg/m^3)	1680
Ground heat capacity (J/(kg·K))	920
Ground conductivity (W/(m·K))	2.25
Ground density (kg/m^3)	2880
Temperature in ground (°C)	$\theta_m + 2$
Geothermal temperature gradient (°C/m)	0.02
Heat capacity of collector tube (J/(kg·K))	930
Conductivity of collector tube (W/(m·K))	0.41
Roughness of collector tube	1.524×10^{-4}
Heat capacity of filling mass (J/(kg·K))	420
Conductivity of filling mass (W/(m·K))	0.6
Density of filling mass (Kg/m^3)	1000

Type of brine liquid	Ethanol
Freezing temperature of brine liquid (°C)	-17
Conductivity of heat carrier	0.41

θ_m: Annual average air temperature (°C)

After the validation of the borehole extension model in IDA-ICE for Oslo climate, the model was tested for a generic office building for three different climatic conditions; Oslo, Stavanger, and Tromsø. The reference building energy supply system for the sensitive and optimization analysis was implemented using the Early Stage Building Optimization (ESBO) plant in IDA ICE (Figure 2(b)). It included peak load heating, base load heating, and heating and cooling distribution systems. The domestic hot water set point temperature was set to 55°C and the supply temperature to the hot water accumulation tank had was controlled by the outdoor compensation curve. To control the temperatures, a 3K dead-band was also considered for ventilation and space heating systems to avoid a high frequency from the actuators. The cold water temperature set points for ventilation air and space cooling units were 5°C and 14°C, respectively. Furthermore, the peak load heating was added to ensure that the heating set point temperatures were maintained in the upper part of accumulation tank all the time. To improve the GSHP efficiency and to avoid a low COP of the heat pump due to oversizing, the sizing of the entire plant was performed as the following: 80% of energy need for heating was covered by the base load heating from the GSHP condenser and the rest (20%) was covered by the peak load heating.
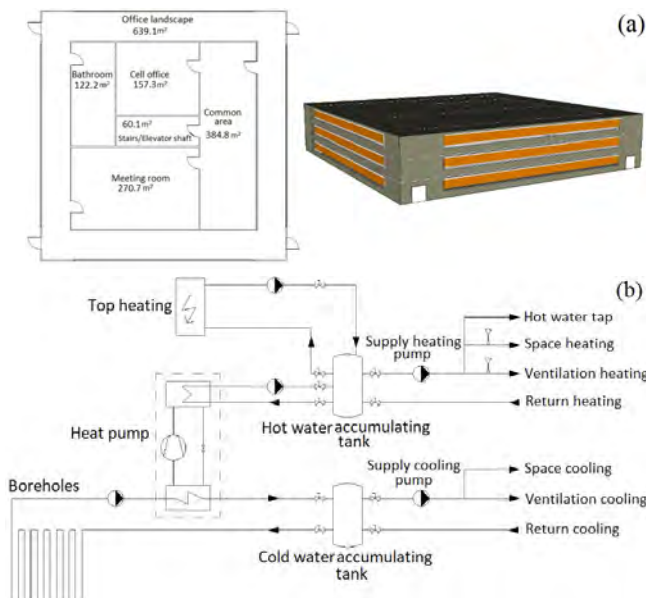
Figure 2. (a) Floor plan and shape of the office building and (b) the simplified schematic of energy supply system for sensitive and optimization study

The details of the building envelope and heating, ventilation, and air conditioning (HVAC) system are shown in Table 2. A hydronic heating system with radiators and convectors was used for space heating and cooling, respectively. The zone temperature set points for heating and cooling were 22 and 24°C, respectively.

Table 2. Details of building envelope, heat gains and HVAC system parameters in the reference case

Parameter	Value	Comment
Supply air temperature (°C)	16	Constant air volume (CAV) system
Supply air supply outside working hours (L/(s·m²))	0.7	Directorate of the Labor Inspectorate, profile usage: weekends, holidays, and non-working hours
Supply airflow during working hours (L/(s·m²))	2.1	Directorate of the Labor Inspectorate, profile usage: from 6:00 to 18:00 o'clock
Heat gain due to equipment (W/m²)	6	NS 3701, profile usage: from 7:00 to 18:00 o'clock, no usage in other times, holidays, and weekends
Heat gain due to occupancy (W/m²)	4	NS 3701, the same as equipment
Heat gain due to lighting (kWh/m²·year)	12.5	NS 3701, the same as equipment
U-Value (external wall/ceiling/floor) (W/(m²·K))	0.1/0.08/0.08	NS 3701
U-Value (door/window) (W/(m²·K))	0.8/0.8	NS 3701
Normalized cold bridge	0.03	NS 3701
Efficiency of ventilation heat recovery	0.83	NS 3701
Specific fan power (kWh/(m³/s))	1	NS 3701
airtightness, n50 (h⁻¹)	0.6	NS 3701

For sensitivity analysis, six parameters were considered and varied with ± 20% compared to the reference case, as shown in Table 3.

Table 3. Parameter values and ranges for sensitive analysis

Parameter	-20	Reference system	+20
Borehole depth (ZHOLE) (m)	175	219	263
Number of boreholes (NHOLE)	8	10	12
Conductivity of filling mass (K1) (W/(m·K))	0.48	0.6	0.72
Conductivity of ground (K2) (W/(m·K))	1.8	2.25	2.7
Mass flow rate (MFLOW) (kg/s)	1.6	2	2.4
Boreholes radius (RHOLE) (m)	0.046	0.0575	0.069

The optimization process was performed by using GenOpt tool with the combination of Particle Swarm

Optimization PSO and Generalized Pattern Search (GPS) with Hooke-Jeeves algorithms. The parameters considered for the optimization study are shown in Table 4. In the optimization process, the objective function was the delivered energy to the building.

Table 4. Range of parameter values considered for the optimization study

Parameter	Range	Description
Borehole depth (m)	50-400	Interval: 50
Number of boreholes	1-20	Interval: 1
Mass flow rate (kg/s)	1-5	Interval: 1
Tank radius (m)	0.1-1	Interval: 0.1
Window U-value (W/(m².K))	0.6, 0.7, 0.8	NA

Results and discussion

Figure 3 shows the variation of the ground temperature in the reference borehole, simulated for ten evenly vertical points at three different cities.
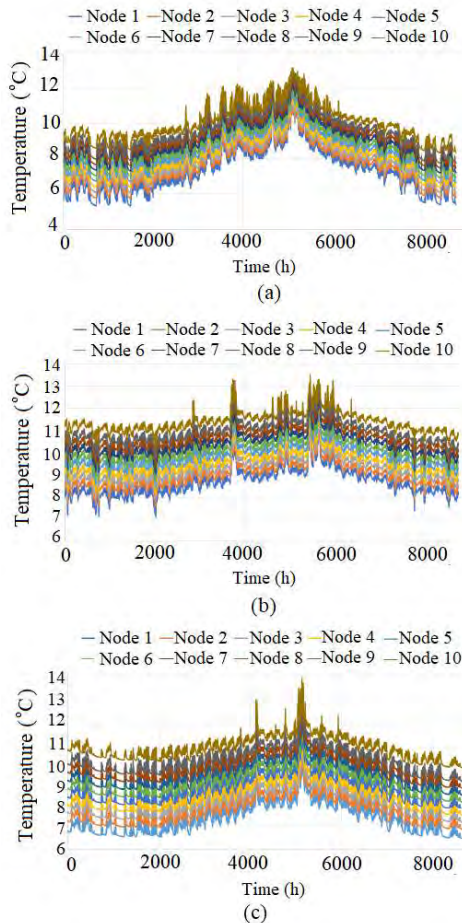
Figure 3. Annual ground temperature variation in the reference system at (a) Oslo, (b) Stavanger, and (c) Tromsø

A significantly higher ground temperature is observed for Stavanger compared to Tromsø and Oslo. The ground temperature was lower in winter and higher in summer due to transfer of heat from/to the ground to/from the

building. It should be noted that the temperatures reached to their original level by the end of the year implying that a significant cooling of the ground did not cause over-discharging of ground on the annual level. However, this may be an issue over longer periods.

With regard to the parameters considered in Table 1, the numerical model of the boreholes was validated by the available measured data for Oslo climate, as shown in Figure 4(a) for the boreholes working fluid (ethanol) temperature at the outlet of boreholes and in Figure 4(b) the heat rate of chargning and discharing in the boreholes. The positive values mean extracting heat from the ground (discharging) and the negative values mean feeding heat to the ground (charging). It should be noted that Figure 4(b) shows the total charging and discharging in the boreholes. The maximum extraction rate from the ground was achieved around 18.3 W/m$_{borehole\ depth}$.
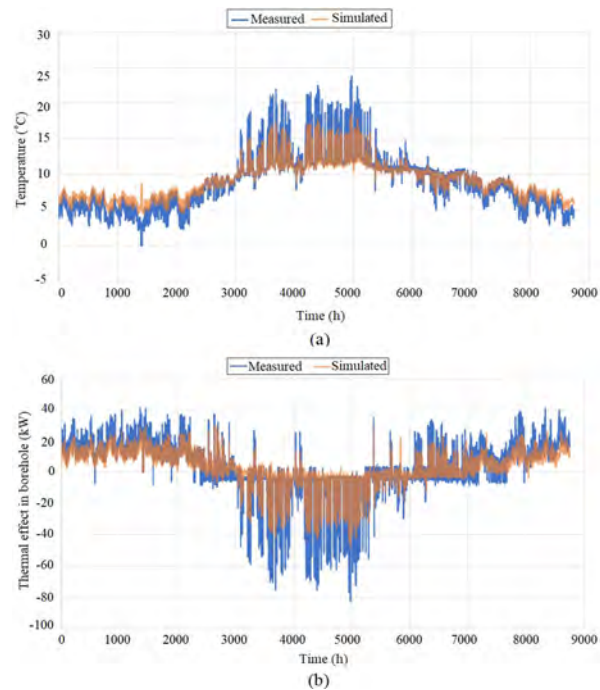
Figure 4. (a) Annual temperature variation of the brine liquid at the outlet of borehole and (b) Annual variation of charging and discharging in the boreholes

As it can be seen from Figure 4, the simulated results were in agreement with the measured data indicating the acceptable performance of the borehole extension model in IDA ICE in replicating the measured data. However, the measured values were higher than the simulated results and the average deviation between the measured and simulated results, e.g. for the brine liquid temperature at the outlet of borehole, was around 0.95 K.

Figure 5 compares the measured and the simulated values of the borehole working fluid temperatures at the outlet of the borehole. The comparison was also quantified using the Coefficient of Determination (R^2) and Coefficient of Variation of Root Mean Square Error (CV_{RMSE}) (ASHRAE), which the latter was defined as follows:

$$CV_{RMSE}(\%) = \frac{1}{\overline{y}}\sqrt{\frac{\sum_{i=1}^{n}(y_i - \hat{y}_i)^2}{n}} \times 100 \qquad (1)$$

where y_i is the simulated value at instance i, $\hat{y}_i$ is the measured value at instance i, $\overline{y}$ is the average of measured data, and n is the number intervals.

As Figure 5 shows R^2 is 96% implying that the variation in simulated temperature well followed the variation in measured temperatures. The CV_{RMSE} was also low, equal to 7% (should be less than 30% according to ASHRAE guideline), which indicated that measured values were in good agreement with the simulated values. It should be noted that the large discrepancies observed in Figure 4 were probably due to hourly averaging of the whole measured data set, shown in Figure 5.
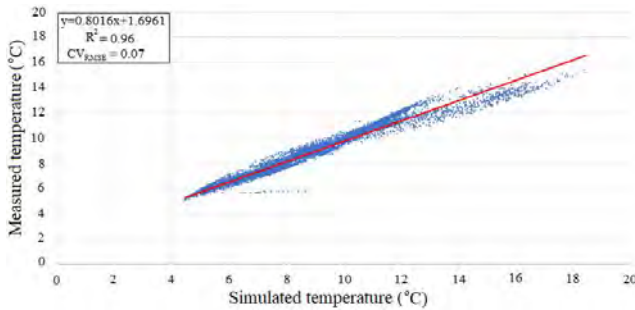
Figure 5. Scatter plot of measured and simulated annual temperature of working fluid at the outlet of borehole

After the borehole model was validated for the Oslo conditions, the model was tested for different climate conditions.

Figure 6 shows a qualitative spatial temperature variation in the ground for Tromsø when the ground temperature was 0°C simulated in IDA-ICE. The number of boreholes in this case was 10. Ground temperature variation reduced as the depth increased so that in far distance from the surface, the temperature remained almost constant and no further temperature variation with depth increase was observed.

The sensitivity analysis based on the parameters shown in Table 3 are presented here. Figure 7 shows the effect of 20% changes in the input parameters, as suggested in Table 3, on the compressor energy use, energy absorbed from the borehole, and the energy supplied by the peak load heating. The borehole depth was the most effective parameter on the borehole performance so that decreasing the borehole depth by 20% led the energy supplied by the peak load heating to increase up to 28%, 108%, and 31% for Oslo, Stavanger, and Tromsø climatic conditions, respectively. The corresponding increase of the borehole depth resulted the energy supplied by the peak load heating to decrease by 21%, 53%, and 22% respectively. Furthermore, the change in borehole parameters did not affect the energy extracted from the borehole and the

compressor energy use as much as the heat supplied by the peak load heating for Stavanger. It is worth mentioning that the change in the borehole filling mass conductivity was not included in the results in Figure 7, because it had negligible effect on the energy use by the compressor, the extracted energy from the borehole, and the heat supplied by the peak load heating.
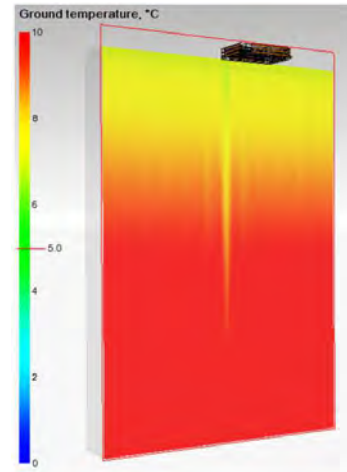
Figure 6. A cross section of temperature variation in the ground around the boreholes on 4th January for Tromsø climate
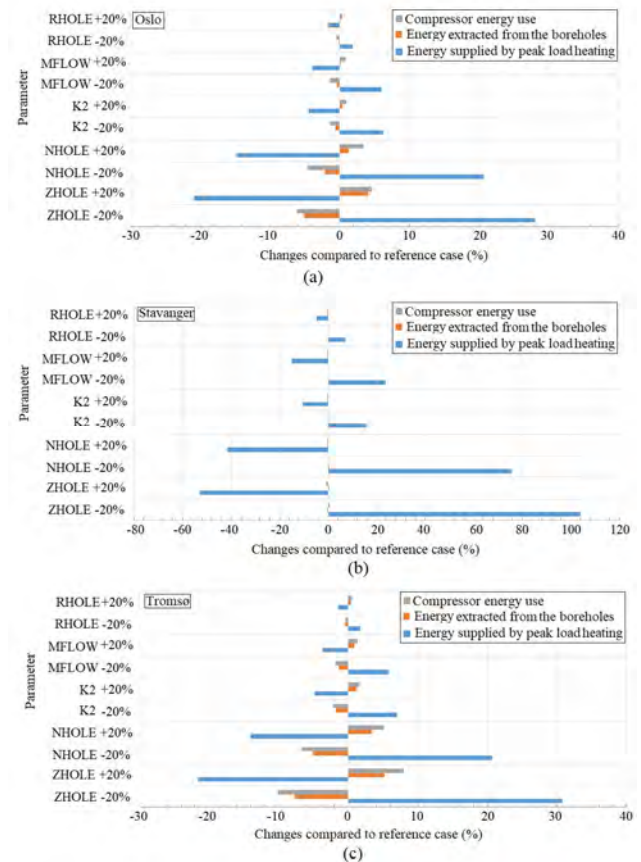
Figure 7. Tornado diagram of different parameters in sensitivity analysis for (a) Oslo, (b) Stavanger, and (c) Tromsø climatic conditions.

Figure 8 shows the impact of different parameters on the COP values at different cities. As it was also observed in Figure 7, the borehole length was the most influential factor on the COP. The COP values at Stavanger did not follow the same trend as in Tromsø and Oslo. The reason was the ratio between the amount of energy used by the compressor and the extraction energy from the borehole. This can be better explained, for example for borehole length, in Figure 9.
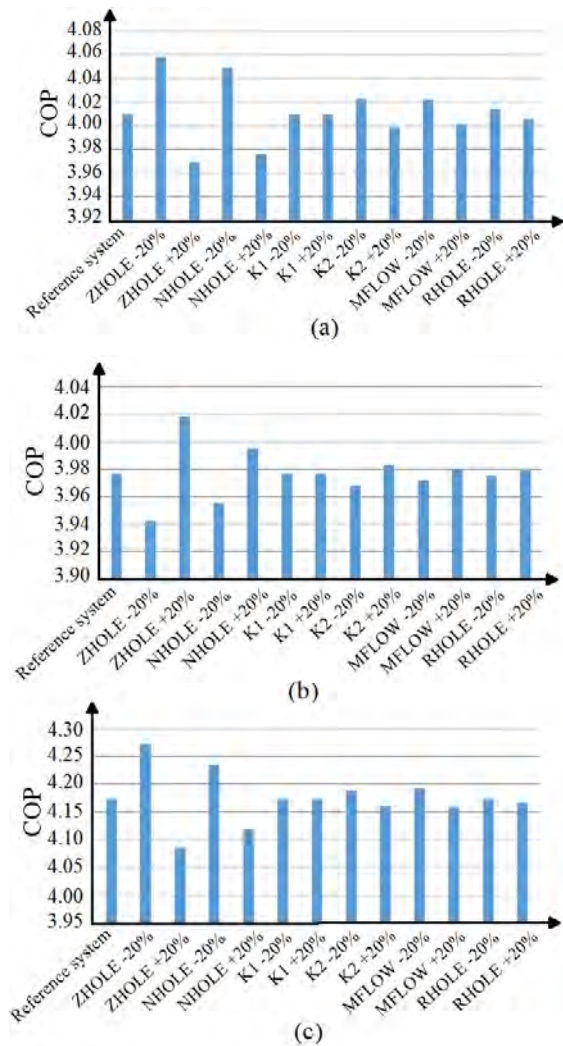
Figure 8. COP values for various parameters in sensitivity analysis for (a) Oslo, (b) Stavanger, and (c) Tromsø climatic conditions.

As Figure 9 shows, in Oslo and Tromsø climate, a decrease in the borehole length yielded a decrease in both the extracted energy from the borehole and the compressor energy use (top picture in Figure 9). However, the ratio of extracted energy from the borehole to the compressor energy use increased as the borehole length decreased, 1.33% and 11.97% for Oslo and Tromsø, respectively. Therefore, the COP increased (cases (c) and (a) in Figure 8). A different trend happened for Stavanger climate; a decrease in the length of borehole

led the extracted energy from the borehole to decrease and the compressor energy use to increase resulting in a decrease in the COP value. It should be also noted that the GSHP could cover almost the whole heating needs in the Stavanger climate so that a trivial amount of energy need for heating was supplied by the peak load heating.
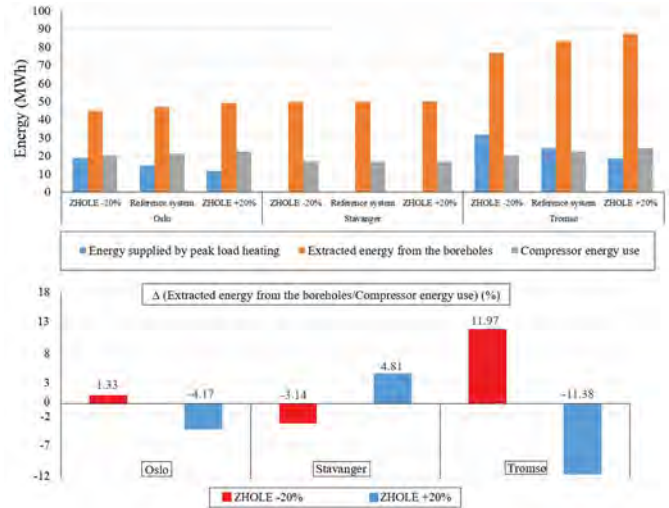
Figure 9. Amount of energy supplied, extracted, and used by different part of GSHP system (top) and ratio variation of borehole extraction energy to compressor energy use (bottom)

Table 5 shows the optimized input parameters, introduced in Table 4, which resulted in minimum delivered energy to the building.

Table 5. Optimized input parameters and the corresponding minimum delivered energy values at three different locations

Parameter	Oslo	Stavanger	Tromsø
Borehole depth (m)	400	400	400
Number of boreholes	20	20	20
Mas flow rate (kg/s)	5	3	5
Tank radius (m)	1	0.2	1
Window U-value (W/(m².K))	0.6	0.7	0.6
Delivered energy of the Reference system (kWh/year)	20 741	17 153	27 193
Delivered energy of the optimal system (kWh/year)	16 127	16 290	23 939

The maximum values of the mass flow rate, length and the number of boreholes, and the tank radius were chosen in the optimization process for the Oslo and Tromsø cases. Nevertheless, the same values did not result in the minimum delivered energy for the Stavanger case. The largest decrease was for the Oslo case, where the annual delivered energy was reduced by 4 614 kWh. In the

Stavanger case, there was a little change, 863 kWh, while for the Tromsø case it reduced by 3 254 kWh. These values correspond to approximately 22%, 5%, and 12% reduction of the delivered energy compared to the reference system in Oslo, Stavanger, and Tromsø cases respectively.

Conclusion

This paper dealt with sensitive analysis and optimization of the GSHP system. The simulations were performed using the building simulation software IDA-ICE and the generic optimization tool GenOpt. In the first step, the ground source borehole model was validated by available measured data and the simulation results were in good agreement with the measured data. The sensitive analysis showed that the borehole depth was the most effective and decreasing the borehole depth by 20% led the energy supplied by the peak load heating to increase up to 28%, 108%, and 31% for Oslo, Stavanger, and Tromsø climatic conditions, respectively. Furthermore, the optimization process revealed that the annual delivered energy to the building was decreased by approximately 22%, 5%, and 12% compared to the reference system in Oslo, Stavanger, and Tromsø cases respectively. Future work on the optimization and sensitive analysis could include a life cycle cost and a life cycle CO_2 emission for different alternatives along with delivered energy simultaneously. It can provide readers with more practical insights about the effective parameters on the system performance.

References

Ally, M.R., Munk, J.D., Baxter, V.D. and Gehl, A.C. (2015). Exergy analysis of a two-stage ground source heat pump with a vertical bore for residential space conditioning under simulated occupancy. *Applied Energy 155*, 502–514.

American Society of Heating, Ventilating, and Air Conditioning Engineers (ASHRAE). Guideline 14-(2014), Measurement of Energy and Demand Savings; Technical Report; American Society of Heating, Ventilating, and Air Conditioning Engineers: Atlanta, GA, USA.

Building Technical Regulations with guidance (2017). (*TEK 17*) (in Norwegian).

Chen, Y., Wang, J., Ma, C. and Shi, G. (2019). Multicriteria performance investigations of a hybrid ground source heat pump system integrated with concentrated photovoltaic thermal solar collectors, *Energy Conversion and Management 197*, 111862.

Directorate of the Labor Inspectorate, Climate and air quality in the workplace (2016) (in Norwegian).

Accessible:https://www.arbeidstilsynet.no/contentass ets/3f86f6d2038348d18540404144f76a22/luftkvalitet -pa-arbeidsplassen.pdf

Emmi, G., Zarrella, A., De Carli, M. and Galgaro, A. (2015). An analysis of solar assisted ground source heat pumps in cold climates, *Energy Conversion and Management 106*, 660–675.

Fadejev, J. and Kurnitski, J. (2015). Geothermal energy piles and boreholes design with heat pump in a whole building simulation software, *Energy and buildings 106*, 23–34.

Madessa, H.B., Torger, B., Bye, P.F. and Erlend, A. (2017). Parametric Study of a Vertically Configured Ground Source Heat Pump System. *Energy Procedia 111*, 1040–1049.

Metz, B., Davidson, Davidson, O., Bosch, P., Dave, R. and Meyer, L. (2007). *Mitigation of climate change*, Cambridge University Press, Cambridge (UK).

Naranjo-Mendoza, C., Oyinlola, M.A., Wright, A.J. and Greenough, R.M. (2019). Experimental study of a domestic solar-assisted ground source heat pump with seasonal underground thermal energy storage through shallow boreholes, *Applied Thermal Engineering 162*, 114218.

Nord, N., Qvistgaard, L.H. and Cao, G. (2016). Identifying key design parameters of the integrated energy system for a residential Zero Emission Building in Norway. *Renewable Energy 87,* 1076–1087.

Nord, N. (2017). Building Energy Efficiency in Cold Climates, *Encyclopedia of Sustainable Technologies*, 149–157.

Norwegian Standard (2012). *Criteria for passive houses and low energy buildings*, *Non-residential buildings*, (*NS-3701*) (in Norwegian).

Norwegian Standard (2014). *Calculation of energy performance of buildings - Method and data*, (*NS 3031*) (in Norwegian).

Norwegian book prices (Norsk Prisbok) (2019). *Norconsult Informasjonssystemer AS*, https://www.norskprisbok.no/WhatIsNP.aspx

Wang, G., Wang, W., Luo, J. and Zhang, Y. (2019). Assessment of three types of shallow geothermal resources and ground-source heat-pump applications in provincial capitals in the Yangtze River Basin, China, *Renewable and Sustainable Energy Reviews 111*, 392–421.

Zhang, P., Wang, B., Wu, W., Shi, W. and Li, X. (2015). Heat recovery from Internet data centers for space heating based on an integrated air conditioner with thermosyphon, *Renewable Energy 80* 396–406.

Solar PVT for heat pumps: Collector development, systems integration, and market potential

Nelson Sommerfeldt[1], Francisco Beltran[1*], Hatef Madani[1]
[1]KTH Royal Institute of Technology, Stockholm, Sweden
*corresponding author: francisco.beltran@energy.kth.se

Abstract

Solar PV/thermal hybrid collectors have been researched for decades, but have never had market success. This paper motivates a research agenda for PVT based on heat pump integration. The market potential is defined and prior research reviewed with an emphasis on systems and collector modelling methods. The result is a research project that works on the component and systems level, with digital and physical prototypes. This project is expected to deliver validated evidence on the advantages of PVT as a compliment to ground source heat pumps and an alternative to air source heat pumps, which can contribute to the decarbonisation of buildings in Europe.

Introduction

Building electrification with heat pumps is a promising technique for heating decarbonisation, particularly if combined with solar energy. Historically, solar heat pump (SHP) research has focused on solar thermal technologies (Poppi et al., 2018), however cost reductions in photovoltaics (PV) has led to an increase in PV based SHP research and a renewed interest in PV-thermal (PVT) hybrid collectors (IEA, 2018). PV installations are increasing rapidly, but PVT has struggled to find success in the market due to issues of reliability, lack of certification standards, confusing range of designs and applications, and high cost relative to alternative pool or domestic hot water (DHW) heating approaches (Good et al., 2015).

PVT collectors combine PV and solar thermal (ST) designs to generate electricity and heat from the same module. Traditionally this meant adding PV cells to the front surface of a glazed ST collector, but more recently manufacturers have been adding heat exchangers to the rear side of traditionally manufactured PV modules.

The application of PVT on the source side of a heat pump offers multiple benefits – the heat pump can receive higher source temperatures for more efficient operation, the lower operating temperature of the collector increases thermal efficiency, and the cooler PV will generate more electricity. However, there are limits to the net energetic benefits a solar collector can have as a heat pump source (Haller and Frank, 2011) and it has been suggested that solar heat should be used for higher-temperature, DHW applications first and heat pump sources second (Kjellsson et al., 2010). This approach assumes that the solar collector should be readily available to prepare DHW, which requires a specific design strategy that is inconsistent with the design of a collector used as a heat pump source – namely, the use of glazing and insulation.

While striving for cost reductions and increased reliability, most PVT collectors on the market today do not use isolative glazing, only glass in contact with the PV cells that protects them from damage (Weiss and Spörk-Dür, 2019). This makes them less thermally efficient than glazed collectors for DHW preparation, but rear-side insulation still makes it possible to reach DHW temperatures, particularly in warmer climates. When operating at the low temperatures used in a heat pump supply circuit (-10° to +20° C), which are often at or below ambient air, the insulation becomes a barrier to efficiency by hindering heat transfer from the air. So in the interest of reducing costs and increasing efficiency, this line of research focuses exclusively on the design of PVT collectors for source side integration of heat pumps.

The objective of this paper is to motivate and describe a research plan for developing a novel, low-cost PVT collector specifically for use in a range of SHP systems. This is achieved by defining specific markets and applications where PVT-SHP can provide more value than alternative solutions, describing the most promising methods of systems integration matched to specific applications, and identifying specific design strategies for PVT collectors for future development. For each stage of the development, appropriate simulation tools are identified, motivated, and described.

This paper is an amalgamation of insights learned over multiple studies performed by the authors during a four year period, and space limitations prevent a complete reporting of model details. References to papers with complete details are provided and the topics presented here are selected to highlight the modelling process and their application towards future development of SHPs.

Applications and market potential

The demand for heat pumping machines is growing in Europe (EHPA, 2019). There are many styles based on heat source, sink, and application, but in buildings it is most common to see heat pumps in single family houses (SFH) with air-to-air or air-to-water configurations. In larger buildings and/or in colder climates, brine-to-water

ground source heat pumps (GSHP) become more common for their improved efficiency over air source heat pumps (AHSP).

SHP designs are extremely diverse and multiple reviews have found that no technical or economically optimal configurations have been found (Chu and Cruickshank, 2014; Mohanraj et al., 2018a; Poppi et al., 2018). Compared to technical aspects, much less attention has been paid to the economic considerations of SHP and their market potential to impact global energy challenges. This study is limited to liquid based PVT collectors integrated with air-to-water and GSHP, which share some common design strategies but utilize different heat sources. PVT can be designed with air as a working fluid in conjunction with an air-to-air heat pump, but the design strategy is considerably different from the liquid based design.

Ground source heat pumps

GSHP rely on the ground's mass to maintain higher temperatures during heating seasons. When the majority or entirety of a load is for heating, the volume of soil/rock surrounding the heat exchanger reduces in temperature. This is usually designed into the system to maintain acceptable performance during its lifetime, however problems can arise if a heat exchanger is undersized.

The primary consequence of undersized ground heat exchangers (GHE) is a reduction in heat pump efficiency resulting in higher electricity use. It can also lead to greater reliance on the direct electric backup heater, which is much more detrimental to efficiency. It is also possible for water inside and around the heat exchanger to freeze, causing frost heaves and damaging the ground at the surface, or potentially damaging the heat exchanger.

Undersized GHEs are not currently a systemic problem, however the issue is growing in more mature markets like Austria, Sweden, and Switzerland. After two to three decades of installations, many buildings will be ready to retrofit a new, more efficient heat pump. The higher efficiency combined with the already degraded ground temperatures means the GHE will be undersized. One solution is to increase the size of the GHE, if the area permits, however this just delays the problem.

PVT can provide benefits in two ways: as a secondary thermal energy source to the heat pump, thereby reducing the load on the ground, and by regenerating the ground with excess solar energy in the summer months. This not only solves the immediate undersizing problem, but will stabilize the GHE temperatures indefinitely. Connecting the PVT in series with the ground, as shown in Figure 1, makes integration with existing systems simple and scalable. It does not require changes to the storage tanks like traditional solar thermal systems, and few if any modifications to the heat pump are required.

Based on installation rates during the 2010's, in 10-15 years most countries in Europe will be routinely upgrading heat pumps leading to an increased potential for undersized GHEs. With approximately 100,000 GSHP

sold each year, this is a smaller but notable market segment that can contribute to PVT's scalable commercialization.

The higher investment cost for GSHP make them suitable for larger multi-family residential or commercial buildings, which are often lacking the land area needed for large GHEs. ASHP alternatives are often unacceptably noisy, leaving a significant part of the building stock inaccessible to heat pumps and electrification. Series connected solar collector simulations have demonstrated the potential for GHE reductions (Bertram et al., 2012; Eslami-nejad et al., 2009; Reda and Laitinen, 2015). PVT in particular has been shown to reduce area requirements by over 80% and remain economically competitive with alternative heating sources (Sommerfeldt and Madani, 2019). Considering over half of the residential building stock in Europe consist of multi-family houses (MFH) (Eurostat, 2015) plus the potential for commercial buildings, PVT could help unlock a large, underserved market for GSHP. This is particularly relevant given the challenges of decarbonizing heat supply in urban building stocks.
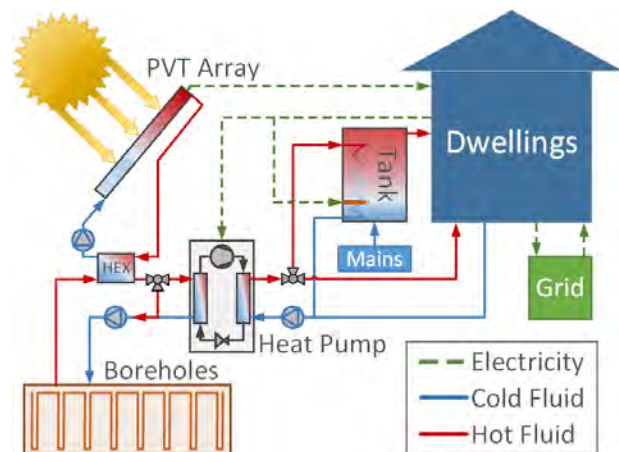
Figure 1: GSHP with series connected PVT

Solar source heat pumps

ASHP make up over 90% of the European heat pump market, with about 45% being air-to-water (EHPA, 2019). One of the main drawbacks to ASHP are disturbances from loud fans in the outdoor heat exchangers. Many SFH have 3-5 kW of PV capacity, corresponding to 20-30 m^2, which would provide a notably larger surface area for an ASHP heat exchanger than the typical fin-and-tube units. With a larger surface area, the need for forced convection is reduced and potentially eliminated, thereby solving the noise problem with ASHP. Even if fans cannot be eliminated, placing them on the roof behind the PVT collectors will help reduce their impact at ground level.

Solar source heat pumps are most often researched as direct expansion systems, where the PVT replaces the evaporator and uses refrigerant as the working fluid, however the most successful systems have relied on refrigerants with high global warming potential (Mohanraj et al., 2018b). There are natural refrigerants

with good performance, however they are flammable and/or require heavy modification to the system. Additionally, most research has been performed in subtropical climates, limiting broader market appeal (Chu and Cruickshank, 2014).

An indirect design, shown in Figure 2, uses a secondary fluid (i.e. a water/glycol mixture) to transfer heat from the PVT to the evaporator inside the heat pump. While the heat exchanger can introduce cost and performance penalties, this approach is more flexible and generalizable for scaling up across multiple markets. It also relies on familiar technologies and approaches within the solar system components, reducing needs for installer training.
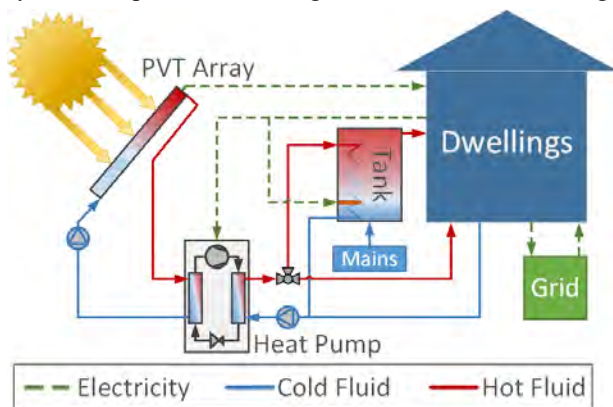
Figure 2: PVT sourced heat pump

Over 500,000 ASHP were sold in Europe in 2018, double the quantity sold in 2012 with expectations for continued growth (EHPA, 2019). After a boom/bust cycle during the 2000's and early 2010's, the solar PV market in Europe is growing again with most systems installed in buildings (IEA, 2019). Combining these two trends gives PVT a larger market to grow with potential to deliver an improved product over ASHP. The performance of a PVT sourced heat pump for Europe is still not well known. A recent laboratory study demonstrated the potential for insulated PVT collectors to meet peak winter loads in a German climate, concluding that the system concept showed promise but should use uninsulated collectors (Schmidt et al., 2018). Even less understood is the economic performance and potential for improvement, however the market potential and scale for a heat pump specific PVT is motivation for further development.

Systems integration and modelling

SHPs are predominantly simulated using quasi-steady state systems modelling tools, such as Matlab/Simulink, Polysun, and TRNSYS. These tools are considered to have an ideal balance between detail, accuracy, and computational resources while also having the flexibility for novel system design. This chapter presents the process of building a complete PVT plus GSHP model in TRNSYS, the auxiliary models used to complete the boundary conditions, and a sampling of results with comparisons. A more thorough description of the study can be found in (Sommerfeldt and Madani, 2019).

Model description

TRNSYS is particularly popular for SHP systems due to the flexibility of design using well-developed libraries of solar and heating system components. A complete systems model is simulated including the building envelope, eight-zone space heating distribution, domestic hot water tanks, heat pump, boreholes, PVT collectors, and auxiliary pumps. The model's goal is to quantify the technical and economic potential for reducing borehole field size when combined with a PVT array in series. This is measured using seasonal performance factor (SPF) considering all auxiliary devices (e.g. pumps) necessary for the function of the complete system, and a 20 year total life cycle cost (TLCC) that includes the residual value of the PVT and boreholes which are assumed to last 30 and 60 years, respectively.

The simulation is run for 20 years, which corresponds to typical heat pump lifetimes and captures long-term temperature changes in the ground due to heat extraction and injection. A three minute time step is used to capture the detailed control response of the heat pump and self-consumption of PV generation. Self-consumption can be reported as 5-10% higher when using a typical 60 minute time step (Cao and Sirén, 2014). One minute time steps are technically possible using the tools presented here, however three minutes was assumed to be a reasonable compromise for processing time. One 20 year simulation requires approximately 3.5 hours on an Intel i7-7600 running at 2.9 GHz.

The target building is a 1980's construction, 2000 m^2 MFH located in Stockholm, Sweden. Weather data representing a typical meteorological year between 1991 and 2010 is generated using Meteonorm 7.2. Atmospheric conditions (e.g. temperature, relative humidity) are generated hourly and linearly interpolated for the three minute time steps, but solar radiation is simulated using one minute time steps using the stochastic Hofmann model (Hofmann et al., 2014) and averaged across three minutes. The resulting space heating demand is 125 kWh/m^2/yr.

Electricity and hot water demand inside the building is generated at one minute intervals using a Markov Chain behavioural model (Widén and Wäckelgård, 2010) and averaged to three minutes. Electrical loads are imposed as an 80/20 split of radiative and convective internal gains and the hot water loads are served by two, fully mixed 1000 l tanks. Specific annual demand for DHW and electric appliances are 30 kWh/m^2/yr and 38 kWh/m^2/yr respectively.

The heat pump is modelled with a black box approach, using a three-dimensional interpolation based on the performance map of a commercially available, 52 kW (nominal) heat pump. The model accepts source temperature, supply temperature, and compressor speed, and returns compressor electricity demand and thermal output. This is a common technique in heat pump systems modelling (Haller et al., 2012; Madani et al., 2011) as it

dramatically reduces the computational needs of a detailed theoretical heat pump model, however it does require empirical data. The compressor speed is PID controlled using a heating supply temperature curve. Auxiliary heaters in the DHW tanks and in series with the heat pump are used to provide supplementary heat in cases where the boreholes are severely undersized. While an auxiliary heater would not normally be used this way in a capacity controlled heat pump installation, this approach directly captures the energetic penalty of not meeting heating comfort demands as opposed to the indoor temperature penalty method.

The baseline borehole field is sized according to a modified ASHRAE method implemented in the web-based GeoDesigner (Rolando et al., 2015) using hourly space and DHW demands from the building model. The result is a field consisting of 12 boreholes with single U-tubes in a 3x4 pattern, 300m deep and 20m spacing. The borehole field is modelled in TRNSYS using Type557a, based on the validated duct storage model (Hellström, 1989). This model is nearly ubiquitous in TRNSYS studies in large part due to being readily available in the pre-packaged libraries and acceptable long-term response. However the short term response has been criticised with alternative models being proposed (De Rosa et al., 2015; Godefroy, 2014), but a workaround proposed by Pärisch et al. (2015) is used here and only relies simple pipe models. Besides accessibility, another benefit of using Type557 is the ease of parametric analysis on length and spacing as compared to a g-function based model.

The system includes a prototype PVT collector being developed specifically for heat pump integration. Empirically derived coefficient models (like the heat pump model) are common but unavailable here due to the developmental nature of the PVT. Therefore a theoretical model is used based on the traditional fin-and-tube design and validated with a detailed finite-volume numerical model and measured performance. Details of the PVT model are presented in the next chapter.

Results

In the full paper, a parametric analysis of borehole length and spacing is considered to quantify the potential reductions due to PVT (Sommerfeldt and Madani, 2019). For brevity, a sample of results are presented, focusing on undersized BHE. The impact of shortened boreholes and various PVT areas on the 20-year average SPF is shown in Figure 3 and TLCC in Figure 4. The borehole (BH) length and PVT area are presented in specific units based on total annual heat demand of the building (326 MWh/yr) to be more generalizable, but for this case the markers represent discrete cases where the farthest right case is the default 12 borehole field (total length 3600 m) and two boreholes (equivalent to 600 m) are removed for each point to the left. The largest PVT array is assumed to fill the entire roof, consisting of 144 collectors equivalent to 234 m^2 and 40 kW$_p$ of PV capacity.

When PVT is added to an adequately sized borehole field, the improvement in SPF is at most 3%. For a system with equivalent performance to the baseline, up to 18% of the total borehole length can be reduced and if a 3% decrease in SPF is acceptable the borehole length can be reduced by up to 33%. These results are comparable to previous studies on PVT plus GSHP simulations in Germany (Bertram et al., 2012) and Canada (Brischoux and Bernier, 2016). For a total borehole length reduced by more than 33% reduction, backup heater usage increases, rapidly degrades SPF, and borehole freezing (indicated by white markers) becomes a potential risk.
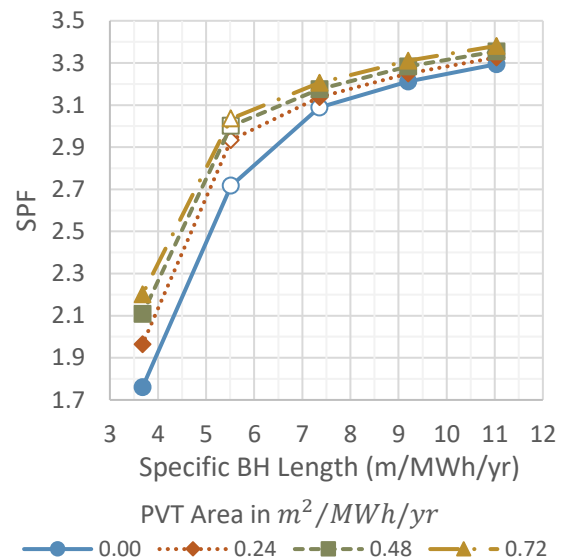
Figure 3: SPF as a function of PVT area and BH length

The TLCC results in Figure 4 suggest that the additional costs for PVT are greater than the savings from reduced borehole length. In the least cost PVT case that avoids borehole freezing (7.3 m/MWh/yr, 0.24 m^2/MWh/yr) the lifetime cost is 4% higher than baseline with a 5% decrease in SPF. For a complex systems model considering long-term economics, this is within reasonable uncertainty.

These results are also highly dependent on Swedish market conditions characterized by low electricity and drilling prices. Low electricity prices reduce the motivation for efficiency and low borehole prices reduce the economic benefits shortened length. Drilling/borehole prices are particularly critical – it is assumed here that boreholes cost approximately €32/m to install, whereas up to €100/m have been used in other European markets (Helpin et al., 2011). For this system, a doubling of borehole cost would make all PVT solutions economically competitive, suggesting the concept will provide greater value to markets outside of Sweden, however comparisons with ASHP and alternative heating sources are needed.

When compared to district heating, which over 90% of Swedish MFH use, GSHP can reduce cost and emissions, however most do not have the requisite land area for

boreholes. PVT can reduce the area needs by over 80% through length and spacing reductions, thereby increasing market potential (Sommerfeldt and Madani, 2019).
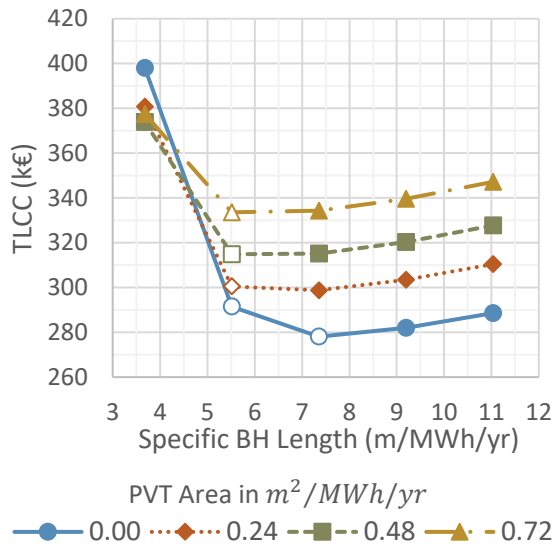
Figure 4:TLCC as a function of PVT area and BH length

Future research

The results presented here in conjunction with the full paper, demonstrate digitally that there is an opportunity for greater GSHP adoption with PVT integration. There are several disparate modelling tools and component models, all of which have been validated, that combine into a single systems model. A challenge with many systems simulation studies is the limited opportunity to test novel concepts in real world applications for full systems validation. Given the risk to system damage from a significantly undersized borehole field, proving this concept in a monitored demonstration is critical to broader market acceptance. The validated model and pilot site would also contribute to further optimization at both the component and system levels.

Broader acceptance will also require expanding simulations to cover additional markets outside of Sweden, and additional applications beyond new systems. For example, the heat pump replacement market described above, which requires the development of a temperature degraded borehole model. The complete systems model presented here is capable of simulating these boundary conditions, however validating them is a crucial next step. High quality, long-term borehole field measurements are rare, however there are opportunities in building demonstration projects that rely on existing, degraded boreholes for validation.

Collector development

This section presents a new review on the design principles of PVT collectors and the recommended features for SHP applications. Model validation is a critical part of prototype development, therefore a brief model description and validation is also presented, with full details available in (Sommerfeldt and Ollas, 2017).

Design principles

For much of the history of PVT design, PV cells were laminated to a typical solar thermal collector as a method for increasing total efficiency (Zondag, 2008). However, the prices for PV modules have dropped dramatically in the last decade due to manufacturing scale and standardization, making it more interesting to flip the design by adding heat exchangers to PV modules. This is typically done by bonding the heat exchanger to the rear side of a PV module using thermo-conductive paste (Aste et al., 2014) or mechanically pressing it into contact and applying a thermo-conducting grease.

Solar thermal absorbers are most commonly built from aluminium and/or copper for their high conductivity and strength. The sheet-and-tube design is most common, however roll-bonded and box-channel designs are potential alternatives (Aste et al., 2014). Sheet-and-tube relies on the absorber to conduct heat to the tubes carrying working fluid, however the small contact surface and imperfect bonding between the tubes and plate hinders heat transfer (Aste et al., 2014). Roll-bonding creates channels between two aluminium sheets that can be formed in nearly any shape, enabling greater surface area contact for the fluid but with higher pressure drops and cost (Bombarda et al., 2016). The box-channel design relies on extrusion, creates the highest surface area contact of the three designs, and can use metallic or polymeric materials (Zondag, 2008).

The performance differences between each design have been tested in several studies, showing that the greater surface area of roll-bond and box-channel absorbers achieve higher efficiencies than sheet-and-tube (Bombarda et al., 2016; Herrando et al., 2019; Kim and Kim, 2012). The gains in surface area can even be enough to overcome lower thermal conductivity of polymers (Herrando et al., 2019).

The use of polymers for solar thermal collectors has been hindered by high temperatures, which lead to rapid degradation of the material. In the case of heat pump integration, the low temperatures can reduce cost in both the PVT collector and the connective piping. Using a box-channel design, polycarbonate has the potential to reduce cost by 22% over a traditional absorber (Herrando et al., 2019). There is also no need for insulation since gains from the ambient air are desired, further reducing costs.

Modelling approach

PVT models are an extension of solar thermal models, which can be categorized by dimension (1D, 2D, 3D) and method (analytical, numerical). The trade-offs are largely between accuracy and computational effort. Zondag et al. (2002), found that in the calculation of daily yield, the error that comes from using a 1D steady-state versus a 3D numerical model is 0.2%. However, Chow (2003) suggests that PVT performance is transient in nature and requires a dynamic model for fluctuating ambient conditions and detailed control strategies. This is largely

an issue of the model being fit for purpose, where detailed heat exchanger design benefits from 3D numerical models, which are the most computationally expensive, and can then be translated into faster 1D/2D analytical models for use in systems analysis.

As demonstrated in the previous chapter, TRNSYS is a powerful tool for complex systems analysis, such as solar heat pumps. Type 560 is a 2D, theoretical PVT model based on the Hottel and Whillier thermal model, later modified by Florschuetz to incorporate PV (Florschuetz, 1979) and is available in the TRNSYS extended library. Being theoretical, the boundary conditions must be validated when working with untested PVT prototypes, as is the case in this study. The goal is to determine the one critical variable that is unavailable via specification sheets and difficult to estimate; thermal resistance between the PV cells and rear side heat exchanger.

Outdoor testing was to provide the necessary empirical data to validate the model, however late in the test cycle, an airlock was discovered with an IR camera, shown in Figure 5**Error! Reference source not found.**, which restricted fluid flow in the left collector. Since Type 560 requires the flow in all runners to be equal, this led to the use of TAITherm, a commercial heat transfer solver that uses a numerical, finite volume approach and allows for individual control of flow in the heat exchanger pipes.
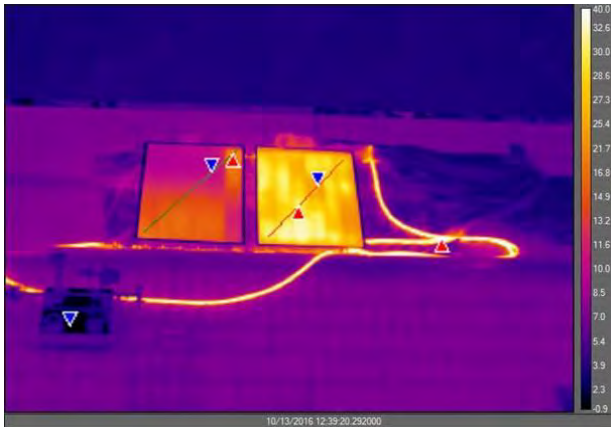
Figure 5: IR image taken during testing

TAITherm uses a 2.5D numerical model using a finite-volume approach. An image of the TAITherm model is shown in Figure 6, which relies on plate and tube surface geometry with assigned thicknesses, connected by 1D conductivity links, and 1D fluid flow model in the tubes to generate convection coefficients. There are two plates in the model; one to represent the PV module with all its layers of glass, silicon, and polymers, and a second to represent the aluminium heat exchanger plate. The plates and tube are thermally linked via a 1D conductivity model and both the front and back surfaces are connected to ambient air nodes with a convection coefficient.

The model is constructed using the known physical geometry and 5-minute measured boundary conditions from the test (i.e. weather and fluid properties). It's tuned considering the flow in each pipe, thermal conductivity

between the PV and heat exchanger, and the rear side convection coefficient. The outlet temperature of the heat transfer fluid is used as the primary calibration measurement and the thermal power output is used as a secondary indicator. Thermal power is calculated using measured volumetric flow rate, fluid density, and inlet temperature with modelled outlet temperature. The validation is measured with mean absolute error (MAE) and the correlation of the outlet temperature and thermal power time series, as well as the differences in total thermal energy generated over the test periods.
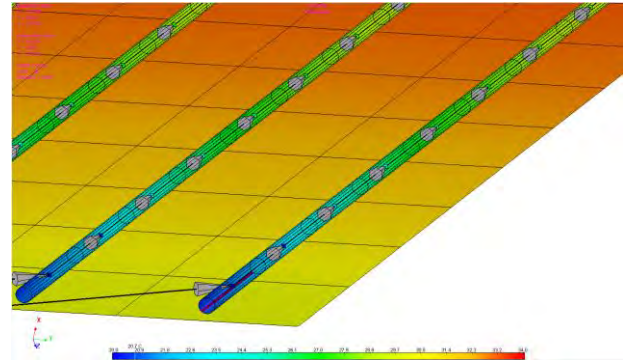
Figure 6: Detailed view of TAITherm model geometry

The surface temperatures in Figure 5**Error! Reference source not found.** are compared with those in the TAITherm model to find that 99%, or effectively all, of the working fluid is passing through the right collector with an insignificant flow through one runner on the left. This made it possible to validate Type 560 directly using the empirical data and test the differences between it and TAITherm. All of the same geometry and climate boundary conditions are applied to Type 560, and tuning performed in an identical manner as TAITherm aside from pipe flow.

Results

The time series results for thermal and electrical energy production are shown in Figure 7. It can be seen that the TAITherm model tracks the measured data more consistently than Type 560, with less pronounced peak and valleys during variable irradiation events. This is confirmed by a lower MAE and higher correlation, and is likely due to the inclusion of the thermal mass, which is missing in Type 560. Mass can be added to Type 560 by using auxiliary models (e.g. pipes) that damp thermal response at the system level, but not at the collector.

The final thermal resistance values range from 0.005 to 0.010 m^2KW^{-1} in TAITherm and 0.010 to 0.040 m^2KW^{-1} in Type 560. Chow describes the thermal resistance between the PV cells and absorbers as being perfect when equal to 0.0001 m^2KW^{-1}, and defective at 0.040 m^2KW^{-1} (Chow, 2003). Given that the heat exchanger is mechanically pressed to the PV module, the high resistance values are not unexpected, but motivate the need for improved design and manufacturing that can improve conductivity while still reducing cost.
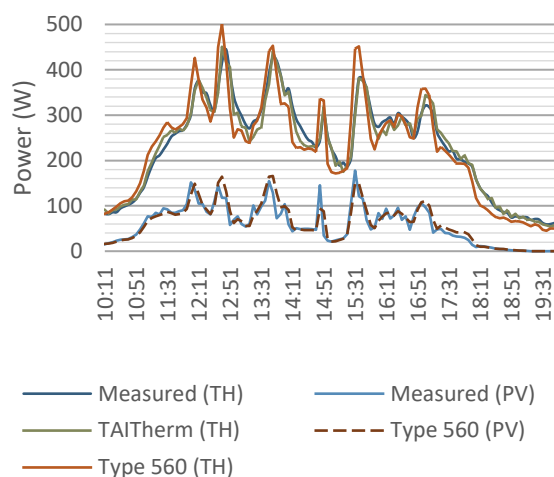
Figure 7: PVT energy production time series

Future research

There has been an increase in PVT research in recent years, primarily boosted by the IEA SHC Task 60. Nevertheless, the PVT heat pump concept is relatively undeveloped and thus has had little design dedicated to PVT collectors as part of a heat pump system. Therefore, there is an opportunity for the development of a novel collector design aimed at maximizing the heat transfer area between absorber and coolant, considering the cost reductions in the materials and manufacturing process afforded by heat pump integration. This can be achieved by developing a 3D numerical models paired with computational fluid dynamics (CFD) to identify optimal flow distribution patterns and heat flux potential. This model can then be transferred over to an analytical model in TRNSYS for rapid computation within a larger, heat pump systems analysis.

Conclusions

This paper set out to motivate and describe research needs for the development of a novel, low-cost PVT collector specifically for use in SHP systems. The rapid growth of the heat pump and PV markets worldwide indicate that there is a growing opportunity for PVT to finally scale up from a niche product to widespread adoption. The systems and PVT modelling methods presented here offers a glimpse into the simulation techniques needed to deliver holistic digital prototypes.

Future work

A new research project started in spring 2020 aims to further the development of PVT heat pumps using the techniques describe here. 3D numerical PVT collector models will be digitally prototyped in COMSOL, leading to physical prototypes validated in an outdoor laboratory. The core goals of the design is to improve conductivity with PV, enhance heat capture from the air, and reduce material and manufacturing costs. Likewise, the new prototypes will be transferred to TRNSYS for systems modelling, where novel configurations and controls will be simulated for multiple markets across Europe. These

models will be validated via a MFH pilot system as well as a lab-scale system installed outdoors.

This research agenda can deliver techno-economically optimized and validated PVT based heat pump system designs for multiple buildings, configurations, and markets around Europe. The results can help build installer and consumer confidence in the concept and contribute towards the continued increase of renewable energy and decarbonisation goals in buildings and cities.

Acknowledgement

References

Aste, N., del Pero, C., Leonforte, F. (2014). Water flat plate PV-thermal collectors: A review. *Sol. Energy 102*, 98–115.

Bertram, E., Glembin, J., Rockendorf, G. (2012). Unglazed PVT collectors as additional heat source in heat pump systems with borehole heat exchanger. *Energy Procedia 30*, 414–423.

Bombarda, P., Di Marcoberardino, G., Lucchini, A., Leva, S., Manzolini, G., Molinaroli, L., Pedranzini, F., Simonetti, R. (2016). Thermal and electric performances of roll-bond flat plate applied to conventional PV modules for heat recovery. *Appl. Therm. Eng. 105*, 304–313.

Brischoux, P., Bernier, M., 2016. Coupling PV/T Collectors with a Ground-Source Heat Pump System in a Double U-tube Borehole, in: *2016 ASHRAE Winter Conference*. ASHRAE, Orlando, Florida, p. OR-16-C046.

Cao, S., Sirén, K. (2014). Impact of simulation time-resolution on the matching of PV production and household electric demand. *Appl. Energy 128*, 192–208.

Chow, T.T. (2003). Performance analysis of photovoltaic-thermal collector by explicit dynamic model. *Sol. Energy 75*, 143–152.

Chu, J., Cruickshank, C.A., (2014). Solar-Assisted Heat Pump Systems: A Review of Existing Studies and Their Applicability to the Canadian Residential Sector. *J. Sol. Energy Eng. 136*, 041013.

De Rosa, M., Ruiz-Calvo, F., Corberán, J.M., Montagud, C., Tagliafico, L.A. (2015). A novel TRNSYS type for short-term borehole heat exchanger simulation: B2G model. *Energy Convers. Manag. 100*, 347–357.

EHPA (2019). European Heat Pump Market and Statistics Report 2019. Brussels.

Eslami-nejad, P., Langlois, A., Chapuis, S., Bernier, M., Faraj, W., 2009. Solar Heat Injection Into Boreholes, in: *4th Canadian Solar Buildings Conference*, Toronto (Canada), June 25-27, 2009.

Eurostat (2015). Housing Statistics [WWW Document]. http://ec.europa.eu/eurostat/statistics-

explained/index.php/Housing_statistics#Further_Eur ostat_information (accessed 9.12.16).

Florschuetz, L.W. (1979). Extension of the Hottel-Whillier model to the analysis of combined photovoltaic/thermal flat plate collectors. *Sol. Energy 22*, 361–366.

Godefroy, V. (2014). Élaboration Et Validation D'Une Suite Évolutive De Modèles D'Échangeurs Géothermiques Verticaux. PhD Thesis.

Good, C., Chen, J., Dai, Y., Hestnes, A.G. (2015). Hybrid Photovoltaic-thermal Systems in Buildings – A Review. Energy Procedia 70, 683–690.

Haller, M.Y., Bertram, E., Dott, R., Afjei, T., Ochs, F., Hadorn, J.-C. (2012). Review of Component Models for the Simulation of Combined Solar and Heat Pump Heating Systems. *Energy Procedia 30*, 611–622.

Haller, M.Y., Frank, E. (2011). On the potential of using heat from solar thermal collectors for heat pump evaporators, in: *ISES Solar World Congress*. Kassel, Germany.

Hellström, G. (1989). Duct Ground Heat Storage Model - Manual for Computer Code. Department of Mathematical Physics, University of Lund, Sweden.

Helpin, V., Kummert, M., Cauret, O. (2011). Experimental and simulation study of hybrid ground source heat pump systems with unglazed solar collectors for french office buildings. *Proc. Build. Simul. 2011 12th Conf. Int. Build. Perform. Simul. Assoc.* 2957–2964.

Herrando, M., Ramos, A., Zabalza, I., Markides, C.N. (2019). A comprehensive assessment of alternative absorber-exchanger designs for hybrid PVT-water collectors. *Appl. Energy 235*, 1583–1602.

Hofmann, M., Riechelmann, S., Crisosto, C., Mubarak, R., Seckmeyer, G. (2014). Improved synthesis of global irradiance with one-minute resolution for PV system simulations. *Int. J. Photoenergy 2014*.

IEA (2019). Trends in photovoltaic applications 2019 (T1-36:2019).

IEA (2018). Solar Heating and Cooling Task 60 - PVT Systems: Application of PVT Collectors and New Solutions in HVAC Systems.

Kim, J.H., Kim, J.T. (2012). The experimental performance of an unglazed PVT collector with two different absorber types. *Int. J. Photoenergy 2012*.

Kjellsson, E., Hellström, G., Perers, B. (2010). Optimization of systems with the combination of ground-source heat pump and solar collectors in dwellings. *Energy 35*, 2667–2673.

Madani, H., Claesson, J., Lundqvist, P. (2011). Capacity control in ground source heat pump systems: Part I: Modeling and simulation. *Int. J. Refrig. 34*, 1338–1347.

Mohanraj, M., Belyayev, Y., Jayaraj, S., Kaltayev, A. (2018a). Research and developments on solar assisted compression heat pump systems – A comprehensive review (Part-B: Applications). *Renew. Sustain. Energy Rev. 83*, 124–155.

Mohanraj, M., Belyayev, Y., Jayaraj, S., Kaltayev, A. (2018b). Research and developments on solar assisted compression heat pump systems – A comprehensive review (Part-A: Modeling and modifications). *Renew. Sustain. Energy Rev. 83*, 124–155.

Nasrin, R., Hasanuzzaman, M., Rahim, N.A. (2018). Effect of high irradiation and cooling on power, energy and performance of a PVT system. *Renew. Energy 116*, 552–569.

Pärisch, P., Mercker, O., Oberdorfer, P., Bertram, E., Tepe, R., Rockendorf, G. (2015). Short-term experiments with borehole heat exchangers and model validation in TRNSYS. *Renew. Energy 74*, 471–477.

Poppi, S., Sommerfeldt, N., Bales, C., Madani, H., Lundqvist, P. (2018). Techno-economic review of solar heat pump systems for residential heating applications. *Renew. Sustain. Energy Rev. 81*, 22–32.

Reda, F., Laitinen, A. (2015). Different strategies for long term performance of SAGSHP to match residential energy requirements in a cold climate. *Energy Build. 86*, 557–572.

Rolando, D., Acuna, J., Fossa, M. (2015). A Web Application for Geothermal Borefield Design. *World Geotherm. Congr.* 2015 19–25.

Schmidt, C., Schäfer, A., Kramer, K. (2018). Single source "solar thermal" heat pump for residential heat supply: Performance with an array of unglazed PVT collectors, in: *12th ISES Eurosun Conference*. Rapperswil, Switzerland.

Sommerfeldt, N., Madani, H. (2019). In-depth techno-economic analysis of PV/Thermal plus ground source heat pump systems for multi-family houses in a heating dominated climate. *Sol. Energy 190*, 44–62.

Sommerfeldt, N., Ollas, P. (2017). Reverse Engineering Prototype Solar PV / Thermal Collector Properties from Empirical Data for Use in TRNSYS Type 560, in: *Proc. of the ISES Solar World Congress 2017*. ISES, Abu Dhabi, pp. 1121–1132.

Weiss, W., Spörk-Dür, M. (2019). Solar Heat Worldwide. IEA Solar Heating and Cooling Programme.

Widén, J., Wäckelgård, E. (2010). A high-resolution stochastic model of domestic activity patterns and electricity demand. *Appl. Energy 87*, 1880–1892.

Zondag, H. (2008). Flat-plate PV-Thermal collectors and systems: A review. *Renew. Sustain. Energy Rev. 12*, 891–959.

Zondag, H. a., de Vries, D.W., van Helden, W.G.J., van Zolingen, R.J.C., van Steenhoven, a. a. (2002). The thermal and electrical yield of a PV-thermal collector. *Sol. Energy 72*, 113–128.

HVAC general, IEQ and ZEB

Chilled water temperature control of self-regulating active chilled beams

Peter Filipsson[1,2*], Anders Trüschel[1], Jonas Gräslund[1,3], Jan-Olof Dalenbäck[1]

[1]Building Services Engineering, Chalmers University of Technology, Gothenburg, Sweden
[2] CIT Energy Management AB, Gothenburg, Sweden
[3]Skanska Commercial Development Nordic AB, Stockholm, Sweden

* corresponding author: filipssp@chalmers.se

Abstract

The flow rate of chilled water in a self-regulating active chilled beam is constant without respect to the actual cooling load. The cooling capacity is instead determined by the room temperature, which gives rise to the self-regulating effect, and also by the centrally controlled chilled water temperature, which is the focus of this paper.

Previous studies have emphasized the benefit of avoiding room-level control equipment, but also highlighted the risk of overcooling with detrimental effects on thermal climate and energy demand. Overcooling may be avoided by supply temperature control, but strategies have not yet been studied in systems operating in cooling mode only.

Simulations are carried out with IDA ICE. The results show that overcooling is effectively avoided by proper control of the chilled water temperature. Desired thermal climate is achieved and the energy demand is in the same order of magnitude as in a system with individually and ideally PI-controlled active chilled beams.

Introduction

The International Energy Agency recently proclaimed the growth in global demand for space cooling as a blind spot of energy policy and one of the most critical energy issues of our time (IEA, 2018). While the global demand for other end-uses of energy in buildings (heating, lighting, cooking etc.) is expected to decline or plateau the coming decades, demand for cooling is expected to increase dramatically (IEA, 2017). Sustainable technologies of meeting this demand are consequently highly desirable.

Active chilled beams

Active chilled beams (ACB) are hydronic cooling equipment connected to the ventilation system and to a chilled water loop. The operation of a common type of ACB is illustrated in Figure 1. Primary air is provided from an air handling unit while chilled water is circulated through a cooling coil inside the ACB. The primary air enters the ACB via a pressure plenum and several nozzles along the beam. The high air velocity generated by the nozzles reduces the static pressure and induces room air (referred to as secondary air) which cools down as it passes the coil before it mixes with the primary air. The mixed air is then discharged into the room through slots along both long sides of the beam and attaches to the ceiling by means of the Coandă effect. The flow rate of secondary air divided by the flow rate of primary air is known as the induction ratio. The flow rate of chilled water is usually controlled as a function of the difference between the room air temperature and the cooling set-point temperature in order to match the cooling capacity with the actual cooling load. In addition, a dew-point control system is usually applied to make sure that the chilled water supply temperature is kept with a margin from the indoor air dew-point in order to avoid condensation forming on the coil surface.
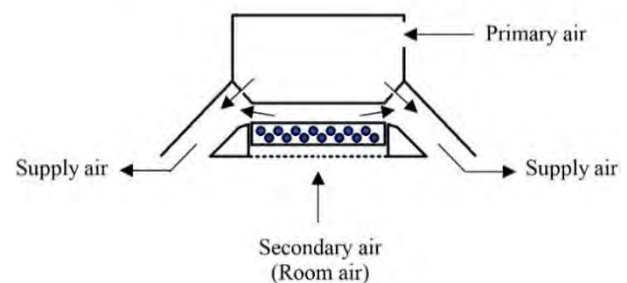
Figure 1: Schematic diagram of an active chilled beam

ACBs are suitable for using chilled water of relatively high temperature, henceforth referred to as high temperature cooling. This provides benefits such as increased use of free cooling, better performance of chillers, reduced risk of condensation (reduced latent load), reduced thermal losses in the chilled water distribution system and less need for individual room control. The latter is supported by a self-regulating effect originating from the fact that the cooling capacity is influenced by the room temperature. This is further discussed in the next section. Active beams may also be used for heating, either with a four-pipe system or a two-pipe system. Four-pipe systems allow versatile control of heating and cooling of each beam. Conventional two-pipe systems are operating either in cooling or heating mode, but innovative configurations with room air tempered water allow simultaneous heating and cooling also in two-pipe systems (Maccarini et al., 2017b).

Self-regulation

The cooling capacity of a comfort cooling system is affected by the room air temperature even if excluding the control system. As room air temperature increases, the driving temperature difference between room air and chilled water increases and consequently also the cooling capacity. As room air temperature decreases, the cooling capacity decreases and reach zero if the air temperature equals the chilled water temperature. In conventional systems, this effect is not enough to maintain the desired thermal climate and a control system is required. With ACBs, it is usually the flow rate of chilled water that is controlled. If designing for a very small temperature difference (i.e. high chilled water temperature), even small changes in air temperature will have large counteracting influence on the cooling capacity, and the conventional control system becomes redundant. The self-regulating effect is often referred to when studying thermally activated building systems (TABS) but has also been emphasized by several researchers investigating ACB systems (Brister, 1995; Henderson et al., 2003; Schultz, 2007; Ruponen et al., 2010; Kosonen & Penttinen, 2017; Maccarini et al., 2017b). The simplicity, robustness and cost-savings of avoiding thermostats, control valves and actuators are the main drivers for designing completely self-regulating systems. The drawbacks are the risk of overcooling, increased circulation pump work and less flexible regarding individual room temperature control.

During operation, the flow rate of chilled water in a self-regulating system is constant. The chilled water supply temperature is equal throughout the system, but may be controlled centrally. Accordingly, pure spatial differences (between locations) in cooling load may be taken care of by having different design cooling capacities while pure temporal variations (over time) may be taken care of by controlling the supply chilled water temperature centrally. The remaining obstacle, the combination of both types (spatiotemporal variations), are up to the self-regulating effect of the system to control. As a consequence, indoor temperature variability is an inherent feature of self-regulating systems. This is in contrast with conventionally controlled systems, which are theoretically able to keep the indoor temperature constant in multiple rooms with different heat gain profiles.

Self-regulating ACB systems have notable similarities as well as differences with TABS. Both systems operate with a small driving temperature difference, implying a strong self-regulating effect and high sensitivity to changes in the chilled water supply temperature. However, the main challenge of control of TABS is the integration with the thermal mass of the building and the associated slow response time. This challenge has attracted a lot of research on developing control strategies of TABS. A comprehensive review of this was presented by Romani et al. (2016). In TABS control strategies, the controlled variables are the supply temperature and the flow rate of chilled water. The most common controlling parameter is the outdoor air temperature and sometimes also with indoor air temperature feedback. In most cases, the instantaneous outdoor air temperature is used. In other cases, the average of the previous hours or the average of the predicted hours is used as input to the controller (Romani et al., 2016).

Previous work on self-regulating active chilled beams

Previous research on self-regulating active beams includes both studies based on simulations and studies based on measurements. Furthermore, it includes active beams for both heating and cooling as well as for cooling only. Kosonen & Penttinen (2017) presented a simulation based study investigating the energy consumption of active beam systems in cold climate. The active beams were used for both heating and cooling, the supply temperature was controlled between 20 °C (cooling mode) and 22 °C (heating mode) in order to keep the indoor air temperature within 21-25 °C. Too low indoor air temperatures during low occupancy outside of the summer season were observed. The authors suggested that this could be avoided by compromising the simplicity of self-regulation by the use of zonal-level control valves. Ruponen et al. (2010) presented simulations comparing a conventional low temperature ACB system with a high temperature ACB system and a self-regulating high temperature ACB system. The main reason for using a high temperature system was to reduce the need for dehumidification of supply air without risk of condensation. The main reason for self-regulation was the simplicity, reliability and reduced need for maintenance. A constant chilled water supply temperature of 20 °C was used in the high temperature systems. This caused excessive cooling which was compensated for by also using more heating. As a solution, the authors called for future research on control of the chilled water supply temperature. Maccarini et al. (2017a) compared different control strategies for active beam systems used for both heating and cooling. With all strategies, the water supply temperature was controlled within 20-23 °C and kept the indoor air temperatures within 20-24 °C. Following four strategies of controlling the supply temperatures were investigated. First, as a function of the outdoor air temperature. Second, as a function of the exhaust air temperature. Third, with respect to the maximum and minimum room air temperatures. As long as these were within the cooling/heating set-points, the supply water temperature equaled the return water temperature. The fourth and final strategy was as a function of the outdoor air temperature (as in the first strategy). In addition, the flow rate was reduced on system level (proportional in each beam) with respect to the maximum and minimum room air temperatures (as in the third strategy). Regarding energy performance, no significant difference

was noticed neither between the first and second nor between the third and the fourth strategy. Strategy three and four required 7-10 % less energy than strategy one and two, but on the other hand, they also required measurements of air temperature in each room of the building as input to the controller.

Controlling the supply water temperature as a function of the outdoor air temperature has also been included in studies of measurements in real buildings. Maccarini et al. (2019) investigated a self-regulating active beam system used for both heating and cooling. Supply water temperature was controlled within 20-23 °C, indoor air temperatures were measured at two positions during a summer day and a winter day and it was concluded that the system was able to provide good thermal conditions (21.0-23.2 °C). Filipsson et al. (2020a) presented the operation and performance of a self-regulating ACB system where heating was provided from a separate radiator system. The ACBs were supplied chilled water of 20.0-21.5 °C controlled as a function of the outdoor air temperature. Indoor air temperatures in the open-plan offices were measured all the year round in 37 positions. It was concluded that the indoor air temperatures were both uniform and stable. The average was 22.3 °C annually and 22.6 °C during summer. The authors called for adjusted control of the chilled water temperature as a way to obtain larger differences between summer and winter, which is suggested by applicable standards and guidelines (CEN, 2019).

Objective

The objective of the work presented in this paper is to compare different strategies of controlling the chilled water supply temperature of a self-regulating active chilled beam system. These are compared with respect to energy use and indoor operative temperature.

Method

The work presented in this paper is based on simulations carried out in the building performance simulation software IDA ICE (EQUA Simulation AB, 2018). IDA ICE has been validated in several research projects, both by measurements (Loutzenhiser et al., 2007) and by inter-model comparison through ANSI/ASHRAE Standard 140-2004 (EQUA Simulation AB, 2010).

The building

The model consisted of one floor of an office building with location and climate representing Stockholm, Sweden. The total area of the simulated office floor was 600 m^2 (20 x 30 m) whereof 500 m^2 was open-plan offices, two meeting rooms of 25 m^2 each and one larger meeting room of 50 m^2. During working hours, the doors to the meeting rooms were open for 15 minutes every

two hours. During nights and weekends, they were open at all times. The open-plan office was divided into five separate zones in order to model spatial differences in this area. The eight zones in total are illustrated in Figure 2.
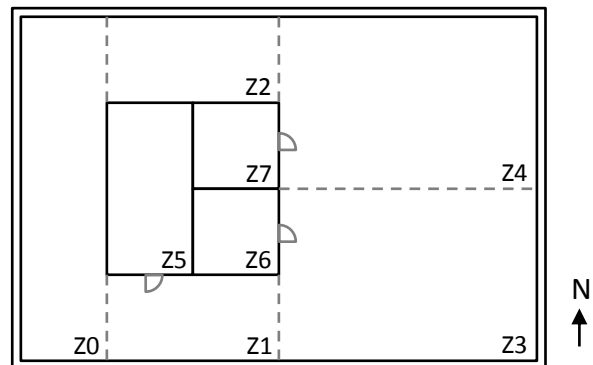
Figure 2: Plan view of the modelled office floor.

Exterior walls consisted of 20 cm light insulation covered by concrete, 22 cm on the inside and 7.5 cm on the outside. Interior walls consisted of 3 cm light insulation between air gaps of 3.2 cm and plasterboards of 2.6 cm on each side. Windows with a g-value of 0.5 and a U-value of 1.2 W/m^{2}K covered 32 % of each façade. Internal blinds, reducing the g-value by 35 %, were drawn when solar radiation exceeded 100 W/m^2. Horizontal shading was represented by surrounding buildings of the same height as the modelled building at a distance of 10 m.

The floor consisted of 0.5 cm floor coating on top of 2 cm lightweight concrete and 15 cm concrete. A suspended ceiling of 3 cm light insulation material was located 50 cm beneath the concrete roof. The volume between the suspended ceiling and the concrete roof was modelled as separate zones.

Surface area of furniture was 1.8 m^2 per m^2 floor area. Material properties of furniture were in accordance to what Johra et al. (2017) specifies as equivalent indoor content material. The furniture was interacting with the energy balance only by convection while its influence on radiation was not taken into account.

The internal heat gain

Levels and schedules of internal heat gain were modelled as declared in Figure 3. Heat gain represented by the white area was included when sizing the ACB system but not when simulating the full-year operation. The reason was to take into account that the actual use of a building differs from the design conditions.
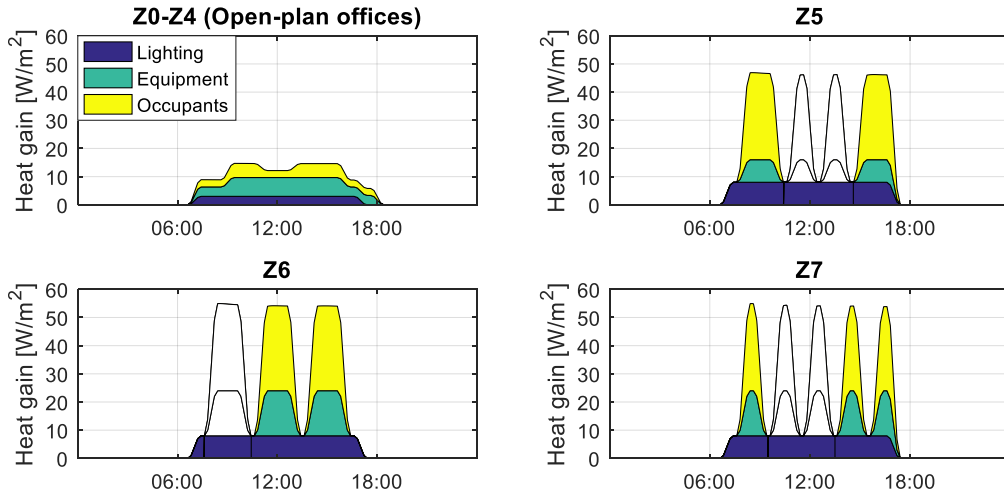
Figure 3: Internal heat gain (white area was included only when sizing the ACBs and not in subsequent simulations).

The HVAC system

Two modifications were made to the default ACB model in IDA ICE. First, the induction ratio of the ACBs was taken into account when determining internal convective heat transfer in the zones. An induction ratio of five was used. Second, the convective heat transfer at the ceiling was determined by the supply air temperature, in contrast to the other surfaces where it was determined by the zone/exhaust air temperature. These modifications were supported by the results presented in a previous paper (Filipsson et al., 2020b).

Ventilation air flow rate of 1.50 l/sm^2 was in operation between 06:00 and 19:00. The primary air temperature was 20.0 °C when outdoor air temperature exceeded 10 °C, 21.0 °C when outdoor air temperature was below -10 °C and linearly interpolated in between. During June-August, the ventilation was turned on at 4:00 on Mondays in order to purge excess heat accumulated during the weekend. Chilled water flow and ventilation were interlocked, hence no cooling from the ACB system when the ventilation was not in operation. For reasons of indoor air quality, meeting rooms were supplied additional ventilation air flow when occupied.

This additional air flow was 1.65 l/sm^2 and supplied through a separate supply air device by-passing the ACBs.

The relatively high temperature of chilled water allowed using the chilled water loop to preheat the incoming outdoor air. This was utilized as long as there was a heating demand of supply air, a cooling demand in the chilled water loop and the outdoor air temperature was at least 3 °C lower than the chilled water supply set-point. Henceforth, this is referred to as free cooling from AHU. Due to the constant flow of chilled water close to room air temperature, some ACBs occasionally provided heating instead of cooling. This implied an internal transfer of heat between zones and is henceforth referred to as free internal cooling.

Heating was supplied through hydronic radiators. These were P-controlled with respect to the indoor air temperature with a proportional band of 1.0 °C (20.5-21.5 °C). The temperature transfer efficiency of the exhaust air recovery unit was 80 %, both in heating and cooling mode. A schematic illustration of the HVAC system is presented in Figure 4.
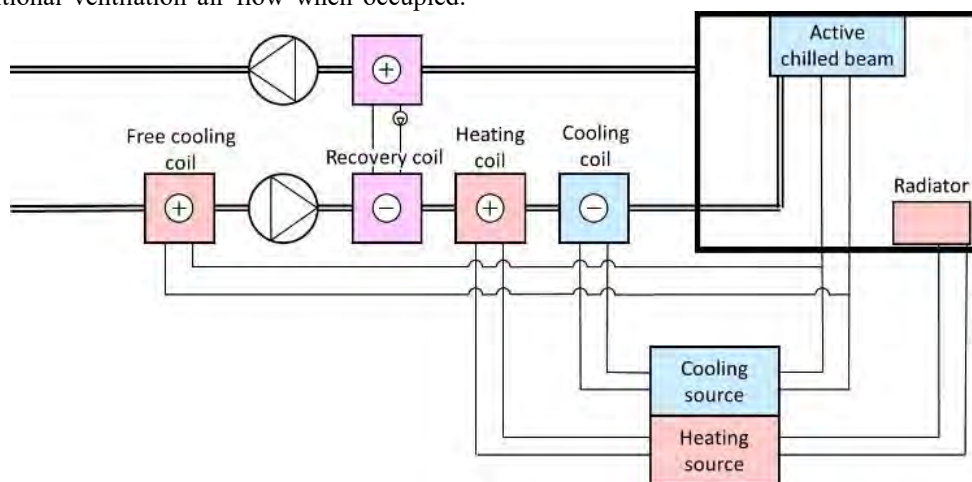
Figure 4: Schematic illustration of the HVAC system

The sources of heating and cooling are generic in this study. In reality, they could be district heating/cooling, heat pump/chiller etc.

The control strategies

The investigated control strategies are listed in Table 1. Regardless of strategy, the chilled water supply temperature was limited to be as least 20 °C.

Table 1: List of included control strategies.

Name	Chilled water supply temperature	Chilled water flow rate
CON20	20 °C	Constant
OA1021	$f(t_{oa})$	Constant
OA1522	$f(t_{oa})$	Constant
EA24	$f(t_{ea})$	Constant
TOP25	$f(\max(t_{op,z}))$	Constant
PI23	20 °C	$f(t_{a,z})$
PI24	20 °C	$f(t_{a,z})$

In Table 1, t_{oa} is the outdoor air temperature, t_{ea} is the exhaust air temperature, $t_{op,z}$ and $t_{a,z}$ is the operative temperature and air temperature in each zone. In strategy CON20, the chilled water supply temperature was constant at 20 °C which means that it provided as much cooling as possible. In contrast, strategy TOP25 aimed at keeping the maximum operative temperature at 25.0 °C, which can be seen as keeping the provided cooling to a minimum. Strategies OA1021 and OA1522 controlled the chilled water supply temperatures as functions of the outdoor air temperature. These functions are presented in Figure 5.
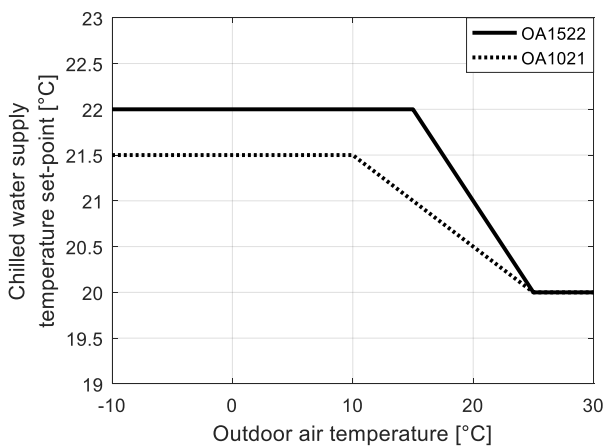
Figure 5: Chilled water supply temperatures as functions of the outdoor air temperature.

In strategy EA24, the chilled water supply temperature was controlled with respect to the exhaust air temperature. The control was aiming for a constant exhaust air temperature of 24 °C.

Strategies PI23 and PI24 were not self-regulating. These had ACBs individually controlled in each zone and the chilled water flow rates were PI-controlled with room air temperature set-points of 23.0 °C and 24.0 °C respectively.

The design cooling capacity of the ACBs was equal in all investigated control strategies. They were sized to obtain a maximum operative temperature of 25.0 °C when using the strategy of a constant supply chilled water temperature at 20 °C (CON20) and design heat gain schedule according to Figure 3.

Results

The results are divided into two parts. The first part is about the energy demand and the second part is about the thermal climate.

Energy

The annual amounts of energy delivered from the cooling and heating sources (see Figure 4) are presented in Figure 6. Energy required for coil cooling is relatively small and very similar in all strategies. The cooling recovery system is the reason why they are not totally equal, since strategies causing low indoor air temperatures require less coil cooling thanks to the recovery coil. Energy required by the heating coil differs slightly more between the strategies. Differences are partly explained by the heat recovery system but to a larger extent by the operation of the free cooling coil. Strategies better able to utilize the free cooling require less energy for the heating coil. This applies to strategies with low chilled water temperature coinciding with low outdoor air temperature (especially CON20). On the other hand, these strategies require more energy for radiator heating since this causes simultaneous and opposing radiator heating and ACB cooling. This unfortunate situation is especially obvious when looking at the radiator heat demand. It also requires excessive use of ACB cooling, but due to utilization of the free cooling coil, this is less detrimental.
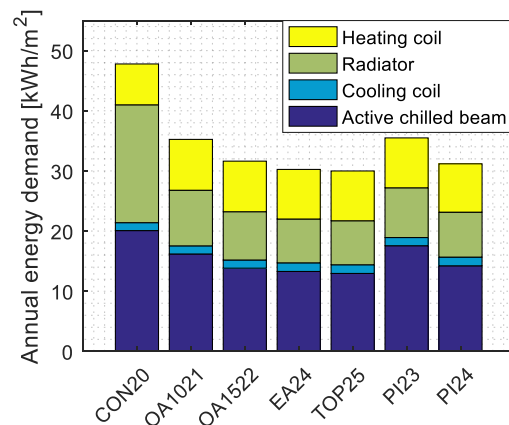
Figure 6: Demand for heating and cooling with each control strategy.

In Figure 6, the cooling energy required by the ACB system included only the part delivered from the cooling source. In Figure 7, the part delivered from the free cooling coil and from cold to warm zones is presented.
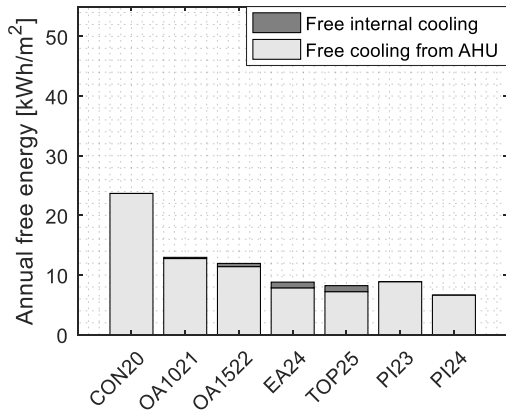
Figure 7: Cooling from cold zones (free internal cooling) and from the supply air (free AHU cooling).

The free internal cooling relies on spatial variability in indoor air temperatures. The free internal cooling happens primarily during winter when the meeting rooms are cooled by the chilled water at the same time as the open-plan offices are heated by the chilled water. Since the cooling source it unable to provide heating, the chilled water temperature do not always reach its set-point. In Figure 8, both set-point and the actual chilled water supply temperature of strategy OA1522 is presented. As seen, during times of low outdoor air temperature, the water is chilled by the indoor air, hence are actual values lower than the set-point.
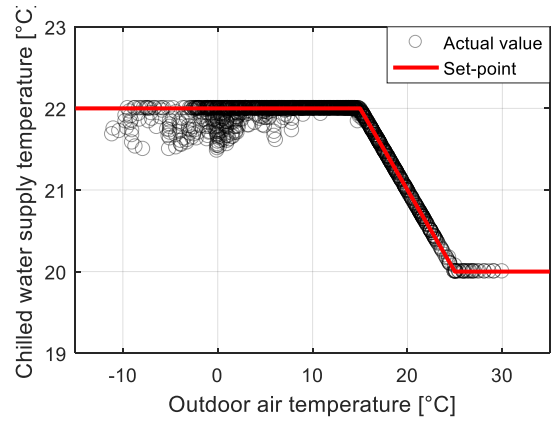
Figure 8: Chilled water supply temperature in OA1522

Thermal climate

The operative temperatures of all zones in the open-plan offices during weekdays 08:00-17:00 in a winter week, a spring week and a summer week are presented in Figure 9. The boxplot illustrates the minimum, maximum, median and the interquartile range. During operation of the HVAC-system in the summer week, the outdoor air temperature varied between 12 and 31 °C. Corresponding range was between 6 and 18 °C during the spring week and between -11 and -4 °C during the winter week. The green lines in the figure refer to the default indoor temperature ranges (for buildings with a normal level of expectation) suggested by standard EN 16798-1:2019 (CEN, 2019) to be used for energy calculations. These are based on the concept of predicted mean vote and correspond to an activity level of 1.2 met, winter clothing of 1.0 clo and summer clothing of 0.5 clo. The standard does not suggest temperature ranges to be used during spring and autumn.
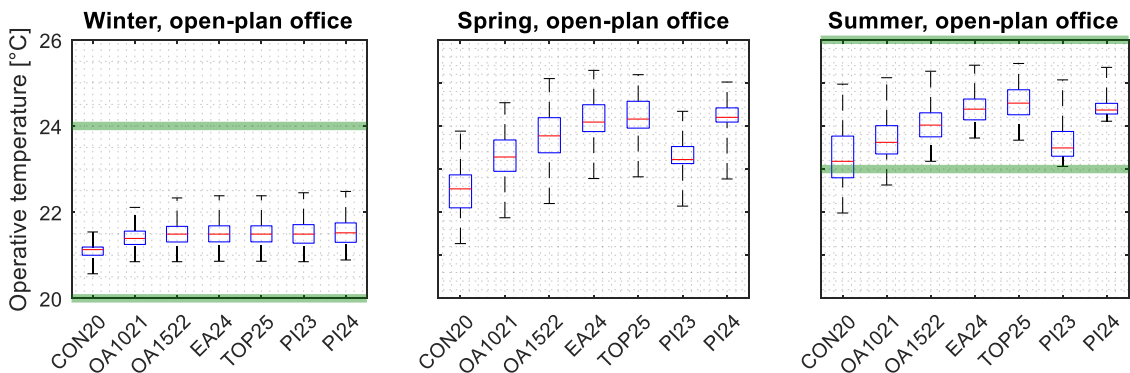
Figure 9: Operative temperature in the open-plan offices during a winter/spring/summer week.
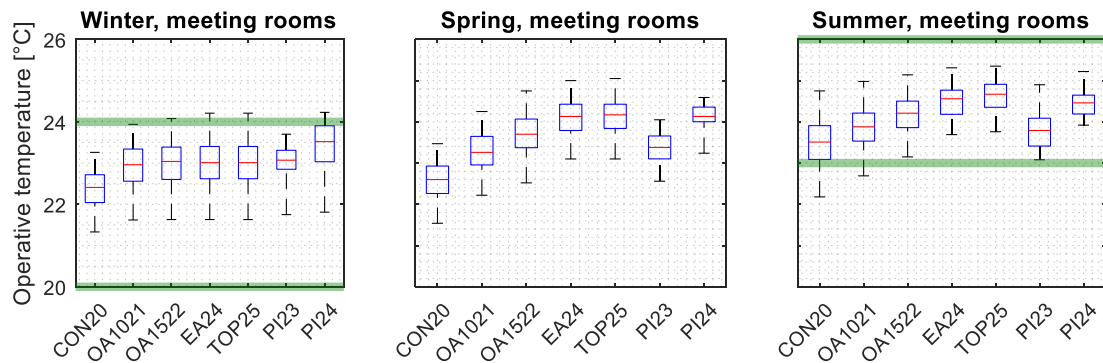
Figure 10: Operative temperature in the meeting rooms during a winter/spring/summer week.

As seen in Figure 9, CON20 is always keeping temperatures lower than any other strategy. Higher operative temperatures (during spring and summer) are associated with lower energy use (see Figure 6). Compared to TOP25, OA1021 implies around 0.9 °C lower operative temperatures during spring and summer, and requires 17 % more energy for heating and cooling. The results of EA24 are very similar to TOP25. EA24 gives slightly lower operative temperatures during spring and summer, and also slightly higher energy use. The non-self-regulating strategies, PI23 and PI24, generally keep the temperature within a narrower range than the self-regulating strategies, especially PI24 during the summer week.

The operative temperatures in the meeting rooms during weekdays 08:00-17:00 in the winter week, the spring week and the summer week are presented in *Figure 10*.

The main difference from the open-plan offices is that the seasonal variations are much less pronounced in the meeting rooms, as a consequence of not being exposed to the exterior walls. Furthermore, during the winter week, the operative temperature is both considerably higher and more variable in the meeting rooms.

Discussion

Self-regulation implies that the flow rate of chilled water is constant without respect to the actual cooling load. Inherent features of such operation are indoor temperature variability and a risk of overcooling. Overcooling and too low room temperatures have been reported in previous studies of self-regulating ACBs (Ruponen et al., 2010) and also of self-regulating active beams used for both heating and cooling (Kosonen & Penttinen, 2017). Indicated by the results of the present study, excessive use of energy may effectively be avoided by controlling the chilled water supply temperature. Most importantly, the chilled water supply temperature should exceed the heating set-point during the heating season. Even though free cooling is supplied to the ACBs, simultaneous operation of radiators and ACBs causes excessive use of energy for heating.

In the investigated strategies in general, there was a trade-off between low energy demand and low temperatures during summer, spring and autumn.

Regarding the energy demand, differences between self-regulating and non-self-regulating strategies were not larger than the difference between having a cooling set-point of 24 °C and 23 °C in a conventionally controlled system.

Strategy TOP25 requires measurements of the operative temperature in each zone as input to the controller and is therefore not a very practical option. The non-self-regulating strategies PI23 and PI24 require the indoor air temperature to be measured in each zone plus thermostats, control valves and actuators for the control of flow of chilled water in each ACB. On the other hand, these require slightly less electricity for the circulation pump. It shall be noted that PI23 and PI24 were ideal controllers modulating the flow rate of chilled water. In conventional systems in reality, simple on/off-control is much more common, hence less able to keep the indoor temperature within such a tight range.

Strategy OA1522 and EA24 both implied low energy use and acceptable thermal climate. EA24 required less energy, but on the other hand, also slightly high temperature in the meeting rooms during the winter week. This may be avoided by decreasing the exhaust air temperature set-point during winter. However, this increases the risk of simultaneous heating and cooling in the open-plan office.

Control of the heating system was made with P-control with respect to the room air temperature and a proportional band of 1.0 °C (20.5-21.5 °C). A wider band or a higher heating set-point would increase the occurrence of simultaneous heating and cooling.

For reasons of indoor air quality, the meeting rooms were supplied additional air flow during occupancy. Since the primary air temperature is lower than the room air temperature, this provides cooling and supports the stability of the indoor temperatures. Absence of this additional air flow would require larger ACBs in order to meet the design criterion. These ACBs would to a larger extent provide cooling also when the meeting rooms were unoccupied, hence causing larger temperature variability. Another factor that helps the self-regulation is the openings of doors to the meeting rooms. Less door openings would cause larger differences between the open-plan offices and the meeting rooms which would

cause uncomfortably high temperature in the meeting rooms during the winter week.

All results presented are valid under the specific conditions of this study and should not be generalized without caution.

Conclusions

Under the conditions and assumptions made in this study, self-regulating active chilled beams are able to provide desired thermal climate without using more energy for cooling and heating than a conventional system with individually controlled active chilled beams. Controlling the chilled water supply temperature as a function of the temperature of outdoor air or exhaust air are two feasible options with similar results. Although associated with higher variability, self-regulating active chilled beams are able to keep the operative temperature within comfortable limits.

Acknowledgement

References

Brister, A. (1995). Chilled beams provide perpetual cooling. *Building Services*, 17-20.

CEN (2019). EN 16798-1:2019 Energy Performance of Buildings - Ventilation for Buildings – Part 1: Indoor environmental input parameters for design and assessment of energy performance of buildings addressing indoor air quality, thermal environment, lighting acoustics – Module M1-6.

EQUA Simulation AB (2010). Validation of IDA Indoor Climate and Energy 4.0 build 4 with respect to ANSI/ASHRAE Standard 140-2004. http://www.equaonline.com/iceuser/validation/ASHRAE140-2004.pdf

EQUA Simulation AB (2018). IDA Indoor climate and energy, Version 4.8 [Computer Software].

Filipsson, P., Trüschel, A., Gräslund, J., & Dalenbäck, J. O. (2020a). Performance evaluation of a direct ground-coupled self-regulating active chilled beam system. *Energy and Buildings*, 209, 109691.

Filipsson, P., Trüschel, A., Gräslund, J., & Dalenbäck, J. O. (2020b). Modelling of rooms with active chilled beams. *Journal of Building Performance Simulation*, *13*(4), 409-418.

Henderson, M., Mech, B. E., & Mieaust, M. (2003). Application of chilled technology in modern office buildings. In Natural Hybrid or Air-conditioning Conference.

IEA. Space cooling: More access, more comfort, less energy, Energy Efficiency Insights Brief. International Energy Agency (2017).

IEA. The Future of Cooling - Opportunities for energy-efficient air conditioning, International Energy Agency (2018).

Johra, H., Heiselberg, P., & Le Dréau, J. (2017). Numerical analysis of the impact of thermal inertia from the furniture/indoor content and phase change materials on the building energy flexibility. In *Proceedings of 15th IBPSA Conference, International Building Performance Simulation Association*, San Francisco, CA, USA.

Kosonen, R., & Penttinen, J. (2017). The effect of free cooling and demand-based ventilation on energy consumption of self-regulating and traditional chilled beam systems in cold climate. *Indoor and Built Environment*, 26(2), 256-271.

Loutzenhiser, P., Manz, H., & Maxwell, G. (2007). Empirical validations of shading/daylighting/load interactions in building energy simulation tools. *A Report for the International energy Agency SHC Task, 34*.

Maccarini, A., Hultmark, G., Afshari, A., & Bergsøe, N. C. (2017a). Analysis of control strategies for a novel HVAC system equipped with a room-temperature water loop. In *The 15th International Conference of IBPSAConference of International Building Performance Simulation Association* (pp. 831-838). IBPSA.

Maccarini, A., Hultmark, G., Bergsøe, N. C., & Afshari, A. (2019). Full-scale operation of a novel two-pipe active beam system for simultaneous heating and cooling of office buildings. In *E3S Web of Conferences* (Vol. 111). EDP Sciences.

Maccarini, A., Wetter, M., Afshari, A., Hultmark, G., Bergsøe, N. C., & Vorre, A. (2017b). Energy saving potential of a two-pipe system for simultaneous heating and cooling of office buildings. *Energy and Buildings*, 134, 234-247.

Romaní, J., de Gracia, A., & Cabeza, L. F. (2016). Simulation and control of thermally activated building systems (TABS). *Energy and Buildings*, 127, 22-42.

Ruponen, M., Itkonen, H., Mustakallio, P., Jokisalo, J. (2010). Energy savings with very high temperature cooling water active chilled beam system. Clima 2010: 10th REHVA World Congress.

Schultz, C. C. (2007). Next-generation cooling is looking up. *Engineered Systems*, 24(5), 64-67.

Energy performance of an office building by using adaptive approach to occupant behaviour and environment control

Himanshu Patel Tuniki[1*], Andrius Jurelionis[1], Monika Dobrovolskytė[2]

[1]Faculty of Civil Engineering and Architecture, Kaunas University of Technology, Kaunas, Lithuania

[2]YIT Lietuva, Kaunas, Lithuania

* corresponding author: himanshu.tuniki@ktu.edu

Abstract

The predicted percentage of dissatisfied (PPD) value indicates the percentage of people dissatisfied with thermal environment, as it depends not only on the environment itself, but on physical, psychological, or behavioural aspects as well. Flexible and adaptive occupant behaviour provides more opportunities for both reaching higher perceived levels of comfort and energy savings. In this research, the software simulation tool IDA-ICE has been used to analyse the building performance of the office building under two scenarios, an adaptive case, and a non-adaptive case. One pattern was based on standard clothing levels, while the other dealt with the possibility for the occupants to adjust in terms of clothing and window operation with respect to the air temperature. The analysis was based on the concept that coping with dissatisfaction can be linked to lower PPD values, and adaptive models can be incorporated into dynamic building energy performance simulations. The results show that there are noticeable differences in the energy used per m^2, cooling and thermal dissatisfaction, upon adopting adaptive approach with respect to clothing, Predicted Mean Vote (PMV) value and the window opening behaviour. Certain occupant behaviours aimed at maintaining thermal comfort that can both increase the accuracy of energy performance predictions and lead to increased energy savings in office buildings.

Introduction

The energy consumption rates vary depending on the type of building. Specifically, in the case of office buildings, where the consumption is dependent more on comfort than necessity. Importance is to be given to the satisfaction of occupants as it affects their productivity (Mostavi, Asadi, & Ramaji, 2016). The relationship between the occupant satisfaction and the energy consumption has been investigated in various studies. Owing to the subjective nature of these studies, the broader conclusions inferred are limited to those specific studies itself. But the specific conclusions and the commonalities can be understood and applied to other scenarios. Ultimately, it is the mind-set of the occupants and their decision making strategies for achieving comfort that makes a difference in meeting the energy efficiency goals (Nižetić, 2017). The sense of comfort for the occupants is enough to influence their behaviour towards the surroundings. It has been given that the occupants would first take on window operation, changing clothes, etc., as adaptations to cater for thermal comfort needs (KC, Rijal, Shukuya, & Yoshida, 2018). A study has shown that the higher window-to-wall ratio increases occupant satisfaction, but without a provision for window shading or blinds, the satisfaction could decrease owing to the lack of privacy (Hong, Lee, Yeom, & Jeong, 2019). Similarly, there are other factors that affect the occupant comfort variable such as, the activity level, clothing (CLO) value, level of interaction with the temperature controls, etc. Activity level, which is measured in MET, is directly linked to the occupant comfort, and would lead to higher interaction with the building temperature controls. This can be regarded as a form of occupant adaptation. If the choice of interaction is given to them for adjusting controls, i.e., manual temperature adjustment system, a rise in satisfaction can be observed. The complication with an occupant demand driven approach is that, each individuals' thermal adaptation influences their response to comfort which affects the overall predicted percentage of dissatisfied (PPD) rate (Aguilera, Kazanci, & Toftum, 2019). Similar is the case with the occupants' behaviour of adapting to the environment in the form of window operation (Chen, Tong, Samuelson, Wu, & Malkawi, 2019). Hence, higher satisfaction levels can be achieved by imparting a sense of being provided with an option to choose to alter the surroundings. In shared office spaces, there is a higher probability of interaction when the element is closer to the occupant (Marín-Restrepo, Trebilcock, & Gillott, 2020). The clothing level, which is measured in CLO, also has a direct impact on the occupant satisfaction. Usually, office environments have strict dress codes which could impact the interaction with temperature controls, as the clothing adaptation for occupants varies in direct relationship with the indoor temperature (Indraganti & Boussaa, 2017).

The behavioural responses of occupants are merely fuelled by their expectations of thermal comfort, from past experiences of regulation and comfortable indoor environments (Auliciems & de Dear, 1998). The various adaptations that occupants would take on and the implications that these actions have on the energy consumptions have been analysed in this paper. The focus is on the adaptations and the energy consumption rates within an office building, which can help in identifying

different ways of saving energy. This can be accomplished by quantifying the energy savings, by the means of IDA ICE software simulations and a questionnaire survey. Various instances of occupant adaptations to the indoor environment are considered. The simulation results from an adaptive case and a non-adaptive case are compared and the results are analysed.

Methods

Case study building

The object of the research is a newly constructed office building in Vilnius, Lithuania (Figure 1). The building has ten floors, premises are rented to various companies and a café is located on the ground floor. All floors of the building are ventilated by mechanical ventilation systems.

Figure 1 Photo of the building

The facade structures of the building are made of painted aluminum profile and glazed with 54-millimeter-thick glass packages. The facade wall constructions are made of painted aluminum profile and filled with thermal insulation filler. The windows of the office building are tilted inwards, made of painted aluminum profile with thermal insulation, glazed with double-glazed units (U value - 1.3 W/m^2·K). The main heat source of the building is district heating. For the ventilation of the premises two ventilation units with rotary heat exchangers are installed. The first is for ventilation of 1 - 5 floors and the second for ventilation of 6 - 10 floors. The units are installed in the technical room on the technical floor. Fresh air is taken through the air intake grille on the north side of the building and removed above the roof. Air cooling units of the variable refrigerant volume (VRV) type are installed for the supply of cold to ventilation equipment. A separate ventilation unit designed to ventilate the cafe is also installed on the technical floor. For the ventilation of other premises, such as toilets, a separate ventilation unit with plate heat exchangers and a heat recovery unit is installed. The air in the premises is cooled by supplying cooled air to the premises through ducts and by cooling the air in the premises with local cooling devices, thus maintaining the

necessary room parameters. A separate three-pipe cooling unit of variable refrigerant volume type is designed for each floor. The office rooms are equipped with ducted air conditioners that supply cooled air through air supply distributors. The specific fan energy consumption per air volume unit of the building's HVAC system is 0.000275 kWh/m^3, and the Seasonal Energy Efficiency Ratio (SEER) value is 3.50, for cooling. The HVAC systems design have an 83% heat recovery efficiency.
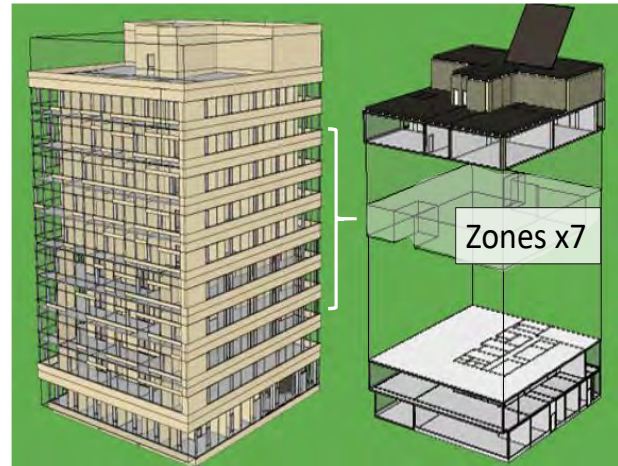
Figure 2 Research building model in IDA ICE environment before and after zone multiplication

Table 1 Building Performance Metrics for 2018

Primary energy consumption of the actual building (kWh/m^2)	175.3
Energy consumption (from simulation) (kWh/m^2)	161.9

IDA ICE Model description

Based on the architectural design of the building a model was created in the IDA ICE environment. The development of the model aims to reproduce the design solutions of the building as accurately as possible. To speed up the simulations a zone multiplier function is used. Buildings often have zones that are identical or very similar. After detailing one zone in this way, the parameters are applied to other zones assigned to the same functional group. This helps to perform simulations faster and to review various options. The object of the research also has identical zones in some floors.

Energy consumption data

The analysis of the energy consumption of a building was performed. Firstly, reports of electricity, heating, and water consumption of the building for the period of 2018 year (Table 1) were received from the company's property manager. Electricity costs include lighting, cooling, and the cost of hot water as it is prepared by electric heaters. Based on the data received, an overall summary of the costs of the building was compiled (Figure 3). The results of the analysis show that the highest costs in terms of the energy consumption of a building are for electricity (28%).

As electricity costs are the biggest part of all building costs, further review of the data was done. It showed that most of the electricity is consumed in autumn and winter when the need for lighting in the premises increases and more hot water is used. Using the Building Management System (BMS), the annual electricity consumption of the building was calculated and spread out according to the need for ventilation, cooling, lighting, and other equipment.
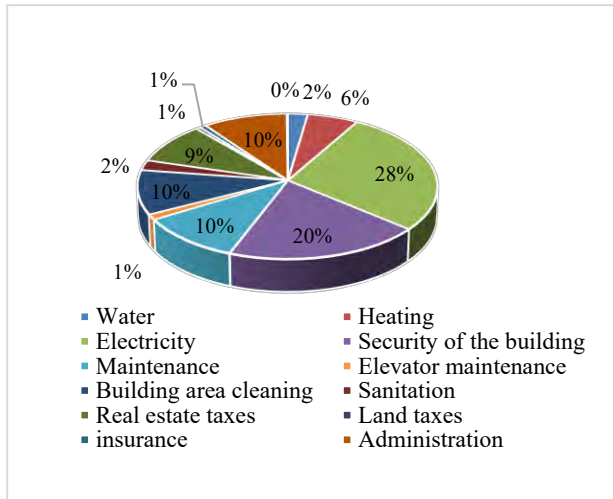
Figure 3 Annual building costs
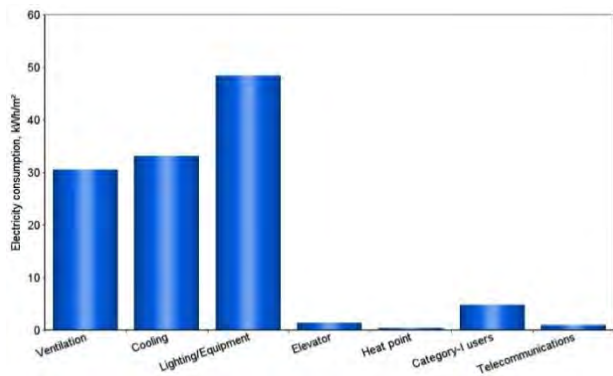
Figure 4 Electricity consumption analysis

It can be seen from Figure 4 that the largest part of electricity consumption is consumed by ventilation, cooling, lighting and equipment systems, which includes not only lighting devices, but also computer equipment, electrical appliances and electric hot water heaters.

Questionnaire survey

The subjects targeted for this questionnaire survey were the occupants in the office building. The survey was designed to gather the data from occupants, regarding the indoor environment and their individual attributes. The survey comprised of 16 questions and was designed using online tools. The survey aims to gather the basic information from the occupants pertaining to their age, gender, duties, physical activities, working hours in office, etc. This is to draw inferences from the survey

responders about their backgrounds, which would help in understanding their comfort perceptions and expectations (Derks, Mishra, Loomans, & Kort, 2018; Khalid, Zaki, Rijal, & Yakub, 2019). Further questions focused on their comfort adaptations, i.e., the possibility to modify their clothing, the heating/cooling systems, and the operation of windows. Attempting to modify the surroundings to meet the comfort expectations is the nature of adaptation. Hence, the occupants' adaptations are a precursor to their comfort and satisfaction (Choi & Moon, 2017). The data gathered from the survey, regarding clothing, activity, and window operation, will be necessary to simulate the indoor environment. The CLO and MET values can be noted from the survey responses that could define the occupant behaviour. The hours of operation of the occupants (as received from the survey) can also be fed to the software. This information is intended to be used as the input data for the IDA ICE software simulations.

The software has the option which allows for designing algorithms for the working logic of HVAC components, window opening control, shading control, etc. within the building. Utilizing this feature, the occupant behaviour was linked to the window operation, for the simulation. The first case is the 'Non-Adaptive Case' scenario, which uses the standard values of clothing for summer, winter, autumn, and spring seasons. The activity level and working hours of the occupants are obtained from the survey results. These settings were applied for all the zones in the building and the simulation was run from January 2018 to December 2019. The 'Adaptive Case' is simulated with the window opening control which will be linked to the air temperature, in a way that they are opened when the air temperature is equal to or higher than 24 °C within the indoor environment. This algorithm can be designed through the creation of macro controls for the windows. Within the macro, the zone is linked to a PI controller as a function of air temperature along with a set-point. The output signal from the PI controller is connected to the window opening control. The same algorithm is then used for all the zones in the building with windows. Also, the clothing values of occupants are used as per the results of the survey, which were taken separately for each season. The Predicted Mean Vote (PMV) value for both the adaptive and the non-adaptive cases is different. For the non-adaptive case, the flexibility to change the clothing is lower. Differences in the simulation results are expected when the adaptive case has slightly higher flexibility with clothing. Upon running the simulations for these three scenarios for the years 2018 and 2019, the results are analysed for variations and the PPD values would be observed as to how they change under the two different scenarios. This methodology focuses on analysing the difference in energy consumption rates when adaptive measures are adopted by the building occupants and systems. Thereby, exposing the potential and scope for further energy saving techniques while maintaining the comfort of occupants.

Results

Survey results

The survey received 48 responses from the building occupants, out of which 28 were from women and 20 were from men. Around 77% of them spend 8 to 9 hours a day in the office (Figure 5) and 79% of them spend maximum time of their work sitting in front of a computer (Figure 6), which make their responses dependable and relevant to the study. The MET value for concerned activities is taken as 1.2, which has been used in all the simulations and this value has been derived from the survey results.
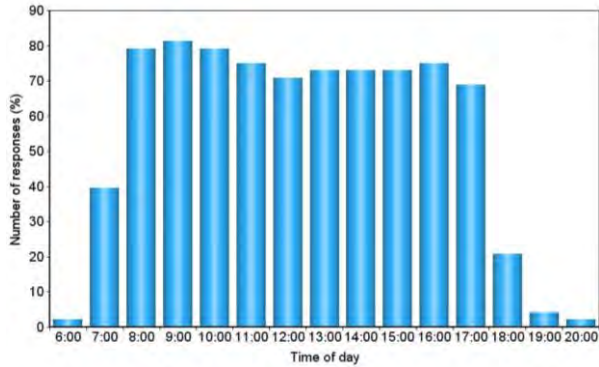
Figure 5 Survey responses for occupants' working hours
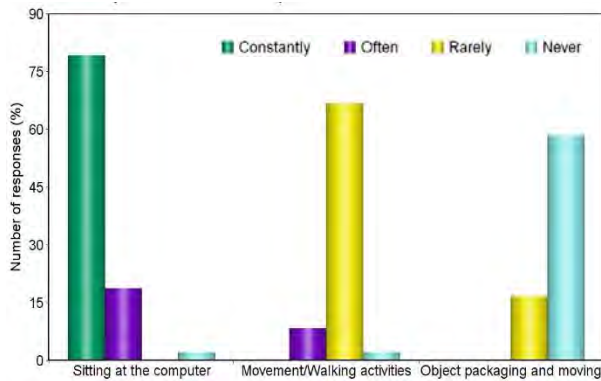
Figure 6 Survey responses for physical activities

The occupants' workplaces were situated on different floors of the building. The maximum number of responses belonging to a single floor were received from the fifth floor which was about 31% while about 22% and 13% of them were from the sixth and second floors, respectively. The remaining respondents were scattered on multiple floors, giving a diverse range of responses covering a significant portion of the building. Focusing on the commonalities among the responses, it has been found that more than half of them had office spaces that had windows facing either southwest or northwest. There is no strict dress code for the employees hence their usual office attire was allowed in the questionnaire. The CLO values were taken from the standard ISO 7730 standard (2005) (International Organisation for Standardisation, 2005) for the base case scenario. Wide range of clothing options were provided within the survey for the respondents to choose their typical office attire. The

survey results revealed the choice of attire of the occupants during various seasons in a year and also the level of flexibility they have with altering their clothing (Yao, Yang, Zhuang, Shao, & Yuan, 2018). To achieve the comfort levels, occupants tend to alter their clothing either by taking off their jacket, scarf, etc. when it is hot and putting them on when it is cold. Taking their responses into consideration and allowing for adaptive clothing, the clothing values were taken as shown in Table 2. Since clothing depends on the seasonal variation, the CLO values are different during different times of the year. For the two-year simulation, each season was assigned an appropriate CLO value with the help of rules and schedule options within the software IDA ICE.

Table 2 Clothing values for simulations

	Summer	Winter	Spring/ Autumn
CLO value for Non-Adaptive Case	0.5 ± 0.1	0.9 ± 0.1	0.7 ± 0.1
CLO value for Adaptive Case	0.4 ± 0.2	1.04 ± 0.2	0.76 ± 0.2

The adaptive behaviour of the occupants is heavily influenced by the indoor atmosphere (air temperature, relative humidity, etc.). To obtain these details, the respondents were asked to give their thermal sensation vote pertaining to the indoor atmosphere. A significant number of them responded that the indoor environment in comfortable during the spring/autumn season. Yet, the responses point out that the indoor environment is hotter during summer and colder during winter (Figure 7).
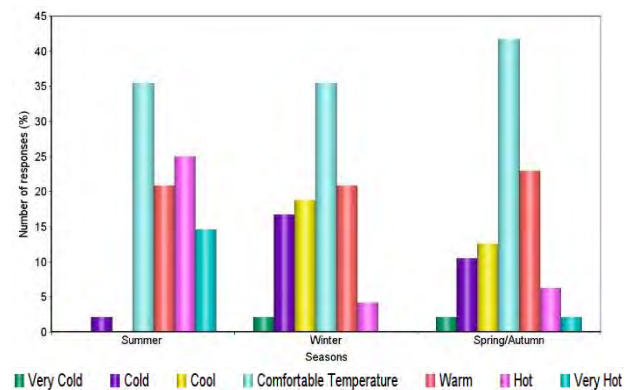
Figure 7 Level of thermal comfort in office during different seasons

Software simulation results

As mentioned earlier, an algorithm was used to run the macros for windows by linking the zone to the opening control as a function of air temperature. This algorithm is used in the adaptive case, where the temperature set point for opening the windows is when the air temperature in the zones is 24°C and above based on the non-adaptive case results. These settings were applied along with the

appropriate PMV values and the clothing schedule for both the case scenarios (Table 2). The simulation results show that the differences between both the cases vary by a slight margin. The total energy used by the building per m^2 is reduced for the adaptive case, as shown in Table 4. The overall thermal dissatisfaction of the occupants is reduced upon introducing occupant adaptations. Since the difference in values is not significant, more control over window opening for the occupants, may be given. The results show that they would feel more comfortable with having control over the windows. This could either be the psychological or physiological satisfaction of the occupants. In addition, the air temperature set point for window algorithm, probably if higher, may have resulted in a larger gap between the adaptive and non-adaptive case scenarios. Yet, in the building the occupants are satisfied with the indoor environment just as received through the survey result in Figure 7. The electric cooling and heating results show that the adaptive case has seen a slight reduction.

Table 3 Simulation case scenarios

	Non-Adaptive case	Adaptive case
Clothing level	Standard values	From survey results
PMV	-1 to +1	-2 to +2
Window opening	-	Based on air temperature

Table 4 Differences in scenario results from 2018 to 2019

	Non-Adaptive case	Adaptive case
Lighting (kWh/m²)	147.3	147.3
Electric cooling (kWh/m²)	14.6	13.9
HVAC (kWh/m²)	58.6	58.6
Electric heating (kWh/m²)	7.9	7.0
Tenant electric (kWh/m²)	110.5	110.5
PV production (kWh/m²)	21.8	21.8
Total used energy (kWh/m²)	317.2	315.6
Total occupant hours with thermal dissatisfaction (%)	19	18
Mean PPD value of all zones (%)	8.76	8.12

Conclusion

This paper has shown the data collection methods and the energy simulation results of a real office building. The results show that the occupants' adjustments with respect to clothing, do not yield a considerable change in the energy consumption rate. However, the values of PMV and CLO assumed for the simulation could be higher by giving more freedom to the occupants, without compromising energy efficiency of the building. In addition to the different CLO values (Table 3), the adaptive case also included window operation. Results prove that the occupants maybe given more control over HVAC controls with no significant change in the energy consumption. Also, further simulations maybe carried out for each season separately to focus more on the smaller variations between variables. For future research, more variables will be introduced to observe their influence over the occupant comfort levels.

References

Aguilera, J. J., Kazanci, O. B., & Toftum, J. (2019). Thermal adaptation in occupant-driven HVAC control. *Journal of Building Engineering*, *25*(May), 100846. https://doi.org/10.1016/j.jobe.2019.100846

Auliciems, A., & de Dear, R. (1998). *Thermal Adaptation and Variable Indoor Climate Control*. 61–86. https://doi.org/10.1007/978-3-642-80419-9_3

Chen, Y., Tong, Z., Samuelson, H., Wu, W., & Malkawi, A. (2019). Realizing natural ventilation potential through window control: The impact of occupant behavior. *Energy Procedia*, *158*, 3215–3221. https://doi.org/10.1016/j.egypro.2019.01.1004

Choi, J. H., & Moon, J. (2017). Impacts of human and spatial factors on user satisfaction in office environments. *Building and Environment*, *114*, 23–35. https://doi.org/10.1016/j.buildenv.2016.12.003

Derks, M. T. H., Mishra, A. K., Loomans, M. G. L. C., & Kort, H. S. M. (2018). Understanding thermal comfort perception of nurses in a hospital ward work environment. *Building and Environment*, *140*(March), 119–127. https://doi.org/10.1016/j.buildenv.2018.05.039

Hong, T., Lee, M., Yeom, S., & Jeong, K. (2019). Occupant responses on satisfaction with window size in physical and virtual built environments. *Building and Environment*, *166*(September). https://doi.org/10.1016/j.buildenv.2019.106409

Indraganti, M., & Boussaa, D. (2017). Comfort temperature and occupant adaptive behavior in offices in Qatar during summer. *Energy and Buildings*, *150*, 23–36. https://doi.org/10.1016/j.enbuild.2017.05.063

International Organisation for Standardisation. (2005). *ISO 7730:2005 Ergonomics of the thermal environment — Analytical determination and interpretation of thermal comfort using calculation of the PMV and PPD indices and local thermal comfort*

criteria. Retrieved from https://www.iso.org/standard/39155.html

KC, R., Rijal, H. B., Shukuya, M., & Yoshida, K. (2018). An in-situ study on occupants' behaviors for adaptive thermal comfort in a Japanese HEMS condominium. *Journal of Building Engineering*, *19*(May), 402–411. https://doi.org/10.1016/j.jobe.2018.05.013

Khalid, W., Zaki, S. A., Rijal, H. B., & Yakub, F. (2019). Investigation of comfort temperature and thermal adaptation for patients and visitors in Malaysian hospitals. *Energy and Buildings*, *183*, 484–499. https://doi.org/10.1016/j.enbuild.2018.11.019

Marín-Restrepo, L., Trebilcock, M., & Gillott, M. (2020). Occupant action patterns regarding spatial and human factors in office environments. *Energy and Buildings*, *214*. https://doi.org/10.1016/j.enbuild.2020.109889

Mostavi, E., Asadi, S., & Ramaji, I. J. (2016). Completing the Missing Puzzle Piece of the Building Design Process: Modeling and Identifying Occupants' Satisfaction Level in Commercial Buildings. *Construction Research Congress 2016: Old and New Construction Technologies Converge in Historic San Juan - Proceedings of the 2016 Construction Research Congress, CRC 2016*, (April 2020), 1112–1121. https://doi.org/10.1061/9780784479827.112

Nižetić, S. (2017). Realisation barriers in energy efficiency projects in Croatian public buildings: a critic overview and proposals. *International Journal of Sustainable Energy*, *36*(9), 901–913. https://doi.org/10.1080/14786451.2015.1127236

Yao, J., Yang, F., Zhuang, Z., Shao, Y., & Yuan, P. F. (2018). The effect of personal and microclimatic variables on outdoor thermal comfort: A field study in a cold season in Lujiazui CBD, Shanghai. *Sustainable Cities and Society*, *39*(February), 181–188. https://doi.org/10.1016/j.scs.2018.02.025

Domestic hot water decomposition from measured total heat load in Norwegian buildings

Synne Krekling Lien[1*], Dmytro Ivanko[2], Igor Sartori[1]

[1]SINTEF Community, Oslo, Norway
[2]NTNU Department of Energy and Process Engineering, Trondheim, Norway

*corresponding author: synne.lien@sintef.no

Abstract

In Nordic climates, the energy use in buildings is dominated by space heating (SH) and domestic hot water (DHW). Heat load measurements with hourly resolution from smart meters are now becoming the standard. However, in most cases, only the total heat use in the building is metered, without separation into DHW and SH use. The analysis performed in this work is aimed at comparing and verifying different methods for estimating typical DHW load profiles by decomposition of heat load measurements into SH and DHW. Three methods have been used for the decomposition of the same set of measurements of the heat load from 78 buildings comprised of apartments and hotels: the seasonal method, the energy signature method and hybrid summer-signature method. All three methods have limitations, but in this article it is shown that the hybrid-summer signature method, which is a new method that is proposed in this article, has the closest similarity to measurements of DHW energy use from similar buildings.

Introduction

The building stock is the most energy demanding sector in Norway. According to (Abrahamsen and Bergh, 2011), it accounts for about 40% of the total energy consumption. A characteristic feature of energy use in buildings in Norway is a high demand for space heating (SH) and domestic hot water (DHW) (Unander et al., 2004). For this reason, a huge potential for increasing energy efficiency in buildings in Norway can be gained through better design and operation of SH and DHW systems.

Analysis of energy use in existing buildings is a powerful instrument for achieving energy savings in buildings, performing better design and dimensioning of the energy systems, as well as introducing energy planning and demand-side management. The European Directive 2018/844 prescribes that energy analysis for building stock should include typical energy consumption for SH, DHW, and other technical systems in a building. However, the heat meter systems in most buildings are simplified and do not allow us to perform energy analysis in a proper way, and a significant share of buildings in Norway uses only a single heat meter for the total heat use. The readings from the meter are not separated into SH and DHW heat use. Experience shows that SH and DHW systems are technically detached. The factors affecting the energy performance in these two systems and are different

(Tereshchenko et al., 2019). Accordingly, it is crucial to conduct the analysis of heat use in SH and DHW systems independently (Cai et al., 2018). Despite the obvious drawback of simplified heat metering systems, the measured total heat use still contains valuable information about the DHW and SH systems performance. However, to use this information correctly, the reliable and accurate method for extracting the DHW and SH heat use profiles from the total heat use should be applied.

Currently, there are no generally accepted recommendations on how to separate the SH Acknowledgment and DHW profiles from the total heat use. The several approaches for decomposing the SH and DHW profiles from the total heat use that can be found in scientific publications are discussed in the text below.

In the article (Tereshchenko et al., 2019), the energy signature curve (ESC) was used to find temperature-dependent and temperature-independent part of the heat use in a Norwegian school. The temperature-independent part in ESC represents the DHW heat use. Based on this assumption, the DHW heat use profiles for working days and weekends were found. When the DHW heat use profiles are known, the profiles for SH can be extracted from the total heat use.

The modification of the ESC approach that takes into account the monthly variation of DHW heat use in dwelling in the United Kingdom (UK) is proposed in (Burzynski et al., 2012). The authors in (Burzynski et al., 2012) consider the days when the outdoor temperature is higher than the base temperature (Tereshchenko et al., 2019) as only the DHW heat use in the building. Hence, the DHW heat use profiles for several warm months can be found. After that, the DHW monthly variation factors from the UK national standard "The government's standard assessment procedure for energy rating of dwellings" were used to extrapolate the DHW heat use from warm months to other months of the year (Burzynski et al., 2012).

Linear regression models were used to extract DHW heat use profiles from the total heat delivery in (Sørensen et al., 2019). A model for total heat delivery was built with using the outdoor temperature, separate hours of each day, weekdays and holidays as an input for the modelling. When estimating the DHW heat use, the authors set the outdoor temperature in the models equal to the break-point temperature, before calculating the DHW daily load profile with hourly mean values (Sorensen et al., 2019).

A time series method for extracting DHW heat use spikes from the total heat use is presented in (Bacher et al., 2016). The method uses the fact that the SH heat use changes gradually during the day due to changes in outdoor temperature and user behaviour. DHW heat use does on the other hand create short-lived spikes in the total heat use time series. In order to identify the slow changes of SH heat use, the authors in (Bacher et al., 2016) propose to apply a non-parametric kernel smoother. All heat use values which lie above the kernel smoother are considered to be DHW heat use spikes.

Another method for detecting the SH and DHW heat use profile is proposed in (Marszal et al., 2019). The method consists of the following steps: 1) the daily profile for the total heat use in an average summer day is identified; 2) the non-DHW use is calculated as a minimum of total heat use profile for an average summer day or average for hours from 0:00–04:00 o'clock; 3) the DHW profiles are calculated by deducting the non-DHW heat use from the value of the heat use at each hour of the day.

An investigation of SH and DHW heat load measurements is shown in (Riachi et al., 2014). Here, the authors propose to model the DHW heat use based on the volumetric DHW use, the building activity, and the type of DHW system within the building. The SH loads are estimated according to the changes in outdoor temperatures, the building setpoint temperature, the night setbacks, and days of the week.

An alternative modelling approach that couples of the behavioural, stochastic, and energy balance models is proposed in (Fischer et al., 2016). The SH model in this approach uses a simplified physical method with a behavioural model for standardised buildings. The characteristics of the DHW heat use is found as a result of the SH model.

The literature review shows that the issue of extracting the SH and DHW profiles from the total heat use is not solved yet. The methods described above require extensive knowledge about the characteristics of the DHW and SH systems, the monthly variation factors for DHW heat use and/or users behaviour in buildings. Usually, when an energy analysis is conducted on a group of buildings, this information is not available. Several of the methods described are not verified with actual measurements (Bacher et al., 2016). For this reason, the comparison and further investigation of methods for identifying DHW and SH profiles from the total heat use in buildings are required.

Methodology

The analysis performed in this work is aimed at comparing and verifying different methods for estimating typical DHW load profiles for different building types by decomposition of heat load measurements into SH and DHW. Three methods have been tested for the decomposition of the same total heat use data from measurements: measurements: the seasonal method, the energy signature method and the hybrid summer-signature

method. The seasonal method and the energy signature method are classical methods. Meantime, the hybrid summer-signature is a new method proposed in this article The results from the decomposition with each method have then been compared against each other and against measurement of DHW heat loads, profiles from the national standard, as well as other studies conducted on decomposition and measurements of DHW in Norwegian buildings.

Measurements

DHW use is significantly influenced by user behaviour and the number of occupants in a building. For this reason, the analysis was performed on measurement data from a large number of buildings. In total, data from 78 Norwegian buildings have been used in this analysis. The buildings are comprised apartments and hotels. None of the buildings are considered to be passive houses or low energy buildings (very energy efficient). The measurements gathered for each building contain between 1-3 years of hourly data on the outdoor temperature and the total heat load (HtTot) in each building. The total heat load is assumed to be the sum of energy use for SH and DHW. The HtTot is covered by district heating in all buildings. The buildings are not registered with secondary heating and/or heat storage inside the buildings, however it is uncertain whether this is actually true for all of them. Table 1 shows an overview of the number of buildings within each building category that were analysed in this paper.

Table 1: Number of buildings sorted by building category.

Building category	Number of buildings
Apartment blocks	58
Hotels	20
Total	**78**

Decomposition method 1: Seasonal method (SM)

The seasonal method – which is sometimes referred to as the summer method - assumes that there is no demand for SH during the summer time (between June 1st and August 31st) in any of the buildings, and that the HtTot during the summer months is used only for DHW purposes. For each building, a typical DHW profile for workdays and weekends is created by extracting the average value for HtTot for every hour of the day during the summer period. SH is assumed to be zero in the summer. SH energy use for the rest of the year is identified as a difference between the measured heat load in the building and typical DHW profiles.

There are two approaches to treat holidays in seasonal method. The first approach ignores holidays when creating the typical DHW profile with the seasonal method. The second approach assumes that for a building there will be at least 30 days within each year when there will be little-to-no operation of SH and DHW systems due to the residents/users being away during the holidays. Most of these days will occur during the summer months.

Therefore, the way of identifying holidays is to mark the 30 days with the lowest heat load out of the warmest days within each year. These data should be eliminated from analysis to take effect of holidays into consideration.

Decomposition method 2: Energy signature method (ES)

In the energy signature method, an energy signature curve (ESC) is created for each building. The ESC shows the relationship between the total heat load in an observed building and the outdoor temperature, as shown in Figure 1. For a typical building, the ESC consists of two parts, divided by the change point temperature (CPT). The CPT is a critical temperature that indicates when the heating season ends. It is assumed that when the outdoor temperature is higher than the CPT, the SH system does not work and the heat use in the building is mainly related to the DHW use.
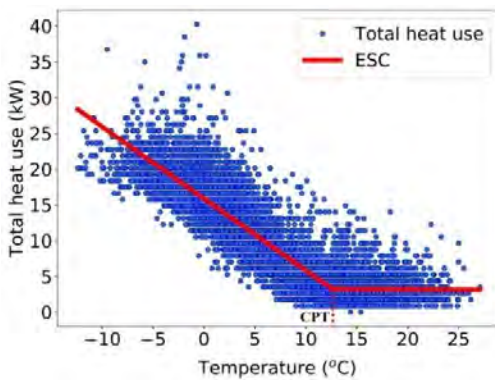
Figure 1: An example of the energy signature curve for the considered apartment building (Csoknyai et al., 2019).

The CPT can be identified by using the piecewise regression method. This method allowed us to find the CPT and construct separate models for the two parts of the ESC, as shown in Equation 1:

$$f(x) = \begin{cases} \beta_0 + \beta_1(x - CPT) + \varepsilon & If\ x < CPT \\ \beta_0 + \beta_2(x - CPT) + \varepsilon & If\ x > CPT \end{cases} \quad (1)$$

where $f(x)$ is a model for the ESC, x is the outdoor temperature, $\beta_0, \beta_1, \beta_2$ are the coefficients of the piecewise model, and ε is the residual error.

Using Equation (1), the CPT values were determined for the considered buildings. After, based on the ESD, the heat use when SH system is not operating, and DHW is the main energy consumer in the buildings was identified. Finally, the DHW heat use profiles for each building and building categories were calculated.

Decomposition method 3: Hybrid summer signature method (Hybrid SM-ES)

In order to improve the existing methods for HtTot decomposition, the authors propose a hybrid SM-ES method that takes aadditional features of SH and DHW systems performance into account. Buildings with ventilation systems might have a heating demand for heating of ventilation air during the summertime in the hours when the outdoor temperature is low – such as in the night time, in the early morning hours and on particularly cold days. By simply extracting the average value for heat load for every hour of the day during the summer (as is done in the seasonal method and to a certain extent in energy signature method), heating of ventilation air may be faulty interpreted as heating of DHW.

When using the hybrid summer signature method, the summer values for the heat load (HtTot) and outdoor temperature (Tout) for every hour of the day are plotted with the Temperature at the X-axis and the heat load on the Y-axis (in an so-called Energy-Temperature-/ET-curve). Linear regression is then used to calculate the expected value for HtTot for the given hour at a given temperature, as shown in Figure 2. When the interpolation is done at higher temperatures it can be assumed that there will be no space heating in the building, and that the interpolated value for the heat load is used solely for DHW heating purposes. In Norwegian buildings, the heating of ventilation air stops at above 16°C. Therefore, the typical DHW profiles created with the hybrid summer signature method has been tested at 16°C, 18°C and 20°C.
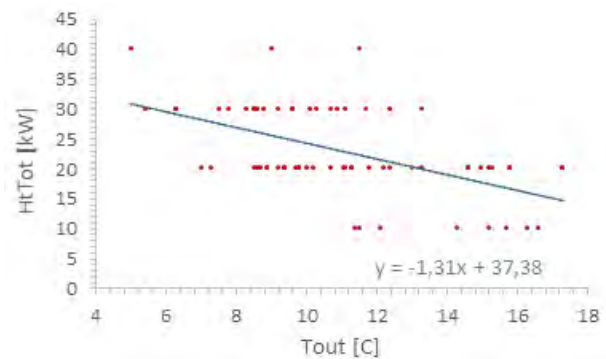
Figure 2 Tout and HtTot in one of the considered apartments on weekdays at 07:00.

In some buildings, the obtained value from the SM-ES method will become negative in some hours when the heat load is interpolated at higher temperatures, such as 20°C. When this occurs, the heat load is set to zero. In order to reduce the number of hours that get negative values for heating, whilst still aiming to reduce the effects of ventilation heating, the linear regression is performed at 18°C in this analysis.

Results

The test data (measurements of HtTot from the 78 apartments and hotels) have been decomposed into DHW and SH using three methods: the seasonal method (SM),

the energy signature method (ES-1) and the hybrid seasonal signature method (Hybrid SM-ES).

The results have been compared to different reference data:

- An application of the energy signature method on a different set of measurements of HtTot (Lindberg, 2017) (ES-2)
- Actual measurements of DHW use from three different sources (REF-1 from (Walnum et al., 2019), REF-2 from (Bagge et al., 2015) and REF-3 from (ElDek, 2020)).
- Normative inout data for DHW energy use for building modelling from the national standard "SN-NSPEK 3031:2020: Energy performance of buildings. Calculation of energy needs and energy supply".

The reference data is collected from different sources with differences in methodologies, system boundaries and building types. An overview of the modelling and the reference data sources is given in Table 2.

Table 2 Overview of simulation and reference data.

		Description	#	Sirc. losses	Energy supply
Test data	SM-1	Seasonal method without (1) and with marking (2) of holidays.	58 apartment blocks, 20 Htl	Yes	DH
	SM-2				
	Hybrid SM-ES 18	Seasonal method with linear regression at 18°C			
	ES-1	Energy signature 1			
References	ES-2	Reference Energy signature values for apartments (Pedersen, 2007) and for hotels (Lindberg et al., 2019).	53 dwellings, 7 hotels	Yes	DH
	REF-1	Reference 1 from measurements. Flow and energy measurements on pipes in Norwegian hotels and apartments. (Walnum et al., 2019)	2 Apt. blocks 3 hotels.	Yes / No	DH and EL
	REF-2	Reference 2 from measurements. Flow measurements on pipes in Swedish apartments, later converted into energy with a fix conversion factor. Individual metering for each unit. (Bagge et al., 2015)	4 apt. blocks with 1000 units.	No	NA
	REF-3	Reference 3, measurements of DHW energy use in single family houses. Energy measurement on socket (ElDek, 2020)	Unknown.	Yes	EL
	NORM	SN-NSPEK 3031:2020. Normative values of net energy demand for heating of DHW used in building modelling	-	No	-

Daily profiles

To evaluate the different decomposition methods, the typical daily profiles for DHW energy use in hotels and apartments have been created based on the test data. These daily profiles have been compared to the daily reference profiles for DHW energy use in apartments and hotels.

The reference daily profiles on DHW energy use from measurements in apartments are shown in Figure 3 (Weekdays) and Figure 4 (weekends). The reference

measurements have been gathered from three different sources: REF-1 and REF-3 come from measurements of DHW energy use in Norwegian apartment buildings, while REF-2 is gathered from the measurement of DHW use in 1000 Swedish apartments. REF-2 is plotted in the figures with a spread from the lowest 10th percentile to the highest 10th percentile of DHW energy use from all of the apartment units, indicating a large spread in DHW energy use between different users. The apartment references indicate that usually during weekdays, apartment blocks will have a high morning peak and evening peak for DHW energy use, with a significant reduction in DHW energy use during the night time. On weekends, the references indicate that apartments typically will have a higher morning peak at a later time of day (compared to workdays), with higher consumption of DHW energy use throughout the day, but still with a low consumption during the night time.

Figure 5 and Figure 6 show the typical profiles for apartments created from the test data with the different decomposition methods, plotted against REF-2, the reference energy signature profiles (ES-2) and normative values for DHW energy consumption (NORM). The seasonal-method profiles (SM-1 and SM-2) and the energy signature profiles (ES-1 and ES-2) show higher values for most hours compared to the typical profiles obtained from measurements, with little reduction in energy consumption during the night time. The hybrid SM-ES 18 profiles are closer to the average profile from REF-2, and show a more significant reduction in the energy consumption during the night time, although the typical daily profile from the Hybrid SM-ES method creates a "flatter" daily profile for the apartments with less significant morning and evening peaks, compared to the other decomposition methods.

The typical daily profile for hotels (regardless of weekdays/weekends) from the test data and from the references is shown in Figure 7. All of the daily profiles for DHW energy consumption in hotels indicate a high morning peak, and a slight increase in DHW consumption towards the evening/night, with a decrease in energy use during the night. The Hybrid SM-ES method has a bigger decrease in energy use during the night compared to the other decomposition methods. The weekend and weekday DHW profiles are not plotted individually for hotels, as the reference values don't separate between different days in the typical profile. The test data does however indicate a later morning peak in hotels on weekends compared to weekends regardless of the decomposition method used.
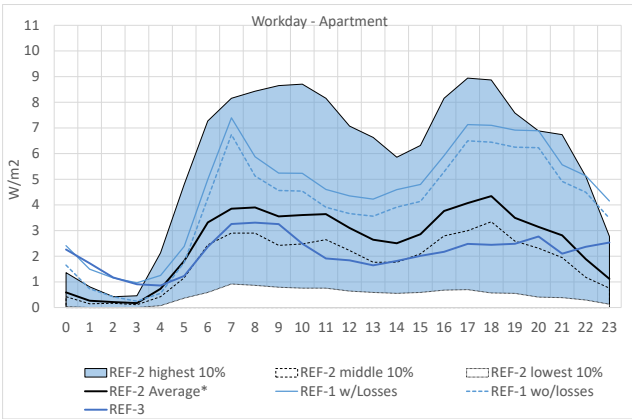
Figure 3 Reference measurements of DHW energy on weekdays in apartments.
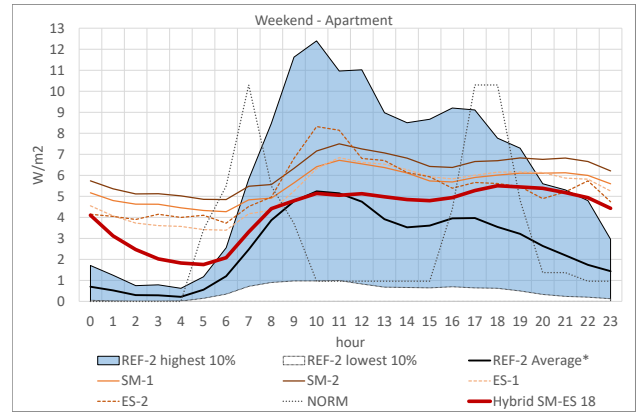
Figure 6 Average weekend profiles for DHW energy use in apartments created for the test buildings with different methods compared against REF-2 and NORM.
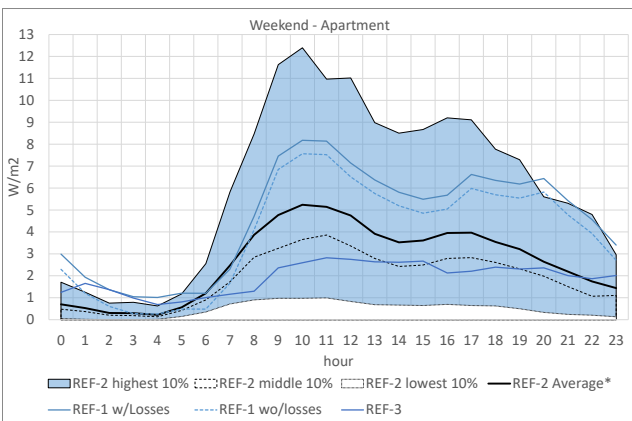
Figure 4 Reference measurements of DHW energy on weekends in apartment buildings.
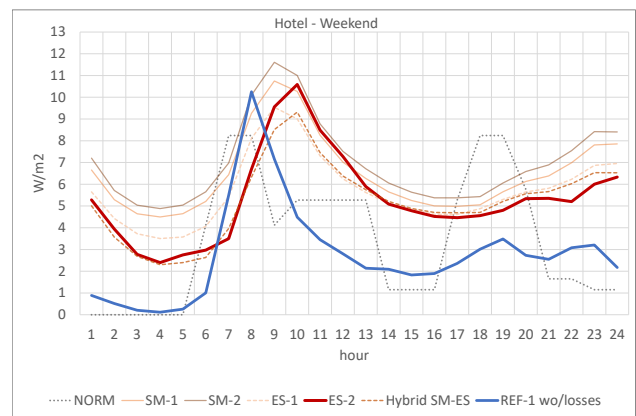
Figure 7 Average daily profiles for DHW energy use in hotels created for the test data with different methods compared against REF-1 and NORM.
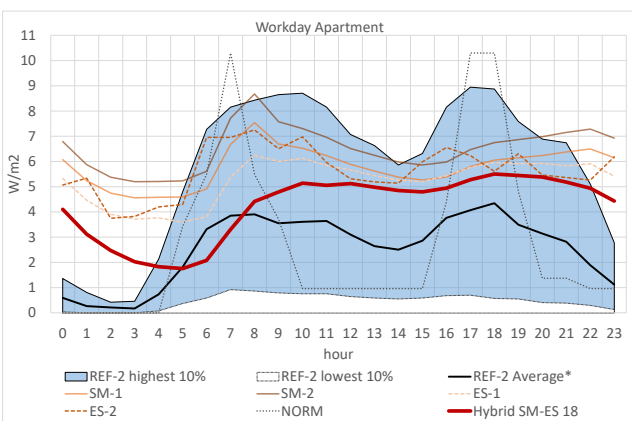
Figure 5 Average weekday profiles for DHW energy use in apartments created for the test buildings with different methods compared against REF-2 and NORM.
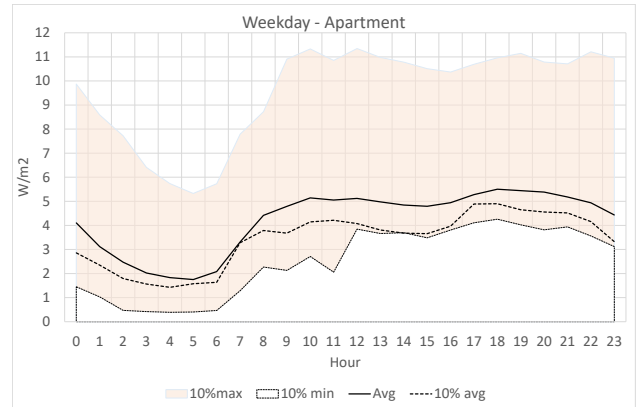
Figure 8 Variation in daily profiles for the apartment test data on weekdays created with Hybrid SM-ES method at 18°C.
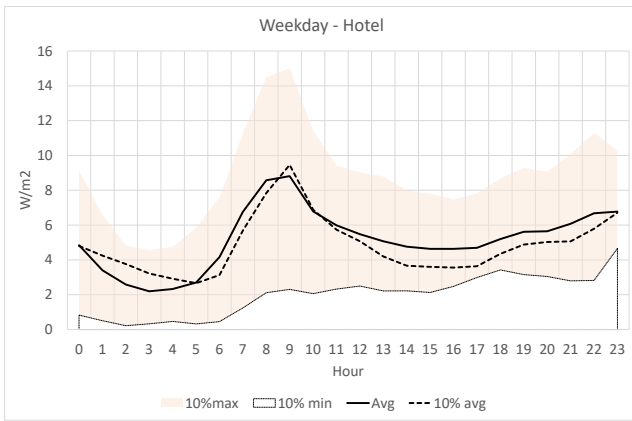
Figure 9 Variation in daily profiles for the hotel test data on weekdays created with Hybrid SM-ES method at 18°C.

The average daily profiles for DHW energy use in apartments and hotels created with the hybrid SM-ES-method has the resulting profile which is the most similar to the typical profiles obtained from actual measurements on the building category level. However, there is a large variation in the typical DHW energy consumption between all the buildings in the test data. Figure 8 and Figure 9 show the variation between the typical profiles created with the hybrid SM-ES method for the 78 apartments and hotels respectively, from the lowest 10th percentile to the highest 10th percentile.

Annual energy use for DHW

The different methods for extracting the DHW energy use give different results on the annual consumption of energy use for DHW. The spread of the resulting annual energy use for DHW in the 78 test data is shown in the boxplots in Figure 10 and Figure 11 for apartments and hotels respectively.
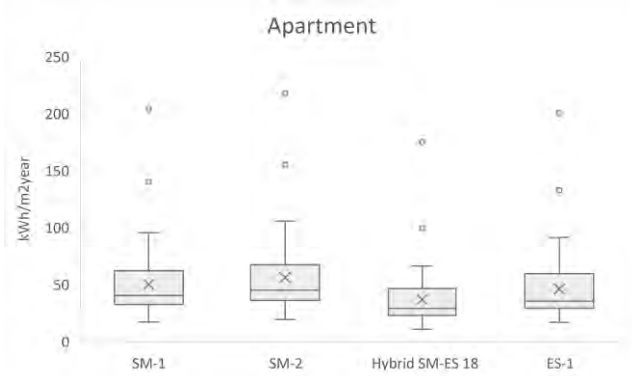
Figure 10 Boxplots of annual specific energy use for DHW decomposed with different methods in 58 apartment blocks.
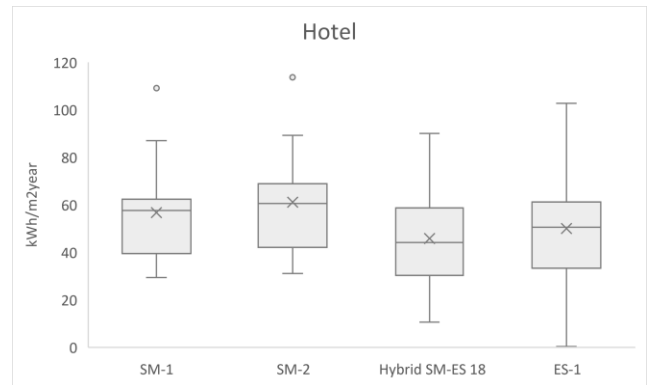
Figure 11 Boxplots of annual specific energy use for DHW decomposed with different methods in 20 hotels.

The mean annual energy consumption is the lowest when the hybrid SM-ES method at 18°C is used, and highest when the SM-2 method is used.

The mean annual specific energy use for DHW created for the test data with the different methods, as well as the mean energy use from the references is listed in Table 3. The results show that all the decomposition methods used on the test data have resulted in higher annual energy use for DHW in both apartments and hotels compared to most of the references. The exception is REF-1 with circulation losses which have higher annual consumption than the resulting mean created with SM-ES-18 for apartments.

Table 3 Mean annual energy use DHW Heating.

	Method	Apartment [kWh/m²year]	Hotel [kWh/m²year]
Test data	SM-1	50.2	56.9
	SM-2	56.3	61.3
	Hybrid SM-ES 16	42.4	50.5
	Hybrid SM-ES 18	37.0	46.0
	Hybrid SM-ES 20	31.8	41.9
	ES-1	45.9	50.0
Reference data	ES-2	48.8	46.9
	NORM	25.1	30.1
	REF-1 w/Losses	40.2	24.5
	REF-1 wo/losses	34.3	-
	REF-2	22.7	-
	REF-3	18.2	-

Discussion

The comparison of decomposition methods is nescessary in order to create realistic energy profiles for achiving energy efficiency in buildings. The proposed Hybrid SM-ES method has showed good results and can be applied in practice.

The simple seasonal method assumes that there is no SH energy use during the summer, however this may not be true for all buildings, especially the buildings with ventilation systems, where the ventilation air is heated before being supplied in the building. By following traditional methods, heating of ventilation air may be faulty interpreted as heating of DHW, resulting in an

overestimated total annual demand for heating of DHW, as well as overestimating the hourly energy demand for DHW, especially at night and in the early morning hours when the outdoor temperature is lower, and the heating of ventilation air is higher. An alternative to the simple seasonal method would be to sort the heat load data by outdoor temperature, and look at the warmest days/hours instead of the summer dates. For buildings in colder climates, there may not be enough data points for higher temperatures (above 16°C) at all hours of the day. The hybrid seasonal-signature method offers an alternative approach where the expected value for the heat load is interpolated at higher temperatures. The hybrid summer-signature method shares similarities with (Burzynski et al., 2012), however, it doesn't identify the CPT/break point temperature for each building, and only measurements from the summer season are collected before the linear regression is applied. In some buildings, the interpolated value results in negative values when the SM-ES method is applied, especially when the heat load is interpreted at higher temperatures (20°C). When this occurs, the heat load is set to zero. Negative values suggest that the values should be low – and close to zero, however this is an underestimation as in reality, the circulation losses will be above 0. If the heat load is interpolated at too high temperatures, the resulting DHW value can get too low. Establishing the most suitable temperature for the interpolation must be balanced between reducing the effects of ventilation heating during the night, whilst not underestimating the heat load for DHW energy use during the day.

The energy signature method is a widely used method for extracting the DHW energy use from heat load measurements. The ES-method is based on Piecewise Regression and optimization. If the ES-method is applied to a dataset without a classical shape, where there for instance is little dependence between the heat load and the outdoor temperatures, where there are a significant amount of data points, or where there heat is being turned off at different times (e.g. due to heat storages being used, load controls or other factors), the ES-algorithm will not work normally. Due to this, the ES-method will not be applicable to all datasets, and has not been possible to apply to all files in the test data set.

All typical profiles created from the test data with the different decomposition method show a time-shift compared to the measurements. This could be due to a difference in the registration of data, or different user behaviour in the different data sets.

In all three methods, it is assumed that there is no seasonal variation in the DHW consumption, however (Bagge et al., 2015) has found a seasonal dependence of DHW consumption in apartment blocks, with higher consumption in the winter months. One could also assume that tourist oriented hotels have higher consumption in the summer months, while congress and business oriented hotels have higher consumption outside the summer months. Seasonal variation in DHW is also supported by (Gerin et al., 2014). The methods could be improved by combining the typical DHW-profiles with seasonal coefficients for DHW from (Gerin et al., 2014) or create coefficients based on (Bagge et al., 2015).

The comparison of the DHW energy use in the test data created with the different methods and the measurements indicate that all methods for decomposition likely overestimates the energy use for DHW purposes in apartments and hotels. As the modelled DHW energy use might be used for dimensioning purposes, this is considered to be preferred compared to underestimation of DHW energy use.

Conclusion

Analysis of energy use in existing buildings is a powerful instrument for achieving energy savings in buildings, performing better design and dimensioning of the energy systems, as well as introducing energy planning and demand-side management. Currently, there are no generally accepted recommendations on how to separate the SH and DHW profiles from the total heat use. The aim of the analysis performed in this work has been to compare and verify different methods for estimating typical DHW load profiles by decomposition of heat load measurements into SH and DHW. Three methods have been used for the decomposition of the heat load from 78 apartments and hotels: the seasonal method, the energy signature method and hybrid summer-signature method. All methods have limitations in creating the typical DHW-profile for a building. The hybrid-summer signature method with linear regression at 18°C gave the best results for the decomposition of DHW compared to the measurements for the test data used in this analysis. A similar comparison of the resulting SH energy use profiles with verification against SH measurements should be conducted in further work in order to further evaluate this method.

Acknowledgment

References

Abrahamsen, A. S., & Bergh, M. (2011). Energibruk i bygninger for tjenesteytende virksomhet. 2008.

Bacher, P., de Saint-Aubain, P. A., Christiansen, L. E., & Madsen, H. (2016). Non-parametric method for separating domestic hot water heating spikes and space heating. *Energy and Buildings, 130*, 107-112.

Bagge, H., Johansson, D., & Lindstrii, L. (2015). BRUKARRELATERAD ENERGIANVÄNDNING Mätning och analys av

hushållsel och tappvarmvatten. *LÅGAN - För Energieffektiva Byggnader*.

Burzynski, R., Crane, M., Yao, R., & Becerra, V. (2012). Space heating and hot water demand analysis of dwellings connected to district heating scheme in UK. *Journal of Central South University, 19*(6), 1629-1638.

Cai, H., Ziras, C., You, S., Li, R., Honore, K., & Bindner, H. W. (2018). Demand side management in urban district heating networks. *Applied Energy, 230*, 506-518.

Csoknyai, T., Legardeur, J., Akle, A. A., & Horvath, M. (2019). Analysis of energy consumption profiles in residential buildings and impact assessment of a serious game on occupants' behavior. *Energy and Buildings, 196*, 1-20.

ElDek. (2020). Data obtain from personal communication with Hanne Sæle [or Project Leader, or Contact Person] in April 2020. https://www.sintef.no/en/projects/eldek-electricity-demand-knowledge/, accessed on 07/05/2020.

European Commission, Directive (EU) 2018/844 of the European Parliament and of the Council, Available from: https://eur-lex.europa.eu/legalcontent/EN/TXT/?uri=uriserv%3AOJ.L_.2018.156.01.0075.01.ENG (Accessed October 16, 2019).

Fischer, D., Wolf, T., Scherer, J., & Wille-Haussmann, B. (2016). A stochastic bottom-up model for space heating and domestic hot water load profiles for German households. *Energy and Buildings, 124*, 120-128.

Gerin, O., Bleys, B., & De Cuyper, K. (2014). *Seasonal variation of hot and cold water consumption in apartment buildings*. Paper presented at the CIBW062 Symposium 2014.

The government's standard assessment procedure for energy rating of dwellings. (2019). In *Building Research Establishment, Watford, UK* (pp. 180): BRE Garston, Watford.

Lindberg, K. B., Bakker, S. J., & Sartori, I. (2019). Modelling electric and heat load profiles of non-residential buildings for use in long-term aggregate load forecasts. *Utilities Policy 58, 58*, 62-88.

Marszal, A. J., Zhang, C., Pomianowski, M. Z., Heiselberg, P. K., Gram-Hanssen, K., & Hansen, A. R. (2019). Simple methodology to estimate the mean hourly and the daily profiles of domestic hot water demand from hourly total heating readings. *Energy and Buildings, 184*, 53-64.

Pedersen, L. (2007a). *Doctoral Thesis. Load Modelling of Buildings in Mixed Energy Distribution Systems. of Energy and Process Engineering.* Trondheim: NTNU,

Pedersen, L. (2007b). *Load Modelling of Buildings in Mixed Energy Distribution Systems.* (PhD Thesis).

Riachi, Y., Rangod, N., & Guillemot, B. (2014). *A numerical model for determining hourly heating and DHW loads in district heating systems.* Paper presented at the The 14th International Symposium on District Heating and Cooling.

Sørensen, A. L., Lindberg, K. B., Walnum, H. T., Sartori, I. Aakenes, U. R. & Andresen, I. (2019). Heat Analysis for Energy Management in Neighbourhoods: Case Study of a Large Housing Cooperative in Norway. *IOP Conference Series: Materials Science and Engineering, 609*, pp. 1-7.

Tereshchenko, T., Ivanko, D., Nord, N., & Sartori, I. (2019). Analysis of energy signatures and planning of heating and domestic hot water energy use in buildings in Norway. *E3S Web of Conferences, 111*(06009), p. 1-8.

Unander, F., Ettestøl, I., Ting, M., & Schipper, L. (2004). Residential energy use: an international perspective on long-term trends in Denmark, Norway and Sweden. *Energy policy, 32*(12), 1395-1404.

Walnum, H., Sørensen, Å. L., Ludvigsen, B., & Ivanko, D. (2019). Energy consumption for domestic hot water use in Norwegian hotels and nursing homes. *IOP Conference Series: Materials Science and Engineering, 609*. doi:10.1088/1757-899X/609/5/052020

Appendix

The hybrid SM-ES method at 18 degrees was applied to 198 buildings from different building categories with measurements of HtTot. This table shows the resulting typical profile for DHW energy use in different building categories. n= the number of buildings in the test data within the building category.

Hour	Apartment n = 58 WD	WE	Hotel n = 20 WD	WE	Nurs. home n = 31 WD	WE	Office n = 49 WD	WE	School n = 40 WD	WE
0	4.10	3.93	4.85	5.42	2.92	3.09	1.26	1.35	1.49	1.57
1	3.12	3.38	3.40	3.98	2.81	2.92	1.20	1.27	1.42	1.48
2	2.47	2.96	2.58	2.95	2.62	2.78	1.19	1.30	1.31	1.50
3	2.02	2.74	2.19	2.57	2.77	2.79	1.11	1.00	1.23	1.44
4	1.83	2.28	2.33	2.56	3.06	3.01	1.17	1.11	1.13	1.29
5	1.75	2.03	2.70	2.48	3.40	3.19	1.15	1.10	1.22	1.32
6	2.08	2.02	4.17	3.47	3.82	3.55	1.57	1.29	1.39	1.52
7	3.31	2.48	6.76	5.23	4.40	3.88	1.64	1.31	1.41	1.57
8	4.42	3.10	8.58	8.36	5.17	4.63	1.97	1.46	1.84	1.67
9	4.79	4.09	8.81	10.59	6.39	5.32	2.20	1.49	2.52	1.74
10	5.14	5.26	6.79	9.12	6.62	5.30	2.37	1.55	2.83	1.88
11	5.05	5.68	5.99	7.35	6.56	5.33	2.56	1.75	3.01	1.93
12	5.12	5.80	5.48	6.43	6.35	5.38	2.67	1.74	3.22	1.97
13	4.98	5.77	5.07	5.57	6.19	5.35	2.67	1.82	3.30	2.09
14	4.85	5.64	4.76	5.20	6.17	5.36	2.62	1.84	3.28	2.07
15	4.80	5.29	4.63	4.88	5.79	5.13	2.56	1.77	3.34	2.19
16	4.94	5.16	4.64	4.82	5.24	4.87	2.36	1.76	2.94	2.06
17	5.28	5.24	4.70	4.72	5.13	4.83	2.15	1.79	2.63	2.09
18	5.50	5.40	5.19	5.26	4.82	4.73	2.00	1.78	2.44	2.08
19	5.44	5.35	5.62	5.44	4.69	4.62	1.94	1.64	2.25	1.99
20	5.38	5.24	5.64	5.71	4.57	4.51	1.79	1.65	2.07	1.98
21	5.18	4.80	6.07	5.91	4.21	4.00	1.68	1.49	1.89	1.89
22	4.94	4.37	6.68	6.16	3.72	3.63	1.56	1.34	1.68	1.68
23	4.43	4.09	6.78	5.90	3.23	3.10	1.32	1.24	1.53	1.54

Numerical analysis of heat recovery options in old Finnish apartment buildings

Janne Hirvonen[1*], Juha Jokisalo[1], Risto Kosonen[1]
[1]Aalto University, Espoo, Finland
*corresponding author: janne.p.hirvonen@aalto.fi

Abstract

Ventilation heat recovery in residential buildings is well established. However, waste heat recovery from sewage is focused on industrial applications and is not commonly done in Finland at the residential building level. This study examines the CO_2 emission reduction potential of heat recovery from sewage and ventilation exhaust air in various configurations in an apartment building built before ventilation heat recovery systems were mandatory. The study was done by dynamic simulation using TRNSYS and the IDA-ICE building simulation software. The lowest costs and emissions were obtained by combining both the exhaust air and sewage heat recovery using heat pumps. Thus, heat recovery can reduce emissions even while lowering life cycle costs. CO_2 emissions were reduced by 12 to 50% using a series connection between district heating and waste heat sources and 21 to 37% using a parallel connection. Utilities enforce the use of parallel connection, which reduces heat recovery potential. With heat exchanger based ventilation heat recovery, the emissions were reduced by 23 to 29%. The key performance indicator for energy efficiency is the primary energy consumption. However, systems with similar primary energy consumption can have very different emissions. The mismatch between emissions and primary energy use suggests a need for a policy update.

Introduction

The Finnish building code introduced the requirement of ventilation heat recovery for residential buildings in 2003 (Ministry of the Environment, 2017). However, most Finnish apartment buildings have been built before this and have no ventilation heat recovery (HR), which wastes a lot of energy. In addition, there is no requirement of recovering heat from sewage even in new buildings. Sewage heat is typically recovered in a centralized manner in waste water treatment plants or even in district heating facilities (Helen Oy, 2020). However, while a far-away treatment plant might recover 10 to 30% of the original energy content in the sewage, on-site recovery at the waste producing site could allow 70 to 90% recovery (Mazhar et al., 2018). This spells out the need for improved heat recovery systems implemented directly at the building.

Exhaust air pumps (EAHP) are quite a well established technology. Various EAHP configurations have been analysed in (Thalfeldt et al., 2018). Special focus was given on integrating the EAHP with district heating (DH), which is also the most common heating type for apartment buildings in Finland. EAHP systems could cover almost all heating needs in summer, but raised the average DH return temperatures. Three EAHP connections were analysed, including series and parallel connection, but no significant performance differences were found between the cases. This was attributed to prioritizing production of domestic hot water (DHW). Study by (Kensby et al., 2017) revealed the non-correlation of district heating and electricity prices. It showed that costs could be reduced by optimizing the heat source timing in a DH/EAHP hybrid, instead of always using the EAHP for base load generation. Advanced control algorithms for a solar electric EAHP hybrid systems were examined in (Psimopoulos et al., 2019). Various priorities between battery and thermal energy storage and between space heating or hot water focus were examined. The value of heat pump control algorithms was greater if no battery electric storage was available.

Ventilation heat recovery was examined in (Ploskić and Wang, 2018). Sewage HR was connected to the inlet air supply of a low-energy house in northern Sweden to reduce ventilation heating demand. Using the waste heat, the ventilation system could more often meet the air supply temperature requirement and reduced the ventilation heating demand by up to 40%. Similarly, sewage HR and geothermal energy were used to reduce frosting in ventilation heat recovery (Nourozi et al., 2019). The sewage HR system did more than halve the total defrosting time in the air-handling unit, but major use of recovered sewage heat reduced the temperature efficiency of the ventilation HR system. The buildings in these studies utilized a mechanical balanced ventilation system, which is not installed in most Finnish apartment buildings. Another study found that sewage HR could cover 80% of DHW heating demand (Hervás-Blasco et al., 2020). This system utilized two connected hot water storage tanks. Comparison was made between infinite available sewage and finite, but constant availability and finite, but variable availability. With proper system design (heat pump or tank sizing), the variability had only a minor impact on system performance.

This study examines the CO_2 emission reduction potential and cost-effectiveness of various hybrid heat recovery solutions in Finnish apartment buildings. It compares the stand-alone ventilation or sewage heat recovery systems to combined systems with both HR methods integrated.

Ideal heat pump connections are compared to systems that are commonly accepted by utilities.

Methods

Building description

The Helsinki municipal housing company (Heka Ltd.), which is the biggest lessor in Finland, owns 531 buildings, with a combined net heated floor area of 2 815 000 m^2. Requirements of ventilation heat recovery were not added to the Finnish building code until the year 2003, but 85% of Heka's buildings have been built before the year 2000 (Heka Ltd., 2020). With an average heating demand of 197 kWh/m^2/a, there is a great potential for efficiency improvements through ventilation or sewage heat recovery. The buildings use district heating, which in Helsinki is supplied mostly through coal power, adding to the emission benefits of heat recovery. A typical apartment building without any heat recovery systems was modelled in IDA-ICE 4.8 to serve as a calculation basis. The properties of the building are shown in Table 1 and Figure 1. Figure 2 shows a comparison of the monthly heating demand in the existing and simulated buildings. The measured data was from the year 2017, while the simulation was done using the TRY2012 weather data (Kalamees et al., 2012) and corrected using degree day weighting for the year 2017. The simulated heating demand for the whole year was 4.3% lower than the measured demand, showing a good correlation between simulation and practice. Hourly comparison was not an option due to non-matching weather profiles.
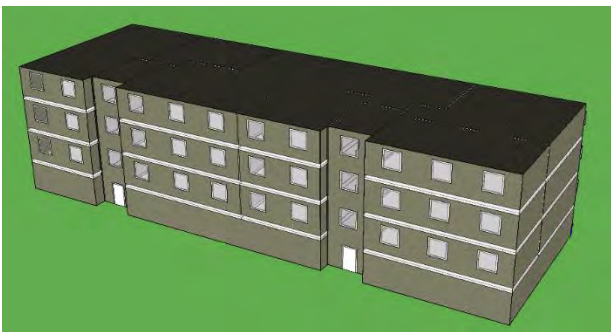
Figure 1. IDA-ICE model of the simulated apartment building.

Water consumption in the reference building was 163 L/resident/day, based on measured data. 40% of this was assumed to be domestic hot water, as is instructed in the building code (Ministry of the Environment, 2018a). Since only monthly consumption was available, hourly use profiles were based on measured results from other apartment buildings (Koivuniemi, 2005). DHW consumed 49% of the heat used in the reference building, with the remainder used for space heating.

Table 1. Building properties.

Feature	Value	Feature	Value
Construction year	2000	Ventilation	
U-values of envelope (W/m^{2}K)		Type	Mechanical exhaust
External wall	0.28	Heat recovery	-
Floor	0.36	Air change rate (1/h)	0.5
Roof	0.22	SFP (kW/m^3/s)	1.5
External doors	1.4	Water radiators (ºC)	70/40
Windows (triple-glazed, clear)	1.7	Heat distribution efficiency	0.8
Window g-value	0.71	Heating set point (ºC)	
Window direct transmittance	0.64	Living spaces	22
Window light transmittance	0.75	Other spaces	19
Infiltration (estimate)		Domestic hot water demand (L/resident/day)	65
n_{50}, (1/h)	1	Residents	108
q_{50} m^3/(h m^2)	2.60	Heated net area (m^2)	3855
		Envelope area (m^2)	1608
		Window area (m^2)	315
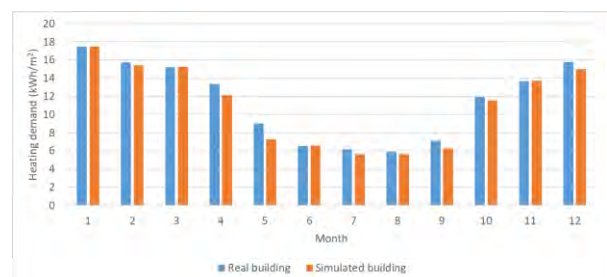
Figure 2. Measured and simulated heating demand of the apartment building.

Energy system options

The reference building had mechanical exhaust ventilation with no heat recovery systems. In this paper we compare the cost-effectiveness of various methods of heat recovery. We analyze combinations of ventilation heat recovery with heat exchangers (HX) or an exhaust air heat pump and sewage heat recovery with heat exchangers or a heat pump. The examined scenarios are shown in Table 2. In cases 2 and 3, a mechanical balanced ventilation system was installed. In cases 4 to 8, EAHP and sewage HR systems were connected to the district heating system in an ideal manner i.e. in series, preheating

the circulating fluid. In cases marked with B, regulation-acceptable parallel connections were used instead.

Table 2. Examined scenarios with different heat recovery options.

Scenario	Ventilation type	Ventilation HR	Sewage HR
1	Exhaust	-	-
2	Balanced	HX	-
3	Balanced + VAV	HX	-
4	Exhaust	EAHP	-
5	Exhaust	-	HX
6	Exhaust	-	HP
7	Exhaust	EAHP	HX
8	Exhaust	EAHP	HP
4 B	Exhaust	EAHP	-
6 B	Exhaust	-	HP
8 B	Exhaust	EAHP	HP

Energy system model

The building was modelled using the dynamic building energy simulation tool IDA-ICE 4.8. The IDA-ICE model was used to calculate the heating demand under all different ventilation systems (Scenarios 1 to 3). The heating demand profile from Scenario 1 (which includes space heating (SH), ventilation heating and domestic hot water) was used as an input for the remaining scenarios. The energy systems for these scenarios were simulated using TRNSYS 17, to allow more flexibility in the system design. The TRNSYS model consisted of heat exchangers (Type 91), flow mixers/splitters (Type 11h, 11f), stratified thermal storage tanks (Type 534) and a custom heat pump model.

Heat pump performance was based on the NIBE F1345-60 heat pump (NIBE AB, 2017). Flow rates of source and load side were determined from the HP data sheet. Part-load operation was allowed, in which case the power and flow rates were adjusted in the same proportion. Figure 3 shows the thermal power of the F1345 60 kW heat pump under different heat source temperatures (x-axis) and load-side temperatures (separate lines for 35, 50 and 65 °C). The power values were linearly scaled down for the smaller heat pumps utilized in this study.

Scenario 1 used mechanical exhaust ventilation, where the exhaust air from rooms was blown outdoors without any heat recovery. In Scenario 2, a constant flow mechanical balanced ventilation system was used instead. Now, heat from exhaust air was recovered using a heat exchanger with 70% temperature efficiency. This exceeds the minimum requirement (Saari and Airaksinen, 2012), but is still lower than some commercial products. The supply air temperature was 17 °C. Scenario 3 was otherwise the same, but variable air flow ventilation (VAV) was utilized. The air flow was 0.14 L/s/m² when a

room was unoccupied and increased linearly to 0.36 L/s/m² at full occupancy.
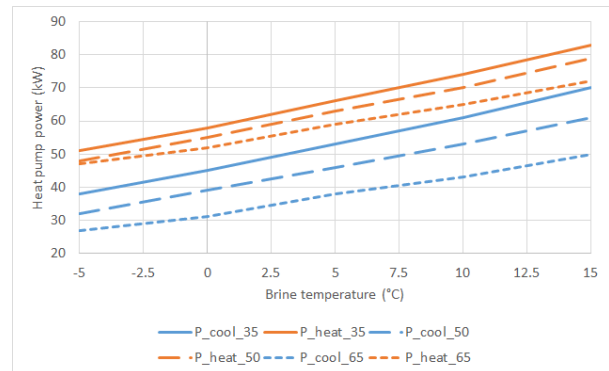
Figure 3. Heating and cooling power of the heat pump NIBE F1345-60. Blue lines represent the cooling power of the heat source and orange lines the heating power of the load. The numbers in the legend signify the output temperature (°C).

Heat recovery series connection

Scenarios 4 to 8 utilized a series connection between the heat recovery and district heating. Any waste heat was first used to preheat the return flow from the space heating circuit and the cold water in the DHW circuit. A stratified primary storage tank (TRNSYS Type 534) with 2 m³ volume was used with the EAHP. A separate 2 m³ secondary tank was used for sewage heat recovery in the DHW circuit. When in use, the EAHP capacity was 30 kW$_{th}$ and the sewage HP capacity was 15 kW$_{th}$. The heat recovery system configuration is shown in Figure 4. The figure shows the most complex configuration, Scenario 8, with two heat pumps and two storage tanks. Other scenarios can be obtained by removing either heat pump or the sewage tank from the system. The connection between waste heat and district heating is shown in Figure 5 (series) and (parallel).

When operating the EAHP, waste heat from the exhaust air was transferred to a brine circuit via a HX. The brine was used as a heat source for the EAHP. The EAHP was activated on full power whenever the primary storage tank temperature was 5 °C below the set point. The idea was to keep the share of EAHP use high, while reducing the amount of on-off-switching. In addition, the heating demand on the load-side was monitored and the EAHP was operated on partial power relative to the demand to slow down the temperature decay in the tank. The set point was determined by the SH control curve, but it was at least 45 °C and a maximum of 60 °C. SH flow was preheated in the primary tank before utilizing district heating to get to the required temperature level.
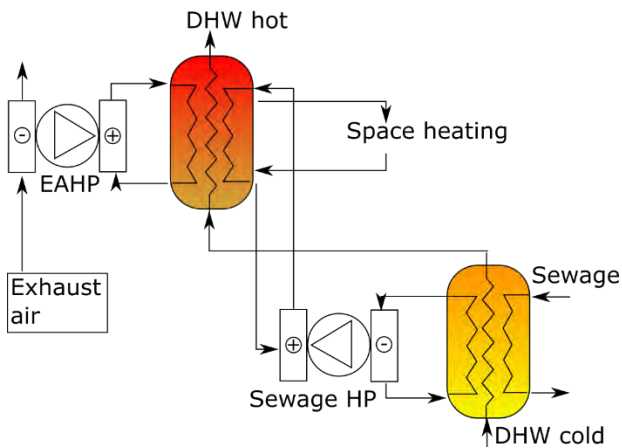
Figure 4. Schematic of the heat recovery system with both exhaust air and sewage HR using heat pumps.

Sewage HR was arranged through a secondary thermal storage tank. Sewage flow at 20 °C was pumped through the secondary tank's heat exchanger to recover the waste heat. Average sewage temperatures of 23 °C have been measured in Finland (Koikkalainen, 2016). However, a conservative temperature value was used to compensate for the ideal heat recovery tank. The sewage flow rate equalled the total water consumption, not only the DHW consumption, as even cold water gets warmed up in the piping between times of use. DHW was preheated by letting the cold inlet water at 5 °C flow through the secondary tank. When a heat pump was used for sewage HR, the secondary sewage tank was used as a heat source and the primary SH tank as a heat sink. The sewage HP was prioritized over the EAHP by the use of a higher set point, to take advantage of the higher heat source temperature provided by the sewage. In the series connection case, both the DHW and SH supply flows were preheated in the primary tank before using DH to prime the flow to the final temperature.
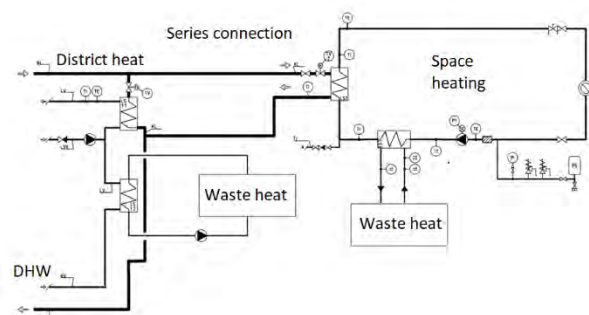
Figure 5. Series connection of waste heat and DH.

Heat recovery parallel connection

Scenarios 4 B, 6 B and 8 B were similar to the base scenarios. However, district heating companies wish to minimize the return temperature of the DH flow and generally don't allow a series connection for secondary heating systems. In the B scenarios a parallel connection for waste heat was used instead (). In the SH circuit (right

side), the return flow was split into two parts,
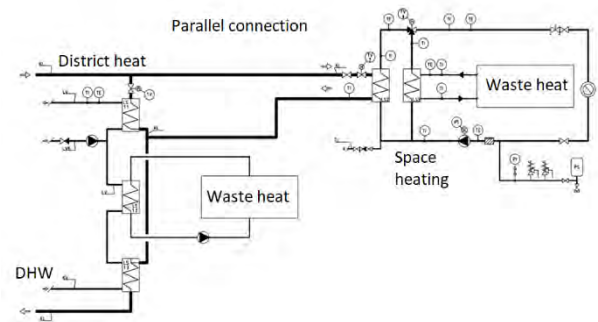
Figure 6. Parallel connection of waste heat and DH.

one going to the primary HR tank (Waste heat) and one to the DH HX, both at the same temperature. The heated flows were then mixed. The DH flow was adjusted to obtain the desired final temperature. Waste heat was not used for preheating, but had equal priority to district heating. This raised the required output temperature for heat pumps and reduced the share of energy produced with waste heat.

The DHW loop in the parallel configuration (left side of) contains three heat exchangers. The return flow from the DH circuit was used to preheat the cold DHW flow (lowest HX). The preheated DHW was further heated by waste heat from the primary HR tank (middle HX) and raised to the final temperature by another DH HX (top HX). Because in the parallel connection DHW preheating was done with district heating, the water temperature was so high that sewage HR using only the low temperature tank without heat pump was not feasible.

Primary energy, emissions and costs

Finland utilizes primary energy factors (PEF) to convert the combined electricity and district heating consumption into a single energy efficiency parameter, the primary energy consumption (PE). District heating has a PEF of 0.5 and electricity a PEF of 1.2 (Finlex, 2017). The PE consumption of the reference case was 107 kWh/m^2/a. For reference, the Finnish limit for a new nearly zero energy apartment building is 90 kWh/m^2/a (Ministry of the Environment, 2018b). The results of this study were not generated using all the background assumptions required for official PE accounting (the "E-luku") and are not directly comparable to the nearly zero energy building (nZEB) limit, which is only used for new buildings.

CO_2 emissions of the building were calculated using an emission factor of 164 kg-CO_2/MWh for district heating (Motiva Oy, 2017) and an average emissions factor of 132 kg-CO_2/MWh for electricity (Finnish Energy, 2017). The emission factors of electricity were determined separately for each month, such that during summer the minimum emission factor was 81 kg-CO_2/MWh and in winter the maximum emission factor was 174 kg-CO_2/MWh.

The cost of district heating had a fixed monthly component based on annual peak power demand and a

consumption based component dependent on the season. The consumption price was 37 €/MWh from May to September, 64 €/MWh from October to December and 72 €/MWh from January to April. The price of electricity was a constant 122 €/MWh through the whole year.

The life cycle costs (LCC) were calculated over the time period n of 30 years. Interest rate i was 3% and the energy price escalation rate e was 2%. The LCC was calculated as follows:

$$r_e = \frac{i - e}{1 - e}$$

$$a = \frac{1 - (1 + i)^n}{i}$$

$$a_e = \frac{1 - (1 + r_e)^n}{i}$$

$$LCC = C_{investment} + a C_{maintenance} + a_e C_{energy}$$

where $C_{investment}$ is the initial investment cost of the building retrofit, $C_{maintenance}$ is the annual maintenance cost and C_{energy} is the combined annual cost of district heating and electricity consumption.

Results

The main results of the study are presented in Figure 7. It shows the district heating and electricity demand in the building in each scenario, as well as the annual CO_2 emissions. Shown above the bars are the primary energy consumption and the heat recovery rate as a percentage of demand, as well as the annual peak DH power consumption. Cases 4, 6 and 8 and their B counterparts are shown in different shades of colour to identify the scenario pairs.

The annual emissions in the reference case were 105 t-CO_2. As expected, the lowest emissions resulted from the use of both the EAHP and the sewage HR with HP (Scenario 8). Using the ideal series connection, the emissions dropped by over 50% to 52 t-CO_2. With the

more acceptable parallel connection (Scenario 8 B), the emission s were 66 t-CO_2. Using the series connection, the PE value fell to 79 kWh/m²/a. With the parallel connection, the PE consumption was 93 kWh/m²/a. The parallel connection guarantees the cooling of district heating flow, which suffers from high return temperatures in the series connection. The series connection allows the heat pumps to operate on lower temperatures, which increases the amount of heat generated while restricting the rise of electricity consumption. This is also evident between Scenarios 4 and 4 B, which have almost the same amount of heat recovered. Due to the lower COP in the B case, less DH was replaced by the heat recovery system. In Scenario 4, the seasonal COP over the whole year was 5.33, while in Scenario 4 B it was 4.45. The worse heat pump performance had a direct effect on the emissions in the all the B scenarios. Emissions in Scenarios 4 B, 6 B and 8 B were 11%, 8% and 26% higher than in the series connected versions.

Figure 8 shows the cost distribution in each scenario. District heating costs are divided between consumption based energy cost and fixed cost based on annual maximum power demand. The lowest cost case was Scenario 8, which also had the lowest emissions. Investment costs were highest in Scenarios 2 and 3, which included a replacement of the ventilation system. Scenario 8 was the only one where the electricity costs exceeded the cost of district heating, due to the effective reduction of DH demand and increased electricity use by heat pumps.

Sewage HR with just a HX (Scenario 5) had the lowest investment cost, but it was the least effective way of reducing emissions. This was because of the limited temperature range in the heat recovery of DHW. The 5 °C inlet water was preheated to 20 °C by the sewage HR system (set point of DHW was 55 °C), but the energy was
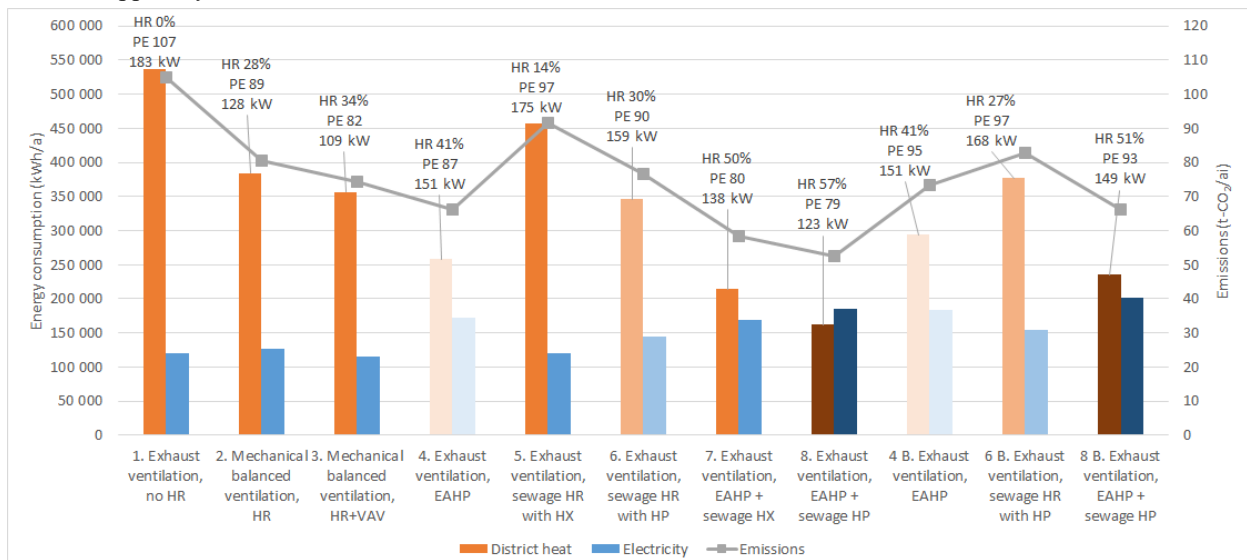
Figure 7. Annual district heating and electricity use and CO_2 emissions in the apartment building under different scenarios. Also shown are the heat recovery, primary energy use and annual peak DH power demand.
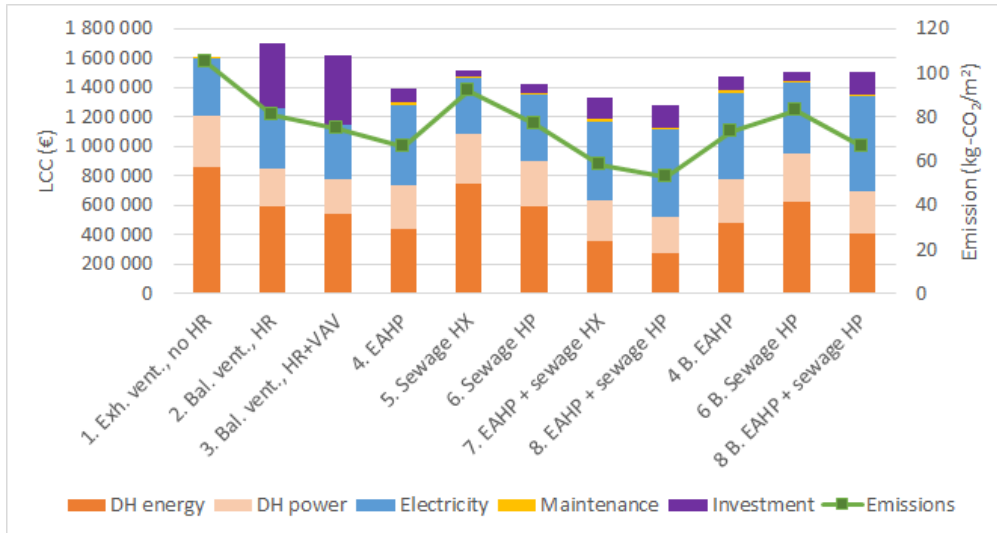
Figure 8. LCC distribution of each retrofit option.

only used in the DHW circuit, not for SH. Using the utility-acceptable connection, this setup was not considered feasible.

The combined benefit of both the sewage and ventilation heat recovery systems was less than the sum of the individual benefits. DH consumption was reduced by 70% in Scenario 8, while the sum of the reduction in Scenarios 4 and 6 was 87%. With the parallel connection, Scenario 8 B had a 56% reduction in DH demand, while the combined reduction in Scenarios 4 B and 6 B was 75%.

Replacing the old exhaust ventilation system with mechanical balanced ventilation (Scenario 2) was about as effective in reducing DH use and emissions as the parallel-connected sewage HR with HP (Scenario 6 B). The electricity use remained at a lower level, which would imply the ventilation retrofit to be a superior choice.

However, as shown in Figure 8, the investment costs and LCC of Scenario 2 were much higher. Adding the VAV (Scenario 3) lowered both life cycle cost and emissions, but the LCC was still higher than in any of the retrofit scenarios with the original ventilation system. On the other hand, the primary energy use in Scenarios 2 and 3 was below many of the heat pump scenarios. Specifically, the PE consumption of Scenarios 2 and 3 was lower than in Scenario 8 B. Conversely, the CO_2 emission were lower in Scenario 8 B. This highlights an issue in the Finnish building code: Primary energy consumption can go up, even while emissions are decreased.

Figure 9 shows the monthly district heating and electricity use in the lowest emission utility-acceptable scenario, 8 B. It shows the district heating energy saved compared to the reference building as well as the increased electricity use resulting from the heat pumps. From June to August, 92% of heating demand was covered by the
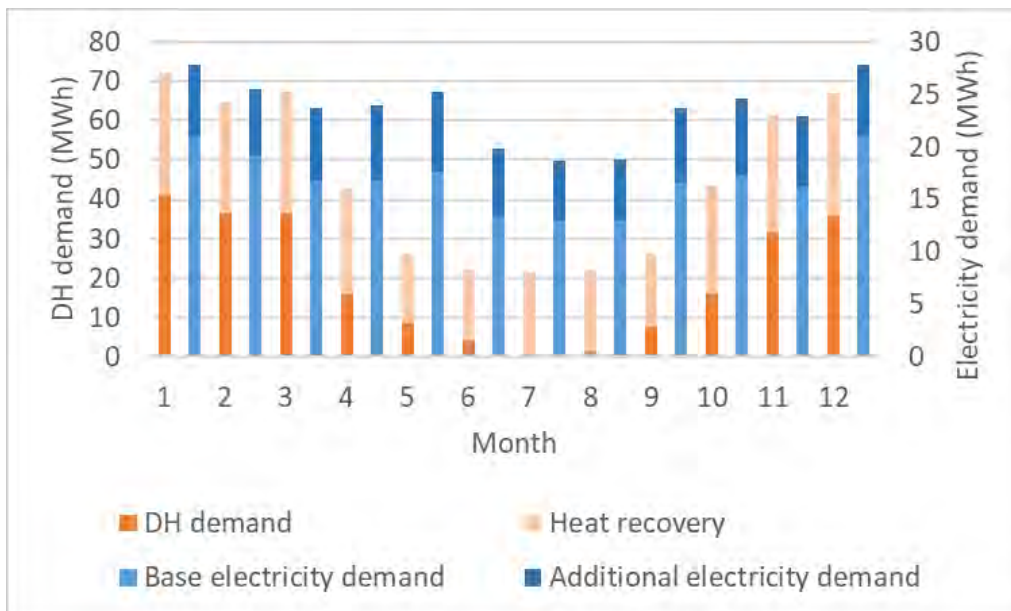
Figure 9. Recovered heat and additional electricity demand in Scenario 8 B vs. the reference.

heat recovery systems. From November to March, the recovered heat covered 45% of heating demand.

Discussion

While the energy demand of the simulated reference building was quite close to the measured data, there were some limitations in the accuracy of the study. The heat pump model was based on linearly fitted power curves and nominal flow rates, but did not take into account pressure changes in the heat transfer fluids. The seasonal COPs of the heat pumps were quite high (4 to 5), which may be a result of omitting some details. In the parallel connection scenarios, the DH flow was perfectly adjusted every timestep to match energy demand alongside the heat pump generation. This helped to minimize wasted energy.

The heat recovery from ventilation and sewage was handled using two separate heat pumps. This way each HR component could be added or removed without adjustment to the other. It would also be possible to run both waste heat streams through the same singular heat pump. This would have some effect on the average temperature of the heat source. Which configuration would perform better is a good topic for further study.

There are some issues which can limit sewage heat recovery potential. Here it was assumed that all sewage flows go through a single pipe where they can be easily routed to the HR system. If a building has many independent sewage outlets, it might not be cost-effective to recover heat. Here a plug flow tank model was used to collect the sewage heat allowing perfect recovery. In practice, the limited capacity of internal heat exchangers could prevent taking advantage of the peak waste flows. In a building with more residents, the ratio of peak to average sewage flow goes down, making it easier to recover heat. Conversely, sewage HR can be challenging in very small residential units. An ideal heat exchanger was used for sewage heat recovery in this study, but the sewage temperature was assumed to be lower than what has been measured in practice. This should reduce the chance of having too optimistic results.

The control algorithm of the heat pumps was not optimized. For example, district heating is very cheap in summer and it might make sense to turn off the heat pumps completely for this part of the year. This is a potential topic for future study. Unlike in (Thalfeldt et al., 2018), significant performance differences were discovered between the series and parallel EAHP connections. This was likely because of prioritizing space heating instead of DHW.

Conclusions

The installation of heat pumps was a more cost-effective way to reduce emissions than a ventilation retrofit. Heat recovery from ventilation had more potential than HR from sewage. The lowest LCC and the lowest emissions were provided by Scenario 8, which utilized both the ventilation and sewage heat recovery system with a HP,

using a series connection with respect to district heating. Combining both the HR methods in a hybrid system provided diminishing returns, as there was some overlap in their operation and the combined benefit was less than the sum of their parts.

Using a series connection between heat pumps and district heating helped achieve lower primary energy consumption and emissions than the parallel connection. This contrasts previous findings where no differences were found. The likely reason is that the EAHP control prioritized space heating instead of DHW. Using the series connection for HP, emissions were reduced by 12 to 50% depending on the HR methods, compared to 21 to 37% with parallel connection. However, it could be possible to improve the performance of the parallel connected heat pumps using better control algorithms or connection configurations, especially when two waste heat sources are in use. One avenue of research would be to store excess heat in the ground during summer, to improve heat pump performance in the winter.

In some cases, a major drop in emissions could be accompanied by no change in primary energy consumption. This suggests that there is a need for a policy update so that the building code takes actual emission performance into account better. The series connection of waste heat recovery was found to be more effective, but it is not typically allowed because of undesirably high DH return temperature. Finding a use for higher temperature DH return flows would be a worthy topic of research.

Acknowledgement

References

Finlex, 2017. Valtioneuvoston asetus rakennuksissa käytettävien energiamuotojen kertoimien lukuarvoista 788/2017 (Government decree on the values of energy conversion factors), 788/2017.

Finnish Energy, 2017. Emission factors of Finnish electricity, email contact.

Heka Ltd., 2020. Annual report 2019 (In Finnish). Heka Ltd., Helsinki.

Helen Oy, 2020. Helen continues to invest in carbon neutrality: one of the world's largest heat pumps

planned for Helsinki, enabling faster reduction in the use of coal [WWW Document]. URL https://www.helen.fi/en/news/2020/new-heat-pump (accessed 8.4.20).

Hervás-Blasco, E., Navarro-Peris, E., Corberán, J.M., 2020. Closing the residential energy loop: Grey-water heat recovery system for domestic hot water production based on heat pumps. Energy and Buildings 216, 109962. https://doi.org/10.1016/j.enbuild.2020.109962

Kalamees, T., Jylhä, K., Tietäväinen, H., Jokisalo, J., Ilomets, S., Hyvönen, R., Saku, S., 2012. Development of weighting factors for climate variables for selecting the energy reference year according to the EN ISO 15927-4 standard. Energy and Buildings 47, 53–60.

Kensby, J., Trüschel, A., Dalenbäck, J.O., 2017. Heat source shifting in buildings supplied by district heating and exhaust air heat pump. Energy Procedia, 15th International Symposium on District Heating and Cooling, DHC15-2016, 4-7 September 2016, Seoul, South Korea 116, 470–480. https://doi.org/10.1016/j.egypro.2017.05.094

Koikkalainen, E.-P., 2016. Management of energy flows and power peaks in high-rise buildings (M.Sc. thesis). Aalto University, Espoo, Finland.

Koivuniemi, J., 2005. Lämpimän käyttöveden mitoitusvirtaama ja lämpötilakriteerit veden mikrobiologisen laadun kannalta kaukolämmitetyissä taloissa [Domestic hot water design flow and temperature criteria as pertains to water microbiological quality in district heated houses, In Finnish] (M.Sc. thesis). Helsinki University of Technology.

Mazhar, A.R., Liu, S., Shukla, A., 2018. A Key Review of Non-Industrial Greywater Heat Harnessing. Energies 11, 386. https://doi.org/10.3390/en11020386

Ministry of the Environment, 2018a. Rakennuksen energiankulutuksen ja lämmitystehon tarpeen laskenta (Calculation of the energy consumption and heating power in a building).

Ministry of the Environment, 2018b. Ympäristöministeriön asetus uuden rakennuksen energiatehokkuudesta (1010/2017) (Decree of the Ministry of the Environment on the energy performance of the new building (1010/2017) [In Finnish].

Ministry of the Environment, 2017. Directive on building energy certificates, Attachment 1 [In Finnish].

Motiva Oy, 2017. CO2-päästökertoimet [WWW Document]. Motiva. URL https://www.motiva.fi/ratkaisut/energiankaytto_suomessa/co2-laskentaohje_energiankulutuksen_hiilidioksidip aastojen_laskentaan/co2-paastokertoimet (accessed 1.14.18).

NIBE AB, 2017. NIBE F1345 heat pump technical manual.

Nourozi, B., Wang, Q., Ploskić, A., 2019. Maximizing thermal performance of building ventilation using geothermal and wastewater heat. Resources, Conservation and Recycling 143, 90–98. https://doi.org/10.1016/j.resconrec.2018.12.025

Ploskić, A., Wang, Q., 2018. Evaluating the potential of reducing peak heating load of a multi-family house using novel heat recovery system. Applied Thermal Engineering 130, 1182–1190. https://doi.org/10.1016/j.applthermaleng.2017.11.072

Psimopoulos, E., Bee, E., Widén, J., Bales, C., 2019. Techno-economic analysis of control algorithms for an exhaust air heat pump system for detached houses coupled to a photovoltaic system. Applied Energy 249, 355–367. https://doi.org/10.1016/j.apenergy.2019.04.080

Saari, A., Airaksinen, M., 2012. Energiatehokkuutta koskevien vähimmäisvaatimusten kustannusoptimaalisten tasojen laskenta [In Finnish].

Thalfeldt, M., Kurnitski, J., Latõsov, E., 2018. Exhaust air heat pump connection schemes and balanced heat recovery ventilation effect on district heat energy use and return temperature. Applied Thermal Engineering 128, 402–414. https://doi.org/10.1016/j.applthermaleng.2017.09.033

Simplified Tool for Pre-Designing Ventilation Air Flow in Greenland

Jørgen Erik Christensen[1*], William Kristian Krogh Vergo[1], Joan Ferris Gimeno[2]
[1]Department of Civil Engineering, Kongens Lyngby, Denmark
[2]Plan 1 Cobblestone Architects A/S, Valby, Denmark
* *Jørgen Erik Christensen: jerik@byg.dtu.dk*

Abstract

Few inhabitants in Greenland results in few small consulting companies, and they do not invest in building thermal simulation programs since they are too expensive and the use will be very limited. The aim of the paper is to describe a simplified thermal calculating design tool TCD2 for pre-designing ventilation air flow in Greenland, and thereby improving the level of calculation of the thermal indoor climate in Greenlandic buildings. In this phase, it has never been the intention to make a full validation of TCD2; however, this will take place during the next phase. The preliminary results show that the proposed design ventilation air volumes by TCD2 for annual simulations in BSim and IDA ICE meet the typical Danish/Greenlandic requirements, which are a given number of hours above 26 ºC and 27 ºC in the working hours, thus indicating that TCD2 is an alternative on the safe side to more advanced programs.

Introduction

Background

The development of TCD2 – Thermal Calculation by Design was originally done for teaching purposes, so it could be used for ventilations courses at Technical University of Denmark. Joan Ferris Gimeno and Jørgen Erik Christensen developed the program. It is easy to calculate the ventilation that maintains an acceptable atmospheric indoor climate according to DS_EN 16798-1:2019 (2019) that includes building emissions and CO_2 emissions. The challenge is to estimate the necessary ventilation for thermal comfort. In order to calculate the thermal comfort, it is necessary to apply dynamic building simulation programs like BSim and IDA ICE. However, it has been a problem that students with no knowledge of these types of programs should spend a disproportionate amount of time familiarizing themselves with these programs. In addition the students never reach the necessary user level to make proper simulations. Instead this knowledge will be taught in other courses, where the focus is only on BSim or IDA ICE. Since the focus of the ventilation courses must be on ventilation, the decision was made to drop these more complex programs and instead develop a simplified program in Excel for calculating the thermal indoor climate.

In connection with the ventilation courses, two programs have been developed. They can fulfil different requirements in a fast and clear way in order to give the student a broader practical experience of sizing ventilation systems: TCD2 – Thermal indoor climate design and TCD Vent – Design of the overall ventilation system.

For a specific location to simulate the indoor air temperature and ventilation need, the program TCD2 applies a design day, which is a warm day with clear skies. The purpose of the program is mainly the development of a simplified thermal calculating design tool. During the early design phase, exact airflow is not required; but rather an estimate of the total ventilation air volume and the design pressure loss to the critical diffuser in order to be able to design the aggregate unit.

Greenland

Greenland has approximately 57,000 inhabitants. The average monthly temperature in Greenland is between -9 and +7 °C. The low temperatures have led to the false conclusion that overheating problems in Greenland are almost non-existent. In general, there is hardly no verification of the thermal indoor climate, only a basic calculation to prove that the requirements for a satisfactory atmospheric indoor climate are fulfilled. According to the Greenlandic Building regulation's (Bygningsreglement, 2006) chapter 11.5, the user must ensure that appropriate temperature conditions are achieved; but this is usually not normal practise. This is the main reason for this paper, since major problems could arise in Greenland from not performing thermal indoor climate validation.

This paper deals specifically with overheating problems in Nuuk. Greenland is situated between latitude 59° N and 82° N, which means most cities have 24 hours of sunlight in the summertime. In addition, the solar radiation hits the vertical windows at a very low angle, resulting in maximum transmission of direct solar radiation through the windows. The consequence is a significant amount of transmitted solar radiation into the buildings through the windows. Even when the outside air temperature in the summertime is low, it will not cool the building due to the low U-values of the external construction in new-built buildings. The minimum ventilation air temperature can only be around 16 ºC to avoid undercooling and if the ventilation system has been designed according to the atmospheric indoor climate, this will result in a limited cooling effect in the ventilation system.

Because there are so few inhabitants in Greenland, the consulting companies are few and small and do not invest in building thermal simulation programs like BSim, IDA ICE, IES-VE, etc. since they are too expensive and the use will be very limited. This means that no competencies will be achieved. To deal with the challenge, the simple Excel

based program TCD2 can be used for analysing the overheating problems in buildings.

Ventilation airflow

When analysing the indoor climate, there are many factors to contemplate. It is therefore not possible to use standard solutions in all cases. There will be a need to consider the activities and processes that will occur in the actual building.

In many cases, it is required during the early design phase to make calculations of air volumes in order to get an estimate of the size of the overall ventilation system: Ducts, valves, air handling units, etc. These components need to be sized to satisfy the indoor thermal comfort.

At this stage, only limited resources are available for this estimate, and there is no money for calculations with building thermal simulation programs such as BSim, ICE-ICE, IES-VE, etc. There is a need to use methods that are very user-friendly and can produce results in a short time.

To achieve sufficient ventilation, it is necessary to provide an acceptable indoor climate for both the atmospheric and the thermal indoor climate. Three requirements are applied to determine the size of the ventilation: 1) authority regulations (minimum requirements), 2) atmospheric indoor climate, 3) thermal indoor climate.

The largest value is applied for sizing, which in most cases will be the value for dimensioning the thermal indoor climate. The designer must always ensure to fulfil the atmospheric indoor climate. Calculating the thermal indoor climate is the focus of this paper, further elaboration of the first two items will not be included. In most cases, the thermal indoor climate has the highest value for ventilation air, hence the dimensionally highest value. Various methods can be applied in order to calculate the required amount of ventilation air:

1. Maximum hourly average indoor temperature
2. Daily average indoor temperature
3. Simulation on an hourly basis using building thermal simulation programs

The first two methods are older methods before the invention of the computer, when the use of hand calculations was common. The two methods give an overview of the influence of the different parameters. If the project is in an initial phase, when only a need to estimate for the size of the ventilation system is required, the two first methods are applied in practice.

Focusing on the hour with the highest external and internal loads, Method 1 'Maximum hourly average indoor temperature' will result in very oversized systems, increasing the cost of the overall project, along with having a system that does not run optimally in normal operating mode. Applying Method 2 'Daytime average temperature' for a warm day with clear skies will result in lower ventilation air volumes than method 1. However, both methods are associated with great uncertainty.

The use of dynamic thermal simulation programs is therefore the most widely applied method, Method 3. Nevertheless, attention must be drawn to the fact that several of the large simulation programs are very

complex, and incorrect use can easily lead to completely misleading results. Program results never get better than their users. Here, TCD2 can be advantageous since using it provides an extra control of results from the complex programs and helps detect errors. In addition, TCD2 is a much simpler tool to apply.

Methods

The thermal indoor climate and energy consumption of a room is the result of a complicated interaction between the design of the building, the thermal loads, the ventilations system, and the outdoor climate. To account for this, it is necessary to calculate a heat balance for the room. For a room the supplied heat flow must be equal to the heat flow carried away, considering the heat effect supplied or emitted from heat accumulating in building parts.

Thermal loads. The thermal loads matter a great deal in the heat balance and it is therefore important to determine them as accurately as possible. However, during the early stage of planning when the user makes decisions, uncertainty is high, since only limited knowledge of the building is available. For this reason a simplified method can be used since only limited data is available and there is no need for a detailed simulation.

The thermal loads transmit heat to the room air and/or room surfaces. It is important to distinguish between these two types of heat transfer because heat transfer to the room air will temporarily give a different temperature course than heat transfer to the surfaces. There will be a greater rise in temperature if most of the energy is transmitted directly to the room air rather than to the surrounding surfaces. The exterior gain is solar radiation, applied as radiation only to the surfaces contrary to the ventilation air, which applies directly to the room air. However, given the other uncertain assumptions, it is accurate enough to apply according to estimates. For most low-temperature heat sources, such as persons, it is a good estimate to apply half of what is emitted as convection heat and the other half as radiant heat.

Outdoor temperature. The outdoor temperature used in TCD2 simplifies to a cosine function around the air's daily average temperature plus/minus the amplitude of the outdoor air temperature with a maximum at a specific time.

The simulation model

The foundation of the simulation model in TCD2 is a simplified model for the heat balance and was originally developed by Bo Adamson (Adamson, 1968) and Bo Andersen (Becher, 1971) and described by Jørgen Erik Christensen in (Hansen et al., 1988). The model was applied in tsbi 2.1 (Johnsen, 1985), which is the precursor of the calculation model tsbi5 in the BSim program.

The most important thermal climate factors are the indoor air temperature and the internal surface temperature. In order to calculate them at different times, it is necessary to establish heat balance equations for the room air, for the surfaces and for the instantaneous heat conduction through the adjacent walls.

The foundations of the simplifications of the model are that all internal surface temperatures are equal and that the calculation of the instantaneous heat conduction in the walls is solved by introducing fictitious, infinitely thin heat accumulating layers with the same temperature. These layers describe the room's heat capacity. Consequently, it will only be necessary to establish three heat balance equations: The heat balance of the room air, the heat balance of the surfaces and the heat balance of the heat accumulating layers. These balances have three unknown temperatures: The room indoor air temperature, internal surface temperatures, and the temperature of the heat-accumulating layer. In (Hansen et al., 1988) a description of the simulation model can be found.

Internal Heat Loads. The internal heat gains of a room are divided into heat gains from equipment, occupants, and lighting. In TCD2 these values are based on predesigned values from (Christensen, 2017) and guidelines written by (Vorre et al., 2017).

Model for the solar radiation through glass panes – Reference year

William Kristian Krogh Vergo and Jørgen Erik Christensen created the method for developing the weather data. The first step in the process of creating weather data for TCD2 is using BSim to create a fictitious reference year. The result of this process shall be a reference year consisting of perfect cloudless days on two selected dates, the 6th and the 21st, of each month. All other dates are of no interest. To create this, it is necessary to find cloudless days during the reference year for Nuuk, which has the coordinates 64.17 N, 51.87 W and the time zone UTC-3.

Most of the cloudless days are from observed data in the reference year that have gone through a manual screening process in BSim. The selected data are transferred to Excel and processed.

If the day has a few hours with some cloud cover, an empirically weighted formula for adjustment will be used. The direct radiation is adjusted up and the diffuse radiation is adjusted down. The adjustment is designed so that the changed values will not exceed a natural cloudless hour from the weather data set during the same period of the year.

The solar radiation is evenly distributed throughout the day. Symmetry is formed around 12 a.m. true solar time since the sun is at the highest point in the sky. In addition to this, symmetry is formed around 21 June by "adding" days. This means that if there is a cloudless day on 12 June (minus nine days), then it is assumed that the same day will occur on 30 June (plus nine days). This resulting in a mirrored duplicate for each cloudless day around 21 June. The reason for this is that it is difficult to find perfect cloudless days in the northernmost climates, since there is always some haze and light clouds that require compensation. Some cloudless days are required to be able to perform the next step, where a regression analysis of the direct and diffuse solar incidence is performed throughout the year. The regression analysis is done in Excel and formed for Nuuk, Greenland, a second-degree

polynomial formula, see Figure 1 and formula 1 for the direct normal radiation and formula 2 for the diffuse radiation.

Direct normal radiation:

$$y = -0{,}7014x^2 + 241{,}27x - 10391, R^2 = 0.9605 \quad (1)$$

Diffuse radiation:

$$y = -0{,}0804x^2 + 27{,}655x - 30{,}846; R^2 = 0{,}766 \quad (2)$$

Normal rad. as a function of day number

y = -0,7014x² + 241,27x - 10391
R² = 0,9605

● Normal radiation sum for cloudless and mirrored days
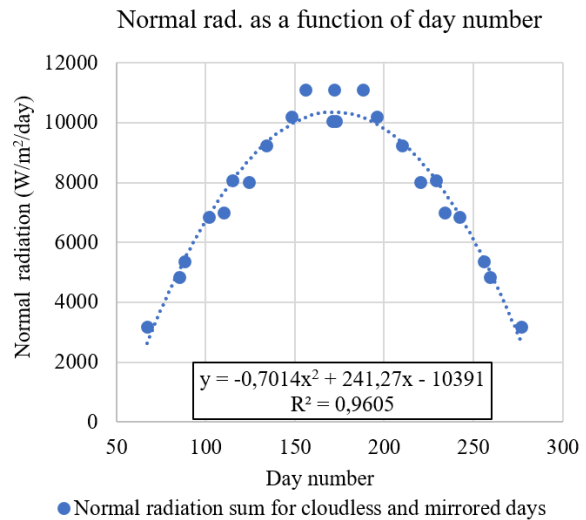
Figure 1: Direct normal radiation as function of the day number.

The formulas are applied to find the diffuse radiation as well as the normal radiation estimated on the desired date for TCD2 for the 6th and 21st of each month. Thereafter, the solar radiation was distributed throughout the day based on a distribution pattern from a "real cloudless day" that was resembling the date. Then the days were eventually corrected for sunrise and sunset on the desired days, which of course have different times than the original days due to the date difference. This means that if the sun rose before 7 a.m. on a truly clear skies day, but did not do it on the desired day, then the sunrise before 7 a.m. was instead distributed over the remaining hours of the day. Then the solar data are ready to be deployed in BSim again. Here they are applied both to create data for use in TCD2 and for direct simulation use in BSim, in order to be able to compare with TCD2 in single days.

Model for the solar radiation through glass panes – TCD2 weather data

TCD2 applies an Excel data file for the transmitted solar radiation through a standard doubled-glazed reference pane with two 4-mm layers of glass and an air gap of 12 mm with a g-value of 0.76 and a U value of 2.8 W /m²K. TCD2 requires the following three parameters on an hourly basis: Direct transmitted solar radiation, diffuse transmitted solar radiation, and ground-reflected transmitted solar radiation. BSim is not able to provide these data directly and for that reason, BSim needs three simulations with two kinds of weather data:

1. Standard weather data – Results of total transmitted solar radiation (ground reflectance = 0,25)
2. Standard weather data – Results of transmitted solar radiation, excluding ground-reflected radiation (ground reflectance = 0)
3. Diffuse weather data, direct solar radiation = 0 – Results of transmitted diffuse solar radiation, excluding direct and ground reflected radiation (ground reflectance = 0)

Based on the three BSim simulations it is possible through simple equations to calculate the values for the transmitted solar radiation for the three necessary components for the TCD2 weather file (a standard reference pane):

- Direct transmitted solar radiation
- Diffuse transmitted solar radiation
- Ground-reflected transmitted solar radiation.

The performance of the weather data is estimated for the seven slopes: 90º (vertical), 75º, 60º, 45º, 30º, 15º, 0º (horizontal), and for the eight orientations: North, northeast, east, southeast, south, southwest, west, northwest. The data are created in BSim with 49 zones (6 slopes · 8 orientations + 1 slope · a fictive direction = 49 zones). The results for the 49 zones from BSim are transferred to an Excel sheet for further calculations.

The selected dates for the weather file are the 6th and 21st of each month. If the user chooses other dates or directions than the ones in the TCD2 weather file, TCD2 makes a linear interpolation. The seven slopes are fixed. All these calculations in the creation of the weather file creates restrictions for the user in terms of choosing different slopes and weather data for other locations. The results for other dates or directions also create some uncertainty in the results.

Model description

The model used is a medium heavy single office with the interior dimensions of 3 m x 4 m x 2.6 m, area 12 m^2 and a volume of 31.2 m^3. The model description is based on (Wittchen et al., 2011) and (Treldal et al., 2011).

The internal load is set to 122 W and consist of 7 W (Working lamp), 25 W (PC screen), 30 W (PC) and general lighting 60 W, (Christensen, 2017) and (Vorre et al., 2017). The occupant has a metabolic rate of 1.2, which emits approximately 100 W as dry heat to the room. The internal load schedules state that the light and equipment are on from 8-16 on weekdays, off at the weekends. The same goes for occupants in the office, except for when they leave for lunch during the period from 12-13 when the load is only half.

The office has a single facade facing the outside, whereas the other five surfaces face a similar room with the same temperature conditions: two sidewalls, back wall, floor, and ceiling. The office is analysed for the four main orientations north, east, south and west. The exterior wall has an area of 10.6 m^2, a U-value 0.13 W/m^{2}K and consists of a medium heavy construction of lightweight concrete and mineral wool insulation, Table 1. The office meets the minimum requirements of the Building Regulations for climate screen (Bygningsreglement, 2018).

Table 1: Structure of the exterior wall with the U-value 0.13 W/m²K – From inside out.

Material	Thick-ness (m)	Thermal Conductivity (W/mK)	R-Value (m²K/W)
Light concrete	0.1	0.17	0.59
Mineral wool	0.25	0.037	6.75
Brick cladding	0.115	0.17	0.68

There is one window in the office and in the standard office (S, 22 % window area of the interior area in the office) with an opening area of 2.6 m^2 (1.98 m^2 glass) and a thermal bridge around the edge of the window set to 0.06 W/m·K. The recess value is set 0 m in BSim and IDA ICE (very low app. 0.1 mm for program reason in BSim). The U-value of the window depends on the type of simulations. In the annual simulations three window areas have been studied: S 22 %, M 30 % and L 55 % window area in relation to the inside area.

A window with a U-value for the glass 2.8 W/m^{2}K, frame 1.4 W/m^{2}K, g-value of 0.76, and light transmission being 0.82 was used for the first simulations with a comparison of solar radiation through the window and the corresponding temperatures. A window with a U-value for the glass 1.1 W/m^{2}K, frame 1.1 W/m^{2}K, g-value of 0.43, and light transmission being 0.71 was used for the last simulations with a comparison of temperatures in the room for the reference years using BSim and IDA ICE.

Results

The results of this paragraph include many different comparisons. The following shows a small part of this work. The results do not give the full picture of the comparison. A more detailed investigation is needed for that. The following simulations are only the first step in the validation of TCD2 in order to create a simplified thermal calculating design tool for pre-designing of airflow for ventilation in Greenland. The purpose has not been to make a full validation of TCD2 for Greenlandic conditions.

Comparison of solar radiation into the room

TCD2 directly applies the solar radiation through a double-glazed standard pane with a g-value of 0.76, as described in the *"Model for the solar radiation through glass panes – TCD2 weather data"*. Therefore, at this initial stage, it will be natural to compare the solar incident between TCD2, BSim, and IDA ICE for this pane.

TCD2 focuses on the date of 21 June and 21 August, both of which are during the summer season. 21 June shows results for the sun being highest in the sky and the most hours above the horizon. On the other hand, this results in the sun hitting the pane with the greatest angle of view, thus giving a smaller solar incident at 12 a.m. on a south-

facing facade. 21 August results in a lower angle of view on the pane, this resulting in a greater solar incident on a south facing pane at 12 a.m. and can therefore become the design factor even if the sun is above the horizon fewer hours than on 21 June.

Without solar shading

The results of the analysis of data without solar shading show that 21 June is dimensioning for east and north, and that 21 August is dimensioning for south.

Table 2 and Figure 2 show a comparison of transmitted solar radiation through a standard double-glazed window with a g-value of 0.76 for TCD2, BSim, and IDA ICE on 21 August for south, east, and north in Nuuk, Greenland, using the weather data developed. The table and Figure show very fine agreement between TCD2 and BSim for both days and directions, except for a small difference for north on 21 June with 4,5 %. The similar results for IDA ICE show relative fine agreement for south, however for east the difference is around 26 % and for north between 39 % and 43 %. In general, the values for IDA ICE are much higher than for TCD2 and BSim.

Figure 2: Comparison of solar radiation through a double-glazed window for TCD2, BSim, and IDA ICE for 21 August for south, east, and north.

Table 2: Daily solar sum difference from TCD2 of the transmitted solar radiation for BSim and IDA ICE.

	% Daily solar sum difference from TCD2			
	21st June		21st August	
Direction	BSim (%)	IDA ICE (%)	BSim (%)	IDA ICE (%)
South	0.1	7,6	0.4	3.7
East	0.1	26.4	0,3	26.2
North	4.5	38.7	-0,7	43.1

The TCD2 solar data is derived from BSim for the same weather data; hence, the expectation for the comparisons will be relatively fine.

IDA ICE applies the Perez diffuse radiation distribution model as default. Originally, creation of solar data for TCD2 derived from BSim applied with the Munier solar radiation model. IDA ICE does not include this model. The Perez model generally shows higher results for the diffuse radiation distribution. This can be noticed especially for the north and east orientated curves, where the IDA ICE results are higher than the others are. This can explain the relatively large difference between BSim/TCD2 and IDA ICE.

With solar shading

In Figure 3 is shown comparisons of solar radiation in W/m^2 for the same window with outside solar shading for TCD2, BSim, and IDA ICE for 21 August for south in Nuuk. The results show fine agreement between TCD2, BSim, and IDA ICE. Larger differences have been measured only in the hours just before and after the use of the outside solar shading

Figure 3: Comparison of solar radiation through a double-glazed window with outside solar shading for TCD2, BSim, and IDA ICE for 21 August for south.

At 9 a.m. and 5 p.m. IDA ICE differs a lot from TCD2 and BSim. This is due to differences in the control strategies of the programs.

Comparison of temperatures in the room for design days

In the first comparisons a standard double-glazed window with a U-value for the glass/frame 2.8 W/m^{2}K was used. To use this window now will not be relevant in practice in Greenland since the U-value is so poor; however, it has only been used to compare results in the first phase. All analyses are for Nuuk, Greenland. The applied weather data are the ones particularly developed for TCD2 for the specially selected design dates with clear skies for the 6th and 21st of each month. These data are applied to create

weather files for BSim and IDA ICE. The weather file for BSim has already been created in the process of producing weather data for TCD2. The outdoor temperature applied to evaluate the initial data has been derived from warm days around the 21 June and 21 August.

No solar shading

In Figure 4, the standard office (S, 22 % window area of the interior area in the office) with no solar shading for south has been analysed for 21 August. The results for the temperatures are fluctuate extremely for the south-facing façade: TCD2 45 ºC – 52.6 ºC, BSim 41.2 ºC – 48.6 ºC, and IDA ICE 39.2 ºC – 48.1 ºC. All together, the temperatures in TCD are around 4 ºC higher than BSim and IDA ICE. This is a relatively big difference even in an extreme situation with very high temperatures. The higher results will be on the safe side for TCD2 compared with the more advanced programs. The reason for the high temperatures in TCD2 is that the program continues to simulate until the heat loss and heat gain during the 24 hours are the same, resulting in a very high asymptotic final temperature. In actual situations, there will be ventilation, solar shading, etc., which will result in much more realistic results – see next section with solar shading.
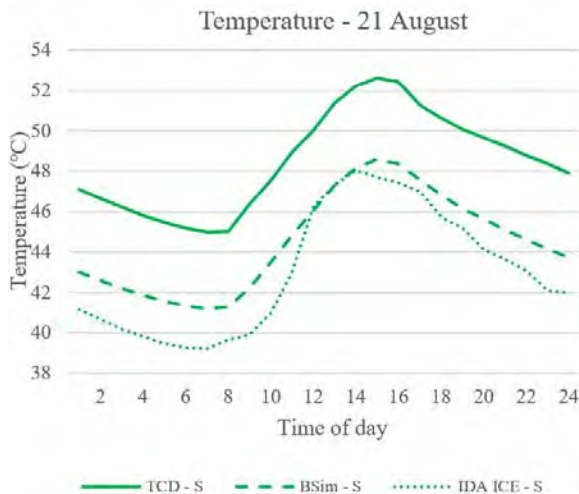
Figure 4: Comparison of temperatures on 21 August between TCD2, BSim, and IDA ICE in the room facing south with a double-glazed window and no solar shading

With outside solar shading

The following example is a study of temperatures with an outside solar shading, Figure 5. Everything else is the same as in the previous paragraph. The temperature results for the south-facing façade are: TCD2 28 ºC – 31.6 ºC, BSim 26.3 ºC – 29.7 ºC and IDA ICE 29.1 ºC – 34.4 ºC. As opposed to the results without solar shading, TCD2 now is 1.1 ºC to 2.8 ºC lower than IDA ICE and 1.7 ºC to 1.9 ºC higher than BSim. It is a little bit surprising that the temperatures are higher in IDA ICE since the daily sum for the solar radiation in TCD2 is lower.
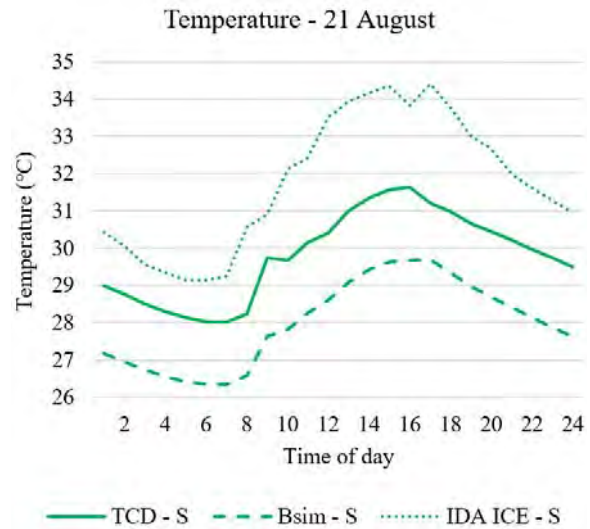
Figure 5: Comparison of temperatures on 21 August between TCD2, BSim, and IDA ICE in the room facing south with a double-glazed window and exterior solar shading.

Comparison of temperatures in the room for reference year

The last comparison of TCD2 (applying a design day with clear skies) is with BSim and IDA ICE (applying the reference year). Analysing with TCD2 includes two design days: 21 June and 21 August. For these two days the results indicate the temperature distribution during a day. Determining the necessary ventilation air volumes is the day with the highest temperature distribution.

The design day is analysed and ventilation air volumes and other factors adjusted so the highest temperature during the day will be between 27 °C and 28 °C. The selected ventilation air volumes are transferred to BSim and IDA ICE and the data implemented. Then the two programs simulate with the reference year to find the number of hours above 26 ° C and 27 °C. According to The Danish building code BR18 (Bygningsreglement, 2018), this limit is recommended to be a maximum of 100 hours above 26 °C and 25 hours above 27 °C during working hours.

Since TCD2 is a simplified program, the intension is that the results from BSim and IDA ICE for the number of hours above 26 °C and 27 °C are significantly lower than the limits of 100 hours and 25 hours respectively using similar data.

In these simulations, the data for the window is a U-value for the glass 1.1 W/m^{2}K, frame 1.1 W/m^{2}K, g-value of 0.43, and light transmission is 0.71.

Using exterior sunshades is a problem due to the harsh weather conditions in Greenland. It is only possible to obtain limited effect of internal sun protection when using modern windows with low U-value. This means that the shading factor will only be approximately 75 %. Hence, it is much more problematic to limit high solar incidence in Greenland than in Denmark, since it is not possible to use

an external solar shade with a shading factor of e.g. ca. 25 %.

Based on these observations an inside screen is used. The inside white/white screen has the data 15 % absorptance, 19 % transmittance, and 66 % reflectance. The calculated shading factor for this window is 71 %.

Three cases have been studied: S 22 %, M 30 % and L 55 % window areas in relation to the inside area. Figure 6 illustrates the estimated temperature distribution for south office S 22 % during 21 August when the objective has been to keep the maximum temperature below approximately 28 °C. Table 3 shows the corresponding values on an annual basis for BSim and IDA ICE.

The results show that the calculated values in TCD2 are within the safe limits for overheating, when compared to the annual simulations in BSim and IDA ICE. However, the number of hours in IDA ICE exceeds the limit of 25 hours for 27 °C for case S 22 %, M 30 % with 11 and 4 hours respectively.
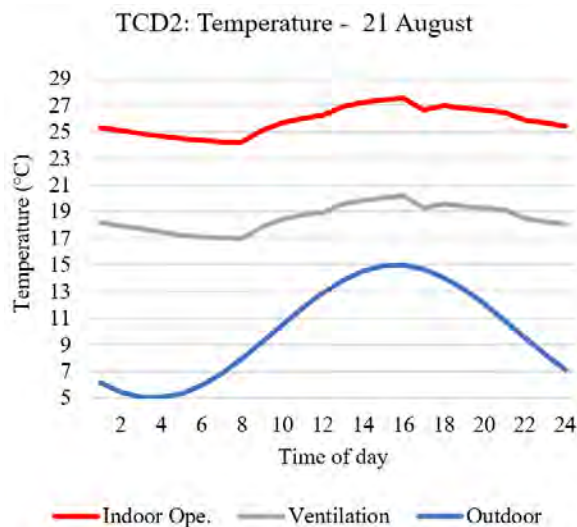
Figure 6: Temperature distribution in TCD2 for 21 August for south in Nuuk. (Ventilation: Ventilation air temperature)

Table 3: Numbers of hours above 26 °C and 27 °C in the working hours for the reference year.

Window % of interior area		Ventilation air ref.	Numbers of hours above specific temperatures in working hours			
			BSim		IDA ICE	
			26 °C	27 °C	26 °C	27 °C
	Hours limit:		100 h	25 h	100 h	25 h
	(%)	(%)	(h)	(h)	(h)	(h)
S	22	100	4	0	71	36
M	30	160	7	0	68	29
L	55	480	6	0	57	13

Discussion

The purpose of the paper was to develop a simplified thermal calculating design tool for pre-designing of airflow for ventilation in Greenland based on the experience of using TCD2 in Denmark. Part of that work is to make a validation of TCD2 up against BSim and IDA ICE. It has never been the intention at this stage to make a full validation of TCD2. The work is only the first step in the process of validation of TCD2. Comparisons made for Danish conditions for hot sunny periods show fine results compared to BSim.

Why IDA ICE differs in solar radiation

In IDA ICE the default diffuse radiation distribution model was developed by Perez. The Munier model used originally in BSim (and the data for TCD) has not been implemented in IDA ICE. Munier states relative constant values for the diffuse for all directions. The Perez model generally states higher results for the diffuse distribution. It is especially obvious from the north orientated curves that the IDA ICE results are higher than the others are. The Perez model also depends more on the direction than Munier.

In general, the temperatures in TCD2 are higher than in BSim, which is on the safe side. The temperature distribution is very similar in TCD2, BSim, and IDA ICE. The difference between TCD2 and BSim is reduced when the temperature level is lower. The comparison between TCD2 and IDA ICE shows no similar clear results, which is due to the difference in solar models between TCD2/BSim and IDA ICE.

Comparison of temperatures in the room for reference years

Comparisons of TCD2 for the dimensional design day with BSim and IDA ICE applying the reference year is the most interesting. The intention is to use TCD2 for pre-designing airflow for ventilation in Greenland instead of the more complicated dynamic building simulation programs like BSim and IDA ICE. The work shows that the use of data from TCD2 indicates a number of hours above 26 ° C and 27 °C, using BSim and IDA ICE for the reference year. The results are on the safe side, since the number of hours in general are lower than the recommendation from BR18 (Bygningsreglement, 2018) setting the maximum during working hours to 100 hours above 26 °C and 25 hours above 27 °C. In two of the cases IDA ICE exceeds the limit for 27 °C for case S 22 %, M 30 % with 11 and 4 hours respectively.

In order to give a better recommendation of how to apply TCD2 on Greenlandic conditions more work will be necessary.

Conclusion

It is a fact that Greenland is dealing with overheating problems. The location between latitude 59 ° N to 82 ° N means the solar radiation hits the vertical windows at a very low angle, resulting in maximum transmission of direct solar radiation through the windows. In addition,

there is sunlight 24 hours per day in the summertime. The consequences are that more solar radiation is transmitted through the windows into the buildings than on more southern locations like Denmark.

The few and small consulting companies in Greenland do not invest in building simulation programs. However, there is a need for a simple inexpensive program for analysing overheating problems in buildings. One possibility could be the use of TCD2, and showing pre-validation of this method is the purpose for this paper.

The preliminary results for comparing TCD2 for design days with annual simulations with the reference year for BSim and IDA ICE show more work is necessary in the future.

Acknowledgement

Kathrine Breinstrup Butler and Natacha Hajj for basic work on model development and validation, DTU.

Thomas Raahauge Andersen for development of the 49 zones model for BSim, DTU.

Charlotte Kira Treschow for the development of TCD Vent

References

Adamson B. (1968). *Värmebalans vid rum och byggnadder*. Tekniska Högskolan i Lund (Sweden).

Bari A., Ardeshir B., Mackay D.M. & Dayanandan S., (2016), *Applied Mathematics and Omics to Assess Crop Genetic Resources for Climate*, 1st Edition, p. 14. ISBN 9781498730136, CRC Press, Taylor & Francis Group, Informa UK Limited (UK).

Becher B. (1971). *Varme og Ventilation 1*. Bo Andersen: Chapter 5 Bygningers varmebalance. [Heating and Ventilation 1. Bo Andersen: Chapter 5 Heat balance of buildings]. pp 118-123. Teknisk forlag. Copenhagen (Denmark).

Bygningsreglement, Grønland. (2006). [Greenlandic Building regulation 2006]. Chapter 11.5 – Indoor Climate, Temperature , viewed 15 May 2020, from http://byginfo.gl/media/1131/br2006dk.pdf (Greenland).

Bygningsreglement – BR18, Danmark. (2018). [Danish Building regulation 2018]. viewed 15 May 2020, from https://bygningsreglementet.dk/ (Denmark).

BSim (Building Simulation). *Integrated computer tool for design of buildings and installations*. The Danish Building Research Institute. Aalborg University (Denmark).

Christensen, J.E. (2017). *Bygningsdynamik – kapitel 12, Energirigtigt drift af det rette indeklima i bygninger – EnDrIn*. [Building Dynamic – chapter 12, Right operation of buildings with respect to indoor climate and energy consumption]. ELFORSK 2017, Project number 348-006 (Denmark).

DS_EN 16798-1:2019. (2019). *Energy performance of buildings – Ventilation for buildings – Part 1:Indoor environmental input parameters for design and assenssment of energy performance of buildings addressing indoor air quality, thermal environment, lighthing and acoustics – Module M1-6*. Danish Standard. Nordhavn (Denmark).

DS 474:1993 (rettet 2017-udgave). (1993). *Dansk Standard, Norm for specifikation af termisk indeklima*. [Danish Standard 474:1993 (Corrrected 2017-edition. Code for Indoor Thermal Climate], Danish Standard. Nordhavn (Denmark).

Hansen, H.E., Kjerulf-Jensen, P., & Stampe, O.B. (1988). *DANVAK – Varme- og klimateknik grundbog*. Jørgen Erik Christensen Kapitel 4 – Varmebalance. [Heating and climate engineering basic book, Chapter 4 Heat Balance]. 1st Edition, pp. 91-108.. Teknisk forlag, ISBN 87-982652-1-0. Copenhagen (Denmark).

Johnsen K. (1985). *Brugervejledning for edb-programmet, tsbi, termisk simulering af bygninger og installationer*. [User Guide for the computer program, tsbi, thermal simulation of buildings and installations]. SBI forlag. ISBN 87-563-0611-3. Hørsholm (Denmark).

tsbi3 – *termisk simulering af bygninger og installationer*. [tsbi3 – thermal simulation of buildings and installations]. The Danish Building Research Institute. Aalborg University (Denmark).

Treldal, J., Radish, N.H., Hansen E.J.d.P., & Wittchen, K.B. (2011). *Energioptimering af kontorbygninger*. [Energy optimization of office building]. 2011. ISBN 978-87-563-1545-6. The Danish Building Research Institute. Aalborg University (Denmark).

Vorre, M.H., Wagner, M.H., Maagaard, S.E., Noyé, P.L., Lynge, N. & Mortensen, L. (2017). *Branchevejledning for indeklimaberegninger*. [Industry guidelines for indoor climate calculations]. InnoBYG / The Danish Building Research Institute, ISBN 978-87-563-1850-1 (Denmark).

Vergo, W.K.K (2018). *Development of solar data from weather data for calculation of thermal indoor climate in Greenland*, Report, Technical University of Denmark, Department of Civil Engineering, Kgs. Lyngby (Denmark).

Wittchen, K.B., Hansen E.J.d.P., Radish, N.H. & Treldal, J. (2011). *Energioptimering af kontorbygninger*. [Energy optimization of office building]. 2011. ISBN 978-87-563-1523-4. The Danish Building Research Institute. Aalborg University (Denmark).

From TEK17 to ZEB-O – A case study for a residential building in northern Norway

John Clauß[1*], Eivind Nygård[2], Judith Thomsen[1]

[1] SINTEF Community, Trondheim, Norway
[2] Gunvald Johansen Bygg AS, Bodø, Norway
* *john.clauss@sintef.no*

Abstract

With a strong focus on reducing emissions from the building sector, it is important that new buildings can compensate for emissions caused during their operation by on-site renewable electricity generation. In academia, there is consensus on measures to achieve a so-called zero emission balance, but there are still mostly pilot projects that have a focus on emission analysis during the planning process of buildings. This work is associated to the Sjøsiden project of Gunvald Johansen Bygg AS, a local entrepreneur in the city of Bodø (Northern Norway). The main goal of this study is to assess the most suitable energy system for the Sjøsiden project in order to approach a zero emission balance, taking into consideration the local conditions in Northern Norway. Three different energy systems are analysed for this project using the dynamic building performance simulation tool IDA ICE, Version 4.8. This work confirms previous findings that a building with passive house standard equipped with a heat pump and photovoltaic panels gets closest to achieving a zero emission balance. In the end, practical implications for zero emission buildings are discussed.

Introduction

In recent years, research related to energy use in buildings has moved from single building level towards neighbourhood level, not only in Norway, but also internationally. This is evident from several international projects, such as CityXchange, Synikia, IEA EBC Annex 83 on Positive Energy Districts. In Norway, the Research on Centre on Zero Emission Neighbourhoods in Smart Cities aims to develop sustainable areas that have zero emissions related to buildings, building operation and transport.

Zero Energy Buildings

Sartori et al. (Sartori, Napolitano, & Voss, 2012) defined a framework for Net Zero Energy Buildings, also called Net ZEB. Net ZEBs are usually all-electric buildings, where *Net ZEB* refers to buildings that are connected to the electricity grid and that can do both, consume and generate electricity onsite. These buildings achieve a balance between the electricity imported from the grid and exported from the building to the grid over a certain time horizon, usually one year.

Regarding the design of a Net ZEB, starting from a reference building, the first goal is an improved energy efficiency (Figure 1). This is usually achieved by improving the energy performance of the building envelope, for example by increasing the thermal insulation and by improving the air tightness of the building envelope to decrease the building heating needs. To achieve a Net ZEB balance, local electricity generation (e.g. from photovoltaic panels) is required. This Net ZEB balance is achieved by designing an onsite photovoltaic (PV) system so that the electricity generated onsite can compensate for the energy use of the building throughout the evaluation horizon.
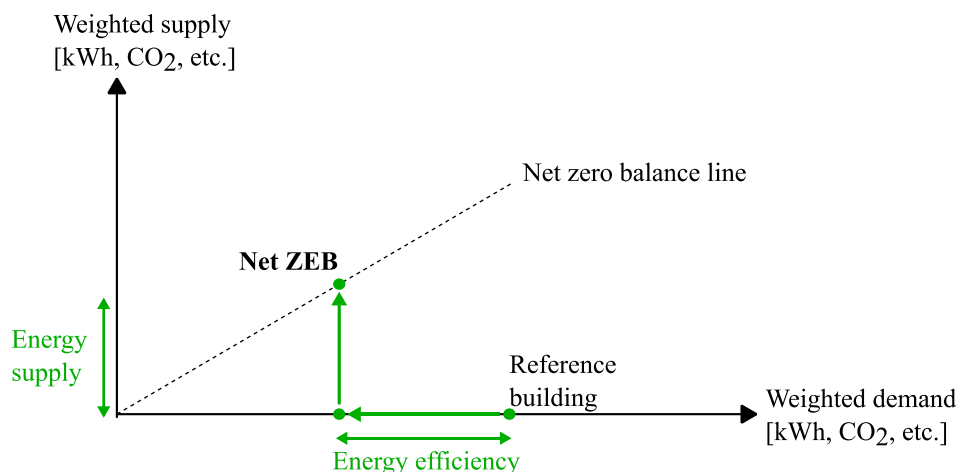
Figure 1: Concept of Net ZEB balance (adapted from *(Sartori et al., 2012)*).

Zero Emission Buildings

In an international perspective, ZEB is usually related to zero energy buildings, whereas in Norway ZEB is related to zero emission buildings.

The Norwegian Research Centre on Zero Emission Buildings (FME ZEB) decided to focus on emissions rather than energy and thus, a zero emission building is defined and evaluated based on the calculated GHG emissions during the lifetime of the building (Mamo Fufa, Dahl Schlanbusch, Sørnes, Inman, & Andresen, 2016). The GHG emissions are calculated with the help of CO_2 equivalent ($CO_{2eq.}$) conversion factors for each energy carrier ($kgCO_{2eq}/kWh$) and building material ($kgCO_{2eq}/m$, $kgCO_{2eq}/m^2$, $kgCO_{2eq}/m^3$, $kgCO_{2eq}/kg$).

As the ZEB Centre definition is ambitious, a stepwise approach with different ambition levels was developed to allow for the possibility to consider different stages of the building life-cycle for the evaluation of a zero emission balance. Figure 3 provides an overview of the different ambition levels defined by Fufa et al. (Mamo Fufa et al., 2016). These levels are briefly described in the following. Emissions are compensated for with renewable energy generation:

- ZEB-O – EQ: Emissions related to the energy use from the operational phase (O), excluding appliances and equipment (EQ)
- ZEB-O: Emissions related to all energy use during operation phase
- ZEB-OM: Emissions related to all operational phase and embodied emissions from materials (M)
- ZEB-COM: Same as ZEB-OM and additionally emissions related to the construction phase (C). The construction phase considers the transport of materials and products to the building site and the construction installation process.

When targeting a ZEB ambition level, it is of outmost importance to have an integrated design process, which *"involves establishing clear goals, employing multi-disciplinary cooperation from the early design stages, implementing a high level of energy integration and* *synergy of systems, and using modern performance prediction tools throughout the process to improve the environmental performance of a building"* (Andresen, Wiik, Fufa, & Gustavsen, 2019).

This approach is still rather theoretical for entrepreneurs and this project aims to bridge the industry and research sector. This work assesses three different energy systems for the Sjøsiden project in Bodø to approach a zero emission balance, taking into consideration the local climate conditions in Northern Norway. The paper also investigates measures that can be applied to satisfy a zero emission balance. The gained knowledge is of value for entrepreneurs with regards to building design.

Methods

This section introduces the building and describes the methodology of the energy system analysis.

Description of the building

The two-family house (TFH) is a three-story building and has a heated floor area of 711 m^2. A sketch of the THF is presented in Figure 2.

Figure 2. Simplified sketch of the two-family house.

Simulation setup

Different energy systems are simulated using the dynamic building simulation software tool IDA ICE Version 4.8.
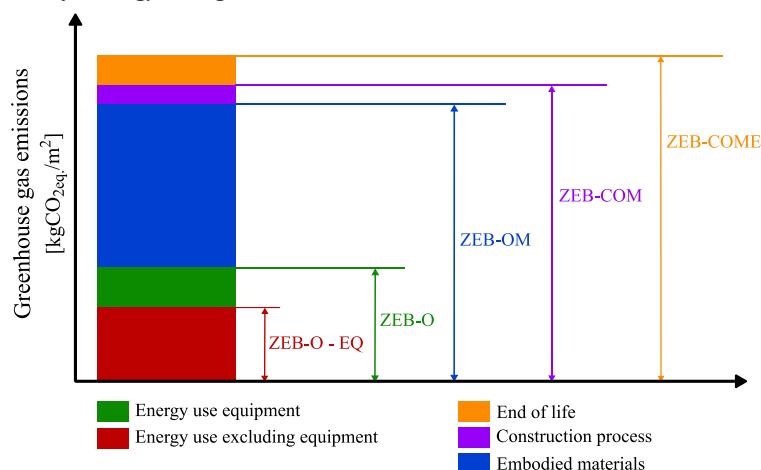
Figure 3. ZEB ambition levels (explanation in the text above; GHG emissions calculated as kg $CO_{2eq.}$ per m^2 heated floor area per year distributed over a 60-years life time).

IDA ICE applies equation-based modeling and allows to investigate building energy systems and to evaluate the energy use of buildings. IDA ICE has been validated in several studies (EQUA Simulation AB, 2010; EQUA Simulation AB & EQUA Simulation Finland Oy, 2010). The energy system analysis uses the results from the dynamic simulations in IDA ICE as input for further evaluation of the carbon footprint of the tested systems during annual operation. Regarding the simulations, the following simplifications and assumptions are taken:

- Local climate data for Bodø is taken into account. An ASHRAE IWEC2 weather file is applied. It contains hourly values for the dry-bulb temperature, relative humidity, direction and speed of the wind, and direct and diffuse solar radiation.
- Specifications according to Norwegian building regulation TEK17 are considered to achieve a required minimum energy efficiency of the buildings.
  - Requirements for minimum U-values of the building envelope and windows (Table 1).
  - Requirements for ventilation as well as internal heat gains from occupants, lighting and electrical appliances.
- Schedules for occupancy, lighting and the use of electric appliances based on SN-TS 3031:2016.
- Regarding thermal zoning in buildings, the room layout is simplified by creating one zone per floor per apartment/housing unit, since the main focus of this work is the energy system analysis and less on the detailed thermal comfort. Assuming that the heating temperature set-point is 21°C in each zone, there are only slight differences in the heating energy use compared to having one zone per room.

Table 1. Building envelope properties for the TEK17 building.

Properties	Unit	TEK17
U-value external walls	$W/(m^2{*}K)$	≤ 0.18
U-value roof	$W/(m^2{*}K)$	≤ 0.13
U-value external floor	$W/(m^2{*}K)$	≤ 0.10
U-value windows/doors	$W/(m^2{*}K)$	≤ 0.80
Thermal bridges	$W/(m^2{*}K)$	≤ 0.05
Air handling unit heat recovery effectiveness	%	> 80
Infiltration at 50 Pa, n_{50}	h^{-1}	≤ 0.6

Simulation procedure for the energy system analysis

The energy systems considered in the analysis are district heating (DH), combined heat-and-power (CHP) and a seawater heat pump (SWHP). The "reference" system is DH because by regulation there is an obligation to connect to DH if the infrastructure is in place. There is one annual simulation for each energy system.

Regarding the sizing of the heating system, a heating load simulation (HLS) at design outdoor temperature is performed. This approach is used to determine the thermal load (peak power) that needs to be covered by the energy system and thus the heat distribution system. This distribution system can be sized for a given design outdoor temperature (DOT), which is -15 °C for Bodø according to (Sintef Byggforsk, 2012). No internal heat gains are considered for this evaluation. The peak power presented in Table 3 shows the peak power for space heating and DHW at the time of the total maximum peak power.

Performance evaluation

The three energy systems are evaluated based on the annual energy use and annual emissions during building operation (Table 7).

The energy use considers the delivered energy for heating and the delivered electricity for lighting and electrical appliances. Lighting and appliances are included because they impact the total amount of energy to be delivered to the building and the amount of PV electricity that can be used on-site or exported to the grid.

For the sake of clarity, different operation strategies are not considered in this report, but are of course worth to be investigated in future work.

Each electricity or heat generating technology has a specific $CO_{2eq.}$ factor, which is used to determine the total annual emissions and the ZEB balance. The Norwegian Standard NS3720 recommends to calculate the emissions from electricity for two different scenarios: i) 18 $gCO_{2eq.}$/kWh, which is the current average factor for the Norwegian electricity grid and ii) 136 $gCO_{2eq.}$/kWh, which is the assumed average $CO_{2eq.}$ intensity of the European electricity grid for the period 2015 to 2075. Referring to NS3720, two scenarios are used in this report (Table 2): (1) current Norwegian $CO_{2eq.}$ factor for electricity and (2) estimated future $CO_{2eq.}$ factor for electricity. The $CO_{2eq.}$ factors for biomass are chosen based on NS3720, which proposes a bandwidth between 8.5 to 130 $gCO_{2eq.}$/kWh as a factor.

Table 2: Emission factors for two scenarios, S1 and S2 (* value according to the FME ZEB).

Energy carrier	$CO_{2eq.}$ factor [$gCO_{2eq.}$/kWh]	
	S1: current $CO_{2eq.}$ factor for El.	S2: estimated future $CO_{2eq.}$ factor for El.
Solid biomass	12	50
Electricity	18	132*

Energy System Analysis

The energy system analysis is done on a higher level, meaning that the aim of the project is the evaluation of the energy systems based on the maximum power need and total annual energy demand. Different control strategies for the operation of the energy systems are not evaluated. This project focuses on energy systems installed to meet the required heating demand of the building. For all three energy systems, DH, CHP and SWHP, it is assumed that the building is directly connected to the energy system.

An HLS at the design outdoor temperature -15 °C is performed for the buildings. An overview of the resulting

heating needs for SH and DHW heating is given in Table 3. The specific characteristics for each energy system are discussed in the remainder of this section. The based load system covers both SH and DHW and the electric auxiliary heater supports the base load whenever required.

Table 3: Thermal capacities resulting from the heat load simulation at DOT -15 °C for the two-family house.

Characteristics	Peak thermal capacity
Space heating: Peak power / thermal capacity [kW]	18
DHW: Peak power [kW]	9

All three energy systems can be combined with on-site PV panels for electricity generation, so that it is possible to evaluate whether the buildings could reach a certain ZEB ambition level. The energy systems are evaluated for each building separately.

Photovoltaic panels

PV panels for on-site electricity generation are considered in combination with the three other technologies. With regards to zero emission buildings/neighborhoods, the electricity generation from PV panels is used to compensate for emissions from the building. In this project, it is assumed that PV panels would be installed on the roofs of the three buildings leading to a total PV area of 260 m^2. The efficiency of the PV panels is set to 17 % which is a typical efficiency of PV panels available on the market. Tilt angles of the panels follow the roof tilt angle (11°). The PV panels are facing south.

The assumption that PV panels are installed on the entire roof area provides a best-case scenario. The scenario is examined to see if ZEB-O could be achieved at all. It is more realistic to have a PV area that is smaller than the roof area. With a certain tilt angle, there would be several rows of PV panels, thus causing shadowing effects. In detailed planning of the PV system, there should be an optimal solution between tilt angle, and thus distances between several rows of PV panels to avoid shadow effect, and the location of the PV system. Optimization should aim for a maximum energy generation for a given location. It is obvious that the installation of several rows will lead to a lower total area of PV panels, and thus lower annual electricity generation

District heating

District heating supplies heat for DHW heating and space heating. The required temperature for DHW is 55 °C. The energy use from DH considers the delivered energy that is needed to cover the heating demand of the building for both, SH and DHW.

Table 4: Simulation data input for the DH system.

Characteristics	Thermal System	
	Base heating	Peak heating
Thermal capacity	Unlimited	Not required
Thermal eff. [%]	90	-

Heat losses from the pipes of the DH system are not considered in the analysis. Input data for the simulation of the DH system are presented in Table 4. The peak power is provided by an electric auxiliary heater

Combined heat and power (CHP)

A CHP plant typically uses biofuels which can be solid biomass or biogas. Solid biomass has a rather low electric efficiency, but also a rather low $CO_{2eq.}$ factor which is advantageous with regards to achieving a ZEB balance. Compared to solid biomass, biogas has a higher electric efficiency, but also a higher $CO_{2eq.}$ factor. In this study, the heating efficiency of 69 % and the electricity production efficiency of 11 % is set in accordance with SN/TS3031:2016. The CHP plant is used to supply DHW and SH. The peak power is provided by an electric auxiliary heater.

Table 5: Characteristics of the CHP system.

Characteristics	Thermal System	
	Base heating	Peak heating
Thermal capacity [kW]	20	10
Thermal/el. eff. [%]	69 / 11	90

Seawater heat pump (SWHP)

A modulating SWHP is evaluated as a third alternative. This choice is based on the geographical conditions since the Sjøsiden neighborhood is located right at the shoreline. The thermal capacity of the simulated heat pump is presented in Table 6. The peak power is provided by an electric auxiliary heater.

Table 6: Characteristics of the SWHP system.

Characteristics	Thermal System	
	Base heating	Peak heating
Thermal capacity [kW]	20	10
Electric eff. [%]	Nominal COP 4	100

Results

The results show that the SWHP leads to a lower annual energy use for heating and to lower annual carbon emissions compared to the DH system and a CHP plant (see Table 7). The energy use for the CHP plant is higher than the energy use for the DH system because more energy must be delivered to meet the same demand due to the lower thermal efficiency of the CHP plant.

Regarding the two scenarios for carbon emissions, S1 and S2, it is shown that the total annual carbon emissions are very dependent on the choice of $CO_{2eq.}$ factor. It can be seen in Table 7 that the total emissions for the CHP plant are higher than for the DH system for scenario S1, whereas they are lower compared to the DH system for scenario S2. This difference is due to the choice of emission factors and their respective ratio (S1: 12 vs. 18 and S2: 50 vs. 132). The importance of the exported electricity generated from the CHP plant increases in

scenario S2. A detailed overview of the results is presented in Table 8.

Table 7: Annual energy use and emissions for the three investigated energy systems.

Performance indicator	District heating	CHP plant	Seawater heat pump
Two-family building (711 m² heated floor area)			
Energy [kWh/m²/year]	65	75	17
Emissions S1 [kgCO$_{2eq.}$/year]	541	606	218
Emissions S2 [kgCO$_{2eq.}$/year]	2164	2091	1599

A cost analysis has not been performed in this study, but it can be referred to a report by Sartori et al. (Sartori, Skeie, Sørnes, & Andresen, 2018), who have performed an analysis of possible energy system at Zero Village Bergen.

Table 8: Detailed overview over annual energy balance and annual emissions.

		Energy system		
		DH	CHP	SWHP
DH	[kWh/y]	47503	0	0
CHP	[kWh/y]	0	61690	0
El$_{Import}$	[kWh/y]	15459	10035	27591
El$_{Export}$	[kWh/y]	17059	17662	15478
El$_{Balance}$	**[kWh/y]**	**-1600**	**-7627**	**12113**
E$_{Balance}$	**[kWh/y]**	**45903**	**54333**	**12113**
Em$_{S1}$	**[kg/y]**	**541**	**606**	**218**
Em$_{S2}$	**[kg/y]**	**2164**	**2091**	**1599**

They compared DH, a CHP plant and a ground-source heat pump also with regards to global costs of the energy systems and found that the ground-source heat pump leads to the lower global costs even though the investment costs were much higher compared to DH. A similar trend could be expected for the SWHP for the Sjøsiden project.

Case study

Results show that it was not possible to reach a ZEB balance with a building that meets the requirements of the building code TEK17.

A case study has been performed to investigate which measures have to be taken to upgrade a TEK17 building to a ZEB-O using the specific case of Sjøsiden. The following measures are investigated in combination with the CHP plant and the SWHP:

- Upgrade insulation level from TEK17 to Passive House (PH – NS3700),
- Increase the efficiency of the PV panels from 17 % to 22%.

The balance for the DH system lies between the SWHP and the CHP plant.

Here it is pointed out that it is important to know which ZEB ambition level one is aiming for. As a reminder, common procedure to achieve a ZEB balance focuses first on (1) reducing the energy demand of a building and then (2) designing the on-site electricity (or heat) generation based on the energy demand.

Therefore, the first measures to be taken in this case study are the upgrading of the building envelope to PH standard by increasing the insulation level, improving the U-values of windows and doors and by improving the air-tightness of the building envelope. Once the heating needs of the building are reduced, the on-site renewable energy generation technology can be dimensioned for the PH case. To reach the ZEB-O ambition level, the PV panels have to generate enough electricity to compensate for all emissions from the operational phase during the lifetime of the building. Shown graphically in Figure 4, this means that the symbol has to be above the diagonal line; the further above the line, the more emissions can be compensated for, thus being also able to reach more ambitious ZEB-levels (Figure 3). The analysis in Figure 4 applies the CO$_{2eq.}$ factors for scenario S1 (biomass: 12 gCO$_{2eq.}$/kWh; electricity: 18 gCO$_{2eq.}$/kWh).

It is shown in Figure 4, that improving the building envelope from TEK17 to PH standard "moves the building" further towards the left, as the heating needs are decreased and thus less energy has to be delivered to the building to cover those needs. For this specific case study, the insulation thickness of the external walls, the roof and the floor were increased by 12 cm, 10 cm and 4 cm respectively to reach the desired U-value.

Several conclusions can be drawn from Figure 4:

1. Comparing the three energy systems for the reference building (TEK17), the building is not able to achieve a ZEB-O level for any of the three energy systems. However, the SWHP helps to reduce the imported energy (and thus emissions) significantly compared to DH and CHP.
2. For both, the SWHP and CHP, it helps to improve the building envelope to PH standard to decrease energy imports (*CHP-PH*, *SWHP-PH*).
3. A rather simple measure is the installation of PV panels with a higher efficiency. With continuously decreasing costs and at the same time improving efficiency for PV panels, the application of PV panels with efficiencies around 20 % to 25 % becomes more cost-effective. It is shown that an efficiency improvement from 17 % to 22 % leads to more exported energy/emissions since more energy can be harvested, but not necessarily self-consumed on-site.
   a. The two-family house in combination with a SWHP almost achieves a ZEB-O level, if the building envelope would be improved to PH
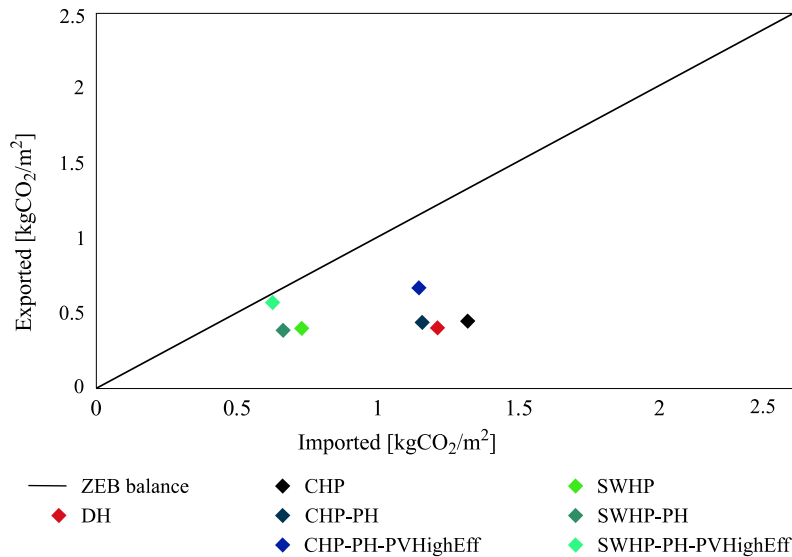
Figure 4: ZEB balance for the two-family house to reach the ZEB-O ambition level.

.

standard and if the PV panel efficiency is increased by 5 %. Again, this is the case, if the size of the PV area corresponds to the total roof area.

b. This is an important finding because it shows that rather simple measures can lead to achieving a ZEB-O level (in combination with a heat pump system), especially considering further improvements in electric efficiency and thus cost-efficiency of PV panels.

c. Regarding the TFH in combination with a CHP plant, the total PV panel area must also be increased additionally to an improved building envelope and an increased PV efficiency, to achieve a ZEB-O level. This can be challenging in a residential area where space for the placement of PV panels often is limited.

4. If the measures were taken in combination with the DH system, the effect of the measures on the ZEB balance would be rather similar to the effect in combination with the CHP plant

This case study demonstrates that it is important to think about relevant solutions for the energy system already during planning phase, if one is aiming for a zero emission building.

Discussion

The discussion focuses on, and tries to put awareness on practical issues faced by entrepreneurs during the early planning phase and construction process for zero emission buildings.

A few relevant challenges and questions are:

- *Regarding building operation:*
  - In this project, the energy systems are evaluated for one building, which is not connected to its neighboring buildings. With regards to interaction between buildings in a neighborhood, it is recommended to integrate the buildings into one energy system to evaluate the energy use of the buildings combined. This will be important when the focus is on the exchange of surplus electricity between buildings and thus feasible operation strategies.
  - Different operation strategies of the energy systems during operational phase are not considered in this project, but it is important to think about desired goals of operation strategies of the energy systems. Operation strategies also influence the choice and dimensioning of system components and relevant operation strategies are thus important to consider from the early design process on.
- *Regarding regulations, business models and costs:*
  - National or municipality regulations, project costs and business models for building and energy system operation go hand-in-hand as they often influence each other.
  - With regards to the choice of energy systems, how can entrepreneurs choose if to connect to DH or not, if the buildings to be constructed are situated in a concession area for DH? Should entrepreneurs be responsible for taking the decision, or the municipality?
  - With regards to achieving a ZEB or ZEN, how would it be possible to attribute more common space to PV panels rather than green area? If so, how would that be accepted by inhabitants?
  - How does the local zoning plan consider the businesses of entrepreneurs? For example, if ZEBs are to be built instead of TEK17 buildings, extra insulation in the walls should be installed to decrease building heating needs which leads to thicker walls. If more insulation is put on the inside, living area is decreased and thus sellable living area. This is a

drawback especially for apartment buildings, which often already have rather narrow rooms, so that it could not be functional to decrease the apartment width even more. If the insulation is to be put outside, the dimensions of the buildings increase, but the distance between the buildings still has to be kept according to the zoning plan. If many buildings are to be built, it could be necessary to adjust the zoning plan accordingly because otherwise, the increased building dimensions comes at the cost of decreased common area. This problem should ideally be considered during the planning phase already so that architects can take it into account.

- Regarding costs and business models there are uncertainties with no simple answers provided by today's models; e.g., who is owning what of the energy system? If a local heating grid is to be built, who is responsible for operating and maintaining it? Who takes the investment costs for a new energy system? If a heat pump supplies heat to a local heating grid, who owns and operates the heat pump? Who owns on-site PV panels, what is the payback time and who gets the possible savings from sold PV electricity?
- What is the value of the energy systems from a private economic and public economic point of view? If there is an obligation to connect to district heating, is it feasible to establish a local heating grid and operate a heat pump to supply heat?
- Starting from the ZEB definition how can the ZEN definition be defined in order to make use of district heating, even if a ZEB could not? For now, the ZEB balance is purely energy-based and thus favors the technologies that use the least energy to cover the demand.

Conclusion

An energy system analysis has been performed for a two-family house at the Sjøsiden neighborhood in Bodø. The energy systems considered in the analysis are district heating (DH), combined heat and power (CHP) and a seawater heat pump (SWHP). The "reference" system is DH because by regulation there is an obligation to connect to DH if it the infrastructure is in place. The performance of the systems is evaluated based on the annual energy use and resulting annual emissions of the buildings. A case study is performed investigating different measures to "upgrade" the building from TEK17 to a ZEB-O.

It has been found that the TEK17 building does not reach a zero emission balance for any of the three energy systems. Therefore, the envelope of the building has been improved to passive house standard and the efficiency of the PV panels has been increased from 17 % to 22 %. Confirming findings from literature, it is found that the SWHP reaches the zero emission balance easier than DH or a CHP plant. If a SWHP is used, it is almost sufficient to improve the building envelope and the PV efficiency. From a practical point-of-view and based on the ongoing

development of PV efficiency, cost-effective PV panels with an even higher efficiency will be available in the (near) future, so that the zero emission balance of the case study building could be achieved by installing highly-efficient PV panels. This is important for a residential area where space for PV panels is limited. For the DH system or the CHP plant, it is not sufficient to only improve the building envelope and the PV efficiency, but it would also be required to increase the total PV area to generate enough electricity to compensate for the imported electricity.

Acknowledgement

Nomenclature

CHP	Combined heat and power
DH	District heating
E	Energy
Eff.	Efficiency
EF	Emission factor
el.	Electric
El	Electricity
Em	Emissions
EQ	Equipment
M	Materials
O	Operation
PH	Passive house
SWHP	Seawater heat pump
TEK17	Norwegian building regulation
TFH	Two-family house
ZEB	Zero energy building / Zero emission building
ZEN	Zero emission neighbourhoods

References

Andresen, I., Wiik, M. K., Fufa, S. M., & Gustavsen, A. (2019). The Norwegian ZEB definition and lessons learnt from nine pilot zero emission building projects. *IOP Conference Series: Earth and Environmental Science - Proceedings of the 1st Nordic ZEB+ Conference*. Trondheim.

EQUA Simulation AB. (2010). *Validation of IDA Indoor Climate and Energy 4.0 build 4 with respect to ANSI/ASHRAE Standard 140-2004*. Retrieved from http://www.equaonline.com/iceuser/validation/ASHRAE140-2004.pdf

EQUA Simulation AB, & EQUA Simulation Finland Oy. (2010). *Validation of IDA Indoor Climate and Energy 4.0 with respect to CEN Standards EN 15255-2007 and EN 15265-2007*. Retrieved from http://www.equaonline.com/iceuser/validation/CEN_VALIDATION_EN_15255_AND_15265.pdf

Mamo Fufa, S., Dahl Schlanbusch, R., Sørnes, K., Inman,

M., & Andresen, I. (2016). *A Norwegian ZEB Definition Guideline*. Retrieved from www.ntnu.no

Sartori, I., Napolitano, A., & Voss, K. (2012). Net zero energy buildings: A consistent definition framework. *Energy and Buildings*. https://doi.org/10.1016/j.enbuild.2012.01.032

Sartori, I., Skeie, K. S., Sørnes, K., & Andresen, I. (2018). *Zero Village Bergen Energy system analysis*.

Retrieved from https://fmezen.no/wp-content/uploads/2018/05/ZEB-pr-report-no-40.pdf

Sintef Byggforsk. (2012). *451.021 Klimadata for termisk dimensjonering og frostsikring*. *2014*(November 1, 2014). Retrieved from http://bks.byggforsk.no/DocumentView.aspx?documentId=204&sectionId=2#tab3

Data-driven Models and BPS Education

Influence of Data Pre-Processing Techniques and Data Quality for Low-Order Stochastic Grey-Box Models of Residential Buildings

Xingji Yu[1]*, Laurent Georges[1]

[1]Department of Energy and Process Engineering, Faculty of Engineering, NTNU - Norwegian University of Science and Technology, Kolbjørn Hejes vei 1a, 7034 Trondheim, Norway

*corresponding author: xingji.yu@ntnu.no

Abstract

Model Predictive Control (MPC) has proved to be a key technology to activate the energy flexibility of buildings. A reliable control-based model should be developed to implement an efficient optimal control. Grey-box models, as a combination of physical knowledge and experiment data, have been widely used in the literature. However, in the identification process of grey-box models, many factors affect the results. This paper uses data from virtual experiments in IDA-ICE to investigate the influence of the optimization methods, the filtering methods, the training dataset and the sampling time interval on stochastic grey-box models. It shows that global optimization increases the chance to avoid a local minimum. Pre-filtering methods have a small influence on the model quality. Larger data sampling time will cause the identified parameters to become non-physical. However, the simulation performance of the model is kept almost unchanged.

Introduction

The share of Renewable Energy Sources (RES) is increasing constantly in today's energy system. The volatile property of RES generation has brought notable challenges to the grid. Thus, flexible loads become a requirement to further increase the penetration of RES. Demand response (DR) is considered to be one of the key components to provide flexibility in smart grid [1]. DR can be described as the interaction and responsiveness of the end-use customer to a penalty signal (e.g. price signal, CO_2 intensity factor for electricity) [2]. In addition, due to the continuous increase of the electric consumption of households and the introduction of electric vehicles, DR can be used for peak-shaving in order to avoid congestion in the distribution grid [3]. Consequently, peak-shaving would enable to minimize or postpone the reinforcement of these grids.

About 25% of the final energy consumption is consumed by buildings and more than 65% of this energy is used for heating and cooling demand in European households, which makes HVAC systems a promising candidate for demand response [4]. In Nordic countries, the space-heating season is long and cold, the energy consumption is mainly related to space-heating. The thermal mass of buildings can be a significant heat storage [5,6]. When using the thermal mass to perform DR, the heating demand will be shifted optimally, while the thermal comfort constraints can still be respected [7]. The targets of DR in buildings are usually the reduction of peak load, lower CO_2 emissions, maximize the use of RES or minimize energy cost [8]. Model predictive control (MPC) is often considered as an important technique to perform demand response (DR) using the thermal mass of the building. The logic of MPC in a building is that the control agent (computers, built-in intelligent devices, etc.) takes the predictions of future disturbances (weather data, power generation from RES, etc.) and the system constraints into an optimization problem and generate an optimal control decision at each control time step. Thus, it is important that the dynamic model embedded in the MPC controller has decent prediction accuracy. A poor-quality model could lead to suboptimal performance, such as increased energy costs, violation of the thermal comfort or even be counterproductive for the electricity grid. In addition, the model identification should also be low-cost to make the investment costs of MPC sufficiently low.

Control models for MPC controller can be divided into three main categories, namely white-, black- and grey-box models. White-box models are based on physical laws, which require detailed knowledge of the system, the underlying physical process and parameters. In practice, it is too complicated and time-consuming to access all the information and to keep it updated during the building's operational lifetime. This type of model usually has higher accuracy but is mathematically more complex, which may cause challenges for the MPC optimizer. This fact makes this kind of model sometimes too complex for MPC [4]. Black-box models are pure data-driven methods considering only measured inputs and outputs from the system. The physical knowledge of the system is not needed. However, this method requires a larger amount of data for training and the precision of black-box models is significantly influenced by the data quality. Black-box models are known to have lower generalization (extrapolation) properties. Grey-box modelling is a combination of physical knowledge and statistical methods. Since the grey-box models have a model structure based on physical knowledge, grey-box models usually require less experimental data compared to black-box models and are hopefully less sensitive to data quality [9].

A common way to create Linear Time Invariant (LTI) grey-box models for buildings is to use lumped capacitance models (RC models). The thermal conditions of the building are expressed with an electrical circuit analogy [10]. This paper mainly focuses on five specific

factors influencing the grey-box modelling of the building thermal dynamics. The first aspect (Q1) is data preprocessing. Few publications are addressing the importance of data preprocessing for building thermal dynamics. The topic is discussed in other disciplines, like [11] in process engineering, but not in building science. The second aspect (Q2) is the convexity of the optimization problem. Except for models with an extremely simple structure like first-order models, the optimization problem for identifying parameters of the grey-box models is not convex. Therefore, grey-box models are very sensitive to initial guess and the search method (i.e. the optimizer). For instance, Generic Algorithm (GA) combined with gradient-based optimization is used in the paper [12] to avoid the identification results ending up in a local minimum. The selection of the optimization algorithm to avoid the local minimum will be discussed in this paper. The third aspect (Q3) is how data quality (e.g. level of excitation signal and amount of data) influences the identification results. It is often said that the temperature of the ventilation extract air is a good image of the average building temperature and is reliable to identify a grey-box model, see e.g. [13]. Thus, the fourth aspect (Q4) is about the selection of the representative indoor temperature for system identification. The last aspect (Q5) considers the sensitivity of the grey-box parameters to the selection of the data sampling time (Ts). The theoretical analysis of Ljung showed that the continuous grey-box models are sensitive to the selection of the sampling time that should be taken lower than the shortest time of the system to be investigated [14]. This analysis needs to be repeated for building applications. All the research in this paper is performed using stochastic grey-box models in innovation form using the disturbance matrix K and the MATLAB identification toolbox.

Methodology

Dataset and virtual experiments

IDA ICE is a detailed dynamic simulation tool for studying thermal indoor climate as well as the energy consumption of buildings. A two-storey detached house with a heated floor area of 160 m² is used as virtual experiment for our case study. The three-dimensional geometry of the building from IDA ICE is shown in Fig. 1. The building is constructed in wood (i.e. lightweight construction) and complies with the requirement of the Norwegian passive house standard, NS 3700 [15]. The detailed description of the building construction can be found in [16]. The building is equipped with balanced mechanical ventilation with a heat recovery unit. The heat exchanger is here modelled using a constant effectiveness of 85% without bypass, like a plate heat exchanger.
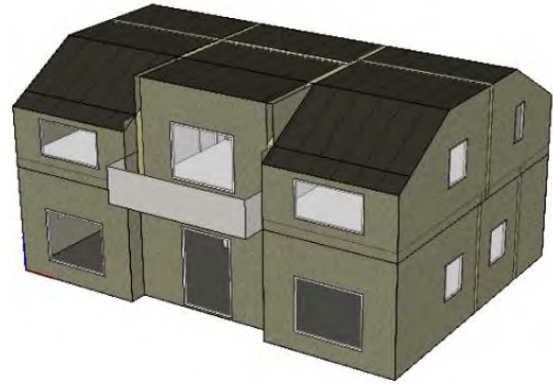
Figure 1: 3D geometry of the building model in IDA ICE (showing the southwest façade).

The building is simulated with a multi-zone model with open internal doors. IDA ICE has an embedded ventilation network model which accounts for the large bidirectional airflow through open doorways. This large convective heat transfer leads to relatively uniform air temperatures in the entire building. However, bathrooms are kept separated with closed doors. Following the cascade ventilation principle, ventilation air is supplied in living areas and bedrooms and mostly extracted in wet rooms (i.e. bathrooms and the laundry). The space-heating was performed using an electrical heater in this case study. Direct electricity is a most common way to heat small residential buildings in Norway [17] . The hourly profiles of internal heat gains for artificial lighting, electric appliances and occupancy is taken from a Norwegian standard [18].

Two types of excitation signals are used to activate the thermal mass of the building in order to collect data for system identification. The first signal is called Pseudo-Random Binary Signal (PRBS) with a minimum and maximum step of 10 and 80 min, respectively. The reason for choosing a PRBS signal is that it approximates white noise, which can activate the dynamic system in a large spectrum of frequencies [19,20]. The other excitation signal is an intermittent set-point, which means that the temperature set-point changes between daytime and night-time (i.e. night setback). In this case, an on-off control is implemented in IDA ICE to track the temperature set-point, like in real direct electric radiators. Both excitation signals are applied to an electric radiator placed in each zone, except for bathrooms as these rooms are relatively small and typically heated by floor heating (with significant thermal inertia). Five different periods with specific weather conditions are implemented in the virtual experiments, as described in the table below.

IDA ICE uses a time-varying time-step so that the data is not generated at constant time intervals. The data output from IDA ICE is therefore interpolated on a uniform time discretization of 2.5 min (thus well shorter than the 10 min time interval of the PRBS).

Type	Outdoor Temperature	Sky	Date	Duration
Very Cold	-10 °C	Clear sky	12/13 /2019	One week
Cold	0 °C	Overcast	12/24 /2019	One week
Cold	0 °C	Clear sky	3/23/ 2019	One week
Mild	5 °C	Overcast	11/23 /2019	One week

Grey-box model structure and identification

The main purpose of this paper is not to investigate the grey-box model structure. This topic is already discussed in previous works [21–23]. Only first-order (1R1C) and second-order (3R2C) grey-box models are considered in this paper with a single temperature node inside the building (i.e. mono-zone model). Preliminary tests have shown that a third-order model would be over-fitted for this test case. Higher-order models can cause over-parameterization more easily, which has been shown in the papers [23,24]. The structure of the two grey-box models follows a RC-formalism. The lumped resistance and capacitance as well as the physical interpretation of these parameters can be found in Figures 2 and 3 below. The free parameters of these grey-box models are calibrated using the IDA ICE data. The ventilation exhaust air temperature or the volume-averaged temperature can be selected to represent the measured interior node Ti and their respective model performance will be compared.
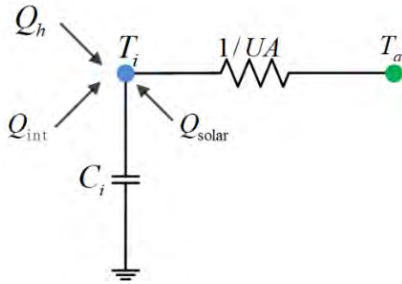
Figure 2: First-order model (1R1C)

T_i Temperature of interior heat capacity [°C].

T_a The outdoor (or ambient) temperature [°C].

C_i Heat capacity of the building [kWh/K].

R ($1/UA$) Overall heat resistance between the building and the ambient, including ventilation [K/kW].

Q_{int} Internal heat gain from artificial lighting, people and electric appliances [kW].

Q_{solar} Heat gain from solar radiation [kW].

Q_h Heat gain from the electric heater [kW].
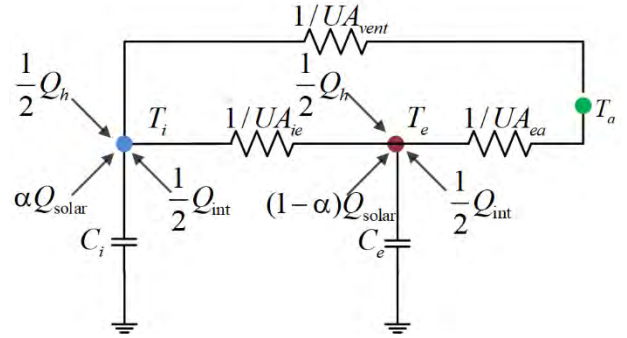
Figure 3: Second-order model (3R2C)

T_e Temperature of the building envelope [°C].

T_a The outdoor temperature [°C].

C_i Heat capacity of the building combining the thermal mass of the air, the furniture, internal walls and, potentially, the first centimetres of external walls [kWh/K].

C_e Heat capacity of the node Te [kWh/K].

R_{ie} ($1/UA_{ie}$) Heat resistance between the building envelope and the interior [K/kW].

R_{ea} ($1/UA_{ea}$) Heat resistance between the ambient and the building envelope [K/kW].

R_{vent} ($1/UA_{vent}$) Heat resistance between the ambient and the interior [K/kW].

α Fraction of solar gains to air node.

The internal gains and solar gains are computed exactly by IDA ICE. In this work, they are not identified and are introduced directly in the grey-box model. Consequently, in the 3R2C model, only the coefficient α to distribute the solar gains between the two temperature nodes needs to be identified regarding gains. In real application, gains are not known exactly. However, simplifying the problem enables to emphasize the specific research questions of the article.

The MATLAB identification toolbox is used for model identification. In grey-box models, the continuous time model is first discretized in order to identify the model parameters using discrete measurement data. The discretization assumes the input data to be piecewise constant during each time interval (i.e. zero-order hold). Regarding the optimization problem, the initialization value of the model parameters and their corresponding range (i.e. minimum and maximum values) should be defined. The optimizer will then iterate to find the parameters that minimize the Normalized Root Mean Square Error (NRMSE) of the one-step ahead prediction. Then, the toolbox covert the discrete time model back to continuous time:

$$\dot{x}(t) = \mathbf{A}\,x(t) + \mathbf{B}\,u(t) + \mathbf{K}\,e(t) \quad (1)$$

$$\dot{y}(t) = \mathbf{C}\,x(t) + e(t) \quad (2)$$

where x is the state vector and A, B and C are the system matrices. u is the input vector (T_a, Q_{solar}, Q_{int}, Q_h) and y is the output (indoor temperature, T_i). K is the disturbance

matrix of the innovation form (Kalman gain). It is a transformed representation from the general process [25].

Influence of the optimizer

In MATLAB, the function *greyest* identifying the model parameters has four different gradient-based iterative search methods, used in sequence. However, preliminary tests using the 3R2C model show a quick converge to a local minimum close to the initial estimate of the parameters. A similar behavior is also reported in the paper [12]. The authors used GA combined with gradient-based optimization to overcome the non-convexity of the optimization problem. Consequently, a global optimization algorithm has been implemented in this paper. Instead of the GA method, the first stage optimization uses particle swarm optimization (PSO) while the second stage uses the default *greyest* function to further polish the results. Each optimization method is able to identify the parameters' value and their corresponding variance. For each case, the optimizer giving the lowest NMRSE for the one-step ahead prediction is selected and provides the selected model parameters.

Pre-filtering methods

In real-life applications, it is difficult to guarantee that the measurement data will be sampled at a higher frequency (Ts) than the highest frequency of the system (here 10 min, imposed by the PRBS). For instance, the Advanced Metering System (AMS) in Norway has a typical time interval of 15 min [26]. It is important to investigate the influence of data pre-processing by low-level digital measurement devices before they log the data at an appropriate time interval. Temperature sensors can register data at a very high frequency (here 2.5 min). This data can be pre-processed before being sampled and logged at a longer time interval (Ts > 2.5 min). A low-pass discrete filter can first be applied, such as a moving average (MA) or a finite impulse response (FIR). Without this low-pass filter (i.e. direct sampling), the aliasing error may be high. With MA, the aliasing error is smaller but still present while the FIR (applied with a sufficient order) would lead to negligible aliasing. By comparing the performance of (MA + sampling), (FIR + sampling) and the direct sampling on the parameter identification, it is possible to understand the influence of aliasing. The low-pass filter is applied to all the input and output variables of the model. If the filter introduces a time delay (like MA), this delay is the same for all variables and will thus not affect the model. The situation would be more complex if the low-pass filter is only applied to a subset of the input or output variables.

Results

Influence of the optimizer (Q2)

Five datasets using the four PRBS signals and the intermittent on-off heating during the full heating season (FHS) are used to investigate the influence of the optimizer. The two optimization methods do not show much difference for the 1R1C model. In most cases, the two optimization methods converge to the same parameter values. However, the identified parameters from *greyest* function are not identical for the 3R2C model. This implies that the optimization is already non-convex from the second-order model, this conclusion is also confirmed in Arendt et al. [12]. The best optimizer leading to lowest NRMSE for the second-order model can be found in Table 2 (with different time intervals, excitation signals and filters). The figure shows that global optimization is selected for all cases no matter the time interval or filtering method.

Table 2: Best optimizer for the four PRBS and FHS experiments.

Sampling time	Type	Direct sampling	Averaging filter	FIR filter
2.5min	PRBS1	Global	Global	Global
	PRBS2	Global	Global	Global
	PRBS3	Global	Global	Global
	PRBS4	Global	Global	Global
	FHS	Global	Global	Global
15min	PRBS1	Global	Global	Global
	PRBS2	Global	Global	Global
	PRBS3	Global	Global	Global
	PRBS4	Global	Global	Global
	FHS	Global	Global	Global
30min	PRBS1	Global	Global	Global
	PRBS2	Global	Global	Global
	PRBS3	Global	Global	Global
	PRBS4	Global	Global	Global
	FHS	Global	Global	Global
60min	PRBS1	Global	Global	Global
	PRBS2	Global	Global	Global
	PRBS3	Global	Global	Global
	PRBS4	Global	Global	Global
	FHS	Global	Global	Global

Since the datasets contain different excitation signals and weather conditions, it is a strong proof that global optimization can give more robust and higher-quality results when the optimization problem is not convex. In other words, the global optimization algorithm can increase the chance to avoid a local minimum in the grey-box identification process.

Influence of the selection of input (Q4)

While the one-step prediction is used to train the models, the simulation performance is more relevant for MPC applications. Therefore, the simulation NRMSE fitting is mainly used as the performance index in this subsection. Table 3 and Table 4 compare the cross-validation simulation performance using the volume-averaged air temperature and the extracted air as representative indoor temperature respectively. Only datasets trained with the original 2.5 min sampling time is used to avoid the influence of other factors (e.g. dataset, discretization error and pre-filtering method).

Table 3:Simulation NRMSE fitting using the volume-averaged air temperature (Ts = 2.5min)

Training dataset	Validation dataset and simulation NRMSE fitting				
	PRBS1	PRBS2	PRBS3	PRBS4	FHS
PRBS1	84.25%	74.96%	0.53%	72.34%	-17.72%
PRBS2	77.10%	74.16%	24.25%	60.58%	9.49%
PRBS3	39.36%	34.03%	64.20%	14.41%	33.24%
PRBS4	82.19%	69.36%	-17.69%	78.45%	-42.34%
FHS	45.95%	41.11%	69.06%	20.59%	39.17%

Table 4:Simulation NRMSE fitting using the extracted ventilation air temperature (Ts = 2.5 min)

Training dataset	Validation dataset and simulation NRMSE fitting				
	PRBS1	PRBS2	PRBS3	PRBS4	FHS
PRBS1	90.21%	70.83%	16.97%	79.05%	-94.10%
PRBS2	73.51%	81.86%	29.88%	71.77%	-74.10%
PRBS3	30.44%	43.28%	68.02%	25.09%	-15.82%
PRBS4	78.70%	73.55%	-10.68%	83.63%	-155.32%
FHS	78.11%	71.50%	52.43%	64.46%	25.33%

In general, simulation performance with the two different representative temperatures are following the same trend. The simulation NRMSE fitting is higher for the original training dataset and lower for the validation datasets. The model identified from the intermittent set-point and on-off control dataset during the FHS presents higher performance on the validation datasets: the validation fitting is acceptable at each period never completely collapsing. Models trained from the PRBS excitation signals of one week have a good simulation NRMSE fitting on their own training data but largely fail in some cross-validation datasets. Simulation results from extracted air temperature show a slightly higher simulation NRMSE fitting value for the original training dataset. However, models trained with extracted air temperature show worse simulation NRMSE fitting compared with volume-averaged temperature when they are trained and validated with the FHS dataset (values in red in Table 3. Thus, the volume-averaged air temperature is a more balanced choice of representative indoor temperature. The exhaust air temperature is not always the best option to train the model and this conclusion could be even more severe if all the internal doors inside the building were closed.

Influence of pre-filtering methods and data-quality (Q1, Q3 and Q5)

Figures 4 to 6 show three key identified parameters for the second-order model. For the value of the total heat transfer coefficient in Figure 4, the estimated value from a step-response of the heating power applied in IDA-ICE is about 85 W/K. Figure 4 shows that most of the results are close to the estimation from IDA-ICE. When the Ts is increased to 60 min, some values using the FIR filter or
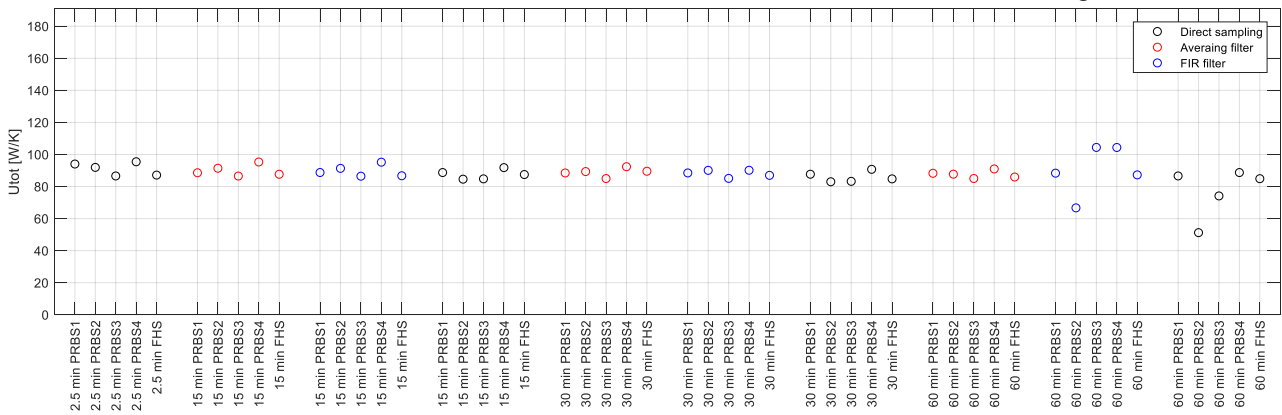
Figure 4: Identified Utot of the 3R2C model (variance is not given as Utot combines the 3R)
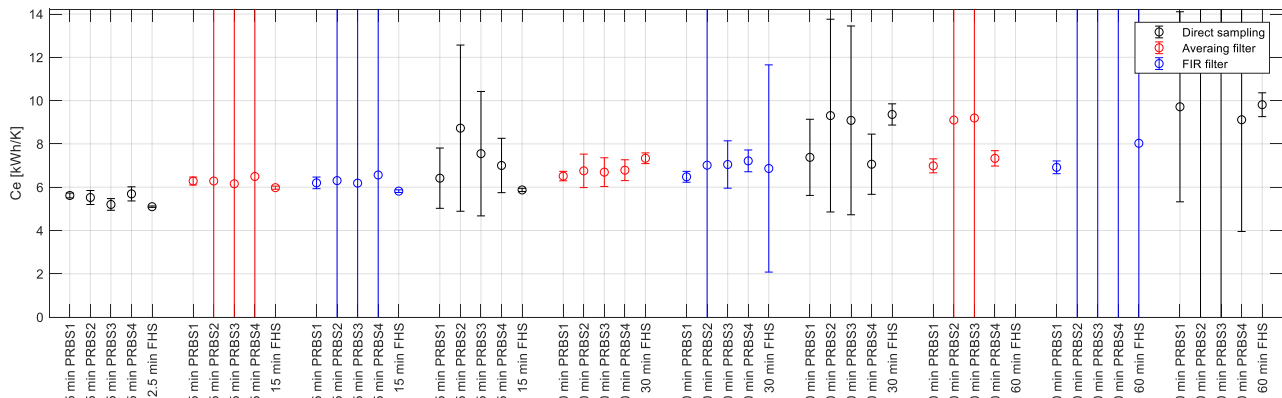
Figure 5: Identified Ce of the 3R2C model
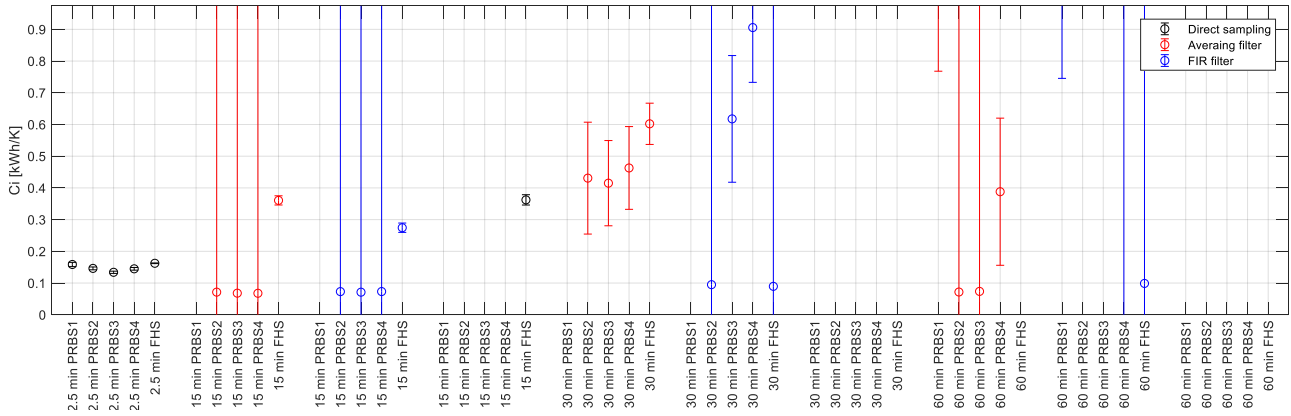
Figure 6: Identified Ci of the 3R2C model

direct sampling starts to depart from the estimated value. Figure 5 shows the value and variance of the heat capacitance of the external wall C_e. Regarding the value of C_e, direct sampling has the tendency to generate a larger capacitance value with increasing sampling time. Some values are not visible because completely outside the y-axis limits of the graph. The same problem is even more pronounced for the value of the heat capacitance C_i in Figure 6. The value of C_i diverges quickly when Ts is increased for every pre-filtering method. Although it shows that the low-pass filter, especially the moving-average, can improve the results of identified value for these key parameters. Regarding the variance of the parameters, it is very limited for the sampling time of 2.5 min. Like the parameter value, the parameter variance increases with the sampling time. However, this increase of the variance is less systematic and regular than for the parameter value.

Regarding the influence of filters, FIR does not show a significant advantage over the moving-average for the identification even though the FIR filter is theoretically better. On the contrary, FIR filter sometimes has worse results than the moving-average filter when Ts is large.

Another important conclusion can be found. The FHS dataset has more stable identified parameters (both values and variance) than the PRBS datasets. This shows that a dataset generated from a normal building operation over a long time period with comfortable indoor temperatures (and thus possible occupancy) can give equivalent or even better parameter identification than a short training period using a better excitation signal (here PRBS) but leading to uncomfortable indoor temperatures, probably preventing occupancy.

The simulation performance is shown in Figure 7 taking the FHS period to train the model. For the sake of the conciseness, the other cases using the other training
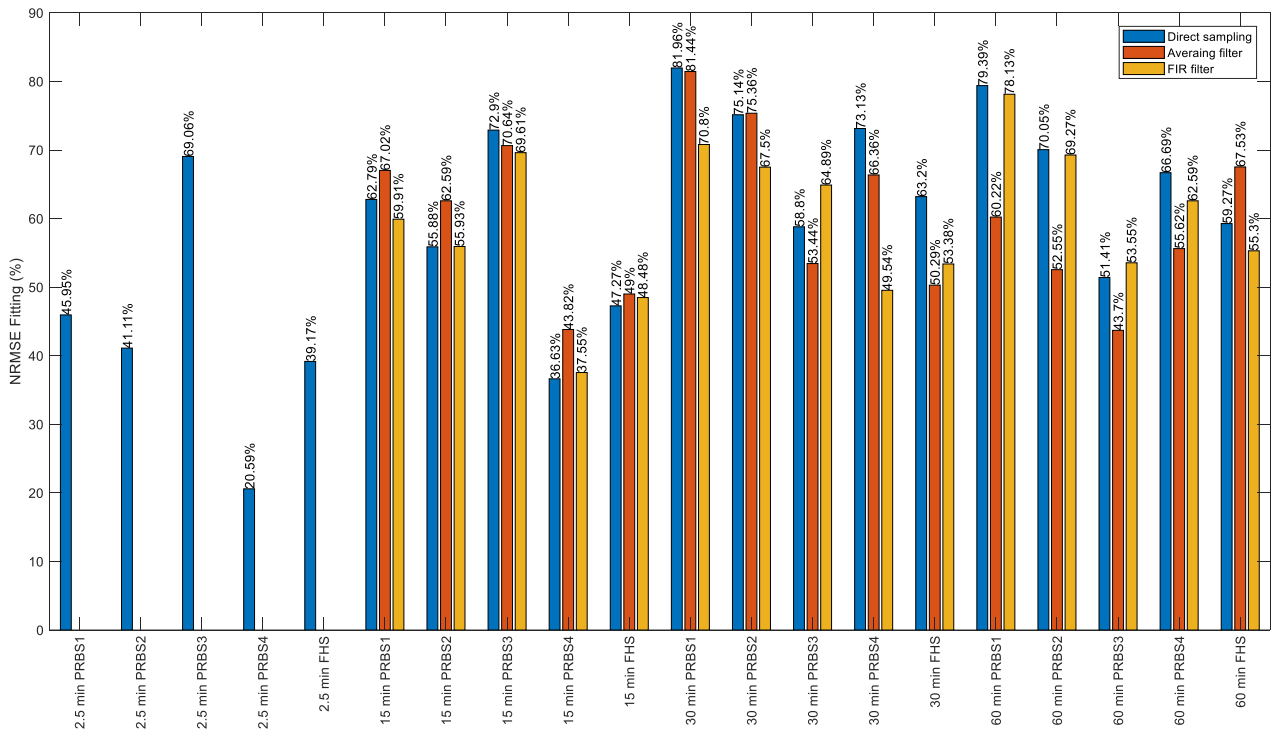
Figure 7: Simulation performance of the models trained using the FHS dataset.

periods are not reported but they give similar conclusions. Unlike, the parameter value and variance, it is clear that the increase of the sampling time (Ts) does not degrade the simulation performance. In some cases, even though the identified parameters have non-physical value or variance, this does not alter the simulation performance. The simulation performance is the main property of interest for the application of MPC. This demonstrates that training of a model for MPC application or characterization of the building thermal properties does not require the same quality of the input data. For instance, the pre-filtering methods (MA, FIR or direct sampling) do not affect much the simulation performance as well. It is difficult to rank the three pre-filtering methods as their relative performance changes between the validation cases.

Conclusions

The sampling time (Ts) of data should be limited to guarantee the physical meaning of the parameter value and variance. Larger Ts can result in non-physical parameter values and variance (Q5). If a small Ts is not applicable, the data should be low-pass filtered before being sampled even though this measure alone does not guarantee that the parameters will be physical for all Ts. This answers the first question in the introduction (Q1). More than the data pre-filtering, the selection of the right sampling time is the dominating factor to guarantee the physical meaning of the parameters. Nevertheless, sampling time and pre-filtering do not seem to affect the simulation performance of the identified models, which is a positive conclusion for MPC applications.

Even if a grey-box model has good simulation performance, having meaningful physical parameters in the model remains interesting. Firstly, it increases the physical understanding of the system, it enables to create benchmark values for other buildings of the same category. Secondly, if the parameters have not physical meaning, the model may have no additional value compared to a pure black-box model. However, to conclude this, the simulation performance of black-box models should be compared as well.

Regarding the selection of the optimizer (Q2), the results show that only the oversimple structure of the first-order model shows convexity property. Significant non-convexity already emerged from the second-order grey-box model. When applying the four different gradient-based iterative optimizers, the trained second-order grey-box model has lower NRMSE for the one-step ahead prediction compared to the model from global optimization. Therefore, it is better to use global optimization to increase the chance of avoiding a local minimum.

It is hard to say whether PRBS or FHS is a better option from the results that we observe. Since it also depends on the target period of the model (better fitting on a certain period or longer period of the FHS). However, it is clear that with a larger amount of data (longer observation period or more samples with smaller sampling time), the chance to identify a model with higher fitting and more physical parameters can be increased. This answers the third question (Q3) of the introduction. The data quality does influence the identified results of the grey-box model. Nevertheless, it is not always realistic to use the PRBS signal to excite the building's thermal mass with normal occupancy in the residential building. Data from normal operation (here intermittent on-off heating) over long periods seems more accessible. The results of this paper also show that an acceptable model can be obtained with normal building operations if large amount of data is accessible.

The selection of the correct input and output is also important for system identification (Q4). In the case study, the identified results from volume-averaged temperatures are better than those from the extracted air temperature. This proves that the correct selection of the representative indoor temperature of the building can increase the model quality and that choosing the extracted air temperature does not systematically give the best performance.

This work has answered some questions for the identification of stochastic grey-box models. However, the data in this paper is based on the results of virtual experiments without measurement noise. For future work, it will be worth investigating the influence of the measurement noise on the identification results. In addition, complementary pre-processing methods to increase the chance to identify parameters with a physical value is also an interesting topic.

Acknowledgement

References

[1]   A. Losi, P. Mancarella, A. Vicino, Integration of demand response into the electricity chain: challenges, opportunities, and Smart Grid solutions, John Wiley & Sons, 2015.

[2]   P. Siano, Demand response and smart grids — A survey, Renew. Sustain. Energy Rev. 30 (2014) 461–478. https://doi.org/10.1016/j.rser.2013.10.022.

[3]   J. Hu, H. Morais, T. Sousa, M. Lind, Electric vehicle fleet management in smart grids: A review of services, optimization and control aspects, Renew. Sustain. Energy Rev. 56 (2016) 1207–1226. https://doi.org/10.1016/j.rser.2015.12.014.

[4]   G. Steindl, W. Kastner, V. Stangl, Comparison of Data-Driven Thermal Building Models for Model Predictive Control, J. Sustain. Dev. Energy, Water Environ. Syst. 7 (2019) 730–742. https://doi.org/10.13044/j.sdewes.d7.0286.

[5] J. Le Dréau, P. Heiselberg, Energy flexibility of residential buildings using short term heat storage in the thermal mass, Energy. 111 (2016) 991–1002. https://doi.org/10.1016/j.energy.2016.05.076.

[6] G. Reynders, Quantifying the impact of building design on the potential of structural strorage for active demand response in residential buildings, 2015. https://doi.org/10.13140/RG.2.1.3630.2805.

[7] M. Dahl Knudsen, S. Petersen, Demand response potential of model predictive control of space heating based on price and carbon dioxide intensity signals, Energy Build. 125 (2016) 196–204. https://doi.org/10.1016/j.enbuild.2016.04.053.

[8] B.P. Esther, K.S. Kumar, A survey on residential Demand Side Management architecture , approaches , optimization models and methods, Renew. Sustain. Energy Rev. 59 (2016) 342–351. https://doi.org/10.1016/j.rser.2015.12.282.

[9] T.P. Bohlin, Practical Grey-box Process Identification, Springer London, 2006. https://doi.org/10.1007/1-84628-403-1.

[10] J.A. Crabb, N. Murdoch, J.M. Penman, A simplified thermal response model, Build. Serv. Eng. Res. Technol. 8 (1987) 13–19.

[11] J.F. van Impe, P.A. Vanrolleghem, D.M. Iserentant, Advanced instrumentation, data interpretation, and control of biotechnological processes, Springer Science & Business Media, 2013.

[12] K. Arendt, M. Jradi, M. Wetter, C.T. Veje, ModestPy: An Open-Source Python Tool for Parameter Estimation in Functional Mock-up Units, in: Proc. Am. Model. Conf. 2018, Oct. 9-10, Somb. Conf. Center, Cambridge MA, USA, 2019: pp. 121–130. https://doi.org/10.3384/ecp18154121.

[13] A. Afram, A.S. Fung, F. Janabi-Sharifi, K. Raahemifar, Development and performance comparison of low-order black-box models for a residential HVAC system, J. Build. Eng. 15 (2018) 137–155. https://doi.org/10.1016/j.jobe.2017.11.021.

[14] L. Ljung, A.G. Wills, Issues in sampling and estimating continuous-time models with stochastic disturbances, in: IFAC Proc. Vol., 2008. https://doi.org/10.3182/20080706-5-KR-1001.0271.

[15] S. Norge, NS 3700: 2013 Criteria for passive houses and low energy buildings-Residential buildings, (2013).

[16] T. Johnsen, K. Taksdal, J. Clauß, X. Yu, L. Georges, Influence of thermal zoning and electric radiator control on the energy flexibility potential of Norwegian detached houses, E3S Web Conf. 111 (2019) 06030. https://doi.org/10.1051/e3sconf/201911106030.

[17] A.C. Bøeng, B. Halvorsen, B.M. Larsen, Kartlegging av oppvarmingsutstyr i husholdningene, Rapp. 2014/45. (2014). https://www.ssb.no/energi-og-industri/artikler-og-publikasjoner/kartlegging-av-oppvarmingsutstyr-i-husholdningene.

[18] S. Norge, SN/TS 3031: 2016 Energy performance of buildings, Calc. Energy Needs Energy Supply. (2016).

[19] P. Bacher, H. Madsen, Identifying suitable models for the heat dynamics of buildings, Energy Build. 43 (2011) 1511–1522. https://doi.org/10.1016/j.enbuild.2011.02.005.

[20] N.R. Kristensen, H. Madsen, S.B. Jørgensen, Parameter estimation in stochastic grey-box models, Automatica. 40 (2004) 225–237. https://doi.org/10.1016/j.automatica.2003.10.00.

[21] R.E. Hedegaard, T.H. Pedersen, M.D. Knudsen, S. Petersen, Towards practical model predictive control of residential space heating: Eliminating the need for weather measurements, Energy Build. 170 (2018) 206–216. https://doi.org/10.1016/j.enbuild.2018.04.014.

[22] R.E. Hedegaard, T. Pedersen, M.D. Knudsen, S. Petersen, Identifying a comfortable excitation signal for generating building models for model predictive control: a simulation study, in: CLIMA2016 12th REHVA World Congr. World Congr., Aalborg Universitet, 2016. https://doi.org/https://doi.org10.3384/ecp18154121.

[23] X. Yu, L. Georges, M.D. Knudsen, I. Sartori, L. Imsland, Investigation of the Model Structure for Low-Order Grey-Box Modelling of Residential Buildings, in: Proc. Build. Simul. 2019 16th Conf. IBPSA, International Building Performance Simulation Association (IBPSA), 2019. https://doi.org/10.26868/25222708.2019.211209.

[24] O.M. Brastein, D.W.U. Perera, C. Pfeifer, N.O. Skeie, Parameter estimation for grey-box models of building thermal behaviour, Energy Build. 169 (2018) 58–68. https://doi.org/10.1016/j.enbuild.2018.03.057.

[25] K.J. Åström, Introduction to stochastic control theory, Courier Corporation, 2012.

[26] Advanced Metering System (AMS) Status and plans for installation per Q2 2016, 2016. https://www.nve.no/energy-market-and-regulation/retail-market/smart-metering-ams/.

Data-based calibration of physics-based thermal models of single-family houses

Virginia Amato[1*], Michael Dahl Knudsen[1], Steffen Petersen[1]
[1]Department of Engineering, Aarhus University, 8000 Aarhus C, Denmark
* corresponding author: viam@eng.au.dk

Abstract

The calibration of building energy simulation models is crucial for addressing the issue of the discrepancy between the simulation output and real-world measurements. The majority of current research studies have used monthly utility bills as calibration data. In this study an automated optimization algorithm was implemented to calibrate an energy model of a single-family house using daily and hourly energy consumption data. The performance of the calibrated model was tested on a different dataset and the simulation output matched the measurements with a daily CV(RMSE) of 14%. This study demonstrates that the calibration using currently available district heating data can significantly improve the performance of building energy simulation.

Introduction

Building energy simulation can be classified in two main categories: physics-based models, which apply physical laws to predict the system behaviour, and data-based models, which estimate the system properties based on statistical analysis of measured data. The advantage of (detailed) physics-based models is the ability to predict the system behaviour under previously unseen boundary conditions. Physics-based building energy simulation tools are therefore suitable for predicting the thermal performance of buildings e.g. during the building design process, in energy retrofit projects, and for various research purposes like testing and developing predictive control systems. However, many studies have documented that there are often significant discrepancies between simulation results and measurements (Coakley et al. 2014; Petersen et al. 2012). The major reason is that the inputs to the simulation model does not correspond to the actual conditions. Therefore, current literature describes different approaches for the calibration of the simulation model to fit the measured data.

The calibration methods are divided by Coakley et al. (2014) into two main approaches: manual and automated. Current research has investigated different methods for automated calibration; among these are optimization-based methods. Optimization methods normally consist in a minimization problem where an optimal set of parameters is found in order to minimize an objective function stating the deviation between the simulated output and the measurements. Sun and Reddy (2006) developed a four-step approach that consist in sensitivity analysis, identifiability analysis, uncertainty analysis and optimization with a gradient-based algorithm. In order to avoid the risk of local minima which are typical of gradient-based methods, different algorithms based on global search have been investigated in other studies. In Asadi et al. (2019), the implemented method is a Harmony Search algorithm, which generates the next iterations either with a random solution or choosing the saved solution with the lowest simulation error. Other studies used population-based approaches, where a group of solutions is generated in each iteration, for example using a particle swarm algorithm as in Yang et al. (2016) or a genetic algorithm as in Martínez et al. (2020). To take the uncertainties of the under-determined calibration process into consideration, Reddy et al. (2007) selected a small number of the best solutions to predict the energy use of the model instead of choosing only one solution.

Current research studies have generally used utility bills on a monthly basis as calibration data (Coakley et al. 2011). Recently, the development and roll-out of e.g. smart heat meters and IoT-based sensors technology has made data with higher resolution more available, data that potentially can improve the robustness of model calibration. In the study by Monetti et al. (2015) hourly data were used to calibrate a building energy model coupling the EnergyPlus building simulation tool and the GenOpt optimization program. The case study was a small building used exclusively for indoor climate experiments, without any occupant and conditioned by means of electric resistances. The validation was based on performance limits set out by ASHRAE Guideline 14 and the results of the calibrated model were found consistent with those thresholds. Another calibration study that utilized hourly data was performed by Asadi at al. (2019). The case study was a large office building and one hundred different independent variables were calibrated. The calibrated model was able to predict the electricity consumption with a proper accuracy after 500 iterations.

In contrast to the previous mentioned studies, the aim of this study is to develop a calibration method that can be suitable for single-family houses, addressing the issue of the low resolution of district heating data and unmeasured indoor temperature, while at the same time keeping the computational complexity low.

Methodology

The calibration method applied in this study was an iterative process between the calibration algorithm and the building energy simulation model made in EnergyPlus, a high-fidelity building energy simulation tool (Crawley et al. 2001). The model was used for co-simulation with Matlab where the calibration algorithm was implemented. The procedure used was similar to the optimization program GenOpt for the minimization of an objective function evaluated by an external simulation program (Wetter 2016). A first input file for the EnergyPlus model was written assigning initial guess values to the calibration variables. Based on output from EnergyPlus, the Matlab code calculated the new input parameters and wrote them in the input file for the next EnergyPlus simulation in the calibration iteration. The process continued until the maximum number of iterations was reached or the convergence criteria were met. The flow diagram is shown in Figure 1.
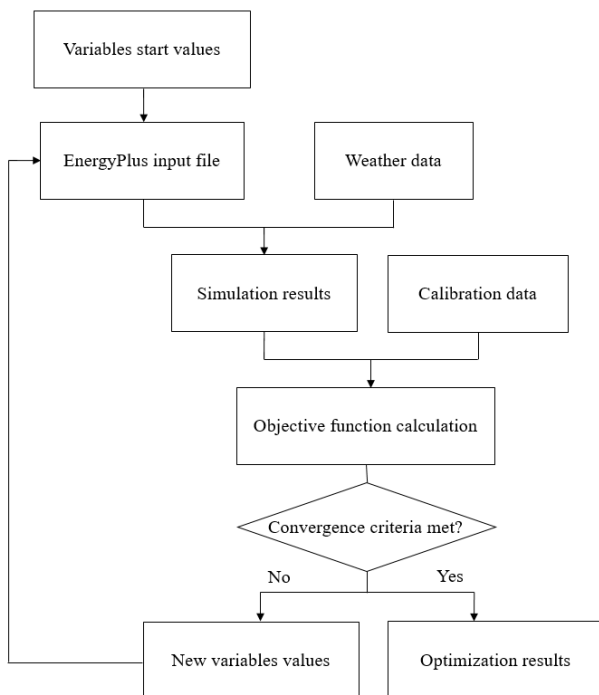

Figure 1: Flow diagram of the calibration process

Building model

The first step of the methodology was to build an energy simulation model using all the information currently available about the building. The case study is a typical single-family house from 1968 located in Aarhus, Denmark, occupied by four people (two adults, two children). The floor area is approximately 180 m² and has 15 rooms distributed on one floor. District heating supplies the radiator-based space heating and domestic hot water. The geometry and initial assumptions about the thermal properties of the constructions was based on as-built drawings. In order to reduce the complexity of the

model, the building was modelled as one thermal zone, while the walls that separate the different rooms were considered as internal mass. Since EnergyPlus models the heat conduction through surfaces is modelled as a one-dimensional problem, thermal bridges cannot be directly modelled. Instead, the contribution of thermal bridges was accounted for with an additional heat loss through the building envelope, hence by increasing the thermal conductivity of the materials.

Hourly electricity consumption data were used to generate a daily profile of the internal heat gains. The heat dissipated by lighting and other electrical equipment was assumed to be a fraction of the electricity consumption recorded every hour, and the daily pattern observed in the data was used as schedule throughout the year for the heat gains in the EnergyPlus model. The occupancy schedule was determined from the time of the day when electrical appliances were used and from the assumptions that all occupants are present during the night.

The weather data included were the outdoor air temperature and the global solar radiation, with a resolution of $1 \cdot 10^{-9}$ °C and $1 \cdot 10^{-9}$ W/m², respectively, measured by a near-by weather station. Other meteorological data such as humidity and wind speed were set to standard values in the EnergyPlus model because they were not measured, and it was assumed that they do not have a major impact on heat consumption.

Calibration data

The output data used to calibrate the model is the energy consumed for space heating. The data available was the cumulative district energy consumed, recorded on an hourly basis with a reading resolution of 1 kWh. This resolution does not give the true hourly value as there might be a consumption of 1 kWh spread across several hours. Two different possibilities were investigated to overcome this issue in the calibration: 1) The hourly truncated data were aggregated into larger time resolutions, as in Kristensen et al. (2017); 2) the data were smoothed using a moving average.

The available district heating data was the sum of space heating and domestic hot water. Domestic hot water consumption thus had to be disaggregated from the total. For a daily resolution, the domestic hot water consumption was calibrated assuming the consumption was constant in each day. For an hourly resolution, different approaches were used in an attempt to identify the profile of the consumption during the day: 1) analysing the district heating data measured during the summer when the radiators are switched off; 2) Indoor air relative humidity logged every 5 minutes in the bathroom was used to detect the time of the day when occupants took showers. However, a clear daily pattern could not be seen in summer, and it was not possible to identify a sound correlation between energy consumption peaks and periods with high/peak humidity. This can be explained to some extent by the low reading resolution of the heating energy meter. Therefore, a constant value was assumed

for this study, while a more accurate way to separate the domestic hot water consumption will be the object of future work.

Sensitivity analysis

The calibration of building energy simulation models is an over-parameterized problem where the parameters cannot be uniquely defined. Therefore, it is crucial to reduce the number of parameters to be calibrated. The first task of the study was to identify the set of parameters that drive the majority of the model output variation. The method used was the screening method by Morris (1991), which is the most common screening technique used for sensitivity analysis in relation to calibration of building simulation models (Fabrizio et al. 2015). First, a minimum and maximum value for each input parameter x_i for $i = 1,2,...,k$, where k is the number of parameters included was defined. These ranges were divided into $p=4$ number of points, called levels, equally distant from each other, forming a grid of input parameter values, Ω. The Morris method then employs a random one-at-a-time (OAT) sampling procedure to generate trajectories through Ω with each trajectory comprising $k+1$ random model realisations from Ω. The sampling procedure was repeated for $r=100$ trajectories creating a global set of $r \cdot (k+1)$ building energy models to be simulated. The elementary effect EE_i of each input parameter x_i for every set of $k+1$ models was calculated from the ratio between the variation in output and the variation in input:

$$EE_i = \frac{Y(x_1,...,x_i+\Delta,...,x_k)-Y(x_1,...,x_i,...,x_k)}{\Delta} \quad (1)$$

where $Y(x_1, ..., x_k)$ is the simulation output, in this case the heating demand, and Δ is the distance between each parameter level.

Finally, the influence of each parameter μ_i can be ranked by calculating the absolute mean of the elementary effects following different trajectories (Saltelli et al. 2004):

$$\mu_i = \frac{\sum_{t=1}^{r}|EE_{i,t}|}{r} \quad (2)$$

The chosen values of p and r are aligned with the findings of Petersen et al. (2019) who found that a reliable outcome of deploying the Morris method for SA applied to a high fidelity BEM (like Energy Plus) is generated by choosing $p \geq 4$ and then run simulations for $r \geq 100$.

The selection of the parameters to include in the Morris analysis was made based on literature review and on the quality and reliability of the available building information. The geometric properties of the building were known with high degree of confidence because they were determined from direct measurements and drawings and therefore they were not included. Instead, there was more uncertainty involved with the thermal properties of the building envelope, such as the U-values and the heat storage capacities. Therefore, the sensitivity of the simulation output to the thermal conductivity and to the specific heat of the insulation material of the main structures was analysed. The set of studied parameters was extended with the infiltration flow rate, the solar transmittance of the window glazing, the internal heat gains intensity and the set-point temperature for space heating. The heat gains from lighting and other electrical equipment were combined in one parameter. As mentioned in the previous section, a scalable equipment schedule was estimated from the electricity consumption data, and the maximum intensity was the parameter used for the sensitivity analysis. The level of occupancy outside of working hours was known and the heat gains from occupants were not analyzed in this study. The results obtained are shown in Table 1.

From the assessment of the results of this analysis the parameters with the highest influence are: the conductivity of the external wall insulation, the infiltration rate, the heating set-point temperature and the domestic hot water consumption. These parameters were selected as calibration variables.

Table 1: Results from sensitivity analysis

Parameter	Unit	Minimum	Maximum	μ
Set-point temperature	°C	18	24	2.030
Infiltration flow rate	l/(s·m²)	0.32	1.28	0.544
External wall insulation conductivity	W/(m·K)	0.02	0.07	0.244
Domestic hot water consumption	kWh/h	200	700	0.130
Window glazing solar factor	-	0.30	0.80	0.085
Window glazing conductivity	W/(m·K)	0.03	0.07	0.053
Roof insulation conductivity	W/(m·K)	0.02	0.07	0.052
Internal heat gain maximum intensity	W/m²	0.80	1.50	0.024
External wall specific heat	J/(kg·K)	400	1200	$2.375 \cdot 10^{-3}$
Internal wall specific heat	J/(kg·K)	400	1200	$9.765 \cdot 10^{-5}$

Optimization algorithm

The objective function to be minimized is a goodness-of-fit function which is calculated combining the mean bias error with the coefficient of variation of root mean squared error. The mean bias error (MBE) is calculated from the sum of the differences between the observed and simulated values, normalized by the sum of the observed values, as follows:

$$MBE \ [\%] = \frac{\sum_{t=1}^{T}(y_t - \hat{y}_t)}{\sum_{t=1}^{T} y_t} \cdot 100 \qquad (3)$$

where $\hat{y}_t$ is the simulated output at time step t, y_t is the measured value at time step t, and T is the total number of time steps.

CV(RMSE) is calculated by normalizing the root mean squared error to the mean of the observed values, as in the following equations:

$$CV(RMSE) \ [\%] = \frac{RMSE}{\bar{y}} \cdot 100 \qquad (4)$$

$$RMSE = \sqrt{\frac{\sum_{t=1}^{T}(y_t - \hat{y}_t)^2}{T}} \qquad (5)$$

$$\bar{y} = \sum_{t=1}^{T} \frac{y_t}{T} \qquad (6)$$

The goodness-of-fit function is calculated from a weighted sum of the CV(RMSE) and the MBE.

$$GOF = \sqrt{\frac{w_{CV}^2 CV^2 + w_{MBE}^2 MBE^2}{w_{CV}^2 + w_{MBE}^2}} \qquad (7)$$

where $(w_{cv} + w_{mbe}) = 1$. The ratio between the weighting factors was chosen to be $w_{cv}:w_{mbe} = 1:3$ as in Reddy at al. (2007).

Different algorithms can be applied to minimize the objective function, some of which evaluate the gradient of the objective function, while others are stochastic meta-heuristic methods (Wetter et al. 2004). Based on the assumption of an objective function without discontinuities, a simple gradient descent algorithm was implemented. The variables of each iteration are changed by moving in the direction of the negative of the gradient of the objective function. The step size for moving is proportional to the gradient and to a defined learning rate. Thus, the values are updated using the following equation:

$$x_{i,t} = x_{i,t-1} - \alpha \frac{\delta}{\delta_{x_i}} GOF(x_{1,t-1}, \dots, x_{N,t-1}) \qquad (8)$$

Where $x_{i,t}$ is the value of the variable x_i in the iteration t, α is the learning rate, N is the number of variables and $\frac{\delta}{\delta_{x_i}} GOF(x_i, \dots, x_N)$ is the partial derivative of the objective function with the respect to the calibration variable x_i. Since the analytical gradient calculation was not practicable, an approximate derivative was calculated using finite difference with a proper step size.

Results

The algorithm was run using a training period which extends from the 25th of September 2018 to the 28th of March 2019. The objective function was evaluated using two different dataset: daily aggregated data or hourly data. It was found that after the tenth iteration the GOF function only improved by a negligible amount and therefore the calibration algorithm was run for 10 iterations.

The error indices obtained are shown in Table 2. In addition to MBE and CV(RMSE), the third metrics introduced for model validation is the fit ratio, which is calculated as follows:

$$FIT \ [\%] = \left\{ 1 - \frac{\sqrt{\sum_{t=1}^{T}(y_t - \hat{y}_t)^2}}{\sqrt{\sum_{t=1}^{T}(y_t - \bar{y})^2}} \right\} \cdot 100 \qquad (9)$$

The fit ratio is a measure of the performance of the model compared to a benchmark naive model where the prediction is the mean of the observations. It is positive when the RMSE of the model is lower than the standard deviation, which is the RMSE of the benchmark model.

The results in Table 2 show that the optimization algorithm succeeded in eliminating the mean bias error and in reducing considerably the CV(RMSE).

The measured and simulated energy consumption with a daily and hourly temporal resolution can be observed in Figure 2 and 3, respectively.

The values of the calibration parameters before and after the calibration can be read in Table 3. It can be immediately seen that the solutions obtained do not show a significant variation depending on the temporal aggregation used.

Table 2: Error indices (training dataset)

	Daily data		Hourly data	
	Initial model	Calibrated model	Initial model	Calibrated model
CV(RMSE) [%]	31.99	13.03	43.65	21.47
MBE [%]	- 28.21	- 0.11	- 36.35	0.09
FIT[%]	- 0.06	56.52	- 26.36	37.37
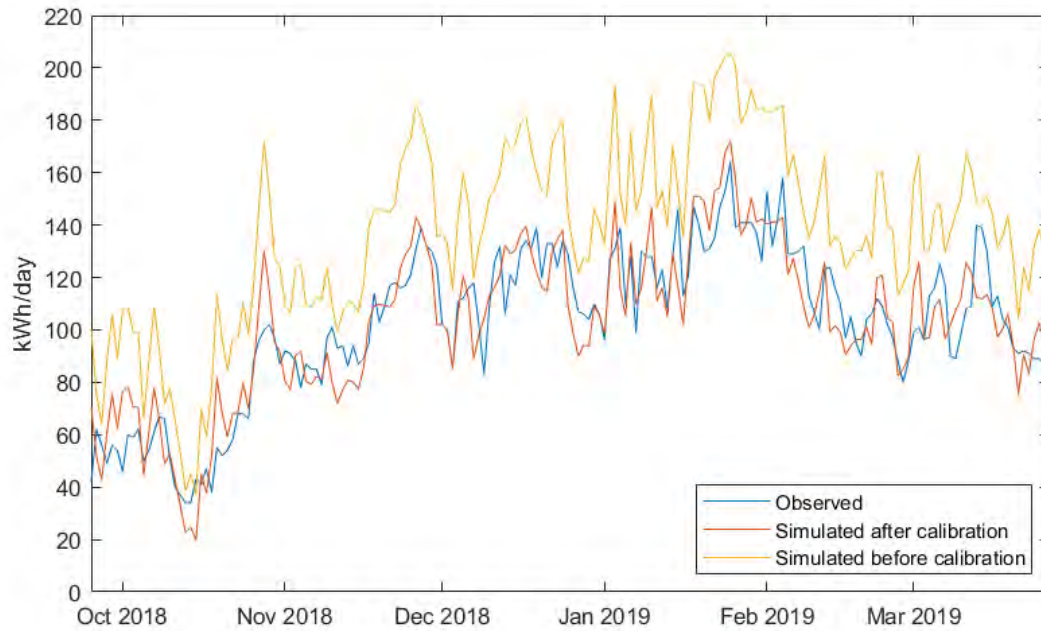
Figure 2: Observed and simulated data with daily resolution (training dataset)
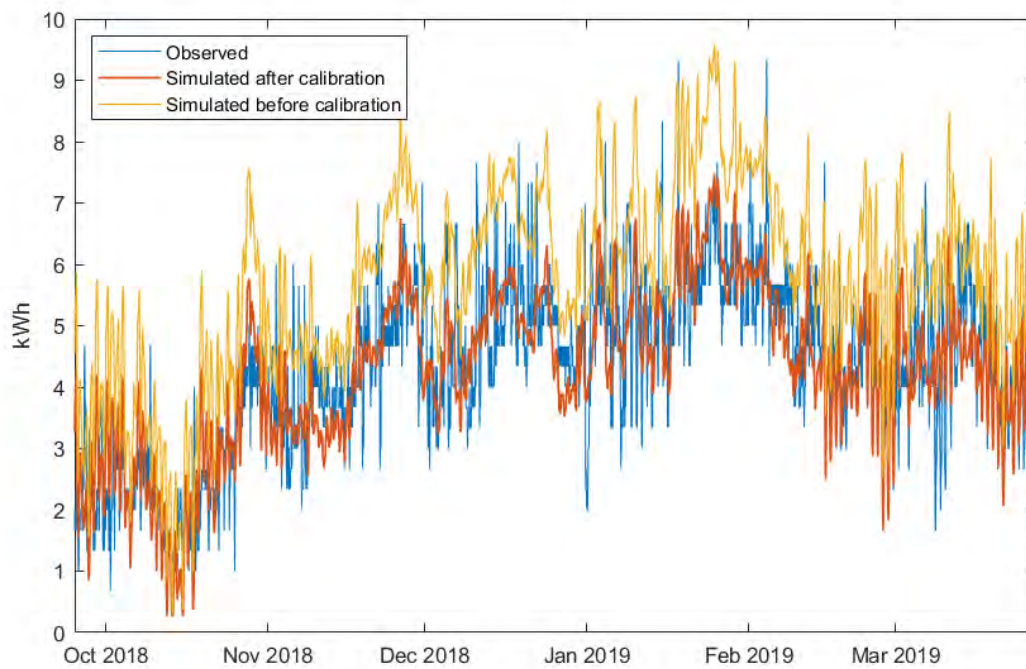
Figure 3: Observed and simulated data with hourly resolution (training dataset)

Table 3: Values of the calibration variables (training dataset)

	Initial model	Calibrated model	
		Daily data	Hourly data
λ_{wall} **[W/mK]**	0.045	0.0424	0.0423
Infiltration [l/(sm^2)]	0.960	0.705	0.704
S.P. temp. [°C]	21.000	19.736	19.750
DHW [kWh/day]	7.200	6.557	6.471
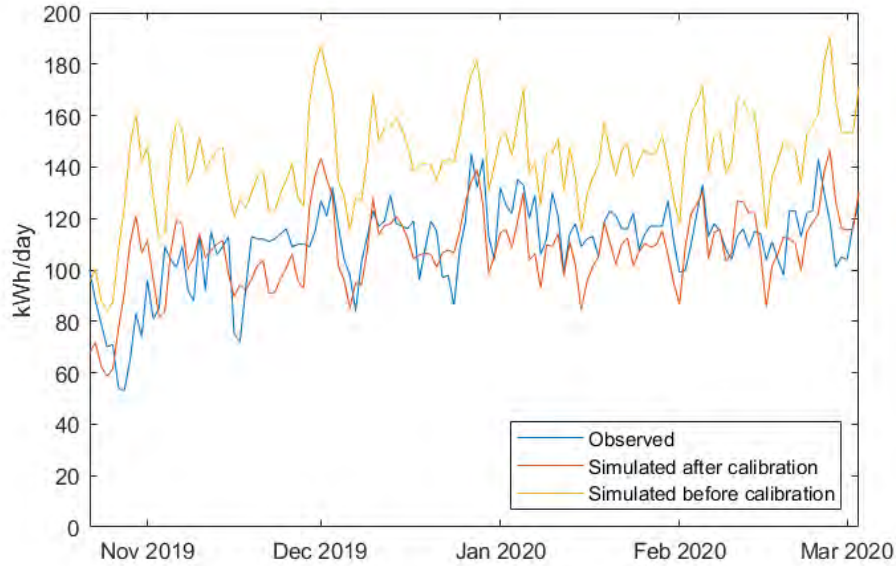
Figure 4: Observed and simulated data with daily resolution (validation dataset)

The robustness of the method was evaluated by testing the performance of the calibrated model with a different dataset. The parameters values estimated on the training dataset were used as input values and a simulation was performed using the data of four months of the heating season 2019/2020, from the 22th of October until the 3rd of March. The set of parameters selected was the one obtained with daily aggregation because it was the one fitting best the training dataset. The model was used to make predictions on a daily basis. The simulation output and the observations are shown in Figure 4 and the statistical indices obtained are summarized in Table 4.

Table 4: Error indices (validation dataset)

	Initial model	Calibrated model
CV(RMSE) [%]	36.54	13.97
MBE [%]	- 26.19	2.04
FIT[%]	- 127.49	12.46

The residuals normalized by the maximum value of the observations are plotted in Figure 5 and in Figure 6 as a function of the outdoor temperature and of the solar radiation rate transmitted through the window. The residuals are positively correlated with the outdoor temperature (the correlation coefficient calculated is 0.46), while there is a negative correlation with the solar radiation (the correlation coefficient is -0.49).
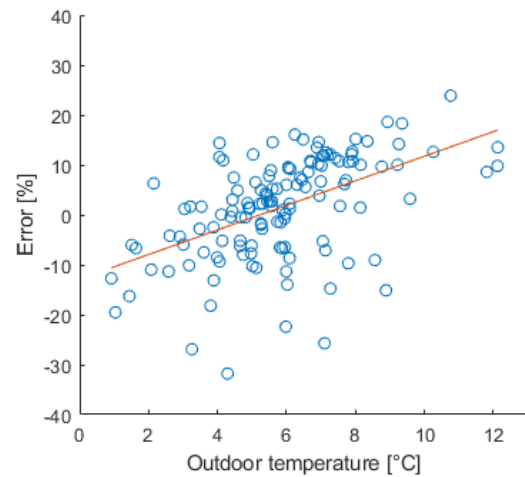
Figure 5: Residuals as a function of the outdoor temperature (validation dataset)
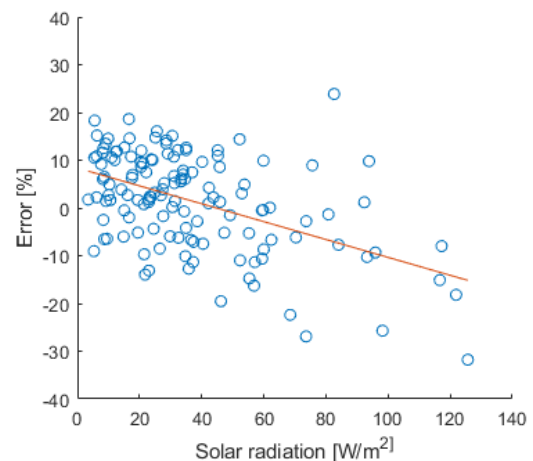
Figure 6: Residuals as a function of the solar radiation (validation dataset)

Discussion

From the assessment of the statistical indices of the residuals and of the final parameters values several considerations can be made about the calibration process.

As expected, the simulation error increases with the temporal resolution because of the larger dataset to fit and because of the significant noise present in the hourly data. Furthermore, there is more uncertainty involved with hourly data because a profile for the domestic hot water consumed during the day was not defined. However, the final values of the calibration variables obtained using different temporal aggregations do not differ significantly from each other.

The energy consumption of the initial model was higher than the measurements. The positive mean bias error was removed by the algorithm by choosing a lower insulation conductivity, infiltration rate, temperature set-point and domestic hot water consumption. Despite that, the final values are still comparable with the initial guesses, that were based on prior information. This demonstrates that the building descriptions and the initial assumptions were valid to some extent.

The calibration parameters were tuned to minimize the discrepancy between the simulation output and the training dataset. However, the goal of a building energy model is the ability to predict the system behaviour under any unseen condition. Although the model performance is reduced on the validation data compared to the training data, the performance is still signicantly better than the one of the not calibrated model. Nevertheless, the mild correlation between residuals and outdoor temperature and solar radiation suggests that the model does not perfectly describe how these inputs relate to the output.

Conclusion

The aim of this paper was to develop and test a calibration method for a single-family house using district heating data. The approach implemented was a calibration algorithm based on numerical optimization. The calibration was performed on a training dataset of six months and the performance of the calibrated model was tested on a different dataset of four months. The validation of the model was based on the assessment of the mean bias error and of the normalized root mean square error on a different dataset.

The calibration method significantly improved the performance of the uncalibrated model both on the training and on the validation dataset. Furthermore, the parameters estimated were not strongly affected to changes in temporal resolution of the calibration data.

Several challenges and possible improvements have been identified for future work. The study has highlighted the limits of the calibration data due to the truncation and to the indeterminacy of the share of domestic hot water in the total energy consumption, especially on an hourly level. The issue could be solved in future studies by utilizing meters with higher reading resolution and separate sensors for the domestic hot water circuit.

Furthermore, there is a level of uncertainty involved with the estimated values of the calibration parameters, because a solution that yields to a good model fit could be a local optimum (Reddy et al. 2007). The optimization algorithm implemented could be improved and used in combination with other algorithms in order to ensure the convergence to a unique optimal solution.

Finally, since the simulation error is correlated to the weather input data even after the calibration, the model could be further improved by extending or modifying the set of calibration parameters (for example including the glazing solar factor).

Acknowledgement

References

Asadi, S., E. Mostavi, D. Boussaa, and M. Indaganti (2019). Building energy model calibration using automated optimization-based algorithm. *Energy & Buildings 198*, 106-114.

Coakley, D., P. Raftery, and M. Keane (2014). A review of methods to match building energy simulation models to measured data. *Renewables and Sustainable Energy Reviews 37,* 123-141.

Coakley, D., P.Raftery, P. Molloy, and G.White (2011). Calibration of a detailed BES model to measured data using an evidence-based analytical optimisation approach. *Proceedings of Building Simulation 2011: 12th Conference of International Building Performance Simulation Association* Sydney (Australia), 14-16 November 2011.

Crawley, D.B., and L.K. Lawrie (2001). EnergyPlus: creating a new-generation building energy simulation program. *Energy and Buildings 33,* 319-331.

Fabrizio, E. and V. Monetti (2015). Methodologies and advancements in the calibration of building energy models. *Energies 8*, 2548-2574.

Kristensen, M.H., R. Choudhary, S. Petersen. (2017) Bayesian calibration of building energy models: Comparison of predictive accuracy using metered utility data of different temporal resolution. *Energy Procedia 122,* 277-282.

Martínez, S., P. Eguía, E. Granada, A. Moazami and M.Hamdy (2020). A performance comparison of multi-objective optimization-based approaches for

calibrating white-box building energy models. *Energy & Buildings 216.*

Monetti, V., E. Davin, E. Fabrizio, P. Andre, and M. Filippi (2015). Calibration of building energy simulation models based on optimization: a case study. *Energy Procedia 78*, 2971-2976.

Morris, M.D. (1991). Factorial sampling plans for preliminary computational experiments. *Technometrics 33* (2), 161–174.

Petersen S. and Hviid C.A. (2012) The European Energy Performance of Buildings Directive: Comparison of calculated and actual energy use in a Danish office building. *1st IBPSA-England Conference*. Loughborough (England), 2012.

Petersen S., M.H. Kristensen, and M.D. Knudsen (2019). Prerequisites for reliable sensitivity analysis of a high fidelity building energy model. *Energy and Buildings* 183, 1-16.

Saltelli, A., S. Tarantola, F. Campolongo and M. Ratto (2004). *Sensitivity analysis in practice : A guide to assessing scientific models*. John Wiley & Sons Ltd. West Sussex (England).

Sun, J. and T.A. Reddy (2006). Calibration of building energy simulation programs using the analytic optimization approach. *HVAC & Research* 12:1, 177–196.

Reddy, T.A., I. Maor, and C. Panjapornpon (2007). Calibrating detailed building energy simulation programs with measured data – part I: General methodology. *HVAC & Research* 13:2, 221–341.

Wetter, M. and J. Wright (2004). A comparison of deterministic and probabilistic optimization algorithms for nonsmooth simulation-based optimization. *Building and Environment 39,* 989-999

Wetter, M. (2016). *GenOpt User Manual Version 3.1.1.* Lawrence Berkeley National Laboratory.

Yang, T., Y. Pan, J. Mao, Y. Wang, and Z. Huang (2016). An automated optimization method for calibrating building energy simulation models with measured data: Orientation and a case study. *Applied Energy* 179, 1220–1231

ASHRAE. *Guideline 14-2002: Measurement of energy and demand savings.* Atlanta: American Society of Heating, Refrigerating and Air-Conditioning Engineers; 2002

Identifying grey-box models of Norwegian apartment block archetypes

Marius Bagle[1*], Harald Taxt Walnum[1], Igor Sartori[1]

[1]SINTEF Community, Oslo, Norway

corresponding author: marius.bagle@sintef.no

Abstract

Identification of grey-box models to describe the heat dynamics of buildings is treated extensively in literature, However, to identify these models, data from controlled heating experiments is needed, which is not feasible in many cases. In this work, the aim is to overcome this threshold by using datasets from simulations of detailed white-box models to identify the grey-box models. Given that the white-box models are validated and calibrated against real measurement data, the need for real measurement data is bypassed, thus enabling the use of grey-box models identified from simulation data in real - world predictive controllers. The results show that a three-state grey-box model is able to capture the heat dynamics of the white-box model over a time period of ~1 week in the summer months.

Introduction

A potentially large amount of flexibility resides in the space heating of residential buildings. To realize this potential, it is necessary to model heat demand with models that are accurate enough and suitable for real time control. Purely physical (white-box) models are ill-suited for the purpose due to the level of detail required, the high uncertainties associated with knowledge of key technical parameters and the difficulty to treat non-technical features such as user behavior. Well-suited for this purpose are grey-box models, which combine a relatively simple physical descriptions of the building with data-driven inference of key parameters. In (Xingji Y., Laurent, & Sartori, 2019), the validation performance of grey-box models based on physical knowledge of buildings and grey-box models extracted from technical standards are compared. In (Walnum, Sartori, & Lindberg, 2019), a backward selection procedure is used; by removing elements in the model and testing the different permutations in validation. In both papers, measurement data from a controlled heating experiment on a real building is used. This is the challenge with grey-box models. In addition to energy use and weather data, the indoor temperature should also be known, with the same hourly or sub-hourly resolution. Such data are scarcely available in most cases. Furthermore, it is not given that measurements from normal operation of buildings provide datasets that are 'rich' enough (containing enough statistical variability) to successfully drive the identification process. In (Sourbron, Verhelst, & Helsen, 2012), the authors conclude that the building

control system should cause sufficient excitation of the building components whenever possible in test periods. This paper presents a method that aims at overcoming this bottleneck by combining features of both white-box and grey-box modelling. A set of white-box models (specifically, IDA-ICE models) representing the Norwegian stock of apartment blocks is available, based on ca. 20 archetypes previously developed in the TABULA/EPISCOPE project (Rønneseth & Sartori, 2018). Validation of the hourly load profiles of such archetypes against a large dataset of measurements is undergoing in a parallel research activity. Provided that load profiles are validated, it is legitimate to assume that the indoor temperature profiles from the IDA-ICE archetypes are also representative for the real building stock. Under this assumption, the grey-box models can be identified from simulation of the archetypes. A Pseudo Random Binary Sequence (PRBS), aiming at exploring a wide and rapidly changing set of indoor temperatures around the comfort zone, is applied as the control signal for the heating system. Finally, validation of the identified models will focus on short term predictions (one day to one week) as this is the typical range of control horizon for predictive controllers.

Methods

For the model identification process, datasets from IDA-ICE simulations, using archetype models of Norwegian apartment blocks is used. Datasets from twenty-one variations of eight archetypes have been made available through a parallel activity in ZEN.

Table 1. Overview of archetypes.

Name	Building year	# of floors/apartments	Floor area [m²]
AB_01	< 1956	4 / 8	557
AB_02	1956-1970	4 / 16	1115
AB_03	1971-1980	4 / 24	1672
AB_04	1981-1990	4 / 24	1672
AB_05	1991-2000	4 / 24	1672
AB_06	2001-2010	4 / 24	1672
AB_07	2011-2020	4 / 24	1672
AB_08	>2020	4 / 24	1672

Each archetype is a representative apartment block from each decade, with the exception of "AB_01", which represents apartment blocks built before 1956, and "AB_08", representing the passive house standard. The building standard (most importantly, the insulation) improves as the buildings get newer. Table 1 summarizes the archetypes.

Figure 1 shows the standard layout of the archetypes as they are modelled in IDA-ICE. A common method used when modelling multi-story buildings is to use a three-story building, with multipliers for the middle zones. This reduces both modelling and simulation time, without sacrificing accuracy in the results. Each apartment consists of three zones: living room, bedroom and bathroom (Rønneseth & Sartori, 2018). However, because the controlled heating input in the living room and bedroom is waterborne (district heating), and the bathroom is equipped with electric floor heating, the bathroom is disregarded. To find a representative temperature for the apartment block, a weighted average of the temperatures is taken, with the temperatures on the middle floor weighted by 2, since we are dealing with 4 floors.
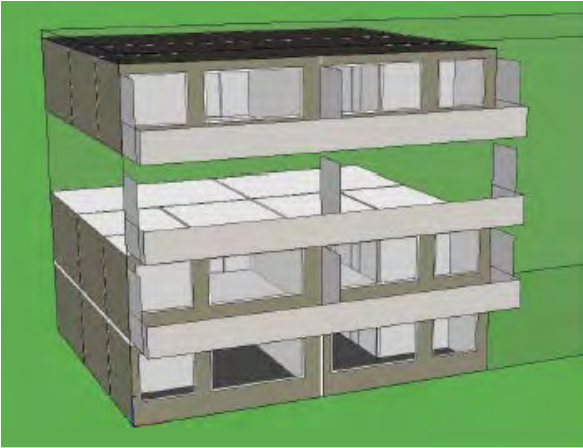
Figure 1. Apartment block layout in IDA-ICE (Rønneseth & Sartori, 2018)*.*

The IDA-ICE simulations are done for a typical meteorological year (TMY) (Renné, 2016), with a Pseudo-random binary signal (PRBS) applied to the heating control system. The signal is applied from the 1st to the 20th in every month of the year. One issue with the signal is that it is applied to the zone-level heaters in the IDA-ICE models, while there still is a weather compensation curve modulating the supply temperature of the waterborne heating system. Thus, the signal is not a true PRBS, since the heating power has a certain dependancy on the outdoor temperature. Figure 2 shows the extracted dataset for "AB_03" in May. We see that the indoor temperature yTi is allowed to deviate substantially from normal comfort limits.
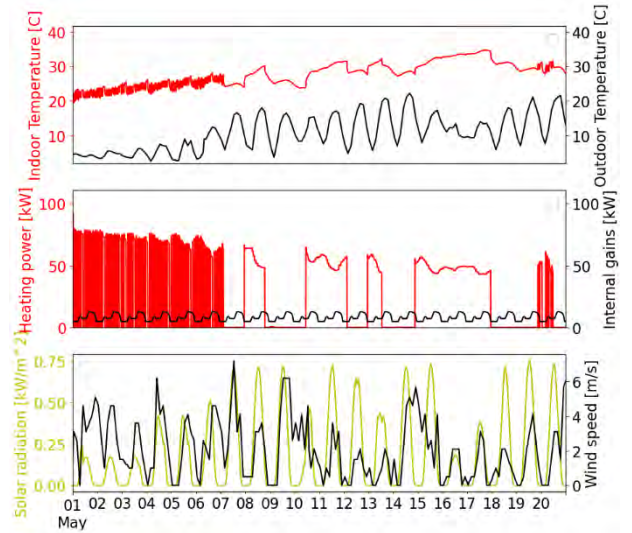
Figure 2. Example input dataset.

To identify suitable models from the data, the forward selection procedure in (Bacher & Madsen, 2011), which uses maximum likelihood estimation, is employed. Consider a series of measurements:

$$Y_n = [y_n, y_{n-1}, \ldots, y_1, y_0] \qquad (1)$$

The likelihood function is the joint probability density:

$$L(\theta; Y_n) = p(Y_n|\theta) \qquad (2)$$

where θ is the vector of model parameters. Another way to write this is:

$$L(\theta; Y_n) = \left(\prod_{k=1}^{N} p(Y_k|Y_{k-1}, \theta) \right) p(Y_0|\theta) \qquad (3)$$

i.e. as a product of conditional densities, with $p(Y_0|\theta)$ as a parameterization of the starting conditions (Kristensen, Madsen, & Jørgensen, 2004). The set of parameters $\hat{\theta}$ that maximizes the likelihood of the model is then found by solving to the optimization problem:

$$\hat{\theta} = arg \max_{\theta}\{ L(\theta; Y_N)\} \qquad (4)$$

The software CTSM-R, developed at DTU, is used to identify the models. CTSM-R, or Continuous Stochastic Time Modelling in R, is an R package providing a framework for identifying and estimating stochastic grey-box models. A grey-box model consists of a set of stochastic differential equations coupled with a set of discrete time observation equations, which describe the dynamics of a physical system and how it is observed. The grey-box models can include both system and measurement noise, and both nonlinear and nonstationary systems can be modelled using CTSM-R . Internally, it uses an extended Kalman filter to set up the conditional densities from the parametrized initial conditions, and a quasi-Newton method for solving the optmization problem (Madsen, 2018). An issue with gradient-based methods in general is that it finds a local optimum, i.e., there is no guarantee that the solution found is the most optimal on the entire parameter space.

A forward selection process is employed by utilizing a statistical test, in which each model considered is a subset of a larger model (Bacher & Madsen, 2011). The starting point for the procedure is the smallest feasible model, and possible improvements are added successively until the maximum amount of information is extracted from the data. The criteria for this is a statistical testing procedure involving likelihood-ratio tests: when the p-value is below a certain limit (e.g. 0.05, which corresponds to a 95 %-confidence level), the more complex model is selected in favor of the simpler model. If no additions yield a p-value below the limit, we have found a sufficient model. We start the selection procedure with the smallest feasible model:

Figure 3. Model Ti

$$dT_i = \frac{1}{R_{ia}C_i}(T_a - T_i)dt + \frac{1}{C_i}(P_s + P_h + P_{int})dt + \sigma_i d\omega_i \quad (5)$$

$$Y_k = T_{i,k} + e_i \quad (6)$$

with descriptions of the variables and parameters listed below. Since we are dealing with mathematical models, it is most accurate to characterize the descri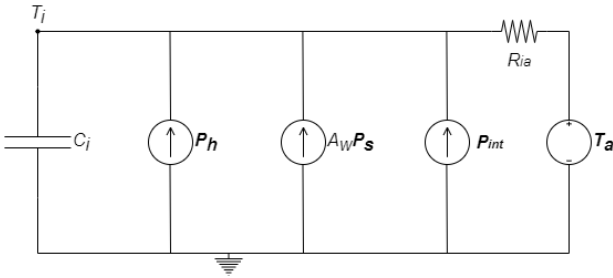ptions as *interpretations* in the case of parameters found with maximum likelihood estimation. The physical meaning for the same parameter will change as the model order increases (Bacher & Madsen, 2011):

T_i – Indoor air temperature

T_a – Outdoor temperature

C_i – Thermal capacitance of interior

R_{ia} – Thermal resistance from interior to ambient

A_w – Effective window area

σ_i – Variance of the Wiener (stochastic) process

Following the example of (Bacher & Madsen, 2011), states to add in the forward selection process are T_m and T_e. They represent the temperature of the heat transportation medium and building envelope respectively. For conciseness,
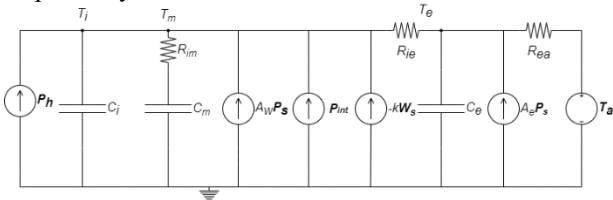
Figure 4. Model TiTeTmAeWs

only the equations and circuit diagram for the complete model *TiTeTmAeWs* are shown here. These two additional states result in two additional state equations. Furthermore, a renaming of the resistance associated with the interior from R_{ia} (directly from interior to ambient) to R_{ie} (from interior to envelope) is necessary, as well as substituting T_a with T_e in equation 5:

$$dT_i = \frac{1}{R_{ie}C_i}(T_e - T_i)dt + \frac{1}{R_{im}C_i}(T_m - T_i)dt$$
$$+ \frac{1}{C_i}(P_s + P_h + P_{int} - k * Ws)dt + \sigma_i d\omega_i \quad (7)$$

$$dT_m = \frac{1}{R_{im}C_m}(T_i - T_m) + \sigma_m d\omega_m \quad (8)$$

$$dT_e = \frac{1}{R_{ie}C_e}(T_i - T_e)dt + \frac{1}{R_{ea}C_e}(T_a - T_e)dt + \sigma_e d\omega_e \quad (9)$$

where the added parameters are:

T_e - Envelope temperature

T_m – Medium temperature

R_{ie} - Thermal resistance from interior to envelope

R_{ea} - Thermal resistance from envelope to ambient

R_{im} – Thermal resistance from interior to medium

C_m – Thermal capacitance of medium

C_e - Thermal capacitance for the envelope

σ_e – Wiener process variance for T_e

σ_m – Wiener process variance for T_m

k – Wind heat transmission coefficient [unit: $\frac{K*s}{kWh*m}$]

Generally, the grey-box models considered in this work can be expressed as continuous, stochastic state-space matrix equations. This can be written as:

$$d\mathbf{T} = \mathbf{A}\mathbf{T}dt + \mathbf{B}\mathbf{U}dt + \mathbf{E}\mathbf{V}dt + d\boldsymbol{\omega} \quad (10)$$

where $\mathbf{T}$ is the temperature state vector, $\mathbf{U}$ is the controllable input vector, and the transition matrices $\mathbf{A}$ and $\mathbf{B}$ consist of simple parameters only to preserve model linearity. This also applies to the matrix $\mathbf{E}$, which contains the coefficients for the disturbance vector $\mathbf{V}$, where uncontrolled heating inputs are lumped. The term $d\boldsymbol{\omega}$ represents the stochastic part of the model, which is represented by the Wiener process.

After model identification and p-value testing, models are validated using datasets from normal operation, i.e. the heating control system trying to maintain a constant set-point temperature (no nighttime setback). Figure 5 shows the entire model identification process, from IDA-ICE simulation to validation of the models. Processes are colored green, data is colored light blue, and decisions purple. Notice the stippled lines around the IDA-ICE simulation with PRBS-signals, which is an ongoing parallel research activity.

Figure 5. Flowchart of the model identification process.

Results

Due to the large number of archetypes and models that have been investigated in the work leading up to this paper, the presentation of results will be limited to the archetype "AB_03" variant 2 for space considerations (apartment block from the seventies, windows changed, renovated). We consider this to be a good representation of the "average" apartment block in the Norwegian building stock. Furthermore, of all the models identified, the ones from the training dat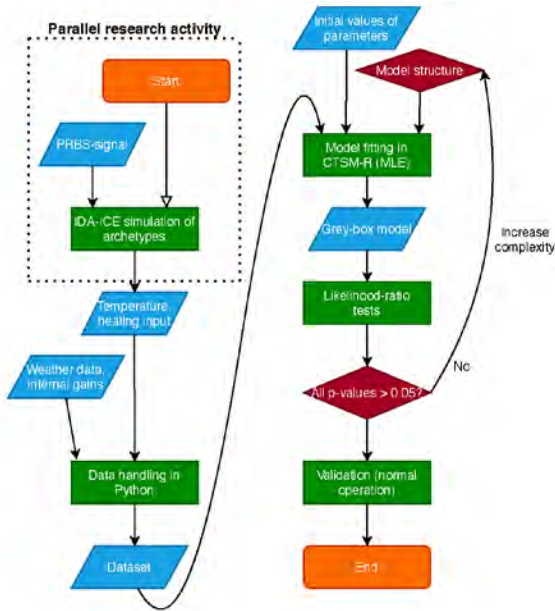aset in May are presented, since this month has the most variability with regard to solar radiation and outdoor temperature. For validation, the models identified in CTSM-R, which are continuous time state-space models, are discretized in accordance with the time step of the of the dataset used for training (5 min). First, we consider the results from the p-value test.

Table 2. Forward selection, AB_03 var 2, May

Iteration		Models		
0		*Ti*		
# params		6		
$l(\theta; Y_n)$		389.22		
1	*TiTe*	*TiTm*	*TiAe*	*TiWs*
# params	10	10	n.a.	7
$l(\theta; Y_n)$	1769.12	1773.16	n.a.	389.22
p-value	0	0	n.a.	0.29
2	*TiTeTm*	*TiTeWs*		*TiTeAe*
# params	14	11		11
$l(\theta; Y_n)$	1828.35	1765.28		1470.86
p-value	0	1		1
3	*TiTeTmWs*		*TiTeTmAe*	
# params	15		15	
$l(\theta; Y_n)$	1828.35		1829.27 (?)	
p-value	1		0.17	
4		*TiTeTmAeWs*		
# params		16		
$l(\theta; Y_n)$		1829.27		
p-value		1		

For the May dataset, the p-value test suggests both *TiTe* and *TiTm* as improvements on the one-state model *Ti*, with a p-value of 0 for both. This signifies that the models describe the data significantly better than the one-state model. Since *TiTm* has a slightly higher log-likelihood, this is the model selected in the first iteration. The model with wind speed (**Ws**) added as a disturbance generator does not yield any improvement on the log-likelihood, hence this model is dropped and the extension saved for later. In the next iteration, the only model that yields any improvement is the three-state model *TiTeTm*. The other extensions actually yield lower log-likelihoods than the best models in the previous iteration.

In the third iteration, the extensions **Ae** (splitting of solar gains in internal and envelope parts) and **Ws** do not yield any significant improvements over *TiTeTm*. Strictly speaking, the model selection process should end here, but for completeness, we try fitting the full model. It has the same log-likelihood as *TiTeTmAe*, thus, there is no improvement. Hence, the model selection process is finished, with *TiTeTm* as the "winner".
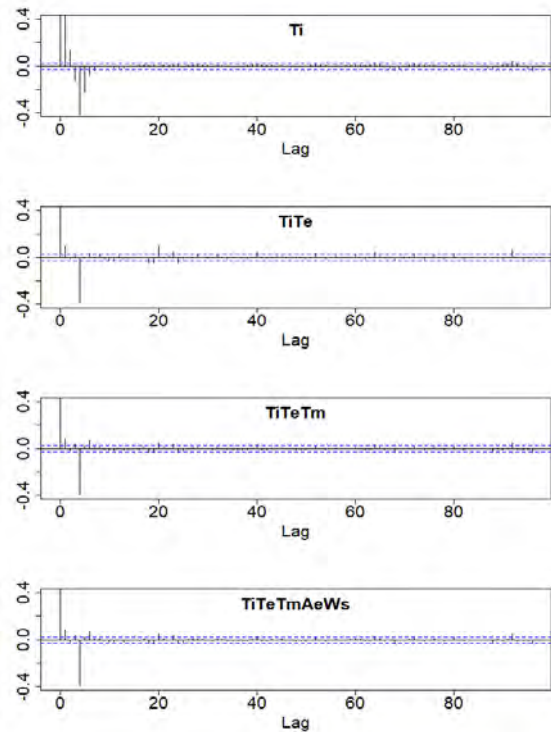
Figure 6. ACF of the residuals

To investigate the assumption of white-noise residuals (effects not captured by the model are uncorrelated and identically and independently distributed), we look at the autocorrelation function of the residuals. It shows the correlation of the residuals $(Y - \hat{Y})$ in the time domain. For this assumption to hold with a 95 % confidence level, ca. 19 of 20 lags have to be inside the blue line in the plots.

Figure 6 shows the autocorrelation of the residuals for a selection of the models considered in the forward selection process. For the one-state model, *Ti*, visual inspection of the ACF-plot tells us that at least 7 out of the

96 lags shown in the plot is outside the 95 % confidence interval, thus, the model does not describe the heat dynamics of the apartment block sufficiently. For the two-state-model, *TiTe,* the lags from timestep zero to seven are dampened, but there is an emergence of lags around timestep 20 that was not present in the previous model. Counting the lags yields 5 terms outside the confidence interval. Hence, this model is also insufficient for describing the heat dynamics. The next model, *TiTeTm,* shows a dampening of the lags around timestep 20, and they appear now to be within the confidence band, and we have three lags outside it. This means that the white-noise assumption on the residuals holds. The complete model, *TiTeTmAeWs,* shows no improvement, and it can be concluded that judging by the autocorrelation plots, the model *TiTeTm* is a sufficient model.

To test the prediction performance of the models identified, we look at the open-loop out-of-sample predictions for a selection of the models (*TiTe, TiTe, TiTeTm*). The validation datasets contain data for normal operation of the heating system, i.e. keeping the zones at a constant 20 degrees Celsius (there is no nighttime lowering of the temperature). In order to get a reasonable estimate of the hidden states (in our case, T_m and T_e), a one-step ahead prediction, where the correct ("measured") temperature is fed back to the model, is run for 48 hours immediately preceding the week selected for open-loop prediction. This should give a better estimate of the hidden states than the naïve approach of simply setting them equal to the value of T_i at the start of the validation period.
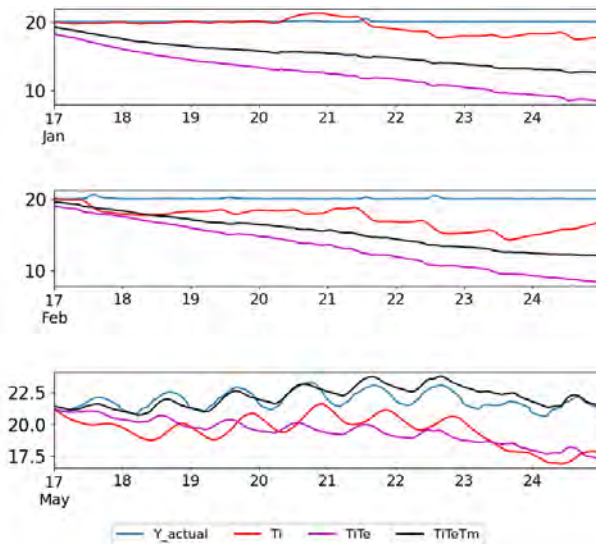
Figure 7. Validation, May models (Jan., Feb., May)

Figure 7 shows the prediction open-loop prediction of the models *Ti, TiTe, TiTeTm* and *TiTeTmAeWs* identified with PRBS-operation in May on validation datasets with normal operation in January, February and May. From the plots, it can be seen that the models generally fails in the winter months of January and February. An exception here is the one-state model *Ti*, which manages to track the actual temperature for almost 4 days. This may be due to

the total capacitance being smaller than for the other models (see table 2.), i.e. needing less heat to maintain the set-point temperature. In addition, the effective window area estimated for *Ti* is on the smaller side, at 11.25 m^2, which makes gives the solar gains relatively little importance in the model, making it more consistent with the moderate solar radiation in January. We see the same trend in February, *Ti* tracks the set-point temperature best, but here there is drop-off after 12 hours, and although the model recovers somewhat, there is a persistent offset of at least 1 degree Celsius. For validation in May, the predictions from *TiTeTm* follows the actual temperature for 4 days, which has to be considered good prediction performance in this context.
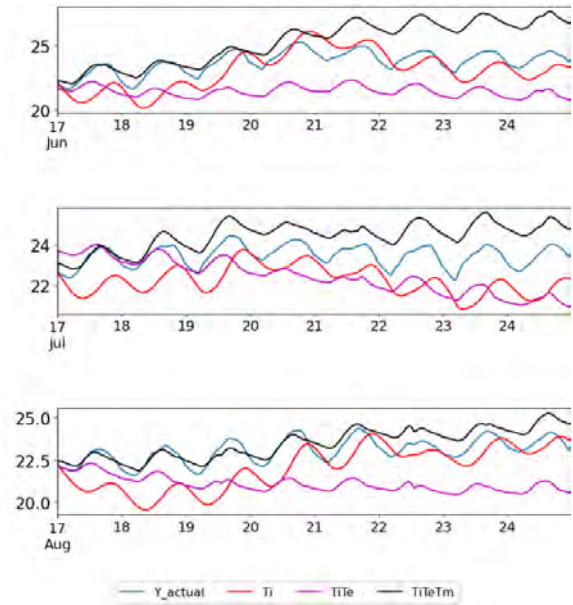
Figure 8. Validation, May models (June, July, Aug.)

Figure 8 shows the open-loop predictions of models identified in May on validation datasets in June, July and August. It can immediately be seen that prediction performance is better in these months than in the winter months. The model *TiTeTm* again appears to have to best performance, although there is an issue with the initial conditions. The temperature (of the interior, "measured") jumps up immediately after the first time step, which signifies that the estimation of the initial values of the hidden states is too high. We can interpret this as one or more of the hidden states having a biased energy balance. Indeed, by looking at table 3, it is seen that the estimated initial value of the medium temperature, T_{m0}, is estimated to -24.6 °C for both the complete model and *TiTeTm*. This is clearly a non-physical situation; the heat transportation medium should not have a temperature that is higher than the envelope. According to (Coninck, Magnusson, Åkesson, & Helsen, 2016), this is a situation in which numerical optimality should be balanced against models with parameters that make sense physically. A less optimal in the numerical sense, i.e. a model with a lower log-likelihood, can be a more beneficial model for prediction and forecasting, given that it has sensible

parameters, not necessarily in the absolute numbers, but at least in relative terms. This non-physicality can also be inferred from the estimated time constants and UA-values[W/°Cm^2]: the time constant of the envelope ranges from 137 to 218 hours as different topologies are considered, and the UA-values range from 0.83 to 7.88. Searching the entire parameter space for both numerically feasible and physically sensible models with a gradient-based method is not a trivial task, and no attempt to solve this in a systematic fashion has been undertaken in this work.

Table 3. Model parameters, identification May

Parameters	*TiTeTmAeWs*	*TiTeTm*	*TiTe*	*Ti*
T_{i0} [°C]	19.39	19.39	19.37	25.47
T_{e0} [°C]	20.08	20.14	19.30	n.a.
T_{m0} [°C]	-24.60	-24.59	n.a.	n.a.
C_i kWh/°C]	8.20	8.27	5.04	75.16
C_e [kWh/°C]	1024	488.3	2939	n.a.
C_m [kWh/°C]	0.30	0.33	n.a.	n.a.
R_{ie} [°C/kW]	0.013	0.013	0.015	*0.49
R_{im}[°C/kW]	0.58	0.55	n.a.	n.a.
R_{ea}[°C/kW]	0.18	0.28	0.075	n.a.
A_w[m^2]	89.39	102.52	81.76	11.25
A_e [m^2]	178.0	n.a.	n.a.	n.a.
e_i	-5.60	-5.61	-16.3	-25.5
σ_i	-8.35	-8.35	-0.63	-0.90
σ_m	3.71	3.66	n.a.	n.a.
σ_e	-0.98	-1.01	-0.72	n.a.
τ_1 [h]	0.102	0.102	0.074	36.99
τ_2[h]	0.184	0.192	n.a.	n.a.
τ_3 [h]	181.06	137.66	218.4	n.a.
C_{tot} [kWh/°C]	1033	496.9	2944	75.16
UA [W/°Cm^2]	0.905	0.835	7.88	1.42

We consider instead models identified in September, which yielded more consistent results. Figure 9 shows the open-loop predictions on the same validation datasets as Figure 8. The prediction performance of *TiTe* especially is improved. Furthermore, the performance of the three-state model *TiTeTm* is also improved, with a closer tracking of the actual temperature in the timeframes where the May models showed satisfactory performance , and a decreased tencency to diverge towards the end of the weeks.

Table 4 shows the time constants and UA-values for a selection of the models identified on the September dataset. The consistency across the model topologies is a significant improvement on the models identified on the May dataset. . The UA-value lies between 1.51 and 1.64, values that can be considered reasonable. The smallest
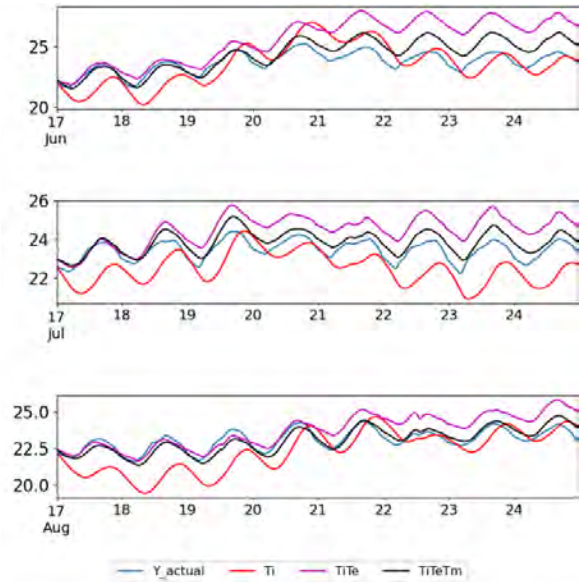
Figure 9. Validation, Sept. models (June, July, Aug.)

time constant is right around the sampling time of 0.0833 hours in the topologies with more than one state. This makes sense, as this is the smallest timeframe in which any dynamics can be captured by the model. If a sampling time of one hour were to be used instead, a small time constant of around 1 hour would be seen instead.

Table 4. Essential model parameters, identification September

Parameters	*TiTeTmAeWs*	*TiTeTm*	*TiTe*	*Ti*
τ_1 [h]	0.073	0.061	0.101	32.84
τ_2 [h]	3.31	2.61	n.a.	n.a.
τ_3 [h]	131.32	125.5	90.78	n.a.
UA [W/°Cm^2]	1.51	1.52	1.64	1.53

Comparing identification results across archetypes is another indicator of the consistency of the results. Due to issues with opitmizer convergence and time limits, this exercise has been limited to the archetypes AB01.5 (old building, renovated windows), AB03, AB07 and AB08 in this work. Table 5 shows the results. There is a difference in how the resistances and capacitances are handled, e.g. for AB_01, the resistances are higher than for AB_07 (which corresponds to TEK10) and AB_08 (passive house standard). On the other hand, if the capacitances are taken into account, the results make more sense. As the building standard increases, the time constants increase. This is in line with the expected: because of better insulation in the walls, there is a larger tendency for the heat to remain in the envelope. As for the UA-value, it decreases in accordance with the building standard, with the exception of AB_03, where it increases.

Table 5. Model parameters across archetypes, TiTe, May dataset

Parameters	AB01.5	AB03	AB07	AB08
T_{i0}[°C]	19.24	19.37	21.16	21.79
T_{e0}[°C]	19.12	19.30	21.11	21.76
C_i [kWh/°C]	1.70	5.04	20.15	26.04
C_e [kWh/°C]	310.8	2939	755.0	892.7
R_{ie} [°C/kW]	0.036	0.015	0.005	0.0045
R_{ea}[°C/kW]	0.39	0.074	0.30	0.39
A_w[m^2]	176.62	81.76	164.8	162.4
e_i	-17.51	-16.28	-8.73	-9.13
σ_i	-0.83	-0.63	-9.83	-10.10
σ_e	-1.04	-0.72	-1.69	-1.74
τ_1 [h]	0.608	0.074	0.104	0.113
τ_2 [h]	122.1	218.4	233.0	355.0
UA [W/°Cm^2]	4.93	7.88	2.33	1.79

Table 6. Estimated/reported parameters (IDA-ICE)

Parameters	AB01.5	AB03	AB07	AB08
C_i [kWh/°C]	0.5	1.5	1.5	1.5
C_e [kWh/°C]	60	160	160	160
UA [W/°Cm^2]	0.98	0.51	0.39	0.25
τ_2 [h] (apprx.)	120	188	246	380

To compare the parameters obtained through model identification in CTSM-R with the parameters of the IDA-ICE models, some assumptions are necessary. Although reports of the simulation models are available, they do not contain any information about the thermal capacity of the apartment blocks. To alleviate this, we use (Standard Norge, 2014) to get approximate values for the capacitances. Assuming a relatively heavy building (100 Wh/Km^2), and a ceiling height of 2.7 m, the envelope thermal capacity can be calculated. The thermal capacity of the interior is more straightforward, taking 0.342 Wh/m^{3}K as the specific heat capacity of air at 15 °C (Dixon, 2007; Jones, 1978). The per floor area normalized heat transfer coefficient UA is found from simulation reports in IDA-ICE. If it is assumed that the most of the thermal resistance is connected to the envelope, an approximation of the long time constant can be found by multiplying the envelope capacitance and the total thermal resistance (inverse of the UA-value), since these are the parameters that dominates the dynamics of the system at low frequencies. Table 6 shows the results of this estimation. As can be seen from the table, both the capacitances and the UA-values are overestimated by a significant margin. However, the time constants are quite close, which means that the overestimation of the capacitances and the underestimation of the resistances balance each other out to yield a seemingly good estimate of the time constants, and hence the heat dynamics of the buildings. Nevertheless, it must be kept in mind that the values we are comparing the estimated model parameters to are estimates themselves, so further investigation into the possibility for a more thourough reporting of the IDA-ICE model is needed.

Discussion

The results from the model identification are varied. For some validation datasets, the open-loop prediction performance may be regarded as sufficiently adequate for MPC application purposes (with prediction horizon typically from one to few days, and actuation of only 1-step ahead control signal in closed loop). This is generally in the months with little to no controllable heat input (summer months). In the winter months, however, only the single-state model *Ti* is able to track the actual temperature. An explanation could be that the indoor temperature – from the IDA ICE archetypes – in these months is almost constant, which is an unrealistic situation in real life. Were there more variability in the measured temperature, the model could perhaps capture these dynamics. This aspect might be improved by changing the low-level controllers of the heating system in the IDA-ICE archetypes, which are now simulated as an ideal PI-controller.

Furthermore, as was mentioned in the Methods section, there is also some modulation of the heating input through a weather compenstion curve in the central heating system in the IDA-ICE model, which means that the heating signal is not pure PRBS. Hence, the heating input in May is significantly smaller than in January. However, in January, the solar radiation is small, so this would mean that the models will have poor prediction performance on the months with more significant solar radiation. May should be a good a compromise with regard to the trade-off between heating and solar. In the results, better prediction and more consistent parameter estimates were shown for September, but the same argument could be made for this month. There is also the possibility of bugs in the IDA-ICE archetype models beyond this. However, since IDA-ICE simulation is not the topic of this paper, this is left for further work.

Another point of uncertainty is the merging and weighing of the temperatures for the different zones. It could be that this simple approach smoothes out dynamics in the temperature that might be needed for better and more consistent results from the model identification. To investigate this further, a model with zoning could be set up. These models, however, would quickly become convoluted, with many parameters and states, and would increase the computational time needed for convergence of the log-likelihood optimization by an order of magnitude.

Nevertheless, it could simply be that there is not enough variability in datasets generated from simulation software to drive the model identification process. This aspect is worth further investigation, especially with respect to the low-level controls (i.e. PI controller) in the simulated heating system, since this maintains an unrealistically constant (and challenging from a statistical analysis viewpoint) indoor temperature.

Conclusion

The software package CTSM-R has been used in order to obtain reduced-order models, based on data from the building simulation program IDA-ICE, obtained by using a Pseudo-random binary signal. A forward selection procedure is employed to find a model that sufficiently describes the data. A three-state model, *TiTeTm*, is found to the best alternative, both in the log-likelihood p-value test, and in the validation performance. In the weeks selected for validation, the models identified on the Septemeber dataset shows better prediction performance than the models identified on the May dataset. These parameters of these models also exhibit more reasonable physical values. In general, the models perform better on the validation datasets when there is no controlled heating input.

Acknowledgement

References

Bacher, P., & Madsen, H. (2011). Identifying suitable models for the heat dynamics of buildings. *Energy and Buildings*, *43*, 1511–1522. https://doi.org/10.1016/j.enbuild.2011.02.005

Coninck, R. De, Magnusson, F., Åkesson, J., & Helsen, L. (2016). Toolbox for development and validation of grey-box building models for forecasting and control. *Journal of Building Performance Simulation*, *9*(3), 288–303. https://doi.org/10.1080/19401493.2015.1046933

Dixon, J. C. (2007). Appendix B: Properties of Air. In *The Shock Absorber Handbook* (pp. 375–378). https://doi.org/10.1002/9780470516430.app2

Jones, F. E. (1978). The Air Density Equation and the Transfer of the Mass Unit. In *Journal of Research of the National Bureau of Standards* (Vol. 83).

Kristensen, N., Madsen, H., & Jørgensen, S. (2004). Parameter Estimation in Stochastic Grey-Box Models. *Automatica*, *40*, 225–237. https://doi.org/10.1016/j.automatica.2003.10.001

Madsen, H. et. al. (2018). *Continuous Time Stochastic Modeling in R User's Guide and Reference Manual*. Retrieved from http://ctsm.info/pdfs/ctsmr-reference.pdf

Renné, D. S. (2016). Resource assessment and site selection for solar heating and cooling systems. In R. Z. Wang & T. S. Ge (Eds.), *Advances in Solar Heating and Cooling* (pp. 13–41). https://doi.org/https://doi.org/10.1016/B978-0-08-100301-5.00002-3

Rønneseth, Ø., & Sartori, I. (2018). *Possibilities for Supplying Norwegian Apartment Blocks With 4 Th Generation District Heating*.

Sourbron, M., Verhelst, C., & Helsen, L. (2012). Building models for model predictive control of office buildings with concrete core activation. *Journal of Building Performance Simulation*, *6*, 1–24. https://doi.org/10.1080/19401493.2012.680497

Standard Norge. (2014). *Calculation of energy performance of buildings - Method and data*. Retrieved from https://www.standard.no/no/Nettbutikk/produktkatalogen/Produktpresentasjon/?ProductID=702386

Walnum, H. T., Sartori, I., & Lindberg, K. B. (2019). Influence of inputs knowledge on Grey-box models for Demand Response in Buildings. *Proceedings of Building Simulation 2019: 16th Conference of IBPSA*.

Xingji Y., Laurent, G. I., & Sartori, I. (2019). Investigation of the Model Structure for Low-Order Grey-Box Modeling of Residential Buildings. *IBPSA Nordic BuildSim Nordic Conference 2019*.

Datasets for grey-box model identification from representative archetypes of apartment blocks in Norway

Hanne L. Bottolfsen[1*], Kamilla H. Andersen[1], John Clauß[2], Igor Sartori[1]
[1]SINTEF Community, Oslo, Norway
[2]SINTEF Community, Trondheim, Norway

*corresponding author: hanne.bottolfsen@sintef.no

Abstract

Grey-box models combine a relatively simple physical description of the building with a data-driven inference of key parameters and are often used for this purpose. A challenge with grey-box models is that the model identification process requires 'rich' datasets, meaning datasets containing enough statistical variability on both heating demand and indoor temperatures. Such datasets are scarcely available, usually only from dedicated experiments in living labs or similar research facilities.

This study aims to present a series of datasets that can be used for the identification of grey-box models of apartment blocks. Special test periods are simulated in IDA ICE during which representative archetypes of apartment blocks in Norway are excited with trains of heating events, Pseudo-Random Binary Sequence (PRBS), aiming at exploring a wide and rapidly changing set of indoor temperatures within and outside the thermal comfort zone.

Introduction

To exploit the energy flexibility potential in buildings, some form of smart control is necessary, that can manipulate the energy use based on external factors, such as weather and energy prices while maintaining thermal comfort for the occupants. In particular, it is expected that the thermal part of the energy demand, such as space heating, can be shifted in time and contribute to increasing flexibility of the demand in the energy system (Jensen, et al. 2017). Such types of controls shall rely on accurate, robust, and simple models of heat demand that are suitable for real-time control.

The aim of this study is to present a series of datasets that can be used for identification of grey-box models of apartment blocks and to describe the method used for creating these datasets.

Based on previously developed archetypes in the TABULA/EPISCOPE project, a set of IDA ICE models, representing apartment blocks in Norway is available. The IDA ICE models was developed in the study (Rønneseth and Sartori 2018).

In parallel with this study, two other studies are carried out. In one research activity the load profiles for the IDA ICE archetype models are validated against empirical datasets, while in the other parallel study the datasets created in this study is used for identification of grey-box models. Provided that the load profiles are validated, it is legitimate to assume that the indoor temperature profiles from the IDA ICE archetypes also are representative for the real building stock (Andersen, et al. 2020). Therefore, heating load and indoor temperature profiles from the IDA ICE models may in theory be used for creating grey-box models of those archetypes, likewise datasets from measurements, where available.

A successful grey-box identification process depends upon 'rich' datasets. To create such 'rich' datasets, simulations using a Pseudo Random Binary Sequence (PRBS) to control the radiators in the archetypes have been run, in addition to simulations with normal operation. Some of the strengths of PRBS-signals is that the signal is deterministic, shows no correlation with external factors and that it can be designed before an experiment (Bacher and Madsen 2010). It has been commonly used as an input signal in order to generate large sets of data with high quality that can be used for identification of black-box models (Royer, Thil, et al., Black-box modeling of buildings thermal behavior using system identification 2014) or as in this study, for identification of grey-box models. Such type of data is scarcely available as it can be challenging or expensive to run in real buildings. Data is therefore usually just available form physical experiments done in research facilities such as living labs. Both (Vogler-Finck, Clauß and Georges 2017) and (Thavlov, Bache and Madsen 2010) have done similar experiments in living labs. As an alternative, dynamic simulation models can be a good solution for increasing the numbers if available datasets.

The datasets generated in this study, both for normal operation and special test periods, are going to be made openly accessible on an internet repository by the time of the BuildSim Nordic conference in October 2020.

Methodologies

In this study, a set of previously developed archetype apartment block models with different age classes is used to run dynamic simulations. The simulation program IDA Indoor Climate and Energy (IDA ICE, EQUA, Sweden), version 4.8, has been used to run thermal simulation experiments. Simulations are run for both normal operation and with Pseudo-Random Binary Sequence (PRBS) control of the heating units (water radiators).

The simulations with PRBS signal control are run to obtain a different thermal behavior of the achetypes than what can be achived during normal operation.

Archetypes

A total of 20 archetypes from the TABULA (Typology Approach for Building Stock Energy Assessment) and EPISCOPE (Energy Performance Indicator Tracking Schemes for the Continuous Optimisation of Refurbishment Processes in European Housing Stocks) projects have been used in this study (TABULA/EPISCOPE u.d.). An archetype is the combination of a building category (here apartment block), age-group and renovation variant.

A detailed description of the archetypes are given in (Brattebø, et al. 2014). These archetypes are also used in other studies, and validation of the models against empirical datasets and numerical simulations is done in a parallel study (Andersen, et al. 2020).

The set of IDA ICE models represents apartment blocks in Norway from the 1950s until 2020, and each archetype represents approx. a ten-year interval. Table 1 presents the age classes and the number of floors and apartments for each of the models.

All apartment blocks for the period 1971 to 2020 consist of four floors and 24 apartments. The oldest archetypes (AB01 and AB02) have eight and 16 apartments distributed to four floors.

Table 1 – Archetypes age classes and size

Model	Age classes	Floors / apartments
AB01	- 1956	4 / 8
AB02	1956-1970	4 / 16
AB03	1971-1980	4 / 24
AB04	1981-1990	4 / 24
AB05	1991-2000	4 / 24
AB06	2001-2010	4 / 24
AB07	2010-2020	4 / 24
AB08	After 2020	4 / 24

In IDA ICE the apartment blocks are modeled with one ground floor, one mid-floor facing zones with the same thermal conditions, and a top floor (Rønneseth and Sartori 2018). 3D-model and floor plan of the model in IDA ICE is shown in Figure 1 and Figure 2.
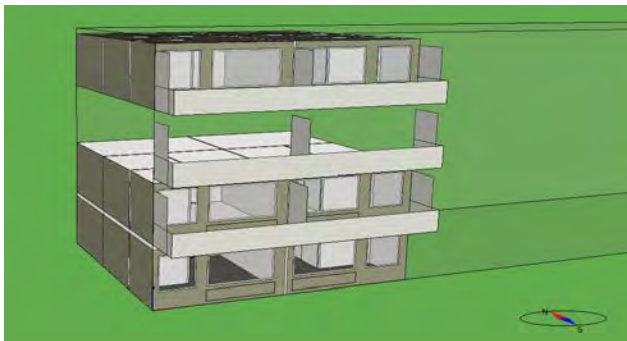
Figure 1 – 3D-model of apartment block in IDA ICE
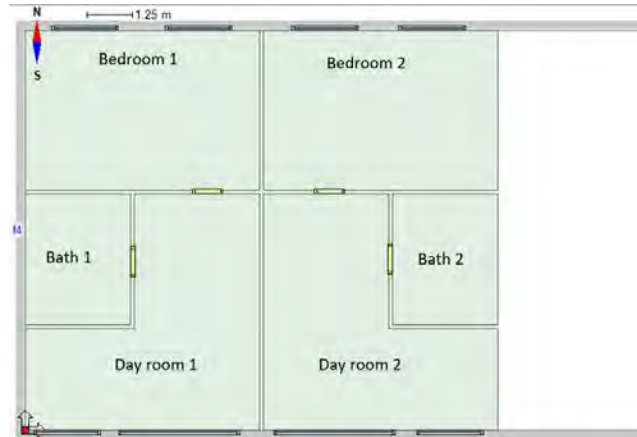
Figure 2 - Floor plan from IDA ICE

Each apartment is 70 m². The size is the same for all floors and consists of three zones with floor area as given in Table 2.

Table 2 - Area of zones in apartment

Room type	Floor area, m²
Dayroom	31,5
Bedroom	28,0
Bath room	10,5

The internal loads in the apratments have not been changed for this study and are the same as in (Rønneseth and Sartori 2018). These loads are set according to SN TS 3031:2016 with the following heat gain:

- Equipment: 17,5 kWh/m²yr, 60 % heat gain
- Lighting: 11,4 kWh/m²yr, 100 % heat gain
- Persons: 13,1 kWh/m²yr, 100 % heat gain

Each zone has a water radiator supplied by district heating. The radiators are dimensioned after the original variant of each archetype, without internal gains and with a dimensioning outdoor temperature (DOT) for Oslo of -20 °C. Setpoints for each zone for normal operation are given in Table 3. The bathroom is excluded in this study as it has electrical heating cables.

Table 3 - Heating setpoint for zone

Room type	Heating setpoint
Dayroom	22 °C
Bedroom	18 °C
Bathroom	24 °C

The district heating supply temperature at max. power is 80/60°C. A weather compensated supply temperature from district heating to the radiators is used in the model. At DOT of -20 °C the supply temperature is 80 °C and the supply temperature follows a linear reduction from 80 °C to 60 °C between outdoor temperatures –20 °C and 17 °C. For all the models a distribution loss of 10 % is included for heat to the zones.

A typical meteorological year for Oslo, Fornebu, has been used in the simulations. The weather file is an IWEC-file (International Weather for Energy Calculations) downloaded from EnergyPlus with a resolution of one hour.

For each age group, in addition to the original building, two different variants of energy upgrade have been modeled in IDA ICE; an intermediate and a standard renovation. Intermediate renovation includes improved windows and thus improved air-tightness. The standard renovation includes, in addition, better envelope insulation, and represents a typical whole-building renovation without particular focus on energy efficiency (Rønneseth and Sartori 2018). Table 4 presents the input values for AB03 and the improvement for the renovated model (standard renovation), compared to the original model. For AB07 (representing the building code of 2010, TEK10) only the intermediate variant is available, and for AB08 (representing the passive house standard) there is just the original variant; this because both archetypes are equal to or better than today's building requirements. Thus we have a total of 21 archetypes.

Table 4 - AB03: Difference in input values for inital model and standard renovation (Brattebø, et al. 2014)

AB03 Initial		
Building component		**U-value [W/m²K]**
Roof: Concrete slab, 180 mm mineral wool, flat roof		0,21
External wall: Timber frame, 100 mm mineral wool, 50 mm thermal bridge barrier		0,34
Windows: Double-glazed window, regular glass, air-filled cavity		2,60
Floor: Concrete floor, 100 mm mineral wool, unheated basement		0,31
Infiltration rate (ACH):		5,0
AB03 Standard renovation		
Building component		**U-value [W/m²K]**
Roof: 180 mm mineral wool replaced with 250 mm mineral wool		0,14
External wall: 50 mm mineral wool added on the outside + brick veneer		0,18
Windows: Double-glazed window, one coated glass, air-filled cavity		1,90
Floor: 50 mm mineral wool added on the cold side (basement)		0,26
Infiltration rate (ACH):		2,0

Normal operation

For simulations with normal operation, no changes are made to the initial archetypes. The radiators are controlled by a PI-controller, which is regulated by the indoor temperature and the heating setpoint.

PRBS-signal

A Pseudo-Random Binary Sequence (PRBS) has been used to control the heat input for the water-borne radiators in the zones for the archetypes. By using PRBS-signal, the heat input for the radiators are excited with trains of heating events of shorter or longer time intervals, leading to a wide and rapidly changing set of indoor temperatures within and outside the comfort zone. The design of the PRBS-signal is described in the following.

Compared to other types of controls, the predefined PRBS-signal will not be affected by any external factors, such as the meteorological data, or limited by setpoints or normally acceptable indoor temperatures. The signal has only two levels, 0 or 1, to turn the radiator off and on. The used PRBS-signal is designed after guidelines given in IEA, EBC Annex 58 (Madsen, et al. 2016). The design of the signal is important, as it will impact the results from the simulations.

For these simulations, the total period of the predefined signal is 468 hours, including an entrance time of 126 hours. For the entrance time the signal has several short time intervals for on/off, while the following period of approx. two weeks, have longer periodes where the signal is on or off, Figure 3.
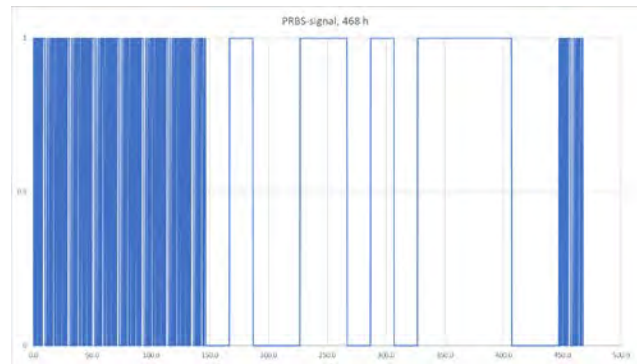
Figure 3 - PRBS-signal

A control module where the PRBS-signal is used as a source has been created in IDA ICE, presented in Figure 4. The control module is applied to each radiator in every zone (dayroom and bedroom).
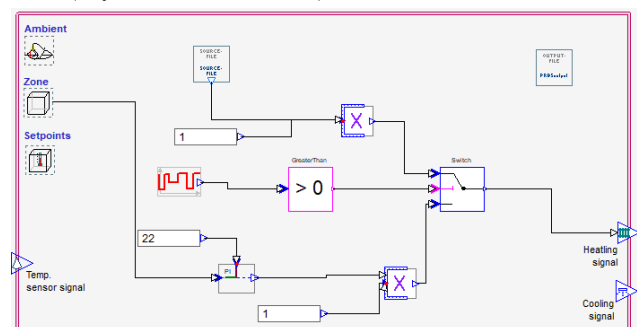
Figure 4 - Control module in IDA ICE

Simulations are run for one year for all archetypes. In the control modul in Figure 4, a source file, which is the predefinend PRBS-signal, is used as an input to control the heating units for the first 468 hours of a month.

Each month of the year starts with a new period of the predefined signal. After the period of 468 hours the control module has a swich-unit that changes the input signal to the PI-controler, shown in the lower part of Figure 4. The swich is controlled by a time schedule. When using the PI-controler the heating units is controlled as normal operation with the same setpoints as given in Table 3. This way, the same PRBS-signal is repeated for each month of the year, leading to a larger set of data.

Results

Even though datasets for a totalt of 21 archetypes have been created, the presentation of the results in this study is limited to four different archetypes. The archetypes AB03, AB03 with standard renovation, AB07 and AB08 is chosen to be a representative selection. Also, datasets from February are used to present the results as this month has usually the lowest average outdoor temperature.

Normal operation

During normal operation the indoor air temperature is almost constant at the zone setpoint. Figure 5 is showing the indoor temperature for two days (12. - 14. February) for the zone (Day room 2 in Figure 1) located in the middle of the building, with only one external wall and a heating setpoint at 22 °C. For all of the archetypes there is a small peak in the indoor temperature around noon on the 13th of February, this peak is related to solar heat gain which has a peak between 10.00 – 12.00.
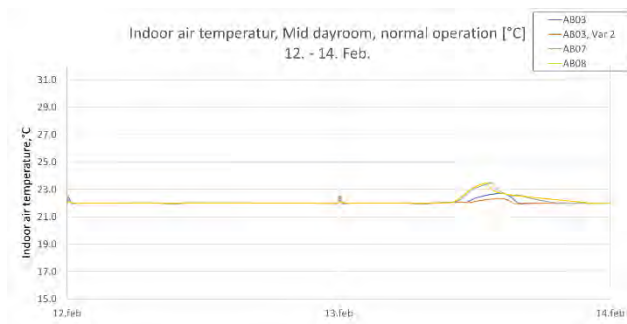
Figure 5 - Indoor air temperature, normal operation, Mid. Dayroom.
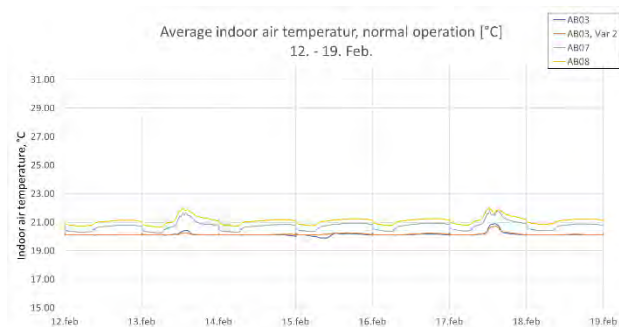
Figure 6 - Average indoor temperature, normal operation

Figure 6 shows the average area-weighted indoor air temperature for each archetype. As the radiators for each zone have been dimensioned after the original variant of each archetype and due to difference in thermal heat loss,

the temperature trend is different for each of the archetypes. In addition, the temperature varies for the different zones, as the indoor temperature also will be influenced by orientation of the room, solar radiation and the different heating setpoints in the different zones

Total heat power from the plant to the zones is shown in Figure 7 for the same week in February as for the average indoor air temperature in Figure 6. The (inverted) outdoor temperature for the same period is shown as a red line in Figure 7. As the supply temperature from the district heating to the radiators is weather compensated the delivered power varies with the outdoor temperature. For this period the outdoor temperature varies between -5 °C and 4 °C.
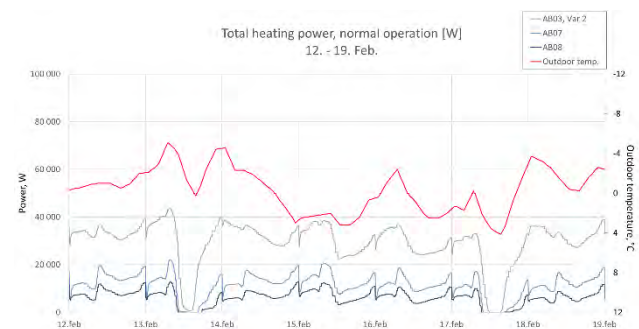
Figure 7 - Total heating power from plant to zones, normal operation

PRBS-signal

In the following Figure 8 to Figure 11, the indoor air temperature and totalt heating power for the plant from the whole simulation period with PRBS-signal is presented. The average indoor air temperature for each archetype is, as previously, weighted based on area and the number of apartment types (different location within the building).

Figure 8 and Figure 9 present the start of the period where the signal has shorter time intervals leading the heating power and indoor temperature to change more rapidly. Figure 10 and Figure 11 presents the period with longer time intervals. Compared to normal operation, the results from simulations with the PRBS-signal shows that a different thermal behavior is obtained for the archetypes and the temperature intervals has a wider range.

Ideally, when applying a PRBS-signal, the heating power curve, in Figure 9 and Figure 11, should be flat when the signal is 1 and the radiators are turned on. But as the signal is applied to the controller of the radiators in each zone and the supply temperature from the plant (representing a district heating substation) to the raditors is weather compensated, the heating power curve will change with the to the outdoor temperature, due to the linear reduction from 80 °C to 60 °C between outdoor temperatures of -20 °C and 17 °C.
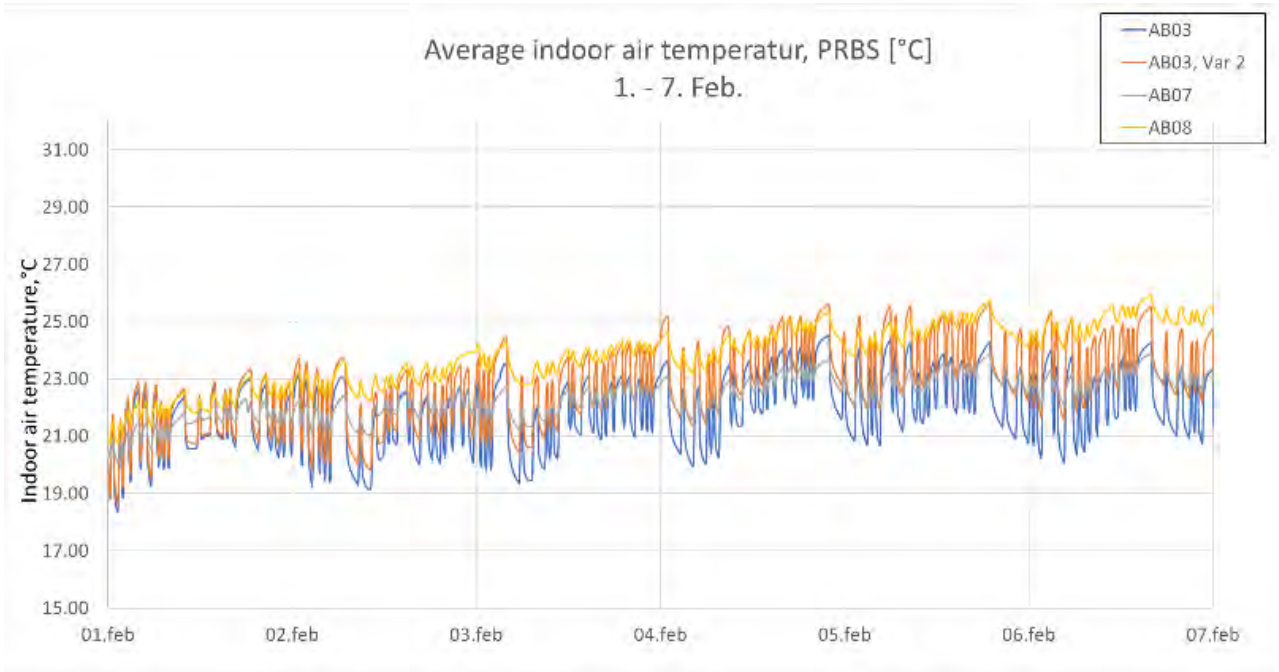
Figure 8 - Average indoor air temperature, PRBS
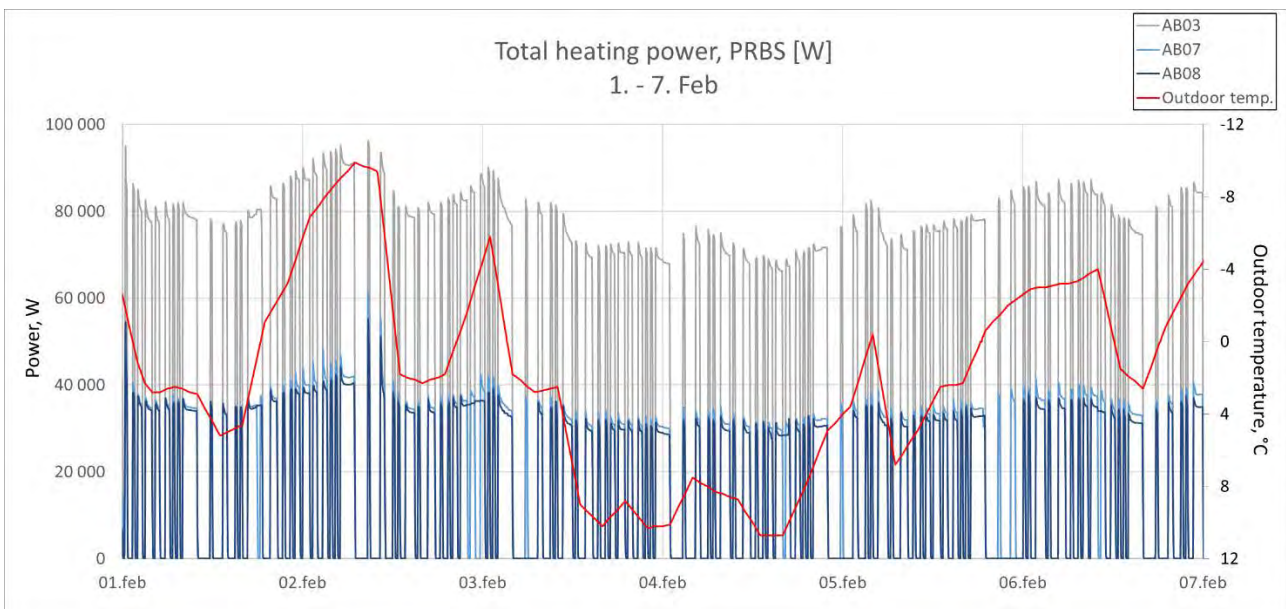
Figure 9 - Total heating power from plant, PRBS
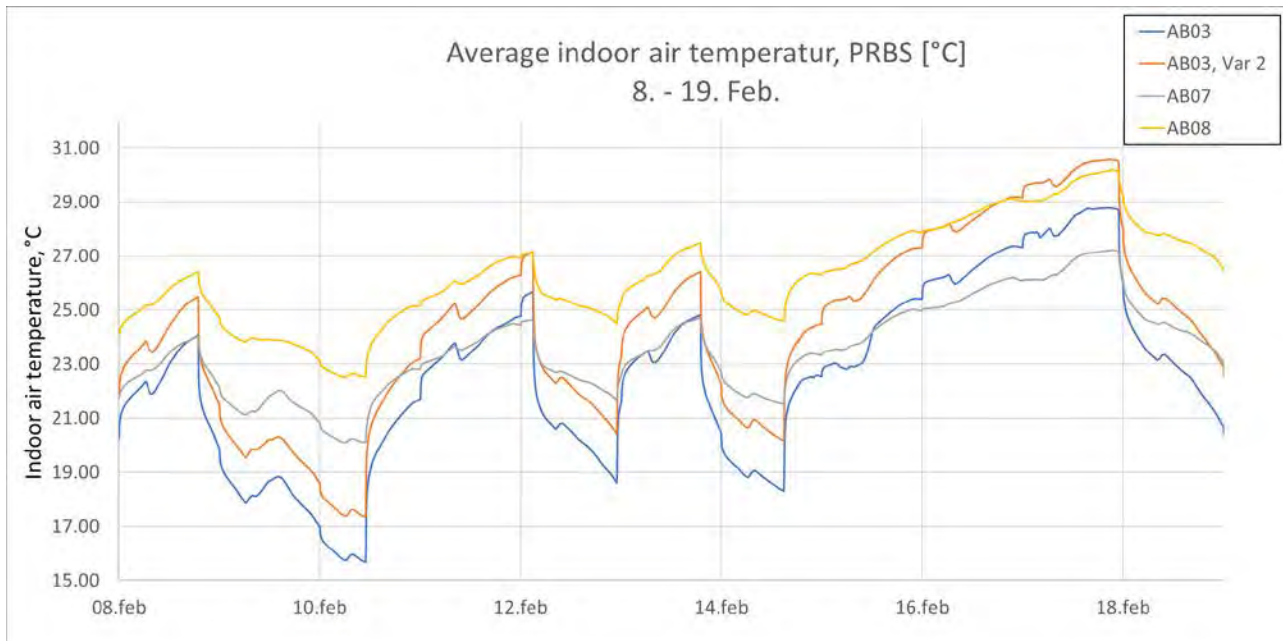
Figure 10 - Avergage indoor air temperature, PRBS
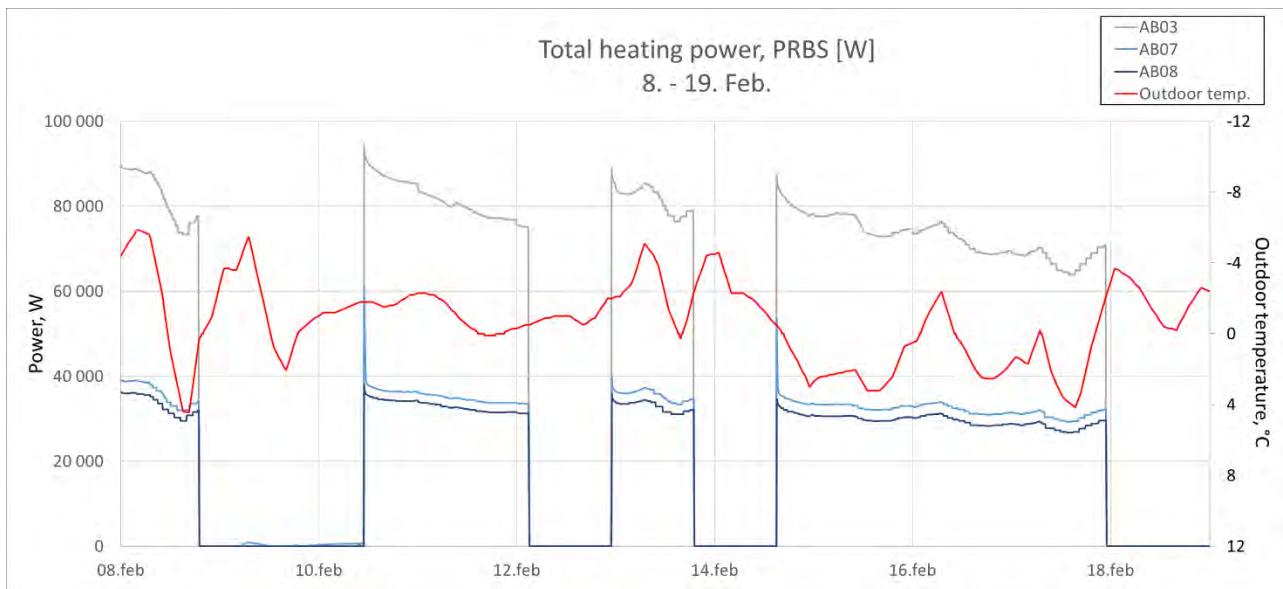
Figure 11 - Total heating power from plant, PRBS

Datasets

After running the simulations in IDA ICE, the data have been extracted from the result files and merged into full datasets in .csv files.

A total of 80 datasets have been created, in two versions: comprehensive and reduced files. This includes datasets for each archetype, including the initial and the two variants of energy upgrade, for both PRBS and normal operation.

The same data is extracted from simulations with PRBS and normal operation. For the comprehensive file, the following data is included with a five-minute resolution:

- Indoor air temperature for each zone
- Room heating for each zone
- Total heat power from the plant
- Weather data; wind, solar radiation, relative humidity, outdoor temperature

For the reduced file, the following data is included with a resolution of one hour:

- Average indoor air temperature
- Total heat power from the plant
- Weather data; wind, solar radiation, relative humidity, outdoor temperature

Conclusion

In this study a large series of datasets from representative archetypes of apartment blocks in Norway have been created.

The datasets consist of values for both normal operation and special test periods. For the special test periods the heat input for the water radiators are excited with trains of heating events of shorter and longer intervals. Simulations with PRBS leads to rich datasets with a wide and rapidly changing set of indoor temperatures within and outside the themal comfort zone.

Values have been extracted from the result files and merged into full datasets in .csv files. The generated datasets, both under normal operation and under special test periods, will be openly available online by the time of the BuildSim Nordic conference in October 2020.

In this study the control module with the PRBS-signal was applied to the water radiator in each zone. For further work the same experiments can be applied directly to the plant so to exclude the influence of the weather compensated supply temperature. This would improve the usefulness of sych datasets, as pointed out in (Bagle, Walnum og Sartori 2020).

Acknowledgment

References

Andersen, Kamilla Heimar, Synne Krekling Lien, Aksel Garvik Fagerheim, Hanne Liland Bottolfsen, og Igor Sartori. 2020. «Validation of Norwegian apartment archetypes based on empirical data and numerical simulations.» *BuildSim Nordic.* Oslo.

Bacher, P., and H. Madsen. 2010. *Experiments and Data for Building Energy Performance Analysis: Financed by The Danish Electricity Saving Trust.* IMM-Technical report-2010-03, Technical University of Denmark, DTU Informatics, Building 321.

Bagle, Marius Eide, Harald Taxt Walnum, og Igor Sartori. 2020. «Identifying grey-box models of Norwegian apartment block archetypes.» *BuildSim Nordic.* Oslo.

Brattebø, Helge, Reyn O'Born, Igor Sartori, Michael Klinski, og Bjørnar Nørstebø. 2014. *Typologier for norske boligbygg - Eksempler på tiltak for energieffektivisering.* Trondheim: NTNU, SINTEF.

Jensen, Søren Østergaard, Anna Marszal-Pomianowska, Roberto Lollini, Wilmer Pasut, Armin Knotzer, Peter Engelmann, Anne Stafford, og Glenn Reynders. 2017. «IEA EBC Annex 67 Energy Flexible Buildings.» *Energy and Buildings* 10.

Madsen, Henrik, Peder Bacher, Geert Bauwens, An-Heleen Deconinck, Glenn Reynders, Staf Roels, Eline Himpe, and Guillaume Lethé. 2016. *Reliable building energy performance characterization based on full-scale dynamic measurements, Report of Subtask 3, part 2:.* Leuven: International Energy Agency, EBC Annex 58.

Royer, Sullivan, Stéphane Thil, Thierry Talbert, and Monique Polit. 2014. "A procedure for modeling buildings and their thermal zones using co-simulation and system identification." *Energy and Buildings, Elsevier, 78, Aug. 2014.*

Royer, Sullivan, Stéphane Thil, Thierry Talbert, og Monique Polit. 2014. «Black-box modeling of buildings thermal behavior using system identification.» *19th IFAC World Congress, Aug. 2014.* Cape Town, South Africa: hal-01292450. 7.

Rønneseth , Øystein , and Igor Sartori . 2018. *Possibilities for Supplying Norwegian Apartment Blocks with 4th Generation District Heating.* SINTEF, ZEN Research Centre.

TABULA/EPISCOPE. u.d. *EPISCOPE and TABULA Website.* https://episcope.eu/building-typology/country/no/.

Thavlov, Anders, Peder Bache, and Henrik Madsen. 2010. *Data for Energy Performance Analysis: Financed by The Danish.* IMM-Technical Report-2010-01, Kgs. Lyngby: Technical University of Denmark, DTU Informatics, Building 321.

Vogler-Finck, Pierre., John Clauß, and Laurent Georges. 2017. *A dataset to support dynamical modeling of the thermal dynamics of a super-insulated building.* Zenodo. 10.5281/zenodo.1034819.

Global Marginal Carbon Footprint Evaluation of Internet Services with Building Energy Models

Eric Kumar, Erica Cochran Hameen, Wei Liang
Carnegie Mellon University, Pittsburgh PA
School of Architecture

Abstract

Over the last decade, operational efficiency optimizations in data center (DC) facilities designs have curtailed their absolute power demands. However, their physical footprint is still growing. This growth in capacity may offset the efficiency gains at best or may even increase the power demand in absolute terms. Such offsetting effects make system level life cycle environmental footprint evaluations complex for distributed services operating in these DCs.

To support system level evaluations for services operating in DCs, this research uses simulated network traffic profiles and coincident energy generation source aware building energy models (BEM) to evaluate the marginal carbon footprint of a globally spanning network of data centers. The result of this research is a prototype of a BEM based framework that can be used in environmental decisions to characterize DC life-cycle costs at internet service levels.

Introduction

Globally distributed internet services are ubiquitous today. These services are driving the demand to build mega-watt scale data center facilities (DC) distributed through out the globe. In a 2015 study data centers were forecast to consume as much as 13% of the global energy production by 2030 (Andrae and Edler, 2015). More optimistic models form the US Department of Energy for the US showed a curtailment with up to fifty percent decline in energy compared to the industry's use of 2% of the power produced by the national grid in 2005 as a result of using state of the art efficiency and consolidation practices (Shehabi, 2016). As more and more parts of society are transitioning to data center dependent online paradigms, the absolute demand of data centers is growing. The volume of growth is exemplified by the capital costs being invested across the world in constructing these data centers.

The growth in data center capital construction costs will reach $89 billion by 2027, a significant increase from the $45 billion spent in 2018 (Insight-Partners, 2019). Capital costs aren't the only commitments for data center owners however. DC owner's also incur significant operational costs throughout the entire operational lives of their facilities.

Over a 20-year life of a continuously operating data-center facility, the use-phase energy costs can exceed its capital costs while having a much larger ecological footprint. Given the accumulation of costs and impacts over the life of data centers, there is a need for a robust model the couples the information technology (IT) and building systems with their energy supply sources through its useful life. In this article a geographically extensible model that accounts for the workloads, building systems, and power utility grid is presented.

In the rest of this paper a model for coincident energy demand and marginal energy costs (MEC) of a set of data centers is proposed and developed. First, the proposed method uses a hybrid model consisting of EnergyPlus and Python programming modules as developed by the researcher in (Kumar, 2020a). For this article, the researcher's original hybrid model is modified as described in the methodology section to be more indicative of the current operations of cloud data centers. Then second, the resulting time series of operational energy demand profile is used as input to a Python based open source MEC simulation tool that is also extended as described in the methodology section.

The MEC calculations are based on the Dispatch Optimized Systems Cost of Energy (DOSCOE) model developed by Platt (Platt et al., 2017). DOSCOE provides a linear programming platform that computes the monetary costs and several environmental emissions associated with operating a mix of dispatch-able and non-dispatch-able energy sources. In this context, dispatch-able energy sources are those that can be controlled to meet demand. Natural gas power plants are examples of dispatch-able sources of energy, where the plant operators can control the mass flow rates of the combustion gases to curtail generation rates. On the contrary are the non-

dispatchable sources, where the energy generation is dependent on extrinsic factors. An example of non-dispatchable energy source is solar; where cloud cover greatly effects the generation rate and no power can be generated at night.

Modeling the costs for a mixture of dispatchable and non-dispatchable generators is complex as most non-dispatchable sources are only accounted for as opportunistic supply sources when sizing the power generation infrastructure. By design the dispatchable generators are sized to meet the full demand in a worst-case condition when no dispatchable power is available (Platt et al., 2017). However, when non-dispatchable power is opportunistically available, it supplements the grid; allowing dispatchable sources to be turned down to part loads. This saves fuel costs for dispatchable sources (ie natural gas generators), but it leaves their physical infrastructure stranded and underutilized.

This research's coupling of the DOSCOE model with a BEM quantifies the monetary and ecological costs associated with operating data centers in grids with mixtures of energy sources bound by physical constraints. The developed model is evaluated by matching the marginal costs of energy with data center demands on hourly intervals. Furthermore, the resulting model is inclusive of the stranded costs of the underutilized power infrastructure.

In the next section, Background, informative context is provided to set the proper use-case for this framework. Then in the Similar Works section, past literature which have quantified the ecological life cycle cost of data centers and internet services are summarized. In the Methodology section, the two main modules of the software implementation of this research are presented. Specifically these modules are a modified version of hybrid building energy model and a novel MEC model based on DOSCOE. After the details of the models are presented, the results are discussed in the Results and Discussion section followed by the Conclusions.

Background

Data centers are critical to modern internet experiences for billions of people. They are the key enablers for disseminating information in real time regardless of people's location. As an example of location agnostic services geographical dispersed infrastructure, Figure 1 illustrates a geographically distributed architecture that enables data centers to provide globally consistent internet experience that have become the status quo over the last decade. Distributed software architectures implemented in the server clusters at the leaf-nodes consist of a collection of autonomous computing resources that appear to its users as a single coherent system (van Steen and Tanenbaum, 2018).
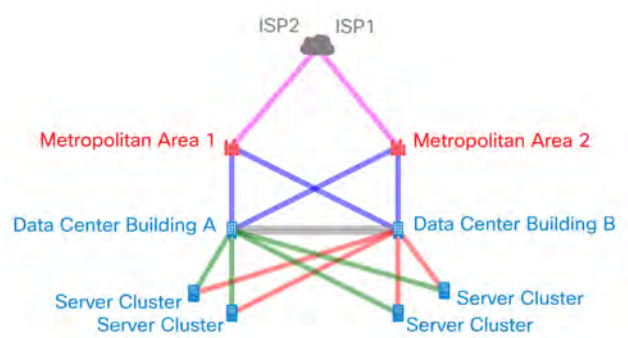
Figure 1: General Topology of data center networks. The 1:1 metropolitan area to building relationships are shown for clarity only. Pink: indicates the first layer - ISP-Metropolitan links (physical). Magenta: indicates the second layer Metropolitan-DC Building with a full mesh connection (physical). Gray: represents the cross-connection between Data Centers (logical). Green/Red: Cluster to Cluster links (logical).

In Figure 1, a data center network stack with three hierarchical WAN layers are shown. The first hierarchical layer, the global level, has a wide area network (WAN) connected to two internet service providers (ISP) as its root node. For the purposes of this work, the WAN is an abstraction of a network that connects a set of data center facilities with each other. The second layer of the global level are the metropolitan regions. In this layer, the ISP links are shown as coming in from top and the outgoing links from the bottom serve local distribution networks to buildings within the metropolitan areas. The final layer of the global level are the data center buildings, where the global network links connect to clusters of servers. Inside each data center there may be another independent hierarchy as shown by the server clusters. The physical network links shown in Figure 1 connect the buildings to each other through the WAN. However, the physical links (pink, magenta) is transparent for the clusters, which directly communicate with each other through logical links (gray, green, red).

Large cloud data center operators have championed WAN systems for global up-time (service availability) and user experience optimizations (Sushant et al., 2013) (Hong and Kandula, 2013). Cloud data centers are a specific class of data centers. They serve business functions that require custom IT and building systems tuned for optimality in total costs of ownership models. These facilities house numerous services that can be controlled by network load balancers, with each data center limited by its physical infrastructure's capacity. As described by Sushant and Hong, the WAN networks can shift loads between data center on command. The efficacy of a strategy for shifting computational loads depends on the capacity headroom of the physical resources at the data center where the loads are shifted to.
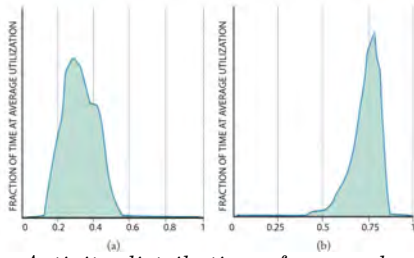
Figure 2: Activity distribution of a sample of 2 clusters, each containing over 20,000 servers, over a period of 3 months. The x-axis indicates the server utilization rates (0 to 1) and the y-axis indicates the fraction of time during the 3 months (Barroso et al., 2018). The figure on the right (b) shows that peak utilization exceeds 75% with little variances over the 3 months, whereas the right figure (a) shows that utilization is below 60% at all times.

The location fungibility enabled by WANs is desirable from a service application performance point of view, as latency can be significantly reduced for specific markets and applications by minimizing the round trip communication times with consumers. Furthermore for cloud DCs, researchers have demonstrated cross awareness of BEMs and network models to optimize DC sustainability (Tripathi et al., 2017; Kiani and Ansari, 2017). Beyond the sustainability gains, there is a potential for meaningful financial incentives by balancing workloads across DC, thus reducing the peak demand on any specific DC and lowering the required physical capacity that must be built.

In the context of BEMs, there is a trade-off with the non-deterministic nature of network load balancing described above. Implementations of load balancing strategies using WAN's make the IT workloads temporally (and geographically) unstable, rendering it elusive for building modelers to reason about. As an example of temporal and geographical instability of data centers, Figure 2 (Barroso et al., 2018) shows the difference in utilization rates for two server clusters from Barroso's operational experience. This behavior of IT loads is something that WAN aware BEMs can help characterize and exploit. One possible means of exploitation is to flatten the peak of each cluster by routing the excessive workloads to another similarly provisioned cluster with lower coincident demands and sufficient building systems capacity headroom. However, building energy simulation need to be aware of more then just energy to make the right environmental decisions. To effectively optimize environmental objectives, BEMs coupled with MEC models can quantify the energy's global warming potential in terms of carbon footprint to shift loads from one building to another.

Based on the literature reviews and references cited, there are no publicly available simulation frameworks that couple the dynamic data center workloads and

the coincident carbon footprint associated with powering their load. The marginal cost of energy coupled building energy model described in this research is the first publicly available tool to allow owners, designers, and researchers to quantify the carbon footprint of data center operations accounting for granular supply and demand matching of power. Next, a literature review of past works concerning the carbon footprint of data-centers and digital services is presented in the Similar Works section.

Similar Works

There are two notable past works that look at the energy footprint for distributed sets of data centers. First, Tripathi considers hardware capital costs alongside with energy acquisition costs to quantify the total costs of ownership in (Tripathi et al., 2017). Tripathi's framework is dynamic in terms of workloads but it is not aware of the building energy dynamics. In the second work, Kiani and Ansari describe a geographical load balancing strategy that exploits green energy mix in the utility grid (Kiani and Ansari, 2017). However, their load balancing scheme doesn't provide insights into how the load balancer evaluates the building energy demands or how the greenness of the energy supply is obtained.

Using a life cycle assessment framework, Whitehead demonstrates a comprehensive data center site level life cycle costs analysis in (Whitehead, 2015). All energy use in Whitehead's models were deduced from annualized PUE values, precluding coincident energy source evaluations with their framework. Similarly the Green Grid's data center life cycle assessment guideline is limited to PUE as their suggested basis for the operational energy proxy (The Green Grid, 2012). The PUE metric is shown in Equation 1, it has proven to be the most popular method for data center operational efficiencies since 2006 (Wikipedia.com, 2020).

$$PUE = \frac{E_{total}}{E_{IT}} \qquad (1)$$

E_{total} = Total Power Used at Facility
E_{IT} = Power Consumed by IT Equipment

Other's have evaluated the costs of internet services (Taylor and Koomey, 2008; Shehabi et al., 2014). Taylor and Koomey quantify the energy and greenhouse gas implications of online Advertising circa 2008. While Shehabi evaluates the energy and greenhouse gas implications of video stream circa 2014 (Shehabi et al., 2014). Together these works provide a taxonomy that can be followed to assess internet service costs in terms of energy use.

Figure 3: Data center locations

Methodology

In this section the MEC model's coupling with the BEM is described. The resulting model maintains a strict partition between the two technical domains. The first part of the model simulates the hourly energy demands of a set of five data centers in EnergyPlus (EP) using the method demonstrated in (Kumar, 2020a). These data centers are distributed across the globe as shown in Figure 3. Then in the second part, the data center demands are matched with the respective region's utility power generation sources for the coincident hour to assess the MEC during that hour. These parts are described in the following subsections.

A fundamental component of the demonstrated implementation of this framework is the network traffic simulator from (Kumar, 2020a). The simulation produces a time-series profile of the network traffic that a hypothetical service will get at a particular data center site. The hypothetical services are based on Wikipedia and segregated according to the natural language of the Wikipedia pages. By segregating services by natural languages allows the treatment of each language as a 'service platform'. With these network simulations, one or more languages can be supported from a single data center with the constraint that the sum of the IT workloads does not exceed the capacity of the data center facility.

Building Energy Model

For the first part, a sufficient building energy demand profile is simulated as in (Kumar, 2020). The IT workload profile characterizing the power and cooling load is obtained by simulating the 50th quantile of daily network traffic to each data center using Kumar's method from (Kumar, 2020b). There are three notable differences between Kumar's orginal BEM and the model presented here. The specific changes are:

1. Setting $2kW/m^2$ as the IT equipment load density to represent cloud DCs with hot-aisle/cold aisle containment resulted in run-time errors. This persistently led to thermal runaway condi-

tions for the Singapore and San Francisco sites in the new model. In order to keep the building envelope form-factor and the construction materials the same, this simulation's IT power load density is changed to $1.0kW/m^2$.

2. In these simulations, the data center model has air distribution flow control with approach temperatures specified. Flow control with approach temperature method calculates the temperature differences between the IT hardware boundaries and the air handling equipment. This method is more representative of modern data-center operations and allows modeling ASHRAE 90.4 Standard's requirement of hot-aisle / cold-aisle compartmentalization. The alternate method in EnergyPlus considers the entire data center room as a well-mixed environment, consistent with the modeling from (Kumar, 2020a). While using the approach temperature method, the cooling setpoint is changed to 27 degrees Celsius from 25 degrees used in (Kumar, 2020a). This 2-degree adjustment corresponds with the approach temperature between the air handling equipment discharge and the inlets of the ITE; as there is no mixing of the supply air before it enters the ITE.

3. As the third and final change, the load distribution values in the EnegyPlus input file (IDF) were revised from the SequentialLoad setting to UniformPLR. In the former, equipment is activated in the order listed in the IDF. With this specification each piece of equipment ramps sequentially from its idle state to full capacity, before subsequent equipment is enabled. In the latter load distribution specification, all equipment are loaded in parallel to each other. Another available setting for load distribution, the Optimal specification, was also tried for this field, but it crashed the simulations.

To validate that the proposed building energy model configurations with the above changes produce reasonable results, each data-center is simulated with two models. In the first model, the economizer for the direct evaporative cooler (DEC) limits are increased while in the second model the default settings are maintained. The summary of the changes are indicated in Table 1, while the comparison of total site energy between the two models for each set of the simulations is illustrated in Figure 4.

In Figure 4, the pairs of simulations for a DC site are presented. In the figure, the red bar indicates the total site energy of the model with economizer limits increased and the IT loads reset by the network coefficient (RL). The blue bar indicates the default economizer values (NoRL) from Kumar and with statically configured IT load profiles (ie cyclic day/time load). From the figure it can be observed that the increased

Figure 4: Total Site annual energy for statically (NoRL) configured IT load and dynamically reset (RL) IT loads.

economizer settings lead to more energy use than the default values for three of the five DCs. This increase in energy demand is attributed to the load resetting, where the network aware model increased the IT load for more hours of the year.

Table 1: Economizer settings for the two models

IDF Object	Variable	Default	Increased
DC-OA	Econ. Max db-C	23	28
DC DEC	Evap. Max db-C	20	28

The next subsection introduces the marginal costs of energy model, which will take the results from the BEM model described above.

Regional Marginal Costs of Energy

The second module requires a time-series profile of the electrical grid's power source attributions, where the intervals of the power generation values match the BEM energy profile. The corresponding site and regional grid model pairs are indicated in Table 2. For this model the energy generation regional grid profiles are obtained from Platt, who provides profiles for 13 US regions in DOSCOE [5]. Singapore and Amsterdam data-centers grid profiles are constructed as described below.

Table 2: Data Center Site and Power Grid

DC ID	DC Location	Regional Grid
SFO	San Francisco, CA	California
CAR	Carrolton, Texas	ERCOT
ASH	Ashburn, VA	Midatlantic
AMS	Amsterdam	Netherlands
SIN	Singapore	Singapore

Each U.S region's grid profile is composed of hourly demands and corresponding production capacity of several power generation technologies. Hourly values for each region's demand, solar, wind, coal, coal with

cryogenic capture, coal amine gas scrubbing, and nuclear are defined. These grid regions are representative of three out of five of the data-center locations being simulated.

For Singapore, the International Energy Agency (IEA) provides a top down view of the annual energy production from various technologies. The IEA data shows that the renewable penetration in the energy supply for Singapore accounted for only 1.6% of the total energy demand in 2016 (IEA, 2017). Due to this negligible contribution from renewable sources and lack of hourly generation data, it is assumed that all demand is met by natural gas power generators, consistent with other sources (USEIA, 2016b). Figure 5 indicates the energy production capacity and the associated carbon emissions for each of the utility grid regions. The demand profile for Singapore in 2016 is obtained from (Singapore-Government, 2016).

For the Amsterdam data center, the energy profile of Netherlands is used. The IEA indicates that in 2018, 12% of Netherlands' energy demands was met by renewable sources. This is a meaningful contribution from renewable, therefore a more granular generation profile is prudent as opposed to Singapore which did not require evaluations of the energy mix at any given time. To formulate a more granular resolution of the Netherlands' generation, the IEA data is supplemented with data from the Open-Power-System-Data to characterize the time series profile of renewable energy (Open-Power-System-Data, 2019). OPSD provides hourly data for the renewable sources only. The balance of the energy demands in the Netherlands is met by fossil fuel-based generators, namely 35% by coal and 42% by natural gas (USEIA, 2016a). The DOSCOE grid profiles don't have any corresponding field for bio-mass, so the bio-mass generation indicated in OPSD is lumped in with the fossil fuel generators. In the discussion section, some validation for this approach is presented. The Netherlands also produces nuclear energy, but only the annual production rates were obtained (USEIA, 2016a). In this works implementation of the DOSCOE, the annual nuclear production for Netherlands is distributed equally over the year and modeled as a constant (non-dispatchable) base load throughout the year.

The MEC coupled BEM algorithm is given below. In the algorithm two inputs are required. The first is DOSCOE[region], it is a two-dimensional array formatted as described in (Platt et al., 2017). It indicates hourly grid profiles of the power demand and power capacity of the available energy sources at the corresponding hour. The second input, traffic.language, is a one-dimensional vector indicating the network traffic to the respective site from Kumar (2020b). In the algorithm, for each language, it's traffic to the respective data center is checked. If there are traces of a language routed to a site, the algo-

rithm performs the BEM simulation by invoking EnergyPlus. This resulting demands from EnergyPlus are then added to the region's grid demand profile. If a language does not have any traffic to a particular site than, the data center site does not do any work and the BEM simulation is bypassed.

Algorithm 1 MEC coupled BEM algorithm

Require: DOSCOE[region] & traffic.language[site]
  for site and region in DC.site and DC.region **do**
    if traffic.language[site].all $! = 0$: **then**
      $DEMAND_{DC} \leftarrow BEM(site, traffic.language)$
      $DOSCOE[region].demand += demand[site]$
    end if
  end for
  CO_2 footprint $= GridSim(region, rps)$

Where $DEMAND_{DC}$ is the marginal demand the data center puts on the power grid,

---

The second step of algorithm quantifies the marginal carbon footprint of the grid with the added data center loads by running DOSCOE's Grid Simulator. In this step, the renewable portfolio standard (rps) argument specifies the percentage of renewable energy mix for the region.

In the next section the results from the methodology are discussed.

Results & Discussions

The resulting values of the carbon footprint for each data center is summarized in Table 3. The energy model for the 491 kW data center has been scaled by 1000 to represent the metro scale of data centers impact of the regional grid. The specific data center model represents only a small fraction of hyper-scale data centers campuses that reach 500-Mega-Watts. The table further indicates the carbon footprint of each of the languages being served from the data centers. The values are indicative of the marginal CO_2 emitted by adding the data center demand to the respective grid.

Table 3 indicates the total marginal carbon footprint for each language in the last row by summing each of the language columns. While the total marginal carbon footprint of each data center is obtained by summing the rows as shown in the last column. The English pages have the most traffic globally and as expected English has the largest marginal carbon footprint due to its data-center operations. Form the physical data center perspective, the model shows that the Ashburn data center has the highest carbon footprint. This can be attributed in part to the energy source's carbon footprint relative to other locations as shown in Figure 5.

Figure 6 is a histogram plot of the PUEs for all the data centers in the evaluated network. Each color in the figure represents a specific data center. The

PUE is indicative of the utilities system efficiencies; namely the cooling and the power distribution The x-axis in Figure 6 indicates the PUE value and the y-axis indicates the number of hours the data centers have at specific values. As a concrete example, the bars representing Netherlands site is labeled as ams-rl_PUE and has most hours at or below a PUE of 1.1. Other data centers also have a PUE of 1.1. Stacking the curves from the different data centers indicates the global network's time spent at a specific PUE. A major influencing factor for the PUE is the local weather conditions.

An understanding of the cooling design weather conditions may help reason about the differences in PUE. Lower PUEs generally coincide with cooler weather, which leads to more favorable thermo-mechanical equipment operating points. In practical terms, cooler temperatures enable facilities to be cooled with economizers for more hours and they also lower the equipment's energy demand when economizers are not fully operational. For the set of the data center analyzed in this work, the ASHRAE cooling design conditions are shown in Table 4 (from ASHRAE. (2009)).

As an implementation detail, the DOSCOE model proved to be quite sensitive to the data structure of the load profiles. For example any null value in the profile resulted in breaking the linear solver. Also, solar and wind energy are required to be non-zero for at least one hour of the year. This requirement is a practical constraint, but in the profile developed for this work the values are arbitrarily set to a low value across all hours. Specifically, the defaults setting used in the work is 0.1 MW for each hour.

Another implementation measure required the discounting of facility's base loads. Without this discount, each model accounted not only the incremen-
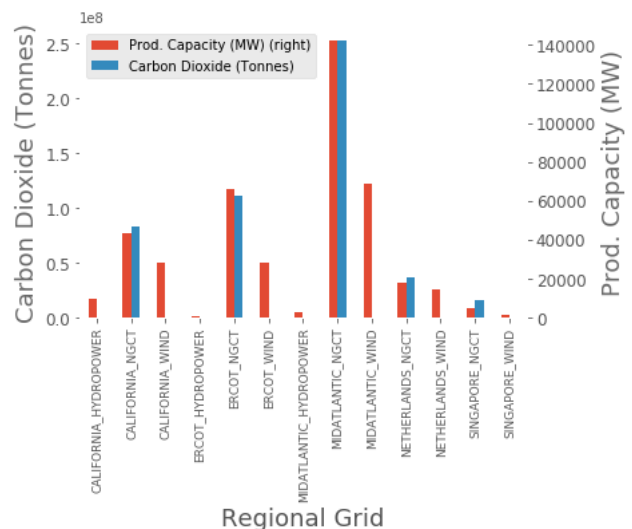

Figure 5: Energy Product Capacity and Carbon Emissions.

Site	German	English	Spanish	French	Japanese	Russian	Chinese	Total
California	0.0	1.24×10^6	0.0	0.0	0.0	0.0	0.0	1.24×10^6
Carollton	0.0	6.59×10^4	1.20×10^6	0.0	0.0	0.0	0.0	1.26×10^6
Ashburn	0.0	4.38×10^6	8.0×10^5	1.17×10^5	0.0	0.0	0.0	1.36×10^6
Amsterdam	2.81×10^5	2.25×10^5	9.85×10^4	2.67×10^5	0.0	3.15×10^5	4.67×10^4	1.23×10^6
Singapore	0.0	3.74×10^5	0.0	3.71×10^4	3.35×10^5	3.91×10^5	7.87×10^4	1.22×10^6
Total	2.81×10^5	2.35×10^6	2.09×10^6	4.21×10^5	3.34×10^5	7.06×10^5	1.25×5	6.31×10^6

Table 3: Data Center Operation Carbon Footprint (Tonnes of CO2 Emitted over the Year)
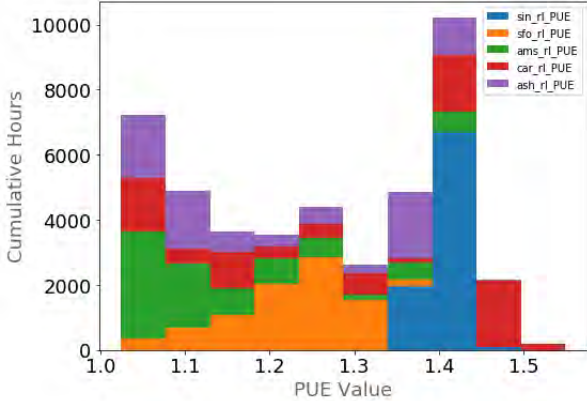
Figure 6: Stacked histogram of PUE from all Data Centers.

DC	0.4%DB	0.4%WB	1%DB	1%WB	2%DB	2%WB
Amsterdam	82	67.5	78.1	66.2	74.6	64.4
Ashburn	93.5	75.1	90.8	74.3	88.2	73
Singapore	91.7	79.4	91.1	79.4	89.9	87.2
Carrolton	100.4	74.5	98.4	74.6	96.2	74.8
San Francisco	83	63	78.3	62.1	74.4	61.2

Table 4: ASHRAE Annual Cooling and Dehumidification Design Conditions in °F ASHRAE. (2009)

tal load placed on the DC from a service's incoming traffic, but also it would account for the entire baseline loads in each EnergyPlus run. For sites with multiple services, this results in significantly over accounting of the base loads, as it would be included for all the services in the DC. To address this issue, a post processing step apportioned the baseline load to each service/language by using the traffic coefficients. For the attributions, an initial condition for the traffic coefficient is set to 0. With this initial condition, the BEM provides the baseline energy required by the data center (i.e. all equipment operating at their lowest turn-down rates). The traffic coefficient scaled this value, bound by the constraint that the sum of the coefficients is strictly equal to 1 for all time-steps of the simulation.

Conclusion

The network dependencies between physically dispersed data center resources make system level building design decisions a challenge to reason about. This research has presented a quantitative method to couple the network dependencies of data centers with

their building energy and grid level marginal costs of energy. The research extended the PUE metric with utility grids to indicate carbon footprint of data centers. Furthermore, as shown in Table 4 the presented method allows analysis of data center systems at global service levels.

As pointed out in the background section, there is a lack of bottoms up building design and carbon footprint models. The modular methodology of this research is a novel means of coupling abstracted service level metrics (WAN traffic in this case) with physics based building energy simulation (EnergyPlus in this case). This integrated tool set can be used by data center system modelers to optimize their deployment across geographical bounds. Future work should consider controlling the network traffic based on building energy simulations to achieve global optimality in real time operational environments.

References

Andrae, A. and T. Edler (2015). On global electricity usage of communication technology: Trends to 2030. In *Challenges*, Volume 6, pp. 117–157.

ASHRAE. (2009). *ASHRAE Handbook: Fundamentals*. Atlanta, GA: ASHRAE.

Barroso, L. A., U. Hozle, and P. Ranganathan (2018). *The Datacenter as a Computer: Designing Warehouse-Scale Machines 3rd ed*. Morgan and Claypool.

Hong, C.-Y. and S. Kandula (2013). Achieving high utilization with software-driven wan. In *SIGCOMM'13 ACM, Hong Kong*.

IEA (2017). International energy data and statistics. Retrieved: March 03, 2020.

Insight-Partners (2019). Data center construction market. Retrieved: May 12, 2020. https://www.theinsightpartners.com/reports/data-center-construction-market.

Kiani, A. and N. Ansari (2017). On the fundamental energy trade-offs of geographical load balancing. Volume 0163-6804/17, pp. 170–175.

Kumar, E. (2020a). Towards energy simulations for proportionally designed and controlled data centers. In *Accepted for Building Simulation and Opti-*

mization 2020. Loughborough (UK), 21-23 September 2020.

Kumar, E. (2020b). Wide area network based data center energy simulations for internet services. In *Accepted for 11th International Conference on Improving Energy Efficiency in Commercial Buildings and Smart Communities*. Frankfurt (Germany), October, 2020.

Open-Power-System-Data (2019). Time series open-power-system-data. Retrieved: April 02, 2020. https://data.openpowersystem-data.org/time_series/20190605.

Platt, J., O. Pritchard, and D. Bryant (2017). Data center construction market 2019-2024 — global industry overview by size, share, future demand, latest research by competitors, segmentation and regional forecast. *SSRN 08*.

Shehabi, A. (2016). United States Data Center Energy Usage, United States Department of Energy.

Shehabi, A., B. Walker, and E. Masanet (2014, may). The energy and greenhouse-gas implications of internet video streaming in the united states. *Environmental Research Letters 9*(5).

(2016). *Half Hourly System Demand. Retrieved: January 02, 2020*. https://data.gov.sg/dataset.

Sushant, J., S. Mandal, J. Ong, A. Singh, U. Holzle, and A. Vahdat (2013). B4: Experience with a globally-deployed software defined WAN. In *SIGCOMM'13 ACM, Hong Kong*.

Taylor, C. and J. Koomey (2008). Estimating the use and greenhouse emissions of internet advertising, IMC squared.

The Green Grid, T. (2012). Data center life cycle assessment guidelines. Retrieved: May 13, 2020. https://www.thegreengrid.org/en/resources/library-and-tools/236-Data-Center-Life-Cycle-Assessment-Guidelines.

Tripathi, R., S. Vignesh, V. Tamarapalli, and D. Medhi (2017). Cost efficient design of fault tolerant geo distributed datacenters. In *IEEE Transactions on Network and Service Management*.

USEIA (2016a). U.S. Energy Information Administration. Retrieved: May 02, 2020. www.eia.gov/international/analysis/country/NLD.

USEIA (2016b). U.S. Energy Information Administration. Retrieved: May 05, 2020. www.eia.gov/international/analysis/country/SGP.

van Steen, M. and A. S. Tanenbaum (2018). *Distributed Systems Third Edition*. Switzerland: Maarten van Steen.

Whitehead, B. (2015). The life cycle assessment of a UK data centre. In *International Journal of Life Cycle Assessments*, Volume 20, pp. 332–349.

Wikipedia.com (2020). Power usage effectiveness. Retrieved: August 01, 2020.

Input Data Workflow, Boundary Conditions, User Interface, BIM

Using inference from user attribution of models to support high resolution modelling

Jon Hand[1*]

[1]University of Strathclyde, Glasgow, Scotland

* corresponding author: jon@esru.strath.ac.uk

Abstract

Air flow networks are for many practitioners a _here-be-dragons_ territory and despite providing useful information short of CFD assessments it has remained a niche activity. The paper discusses how we might transition from user-imposed air flows to computed air flows for long term high frequency assessments within simulation practice. It explores the historical, developmental, domain knowledge and model quality barriers to this transition. It describes the implementation of an inference facility to assist in the creation of flow networks of hundreds of entities and applies this in case studies to show what a new normal might look like.

Introduction

Few developers write about the process of designing the evolution of tools and the nature of how a diverse set of observations leads to conceptual leaps and new facilities. Few practitioners write about how they evolved working practices and found ways to drive their tools outside their usual comfort zone. And the Passive House community attempts extreme design goals with tools that are highly abstracted and would definitely benefit from access to dynamic assessments. This paper combines these perspectives – the author as a practitioner pushing multi-domain simulation projects into new territory who is a Passive House Trainer as well as one of the developers of the ESP-r simulation suite. Scores of projects involving flow networks provide the evidence of current limitations and points of frustration as well as the wealth of information that practitioners might access. They provided a rich testing ground for adaptations of the simulation tool which this paper reports on.

Overcoming inertia

In the early years of simulation practice the simulation community had to choose what to solve and often drew the line at numerical approaches to air flow. We got used to acting as _deities_ who decided on a flow regime and imposed it even if it had little or no basis in physics. The _inertia_ within the simulation community for the habitual use of imposed flows remains considerable. For example, in Gowri (2009) produced guidelines for adapting fixed flow approaches when building pressure tests were available. This may lead to a better match for aggregate performance but the uncertainty has always been in apportioning this single measurement over the scores of leakage paths and across time.

Compliance methods impose a range of _arbitrary_ conventions which usually include imposed air flows. The risk for designers is in forgetting the arbitrary nature of such conventions. Imposing flow values taken from reference books is undermined by the evolving nature of building facades. As facades improve the energy flows associated with unintentional air movement are no longer noise in the system and have become something worth paying attention to. Imposing infiltration _as if we were deities_, is so 1990s.

There is also _inertia_ in how the simulation community zones it's models. Consider the classic core plus perimeter zones for office accommodation layout shown in the Figure 1. The boundary between the core and perimeter was often an effective barrier to air movement at a junction where a host of complex and dynamic flow patterns have been observed. Enlightened practitioners might add some scheduled mixing (and some simulation suites include specific entities to enable this). Ignoring mixing or imposing guesses of mixing rates is so 1990s!

A bit of background. A number of simulation tools are able go beyond user-imposed schedules of infiltration and ventilation to dynamically solve mass flow along with other domains. Some also provide linkages between mass flow and CFD domain. Flow networks are composed of **nodes** (e.g. within thermal zones or at boundary points) and **components** (e.g. openings, cracks, fans, pumps, conduits) and **linkages.** In Figure 2 there is a room node and three boundary nodes and one frame crack, one door undercut and one extract fan which is tied into a temperature control. Typically, there is a one-to-one mapping between internal flow network nodes and thermal zones rather than a mesh of hundreds of CFD cells per thermal zone.

Each tool has its own syntax and its own approach to interacting with the user and although ESP-r is the point of demonstration the observations will likely resonate with practitioners using other tools.

Traditionally networks would be carefully planned/sketched and critical parameters and locations noted prior to inputting the relevant information for the nodes, components and linkages. Work-flows tended towards the pedantic. Clear naming of entities was

assumed to provide the clarity required e.g. 'South door boundary is connected to entrance by crack-under-front-door'. Approaches to the planning and creation of flow networks are covered in (Hand 2020 Chapter 7) and http://www.esru.strath.ac.uk/applications/esp-r/.

Manual approaches work for a few dozen entities. Beyond that its hard work. Depending on the simulation tool, the facilities on offer and user skills, networks of a few dozen entities might be something to celebrate whilst other practitioners manage far greater complexity.
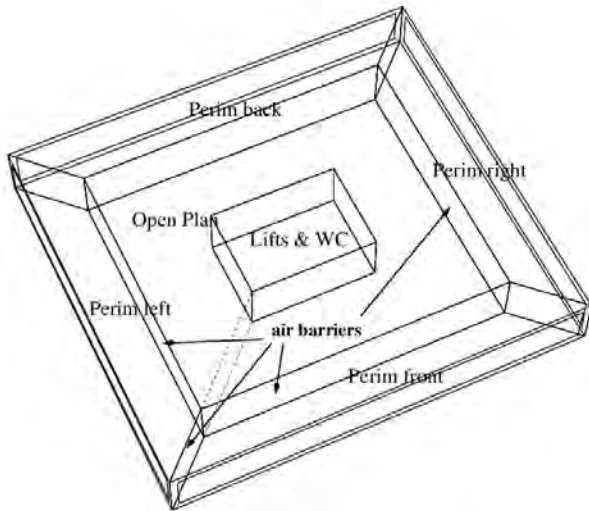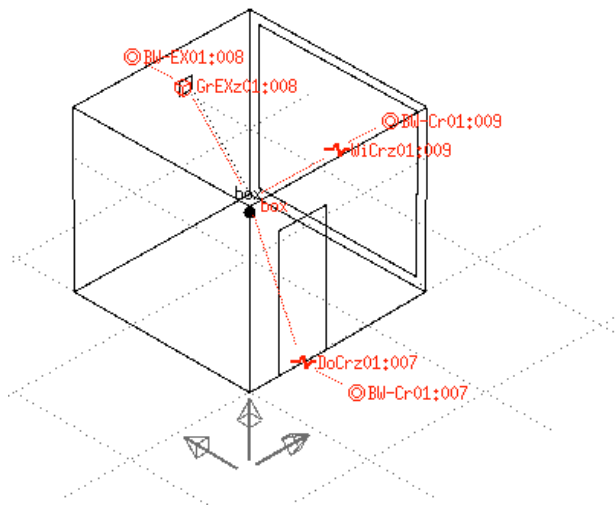

Figure 1: Classic zoning patterns

Figure 2: entities within a flow network

Regions where natural ventilation is a common design approach provided an early focus for the use of air flow assessments. Flow networks are well suited to assessing patterns and risks over long assessment periods when driving forces (wind direction, wind speed, internal conditions) vary considerably. In a UK context the majority of simulation projects our group has been involved in include aspects of natural and mechanical ventilation because they are a traditional approach to controlling overheating. In other regions natural

ventilation is a niche activity and few practitioners are in the habit of using flow networks. Perhaps this hesitancy to deploy flow might be traced to the history of its development and the facilities on offer?

Historical baggage

- Much of the research was carried out decades ago with an initial flurry of interest and research papers.

- Solving mass flows is viewed by many as numerically intensive and, by inference, not to be deployed by default.

- Habits of imposed flows have been difficult to break.

- Mass flow assessments have long been associated with natural ventilation studies.

- It is littered with jargon and assumed to be used by experts.

- Tool work-flows require attention to detail. Flow is usually treated conceptually separate from buildings and systems.

- Inputs focus on the underlying equations rather than information likely to be available to practitioners.

- There is little consensus in the community as to the scope, topology and attribution of flow entities.

- Component representations are often based on curve fits for which there is no clear **provenience** or which presume access to measurements.

Methods for defining and solving mass flow are indeed decades old (Henson 1991, Walton 1989). As these methods were embedded in simulation tools there was an initial tranche of research publications. In addition to Henson's description of the solution techniques underlying ESP-r's method is also documented within the source code (ESRU 2020) and in (Clarke 2001). A terse description of the solution technique from Hensen:

The technique of is to assign an arbitrary pressure to each of the "nodes" participating in a network and representing volumes of air. The flow along each connecting branch - representing either cracks, area openings, or doorways - is the determined from empirical equations relating air flow to pressure difference. The algorithm uses a node-wise Newton-Raphson technique to iteratively adjust nodal pressures until the air mass balance equals zero at each node simultaneously. A convergence device to ensure this end result even for networks involving a mix of large and small flow paths.

The solver is highly efficient, convergence is typically reached with dozens rather than hundreds of iterations.

Having described the methods and demonstrated the facilities there were a few follow-up conference papers and a limited cohort of researchers and practitioners deployed the facilities. This pattern was repeated after air flow was introduced into EnergyPlus (Lixing Gu 2007).

Most readers of these initial review papers would conclude, not unreasonably, that dragons tended to congregate around flow networks and it just slowed everything down. Because the topic is sparsely covered in

journals or in building simulation conferences such perceptions persist. Solving flow networks takes a fraction of CFDs resources and, at least in the case of ESP-r, a minimal increment over scheduled flows - for example a 40 node network solved for a two minute timestep over one week added seven seconds to run time.

It has long been an been considered an art to design a network that captures relationships embedded in a set of construction drawings or gleaned from photographs taken from a site visit. Fragmentation in the simulation community has limited the spread of best-practice guidance and thus flow networks design is a hard-won skill set.

This needs a radical re-think. At the component level practitioners are sometimes asked for values which, with a bit of digging, are possible to acquire or transform from standard sources via well documented methods. These could be revised for practitioner use. And then there are the dragon components which presume you own an entire testing lab because that is what the author of the method had access to. Here we desperately need fresh formulations.

A new normal

Looking back over a decade of projects which included flow networks a number of patterns emerge:

- computational resources are usually **not** the limiting factor in the project
- expertise tends to get re-invented rather than embedded
- there are ubiquitous instances of air flow which follow patterns and can be codified
- it pays to occasionally check the original intent of flow components
- user tasks are constrained by the time needed to envision relationships and locate gaps in networks
- simulation tools are not very good at communicating predictions of flow patterns

These projects also provide valuable usability clues:

- noticing minor user frustrations and instances of ad-hoc note taking,
- noticing points of friction that emerge at magnitude jumps in complexity
- documenting work-flows and instances of re-invention in subsequent projects
- observing what power users take for granted
- noticing that design teams are often not very good at observing air movement

The advent of widespread pressure testing provides anecdotal evidence. However, it is early days for the task of calibrating virtual flows from such tests, in part because overall leakage rates tell us little about how air distributes between rooms and via specific faults in facades. The fault detections carried out during pressure tests indicate:

- real building facades have an abundance of faults
- rain-screens hide any number of faults
- wall cavities and service voids can provide substantial shortcuts for air movement

The advent of high- performance facades has changed the rule sets. Clients are demanding more of design teams and so a number of design patterns are evolving and new classes of design questions are being asked. In order for flow network to supplant imposed flow traditions it needs to impose less friction on workflows and have a clear visibility within the simulation tool. The above bullet points suggest that we want to move the point where we can productivity deal with networks of hundreds of entities. This paper argues for and explores the pervasive inclusion of flow networks as a new normal for high resolution models.

At least for ESP-r, development tends to be incremental. The paper reports on a series of interventions by the author in the code and the data structures of the simulation tool ESP-r to transition from manual creation of the nodes and components to one based on inference. This involved thousands of lines of code, new interface menus as well as the creation of test models and eventually exemplar models for distribution.

As new data structures, menus and inference logic emerged they were tested in live research and consulting projects. Some code interventions save more time in their first use than it took to write them. Some conceptual leaps require extensive adjustments to the code that can take weeks to implement. What follows is a synopsis of the driving forces and code interventions taken.

Firstly, unlike those who have traditionally created flow networks or do blower door tests, design teams are often not very good at observing/envisioning air movement or faults in facades or in construction documents. We need another way to gather the attributes and relationships needed for the creation of flow networks.

So rather than going into a specialist facility focused on flow let's use a different point of interaction. Almost all leakage paths in a building have an analogue to surfaces and zones or system components that we have already created in our simulation models. For example, the user adds a surface representing a door between two rooms. In the past users would signal this intent via the surface name and composition. The idea is to formalize this user intent. Another conceptual leap is to notice patterns in past models and the ad-hoc notes and types of components and linkages power users.

One of the first steps was to introduce a surface USE syntax which could capture the observed patterns. Table 1 shows the matrix of the USE syntax that evolved. In keeping with the constraints of incremental development these were initially embedded in the model files as documentation.

Projects and users with access to this documentation found model quality checking was more straightforward

and the networks were closer to the intent embedded in the planning sketches.

Table 1: Surface USE syntax.

Key phrase	Implemented as
DOOR:CLOSED	Crack around perimeter of surface
DOOR:UNDERCUT	Orifice width of door with user defined height
DOOR:OPEN	Orifice with discharge coefficient and perimeter crack
DOOR:BIDIR	Two way flow with full surface width & perimeter crack
DOOR:ADJ-BIDIR	Two way flow with constrained width and perimeter crack
FRAME:CLOSED	Crack around perimeter of surface
FRAME:VENT	Orifice following a specific rule set
GRILL:CRACK	Crack around perimeter of surface
GRILL:INLET	Fixed volume flow incoming
GRILL:EXTRACT	Fixed volume flow extract
GRILL:OPEN	Orifice with discharge factor
GRILL:DUCT	Conduit with hydraulic diameter and local loss factor
WINDOW:CRACK	Crack around perimeter
WINDOW:OPEN	Orifice with user defined area
WINDOW:SASH	Pair of orifices with user defined areas
WINDOW:BIDIR	Two way flow with full width & perimeter crack
WINDOW:ADJBIDIR	Two way flow with constrained width and perimeter crack

Next it was necessary to address the unintended consequences of focusing on the needs of the solution technique rather than clarity for the user. For example, the ESP-r flow solver requires the difference in height between components and nodes in the network but not their position in space (show image). Fewer numbers is 'good'. Flow networks were usually designed to be as simple as possible but the advent of surface USE attribution suggested rather more complex networks. We had to relax the 'fewer numbers and fewer nodes is good' mantra in order to convert USE documentation into directives used during the creation of networks and support additional views of networks.

The next step was a translation of these key words into flow components which took position, perimeter length and boundary conditions from the surface. In addition, for facade components, a matching boundary node was generated. The expectation was that the user would then traverse the resulting network to fit the specific needs of the project. This greatly reduced input errors but still expected quite a bit of input from the user.

Initially doors and windows flow components were set to match the surface area they were associated with. However, most windows do not open fully and experts would either have planned surfaces to reflect the actual opening area or edit the orifice area so it made sense to allow this kind of transform as the network was being created. Many projects included user edits to constrain the width of bi-directional flow components because many occupants leave doors ajar. This suggested that the key words to signal this as a special case.

Over several projects it became clear that users tended to impose control on doors and windows and fans and it was necessary to add parallel crack connections to the network so there was always a path to a boundary condition when the primary flow path was closed. The code was adapted to create parallel crack connections for components which could be controlled. This resulted in a more complex but future proof network.

Another conceptual leap was that as network complexity grows so does the need for ensuring the user is aware of the immediate context of a flow entity and that feedback takes multiple forms (Figure 3). Feedback to the user involved the introduction of icons on the wireframe display as USE attributes were initially defined and as well as new entries in the control menus. This reminder was critical for work flow tasks involving surface attribution. These same display facilities were used when working in expert mode within the network flow menus to remind users of linked entities.
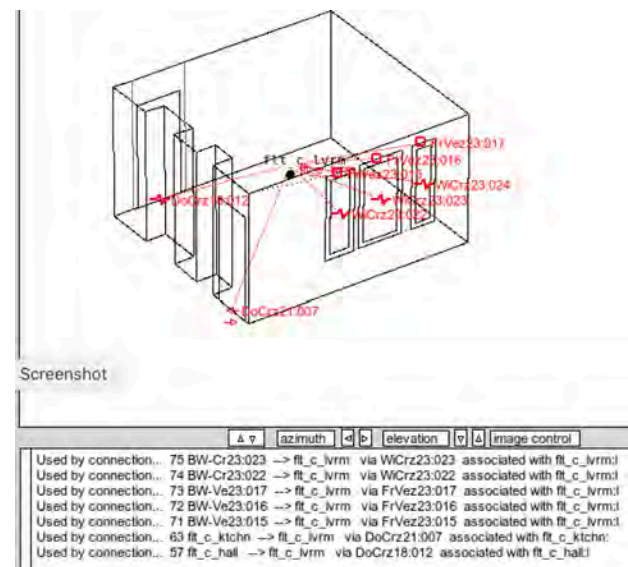

Figure 3: Zone context from within flow facility.

During the initial creation of the network the wireframe display network overlay was also updated as new entities and linkages were added. For small models and simple networks this worked but for larger models the display became overly cluttered and users lost contextual information needed for accurate editing. Another

observation was that once the network had been created and the building evolved the user was forced to jump between the surface attribution menus and the flow attribution menus. It made much more sense to add the functionality within the zone surface attribution facility, as in Figure 4, to avoid the traverse and to offer the same form of feedback as was offered during the initial creation of the model. This further eased user tasks and it was possible to manage rather more complex networks.
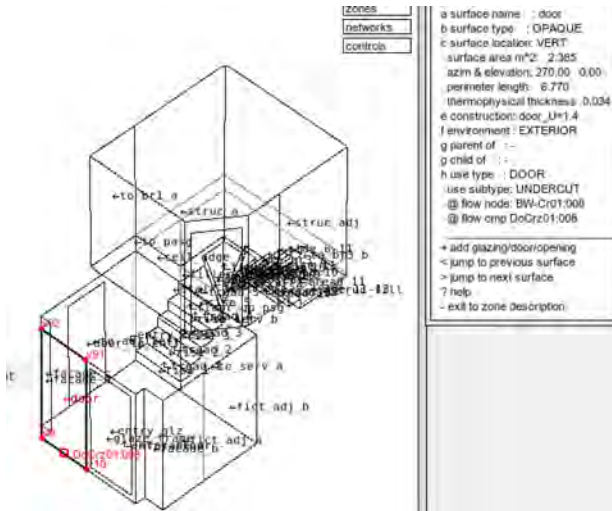

Figure 4: Context of flow components within zone.

Inference and revisiting initial assumptions

In addition to the relative straightforward bookkeeping tasks and interface updates a parallel evolution was considered for considering whether the flows resulting from the USE-to-component conversion were as expected. In the case of DOOR:UNDERCUT some unexpected predictions were found. The author had often used a crack component as 4-5mm undercuts seemed to fit the definition. Passive House suggests door undercuts of 10-15mm so that the pressure drop between rooms is typically in the range of 1Pa. However, beyond ~5mm of undercut the predicted flows were much less than found in the literature. A set of virtual experiments setup to match physical experiments reported in the literature eventually indicated that orifices would be a better fit.

Another issue was the treatment of ubiquitous element of many facades such as so-called trickle vents. Their intent is to ensure a minimal level of background ventilation. It turns out there are standard reporting conventions which provide just enough data to result in a good fit orifice and a well-documented method for converting product reports if experts wish to fine tune their network. A set of virtual experiments were setup to find mappings between published data and flow predictions. Patterns were discovered so that the inference logic could generate a fair set of initial attributes. The accumulation of inference logic is at the early stage but intent is to gradually improve the initial attribution of other ubiquitous flow entities.

The last stage reported on this paper reverts to a focus on natural ventilation. Refurbishment projects in the UK often focus on upgrading the thermal performance of facades and improving air tightness. As expected, this ratchets up occurrences of overheating and as natural ventilation is likely to be used to control overheating it needs to be included in the model. Schedule increased infiltration to mimic occupants opening windows is so 1990s!

Reviewing dozens of models where natural ventilation controls had been manually created a number of patterns emerged. The logic needs to not open windows if it is overly cold or hot outside and it is kind of silly to open windows when the heating or cooling is on. And it would also be convenient to disable natural ventilation controls by ensuring that all windows are closed. The code was extended to create a global facade control preference facility which asks a few high-level questions and then creates the relevant controls for each of the facade components. Experts could, of course, tweak these controls but the time savings in projects was considerable. Of course, natural ventilation is only one of a host of common design intents to which a software agent could have an impact.

Refurbishment Case study

A 2019 refurbishment project is indicative of the practical issues related to designing flow networks to reflect a) the state of the base case and retrofitted buildings, b) representing different ventilation ideas the design team was considering and c) finding that the assessments were tracking in the same direction as other monitoring projects. As is typical in such projects a matrix of ideas to consider needed to be tested and benchmarked against the building prior to refurbishment. The base case consisted of four two-bedroom apartments (on the left of Figure 5) and the refurbishment options included an adjacent building of the same layout which would have an external insulation system applied to all of the apartments. One flat would also have a mechanical extract system and floor heating, another would have the vent system plus skirting board heater, as in Figure 6, and one flat would have the mechanical extract system with a mix of skirting board and conventional radiators.
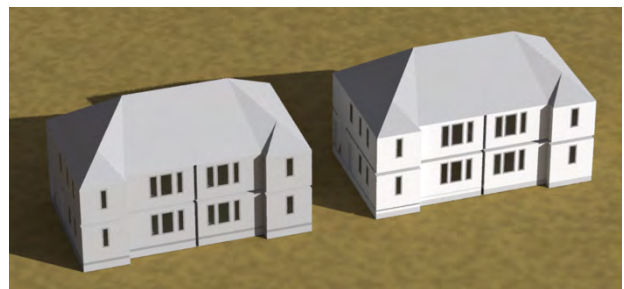

Figure 5: Base-case and refurbished apartments

The mechanical extract was intended to improve indoor air quality and control humidity levels. To limit costs extracts were only connected to the main living space, the

kitchen, bathroom and passage and humidity sensors would open dampers into the main extract chamber. Thus, there were many possible combinations and the pressure imbalance created also influence inter-room flows. The idea was also to use humidity-controlled facade vents.
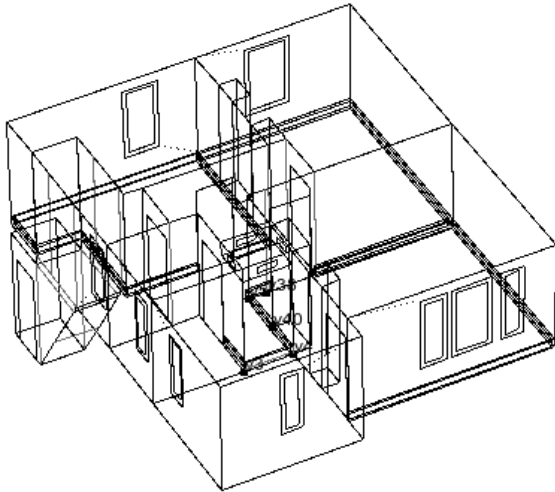
Figure 6: View of flat with explicit skirting board heaters and extract system

A number of refurbishment ideas required explicit representations so the extract mixing boxes, crawl spaces, roof voids, heated floors sections and skirting heating units were treated as separate thermal zones. Considerable diversity was enabled for occupants and humidity generation in various rooms which lead to some obscure corners of the internet to discover heat and humidity associated with various cooking and bathing activities. The resulting model comprised 75 thermal zones. Additional surfaces representing the grills and the casing of the skirting heating and floor structure were included to support detailed comfort assessments. There were 50 room controls to accommodate the various heating regimes and 20 controls for flows associated with the extract system. The flow network included 238 nodes and 253 components - somewhat greater complexity than would have been common a few years ago.

To support the study a virtual test chamber was setup to find a set of component attributes that matched the published pressure drops for the facade vents but it was not possible to find full details of the control logic used in the extract system. Flow controls traditionally sense temperature or humidity but not both so a more complex network was required. There were no pressure tests available so it was not possible to calibrate the facade faults included in the model.

The report to the client focused on the following metrics:

- Peak capacity of heating equipment
- Energy demands over time
- Distribution of temperatures within the flats
- Hours over 25C in each of the rooms

- Response during cold periods
- Frequency of ventilation boost rates (Figure 8)

The findings of the project report related to flow were:

- The design largely suceeds in improving indoor air quality and limiting humidity buildup.
- In cold conditions there is a risk of draft and compensating heating demands.
- It provides only limited overheating protection and trickle vents are marginal in summer conditions.
- Huidity remains high in bedrooms if doors are closed.
- A façade upgrade without addressing ventilation issues lowers heating costs but results in generally lower comfort and air quality.
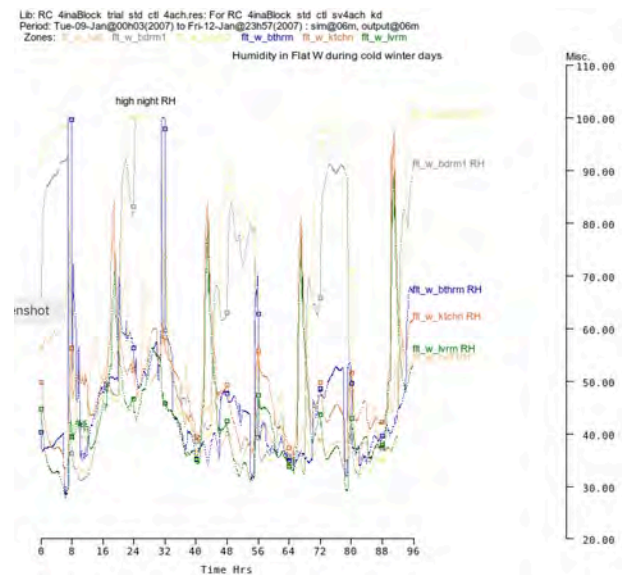
Figure 7: Humidity levels in bedrooms
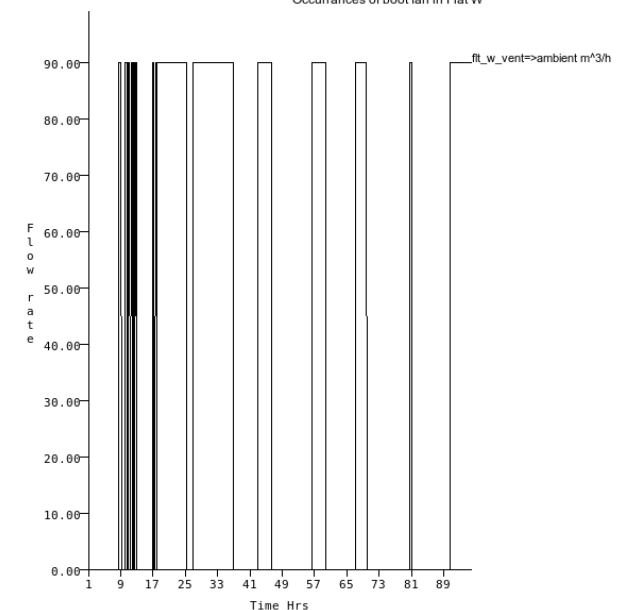
Figure 8: Instances of ventilation boost fan

Although officially sanctioned the efficacy of trickle vents has been questioned in many studies. When

combined with closed doors to bedrooms the reductions in flow had clearly detrimental impacts on air quality and humidity. Revising the model to add extract grills in the bedrooms mitigated much of this risk but would have required more inlets than the extract manifold was designed for. The other finding was the moderating impact of at least partly opening the door between the kitchen and living area. Overheating from cooking was dissipated more readily and helped compensate for the limited heating capacity of both the floor and skirting board heaters.

Resilience testing case study

Some projects are focused on the resilience of buildings, for example, looking for instances of discomfort if particular failures happen in the fabric or operation of a building. Design teams identify what metrics, at what frequency would signal failure. The building is continuously assessed and subjected to random faults at random points in time to see if the expected standard of performance is maintained. When failures are detected the further investigations can be invoked. Air flow assessments are well placed to cope with such continuous assessment scenarios. The 'further investigations' potentially need higher resolution and here is where a mix of air flow and CFD assessments can be used.

A design team was concerned that one of their high performance housing designs (Figure 9) might be at risk from overheating and so a high resolution model (Figure 10) was created with a flow network in place which had been designed to support natural ventilation for overheating (30 nodes 34 components and 34 connections). The model also hosted CFD domains in the primary rooms to support detailed assessments without the overhead of domains in minor spaces. In ESP-r CFD domains are tightly coupled to air flow networks as well as thermal zones and adapt at each timestep to new boundary conditions.
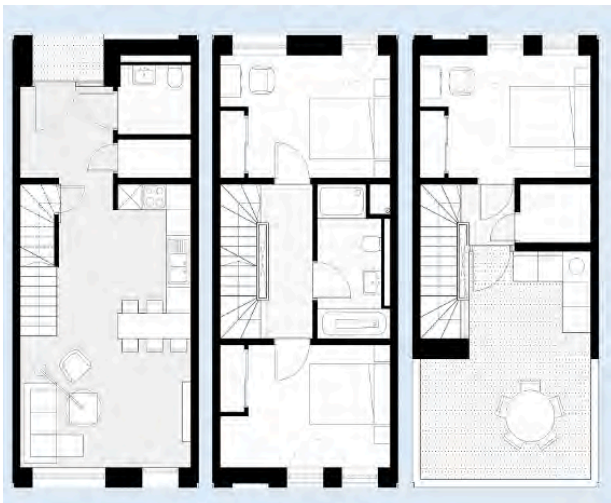
Figure 9: Terrace house for overheating risk assessment.
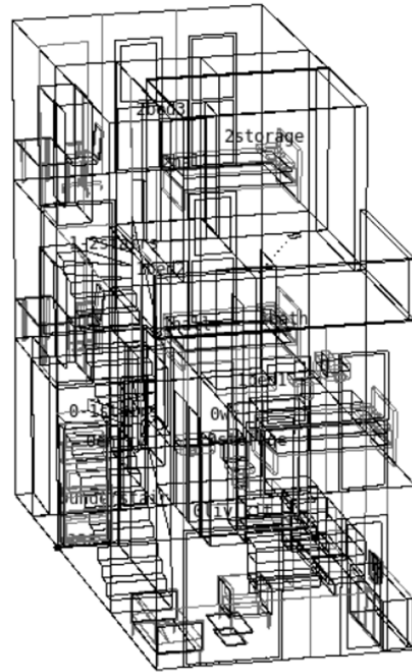
Figure 10: ESP-r model of the house.

Detailed assessments would typically look at patters over a few days at 10 minute interval. Figure 11 shows flow patterns, temperatures and CO_2 concentration in the kitchen/lounge.

Skills acquisition

The approach taken requires practitioners to notice and attribute surfaces within the model. Users need a bit of background as well as hints gleaned from power users (but with the jargon stripped out). There are a number of steps in the process that needed to be documented and it became clear that this worked much better if a number of sessions were captured and then annotated. Users have access to:

- A web page with guidance on how to survey buildings with multiple worked examples and videos of the process of creating networks.

- Exemplar models have been updated or added which demonstrate a number of classic use cases.

A number of practitioners have used the new facilities and the author found fewer faults in these models and also noticed that they were somewhat more complex than those users had managed in the past.
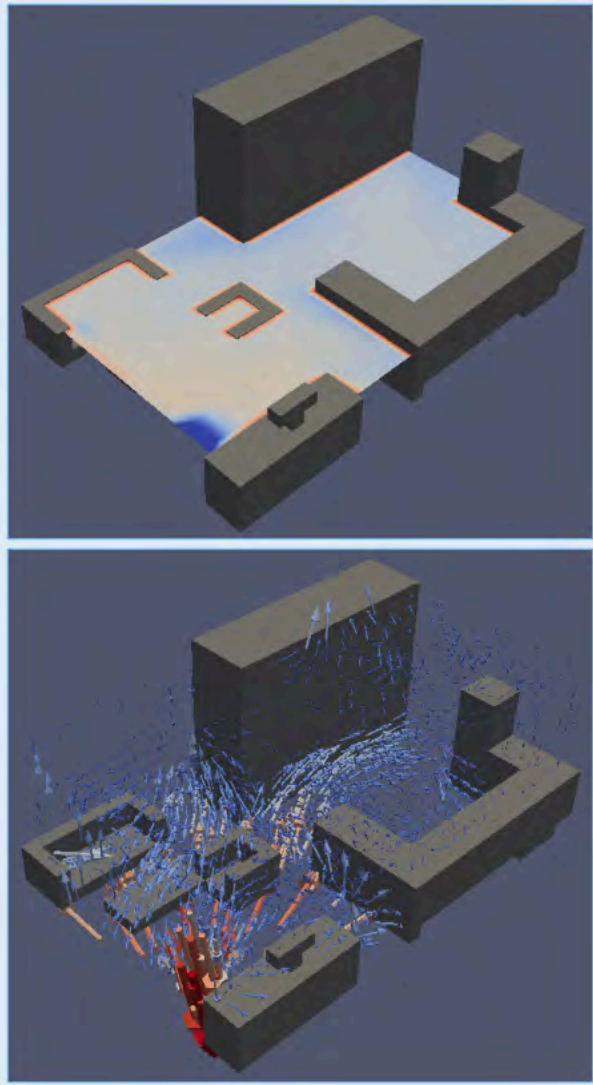
Figure 11: CFD plots in primary rooms.

Conclusion

The approach taken in the work reported is requires that users signal the use of entities in the model. The tool makes inferences which should result in a well-founded model but, crucially, the user gets a veto over what has been generated. Full details are reported and it is assumed that flow experts will be tweaking the network to match their opinions.

The nominal complexity of models has shifted by roughly one magnitude and it is possible now to consider applying air flow assessments within less constrained projects. An ongoing project is looking at eight different construction types in a new neighbourhood of 48 houses with physical and virtual tests carried out on a sample of a dozen houses. Modelling of each room in those dozen houses requires roughly 100 zones and including a mix of mechanical vents and window openings is going to roughly push the network complexity to 300-400 nodes and components.

Parallel work is underway to streamline the creation of CFD domains within ESP-r. Currently users have a number of 'rules' that they need to follow and additional specifications and linkages which must be supplied. The long-term aim is to lower both the friction and expertise needed to work with CFD domains.

This paper has not discussed the state of other simulation tools which feature air flow solutions. Some hide the networks that are created from users. What a strange decision in light of practitioners need to carry out due diligence.

Other tools also have historic baggage that has limited the up-take of flow assessments. The Gu (2007) paper includes a horrific chart showing the relationships between flow related entities for EnergyPlus. Names and numbers for flow entities in IDF files use a different syntax from the legacy flow network files of ESP-r but their focus on feeding the underlying equations obscures how they relate to the building and limit graphic presentation options. See how far you get in five minutes reviewing the simple EnergyPlus house exemplar AirflowNetwork_MultiZone_House_FanModel.idf?

It will be interesting to see the extent to which practitioners are able to leverage the ideas and facilities discussed in this paper and what further evolution might be required to make user imposed flows a niche activity.

Acknowledgement

References

Clarke, J.A. (2001). Energy Simulation in Building Design, Second Edition. Butterworth-Heinemann. (UK).

Gowri K., Winiarski D., Jarnagin R. (2009). *Infiltration Modeling Guidelines for Commercial Building Energy Analys PNNL-18898.* Pacific Northwest National Laboratory, Oak Ridge, TN (USA). https://www.pnnl.gov/main/publications/external/technical_reports/PNNL-18898.pdf

Gu, L., "Airflow Network Modeling in EnergyPlus", 10th International Building Performance Simulation Association Conference and Exhibition on September 3-6, 2007 in Beijing, China

Hensen, J.L.M. (1991). On the thermal interaction of building structure and heating and ventilating system. Glasgow. (UK).

Hand J. A. (2020) Strategies for Deploying Virtual Representation of the Build Environment http://contrasting.no-ip.biz/Strategies/Index.html

Working With a Small and Predictable Performance Gap

Marc Azar[1], Par Carling[2]
[1]EQUA Simulation, Solna, Sweden
[2]EQUA Solutions, Solna, Sweden

Abstract

Much is written about the performance gap. Multiple studies show alarming discrepancies between design and actual building energy performance. Should this prove to be a *universal truth*, the need of more detailed dynamic modeling methods can certainly be put into question. The prevalence, of somewhat antiquated, monthly methods in many current building codes seem to support this view.

In this paper we demonstrate a case supporting the opposite viewpoint. When the motivation and tools are right, sufficient accuracy between prediction and actual energy performance can be achieved. We present a building modelling case, where appropriate data was collected over a period of a full year for an office building with gross floor area of 31,809 meter squared in Stockholm, Sweden. We showcase how by abiding by a Keep it Simple and Straightforward approach in modeling one is able to achieve accurate energy performance predictions without sacrificing on capturing building's dynamics and internal states. However the selected project is not a singularity, but represent the mainstream in state of the art Swedish design practice. We end by highlighting some pitfalls with current guidelines regarding calculating goodness of fit measures between empirical data and a dynamic simulation model, and providing some recommendations for more appropriate metrics.

Introduction

Building commissioning is becoming a vital part of the building construction industry in Sweden, where legislation requires a two year commissioning phase for new constructions. The construction industry has since had to bridge the energy performance gap between initial design models and the physical building in a way that is practical and robust enough for industrial use. Moreover, utilizing a consistent, unbiased, and transparent methodology for building modeling is deemed an important factor for reliable and trustworthy results.

In this paper we describe our methodology behind modeling and simulating a physical building for achieving a small prediction gap. We consider the complex and fast acting dynamics behind the heating and cooling demands of the building, as well as it's underlying custom control structures over a period of a full year. We demonstrate this using the building performance simulation tool IDA ICE,EQUA (EQUA), a commercial tool for whole year building energy and indoor climate simulations, which allows the creation of custom controls and HVAC systems.

The structure of this paper is as follows. In Section II we describe the physical building envelope and zoning, as well as the nature of the collected input data; we also discuss our modeling approach. Section III details the building's HVAC systems and control sequences. along with their implementation within "IDA ICE". In Section IV we present our findings and results, highlighting the attained small prediction gap. We also reflect on the adequacy of the ASHRAE guideline 14-2014,ASHRAE (2014), on describing goodness of fit measures for dynamic simulation models. Conclusions are drawn in Section V.

A Case Study - Gångaren 11

Gångaren 11, the current headquarters of Skandia AB, a Swedish independent banking and insurance group, is located in the central Stockholm district. The office building was built by Skanska AB, a Swedish project development and construction group, throughout 2010-2011, and is certified as a "Green Building". The building houses around 1200 employees, and spans a gross floor area of 31,809 meter squared over a total of eight floors, seven of which are offices. The building also has access to an underground garage, and has a double skin façade with internal blind control, as well as a glazed atrium running through the center of the building. Figure 1 depicts the building envelope. The zoning of each of the office floors consists of dense private offices along the outer and inner perimeters of the envelope. The first floor also includes a kitchen and food court area, along with a small refrigerated room, and three small data center rooms. A sample office floor layout is shown in Figure 2.

Zoning and modeling data

Thermal zones were constructed with accordance to ASHRAE 90.1-2007 appendix G3.1.7-9,ASHRAE (2013). For the office floors, two geometric zone configurations were constructed.

The *perimeter* zones extending 5 meters from the outer building envelope, and the *inner* zones covering the remaining inner space. The atrium was modeled as a separate zone. The office floors were sectioned with respect to orientation, classification,

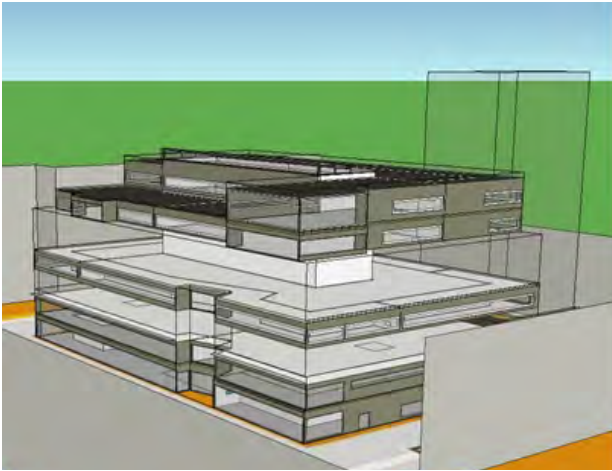*Figure 1: Gångaren 11, double skin façade building envelope*

Figure 2: IDA ICE 3D model view of the Building

and common HVAC systems. Zone multipliers were used for similar zones, while the building body was divided across the top, bottom, and middle floors. A simplification was made for the double skin façade with the total U-value and SHGC abbreviated into a single glazing. the glazing U-values were supplemented by a 10% increase on the rated value to accommodate Swedish climate conditions. Internal and in between blinds, as well as a 100 mm recession in the window frames were accounted for in the model. The average glazing U-value was around 1.4 W/m² K with a SHGC ranging between 0.2 and 0.6. The blinds had a multiplication factor for the SHGC of 0.4 when drawn, and a control schedule set to an upper limit of 150 W/m² of irradiance inside the zone. The ground layer is modeled according to ISO 13370 with 1 meter of soil, while the exterior walls have an average U-value of 0.20 W/m² K, and a roof U-value of 0.13 W/m² K. Thermal bridges were defined per joint type, and infiltration was modeled by an air flow network, with an average leakage over the envelope of 0.6 L/s m² external surface at 50 Pa. Figure 3 shows the building envelope and zoning in IDA ICE.

The weather file, which includes dry-bulb temperature, relative humidity, Direct normal irradiance, Diffuse irradiance, and wind speed & direction, was ob-

tained from the Swedish Meteorological and Hydrological Institute, SMHI, weather service. The service implements a mesoscale analyses system called MESAN for wind, temperature, and humidity measurements, and a modeling system called STRÅNG for global horizontal irradiance, and direct normal irradiance. The measurements have a spatial resolution grid of 11x11 km,MESAN (MESAN); STRANG (STRANG).

HVAC systems and Controls

The building is serviced by district cooling and heating, and has four Air Handling Units with liquid-coupled heat recovery and a free cooling circuit, as well as two air recirculation units dedicated for the atrium. The garage is heated via the return air of one of the AHUs, while the toiletries, recycling room, utilities room, and staircases are serviced by forced exhaust fans. A small ground heating unit, for melting snow, is located in front of the garage entrance.

The rooms are cooled through active chilled beam units, and heating is delivered by water radiators with thermostatic actuators regulating room temperature. Most rooms are supplied with Constant Air Volume flow, except meeting areas and the food court which have a Variable Air Volume flow controlled by dry-bulb temperature. The room set-points are 22^oC, and 23 ^oC for heating and cooling respectively. Winter/Summer mode activates according to outside air temperature.

$$\text{Summer:} \begin{cases} T_{out} & > 17^oC \\ \frac{1}{3} \times \sum_{i=1}^{3} T_{out,i} & > 12^oC \end{cases}$$

$$\text{Winter:} \qquad T_{out} < 5^oC$$

The building has night set back ranging between 5 and 10^oC, depending on outside temperature, from 18:00 till 05:00, except for the month of January. Night ventilation control scheme is as follows:

$$\text{Activate:} \begin{cases} T_{in} & > 23^oC \\ T_{in} - Tout & > 4^oC \end{cases}$$

$$\text{Deactivate:} \begin{cases} T_{in} & < 21^oC \\ T_{out} & < 10^oC \\ T_{in} - Tout & < 2^oC \end{cases}$$

Free cooling is made available whenever $T_{out} < 15^oC$. The free cooling network, recirculates the cold water circuit of the active chilled beam units into a heat exchanger on the supply air side of the Air Handling Units. The control schemes were implemented as is, while the 4 AHUs were lumped into one single AHU. Similarly a single recirculation unit was modeled as a sum of the existing two units supplying the atrium. The kitchen was modeled with a separate AHU, one which contains no heat exchanger. Figures 4 & 5

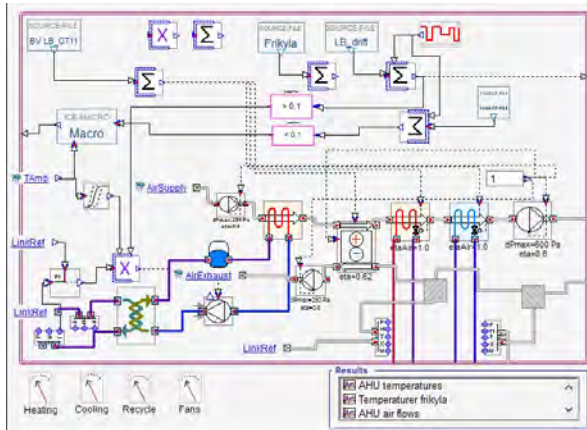show the plant and main Air Handling Unit modeled in IDA ICE.

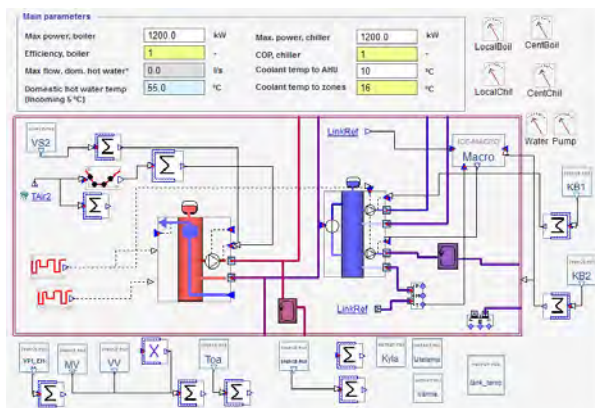*Figure 3: IDA ICE schematic view main AHU*

Figure 4: IDA ICE schematic view of the plant

The main AHU features a cooling coil, heating coil, heat exchanger with 62% efficiency (see subsection C), and the free cooling circuit. The free cooling circuit has an additional control condition in the form of a delay function. The building has a delay control function of one hour, delaying district cooling for a period of 60 min from 07:00 till 08:00, in order to avoid peak surcharges on cooling. The recirculation unit, is equipped with a heating and cooling coil only, at a set-point of 22°C. While the kitchen is modeled with an AHU, also equipped with only a heating and cooling coil, supplying air at a set-point of 19.5^{o}C.

District cooling and heating are modeled with COP of 1 and capped at 1200 kW. The hot water system provides hot water at a proportional set point between 60 and 20 ^oC for outside temperature range of -20 and 20 ^oC for the AHU network, and a set-point between 55 and 15°C for the same range, for the room unit network. To account for pipe and network losses, a tank is modeled at the supply side of the room unit hot water network with a capacity of 10 m^3, and heat loss of around 10% of total hot water consumption. Cold water is provided at a set-point of 10°C for the AHU unit cold water network, and at 15°C for the

room unit cold water network. Two tanks were modeled on the supply side of the cold water network of the AHU and room units, each with a capacity of 7 m^3.

The office building also contains three small server rooms which contribute to processes cooling consumption, and are serviced by the main cold water network in the model. To simulate this, a separate small room was added, where process heat was injected into the zone and removed by a fan coil unit connected to the main AHU network. To quantify the amount of process cooling needed, we analyzed the collected sensor data from the building. Cooling demand at off schedule hours on a cold winter day, i.e when cooling is not required, gives us an estimate of the base process cooling load, as well as cold water network losses in the building. Those were estimated at around 30 kW. Similarly to get an estimate of heating losses in the domestic hot water network, we examine the heating demand of a building at a hot summer day at peak hour, i.e when heating is not required.

The set-points and control schedule are fed into the modeled plant and AHU from the sensor data of the building. While internal gains were estimated from the electricity consumption of the office building. The electricity consumption can also provide us with a control signal for occupancy presence, due to it's high correlation with occupancy presence profile in an office building setup. A high pass filter was applied on the occupancy presence profile in order to remove the baseline value of occupancy presence during nighttime and off working hours. Moreover in an office type building 100% of the electricity consumption can be considered as added heat in the form of radiation and convection, with the exception of the kitchen area where almost all the heat demand is discarded as losses. The distribution of occupancy was uniform with an occupancy density of 1 person per 30 m^2, the figure can be considered sparse but it includes unoccupied spaces.

Domestic hot water was not considered in the model, but was directly fed from measured sensor data from the building. It is often difficult and stochastic to guess and estimate dynamic hot water consumption in a building. The small ground heater was also not included in the simulation model, and was instead fed to the model from measured sensor data.

Preprocessing of Sensor Data

The building has a total of 460 sensor signals, at a frequency of 0.0016 Hz (1 reading every 10 min). A full year worth of measurement data was collected for 2011. The building has an outdoor temperature sensor, however the building's outdoor temperature sensor was peppered with spikes, due to the sensor being unshaded from direct solar radiation. The temperature signal was therefore filtered with a sliding me-

dian filter, and compared with the temperature measurements from the weather file. The two measurements matched well, with an hourly Residual Mean Square Error, $RMSE_h = 0.0029$. The filtered outside temperature sensor was therefore qualified to replace the temperature from the weather file. It is standard practice to use the direct outside temperature sensor from the building's location instead of the weather station temperature readings, due to the prior being a better indication of ground truth.

Accumulated electric power consumption was metered for four different sections in the building; the kitchen area, offices, facilities, and an annex area. The accumulated graphs were differenced to yield instantaneous electric power consumption. Process electricity was subtracted from the total figure, as it was added separately into the model. While only 10% of the kitchen's electricity consumption was considered as heat gains for the kitchen area. All remaining electricity was considered as heat gains, and was uniformly distributed according to floor area across the model, excluding garage, atrium, and storage floor areas.

The electricity consumption of the office areas was converted to a control signal by data normalization:

$$X_{norm} = \frac{X - min(X)}{max(X) - min(X)} \qquad (1)$$

the control signal was multiplied by the occupancy density, and uniformly distributed according to floor area across the model.

The temperature transfer efficiency for the heat exchangers were computed, and estimated at around 62% under normal working conditions.

$$\eta_{supply} = \frac{T_{supply} - T_{inlet}}{T_{return} - T_{inlet}} \qquad (2)$$

By comparing the supply and return temperature transfer efficiencies, we analyzed the flow balance in the building.

$$\eta_{return} = \frac{T_{return} - T_{outlet}}{T_{return} - T_{inlet}} \qquad (3)$$

Since we were lumping the AHU in the model into a single unit, the control signal had to be calculated as the normalization of the total sum of all existing supply fans flow meters. We calculated the measured power of the free cooling circuit from the volumetric flow of the supply fans, and the temperature difference across the cooling coil $T_{in,c}$ and $T_{out,c}$.

$$\dot{Q}_{free,cooling} = \rho * cp_{air} * \Delta T * \dot{V}_{supply} \qquad (4)$$

The outlet temperature of the cooling coil in the free cooling circuit was not measured directly, instead the temperature sensor was located at the inlet of the

heat exchanger after the supply fans. Thus a correction value of 0.3^oC was added to the ΔT term. The Specific Fan Power was then calculated from measured data by dividing the measured power consumption of the fans with their respective volumetric flow rates.

The supply and return rates of the room ventilation inlets and diffusers, were calculated based on the total sum of the volumetric flow rates of the existing AHUs. The sum was then divided uniformly according to gross floor area across all rooms. Fan and pump electricity was summed up for comparison with simulated output data.

The ground heating system's power consumption was calculated knowing the temperature difference across the supply and return pipes, and knowing the working fluid medium to be Propylene glycol. While Domestic Hot water consumption was calculated, with the assumption of incoming cold tap water temperature to be at 10^oC, by differencing the metered volumetric flow to obtain volumetric flow rate measurements.

$$\dot{Q}_{DHW} = cp_{water} * (T_{hot} - 10) * \frac{\delta V_{supply}}{\delta t} \qquad (5)$$

Both the domestic hot water consumption, and the power consumption of the ground heating unit were added to the heating demand output of the simulation model. Finally, by inspecting periods when the DHW supply valve was off in the building, we were also able to estimate the Domestic Hot water loses which were about 9.5 kW, and consequently the losses were added to the model.

Note that all incoming signals from the building's SCADA, Supervisory Control and Data Acquisition, system were transferred by FTP, File Transfer Protocol, in the form of text files, and were pre-processed to remove NaNs by a moving average interpolation.

Post-processing and Results

The model was constructed using IDA ICE. The floor layout, building geometry, along with nearby shading objects were all considered, and modeled as described in the section *Zoning and modeling data*. An additional zone with a small floor surface area was added to simulate the process cooling consumption of the building.

Three AHUs were constructed, one for the kitchen without any heat exchange, one for the atrium representing the two recirculation units, and one main unit servicing the remaining areas. The main AHU has the free cooling circuit, and a heat exchanger. The delay function was also included in the main AHU, which controlled the district cooling distribution to the zones. A separate AHU, acting as a fan coil, was servicing the special process cooling zone.

The modeled plant included the district heating and cooling, along with tanks on the supply side of each.

The cold water tanks were modeled with no losses, since the distribution losses were already accounted for in the process cooling zone.

IDA ICE simulates the plant, AHUs, and all zones as one single entity. By compiling all elements into a state matrix, it avoids any error propagation and discontinuities due to mismatches in time steps. Moreover it solves the state matrix with a variable timestepping mechanism. This means the user does not have to input an appropriate guess for the simulation time step. In this manner, IDA ICE can accurately capture the dynamics of the building, and its custom control structure.

Results

The simulation was performed for the year 2011, and the results were reported every 10 min; matching that of the observation data frequency. Since IDA ICE is transparent, and allows access to any variable in the simulation model, we were able to log in detail the cooling, and heating demand profile of the building. The results represent a full year of collected data at a 10 min interval resolution. Figures 6 & 7 show the full distribution of the error profile over the duration of the collected data for heating and cooling respectively.

It is clear from those profiles that the initial building performance model designed by the KISS principles discussed above describe the actual building performance to a high degree. The maximum error in the heating profile peaks at around 200 kW, while for cooling it peaks at around 1000 kW over the full year profile. For a building this size and data resolution this intricate, it is evident that the initial model without any calibration can indeed predict actual building performance. Figures 8 & 9 show the overlap in dynamics captured by the simulated model.

Refer to Appendix A for comparative threedimensional carpet plots for the total heating, and cooling profile of the building, over a full year, on a daily basis

Discussion

ASHREA guideline 14-2014 provides us with quantifiable measures to evaluate the building performance gap between the simulated model and the actual building. These measures are the Coefficient of Variation of the Residual Mean Square Error, CV(RMSE), along with the Normalized Mean Bias Error, and are required to be less than 30% and 10% respectively for simulated hourly data, and less than 10% and 5% for monthly data. The CV(RMSE) and NMBE are

defined as:

$$CV(RMSE) = 100 * \frac{\sqrt{\frac{\sum_{i=1}^{n}(Y_i - \hat{Y}_i)^2}{n-p}}}{\bar{Y}} \quad (6)$$

$$NMBE = 100 * \frac{\sum_{i=1}^{n}(Y_i - \hat{Y}_i)}{(n-p) * \bar{Y}}$$

n, is the number data measurements, 8760 for a full simulation year.

p, is the degree of freedom in a model, p = 1.

$$(7)$$

For the simulation results obtained we accumulated the 10 min data to hourly data as requested by the guideline, and calculated the goodness of fit metrics on the total delivered energy, as well as on each of the heating and cooling profiles.

Metric/Type	Total	Heating	Cooling
CV(RMSE)hourly	25.5%	23.9%	56.8%
NMBE hourly	-0.2%	-1.3%	1.6%

Metric/Type	Total	Heating	Cooling
CV(RMSE)monthly	6.0%	9.1%	5.5%
NMBE monthly	0.2%	-0.2%	1.0%

Cooling has proved to be particularly difficult to get within the 30% limit of the guideline for the CV(RMSE). This is due to the high dynamic nature of the cooling profile, and having a low mean value in cold climates. Furthermore, it is very difficulty to obtain accurate hourly solar measurements, which have a direct influence on the cooling load. Finally, there was no direct logging for the free-cooling circuit, and thus the free-cooling circuit estimation was done based on air-flow measurements, which can entail high uncertainties. To aggravate things, the indirect measurement of the free cooling system, meant that the pipe losses in that network were hard to estimate and account for in the simulation model.

The issue with the CV(RMSE) metric is twofolds, the first being the normalization with respect to the mean, while the second is the RMSE bias towards outliers. The first point is highlighted when one tries to utilize the CV(RMSE) metric to compare signals with different observed means. For instance large buildings will have a higher mean value, for say heating demand, than a smaller sized office building, and consequently will have a smaller CV(RMSE) measure overshadowing the quality of the fit. This is also evident when we calculate the CV(RMSE) for heating demand profile vs cooling demand profile. That also explains how the total delivered energy CV(RMSE) is usually lower than the individual CV(RMSE) of
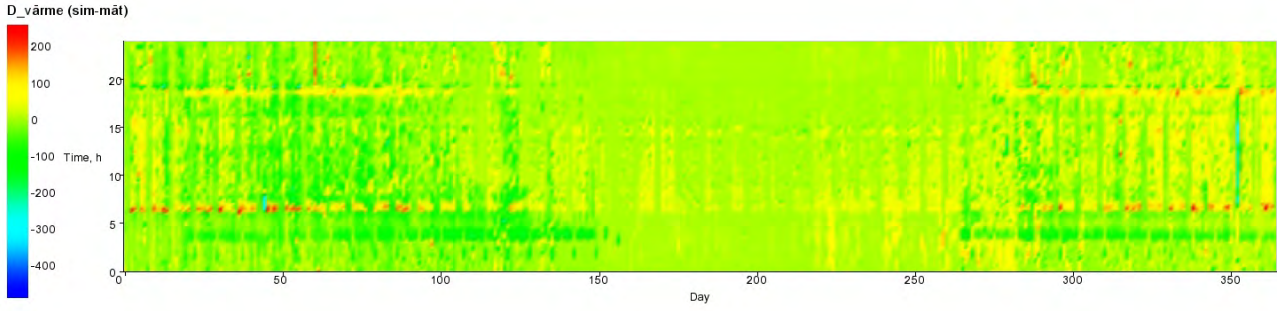
Figure 5: Error in delivered district heating over full year kW, (Simulated-Measured)
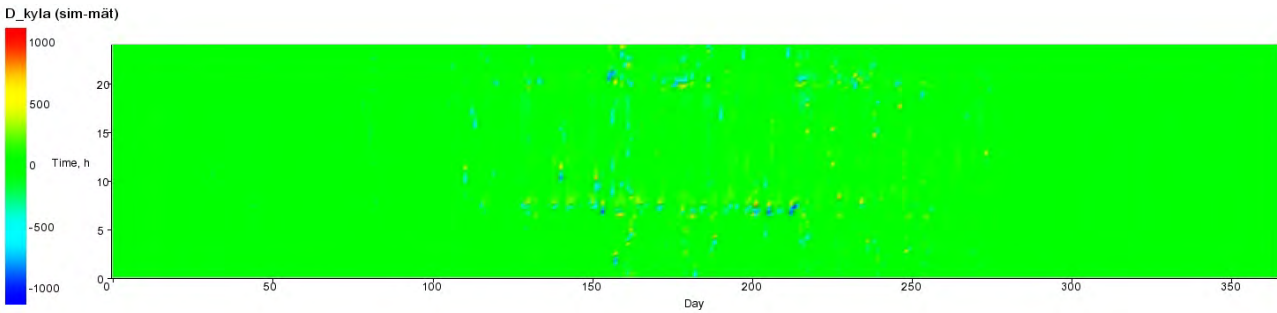
Figure 6: Error in delivered district cooling over full year kW, (Simulated-Measured)
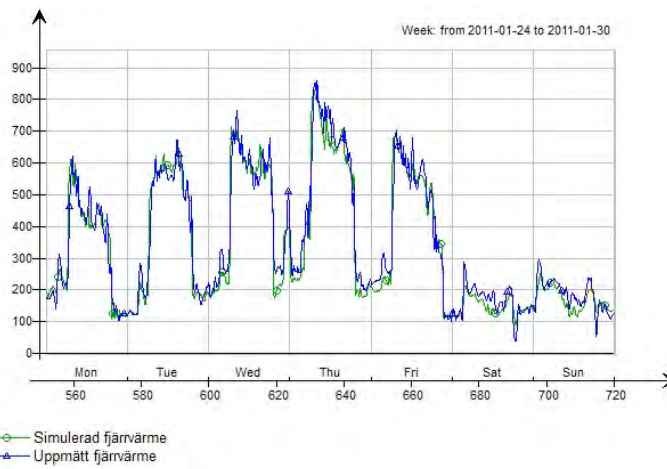
Figure 7: Delivered district heating profile kW, Measured (Blue) vs Simulated (Red), a week in February
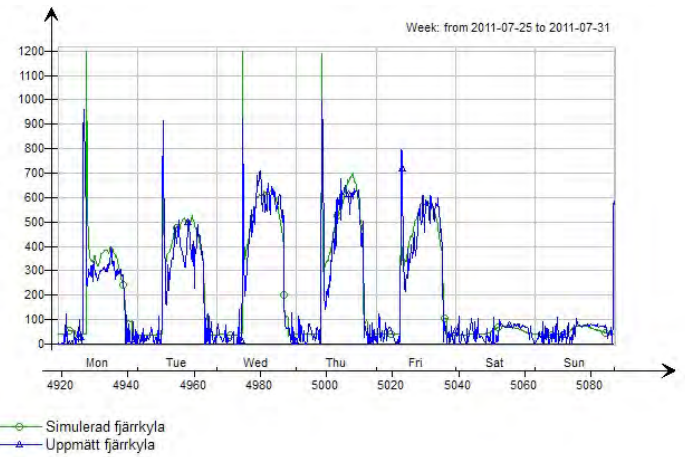
Figure 8: Delivered district cooling profile kW, Measured (Blue) vs Simulated (Red), a week in July

either heating or cooling. An alternative would be to normalize the RMSE with respect to the standard deviation, as in a standard score normalization.

$$Z(RMSE) = 100 * \frac{\sqrt{\frac{\sum_{i=1}^{n}(Y_i - \hat{Y}_i)^2}{n-p}}}{\sigma_Y} \qquad (8)$$

However the metric is still based on the RMSE, which for dynamic simulations is too conservative a measure. Since the RMSE squares the residual error of every data point, which in a full year dynamic simula-

tion translates to 8760 points, this implies that a peak mismatch on any of the measured points will create a large offset in the CV(RMSE) metric. ASHRAE guideline also comments that a well trained artificial neural network is able to achieve a 20% CV(RMSE) error for hourly data. However, this issue becomes less severe when calculating monthly fits, or when reporting over a short exercise period. An alternative would be to rely on a Mean Absolute Error metric,

which less sensitive to outliers and peaks.

$$Z(MAE) = 100 * \frac{\sum_{i=1}^{n} |Y_i - \hat{Y_i}|}{(n-p) * \sigma_Y} \qquad (9)$$

For the same simulation results, applying the new metrics for hourly, and monthly data we have:

Metric/Type	Total	Heating	Cooling
Z(MAE) hourly	22.5%	13.9%	20.9%
Z(MAE) monthly	10.0%	8.1%	5.9%

The new metric reflects more accurately on the quality of the simulation model. It is close to the CV(RMSE) results for Total delivered energy figures for both monthly and hourly data, but is less sensitive to outliers. Hence for heating only or cooling only figures, it gives more realistic and practical results reflecting on the true quality of the simulation model. This evidence is further supported by calculating the Coefficient of Determination, which for hourly cooling calculation is at $r_h^2 = 95.4\%$, for hourly heating $r_h^2 = 97.4\%$, and total hourly cooling and heating at $r_h^2 = 94.7\%$.

On occupancy and the prediction gap

The results show clearly that occupancy, while modeled by direct correlation with the building's electricity consumption profile, was accurately captured. The small prediction gap, shows that using a simple approach with a guesstimate of occupancy density can yield satisfactory end results. That has been the case, at least, for many non-residential buildings and projects, Song et al. (2010).

Conclusion

With proper care, one is able to achieve and work with a small prediction gap. Today's tools allow us to model and predict a building's energy performance accurately, and in an efficient manner. We showed how, abiding by a Keep it Simple and Straightforward approach in modeling, one is able to achieve accurate energy performance predictions, without sacrificing on capturing building's dynamics and internal states. We also argued that current guidelines regarding calculating goodness of fit measures for a dynamic simulation model are too conservative for industrial practice, and we provided some recommendations for more appropriate fitness measures.

Acknowledgment

References

ASHRAE (2013). Energy standard for buildings except low-rise residential buildings. *ASHRAE Standard 90.1-2013*.

ASHRAE (2014). Measurement of energy and demand savings. *Guidline 14-2014 8400*, 0–170.

EQUA Simulation AB - IDA ICE. Accessed: 2018-04-29.

SMHI, Analysmodell. Accessed: 2018-04-29.

Song, C., Z. Qu, N. Blumm, and A.-L. Barabasi (2010, feb). Limits of predictability in human mobility. *Science (New York, N.Y.) 327*(5968), 1018–21.

STRANG - A mesoscale model for solar radiation. Accessed: 2018-04-29.

(a) Measured total delivered energy kW

(b) Simulated total delivered energy kW

(c) (Measured - Simulated) total delivered energy kW

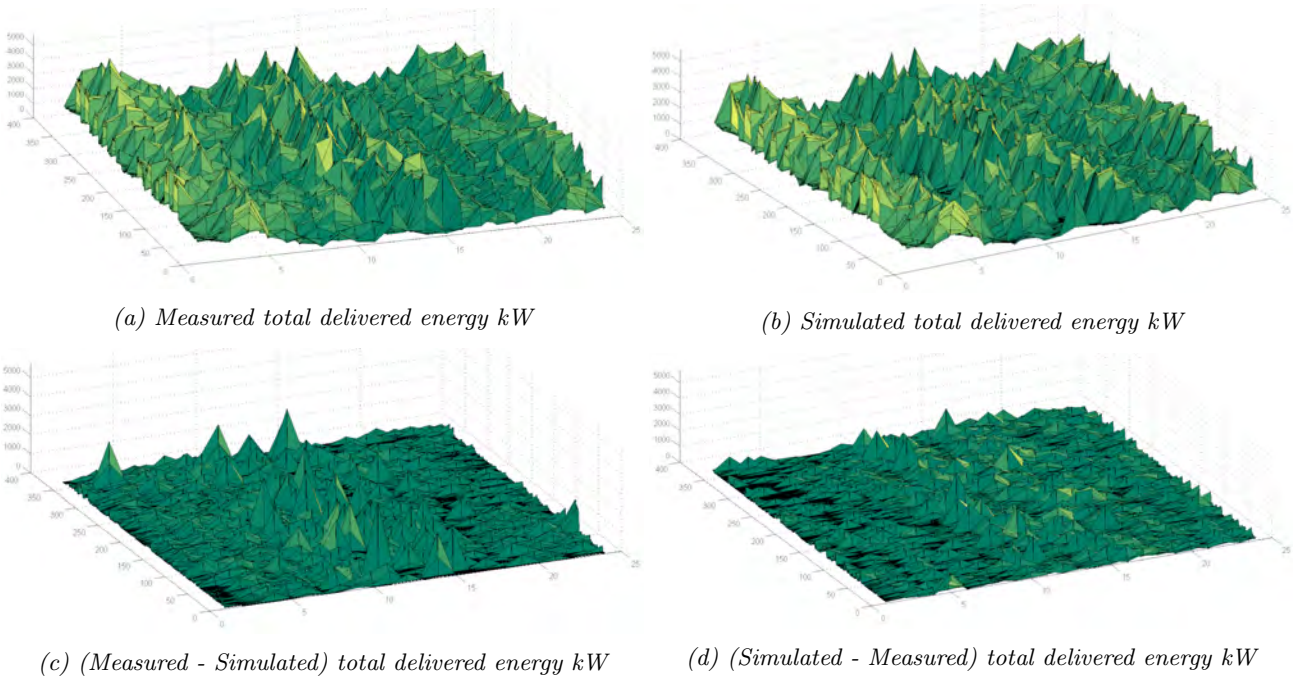*(d) (Simulated - Measured) total delivered energy kW*

Figure 9: x-axis: Hours, y-axis: Days, z-axis: kW
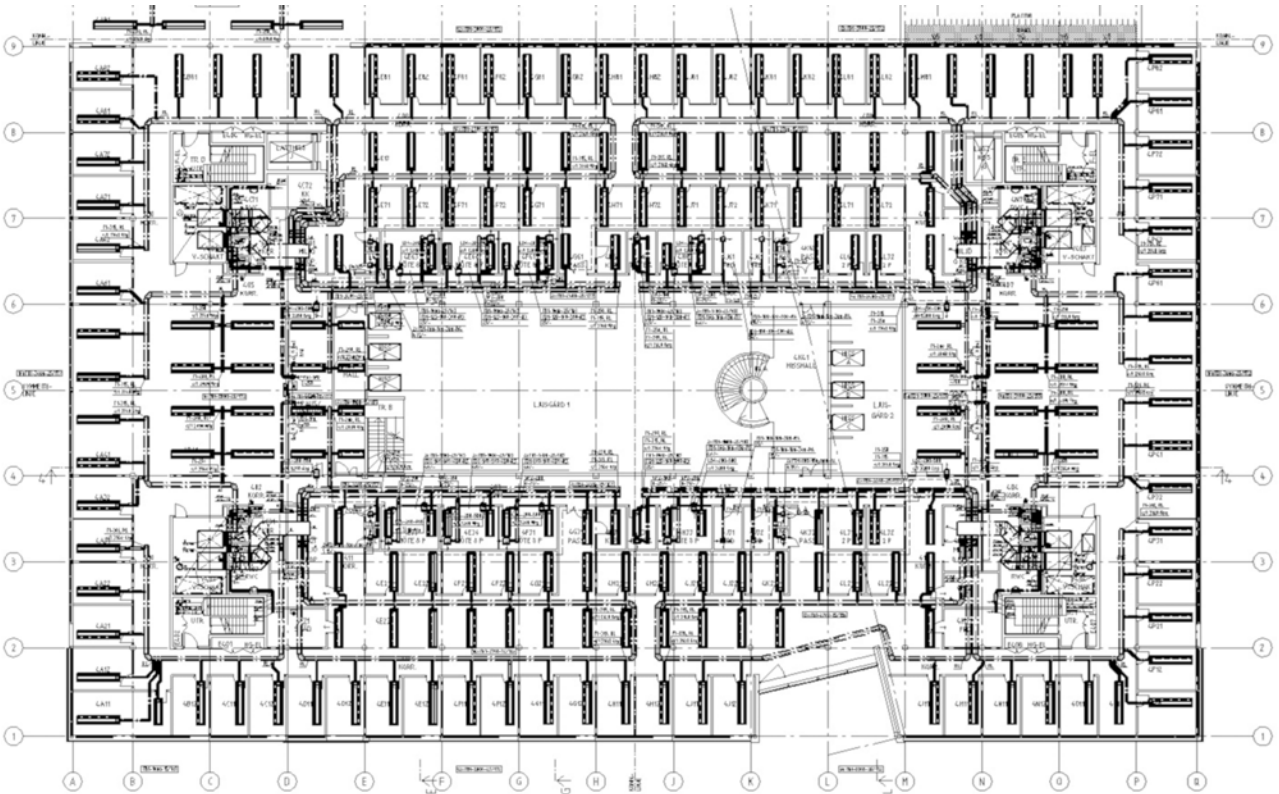

Figure 10: Office floor layout showing active chilled beams network

Exploring possibilities to quantify the qualitative description of occupant behaviour

Jakub Dziedzic[1,*], Da Yan[2], and Vojislav Novakovic[1]

[1] Norwegian University of Science and Technology, Institutt for energi- og prosessteknikk,
Kolbjørn Hejes v 1B, Trondheim, Norway

[2] Tsinghua University, School of Architecture, 100084 Beijing, China

*corresponding author: jakub.w.dziedzic@ntnu.no

Abstract

Human behaviour is a multidisciplinary subject that is being investigated by numerous scientists around the world. The ability to understand and forecast reactions can be beneficial for all scientific branches that are related to this subject. With the increase in the accessibility of personal monitoring systems, a new era of human behaviour research has begun. Currently, in the market, there are many inexpensive and reliable solutions that can grant extra insights into the everyday lives of human beings. Regardless of whether the monitoring solutions are stationary or wearable, they can provide very detailed information with high operational and temporal resolution. Access to these data has advanced our understanding of human routines and habits, but it does not provide insights into the "soft" data that define human beings.

Once the quantitative data has started to enrich scientific databases, the community has started to question whether such information is suitable to detect or record qualitative ("soft") output. Typed text is not included, but it is possible to extract existing data and to obtain "soft" data. This manuscript will try to address this issue. It proposes a straightforward solution that can have great potential for implementation purposes. It investigates the existing literature and tries to evaluate its applicability for numerical implementation. One of the highlights of the manuscript is the proposal of a novel modelling solution that can cooperate with other occupant behaviour-related simulation models. Finally, the manuscript tries to outline future steps to enable the possibility of translating or modelling quantitative input into qualitative output.

Introduction

The possibility of fully re-creating human behaviour can be considered an enormous task if certain boundaries are not stated. The main question depends not only on whether it is even possible but also on the potential simulation goal and the operational resolution. Beyond typically measurable "hard" parameters such as temperature, CO_2 or humidity, which can be adopted in any investigation scenario, there is a "soft" side of data, which is considered qualitative information [1]. Such data deliver a subjective opinion about the subject in question. For example, if a person is asked about whether he or she is comfortable, the obtained answer can be hard to quantify. In most cases, the delivered responses might be similar to answers such as "I am fine" or "I feel slightly uncomfortable". The main issue regarding such qualitative output is its measurable repetitiveness [2]. Does such an input operate on a linear scale? If yes, what is the threshold for a specific answer? How similar or overlapping are specific states? If such output cannot be explained based on a linear model, what kind of model should be implemented? These are very important questions, but presently, even with the existence of social media such as Facebook, Twitter and other applications, it is hard to provide a definite answer regarding such "simple" questions [3]. This can be considered a major limitation if the desire is to translate qualitative data into quantitative output. To overcome this issue, the problem could be potentially reversed engineered in a specific way.

It is nearly impossible to ask building users about their satisfaction level during each activity that they are involved in. Even if such measures were possible, the reliability of the results would be questionable. Constantly questioning test subjects about their status would be more like a burden than a support system. After a very short period, participants would become tired or fed up of being involved in such an extensive study, which consequently would corrupt the collected data [4]. Being involved in an experiment would play a major role in their daily routine, and their answers would reflect this phenomenon. To make such interventions more reliable, their frequency cannot go against participants' comfort. Therefore, the sample rate will be rather small, especially if such information is compared with information that can be gathered about the environment. However, this issue does not automatically discredit the applicability of such data. If test subjects agree to be extensively monitored using in situ methods, such quantitative data can be used to formulate an ontology for labelling various activities [5]. Each discrete action observed can be formulated in sequence or parallel scenarios. If the observed phenomena are repetitive, these activities can be labelled as a routine or a habit. During each intervention, an interviewer might present a list of all observed habits and ask about the purpose, feelings and desires that were associated with such activities. In this way, each recorded activity can be labelled, and with the use of sophisticated deep-learning methods, such data can be used to pre-train and to develop a labelling tool. This tool can help to observe and examine quantitative output.

Labelled data would allow to describe the origin of a specific qualitative output. Proposed solution would act as a supportive machine to define whether the specific qualitative output is embedded in psychology, physiology or a mixture of these parameters. If the repetitive pattern of activities constantly provides similar output and for unknown reasons the response is different, then it will be an indication that the origin is embedded somewhere beyond quantitative observation. Therefore, it will enrich the model structure by providing a new branch of connection to the outcomes of actions. Additionally, conducting such a study will highlight the spectrum of activities that could influence human well-being. Such analytics can be conducted at the individual, group or population level, which might highlight the personality differences among test subjects. Studies that try to reach such a sophisticated level of occupant behaviour description have not been found. There might be many reasons for such a situation, but one of the identified constraints might be a low level of interest in the direct monitoring of occupant actions. This situation is changing with each passing year, but the methodology for fully tracking occupant indoor activities has not yet been established. There are studies that focus on this subject such as [6], [7], but studies that track all indoor activities (to a reasonable extent) have not been found in the existing literature.

Since it is currently not possible to translate qualitative data into quantitative information, it might be possible to develop a methodology (application) for receiving a qualitative output from a simulated occupant. For application purposes, it is necessary to establish a framework and to define all potential functionalities that enable the simulation of a "virtual being". The aim of this manuscript is to define, develop and discuss the possibility of connecting qualitative and quantitative studies about occupant behaviour in residential buildings. The focus is on the possibility of simulating each occupant as a separate "virtual being" and the possibility of obtaining qualitative feedback from them. In this way, the interaction between occupants can be included in the simulation environment. This work is based on a collection of reviewed papers and numerical explorations of modelling practices for re-assembling the typical family. This manuscript has to be considered a hypothetical exploration of the ability to portray the qualitative desires of indoor occupants in a simulated reality. The ability to simulate each particular individual output will open a new dimension with regard to the interaction of virtual occupants. Additionally, this will allow us to formulate a social structure of interactions in which each virtual occupant is an active or passive participant. The motivation among occupants might vary, but it can be considered a main driving force of being involved. For the purpose of explaining each day of the occupants, this is considered a "game". The fulfilment of a specific motivation is considered a "win". Each included virtual being will participate in a "game". For this reason,

such a "game" requires a description of its "mechanics". Studies that focus on simulations of human behaviour can be divided into two main categories: indoor and outdoor simulations.

The occupant is recognized as a crucial part of the building's "metabolic system". This is a relatively fresh concept. Therefore, the current time spent on development has allowed the validation of general theories. The use of the metrics proposed by Fanger is considered a good approximation [8]. The proposed approach bounds all building users and defines the principles for the human-centric design of a building's heating, ventilation and air conditioning (HVAC) system. The solution proposed by Fanger was considered as a state of the art in previous years. It was one of the first attempts to include the "human" factor inside the building. Fanger's studies could be considered a first milestone that establishes a building's users as an important factor during the building design phase. Fanger's discoveries have opened a new methodological branch of building science that focuses on occupant behaviour [9], [10], [11]. Once the subject of interest was introduced, it started to gather a larger audience. It became a foundation for investigating human indoor comfort, and it was extended even further. It has allowed to formulate many highly impactful discoveries about the human indoor environment [12], [13], [14]. Extending the research subject with regard to the impact that an occupant has on a building's energy systems has allowed us to formulate important theories about energy-related occupant behaviour [15], [16]. Currently, research is part of a larger subject that focuses on building energy performance. The combined efforts of scientists who have contributed to the development of this scientific branch have allowed us to formulate a "know-how" [17] guidebook that tries to describe occupant behaviour investigations in a holistic way. Additionally, it summarizes current knowledge about the subject and highlights new challenges [18].

One of the offshoots of occupant behaviour studies has made it possible to formulate and implement numerous numerical models that are now commonly used in commercial building simulation software, such as IDA-ICE, Energy Plus, DeST or Rhinoceros' Grasshopper with LadyBug [19]–[22]. Due to the currently available computational processing power, it is possible to introduce more detailed models that focus on individual building users. Currently, there are no guidelines that limit the complexity of the proposed models. As a rule of thumb, the calculation time should allow forecasts of the near future (for model predictive control applications) or annual simulation. Both applications require a different level of temporal and spatial resolution, but in both approaches, the validation process still requires a huge improvement to check its clarity, applicability and robustness. Typically, such applications have a description of the physical properties of the used materials and a simplified energy equation (selection of the

numerical methods depends on the software used and application purposes). Additionally, the entire simulation can be enriched with a series of probabilistic models focusing on specific occupant-related aspects such as presence, window and blind operations or plug load use. There are a few more sophisticated methods that try to re-create occupant indoor activities, such as those proposed by T. Hong, in which the occupant behaviour model operates as a functional mock-up obFMU [5].

The simulation of occupants outdoors focuses on the behaviour of the crowd. These simulations are mainly applied to model a specific phenomenon in which the crowd is involved, such as setting up proper sidewalls [23], checking the labelling of streets/large areas [24], setting up a time opening for pedestrian lights or designing escape routes from large spaces/buildings [25]. The description of each particular occupant is dependent on the purpose of the simulation. The description of functionalities is simplified, and a specific simulated feature operating on specific distribution to generate a crowd profile. For example, to simulate a pedestrian crossing light, each simulated occupant must obey the lights to a certain extent. However, the factor of following the rules might be time-dependent. Therefore, if a specific waiting time is prolonged, the threshold for breaking the rules decreases. Combined with an extra occupant following functionality, it is possible to produce a significant model for testing the safety of a street. Both functions can be considered occupant attributes, and levels that trigger specific reaction can be individualized and distributed among pedestrians by certain distribution functions.

Previous studies that have tried to portray occupant behaviour have used a representative occupant [26]–[28]. This means that all groups included indoors or outdoors were represented as artificial occupants that hold the sum of all actions. In those cases, there is no individual simulation of behaviour, and all actions are captured in a group-size resolution. The model data obtained in such a manner can be used as a support for future development attempts, but precise information on individual actions plateaus. The data used for these observations were collected mainly from interactions with various controllers (such as a thermostat [16]) and indoor monitoring devices (such as plug load metres or the PIR sensor [16]). Even without high spatial and temporal resolution, it is possible to distinguish a few types of representative energy user archetypes [29], where their behaviour operates on two dimensions related to energy awareness and general wealth. Despite the lack of individualization, such studies can be used to develop a database of all potential activities. It has to be pointed out that such an approach guarantees the stability and direct reproducibility of the study due to the operation on a purely statistical basis. This flattens the specific context (knowledge of users) but delivers a model that is reliable. This model representation of users offers a probabilistic

approach, which is sufficient to a certain extent. If an investigation target focuses on personalized control, it is necessary to implement solutions that involve a more deterministic approach. It is very common to justify and explain occupant behaviour with the use of stochastic methods. Although they are a convenient method for describing repetitive actions, where the initializations might vary due to numerous implications, stochastic methods are a simplification of deeper phenomena [30], [31]. The use of this methodology implies that occupant behaviour is a stochastic process, which contradicts its deterministic nature. Put simply, the actions of occupants depend on proper circumstances and motivations, not a randomized action. Therefore, to create an individualized simulation for a specific building user, it is necessary to operate on a similar structure. The closest method that operates on similar principles is a pre-trained artificial intelligence model.

The urge to define occupants as individual "virtual beings" in a simulated environment is also suggested by other scientific branches, such as medicine [32], and sociology [33], [34]. However, these branches can also be connected by topics focusing on energy usage by various social groups. Most of these studies aim to recognize the current understanding of energy uses inside residential houses from the perspective of their own scientific context [38]–[42]. One investigation subject that can be explored is the impact of ICT on the structure of the family or how occupants understand the concept of energy savings. This study allows for a multidimensional analysis that can be related to sociology, psychology and energy studies. Unfortunately, such studies are carried out in a relatively small group of participants, but they still provide valid and representative output. The utilization of the insights gained allows the construction of a model that relies on a typology of activities, similar to Pavlovian conditioning [40]. Such an application can be a separate model, or if its structure has a modular application, it can be considered a module of a larger occupant behaviour simulator [41].

Aim

From the qualitative research perspective, there are a few models that can be implemented in functional applications, such as the theory of planned behaviour or Maslow's hierarchy of needs [42], [43]. The main issue regarding these modelling approaches is their Eulerian nature. This means that the proposed models have a clear and understandable structure, but their implementation is difficult. For this reason, it is necessary to try to approach this issue with a more Lagrangian approach, where the structure of the model might be more complex and convoluted, but implementation will be more straightforward. The main aim of this manuscript is to define and describe the process of developing an occupant behaviour model/module that delivers qualitative data as an output. Due to the lack of data that can completely support this process, the whole development will rely on

existing studies, discussions and conclusions provided by the literature. Additionally, the whole model/structure is designed from the implementation perspective.

Studies in the literature have shown that there are a few examples of attempts to approach the qualitative output issue. Unfortunately, deeper analysis does unravel the problem is relatively ignored [15]. In this study, the attributes of particular occupants are defined as a trigger to carry out an action, which is counted as the fulfilment of a need/desire. This could be considered a "shallow" ontological approach in which specific needs can be met by a selected driver, which, to a certain extent, is correct, but its structure limits the existence of other options. In other words, models are blocked by this framework.

To address all these issues this manuscript will try to develop a semi-open structure for a framework in which each sub-part of the model is described. To not overextend the subject, the proposed simulated model will be tested to simulate two specific scenarios that were investigated in previous studies.

Methods

First, with regard to the description of model development, it is necessary to define all the vocabulary used and the basic mechanics of the "game". This manuscript is operating on the edge of engineering and sociological studies, and each of these fields has similar terms, but their meaning might vary. Therefore, it is necessary to define an operational library. Each simulated person is considered to be an occupant. Each occupant is simulated individually. The qualitative model output is considered a defined spectrum of answers from simulated occupants that informs the status of goal fulfilment. There is no predefined pathway that will promote fulfilling a goal. The goals are defined as a target of actions or a state that one specific occupant has to obtain to fulfil his or her personal needs. Personal needs are the pre-defined boundaries of each person that cover a spectrum of basic human needs, such as hunger, stamina, and social interaction. Each target has its selected description that defines the conditions for reaching it, what is an acceptable buffer and what is a qualitative outcome. For the purpose of theoretical analysis, this study will limit itself to five specific needs (Entertainment, Hunger, Hygiene, Social interaction, Stamina), which are usually mentioned in research related to the description of personality [44]–[46]. The "game" is a simulated activity with a selected time horizon. A whole "game" has four main layers, and the first layer defines the rules for reaching the target. The second layer focuses on relationships and the relations of the simulated occupants. The third layer focuses on describing the elements of the activities and actions that the occupants have to take to be involved. This layer can be considered a building block for formulating the action. The fourth and final layer describes the occupants individually. The result of each game is ultimately connected to two outcomes, winning or losing. A "win" is an outcome in which the target desire

is fulfilled while staying within the boundaries of personal needs. Losing is considered a state where one or none of the winning elements is not fulfilled. The outcome of the "game" influences the qualitative state of the simulated occupant. Winning boosts the level of well-being, and losing decreases it. Well-being is a one-dimensional variable that operates on a mathematical plane of real numbers. If the value is positive, the occupant reports a positive state, and vice versa for a negative value of well-being. It is a time-dependent variable that aims to obtain a neutral zero value. This process will be called "mood neutralization". The dynamics of this parameter can vary between occupants, but for this approximation, the parameter will be held constant at a selected value. Therefore, each occupant has one linear curve of mood neutralization. To make the description more transparent, each layer of this model will be described in descending order in a separate subsection.
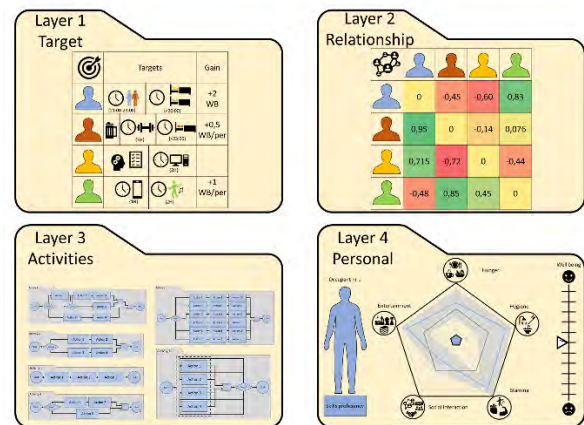
Figure 1. Layer structure of the whole model

The structure of each target is the same in terms of the framework, but the selected conditions have to be defined on an individual level. Such an implementation allows us to formulate means of personalities and allows space for the potential simulation of the personal evolution of the needs of occupants. The qualitative outcome of a simulated activity strictly depends on a buffer of acceptance, which makes acceptance a dynamic variable. If a simulated occupant "wins" the "game" even without being fully in aligned with his or her personal needs but is still inside the buffer zone, the occupant's personal needs will be impacted. If such an event occurs more frequently, the description of personal needs will evolve. It is possible to forecast that if such a numerical simulation is left alone (continuous simulations of daily activity), it will tend to generate "pathological" scenarios where one participant will be overused. This will consequently lead to a reinforced shift in personal needs. Such a situation might happen in real-life scenarios, but in most cases, it will not happen in a short period of time. To counter the development of an excessively accelerated change in personal needs, it is necessary to implement a negative reinforcement. This will gradually reduce the previously

gained modifications of the personal need parameters. In terms of the core structure, in whole "games", there are three times more losing than winning outcomes. Therefore, observing the "personal" evolution during the simulation process must be connected to a constant positive "game" outcome. To implement this functionality, each occupant has to hold a memory of the baseline of each personal need and the changes that occur due to modifications. To make the description more transparent, the whole model structure is presented in Figure 1.

Reaching the target requires performing all the actions in a series of activities. All of the actions are operating on a global time step. Each activity that can be performed in the real life is considered as a series of actions that are defined by the specific activity. The completion of one action depends on the time and effort spent on performing it. It is a cumulative threshold value that triggers a confirmation that the action has been completed. There is no qualitative evaluation of the action performed. If there is an action that does not require constant involvement, in its description, there is an additional "NaN" parameter. This means that the action has at least three threshold cumulative values, where the first defines the amount of time that has to be spent to reach the "NaN" status. The second threshold defines the amount of the cumulative time value until the action will stay inside the "NaN" status. During this time, occupants cannot accelerate the process by using their skills. The third threshold defines the amount of the cumulative value that is necessary to finalize the activity. One activity can have more than one "NaN" status, and its appearance depends on the types of actions that are defined. It is assumed that occupants are aware of the structure of whole actions. During the "NaN" status, occupants gain an additional timeline that can be used to perform any other action. For example, to boil water with the use of an electric kettle, it is not necessary to wait for the entire boiling process. This time can be used to become involved in other actions, which are defined by the activity. Each time step that contributes to the completion of actions reduces the amount of stamina of occupants. From the operational perspective, actions are defined by two variables: time-dependency and score-ability. If an action is time-dependent, this means that its appearance exists during the specific moment in the timeline. If the targeted occupant will not engage in performing the action within a defined time window, this action is concluded and cannot be performed. Scoreable actions are events in which the performance of such actions has a direct influence on the whole activity. Therefore, the outcome has an influence on the entire activity that the occupant was involved in. To summarize, activities can be divided into four groups separated by two variables, (time-depended scoreable; non time-depended scoreable; time-depended non-scoreable; non time-depended and non-scoreable). The visualization of the action block that can be used to model the whole activity process is presented in Figure 2.

Place	Action n		Gain
{Location}	• Time requested	$n=T[s]$	
	• Proficiency mod.	$X*n$	
	• Penalty		
	➤ Entertainment	$-x_1$	$+y_1$
	➤ Hunger	$-x_2$	$+y_2$
	➤ Hygiene	$-x_3$	$+y_3$
	➤ Social interaction	$-x_4$	$+y_4$
	➤ Stamina	$-x_5$	$+y_5$

Figure 2. Action module structure with all necessary inputs and outputs

The completion of a specific activity depends on two functions, proficiency and focus. Proficiency is a fixed function that describes the experience of the occupant in performing a selected action. The more similar the category of actions performed, the more skilled the occupant becomes. The proficiency level accelerates the process of performing an activity. It can be considered a multiplier for its completion since actions are performed based on an accumulation of time steps that occupants use to participate in these actions. The action proficiency level will multiply the value of each time step that was used for these actions. The focus parameter is a survival model that defines the amount of time that a specific occupant will stay focused on an action. The survival model is a probabilistic time function that describes the amount of time that specific phenomena will last. It makes it possible to describe one-dimensional phenomena in which the chances of occurrence increase over time. For example, with this approach, it is possible to simulate the time until a window will be shut once it is opened. Initially, the chances that the window will be closed are small, but once time starts to pass, there are higher chances that it will be closed. This approach is usually supported by a prolonged period of observations. Observed phenomena are investigated based on the time they last, and aggregated data allow us to formulate a distribution. The formulated distribution becomes the foundation of the survival model. This model will be implemented to simulate the focus of the occupant and to provide the solver that will be responsible for simulating the attention time spent. The shape of the curve is dependent on numerous variables, and due to its simplicity, it is possible to introduce its modulators. Some impactful parameters might be age, the time of day, weather conditions, the amount of stamina or open timelines due to the parallel involvement in a few actions.

The simulation of the whole activity requires a precise definition of its sub-elements (actions). The whole sequence of actions has to be defined, with its characteristics, the cumulative time required to complete it, the necessary previous actions and the amount of necessary resources to finish it. The global order within one activity does not have to be fully specified. Some actions have to be followed by other actions, but some can be carried out in parallel. Additionally, an activity has to define the maximum number of occupants who can

conduct the activity. The use of this structure allows the formulation of various scenarios. This requires defining each activity separately, but this allows us to formulate various, more realistic scenarios. The logic of the actions is not directly defined. Therefore, it is possible in such a structure to define unreasonable activities and to observe their impact. The larger the database of defined activities is, the more sophisticated simulations can be conducted. If an activity is completed, it grants specific rewards that are defined by the activity description. An activity can be built from at least one or more actions. With such a structure, it is possible to introduce the utilization of resources. This could be an additional trigger for a new spectrum of activities that rely on the control of resources levels. For the current form of the model, such a feature will be avoided because it would demand a significant effort to define the operational library. For the current state of the model, it is assumed that occupants have access to all the resources necessary to perform each activity.

The relationship layer defines the hierarchical structure of the group. It has a significant impact on the whole model. The time spent on each action can be modified by the number of people who can be involved and the number of people who will be impacted. For example, the time necessary to prepare a meal for one person will be different from that preparation of a meal for a whole family. Additionally, the potential involvement in collaborative efforts can affect the process of completing activities. If there is a difference in the proficiency level among the occupants who are involved in an activity, the occupant with the highest proficiency level will become the supervisor of the task. The supervisor will have a reduced amount of focus on the task because he or she will be controlling the others, but the proficiency level of the supervised occupants will grow faster. The proficiency level can grow to the level of supervisor. These are the rules of the task-based hierarchy that allow us to define the main person responsible for an activity that is being performed. It is assumed that the proficiency parameters are known to each occupant, as well as all other personal need parameters. Each time a task is performed by more than one occupant, the social interaction need parameter of each occupant increases. If an occupant's action involves only one person, the same parameter is reduced. Beyond the local hierarchical system, it is necessary to establish the global hierarchical system among the occupants included in a simulation. This feature will influence the involvement in actions, where a spectrum of activities must be distributed among occupants. If this parameter is left unsupervised, it can produce an uncontrollable artefact. The global hierarchical system is established in the relationship matrix, and it is assumed that the main decision makers are the parents. Therefore, if the list of activities must be distributed among the occupants, occupants representing parents will define who is involved in a specific task. In this structure, it is possible to implement a sub-layer that

represents a negotiation phase, where a child can try to disobey parent and where the combination of basic-need parameters might play a significant role. For the development of the current model, this functionality will not be introduced.

Reaching the target of the "game" requires completing specific subtasks that are dictated by the ongoing daily routines. Each occupant has his or her own targets that he or she is motivated to achieve. Reaching a target requires completing a series of activities. If a target is reached with a successful score, it boosts the well-being variable. The status of well-being can change during the occurrences of various events. The current structure of the "game" assumes that each occupant aims to "win" his or her "game". The main idea of the "game" is to constantly involve the occupants in "play". Their statuses over time will be modified by the actions in which they will be involved, which can be used to evaluate their qualitative response in any selected time step. The initial conditions will play a significant role, especially if there are implications connected with having a low status of well-being variable. The current status of the whole model must be considered an initial approach for building a sophisticated occupant behaviour simulator. The methodology section describes many interactions between the different layers of this model. The interactions vaguely define the components and mechanics behind the model. Access to data that would define more concrete, quantitative connections is currently not available. For this reason, it is necessary to fine tune all the parameters to make a model functional; this will be the focus of the analysis (results) section.

Simulation setup and results

To set up simulations, it is necessary to define a set of specific actions and activities and the target of each occupant. This manuscript will test the scenario of evening routines. The whole set of activities and the necessary actions are displayed in the process graph, in Figure 3. The idea of the simulation scenario is adopted from a study on the influence of ICT on a one daily routine (Activity), family dinner. [36], [47], [48]. In the simulated test case, a family consisting of four members, two parents and two children, was generated.

Initial Penalty						
Activity	Time[s]	Entertainment	Hunger	Hygiene	Social interaction	Stamina
Tea	120	0,1	0	0,1	0,01	0,01
Sandwich	600	0,2	0,1	0,2	0,01	0,01
Tap water	30	0,1	0,1	0,1	0,01	0,01
Table preparation	1000	0,1	0,1	0,1	0,01	0,2
Cutleries	200	0,01	0	0	0,2	0,2
Eat	2000	0,01	0	0	0,3	0,1
Phone	60	0	0,1	0,01	0,1	0,01

Process Penalty [per/s]						
Activity	Time[s]	Entertainment	Hunger	Hygiene	Social interaction	Stamina
Tea	120	0,01	0	0	0	0,05
Sandwich	600	0,01	0,01	0,01	0,01	0,01
Tap water	30	0,01	0,01	0,01	0,01	0,01
Table preparation	1000	0,01	0,01	0,01	0,01	0,1
Cutleries	200	0,01	0,01	0,01	0,02	0,1
Eat	2000	0,01	0	0,01	0,01	0
Phone	60	0,01	0,01	0,01	0,02	0,01

Action Gain								
Activity	Time[s]	Entertainment	Hunger	Hygiene	Social interaction	Stamina	Relations	Well Being
Tea	120	0	0,5	0,1	0	0	0	0
Sandwich	600	0	1	0	0	0	0,05	0
Tap water	30	0	0,2	0	0	0	0,02	0
Table preparation	1000	0	0,2	0	0	0	0,5	0
Cutleries	200	0	0,1	0	0,1	0	0,3	0
Eat	2000	0,5	2	0	0	1	0,5	0,5
Phone	60	0,3	0,2	0	0	0	0,5	0,1

Figure 3. Sample action table with variables necessary for simulation

Setting up this simulation requires performing a series of sensibility analyses to establish the accuracy rates and parameter modifications to reach a balanced output. The analysis of the parameter weights is shown in Figure 4. Setting up the first simulation requires a certain stabilization of the parameters to control the tuning procedure. For this reason, it is assumed that everyone is involved in activities and that occupants have the same initial personal parameters.
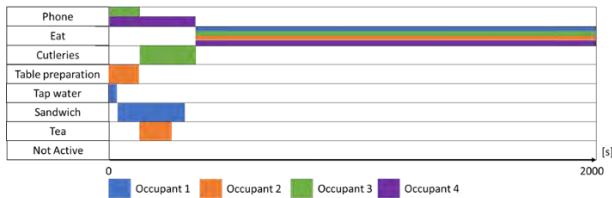

Figure 4. Simulated action sequence results

Each occupant performs his or her action and is a part of the activity process. Their actions do not operate on any dimensions other than time, at least for this approximation of the model. The lack of a physical connection makes it possible to operate on an abstract plane of the whole process, where involvement in a specific action can be visualized. Each occupant has his or her own "game", which can be considered a process. Each occupant has its own needs that are evolving thru the actions that are involved. The results of this simulation of occupants' needs are displayed in Figure 5.
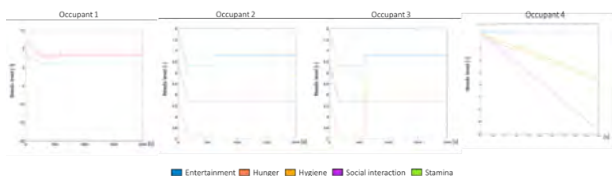

Figure 5. Occupants' needs simulation results.

Discussion

The ability to simulate occupants' qualitative output is a novelty in the research field. Performing validations of this concept would require conducting multiple tests, where trained personnel would collect data for this purpose. It is a challenging task, but with the selection of a specific mechanics, it is possible to narrow down the number observations necessary to complete such a task. Put simply, once the framework is established, it is easier to define the goals of observation.

The proposed model is developed with an application goal. It is recognized that occupant well-being has a significant impact on the performance of occupants, and this parameter must be included. The main issue with "soft" parameters that describe occupants is the lack of knowledge about how to include them in a simulation. The issue is exacerbated if it is assumed that feeling and sensation are a subjective, personal experience. If such a status is accepted, the development of this model has to be defined by each separate person. This would require a detailed "bottom-up" approach, but certainly, it is possible to implement this methodology in small test cases.

The proposed model is built from the engineering perspective, where actions are followed by the reactions of the overall model. Studies that followed a similar procedure or that investigated human behaviour in similar matter were not found. There are many good models proposed in a past, that define human drivers and that describe human dynamics, but none of these descriptions allow us to atomize the content of the investigation. This means that tremendous efforts that were made to develop a structural model do not allow to extract the contents of actions and reactions. Existing studies can be considered inspirational, but the qualitative data that they collected are far from being considered for implementation in numerical simulation. Additionally, current control of status parameters requires more tuning, but this should be fixed once the proper measurements are conducted.

The main disadvantage of the proposed model is its reliance on action, activity and human profile libraries. This requires access to a huge variety of activities to function correctly. Development of vast library is beyond one research group or project. To develop such a database, it is necessary to involve volunteers. With the formulation of a proper survey, participants can be asked to describe their daily routines. Each routine can build from action/activity blocks. These blocks will represent each action that occupants can be involved in. While describing an activity, participants can be asked about the benefits and requirements that are related to routine, activity or action. In this way, it would be possible to develop a crowd-sourced database that defines daily activities. Each similar routine could have multiple, different actions included, or its order may vary. Once the data base is saturated with a significant number of activities, it can be implemented in the proposed model.

The complexity and variety of scenarios can be extended nearly to infinite. Especially if each included in simulation occupant has an extensive list of factors that might influence the motivation and need. Even if the amount of the influential parameters would be limited to a small number, the core design of the proposed numerical solution promotes lack of direct reproducibility, but the reasoning of the actions is capped. Each action can be stopped or initialized based on specific, defined distribution. Each distribution function can be modified or transformed by numerous conditions like weather, health, type of event, date, relationship to other occupants or others. Combination of all of these factors influences occupants engagement in action. If all of these parameters are also time depended, the level of complexity rises exponentially. This is a significant limitation because it does not allow to validate the proposed model on an operational level. The proposed solution can be tested with the use of the stochastic methods, which will blur the main context of the model. It will not draw one single cue of actions, rather a set of cues that are emerging into a

similar status. If the rules of the proposed "game" for increasing well-being status are considered as a correct, the direct link between the motivation of actions and reaching the goal can be measured by means of entropy. It changes the mathematical apparatus and do not discards the story that leads to effect. It instead evaluates each action, or piece of a timeline how it declines from the goal.

Additionally, it is important to discuss the pros and cons between simulation and rule-based modelling. Both approaches are fundamental, but each of them has its flaws. Numerical simulation operates on a non-natural random number generator. If such setup is left running without any supervision (rule), it will not produce any consistent results. Each simulation has to have its limitations that are stated by the set of rules, for example, the level of convergence or boundary conditions. On the other hand, fully rule-based methods will not promote any diversity; the rules are followed until the fulfilment conditions are met. Incorporating occupants simulation by the use of these methods as a seldom solver is inapplicable. It is possible to assume that each person has its plan (cue) of action set in a logical order. However, such a plan could be considered as rational only for them, due to their limitations or personal triads. Therefore, the fully rule-based methodology cannot be applied. Promotion of any diversity among the simulated individuals, requires introduction a certain amount of variety, that can be found in simulation methods. To somehow overcome issue connected with both of these methods, it is necessary to combine positive sides of each approach and overcome existing disadvantages. Such a task is an important limitation because it requires a definition of how rule-based or chaotic is a specific person and their personality.

The development of this model aims to be implemented in a building performance simulator. There are existing building numerical models that could potentially operate on outputs provided by this model [41]. For this purpose, access to an activity scheduler would be a significant asset and would allow to simulate the realistic utilization of energy resources. Currently, the available functional models do not allow us to track the reasoning of individuals. The links of cause and effect are broken by implementing fixed schedule or time-series models [49]–[51]. In proposed model, it would be possible to trigger interaction with a simulated building infrastructure. Therefore, each action would have its own marker. Similar to the block-chain technique, each component of the simulation would hold a permanent record of who was using it and when. Incorporating the well-being status would introduce a new dimension that could influence the energy usage of the building. In particular, the link between occupant thermal comfort and well-being could be established.

Conclusion

The idea presented in this manuscript tries to capture and implement in simulation software artificial qualitative responses of human beings. The main aim is to implement a systematic solution that can be further developed. Due to the limited resources applied, this methodology cannot be extended, but its current state can be used as a reference framework. It is difficult to judge whether such a methodology is fully correct from the social science perspective because the work presented is a mock-up. Its main advantage is the possibility of simulating the human-interaction process, where each included person plays his or her role in reaching his or her goals. The proposed solution has a relatively simple core structure, but the interconnection between parameters starts to increase the level of complexity significantly. The design of the model and its key parameters was selected to be fully used during simulations. This indicates that such similar parameters should be considered when performing a model validation data collection procedure.

Based on existing studies, it is possible to extract pieces of information about how the model delivers qualitative output. The closest approximation can be found not in the scientific literature but in interactive entertainment systems. Pieces of software that focus on a procedural world building environment develop similar simplified tools, but their applicability is questionable. Applications such as Dwarf Fortress or RimWorld focus on a computer simulation of societies where each new application user delivers a unique social network and history of events and relations is shared between non-player characters (NPCs) [52], [53]. It is obvious that it is impossible to program all of the connections between NPCs; therefore, an algorithm that is dedicated to such a task must exist. Additionally, substantial access to the computer's rapid access memory must be held to operate with all of the connections that are delivered during the simulation process. It is expected that the only applicable solution for handling social interaction and simulating qualitative responses can be achieved with the use of procedural techniques. Procedural generated interaction is relatively simple in a core design, but it allows to build advanced scenarios without the extensive influence in software code.

The initial challenge that was presented in this manuscript concerned questioning the possibility of translating qualitative human input into accurate quantitative response output. Such a task can be considered unachievable due to the overcomplexity of human nature. However, the combination of extensive in situ monitoring techniques and the further development of the proposed model can be a solution to this task. It requires appropriate detection ontology, recognition of an observed person, and detection activity that the observed person is performing. Those parameters can be an initial input to pre-training the model that is presented in manuscript. Once the significant training is completed, the monitored occupant can be evaluated in terms of his/hers potential

qualitative output. Such a combined system can be considered a model predictive control for human qualitative response (MPC-HQR). The use of such a technique is blocked not by the current limits of technology but by the critical mass of activity descriptions and number of studies that share similar methodology and framework. Once this status will be changed, collected data can be process with a support of advanced statistical methodologies. The contemporary advancement of machine learning and deep learning techniques makes it possible to precisely classify data without a significant amount of computational time. Usage of this technique with collected information would allow to train a labelling tool for proper qualitative recognition. With this knowledge, it is possible to conclude that once a proper targeted study that aims to collect different activity scenarios is conducted, it will be possible to reach application of MPC-HQR in a relatively short period of time.

Acknowledgement

Reference

1. Hensen, J. L. M. & Lamberts, R. (2012) Building Performance Simulation for Design and Operation. Routledge. London (UK).

2. Hong, T., Yan, D., D'Oca, S. & Chen, C. (2017) Ten questions concerning occupant behavior in buildings: The big picture. Build. Environ. 114, 518–530.

3. Ren, Y., Tomko, M., Salim, F. D., Chan, J. & Sanderson, M. (2018) Understanding the predictability of user demographics from cyber-physical-social behaviours in indoor retail spaces. *EPJ Data Sci*. 7, 1.

4. Wilson, E. B. (1958) *An Introduction to Scientific Research*. Br. J. Philos. Sci. 9,.

5. Hong, T., Sun, H., Chen, Y., Taylor-Lange, S. C. & Yan, D. (2016) An occupant behavior modeling tool for co-simulation. *Energy Build. 117*, 272–281.

6. Jamrozik, A. et al. (2018) A novel methodology to realistically monitor office occupant reactions and environmental conditions using a living lab. *Build. Environ. 130,* 190–199.

7. Delzendeh, E., Wu, S., Lee, A. & Zhou, Y. (2017) The impact of occupants' behaviours on building energy analysis: A research review. *Renew. Sustain. Energy Rev. 80,* 1061–1071.

8. FANGER O. P. (1982) Thermal Comfort -Analysis and Applications. *Environ. Eng.* 128–133.

9. de Dear, R. & Schiller Brager, G. (2001) The adaptive model of thermal comfort and energy conservation in the built environment. *Int. J. Biometeorol. 45,* 100–108.

10. Yan, D. & Hong, T. (2018) *International Energy Agency, EBC Annex 66. Definition and Simulation of Occupant Behavior in Buildings*. Annex 66 Final Report..

11. Parsons, K. (2014) *Human thermal environments: the effects of hot, moderate, and cold environments on human health, comfort, and performance*.CRC.

12. Janda, K. B. (2011) Buildings don't use energy: people do. *Archit. Sci. Rev. 54,* 15–22.

13. Yan, D. et al. (2015) Occupant behavior modeling for building performance simulation: Current state and future challenges. *Energy Build. 107*, 264–278.

14. Wågø, S. & Berker, T. (2014) Architecture as a strategy for reduced energy consumption? An in-depth analysis of residential practices' influence on the energy performance of passive houses. *Smart Sustain. Built Environ. 3*, 192–206.

15. Langevin, J., Wen, J. & Gurian, P. L. (2015) Simulating the human-building interaction: Development and validation of an agent-based model of office occupant behaviors. *Build. Environ.88*,27–45.

16. Dong, B. et al. (2018) Modeling occupancy and behavior for better building design and operation-A critical review. *Build. Simul. 11*, 899–921.

17. Dong, B. et al. (2018) Sensing and Data Acquisition. in Exploring Occupant Behavior in Buildings: *Methods and Challenges*. Springer

18. O'Brien, W., Wagner, A. & Dong, B. (2018) Concluding Remarks and Future Outlook. in Exploring Occupant Behavior in Buildings: *Methods and Challenges*, Springer 307–310

19. EQUA Simulation AB. IDA Indoor Climate and Energy:User Manual.

20. Us Department Of Energy. Energy Plus, Energy Plus Documentation. 67 (2010).

21. DeST. DesT. https://www.dest.com.cn/.

22. Payne, A. & Issa, R. (2009) The Grasshopper Primer. (LIFT architects).

23. Omer, I. & Kaplan, N. (2017) Using space syntax and agent-based approaches for modeling pedestrian volume at the urban scale. *Comput. Environ. Urban Syst. 64,* 57–67.

24. Lee, Y. S. & Malkawi, A. M. (2014) Simulating multiple occupant behaviors in buildings: An agent-based modeling approach. *Energy Build. 69*, 407–416.

25. Rendón Rozo, K., Arellana, J., Santander-Mercado, A. & Jubiz-Diaz, M. (2019) Modelling building emergency evacuation plans considering the dynamic behaviour of pedestrians using agent-based simulation. *Saf. Sci. 113*, 276–284.

26. Semchena, J. H., Faigle, E. M., Thompson, R. J., Mazur, J. F. & Steffens Jr, C. E. (1996) Apparatus and method for controlling an occupant restraint system..

27. Clevenger, C. M. & Haymaker, J. (2006) The impact of the building occupant on energy modeling simulations. in Joint International *Conference on Computing and Decision Making in Civil and Building Engineering*, Montreal, Canada 1–10.

28. O'Brien, W., Gunay, H. B., Tahmasebi, F. & Mahdavi, A. (2017) A preliminary study of representing the inter-occupant diversity in occupant modelling. *J. Build. Perform. Simul. 10*, 509–526.

29. Brounen, D., Kok, N. & Quigley, J. M. (2013) Energy literacy, awareness, and conservation behavior of residential households. *Energy Econ. 38*, 42–50.

30. Wang, C., Yan, D., Sun, H. & Jiang, Y. (2016) A generalized probabilistic formula relating occupant behavior to environmental conditions. *Build. Environ. 95,* 53–62.

31. Gilani, S., O'Brien, W. & Gunay, H. B. (2018) Simulating occupants' impact on building energy performance at different spatial scales. *Build. Environ. 132,* 327–337.

32. van Marken Lichtenbelt, W. D. & Kingma, B. R. (2013) Building and occupant energetics: a physiological hypothesis. *Archit. Sci. Rev. 56*, 48–53.

33. Strengers, Y., Nicholls, L. & Maller, C. (2016) Curious energy consumers: Humans and nonhumans in assemblages of household practice. *J. Consum. Cult. 16*, 761–780.

34. Wang, Z. & Zhang, J. (2019) Agent-based evaluation of humanitarian relief goods supply capability. *Int. J. Disaster Risk Reduct.* 101-105.

35. Gram-Hanssen, K. (2010) Residential heat comfort practices: understanding users. *Build. Res. Inf. 38*, 175–186.

36. Butler, C., Parkhill, K. A. & Pidgeon, N. F. (2016) Energy consumption and everyday life: Choice, values and agency through a practice theoretical lens. *J. Consum. Cult. 16,* 887–907.

37. Brager, G., Zhang, H. & Arens, E. (2015) Evolving opportunities for providing thermal comfort. *Build. Res. Inf. 43*, 274–287.

38. Shove, E. & Walker, G. (2014) What Is Energy For? Social Practice and Energy Demand. Theory, *Cult. Soc. 31*, 41–58.

39. Wilhite, H. (2009) The conditioning of comfort. *Build. Res. Inf. 37*, 84–88.

40. Rescorla, R. A., Wagner, A. R.et.all (1972) A theory of Pavlovian conditioning: Variations in the effectiveness of reinforcement and nonreinforcement. *Class. Cond. Curr. Res. theory 2*, 64–99.

41. Dziedzic, J., Yan, D. & Novakovic, V. (2019) Framework for a transient energy-related occupant behavior agent-based model. *REHVA 2019/05* 39–46.

42. MASLOW, A. H. (1943) *Preface to Motivation Theory*. Psychosom. Med. 5,.

43. Ajzen, I. (1991) The theory of planned behavior. *Organ. Behav. Hum. Decis. Process. 50*, 179–211.

44. Doyal, L. & Gough, I. (1984) A theory of human needs. *Crit. Soc. Policy 4*, 6–38.

45. Alderfer, C. P. (1969) An empirical test of a new theory of human needs. *Organ. Behav. Hum. Perform. 4*, 142–175.

46. Rubenstein, R. E. (2001) Basic human needs: The next steps in theory development. *Int. J. peace Stud. 6*, 51–58.

47. Schelly, C. (2016) Understanding Energy Practices: A Case for Qualitative Research. *Soc. Nat. Resour. 29*, 744–749.

48. Shove, E. (2010) Beyond the ABC: Climate Change Policy and Theories of Social Change. *Environ. Plan. A Econ. Sp. 42*, 1273–1285.

49. Jia, M., Srinivasan, R. S., Ries, R., Weyer, N. & Bharathy, G. (2019) A systematic development and validation approach to a novel agent-based modeling of occupant behaviors in commercial buildings. *Energy Build. 199,* 352–367.

50. Page, J., Robinson, D., Morel, N. & Scartezzini, J. L. (2008) A generalised stochastic model for the simulation of occupant presence. *Energy Build. 40*, 83-98

51. Liang, X., Hong, T. & Shen, G. Q. (2016) Occupancy data analytics and prediction: A case study. *Build. Environ. 102,* 179–192.

52. Dwarf Fortress. https://dwarffortresswiki.org/.

53. RimWorld. https://rimworldwiki.com/wiki/Basics.

Undefined modelling parameters impact on building simulation results: using IDA ICE according to the Estonian methodology for calculating building performance

Henri Sarevet[1*], Martin Kiil[1], Raimo Simson[1], Martin Thalfeldt[1], Jarek Kurnitski[1,2]

[1]Tallinn University of Technology, Department of Civil Engineering and Architecture, Ehitajate tee 5, 19086, Tallinn, Estonia
[2]Aalto University, School of Engineering, Otakaari 4, 02150, Espoo, Finland
* corresponding author: henri.sarevet@taltech.ee

Abstract

The Nordic countries have taken important and strict steps moving towards reducing building energy consumption. Energy performance estimation by dynamic building simulation has become a crucial part of the building design. The performance assessment methodology including pre-determined standardised input parameters vary from country to country. The purpose of this study was to analyse the impact of modelling parameters which are not pre-defined but influence the result, and define specific values to be used in the methodology to reduce the uncertainty and variations in the results. The assessed parameters include the definition of the first day of simulation, e.g. startup date, weekday and calendar year, startup pre-simulation specifics and simulation splitting. The simulations were conducted using dynamic simulation software IDA ICE. Calculations were carried out according to the Estonian national methodology for calculating energy performance of buildings. The study analyses the impact of modelling input data parameters which are not pre-defined in the methodology. The effects of these parameters are illustrated by modelling and simulating multiple typical 5-day usage office buildings. The results show that the startup date can affect the results of the net ventilation heating energy, net ventilation cooling energy or energy performance value over 1 kWh/(m²×a). This study highlights the importance of the initial modelling parameters determination on the building energy consumption calculation results.

Introduction

Building energy efficiency importance and implementation in European Union member states and the need for dynamic simulations, in case of nearly zero energy building (nZEB) and low-energy buildings the detail of the simulations can have large effect on the energy performance assessment results. Although not all the member states require a dynamic simulation to prove compliance with national requirements, experienced clients and developers could be interested in vital information regarding simulations in the early stages of the design. In addition, the decisions for mechanical, electrical and plumbing system (MEP) selection criteria in these buildings is more and more dependant on the cost-benefit analyses. Complex technical systems, including heating, ventilation and air conditioning sub-systems require comprehensive and precise simulations. Mastery of dynamic simulation software is a common part of a heating, ventilation and air conditioning (HVAC) engineer on building energy performance specialist. However, simulation software are useful tools for the user, not giving out answers by itself.

There are many variables and parameters in simulation software tool that are not predetermined by the national regulations and can be chosen freely by the energy efficiency specialist who conducts the calculations. These parameters can have large impact on the simulation results and influence the design decisions regarding building systems and renewable energy production systems in order to achieve nZEB energy performance levels.

In the Estonian energy performance regulations for buildings (Ministry of Economic Affairs and Communications 2018), a detailed methodology is given with specific parameters for building modelling and dynamic simulation creation (Ministry of Economic Affairs and Communications 2015b).

In this paper we have addressed these research questions:

- in what extent the startup date, pre-simulation and simulation splitting affect the results of energy consumption or energy performance calculations;
- which is the most affected of the net room heating and cooling, net ventilation heating and cooling, delivered heating energy and electricity and *EPV* in general.

Methods

In this section, the input, modelling, simulation model creation, simulations and analysis steps of the study are described. The undetermined simulation parameters analysed in this study are not defined by regulations (Ministry of Economic Affairs and Communications 2015b). For running simulations in IDA ICE, the user must choose the calendar input, such as start-up date, weekday and calendar year. Therefore, seven different options for the weekday are available. Secondly, user can define the custom startup length. In this study, we have used 14-day length startup for all the default simulations and compared it with 0, 1, 7 and 31-day pre-simulation options. Finally, we ran simulations with multiple parallel processes, as the simulation was split into 6 sub-simulations (one year into six months). Flow chart of

undetermined modelling parameters are seen on Figure 1. Thus, first day of simulation is labelled as P1, startup pre-simulation as P2 and simulation splitting as P3.
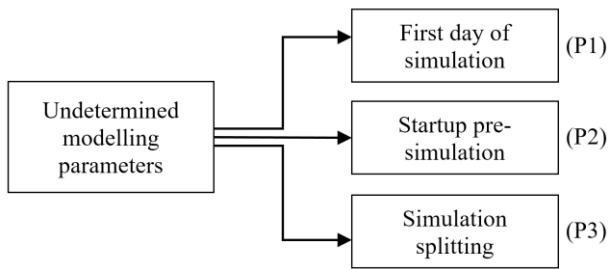

Figure 1: Flow chart of undetermined modelling parameters.

Flow chart of research methodology is seen on Figure 2. Simulation input data is the set of buildings used in this study. To investigate undetermined parameters on the same set of buildings, the main criteria for the buildings is the 5-day usage per week. Otherwise, the first day of simulation impact would be questionable. Therefore, according to Estonian regulation (Ministry of Economic Affairs and Communications 2015b), 5-day usage must be used in energy calculations for office, educational, preschool institution, healthcare and industrial buildings. However, in a multi-purpose building, the *EPV* corresponding to each purpose shall be assigned separately, if heated net floor area exceeds 10% of the total heated floor area (Ministry of Economic Affairs and Communications 2018). Whereas, depending on the remaining building part purposes' efficiencies, single parts of the building can also be below the required criteria independently as the overall *EPV* is decisive.

In this study, we have analysed five office buildings (B1-B5) and five office parts of the buildings (B6-B10), designed between 2015 to 2020. The second criteria were the requirement for at least low-energy building ("B") as *EPV* criteria or the significantly reconstructed building value ("C") (Ministry of Economic Affairs and Communications 2015a). According to issued *EPV* certificates, B1 and B2 met nZEB criteria ("A") and B3 the low-energy ("B") building *EPV* criteria. B4 and B7 were significantly reconstructed to *EPV* corresponding value "C". B5, B6, B8, B9 and B10 to *EPV* corresponding value "D". 3D views of the analysed buildings are provided in Table 1.

Reference buildings are situated in Tallinn or near the capital of Estonia. The highest reference building has eight floors and the lowest has two. The largest analysed office building or part of the building as office is 6890 m² and the smallest is 810 m² by heated net floor area. The reference building MEP system initial data used in analysis includes HVAC information given in the : Building HVAC system information of the analysed office buildings and office parts of the building., domestic hot water information, lighting and appliances energy consumption values (Table 4). In Table 2, heating column consists of heat source and conversion factor values,

building heating system and efficiency factor values and heating auxiliary devices' electricity consumption. The ventilation column includes ventilation supply air temperature, type of the air handling unit heat recovery with efficiency, frost protection temperature, air exchange rate and specific fan power of the air handling units. The cooling column consists of could source with efficiency factor, type of cooling system regarding the room units and condensation losses of the cooling process. The indoor temperature setpoint for heating period is +21°C and for cooling period is +25°C.

Domestic hot water consumption is a default value 6.0 kWh/(m²×a). Default lighting installed power wattage per m² is 10, yet may be varied as other values regarding wattages are allowed to be used, if lighting calculations are conducted in conjunction with the *EPV* evaluation process. Appliances are calculated with default value 12 kWh/(m²×a). Internal gains and schedules are listed in Table 4.

Table 1: 3D views analysed reference office buildings and office parts of the buildings in IDA ICE.

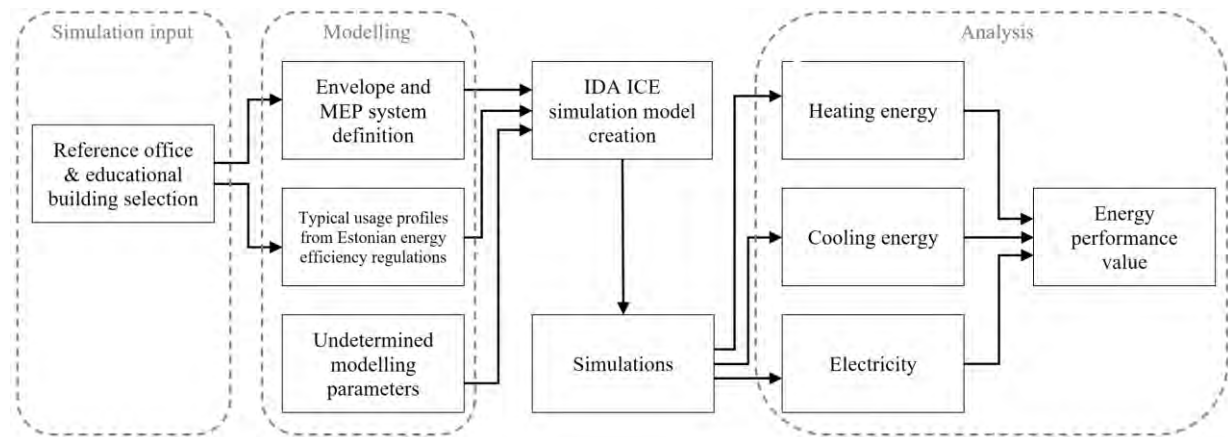| Office buildings	Office parts of the building
Building 1 (B1)	Building 6 (B6)
Building 2 (B2)	Building 7 (B7)
Building 3 (B3)	Building 8 (B8)
Building 4 (B4)	Building 9 (B9)
Building 5 (B5)	Building 10 (B10)

Figure 2: Flow chart of research methodology.

Table 2: Building HVAC system information of the analysed office buildings and office parts of the building.

	Heating				Ventilation				Cooling		
B	Heat source/ conversion factor	Heating system/ efficiency factor	Heating aux. dev. electricity kWh/(m²xa)	Supply air temperature °C	Heat recovery	Efficiency	Frost protection	Air exchange/ SFP	Could source/ efficiency factor	Cooling system	Condensation losses
1	district heating 1.00	underfloor heating 0.92	1.0	20(w) 18(s)	plate heat exch.	0,84/ 0,80	0	2.0 1.78	compressor-driven cooler 3.5	fancoil	0.3/0.2
2	district heating 1.00	underfloor heating 0.92	1.0	18	rotary heat exch.	0.78	-5	2.0 1.80	compressor-driven cooler 3.5	fancoil	0.3/0.2
3	effective district heating 0.90	radiator heating 0.97	0.5	18	rotary heat exch.	0.80	-5	2.0 1.80	compressor-driven cooler 3.9	chilled beam	0.3/0.1
4	district heating 1.00	radiator heating 0.97	0.5	19	rotary / plate heat exch.	0.80	-5/ 0	2.0 1.80	compressor-driven cooler 3.5	fancoil	0.3/0.2
5	gas cond. boiler / AWHP 0,95 / 2,7 / 2	underfloor /radiator heating 0.97	0.5	18	rotary / plate heat exch.	0,80 / 0,84	-5/ 0	2.0 1.30	compressor-driven cooler 3.5	chilled beam	0.2/0.1
6	district heating 1.00	radiator heating 0.97	0.5	18	rotary heat exch.	0.80	-5	2.0 1.80	compressor-driven cooler 3.5	chilled beams	0.3/0.1
7	gas cond. boiler 0.95	underfloor heating 0.93	1.0	18	plate heat exch.	0.80	0	2.0 1.80	split 3.5	fancoil	0
8	gas cond. boiler 0.95	underfloor heating 0.96	1.0	18	plate heat exch	0.80	0	2.0 1.80	compressor-driven cooler 3.5	fancoil	0.3/0.2
9	gas boiler 0.85	radiator heating 0.97	0.5	18	rotary heat exch.	0.80	-5	2.0 2.14	compressor-driven cooler 3.5	chilled beam	0.3/0.1
10	gas. cond. boiler 0.95	underfloor / radiator heating 0.97	1.0	18	rotary heat exch.	0.80	-5	2.0 1.70	compressor-driven cooler 3.5	fancoil	0.3/0.2

Table 3: Building envelope information of the analysed office buildings and office parts of the building.

B	A m²	H/A W/(K×m²)	H/V W/(K×m³)	A_{env}/V m	WWR	WFR	U_{wall} W/(m²×K)	U_{roof} W/(m²×K)	U_{floor} W/(m²×K)	U_{door} W/(m²×K)	U_{window} W/(m²×K)	SF Shading
1	1276	0.43	0.12	0.47	0.36	0.24	0.12	0.09	0.09/0.15	0.9	0.9	0.45, shading E, S, W
2	1329	0.50	0.14	0.58	0.39	0.27	0.10	0.10	0.11	0.8	0.8	0.50 -
3	6890	0.31	0.10	0.24	0.51	0.24	0,15/0,10	0.10	0.11/0.15	1.4	0.65	0.23 0.41 -
4	810	0.84	0.23	0.49	0.33	0.34	0.23	0.13	0.11	1.0	1.0	0.45 -
5	999	0.53	0.16	0.44	0.35	0.29	0,15/0,23	0.11	0.19	1	0.83	0.25/0.30/0.40 -
6	1889	0.60	0.18	0.39	0.55	0.42	0.17	0.12	0.12/0.22	1.2	0.8	0.25 -
7	1613	0.41	0.12	0.46	0.32	0.14	0.17	0.09	0.11	-	0.8	0.30 -
8	1739	0.59	0.15	0.40	0.65	0.29	0.17	0.10	0.08	1.0	1.0	0.50 -
9	5413	0.56	0.16	0.29	0.34	0.21	0.40	0.11	0.19/9.40	1	0,9 / 1,53	0.48 -
10	2190	0.50	0.17	0.35	0.57	0.33	0.16	0.12	0.16	-	0.9	0.31 -

The building envelope information is provided in Table 3. Thermal bridges and infiltration parameters for reference buildings are not brought out in this paper as they are partly different from the regulation-based default values. However, these values are included in the values of *H/A* W/(K×m²) and *H/V* W/(K×m³) with thermal transmittance values indicate the building heat resistance. A_{env}/V ratio represents the compactness of the building. Window-to-floor (*WFR*) and window-to-wall (*WWR*) ratios illustrate the window proportions of the envelope. In addition, window solar factor (*SF*) values and option of shadings are listed in Table 3.

Table 4: Office building internal gains parameters and schedules.
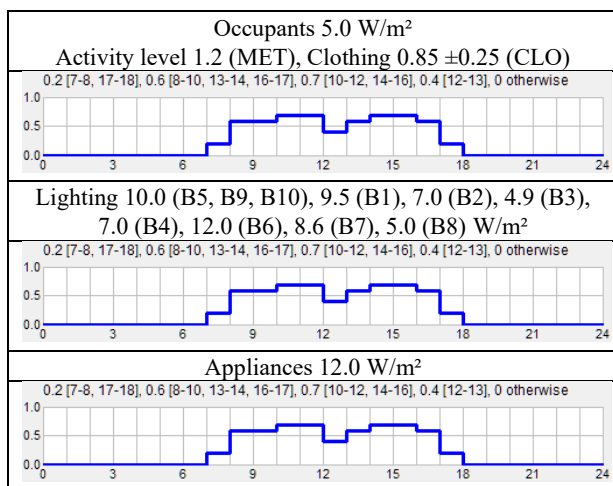
The internal gains and parameters of the reference office buildings are provided in Table 4. Building envelope and MEP system data in this study is provided from the reference building energy performance certificates. Firstly, the energy calculation results are split into net heating, ventilation, cooling, domestic hot water, lighting and appliance energy consumption. Secondly, using heat and cooling source conversion and heating and cooling system efficiency factors, delivered energy is calculated. Finally, the *EPV* is found using primary energy conversion factors. Currently, Estonian regulation sets the *EPV* requirements for nZEB, low-energy building and significantly reconstructed office building as (Ministry of Economic Affairs and Communications 2015a).

- "A" ≤ 100 (nZEB)
- 101 ≤ "B" ≤ 130 (low-energy building)
- 131 ≤ "C" ≤ 160 (significantly reconstructed building)

Therefore, the gap between high efficiency *EPV* for office buildings is 30 units. The simulations were conducted according to the current building energy performance regulations in Estonia (Ministry of Economic Affairs and Communications 2018). Worth noting, that currently, in Estonia, the simplified verification method with a specific energy efficiency calculator for small individual houses is allowed. As an exception, energy calculation software BV^2 is allowed to use in case of major reconstruction of a small individual house, apartment building or barracks.

Estonian local climate data used in this study is based on Estonian test reference year (Kalamees and Kurnitski 2006). The office building models were composed and the simulations were conducted using well validated (Kroph and Zweifel 2002) building simulation software IDA ICE, version 4.8 SP1, EQUA Simulation AB, Stockholm, Sweden (EQUA 2019).

Results and discussion

In this paper, undetermined simulation parameters, such as first day of simulation, startup pre-simulation length and simulation splitting to sub-simulations was analysed.
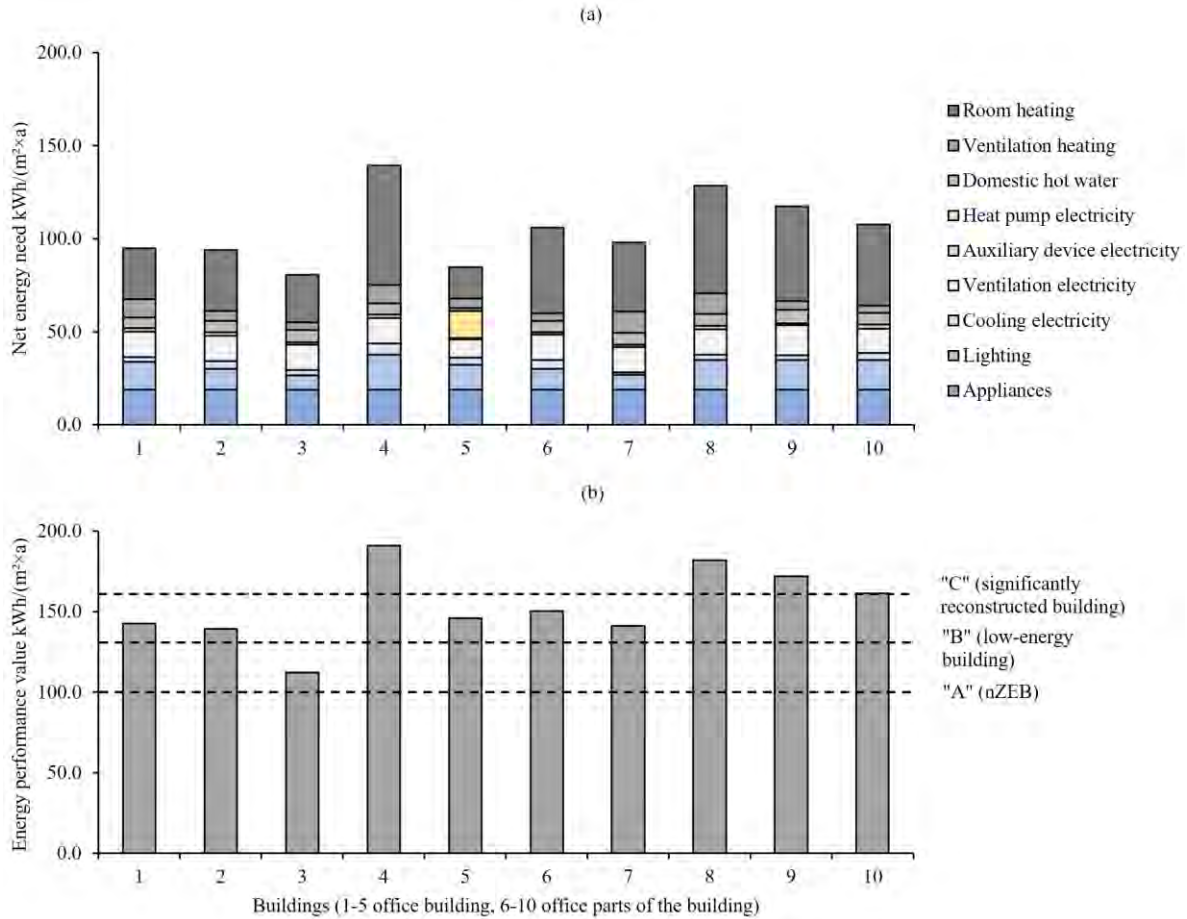
Figure 3: Comparison of base model (a) net energy need kWh/(m²×a) and (b) energy performance value kWh/(m²×a) for reference buildings. EPV is presented without on-site produced energy.

The base model is defined as a year starting with Thursday, using 14-day startup pre-simulation without simulation splitting. The results for each reference building are provided in Figure 3. On the upper part of the figure, the components of net energy need are provided and on the lower part of the figure the *EPV* is presented. For comparison, the on-site produced energy is excluded.

Firstly, room heating and ventilation heating net energy consumption was assessed. The variation of the results is presented on Figure 4. The maximum difference between starting weekday simulation is 0.37 kWh/(m²×a) for room heating and 1.18 kWh/(m²×a) for ventilation heating as the mean values for the reference buildings are 0.08 and 0.43 kWh/(m²×a). For the startup pre-simulation, the maximum differences are 0.52 and 0.04 kWh/(m²×a) and the mean values 0.28 and 0.01 kWh/(m²×a). Regarding simulation splitting, the results vary up to 0.39 and 0.02 kWh/(m²×a) with the mean values of 0.21 kWh/(m²×a) for room heating and for the ventilation heating the difference is close to zero. Ventilation heating has the highest impact, when weekdays for the start of the simulation is exchanged, but obviously insignificant for the startup or the simulation splitting, as the external air temperature is not affected by the building. Opposite to ventilation heating, the room heating is more varied by startup and simulation splitting.
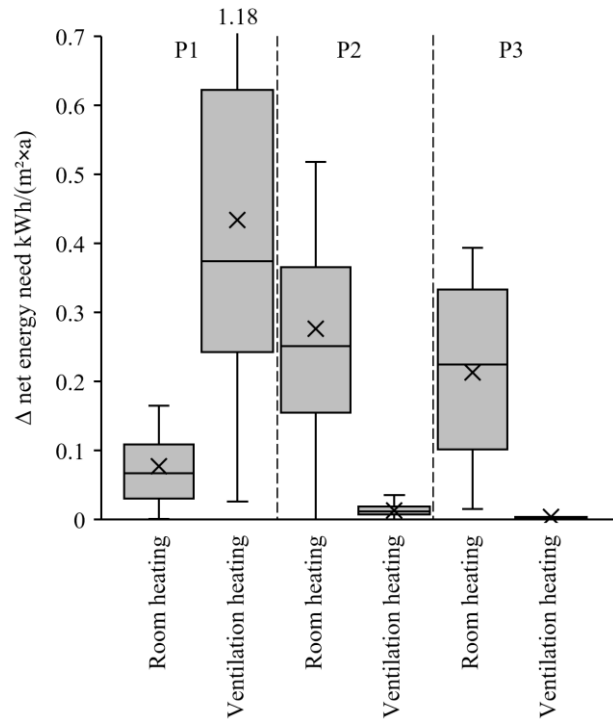

Figure 4: Room heating and ventilation heating net energy need variation with parameters 1 to 3.

Secondly, room cooling and ventilation cooling net energy consumption was assessed. The variation of the results is presented on Figure 5. Similarly, to ventilation heating, the ventilation cooling impact has the highest impact with up to 0.95 kWh/(m²×a) with the mean value of 0.37 kWh/(m²×a). The same results for room cooling are 0.17 and 0.04 kWh/(m²×a). Other simulated parameters do not have any significant effect on the results, except minor effect for room cooling with simulation splitting with the highest and the mean values of 0.08 and 0.03 kWh/(m²×a). Startup simulation does not affect room cooling or ventilation cooling, since simulations were started in the beginning of the calendar year in January. Similarly, to ventilation heating, ventilation cooling is not varied, as the building does not affect the external air temperature.
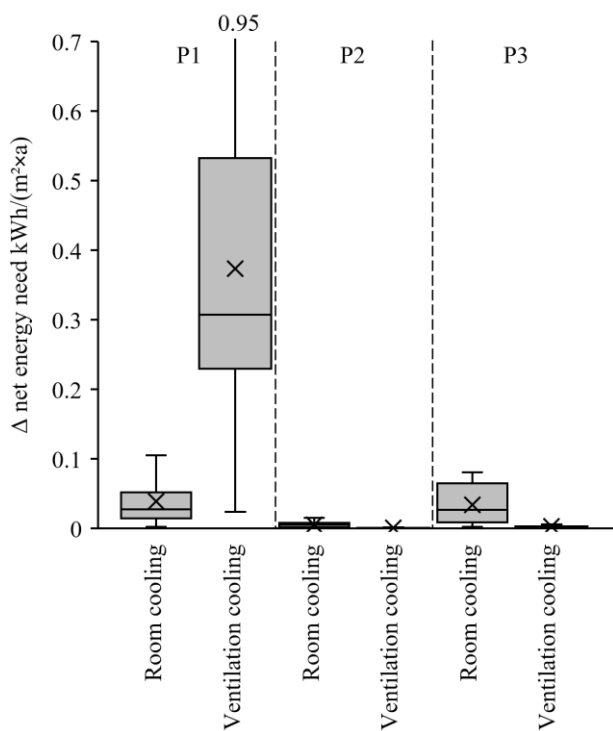

Figure 5: Room cooling and ventilation cooling net energy need variation with parameters 1 to 3.

Finally, delivered heating energy and electricity with *EPV* variation was analysed. For the delivered heating energy, the maximum values are up to 1.19 kWh/(m²×a) for weekday selection, up to 0.58 kWh/(m²×a) for startup pre-simulation comparison and up to 0.41 kWh/(m²×a) for simulation splitting into sub-simulations. As for the electricity, the results are less affected, due to the non-weather-related consumers, such as lighting fixtures and appliances. The effect with startup or simulation splitting is insignificant. The maximum impact regarding start of the simulation weekday comparison results with 0.37 kWh/(m²×a) with the mean value of 0.16 kWh/(m²×a). However, due to the lower impact of the electricity impact, the *EPV* results are correlating with the delivered heating energy. If reference building were more reliable on electrical sources of heating, e.g. heat pump systems,

the results would be more diverse. The maximum impact on EPV is 1.05 kWh/(m²×a) with start of the simulation day comparison with the mean value of 0.45 kWh/(m²×a). Startup comparison shows 0.56 kWh/(m²×a) for the maximum and 0.29 kWh/(m²×a) for the mean *EPV* variation. Simulation splitting has the lowest effect on the *EPV*, as the maximum difference is 0.39 kWh/(m²×a) with the mean difference of 0.21 kWh/(m²×a). The results of delivered heating energy, electricity and *EPV* variation with parameters 1 to 3 are shown on Figure 6.
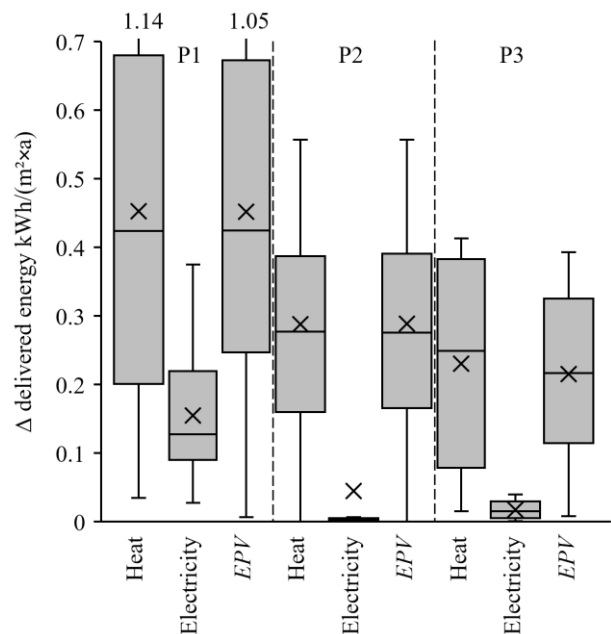

Figure 6: Delivered heating energy, electricity and energy performance value variation with parameters 1 to 3.

The fluctuation of the results shows, that reaching for the higher *EPV* value of the 30-unit gap between the regulation criteria, is approximately 0.5 kWh/(m²×a) on the average (1.7%) and over 1.0 kWh/(m²×a) as the maximum (3.3%) of the analysed buildings. This means, that up to one unit of the *EPV* can be dependant, on the first day of the simulation chosen. Worth recalling, this effect emerges with the 5-day usage buildings. To avoid this uncertainty, the test reference year could be defined to be used with the starting day of Monday as 1st of January for example. Regarding startup length definition and simulation splitting to sub-simulations, the effect on the *EPV* could be up to half of one unit of the *EPV*.

The analysis of this study represents only a few parameters that are undetermined by the local Estonian energy performance regulations. Further studies regarding similar undetermined simulation parameters analysed in this study should include educational and preschool institution buildings, since these buildings are generally half-occupied or empty during the summer holidays. The building energy performance regulations in Estonia guide architects, HVAC engineers and energy performance specialists including developers or building managers to design these buildings without mechanical

cooling systems. However, these calculations including passive methods for maintaining required room air temperature levels must be conducted according to regulations methodology. Therefore, the question arises, in which extent the results are varied for the overheating calculations. In addition, the impact of simulating with different time-step options or the leap year could be assessed. Furthermore, in default simulations daylight saving time is used. Hence, simulating only with summertime or correct schedule including both daylight saving time and summertime should be analysed. Additionally, investigating effect on simulations containing demand-based controlled systems, such as variable air flow ventilation system or occupant or natural lighting-based lighting system, the results variations with the same building models could be assumed.

Conclusion

The aim of this paper is to assess the impact of the undetermined building energy related simulation parameters presented in this study, such as first day of simulation, startup pre-simulation length and simulation splitting to sub-simulations. Five office modern buildings and five office parts of the building, situated in Estonia, were analysed.

The first parameter, consisting of the start of the simulation weekday comparison, showed the highest impact to the results. Depending on the weekday chosen, the net ventilation heating energy may vary up to 1.18 kWh/(m²×a) with the mean value of 0.43 kWh/(m²×a) or the net ventilation cooling energy can vary up to 0.95 kWh/(m²×a) (0.37 kWh/(m²×a) on the average). The delivered heating energy may vary up to 1.19 kWh/(m²×a) (mean value 0.45 kWh/(m²×a)) and the *EPV* up to 1.04 kWh/(m²×a) (mean value 0.45 kWh/(m²×a)). Room cooling and electricity consumption as well as definition of startup pre-simulation or simulation splitting is less sensitive to the overall results. In Estonia, the gap between different *EPV* criteria is 30 kWh/(m²×a) for office buildings. Therefore, up to 1.5% of reaching the desired upper *EPV* criteria is based on pre-simulation definition or dividing simulation into smaller sub-simulations. The gap can be over 3% of the desired result depending on the weekday to be chosen for the startup of the simulation. To avoid uncertainty at given extent for the day at the start of the simulation, a fixed weekday for the start of the whole-year simulation could help.

In conclusion, by the means of the analysed 5-day usage-based office buildings undetermined simulation parameters, we found:

- weekday of the first day of simulation to be considered as an additional variable regarding building energy or energy efficiency calculations;

- startup pre-simulation length and simulation splitting to be less sensible parameters compared to first day of simulation impact.

Acknowledgement

Nomenclature

HVAC	heating, ventilation and air conditioning
MEP	mechanical, electrical and plumbing system
nZEB	nearly zero energy building
A	net heated floor area m²
A_{env}	envelope area of the building m²
EPV	energy performance value kWh/(m²×a)
H	specific heat loss W/K
SF	solar factor
SFP	specific fan power kW/(m³/s)
U	thermal transmittance W/(m²×K)
V	volume of the building m³
WFR	window-to-floor ratio
WWR	window-to-wall ratio

References

EQUA. 2019. "IDA Indoor Climate and Energy 4.8 Equa Simulations AB." 2019. www.equa.se.

Kalamees, Targo, and Jarek Kurnitski. 2006. "Estonian Test Reference Year For," no. June: 40–58.

Kroph, S, and G Zweifel. 2002. "Validation of the Building Simulation Program IDA-ICE According to CEN 13791 'Thermal Performance of Buildings -Calculation of Internal Temperatures of a Room in Summer Without Mechanical Cooling -General Criteria and Validation Procedures.'" HLK Engineering, Hochschule Technik, Architektur Luzern.

Ministry of Economic Affairs and Communications. 2015a. "Estonian Regulation No 36: Requirements for Enerrgy Performance Certificates." State Gazette.

———. 2015b. "Estonian Regulation No 58: Methodology for Calculating Building Energy Performance." State Gazette.

———. 2018. "Estonian Regulation No 63: Minimum Energy Performance Requirements." State Gazette.

The right way to do building simulations? Using Monte Carlo simulations, sensitivity analysis, and metamodeling on a design case

Torben Østergård[1][2]*, Lars Broder Lindgren[2], Rasmus Lund Jensen[1]

[1]Department of the Build Environment, Aalborg, Denmark
[2]MOE Consulting Engineers, Aarhus, Denmark
* corresponding author: to@build.aau.dk

Abstract

Monte Carlo simulations, sensitivity analysis and metamodeling are becoming popular in academia but are rarely applied in real building projects. In this case study, we demonstrate how a combined framework of these methods can aid decision-making in relation to building performance of nine 16-story residential buildings. We describe the processes before, during, and after a meeting between building engineers and the building owner. For preparation, BeDesigner was used to create, run, and analyse 5.000 Be18 simulations in roughly 4 hours. The meeting is initiated with a presentation of sensitivity analysis results to focus the attention towards the most influential design inputs. The 5.000 simulations are visualized with parallel coordinates plots in DataExplorer, which enable decision-makers to observe the consequences of different design choices and regulatory requirements. Real-time sensitivity analysis, TOR, highlights the parameters affected the most by the applied constraints, while histograms indicate favourable or disadvantageous design choices. However, no solutions exist among the 5.000 simulations, which is due to the vastness of the multi-dimensional input space and the decision-makers' numerous requirements. Using metamodels, 500.000 additional input combinations are calculated and from this extensive dataset a variety of solutions are found. It becomes clear that a "no-renewables" ambition necessitates costly counter-measures and makes it difficult to realize the architectural and indoor climate requirements. In conclusion, the combined framework improves the information quality for decision-making and significantly increase the likelihood of finding diverse, high-performing solutions within the same time-frame as traditional practice.

Introduction

Building regulations are gradually being tightened and the number of performance objectives steadily increase. In Denmark, the building energy frame has been reduced by 25% in 2006, 2010 and 2015 while constraints for thermal comfort and daylight have been added or strengthened (Danish Energy Agency, 2020). In 2023, regulations are expected to involve life-cycle-analysis and life-cycle-costs (Ingeniøren, 2020). At the same time, voluntary holistic assessment schemas, such as DGNB, are becoming increasingly popular (Danish Green Building Council, 2020). These circumstances make it harder to find code-compliant solutions and, at the same time, meet the ambitions of different stakeholders, e.g. from the building owner and the architects. In the iterative, interdisciplinary design process, the design team often address many design parameters in search of a solution to all requirements. In this process, building performance simulations (BPS) are used to assess many quantitative requirements while other constraints are evaluated using budget spreadsheets, expert judgement, or past experience. Since such assessments are performed by multiple actors at different companies, most important design decisions are made during interdisciplinary meetings. As building engineer responsible for BPS and code compliance, it is therefore a great challenge to find high-performing solutions and use the information gained from BPS to assist multi-actor decision-making.

First, we outline the typical approach to building simulations in Danish consultancy industry before shifting our attention to trends in academia and software developments. The common approach is to perform a manual parameter study in which a few selected design parameters are varied one-at-a-time based on prior experience and best estimates. The starting point is a reference model constructed on basis of the latest BIM-model combined with initial estimates for construction quality and HVAC system properties. For the parameter study, it is common to manually vary between five to ten design parameters one-at-a-time. The number of parameters and their variations increase when the requirements are difficult to meet. The resulting solutions, and potential design alternatives, are often presented in reports or in slideshows during design meetings. It often requires some compromises to choose a specific option. Sometimes, none of the presented solutions satisfy all stakeholders, e.g. if too costly or aesthetically undesirable, and more alternatives are requested, which require a new parameter study and subsequent meeting. A final note is that the one-at-a-time parameter study only covers a small part of the design space and is most likely to reveal sub-optimal solutions, which depend heavily on a good starting point (Østergård, Jensen and Mikkelsen, 2019).

The traditional one-at-a-time approach is contrasted by statistical methods such as Monte Carlo simulations and multi-objective optimization, which have become

increasingly popular in academia (Tian *et al.*, 2018) (Kheiri, 2018). They make it possible to address a large number of design parameters and explore hundreds or thousands of design combinations. Multi-objective optimizations rely on algorithms to search for high-performing solutions under given constraints. Optimization are mostly done with respect to building control but research also address optimization of building design (Machairas, Tsan-grassoulis and Axarli, 2014). The optimisation usually results in a Pareto front of solutions from which anyone may be selected by making a trade-off between equally important objectives, e.g. energy demand and cost (Longo, Montana and Riva Sanseverino, 2019). However, these solutions may be unfavourable or sub-optimal if not all objectives, for example qualitative ones, have been considered or if the constraints have changed. Another consideration is that optimization try to avoid "poor" designs but such simulations may still contain valuable information, e.g. they can help persuade a stakeholder that a specific design approach yields unsatisfying performance.

The Monte Carlo method, on the other hand, rely on *random* sampling of input combinations, which facilitates sensitivity analysis, Monte Carlo filtering, and the construction of fast metamodels. Sensitivity analysis provide insight into model behaviour and parameter importance, which can help a design team to focus on the most influential inputs and disregard the insignificant ones (Pang *et al.*, 2020). This knowledge can be combined with Monte Carlo filtering, which reveals the consequences of any constraints applied to the simulation inputs or outputs (Østergård, Jensen and Maagaard, 2017a). Lastly, the metamodeling ability means that fast, simplified models of the current building simulation model can be constructed from the Monte Carlo simulations. Valid within the initial input space, metamodels allow for immediate computation of any design configuration and assess specific design changes. With Monte Carlo sampling, no constraints are given on beforehand, which "provides the maximum possible information for use in decision-making" and the search of solution is more flexible than optimization approaches (Wright, Nikolaidou and Hopfe, 2016)(Lee, Pourmousa-vian and Hensen, 2016). In addition, a comparison of structured one-at-a-time optimizations with random Monte Carlo simulations has shown that the latter provides better performing and more diverse solutions – even with the same number of simulations (~30) (Østergård, Jensen and Mikkelsen, 2019).

Initially, the ability to perform automated optimization and Monte Carlo simulations were facilitated by third party "add-ons" or customized scripting, e.g. BEopt, jEPlus, GenOpt, and Matlab. However, in recent years, several developers of BPS software have integrated the capability to define uncertainties and propagate these using random Monte Carlo sampling, e.g. DesignBuilder v. 6 (~2009) and IDA-ICE 4.8 (beta, ~2019). At the same time, it has become less of a burden to compute hundreds or thousands of building simulations due to advances of parallel computing and cloud computing. These developments have made Monte Carlo methods more accessible and easier to use, which may significantly increase their popularity in both academia and industry.

At least in the Nordic countries, the Monte Carlo methods, sensitivity analysis, and metamodeling are still highly uncommon in industry despite the great potentials shown in academia and the recent advances in software applications. This may be due to a number of reasons. First, it necessitates a different workflow for setup, computation, and communication. Stakeholders must also accept another "way-of-thinking". Instead of evaluating few deterministic simulations, design parameters are described by ranges or probabilities and the performance objectives are expressed by distributions. Another possible obstacle could be reluctance by project leaders, or building owners, concerned of increased cost and time for the computation of large numbers of simulations. A final reason may be lack of education or knowledge of these frameworks.

With this paper, we hope to break down the aforementioned barriers. We will demonstrate how to apply a combined framework denoted "MIBS" (Multivariate and Interactive Building Simulations), which rely on Monte Carlo simulations, sensitivity analysis, interactive visualizations, and metamodeling. For this real building case study, the work load and timeframe are comparable to traditional practice, i.e. the efforts needed to perform simulations, analyse results, and communicate the information as part of a multi-actor design process. Throughout the paper, we explain how the MIBS framework differs from typical practice and discuss advantages and disadvantages.

Methods

The case study involves three parts: 1) a meeting preparation phase in which design variations are assessed using building performance simulations and analysed by architectural engineers, 2) a design meeting where multiple decision-makers discuss design alternatives, and 3) subsequent updates of the design. In this section, we describe the building project denoted "Parkbyen", the building requirements, the stakeholder ambitions, the decision-making context, and the software used. We remark that the design process is considered from the perspective of the architectural engineer responsible for building performance simulations and compliance with building code. The building design case is provided by the engineering consultancy company MOE and comparisons of time-frames and workflows in common practice are based on MOEs experience, which are assumed representative for Danish consultancy practice. We remark that the MIBS framework has been applied to more than 10 projects in MOE so this is not an exclusive case.

Building description

The MIBS framework was first introduced to the project late in the conceptual design phase and close to the project delivery for municipal approval. At this point, the project consisted of nine identical, but differently rotated, high-rise buildings – each of 5.622 m² floor area. The façade design and floor plans were relatively fixed, see Figure 1 and 2. In contrast, the constructions and systems were still at a low information level with large variabilities.

Some important characteristics are as follows:

- Heated by district heating
- High heat capacity mainly due to exposed concrete slabs, 129 Wh/K m²
- 62 decentralized air handling units with supply and exhaust ducts leading to the façade in each apartment
- Minimum mechanical ventilation rates, ~0.3 l/s m²
- No mechanical cooling
- 62 decentralized water tanks
- Indoor temperature set point is 20°C (building code)
- Person load is 1.5 W/m² (building code)
- Equipment load is 3.5 W/m² (building code)

Based on experience, we have chosen 16 important design parameters to be varied with the Monte Carlo method, while keeping (supposedly) insignificant inputs fixed, such as pump and hot-water tank properties. The 16 design parameters and their variations are shown on Figure 3. Uniform (discrete or continuous) distributions are used for a several reasons: a) they must describe an unbiased design "variability" where all values are equally possible, b) it makes easier to observe trends when adding constraints, and c) they provide good coverage of the input domain for metamodeling. The variable inputs span an enormous 16-dimensional design space. We "explore" this design space with 5.000 random Monte Carlo simulations, which is considered sufficient to construct accurate metamodels for a more complete coverage of the multidimensional space. The software applications described below have been used to enable this setup.

Performance requirements

At the time the MIBS framework was introduced to the project, the main focus was to balance the design parameters to meet the normative whole-building energy demand without exceeding the budgets. The energy frame for primary energy demand was 30.2 kWh/m² according to Danish building regulations BR18. In terms of thermal comfort, BR18 requires that the temperature in the most critical room must not exceed 27°C for more than 100 hours a year. Daylight requirement is met when the "corrected" glass-to-floor-ratio is at least 10% for each room. The ratio is corrected for shadings, light transmittance, etc. Only a few, "critical" rooms are assessed in terms of thermal comfort and daylight availability at this design stage, see Figure 2. To sum up, the design team had to address three regulatory,

quantitative objectives; primary energy demand, thermal comfort risk, and glass-to-floor-ratio which are often conflicting. E.g., increasing the glazing area may induce overheating or increase energy demand.

Figure 1 Illustration of façade concept and building rotations. Illustration: TRANSFORM.

Figure 2 Floor plan with indication of rooms selected for thermal comfort evaluation (green, blue) and daylight availability (blue, yellow). Illustration: TRANSFORM.

In addition to the regulatory requirements, the building owner requests a solution with no solar cells. To understand the importance of this request, it is worth to notice that due to the frequently strengthened requirements in the building code most new buildings include solar cells. This statement can be supported by the development in medium-sized and large residential building projects in MOE. There, 18 of 27 (67%) projects included solar cells with the BR10 regulations having an energy frame of ~53 kWh/m², which applied from 2010 to 2015. In comparison 16 of 17 (94%) projects included solar cells for BR15 and BR18 project.

Software – BeDesigner and DataExplorer

In Denmark, the normative whole-building energy demand is assessed using the Be18 software, which is based on EN 13790. Be18 includes a module for

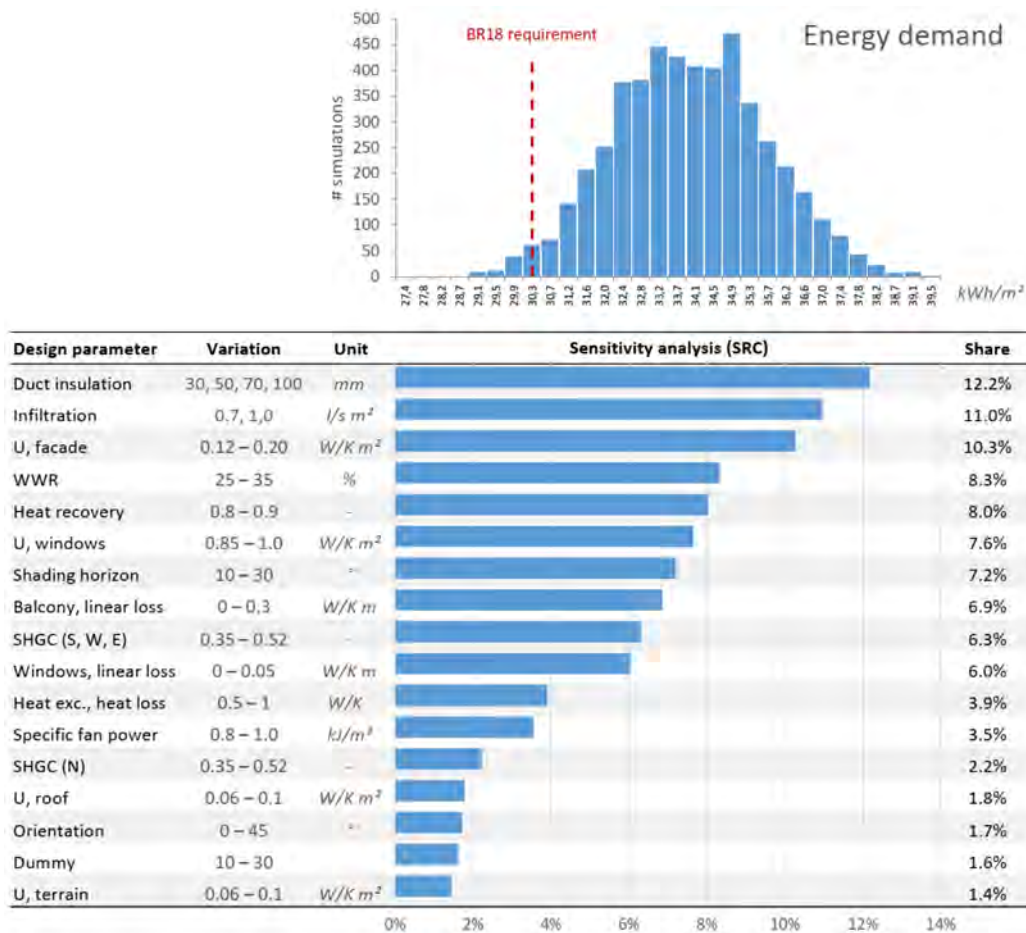| Design parameter	Variation	Unit	Sensitivity analysis (SRC)	Share
Duct insulation	30, 50, 70, 100	mm		12.2%
Infiltration	0.7, 1.0	l/s m²		11.0%
U, facade	0.12 – 0.20	W/K m²		10.3%
WWR	25 – 35	%		8.3%
Heat recovery	0.8 – 0.9	-		8.0%
U, windows	0.85 – 1.0	W/K m²		7.6%
Shading horizon	10 – 30	°		7.2%
Balcony, linear loss	0 – 0.3	W/K m		6.9%
SHGC (S, W, E)	0.35 – 0.52	-		6.3%
Windows, linear loss	0 – 0.05	W/K m		6.0%
Heat exc., heat loss	0.5 – 1	W/K		3.9%
Specific fan power	0.8 – 1.0	kJ/m³		3.5%
SHGC (N)	0.35 – 0.52	-		2.2%
U, roof	0.06 – 0.1	W/K m²		1.8%
Orientation	0 – 45	°		1.7%
Dummy	10 – 30			1.6%
U, terrain	0.06 – 0.1	W/K m²		1.4%

Figure 3 Screenshot from BeDesigner with input variations, distribution of calculated energy demand, and sensitivity analysis (based on standardized regression coefficients).

evaluation of thermal comfort in a "critical" room for residential buildings. Simulation inputs and results are stored in XML files. Based on a reference Be18 model, the novel tool, BeDesigner, is used to define variable inputs and run Monte Carlo simulations with Be18 as "engine" (MOE|BuildingDesign, 2019a). With an Excel interface, the user can quickly select inputs from the reference model and assign probability density functions to represent their uncertainty or variability. Next, a large number of input combinations are constructed from random sampling. After parallel simulations, sensitivity analysis is automatically performed for each output using linear regression (standardised regression coefficients). This shows how much each variable input contribute to the output variation. Thus, sensitivity analysis indicates the parameters relative importance and helps identify which inputs require the most attention and which can be ignored for the time being. The final step in BeDesigner is to create a text-file containing Monte Carlo input and outputs values for further analysis in DataExplorer.

DataExplorer is an online tool for visualization and analysis of multivariate data (MOE|BuildingDesign, 2019b). The simulation data is displayed in an interactive parallel coordinates' plot (PCP), where each simulation is represented by a line showing its input and output values (see Figure 4). The user, or in this case multiple decision-

makers, can search for solutions and test different design strategies by applying constraints to the coordinates.

For each coordinate, a histogram shows the parameter's distribution with the current set of constraints. Initially, the bins are equally wide since we have described input variability using (discrete or continuous) uniform distributions (see top PCP). When adding constraints, some input distributions become skewed. The widest bins therefore indicate favourable input ranges since most of the remaining simulations intersect in those. Thus, histograms help reveal both favourable and disadvantageous input values for the applied constraints range (see bottom PCP). Real-time sensitivity analysis guides the users to those parameters, which have been affected the most by a given set of constraints (Østergård, Jensen and Maagaard, 2017b). This makes it easier to observe the consequences of specific design strategies or criteria.
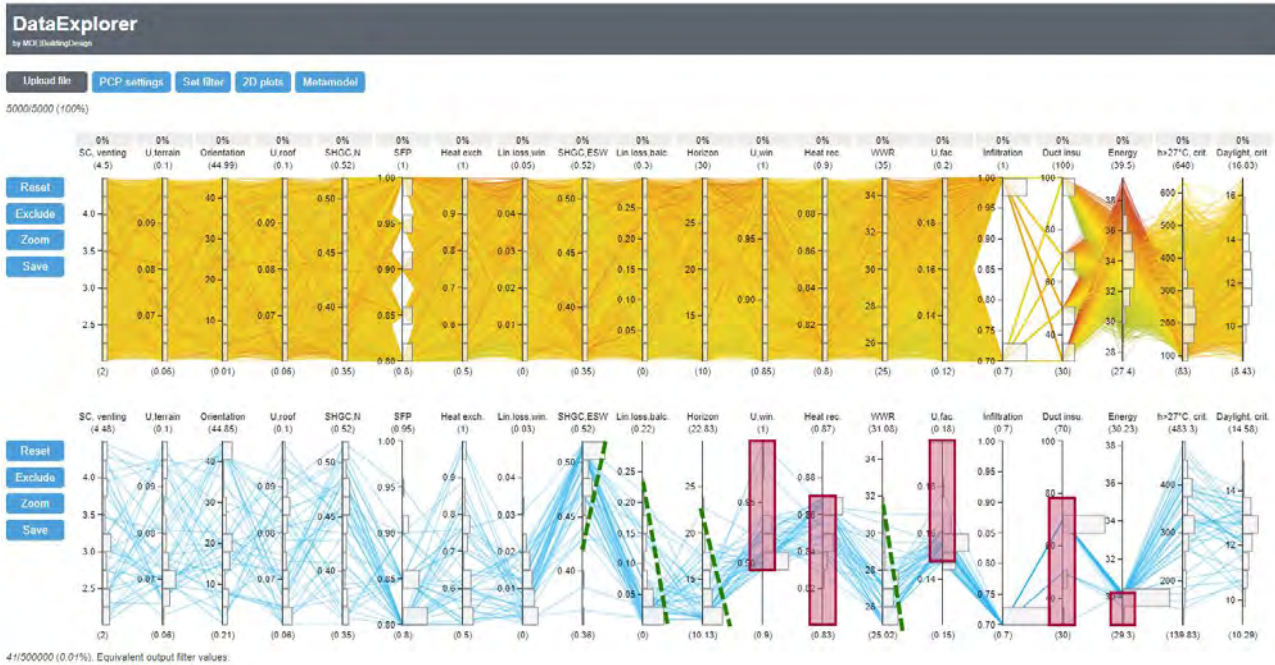
Figure 4 Parallel coordinates plots with 5.000 Be18 simulations (top) and 500.000 metamodel calculations (bottom). Filters are highlighted with red boxes and examples of histogram trends are exaggerated with green, dashed lines.

Finally, DataExplorer enables fast metamodeling using artificial neural networks.[1] Additional design evaluations are often necessary when adding multiple constraints to a large multidimensional dataset. For this case study, the 5.000 randomly selected points cover only a very sparse part of the 16-dimensional design space. But metamodels, "trained" from the 5.000 simulations can calculate 100.000's additional design combinations, in the original space or in a subspace, which allow for a more thorough investigation in a secondary parallel coordinate plot.

The metamodeling feature also address a shortcoming of the PCP visualization that cannot show the expected outcome of changing a single variable by specific amount. To elaborate, the metamodels enable the design team to assess how much an input change, made anywhere in the multidimensional design space, will affect each output on average (and their minimum and maximum output changes), see Figure 5. E.g. the effect of an incremental increase in SHGC (solar heat gain coefficient) of 0.1 will depend on other design parameters, such as WWR (window-wall-ratio), shading, etc., and therefore the effect on energy demand could be 1 kWh/m² on average, but with smaller values when WWR is low and shading high, and vice versa.

Results and discussion

Preparation for design meeting

Based on experience and knowledge of building physics, a total of 16 inputs have been selected as variable parameters. Their variations are defined with either a range (minimum to maximum value) or discrete values as shown on Figure 3. With the Monte Carlo framework, the 16 design parameters are varied randomly 5.000 times. The resulting distribution of energy demand is shown on Figure 3 and ranges from 27.4 to 39.5 kWh/m² year. The first significant learning is that only ~2% of the calculations is within the energy frame – without considering the constraints related to daylight and thermal comfort. Figure 3 also shows the results of the sensitivity analysis, which indicate the inputs' relative contributions to the variation in calculated energy demand. It came as a surprise to the engineers that the variation in ventilation heat recovery has more than twice the effect/influence (~8%) than the variation of specific fan power, SFP (~3.5%). This is valuable information since its easier and cheaper to install a better heat recovery than minimizing pressure loss in the entire ventilation system. Another surprise was that the variation in duct insulation was the most influential design parameter and would therefore require much attention at the design meeting. This parameter is rarely an issue since ducts are often placed in heated installation shafts but, in this case, cold ducts run from decentralized units to the façade.

The sensitivity analysis also provides insight into the influence of the detail level of the horizon angle. At this stage in the project, the same horizon angle had been used for all windows. The reason for this is that the model representation in Be18 is rather limited and as a consequence, it necessitates subjective, time-consuming approximations of the shading angles. Since window

---

[1] Metamodels are constructed from 3-layered feedforward neural network for which the user defines the training and test sizes and the number of neurons in the hidden layer.

positions and building rotations were still uncertain, the engineers chose to simplify the model representation and instead describe this modelling uncertainty by varying the horizon angle for all windows from 10 to 30°. The sensitivity analysis shows that this uncertainty contributes with roughly 7% to the variation in energy demand corresponding to 0.9 kWh/m². This is an approximation but it gives an idea of the possible impact of the simplification of shading objects.[2] Another thing, the horizon angle also affects thermal comfort and daylight. Ultimately, this analysis showed the engineers that the Be18 model had to be refined at a later stage and the design team should include a "buffer" for later design changes (which is common practice).

Even though main focus is on energy demand at this stage, the design team must pay attention to how design decisions may influence thermal comfort and daylight. Notably, thermal comfort may cause a challenge since the distribution of overheating hours for the corner-room (see Figure 2) ranges from 83 to 648 hours. Only 67 of the 5.000 simulations (1.3%) meet the requirement of maximum 100 hours, and this necessitates windows with a SHGC of maximum 0.37. Thus, no simulations meet both the energy frame and the thermal comfort requirement. However, actions can be taken to deal with thermal comfort in a few critical rooms without notably affecting the whole-building energy performance. For example, fixed windows may be made openable to allow for a higher air flow or the SHGC may be lowered for the "critical" rooms only. Regarding daylight, the "corrected" glass-floor-ratio ranges from 8.4 to 16.8% for the "critical" living room. Since most simulations (93%) meet the criterion, daylight seems to be of little concern. Based on these room-level results, the engineers can raise the issue with thermal comfort at the meeting and urge the design team to address it as soon as possible.

The total timeframe for this preparatory work was a roughly four hours. This includes the following: 1) selection of design parameters and definition of their variations; 2) adjusting the reference Be18 model, setting up BeDesigner, and running 5.000 simulations; and 3) interpretation of results and test of design strategies. The reported timeframe excludes the construction of the Be18 reference model, which was already set up with geometry, shading, internal loads, etc. The timeframe is similar to ordinary practice with roughly 10 to 20 manual variations which, hopefully, results in a few solutions.

MIBS framework at the design meeting

The main purpose of the meeting with the building owner and his consultants was to discuss possible solutions to achieve code compliance. The choice of design parameters and their variations was explained to all decision-makers. The distribution of calculated energy demand was presented and the few energy-compliant solutions underlined the difficulty of reaching compliance without renewables. The results from the sensitivity analysis point out that many inputs influence the energy demand. Focus should be on the most important ones, i.e. duct insulation, infiltration/air tightness, and façade insulation, while the decision-makers may somewhat ignore orientation, roof insulation, and ground insulation for the time being. With this background knowledge, the participants used the interactive coordinates plots in DataExplorer to assess the consequences of different design strategies.

By applying filters, some of the initial variations are left out, e.g. duct insulation of 100 mm for aesthetic and spacing reasons, which reduce the design space and potential solutions. Due to the large dimensionality, no solutions remain from the 5.000 Be18 simulations when adding all of the participants' requirements.[3] This issue is overcome by adding 500.000 extra design combinations using the metamodeling feature. Finally, solutions are found but it becomes clear that several costly actions are necessary to accommodate the desired constraints, e.g. 70 mm duct insulation, high airtightness, and a SHGC ≥ 0.47. The latter causes a challenge since, as discovered prior to the meeting, the SHGC for the corner-room has to be 0.37 or less to meet the thermal comfort criterion. Thus, other actions need to be made to ensure thermal comfort in the critical rooms. In the end, it was advised to consider renewables, which would make it easier to meet code compliance and it would provide a "buffer" for later design changes.

For this real-time design space exploration, it is worth mentioning that the construction of metamodels was done in less than a second and calculation of 500.000 new points within 10 seconds. Moreover, metamodels are rarely perfect but with R²-values from 0.96 to 0.99 they are sufficiently accurate to reveal the correct consequences of design choices.[4]

In conclusion, the participants were positive towards this novel framework and the ability to explore (almost) all design options and find solutions in collaboration. It is doubtful that any "no renewables solutions" could be identified without it. However, if considering only a single objective (energy), a few solutions may have been found using the traditional, manual approach by choosing the most expensive options for many design parameters. But some of these may deem too costly or otherwise inappropriate that the solutions would be discarded resulting in the building owner to require more inputs, or other variations, to be considered. Then the entire preparation/simulation process would need to be repeated

---

[2] Assuming a linear model (R² of the linear regression is 0.96) and that model refinements would be within this uncertainty.

[3] Constraints: no solar cells, $U_{facade} \geq 0.15$, $U_{windows} \geq 0.9$ and heat recovery ≤ 0.87, and duct insulation ≤ 70mm.

[4] Inaccurate metamodels with R²~0.4 have been shown to reveal the same trends as the true models when adjusting the constraints slightly (Østergård, Jensen and Maagaard, 2017a).

and a new meeting scheduled. Finally, the framework highlighted the necessity to consider all requirements at the same time, i.e. energy, thermal comfort, and daylight.

Subsequent design changes

A few after the design meeting, the architects shared an updated BIM-model with the engineers. Some windows had been removed, or made smaller, resulting in a reduction of window-wall-ratio from 31.5 to 26.9%. In addition, the heated floor had increased from 5.622 to 5.727 m². Such changes of BIM-models happen frequently over the course of a building design project. Unfortunately, there is not sufficient time and money to update the energy model, and other BPS models, every time. This is partly due to the lack of interoperability between Revit and the Be18 energy model. Thus, the engineers had to consider if it was necessary to spend half a day's work to redo the tedious, manual measurements. As we will show, the MIBS framework helped the engineers to make this decision.

The sensitivity analysis for energy demand shows that WWR is the fourth most influential design parameter so it does impact the energy demand significantly (see Figure 3). But what will a reduction of ~4.6% lead to? Well, that depends on other variable parameters, such as $U_{windows}$, SHGC, and Horizon (shading angle). Based on the metamodels, we can estimate this reduction of WWR while keeping the other parameters uncertain. This is done using the "what-if" table in DataExplorer, which calculates the possible outcomes of the reduction in WWR at 100 random locations in the design space (see (Østergård, Jensen and Maagaard, 2017a) for in-depth explanation). Figure 5 show that a reduction of 4.6% will reduce energy demand by 0.83 kWh/m² on average but depending on the other parameters the energy demand may reduce in the range 0.24 to 0.96 kWh/m². Based on this knowledge, the engineers could choose to postpone the update of the energy model. However, since the floor area had not been varied in the Monte Carlo simulations, we could not assess the consequences of this change using the metamodels. Though, the small increase of floor area was expected to have little, and positive, impact. The decisive argument was the aforementioned uncertainty related to the horizon (shading angle) input. Due to this uncertainty, the engineers chose to refine the inputs related to shading and update the entire energy model according to the new BIM model. Finally, we remark that the information gained from the metamodels could have been use to inform the architects about the expected consequences of changes of window-wall-ratio. Thereby, the architects would not be making changes "in the blind" but with knowledge of the most likely consequences on energy demand (and thermal comfort or daylight in the critical rooms).

	ΔX_i	$X_{i,span}$	Energy
Duct insu.		30 - 100	
Infiltration		0.7 - 1	
U,fac.		0.12 - 0.2	
WWR	-4.6	25 - 35	-0.83 (-0.96 – -0.24)
Heat rec.		0.8 - 0.9	
U,win.		0.85 - 1	

Figure 5 Screenshot of "what-if" table in DataExplorer showing the average (and min-max) response to energy demand by decreasing WWR by 4.6 percentage points.

Conclusion

In this case study, we have applied a Monte Carlo based framework which enables: 1) sensitivity analysis to inform decision-makers of important and insignificant design parameters, 2) construction of fast metamodels that enable an all-encompassing exploration of design alternatives, and 3) real-time Monte Carlo filtering and design feedback. The framework helped assist decision-making for a real building project within the same time-frame as in common practice. The following sums up valuable, project-specific insights gained from the combined framework:

- Less than 2% of 5.000 Be18 simulations met the energy frame stressing the difficulty of finding a "no-renewables" solution.

- Using metamodels to evaluate 500.000 additional combinations, it was possible to find technical solutions to the decision-makers' requirements.

- The conditions, needed to meet all requirements for the whole-building energy demand, would make it difficult to achieve thermal comfort in critical rooms for which other actions would be necessary.

- Inclusion of solar cells was advised to avoid costly solutions and to create a "buffer" for future changes and to meet with thermal comfort criteria.

- Design parameters were ranked with respect to their influence on energy demand which showed some surprises, i.e. duct insulation ranked first and the variation of ventilation heat recovery had more than twice the effect of varying the specific fan power.

- The sensitivity analysis also showed that building's rotation was of little concern.

- Sensitivity analysis revealed the shading angle, horizon, to have considerable importance calling for a refined model.

- The metamodels could be used to estimate the consequences of the reduced window-wall-ratio in the architects' updated BIM-model.

Feedback from meeting participants have been positive and they had no problems to engage with the new type of information and the interactive visualizations. They

appreciated the extent of design alternatives, which provide more confidence in their choices.

In conclusion, this work has demonstrated how a combined framework of Monte Carlo simulations, sensitivity analysis, metamodeling, and interactive visualization can be applied to a real building project. This makes it much more plausible to find diverse, high-performing, and cost-effective solutions, which again reduces the need for additional design iterations and meetings. If requirements for LCA and LCC are added to future building regulations, we can no longer simply add renewables. This would further advocate for a framework enables extensive search of solutions and the ability to assess and balance multiple design parameters.

Finally, we believe that this framework is also applicable for more advanced, time-consuming BPS. The time to set up and analyse results is presumably less than for manual, iterative parameter studies. The extended computational effort can be addressed by parallel or cloud computing and the Monte Carlo simulations may also be run during lunch breaks or overnight or while working on other tasks.

Acknowledgements

References

Danish Energy Agency (2020). *Danish Building Regulations, BR18*. http://bygningsreglementet.dk.

Danish Green Building Council (2020) *Statistik over certificeringer*. https://www.dk-gbc.dk/dgnb/certificering/statistik-over-certificeringer

Ingeniøren (2020) Minister: *Fra 2023 bliver bæredygtighed et krav i byggeriet*. https://ing.dk/artikel/minister-2023-bliver-baeredygtighed-krav-byggeriet-231842

Kheiri, F. (2018). A review on optimization methods applied in energy-efficient building geometry and envelope design. *Renewable and Sustainable Energy Reviews 92,* 897–920. doi: 10.1016/j.rser.2018.04.080

Lee, B., Pourmousavian, N. and Hensen, J. L. M. (2016). Full-factorial design space exploration approach for multi-criteria decision making of the design of industrial halls. *Energy and Buildings 117*, 352–361. doi: 10.1016/j.enbuild.2015.09.028.

Longo, S., Montana, F. and Riva Sanseverino, E. (2019). A review on optimization and cost-optimal methodologies in low-energy buildings design and environmental considerations. *Sustainable Cities and Society 45*, pp. 87–104. doi: 10.1016/j.scs.2018. 11.027.

Machairas, V., Tsangrassoulis, A. and Axarli, K. (2014). Algorithms for optimization of building design: A review'. *Renewable and Sustainable Energy Reviews, 31*, 101–112. doi: 10.1016/j.rser.2013.11.036.

MOE|BuildingDesign (2019a). *BeDesigner*. https://buildingdesign.moe.dk/tools/bedesigner/

MOE|BuildingDesign (2019b). *DataExplorer*. https://buildingdesign.moe.dk/tools/dataexplorer/

Østergård, T., Jensen, R. L. and Maagaard, S. E. (2017a). Early Building Design: Informed decision-making by exploring multidimensional design space using sensitivity analysis. *Energy and Buildings 142*, 8–22. doi: 10.1016/j.enbuild.2017.02.059.

Østergård, T., Jensen, R. L. and Maagaard, S. E. (2017b). Interactive Building Design Space Exploration Using Regionalized Sensitivity Analysis. *Proceedings of the 15th International Conference of the International Building Performance Simulation Association*. San Fransisco (USA), 7-9 August 2017.

Østergård, T., Jensen, R. L. and Mikkelsen, F. S. (2019). The best way to perform building simulations? One-at-a-time optimization vs. Monte Carlo sampling. *Energy and Buildings 208* doi: 10.1016/j.enbuild.2019.109628.

Pang, Z. et al. (2020). The role of sensitivity analysis in the building performance analysis: A critical review. *Energy and Buildings 209*. doi: 10.1016/j.enbuild.2019.109659.

Tian, W. et al. (2018). A review of uncertainty analysis in building energy assessment. *Renewable and Sustainable Energy Reviews 93*, 285–301. doi: 10.1016/j.rser.2018.05.029.

Wright, J., Nikolaidou, E. and Hopfe, C. J. (2016). Exhaustive Search; Does it have a Role in Explorative Design? *Proceedings from BSO2016: Building Simulation and Optimisation Conference*. Newcastle (UK), 12-14 September 2016.

BUILDSIM-NORDIC 2020
Selected papers

This book contains selected papers from the BuildSim-Nordic 2020 conference, October 13th & 14th 2020. The conference was hosted by OsloMet University in Oslo, Norway, and organized in cooperation between the Nordic chapter of IBPSA, OsloMet and NORVAC.

The BuildSim-Nordic 2020 conference is the first in a series of events with a long-term objective to establish a key biannual international conference in building performance simulation, with a strong focus on Nordic countries. The purpose is to create a platform for exchanging ideas, issues, and research findings that facilitates international collaboration and the meeting of minds between practitioners, researchers, and students.

IBPSA-Nordic is a regional affiliate of IBPSA, the International Building Performance Simulation Association, for four countries: Denmark, Finland, Norway and Sweden.

IBPSA-Nordic is linked to IBPSA-World association but acts as an independent organization.

IBPSA-Nordic is a non-profit association.

Four countries form IBPSA-Nordic: Denmark, Finland, Norway and Sweden.

IBPSA-Nordic was founded in 2011 to promote the science and practice of building performance simulation and to improve the energy, environmental and economic performance of buildings and their systems in the four covered countries.

IBPSA-Nordic provides a forum for exchange of knowledge and coordination between research-ers, designers, developers and practitioners in the field of building performance simulation and related issues in the four covered countries.

IBPSA-Nordic will strive to achieve its objectives on the level of each country and on the regional level through various activities (e.g. meetings, seminars, workshops, publications, education pro-grammes, training, coordinated activities with other associations on national and regional levels and holding the biennial regional technical event).

Affiliate of IBPSA   IBPSA

SINTEF Academic Press